THE UNIVERSITY
of EDINBURGH

Systematics, Biomechanics and Ecology of Mammals of the Kilmaluag Formation (Jurassic) of Scotland

Elsa Panciroli

THE UNIVERSITY *of* EDINBURGH

Thesis submitted for the degree of

Doctor of Philosophy

University of Edinburgh

School of Geoscience

Year of Submission 2020

Declaration

I declare that the work submitted herein is entirely my own, except where work has been part of jointly-authored publications. This thesis contains five chapters that have been published in peer-reviewed journals, or are currently in review. Details of these publications are outlined below, and also indicated within the text of the thesis. I confirm that I conceived of and was principle author on all of these works, performing the bulk of the data gathering, analysis, manuscript preparation and revisions based on co-author feedback, unless indicated otherwise below. The appropriate credit has been given where reference has been made to the work of others, including in-text and in the Acknowledgements. No part of this thesis has been submitted for any other degree or professional qualification.

The work presented in Chapter 3.1 was previously published as: Panciroli, E., Walsh, S., Fraser, N., Brusatte, S.L. and Corfe, I. 2017. A reassessment of the postcanine dentition and systematics of the tritylodontid *Stereognathus* (Cynodontia, Tritylodontidae, Mammaliamorpha), from the Middle Jurassic of the UK. *Journal of Vertebrate Paleontology*, 37:1351448. The study was conceived by all of the authors. I carried out data gathering, analysis, manuscript preparation and revisions. I. Corfe provided additional specimens and data. Co-authors provided comments and revisions.

The work presented in Chapter 3.2 was previously published as: Panciroli, E., Benson, R.B.J. and Walsh, S. 2017. The dentary of *Wareolestes rex* (Megazostrodontidae): a new specimen from Scotland and implications for morganucodontan tooth replacement. *Papers in Palaeontology*, 3:373–386. The study was conceived by all of the authors. I carried out data gathering, analysis, manuscript preparation and revisions. R.B.J Benson provided additional specimens and data. Co-authors provided comments and revisions.

The work presented in Chapter 3.3a was previously published as: Panciroli, E., Benson, R.B.J. and Luo, Z.-X. 2019. The mandible and dentition of *Borealestes serendipitus* (Docodonta) from the Middle Jurassic of Skye, Scotland. *Journal of Vertebrate Paleontology*, e1621884. I conceived the study with Z-X. Luo. I carried out data gathering, analysis, manuscript preparation and revisions. R.B.J Benson and Z-X. Luo provided additional specimens, data, comments and revisions.

The work presented in Chapter 3.3c was previously published as: Panciroli, E., Schultz, J.A. and Luo, Z.-X. 2018. Morphology of the petrosal and stapes of *Borealestes* (Mammaliaformes, Docodonta) from the Middle Jurassic of Skye, Scotland. *Papers in Palaeontology*, 5:139–156. The study was conceived by all of the authors. I carried out data gathering, analysis, manuscript preparation and revisions. J. Schultz and Z-X. Luo provided additional data, anatomical observations, comments and revisions.

The work presented in Chapter 3.4 was previously published as: Panciroli E., Benson, R.B.J. and Butler R.J. 2018. New partial dentaries of *Palaeoxonodon ooliticus* (Mammalia, Amphitheriidae) from Scotland, and posterior dentary morphology in stem cladotherians. *Acta Paleontologica Polonica*, 63:197–206. The study was conceived by all of the authors. R.J. Butler also provided specimens. R.B.J. Benson also provided micro CT data. I carried out analysis, manuscript preparation and revisions. Co-authors provided comments and revisions.

Elsa Panciroli
8/01/2020

Abstract: The Middle Jurassic was a pivotal time in the macroevolution of mammals. The earliest mammaliaform branches flourished alongside non-mammalian cynodonts (tritylodontids) and the first crown group mammals. Recent fossil material from China suggests not only that mammaliaforms were unexpectedly ecologically diverse, but that Docodonta had exceptionally high ecomorphological diversity for such a geologically early-diverging clade. Understanding these macroevolutionary patterns is hindered by the paucity of Middle Jurassic material globally. The Kilmaluag Formation of the Isle of Skye, Scotland, provides a rare, exceptionally well-preserved fossil mammaliaform assemblage. The analysis of this material provides new data to answer phylogenetic and ecological questions about Middle Jurassic mammaliaforms.

I utilise synchroton tomographic data of the first skeleton of a Middle Jurassic mammaliaform from the British Isles, *Borealestes serendipitus*. As a basal docodontan, *Borealestes* provides key anatomical information for resolving docodontan phylogenetic relationships. Using these data I clarify the diagnosis of *Borealestes* and identify two new petrosal structures: the trans-cochlear canals anterior and posterior. I perform two phylogenetic analyses: 1) using a large docodontan dataset of dentomandibular characters; 2) an analysis with few docodontans but multiple mammaliaform lineages using dentomandibular, cranial, postcranial and soft tissue characters. These provide conflicting results that suggest the lack of skeletal characters for most docodontan genera impacts the usefulness of an expanded character dataset for resolving docodontan relationships. In the dentomandibular-based phylogenetic analysis I find *Borealestes* belongs to a previously proposed basal docodontan clade along with *Docodon, Docofossor* and *Haldanodon*.

Additionally, using conventional micro computed tomography of multiple teeth and dentaries I describe the anatomy and test the systematic position of *Stereognathus*, *Wareolestes,* and *Palaeoxonodon* material. These data permit the clarification of the diagnosis of *Stereognathus ooliticus* (=*hebridicus*), and

outline previously unknown anatomy, and the identity of disputed lower molars in the holotype, of *Wareolestes*. By combining new *Palaeoxonodon* material with previously collected material from Skye, I find additional characters of the posterior dentary including a deep, anteriorly enclosed masseteric fossa, and mandibular foramen offset from the Meckel's sulcus and positioned below the alveolar plane.

Finally, I explore the ecology and ecomorphology of the mammaliaforms of the Kilmaluag Formation using body mass estimation and biomechanical and morphometric analyses. These analyses support niche partitioning among the Kilmaluag mammaliaform assemblage. They also suggest early mammaliaform biomechanics cannot be easily assessed using morphological datasets of extant, phylogenetically distant eutherian, monotreme and metatherian relatives due to the conserved morphology of many skeletal structures—particularly the calcaneus and astragalus—in early mammaliaform taxa.

Summary: The Middle Jurassic was a pivotal time in the evolution of mammals—the group to which we belong. We often discuss their emergence as taking place after the dramatic extinction of the non-avian dinosaurs around 66 million years ago, but their success-story stretches at least another 150 million years further back in time. The earliest members of this group, the mammaliaforms, flourished alongside the dinosaurs and marine and flying reptiles in the Jurassic. Recent fossil material from China suggests not only that mammaliaforms were unexpectedly ecologically diverse at this time, but that one very early branching group called Docodonta had exceptionally high diversity in their ecological specialisations. Our understanding of the emergence of this diversity is hindered by the lack of Middle Jurassic fossil material globally. The Kilmaluag Formation of the Isle of Skye, Scotland, provides a rare, exceptionally well-preserved fossil mammal assemblage to study. Analysing this material provides new data to help answer questions about Middle Jurassic mammal relationships and ecology.

I gathered and studied computed tomography (micro-CT) scans of the first skeleton of a Middle Jurassic mammaliaform from the British Isles, *Borealestes serendipitus*. *Borealestes* is an early member of Docodonta, and so provides key anatomical information for understanding their family relationships. Using these scans I clarify the anatomy of *Borealestes* and identify new structures in the ear bones that contribute to our larger understanding of the evolution of mammal hearing. I analyse the skeletal anatomy of *Borealestes* alongside other mammals, first using only the shape of the teeth and jaws, then of the entire skeleton. These analyses give conflicting results, but the teeth and jaws support the idea that *Borealestes* is part of a ‘basal docodontan’ group, which includes some of the first docodontans to appear in the fossil record. These analyses suggest that the lack of fossil skeletal material for most docodontans—which are mainly known from just teeth and jaws—limits the usefulness of using whole-skeletons to understand family relationships in this group.

Additionally, I use micro-CT scans of multiple teeth and jaws to describe the anatomy and analyse the family relationships of the close mammal-relative *Stereognathus*, mammaliaform *Wareolestes,* and early mammal *Palaeoxonodon*, all found on the Isle of Skye. These data make it possible to clarify the anatomy of *Stereognathus ooliticus* (previously thought on Skye to be a separate species, *S. hebridicus*). I describe previously unknown anatomy for *Wareolestes*, and combine new *Palaeoxonodon* material with previously collected material from Skye, finding additional characteristics of the jaw that tell us more about its morphology.

Finally, I explore the ecological diversity of the mammaliaforms of the Kilmaluag Formation. I calculate estimates of body mass, and analyse their jaws and skeleton visually, quantitatively, and using engineering principles to find out how anatomy relates to lifestyle in these animals. These analyses support niche-partitioning among the Kilmaluag mammaliaform assemblage. They suggest that the form and function of the skeletons of the earliest mammals in the Middle Jurassic cannot easily be assessed by comparison with living mammals, which are only distantly related to them. This is especially true of the bones of the foot of *Borealestes* used in this study, probably because the shape of these bones more closely resembles their pre-mammalian ancestors, than their living relatives.

Contents

List of Figures Page

List of Tables

Abbreviations

Institutional Abbreviations: BGS, British Geological Survey, London, U.K.; **BRSUG** (formerly UBGM), Geology Museum, University of Bristol, U.K.; **DORCM**, Dorset County Museum, Dorchester, U.K.; **GLRCM**, Gloucester City Museum, Gloucester, U.K.; **NHMUK**, Natural History Museum, London, U.K.; **NMS**, National Museum of Scotland, Edinburgh, U.K.; **OUMNH**, Oxford University Museum of Natural History, Oxford, U.K.

Other abbreviations: FEA, finite element analysis; **MPT**s, most parsimonious trees; **TBR**, tree bisection and re-connection; **µCT**, micro-computed tomorgraphy.

Chapter 1: The Early Evolution of Mammals

1.1 Introduction

Today's extant mammals belong to crown Mammalia, part of the larger clade called Mammaliaformes (Rowe, 1988, McKenna and Bell, 1997). The mammaliaforms have their origins in the Late Triassic, and include all taxa descended from a common ancestor with *Sinoconodon* and *Morganucodon* (McKenna and Bell, 1997; Luo, 2007; Martin, 2018). Understanding the origins of mammaliaforms has been a major goal in vertebrate palaeontology in the last 150 years, and the osteological transformations that occurred at the base of Mammaliformes are now well-known: particularly the development of diphyodont dentition and precise tooth occlusion, acquisition of the squamosal-dentary jaw joint, enlargement of the brain, and development of the single petrosal bone to house the middle ear (Kemp, 2005).

However, the ecology and biomechanics of the earliest mammaliaforms remain poorly known. Until relatively recently, the fossil record for mammals in the Mesozoic was scant and predominantly comprised dentomandibular material. While dentition is taxonomically informative and can provide information about diet through analyses of tooth wear (microwear) (e.g. Gill et al., 2014) and occlusion patterns (e.g. Schultz et al., 2017), more complete cranial or postcranial skeletal material is needed to facilitate biomechanical and ecomorphological analyses.

In the last twenty years the number of well-preserved partial and near-complete skeletons has increased with new finds from China; particularly from the Jurassic Yanliao and Cretaceous Jehol Biotas. The postcranial skeletons of these Chinese Mesozoic mammals have transformed our understanding of the ecological diversity of early mammaliaforms (Luo, 2007; Meng, 2014). The Middle to early Upper Jurassic Yanliao Biota in particular, spans a period of mammal diversification that saw the persistence of early diverging mammaliaforms—including some with unexpectedly derived ecomorphological specialisations, particularly among docodontans—alongside the emergence of crown mammals. This makes it a crucial assemblage for informing our understanding of macroevolutionary patterns in mammals, and the complex ecosystems of the Middle to Late Jurassic.

However, fundamental gaps remain in our knowledge of Mesozoic mammaliaform ecomorphological diversification outside Asia. Only a handful of Middle Jurassic sites are known that contain mammaliaform material, and these remain almost exclusively dentomandibular, often comprising only individual teeth and dentary fragments. Rare more complete Jurassic specimens outside China are only known from the Late Jurassic—for example *Haldanodon* and *Henkelotherium* from Portugal (Lillegraven and Krusat, 1991; Krebs 1991; Martin, 2005) and *Fruitafossor* from the USA (Luo and Wible, 2005). Dental material provides some information on taxonomic diversity, distribution and abundance, but without more complete specimens with postcranial material our understanding of mammaliaform ecological diversification in the Middle Jurassic remains incomplete.

Middle Jurassic fossil material from the Isle of Skye, Scotland, provides a precious new source of data for this crucial time period in the diversification of mammals. The Kilmaluag Formation fauna includes a mammaliamorph outgroup to mammaliaforms (tritylodontids), stem mammaliaforms (morganucodontans and docodontans), and crown mammalians (eutriconodontans and cladotherians). The fossil material is more complete than at most mammal-bearing localities globally, with minimal deformation, and it includes postcrania. This provides a unique case study outside China for examining mammal diversity, niche-partitioning among the multiple lineages present in this ecosystem, and biomechanics in Docodonta, an unusually ecomorphologically diverse stem mammaliaform clade. The wealth of fossils from this locality creates a picture of a diverse Middle Jurassic freshwater environment, and allows us to place these mammals in a broader ecological context.

1.2 Mammal Diversity in the Middle Jurassic

Our enhanced understanding of mammal macroevolution has been made possible by the tenfold increase in fossil mammal material found since 1979 (Luo, 2007). This massive increase has enabled comprehensive meta-analyses of character datasets, shedding light on patterns of taxonomic and ecomorphological change. Throughout the Mesozoic mammaliaforms have undergone four main diversification events: the Late Triassic/Early Jurassic diversification of stem mammaliaforms; the Middle Jurassic diversification of docodonts, basal australosphenidans and theriiforms; a Late Jurassic diversification within theriiforms; and an Early Cretaceous diversification of the eutherian and metatherian lineages (Luo, 2007; Close et al., 2015) (Figure 1.2.1).

The Middle Jurassic diversification of mammaliaforms marks a significant event in mammal macroevolution. At this time there is a coupled taxonomic and ecomorphological diversification, with the emergence and proliferation of distinct order- and family-level lineages including stem mammaliaform docodontans, and crown mammalian multituberculates, eutriconodonts and stem cladotherians (Luo, 2007; Close et al., 2015; Newham et al., 2015). These new lineages occupied new ecological niches, constituting an adaptive radiation—observed by multiple authors (Luo, 2007; Meng, 2014) and more recently supported quantitatively by meta-analyses of rates of taxonomic and morphological evolution (Newham et al., 2014; Close et al., 2015). It appears this resulted in an increased long-term standing diversity of mammaliaforms as a whole, a macroevolutionary event which would not occur again until just after the K-Pg extinction (Close et al., 2015; Close et al., 2019).

The drivers of Middle Jurassic mammal diversification remain uncertain, but several extrinsic and intrinsic factors have been suggested. The breakup of Pangaea, which began in the Early Jurassic, may have resulted in an increase in habitat complexity and availability. The same pattern of increased diversification is seen in other groups including archosaurs (Benson et al., 2014), suggesting they may also have responded to the opening up of ecological opportunity at this time.

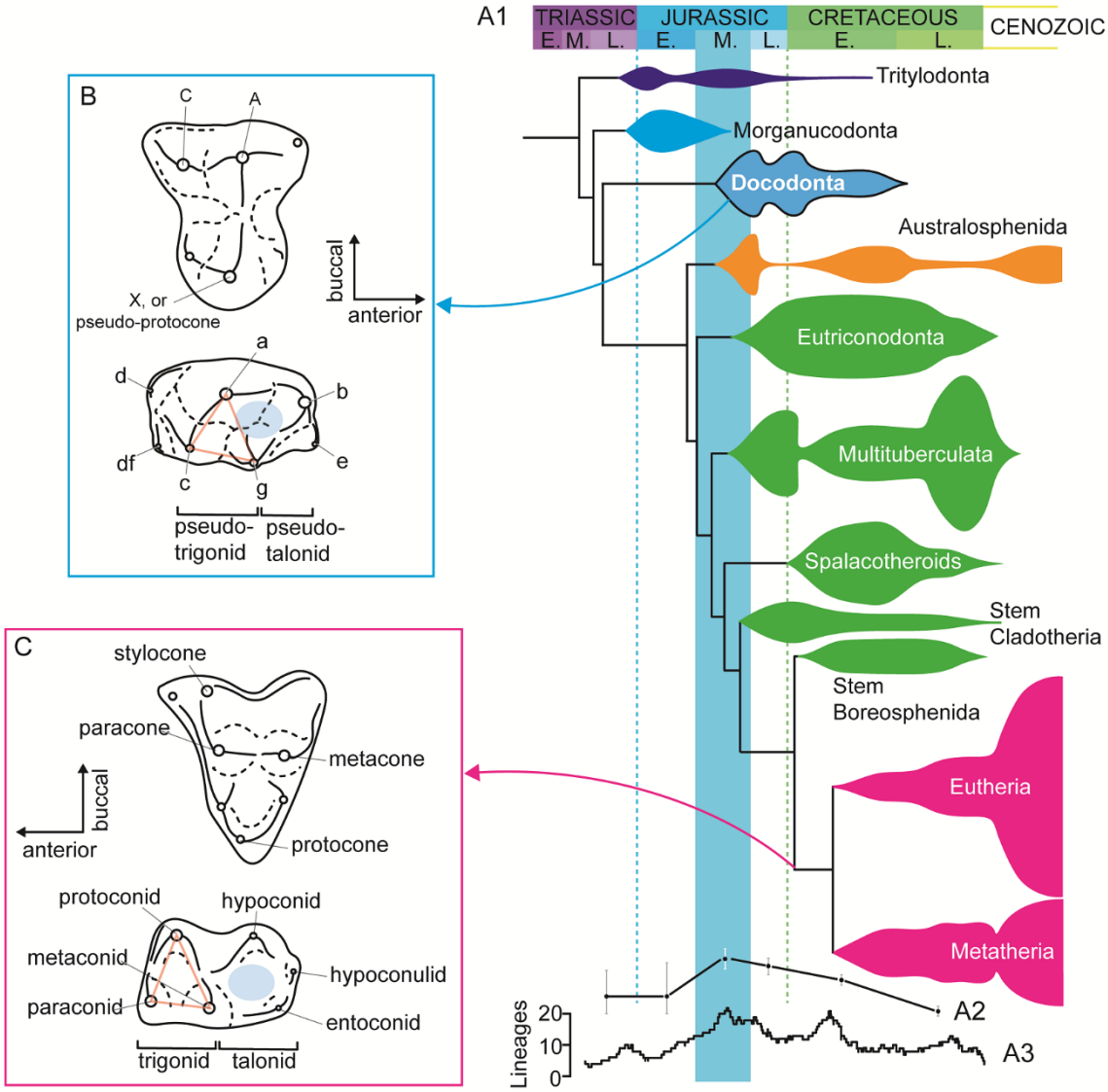

Figure 1.2.1: Simplified tree of major Mesozoic mammal orders, and homologous docodontan pseudo-tribosphenic molars. A1, macroevolution of mammal orders (adapted from Luo, 2007) showing position of Docodonta and with the Middle Jurassic highlighted; A2, weighted mean pairwise disparity of Mesozoic mammals by epoch (from Close et al., 2016); A3, phylogenetic lineage diversity (from Close et al., 2016); B, the pseudo-tribosphenic of docodontans (*Borealestes*) with pseudo-trigonid marked with a red triangle and the pseudotalonid marked with a blue circle; C, the tribosphenic molar of therians (*Kokopellia*, adapted from Davis, 2011), with trigonid marked with a red triangle and the talonid marked with a blue circle.

Multiple anatomical changes may have contributed to the Middle Jurassic diversification of mammals. The early stages of the development of the mammalian middle ear, which evolved homoplastically in three different lineages of mammal, likely contributed to ecological diversification (Luo 2007; Luo 2011; Luo et al., 2016). The transformation from the non-mammalian cynodont middle ear, with its multiple postdentary bones attached to the medial surface of the dentary, to the definitive mammalian middle ear

(DMME) in which these bones are detached from the dentary and fully incorporated into the middle ear, with a coiled cochlea in the inner ear, is well documented (Kemp, 2005; Luo 2011; Luo et al., 2016). The retroarticular process appears in Docodonta in the Middle Jurassic (e.g. Castorocauda, Ji et al., 2006), and precursors to the monotreme DMME are seen in the Middle Jurassic *Henosferus*, which has a subdivided postdentary trough and an angular fossa on the dentary for an ectotympanic ring (Rougier et al., 2007). The cochlear innervation seen in the Late Jurassic *Dryolestes* is a precursor to the coiled cochlea (Luo et al., 2011), and suggests morphological changes in the inner ear were already taking place in Cladotheria by this time.

Another important homologous feature that appeared in at least four lineages of mammaliaforms is the tribosphenic/pseudotribosphenic molar. This is a complex multifunctional tooth arrangement in which a mortar-and-pestle formed by upper and lower cusps and basins permits extensive shearing and grinding functions, making it possible to process a wider range of foodstuffs (Luo, 2007; Davis 2011). Docodontans are the earliest branching mammaliaform group to develop this level of tooth complexity, possessing a pseudotalonid and pseudoprotocone analogous to the talonid and protocone of tribosphenic mammals (see below) (Luo and Martin, 2007) (Figure 1.2.1).

Another possible morphological factor in the Middle Jurassic diversification of mammals was the alteration of the shoulder girdle, permitting a wider range of movement in the upper body and forelimb (Luo, 2015). Docodontans are the earliest mammalian group to lose the procoracoid, and are likely to have possessed a greater range of movement in the pectoral girdle than extant monotremes (Luo, 2015). A rigid interclavicle-clavicle structure—convergent with the furcula of birds—permitted haramiyidans such as the Late Jurassic *Maiopatagium* to evolve gliding capabilities, despite retaining other plesiomorphic shoulder girdle morphologies (Meng et al., 2017).

In order to understand the drivers and patterns of diversification among mammaliformes in the Middle Jurassic, more data are needed on their anatomy and ecomorphology. This helps us understand their ecological role in their palaeonenvironment and ecosystem, and in turn this information can be integrated into broader macroevolutionary analyses.

1.3 Ecological Diversity in Docodontans

The extinct clade Docodonta comprises an early branch of mammaliaforms that fall outside crown Mammalia, making it a key group for informing our understanding of mammal macroevolution (Simpson, 1929; Lillegraven and Krusat, 1991). Initially known from dental and some mandibular material, it was well-established by the end of the twentieth century that their teeth were unusually complex (Jenkins, 1969; Gingerich, 1973; Butler, 1997) (Figure 1.2.1B). Although they share some morphological features with the earliest mammaliaforms of the Late Triassic and Early Jurassic, such as *Morganucodon* (Hopson and Crompton, 1969; Kermack et al., 1973), the unexpected ecological diversity of docodontans in the Middle Jurassic has been one of the most exciting developments to arise from recent fossil discoveries in China (Luo, 2007). Three new docodontan genera with ecomorpholoical specialisms are known from the Yanliao Biota: the semi-aquatic *Castorocauda* (Ji et al., 2006); the fossorial *Docofossor* (Luo et al., 2015); and the arboreal *Agilodocodon* (Meng et al., 2015). Alongside the fossorial-semi-aquatic adaptations of *Haldanodon* from the Late Jurassic of Portugal (Martin, 2005), this signifies an impressive range of ecological specialisation in such an early branch of mammaliaforms (Figure 1.3.1).

The first docodontan for which extensive cranial and postcranial material is known was *Haldanodon exspectatus*, from the Alcobaça Formation in Guimarota Coal Mine in Portugal (Kühne and Krusat, 1972). This Late Jurassic docodontan exhibits adaptations for a fossorial and semi-aquatic lifestyle with its short, robust limb bones and compressed phalanges, the pronounced deltopectoral crest of the humerus and expanded distal joints (Martin, 2005) (Figure 1.3.1C). Although these adaptations suggest an ecomorphological specialism, the morphology is not as substantially derived as the first Chinese docodontan to be published, *Castorocauda lutrasimilus* (Ji et al., 2006), from the Middle Jurassic Yanliao Biota. The exceptional preservation of this articulated skeleton indicates semi-aquatic adaptations similar to that of the modern beaver or otter. The preserved soft tissue impression of the tail indicates it was wide and flattened, and the caudal vertebrae are transversely expanded to support this (Ji et al., 2006). Soft tissues around the hind feet also suggest webbing between the digits. The teeth of *Castorocauda*

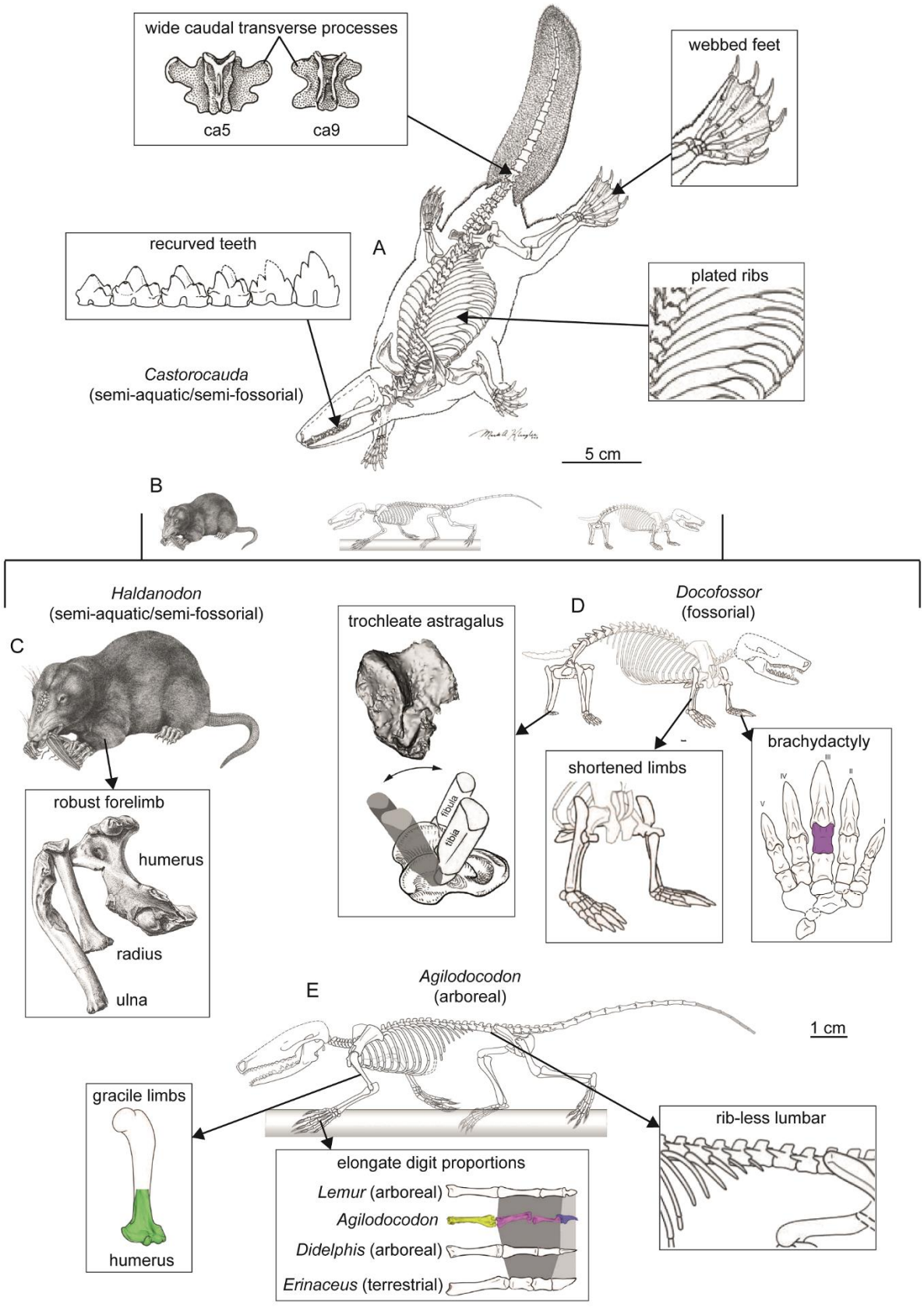
wide caudal transverse processes
ca5
ca9
webbed feet
recurved teeth
A
plated ribs
Castorocauda
(semi-aquatic/semi-fossorial)
5 cm
B
Haldanodon
(semi-aquatic/semi-fossorial)
C
trochleate astragalus
fibula
tibia
D
Docofossor
(fossorial)
shortened limbs
brachydactyly
robust forelimb
humerus
radius
ulna
E
Agilodocodon
(arboreal)
1 cm
gracile limbs
humerus
elongate digit proportions
Lemur (arboreal)
Agilodocodon
Didelphis (arboreal)
Erinaceus (terrestrial)
rib-less lumbar

are slightly recurved, facilitating a diet of aquatic invertebrates or even small fish (Ji et al., 2006) (Figure 1.3.1A). All of these specialised ecomorphologies are seen in modern semi-aquatic mammals, but had never been observed in a Mesozoic mammal previously. *Castorocauda* also has plated ribs, a homoplastic feature among cynodonts that strengthens the trunk (Jenkins, 1971), and may be related to digging. This kind of semi-aquatic, semi-fossorial ecomorphology is also seen in the modern platypus, *Ornithorhynchus anatinus* (Gambaryan et al., 2002).

The semi-aquatic, semi-fossorial adaptations of *Haldanodon* and *Castorocauda* suggested that docodontans as a group may have lived a similar ecological lifestyle to the modern platypus (Ji et al., 2006). The announcement of two new Chinese taxa in 2015 radically altered perceptions of the ecological diversity of this clade. The articulated skeleton of *Agilodocodon scansorius*, also from the Middle Jurassic Yanliao Biota, tells us this taxon was more gracile than other docodontans, and the elongate proportions of the manus and pes are similar to those of modern scansorial and arboreal mammals, notably arboreal diprotodontan marsupials (Meng et al., 2015) (Figure 1.3.1E). This is coupled with a wider range of ankle movement than seen in other docodontans or earlier mammaliaforms. Also unlike other docodontans and most early mammaliaforms, *Agilodocodon* has a distinct rib-less lumbar section of the spine, allowing a wider range of movement in the posterior vertebral column and likely facilitating flexible body movements among branches (Gabe et al., 1967; Meng et al., 2015).

The ecological diversity of docodontans was further expanded by yet another, substantially morphologically derived taxon, *Docofossor brachydactylus* (Luo et al., 2015). This member of the Yanliao Biota has clear adaptations for a fossorial, likely subterranean lifestyle that go beyond those seen in either *Haldanodon* or *Castorocauda*. The robust appendicular skeleton has reduced limb proportions, and reductions in digit segments caused by the fusion of proximal and intermediate phalanges (Luo et al., 2015) (Figure 1.3.1D). The olecranon process is hypertrophied, and a trochleate astragalus allows for

Figure 1.3.1 (previous page): Ecomorphological specialisations among docodontans. A, *Castorocauda lutrasimilus* has semi-aquatic and some semi-fossorial morphological specialisations (adapted from Ji et al., 2006); B, *Haldanodon* (left), *Agilodocodon* (centre), and *Docofossor* (right) to same scale as *Castorocauda*; C, *Haldanodon exspectatus* has semi-aquatic and semi-fossorial specialisations (adapted from Martin and Krebs, 2000); D, *Docofossor brachydactylus* is highly specialised for a fossorial lifestyle (adapted from Luo et al., 2015); E, *Agilodocodon scansorius* has gracile morphology supporting an arboreal lifestyle (Meng et al., 2015). A-B same scale. C-E same scale.

habitual abduction of the foot. The teeth are simplified compared to other docodontans, and the tip of the snout protrudes slightly. All of these features are seen in modern subterranean digging specialists such as the golden moles (Chrysochloridae) (Kindahl, 1949). The same pattern of brachydactyly through symphalangism is seen in *Docofossor* and in golden moles, resulting in a short and widened manus perfect for removing and moving soil substrate (Kindahl, 1949; Luo et al., 2015).

It now seems clear from these four docodontans alone that Docodonta exhibits an unusual amount of within-clade ecological diversity, mirroring that seen among extant therian taxa. It has been hypothesised that the molar complexity of docodontans is one of the reasons for their success (Luo and Martin, 2007) and may also be a key factor in their ability to exploit new niche-space and diversify ecologically (Luo, 2007).

However, a lack of postcranial material for other known docodontan genera means that we currently know little about how this ecomorphological diversity emerged, or how widespread it was across the clade as a whole. At least fourteen genera of Docodonta are known from dentomandibular material from across Laurasia, including: North America (Marsh, 1881; Schultz et al., 2018); Britain (Simpson, 1928; Waldman and Savage, 1972; Kermack et al., 1987; Sigogoneau-Russel, 2003; Panciroli et al., 2018b, in press); Russia (Maschenko et al, 2002; Lopatin and Averianov, 2005; Averianov et al., 2010; Averianov et al., 2018); Mongolia (Tatarinov, 1995); Kyrgyzstan (Martin and Averianov, 2004; Martin et al., 2010); as well as Portugal and China (as outlined above, but also Pfretzschner et al., 2005). There is also a disputed possible docodontan from India (Prasad and Manhas, 2007). They span a temporal range from the Middle Jurassic (Waldman and Savage, 1972; Kermack et al., 1987; Sigogneau-Russell, 2003) to the Early Cretaceous (Maschenko et al., 2002; Sigogneau-Russel, 2003; Averianov et al., 2018), and their greatest taxonomic diversity was in the Middle to early Late Jurassic (Luo and Martin, 2007).

One of the geologically oldest docodontans is *Borealestes*, a genus first discovered in the Bathonian Kilmaluag Formation, Scotland (Waldman and Savage, 1972). Later, a further two genera, *Simpsonodon* and *Krusatodon* and another species of *Borealestes*, *B. mussetae* (=*mussetti*) were found in the contemporaneous Forest Marble Formation of England (Kermack et al., 1987; Sigogneau-Russel, 2003). As some of the geologically oldest docodontan genera, they provide critical information on the emergence of this clade. Their morphology is of particular interest in reconstructing the ecomorphological

macroevolution of Docodonta, but until recently, no cranial or postcranial material of these taxa were known.

Between 1971 and 1982, fieldwork carried out by Dr Michael Waldman and Professor Robert Savage on Jurassic sediments of the Kilmaluag Formation on the Isle of Skye, yielded a wealth of mammal and other vertebrate fossil material (Savage, 1984; Evans et al., 2006). Despite the many mammal specimens collected, only one new genus of mammal was published, the docodontan *Borealestes serendipitus* (Waldman and Savage, 1972). Later research into their original collections suggests they also collected the first specimens of two mammals later named from the Forest Marble Formation, the docodontan *Krusatodon kirtlingtonensis* (Sigogneau-Russel, 2003; Panciroli et al., 2018d) and the cladotherian *Palaeoxondon ooliticus* (Freeman, 1976; Panciroli et al., 2018a).

Among the unpublished collections made by Waldman and Savage were two docodontan skeletons, referred to as 'Block A', now NMS G.1992.47.121.1, and 'Block B', now NMS G.1992.47.122.1. Block A is identified as the partial skeleton of *Borealestes serendipitus*, and Block B as the near-complete skeleton of *Krusatodon* sp. (under study by EP). These fossil skeletons, comprising cranial and postcranial material, provide invaluable information about two of the geologically earliest docodontan genera.

Borealestes has long been considered to belong to a basal docodontan clade, based on the dentomandibular morphology and results of phylogenetic analyses (Sigogneau-Russel, 2003; Martin and Averianov, 2004; Luo and Martin, 2007). With additional postcranial material, these taxonomic relationships can be comprehensively assessed. The ecomorphology of *Borealestes* will have interesting implications for the origins and emergence of ecological diversity in this clade, especially in light of results of revised phylogenetic analyses. The adaptive diversification of lineages is connected with the opening up of ecological opportunity, but this can only be exploited if other factors, such as population distribution and interspecific competition, permit the population to respond to exploit it, and if the biological and morphological characteristics of that lineage make it possible (Wellborn and Langerhans, 2014). With more complete fossil material for *Borealestes*, along with the other mammaliaforms represented in the biodiverse ecosystem of the Kilmaluag Formation, it is possible to explore ecological and biological factors contributing to mammaliaform diversity in the Middle Jurassic.

1.4 Research Questions

Here I summarise the main research questions, addressing two areas of research focus:

- **Diversity and Phylogeny:** the Kilmaluag Formation comprises mammaliaform taxonomic diversity that includes the earliest branching mammaliaforms alongside the first crown group mammals. Through analysis of fossil material from the Kilmaluag Formation I will address the following questions:

  Q1. Is the Kilmaluag Formation mammal assemblage as diverse as geologically contemporaneous sites globally?

  Q2. Does the completeness of fossil mammal material from the Kilmaluag Formation influences the results of phylogenetic analyses for multiple taxa?

  Q3. As a basal docodontan, does* Borealestes *provide key anatomical information for resolving docodontan phylogenetic relationships?

  These questions will be addressed by: exploring the geological context of the Kilmaluag Formation and making comparisons with other sites (Chapter 2); descriptions and phylogenetic analyses of the fossil material found in the Kilmaluag Formation to date (Chapter 3); analysis of *Borealestes* anatomy and phylogeny using dentomandibular and cranial and postcranial characters (Chapter 3.3).

- **Ecology and Ecomorphology:** recent fossil material from China suggests not only that mammaliaforms were unexpectedly ecologically diverse, but that Docodonta had exceptionally high ecomorphological diversity for such a geologically early-diverging clade. Through multiple analyses I will address the following questions:

  Q4. Did niche partitioning take place among mammals in the ecosystem of the Kilmaluag Formation?

  Q5. Can quantitative biomechanical analyses be used to explore the locomotion and ecology of fossil mammal taxa?

Q6. As a basal docodontan, is the locomotor ecology of* Borealestes *conserved (i.e. lacking derived specialisations)?

These questions will be addressed by: establishing the broader ecological context of the Kilmaluag Formation (Chapter 2); body mass estimates (Chapter 4.1); jaw biomechanics using beam theory (Chapter 4.2); and morphometric analysis of postcranial elements of *Borealestes* (Chapter 4.3).

Chapter 2: The Kilmaluag Formation

The first fossils from the diverse ‘vertebrate beds’ of the Kilmaluag Formation on the Isle of Skye, Scotland, were discovered in 1971 by Dr Michael Waldman (Stowe School) (Waldman and Savage, 1972). Between 1971 and 1982 seven field trips were carried out by Waldman and his colleague and mentor, Professor Robert Savage (University of Bristol). Further field work was carried out in the early 2000s by a team from the Natural History Museum in London, NMS, University College London, and the University of Oxford under Professors Susan Evans and Paul Barret. Since 2010 field work has continued led by Dr Stig Walsh at National Museums Scotland and Professor Roger Benson at the University of Oxford, along with myself and Professor Richard Butler of the University of Birmingham. The wealth of material collected by these multiple expeditions has revealed the Kilmaluag Formation as one of the most biodiverse vertebrate fossil localities in Britain, and of global significance both in terms of faunal composition, and the completeness of specimens.

No comprehensive overview of the fossil finds from this Formation has been provided since 2006 (Evans et al., 2006), and as a result the significance of the Kilmaluag Formation is currently underappreciated in the wider scientific community. Here I provide an up-to-date overview of the geology and collections, and make comparisons of the vertebrate faunal assemblage—particularly mammals—with relevant contemporaneous localities from Britain, Europe, Asia and North America. These comparisons provide international context for the Kilmaluag Formation assemblage, and provide evidence regarding proposed global distribution patterns and macroevolutionary trends in various mammal groups and their close relatives.

2.1 Geological Overview

The Kilmaluag Formation (Harris and Hudson, 1980) is part of the Great Estuarine Group (formerly Great Estuarine Series [Judd, 1878, p722]), a series of near-shore shallow marine, varied-salinity lagoon, and freshwater lagoon sediments that are Bathonian in age (Barron et al., 2012) (Figure 2.1.1). The Great Estuarine Group comprises the Middle Jurassic portion of the Sea of Hebrides Basin and Inner Hebrides Basin: tectonically bound basins with sedimentology that reflects fluctuating sea-levels caused by subsidence and uplift (Morton 1987; Mellere & Steel 1996; Hesselbo and Coe, 2000). These Mesozoic sediments are overlain disconformably by Tertiary basalt (Harris and Hudson, 1980).

The Kilmaluag Formation crops out on the Scottish Inner Hebridean islands of Eigg, Skye and Muck, and is approximately 25 m in thickness at the most complete section on the Strathaird Peninsula on Skye (Harris and Hudson, 1980; Morton and Hudson, 1985) (Figure 2.1.1 and 2.1.2). It was formerly known as the Ostracod Limestone, and the base of the formation is defined by the occurrence of ostracod-bearing calcareous mudstones and marls/fissile mudstones (Barron et al., 2012). It is named for the village of Kilmaluag on the Trotternish Peninsula of Skye, where the type section crops out along the shore of Kilmaluag Bay (Harris and Hudson, 1980). Despite being less extensive than exposures on the Strathaird Peninsula in Southern Skye, Kilmaluag was chosen as the locality of the type section as it is accessible and fossiliferous, and the base of the formation can be easily defined to within 3 m (Harris and Hudson, 1980).

Dating for the Kilmaluag Formation has proven problematic due to a lack of clear biostratigraphic correlations, but it is considered to correlate with the *Retrocostatum* Zone, and is Late Bathonian in age (Barron et al., 2012). The similarities in vertebrate faunal composition with Kirtlington Cement Quarry (Forest Marble Formation, see below) in England also support a Late Bathonian age.

Unlike other Formations within the Great Estuarine Group, the Kilmaluag Formation includes predominantly low-salinity and freshwater facies, especially on the Strathaird Peninsula, as demonstrated by the presence of freshwater ostracods *Darwinula* and *Theriosynoecum* (Wakefield, 1995), shallow freshwater to oligohaline

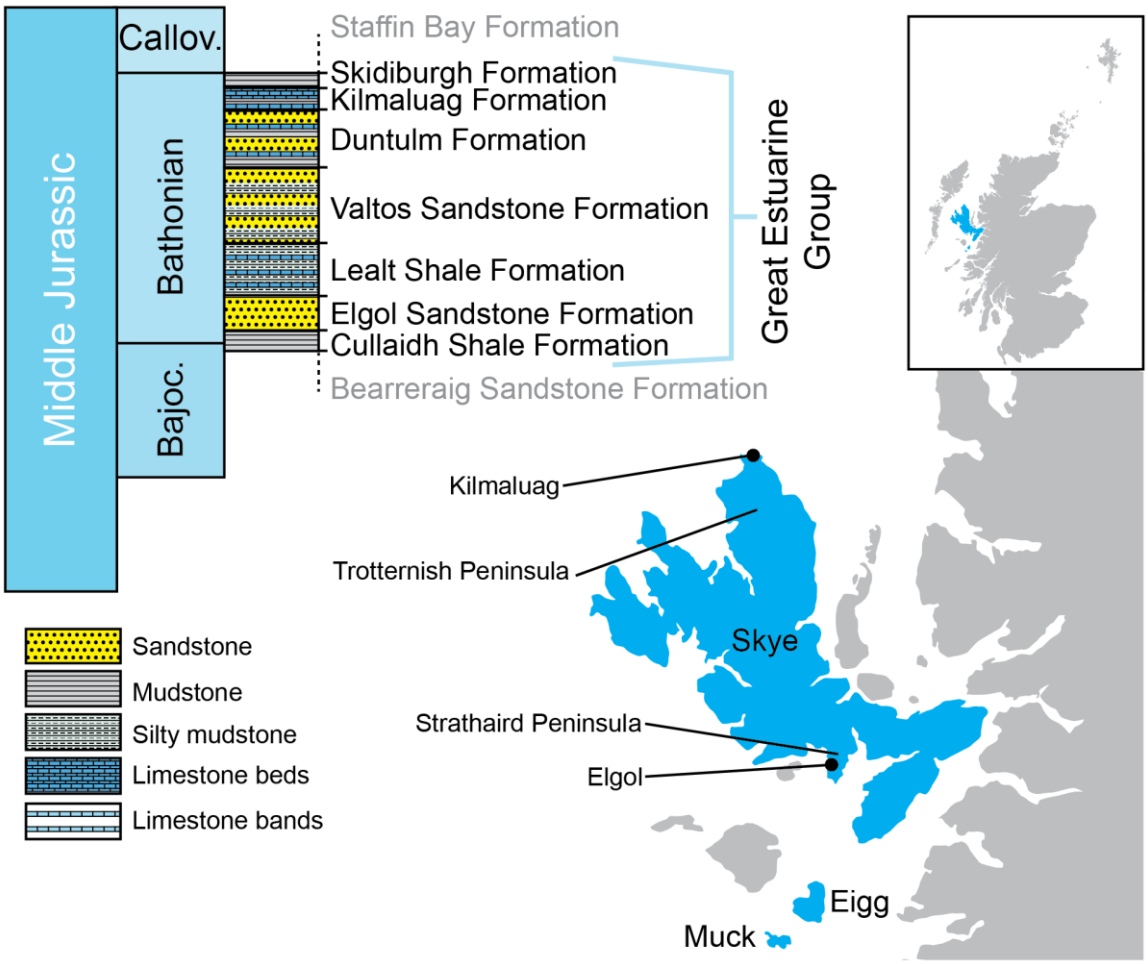

Figure 2.1.1: The location of the Kilmaluag Formation and overview of the stratigraphy of the Great Estuarine Group. Map adapted from Wikimedia. Stratigraphy compiled and adapted from Cohen et al., 2018, Andrews, 1985, and Barron et al., 2012).

Conchostracans, such as *Anthronesteria* and *Pseudograpta* (Pei-Ji and Hudson, 1991), and freshwater gastropods *Viviparus* (Andrews, 1985; Morton and Hudson, 1985; Barron et al., 2012) (Figure 2.1.3).

The Kilmaluag Formation can be divided into two distinct facies: clastic facies in the north of Skye which include sandstones; and argillaceous limestone facies found on the Strathaird Peninsula in southern Skye, and also in small outcrops on Eigg and Muck, which do not include sandstones. Palaeoenvironmental reconstructions of the northern, clastic facies suggest a low-salinity environment of closed lagoons or marginal coastal lakes, fed by small rivers which carried in clastic sediments and plant material (Andrews,

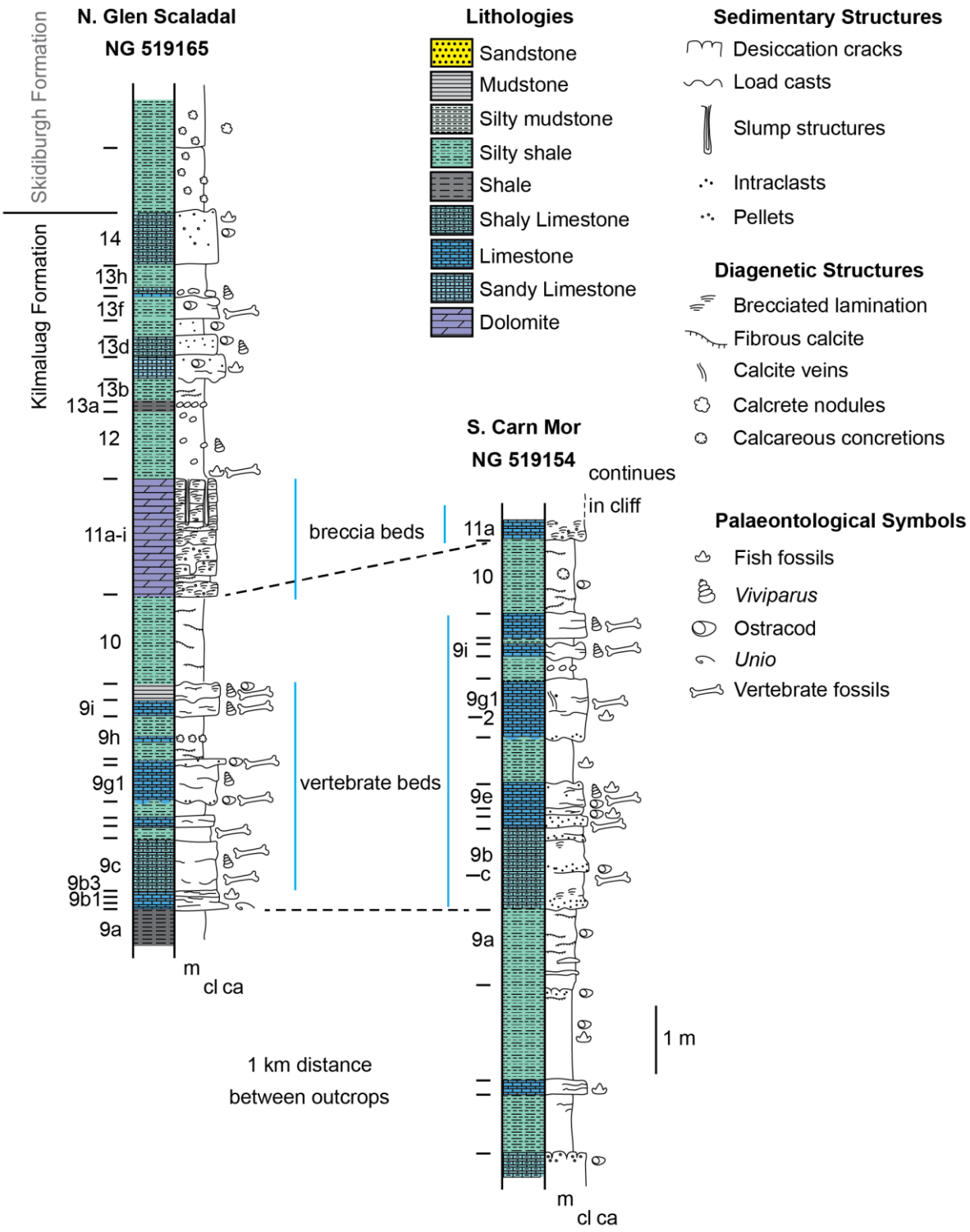

Figure 2.1.2: Stratigraphy of the Kilmaluag Formation at two main fossil collection sites on the Strathaird Peninsula. Adapted from Andrews, 1985.

1985). Multiple layers of desiccation cracks, and reworked desiccation breccias infilling mudcracks, suggest periodic drying out followed by wetter periods of lagoon expansion. There are also rippled sandsheets in some beds, with tuning-fork bifurcations indicative of wave generation (Andrews, 1985).

The southern, argillaceous limestones are depositional rather than diagenetic in origin and contain up to 44% acid-insoluble residues (Andrews, 1985). These beds are altered by localised metamorphism resulting from Palaeogene igneous intrusions (Hesselbo and Coe, 2000). The mud-dominated lower beds, which alternate between muds and muddy-carbonates, represent a low-salinity to freshwater lagoon environment, which evaporated in drier seasons and expanded in wetter seasons (Andrews, 1985). This is supported by alternating clay-rich muds and muddy carbonates dominated by disarticulated ostracod bioclasts and structureless micrite introclasts. Minor dolomites probably represent the dolomitisation of precursor carbonates during extreme periods of desiccation. This would have exposed mudflats, forming desiccation cracks and flat-pebble conglomerates. The argillaceous facies were fed by meteoric waters, unlike the clastic facies in the north. This interpretation of a low-salinity closed lagoon environment is supported by palynoflora that includes *Tasminites* and *Botryoccus* (Riding et al., 1991).

Andrews (1985) informally divided the Kilmaluag Formation into a series of numbered horizons, some of which were grouped together to form the ‘Vertebrate Beds. These beds are highly fossiliferous, and located on the Strathaird Peninsula. They are thought to represent a predominantly wet climatic phase. These thick beds alternate between muddy carbonates, hard blue-grey limestones, micrites, wackestones and breccia conglomerates, and appear to be predominantly freshwater (Andrews, 1985). The lowest MgO content is found in these beds, and in some there is smooth millimetre-scale lamination, and some stromatolitic domed laminations, which suggests a shallow sublittoral depositional environment. Vertebrate fossil remains in the Kilmaluag Formation appear conspicuously black, and are scattered throughout. Also yielding body and trace fossil material are the breccia beds that sit above the vertebrate beds (Andrews, 1985; Marshall, 2003) (Figure 2.1.2). The breccia beds comprise three dolomitic, gradationally bound beds combined into one bedset (Marshall, 2003). Each bed consists of silty micrite which becomes brecciated upwards with desiccation cracked horizons. This evidence, coupled

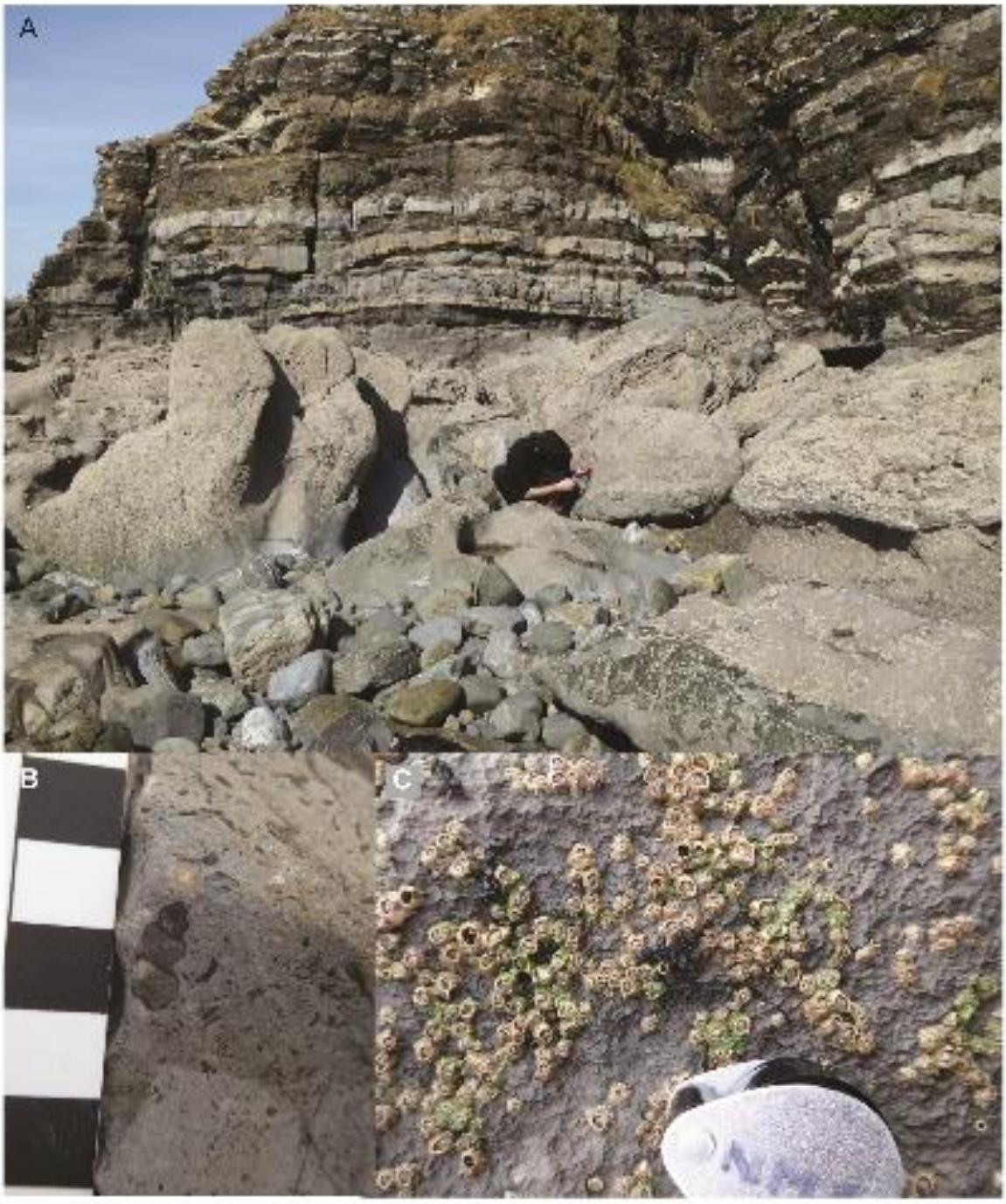

Figure 2.1.3: Outcrops of the Kilmaluag Formation on the Strathaird Peninsula, Isle of Skye, Scotland. A, section at Cladach a Ghlinne; B, example of the *Viviparus* and ostracod-rich limestone; C, a fossil vertebrate at outcrop (black, in centre of picture).

with the lack of fossilised vegetation, suggests these beds represent a barren or sparsely vegetated supralittoral lagoon margin (Marshall, 2003).

2.2 The Fossil Flora and Fauna of the Kilmaluag Formation

Flora

No in-depth palaeobotanical studies have been made of the plant fossils of the Great Estuarine Group. Floral remains mostly comprise poorly preserved fragments, and in the Kilmaluag Formation there are only rare small broken pieces of bark or stem (pers. obs.). A single palynological study was carried out on the Kilmaluag Formation as part of a wider analysis of the Jurassic rocks of the Hebrides Basins, by Riding et al. (1991). They took 16 samples from the Isle of Skye, 12 of them from the type section at Port Gobhlaig in Kilmaluag Bay at the North of the Trotternish Peninsula, and four at Prince Charles's Point, also on the Trotternish Peninsula. No sampling was done on the Strathaird sections. The type section had low diversity, and was dominated by gymnosperm pollen (up to 87%), with <24% pteridophyte spores (Riding et al., 1991:p143). Similar gymnospore-dominated palynomorph assemblages were found in the Prince Charles's Point samples.

Arthropoda

The dominant anthropod fossils known from the Kilmaluag Formation are ostracods, principally *Darwinula* and *Theriosynoecum* (Wakefield, 1995), and conchostracans *Anthronesteria* and *Pseudograpta* (Pei-Ji and Hudson, 1991). Trace-fossil burrows attributable to larger decapods are preserved in the vertebrate beds and breccia beds on the Strathaird peninsula, and are interpreted as dwelling burrows for crabs or shrimps (Marshall, 2003).

Only a handful of other invertebrate fossils are known from the Kilmaluag Formation. Insect-bearing strata were discovered by EP in 2017 at an outcrop of Kilmaluag Formation at Lub Score on the Trotternish Peninsula. Subsequently, multiple specimens have been collected, and currently await description (under study by A. Ross). These mainly comprise beetle wing cases of limited taxonomic value and cannot be assigned above order-level, but continued collection should yield sufficient data to give an indication of insect faunal diversity in the future.

Chondrichthyes and Osteichthyes

Three chondrichthyan and two osteichthyan taxa are known from the Kilmaluag Formation to date. The chondrichthyans are all hybdont sharks: *Acrodus, Hybodus* and an indeterminate hybodont (Rees and Underwood, 2006; Evans et al., 2006). The semionotiform *Lepidotes* and an unidentified actinistian comprise the osteichthyans recovered (Evans et al., 2006). All of these are known from isolated teeth and tooth fragments. In the last decade of fieldwork more fish fossils have been recovered, including partial associated skeletons—these currently await preparation and study.

Lissamphibia

Two lissamphibians are known from the Kilmaluag Formation. A partial associated skeleton of *Marmorerpeton kermacki* comprising vertebrae, skull bones and limb elements as well as isolated elements, has been published (Evans and Waldman 1996), but there are now several *Marmorerpeton* specimens collected since 2010 and awaiting further study. The heavily sculptured skull bones of *Marmorerpeton* suggest an affinity with primitive karaurids. A second more basal salamander, referred to as 'Kirtlington Salamander A' (Evans and Milner, 1994) and known from the Forest Marble Formation at Kirtlington Cement Quarry (Evans and Waldman 1996), is also represented on Skye (currently under study).

Squamata

Several squamates and stem squamates have been reported so far from the Kilmaluag Formation of the Strathaird Peninsula, based predominantly on tooth bearing elements (dentaries and maxilla). Of these, the stem squamate *Marmoretta* is most abundant, and is represented by a partial skeleton, paired posterior portions of mandibles, and two partial maxillae (Waldman and Evans 1994; Evans & Waldman 1996). The skull confirmed previous reconstructions of *Marmoretta*, which was first identified from the Forest Marble Formation at Kirtlington Cement Quarry in Oxfordshire (Evans, 1991). Only the skull and limited aspects of postcranial morphology have been described so far (Waldman and Evans 1994, figs 6–8). However, microCT scans of the Skye specimen indicate a substantially complete skeleton, and await description (pers. com RBJ Benson).

Waldman and Evans (1994) also described the almost complete right and a partial left dentary of *Paramacellodus*, and later reported specimens of other species: fragmentary

cranial remains of a small non-paramacellodid ‘scincomorph’; vertebrae resembling subadult specimens of *Parviraptor*; and (tentatively) a gekkotan-like vertebra (Evans et al., 2006). A new squamate dentary with weakly tricuspid teeth was also found during fieldwork in 2004, and is apparently distinct from other specimens both from Skye and from Kirtlington Cement Quarry (Evans et al., 2006).

Recent fieldwork has extended the number of known squamate fossils substantially, recovering >20 isolated tooth-bearing elements, and several partial or near-complete skeletons. So far these new specimens represent squamates such as *Parviraptor* and the stem-group squamate *Marmoretta* (pers. com RBJ Benson). No rhynchocephalians are currently known, which is consistent with other Middle Jurassic assemblages in the British Isles: only three fragmentary bones of rhynchocephalians were reported previously from Kirtlington Cement Quarry (Evans 1992) despite bulk sampling of large quantities of sediment. The reason for the rarity of rhyncocephalians during this period is currently unexplained.

Testudinata

Turtle fossils are common in the Kilmaluag Formation on the Strathaird Peninsula, mostly comprising broken non-associated fragments of turtle plastron, but also some significant associated material. A new genus and species of stem turtle, *Eileanchelys waldmani* (Anquetin et al., 2009, 2010), was named from material recovered during field work in 2004. This material included the holotype partial skull, and the paratypes, in total comprising at least three associated partial skeletons on the same limestone block. The paratype material includes postcrania and almost complete carapaces.

Eileanchelys waldmani represents one of the earliest recorded aquatic turtles, and one of the few known from the Middle Jurassic. Its mixture of plesiomorphic and derived characters, coupled with unique unusually shaped supernumerary suprapygal and broad first suprapygal contacting the peripherals laterally, make it a key taxon in tracking the morphological evolution of the vomer and basicranium from basalmost to crown-group turtles (Anquetin et al., 2009).

Archosauromorpha

The choristodere *Cteniogenys* is now known from the Kilmaluag Formation from a partial skull (Evans and Waldman, 1996) and multiple dentary fragments, some published and more under study (Evans et al., 2006; RBJ pers. com. 2018).

The first crocodylomorph material described from the Kilmaluag Formation comprised an indeterminate partial postcranial skeleton belonging to an animal approximately one metre long (Waldman and Evans, 1996). This included elements of the right hind limb and scapula, fragments of rib, three dorsal vertebrae and multiple scutes. These authors suggested the small size and postcranial morphology of the material is not goniopholid, although goniopholid teeth are common in other Bathonian sites. A crocodylomorph left pubis, some osteoderms and a single goniopholid tooth were described by Wills et al. (2014), and represent the first figured crocodylomorph material from the Kilmaluag of the Strathaird Peninsula. The pubis was collected in 1992, and the osteoderms and tooth in 2006. These are assigned to indeterminate goniopholid neosuchians. Isolated crocodylomorph material is also included in faunal lists (Evans and Milner 1994; Evans et al. 2006), but not described or figured. Evans et al. (2006) mention atoposaurid material, although it is not figured or described.

Two associated skeletons of pterosaurs are currently under study from the Kilmaluag Formation: one monofenestraten pterosaur (Martin-Silverstone and Barrett, 2018); and one as yet undetermined pterodactyloid taxon (pers. com S Walsh, 2019). Several teeth thought to represent pterosaurs have also been identified (Evans et al., 2006).

Although dinosaur body and ichnological fossils are known from other parts of the Great Estuarine Group (see Clark, 2018 for overview), very little dinosaur material has been recovered from the Kilmaluag Formation to date. However, the scant material that does exist currently comprises the geologically youngest contribution to the dinosaur fossil record in Scotland. The trackways of small bipedal tridactyl dinosaurs at Lub Score on the Trotternish Peninsula (Clark et al., 2005), possibly represent adult and juvenile theropods, most likely the same ichnospecies. They were found in two distinct stratigraphic layers: a silty mudstone, and a sandstone containing darker organic layers. Both are suggested to represent freshwater depositional settings, but exact correlation with stratigraphy in other parts of the Isle of Skye has proven problematic (Clark et al., 2005).

The only dinosaur body fossil remains reported so far from the Kilmaluag Formation are an isolated sauropod tooth, which represents the first dinosaur tooth described from

Scotland (Barrett, 2006), a fragmentary femur, and a theropod tooth, all from the Strathaird Peninsula (Wills et al. 2014). The sauropod tooth is a complete crown with partial root, with morphology suggesting it is referable to either a basal eusauropod or basal titanosauriform (Barrett, 2006).

Mammaliamorpha

The Scottish specimens of the non-mammalian cynodont *Stereognathus* were originally erected in their own species, *S. 'hebridicus'*, based on four isolated upper postcanines, which appeared to be larger than the English *S. ooliticus* (Waldman and Savage 1972). Following detailed morphological comparison of specimens assigned to these two species, with the addition of better-preserved specimens recovered from the Kilmaluag Formation since the 1970s, these species were synonymised under *S. ooliticus* (Panciroli et al., 2017d; Chapter 3.1). *S. ooliticus* in the British Isles is almost entirely represented by isolated postcanine teeth, with only one edentulous fragment of maxilla, and the holotype comprising three postcanines in a fragment of maxilla. Some isolated limb bones from English Jurassic sites, such as Kirtlington, have been assigned to Tritylodontidae (Simpson, 1928; Kühne, 1956), but their further identification as *Stereognathus* is unconfirmed.

The first Mesozoic mammal from Scotland came from the Kilmaluag Formation on the Strathaird Peninsula: the new genus and species of docodont, *Borealestes serendipitus* (Waldman and Savage, 1972; see Chapter 3 herein). This was published alongside the first tritylodontid fossils found in Scotland, *Stereognathus 'hebridicus'*. Only one specimen of *Borealestes* and one of *Stereognathus* were described briefly in 1972, with further specimens collected during fieldwork in the 1970s and 1980s, but not formally described.

Borealestes serendipitus was initially described from a fragment of dentary comprising three premolars and six molars. It was only the third docodont genus to be named (after *Docodon victor* [Marsh 1880] and *Peraiocynodon inexpectatus* [Simpson 1928]—although the latter was synonymised with *Docodon* [Butler 1939], only to be resurrected again later [Sigogneau-Russell 2003]), and the original diagnosis was not comprehensive. Later authors somewhat clarified the diagnosis of *B. serendipitus* for upper and lower molars, and added a second species, based on multiple individual molar teeth found at Kirtlington Cement Quarry (Sigogneau-Russell 2003; Luo and Martin 2007).

There are now multiple dentary fragments of *Borealestes serendipitus* known from the Kilmaluag Formation, along with associated crania and postcrania (see Chapter 2). Most of these specimens were collected in the 1970s, and one almost complete dentary was recovered during fieldwork in 2016, and another in 2018. Together they will provide a great deal more information on this taxon, and clarify the diagnosis of the genus and species.

Further mammaliamorph and mammaliaform material was recovered and included in published faunal lists (Evans and Milner, 1994; Evans et al., 2005), including a molar from the docodont genus *Krusatodon*. A skeleton collected in the 1970s is also confirmed as belonging to *Krusatodon* (under study by EP). Recent fieldwork resulted in the publication of the first crown-group mammal from the Kilmaluag Formation, the cladotherian *Palaeoxonodon ooliticus* (Close et al., 2016), and another mammaliaform, the morganucodontan *Wareolestes rex* (Panciroli et al., 2017b). Both of these species were already known from isolated teeth from the Forest Marble Formation (Freeman, E., 1976, 1979; Butler and Sigogneau-Russell 2016), but the Kilmaluag Formation yielded more complete dentary fragments with teeth. Recently material from *Phascolotherium* was also recovered, and is currently under study.

The dentary of *Palaeoxonodon* recovered from the Kilmaluag Formation has revealed the near complete lower tooth row for this taxon (Close et al., 2016), and a small portion of the posterior portion of the dentary is known from a more recently recovered dentary fragment (Panciroli et al., 2018a; Chapter 3.4). The morphological variation of the tooth row in their more complete specimen led Close et al. (2016) to suggest *Palaeoxonodon leesi, P. freemani,* and *Kennetheridium leesi* (Sigogneau-Russell, 2003) are junior synonyms of *P. ooliticus*.

The dentary of *Wareolestes rex* is the most complete fossil of this taxon, and settles disagreement over the orientation of previously recovered isolated molars within the tooth row (Freeman E., 1979; Hahn et al. 1991; Butler & Sigogneau-Russell 2016; Panciroli et al., 2017b; Chapter 3.2). Replacement teeth present within the dentary also provided information on tooth replacement in this taxon.

Food Web

Based on the flora and fauna described so far from the Kilmaluag Formation, it is possible to create a tentative food web for this Middle Jurassic ecosystem (Figure 2.2.1),

with primary producers and multiple levels of consumer represented. However, at present this represents merely a thought-exercise, and there are some important caveats. It is currently unclear how much time is represented by the vertebrate and breccia beds of the Kilmaluag Formation, and many vertebrate fossils have been recovered from loose boulders so their exact position in the stratigraphical sequence is not known. Therefore we cannot be completely certain that all of the recovered fossil taxa are coeval. To address this, work is currently being undertaken by the University of Birmingham and National Museums Scotland to match the lithology between each bed that crops out on the Strathaird Peninsula with the matrix of fossil material collected from loose boulders to date. This should help constrain the presence of taxa within the sequence.

A second drawback is our currently limited understanding of the deposition of vertebrate material within the Kilmaluag Formation. Fish, lissamphibian, turtle and crocodile material is congruent with the lagoonal environment, but it is not clear how the squamate, mammal or larger archosaur material was deposited. These taxa may have lived around the lagoon margins, or their remains may have been washed into the lagoons from elsewhere, either when fresh or after a period of time decomposing, or within coprolites. For the small vertebrate material in particular, a coprolitic origin is possible. Depending on the consumer, this means these taxa could have lived elsewhere and been transported in the gut of a predator, and in the case of pterosaurs and theropods, these distances could be substantial. Answering this question of origin is a focus on ongoing research at National Museums Scotland and the University of Oxford.

It is likely that even if the exact taxa recovered so far from the Kilmaluag Formation are not coeval, they represent persistent taxonomic groups at this locality and in the vicinity, and in similar habitats across the British Isles in the Middle Jurassic. This makes this preliminary food web a useful first attempt at reconstructing ecological interactions between the flora and fauna of the Kilmaluag Formation. Further study of the placement of taxa within the lithological sequence, and the circumstances of deposition for this fossil material, will improve our ability to confidently reconstruct this Middle Jurassic food web.

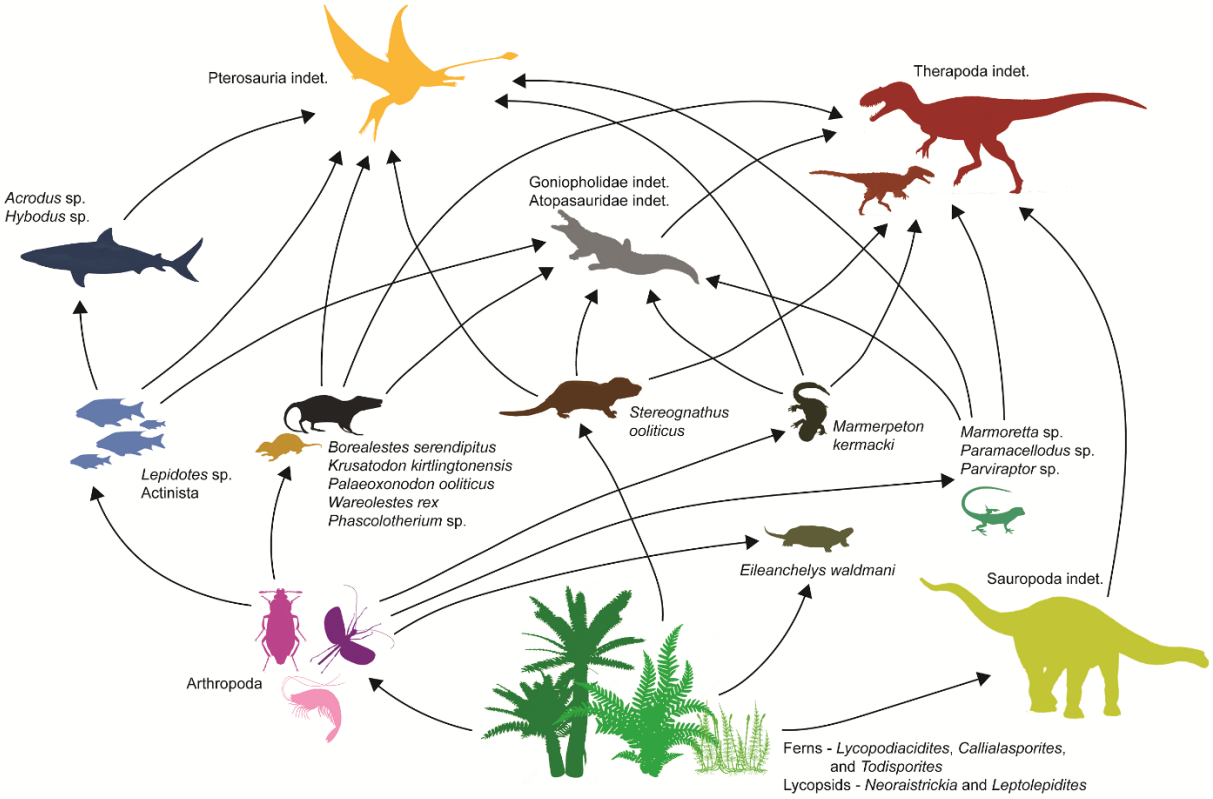

Figure 2.2.1: Food web for the Kilmaluag Formation fauna.

2.3 Comparisons of Vertebrate Fauna with Other Sites

In order to facilitate comparisons between the Kilmaluag Formation vertebrate fauna and a selection of other Jurassic assemblages, faunal tables were compiled from the literature (Table 2.3.1) and a measure of similarity, the Jaccard Index (Jaccard, 1912), was calculated to compare diversity (but not abundance) at order level (Table 2.3.2).

The Forest Marble Formation of England provides the closest comparison to the Kilmaluag Formation, both temporally and in faunal composition (Figure 2.3.1, Table 2.3.1). The Forest Marble Formation is part of the Great Oolite Group, and comprises greenish grey silicate mudstones with cross-bedded limestone units and channel fills (Barron et al., 2011). The vertebrate beds at Kirtlington Cement Quarry near the village of Kirtlington in Oxfordshire comprise an unconsolidated medium brown marl, forming lenses of variable thickness between ooidal limestone (Freeman, E., 1979). These lenses are now thought to be exhausted at surface exposure (Freeman, E., 1979; Freeman, pers. com. 2017). The Forest Marble Formation at Kirtlington represents an estuarine environment, brackish to marine in nature and in the *Retrocostatum* Zone to *Discus* Zone (possibly the *Oppelia aspidoides* Zone, Cope et al., 1980), making it Late Bathonian in age, although the exact dating is uncertain (Evans and Milner, 1994; Barron et al., 2011). Kirtlington Cement Quarry was collected intensively in the 1970s and 1980s, with many tonnes of matrix processed for vertebrate fossils, and it is considered one of the most diverse and productive microvertebrate assemblages in the British Isles (Evans and Milner, 1994).

The Jaccard index supports the similarity between the Forest Marble Formation and the Kilmaluag Formation, with 46% overall similarity, mainly in the number of semionodontiform, turtle, lepidosaur, squamate and choristodere orders (all 50%, see Table 2.3.2). Small vertebrates found in both locailities include the lissamphibian *Marmorerpeton*, leipdosauromorph *Marmoretta*, and choristodere *Cteniogenys* (Table 2.3.1). The larger vertebrate material is also similar between the formations, with goniopholid and atoposaurid crocodylomorphs present in both (38% Jaccard index, Table 2.3.2). Although there is evidence of dinosaur material at both sites, most cannot be identified to a high taxonomic level, meaning comparison is limited, however both formations have yielded theropod material (33%). Many of the same mammaliamorph

and mammaliaform taxa are present in both formations: *Stereognathus*, *Wareolestes*, *Borealestes*, *Krusatodon*, *Phascolotherium* and *Palaeoxonodon* (Table 2.3.1). One of the main differences between the mammaliaform material is the abundance of haramiyids and multituberculates in the Forest Marble Formation—five species to date (Kermack et al, 1998; Butler and Hooker, 2005)—whereas there are currently none known from the Kilmaluag Formation.

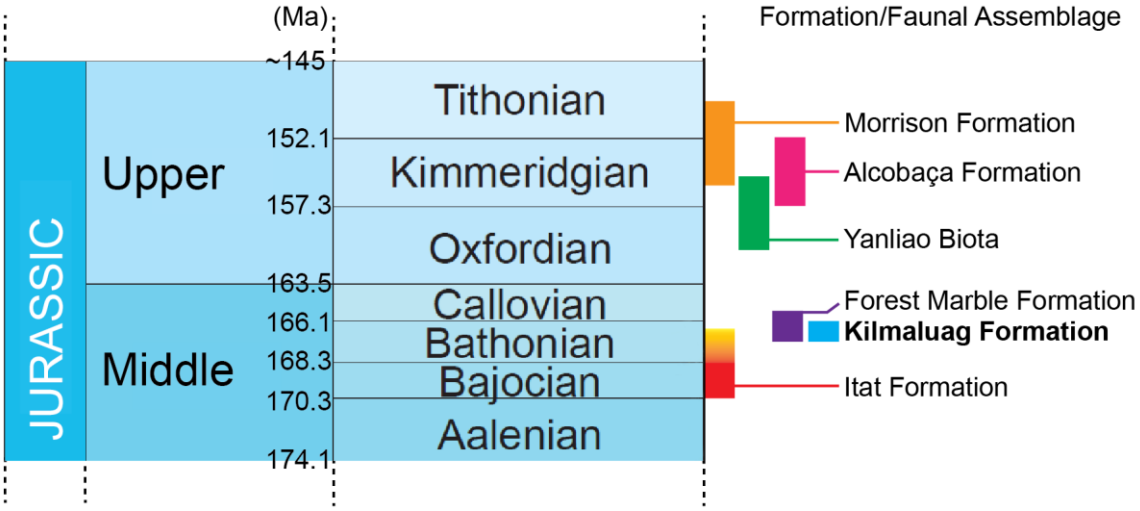

Figure 2.3.1: Approximate ages of the Middle to Late Jurassic localities compared herein. Timescale adapted from Cohen et al., 2018. For dates of Formations see text.

Of similar age, although possibly slightly older than either the Forest Marble Formation or Kilmaluag Formation, the Itat Formation in Russia comprises a series of fossiliferous clays, sandstones and siltstones representing a fluvial floodplain deposit (Averianov et al., 2005, 2016). Fossils from this formation are currently being collected from Berezovsk Quarry in Russia. Similar vertebrate groups are represented in the Itat Formation as in the two British sites (sharing 46% overall order diversity with the Kilmaluag Formation), but the exact genera differ (Table 2.3.1). Dating and stratigraphic correlation for the Itat Formation are uncertain, but if the Kilmaluag, Forest Marble and Itat formations are broadly coeval, the similar faunal composition may reflect regional speciation of well-established groups.

Among the mammaliaform fauna, all three sites have multiple docodontans, and at least one cladotherian. The similarity between the mammaliamorph and mammaliaform diversity in the Itat Formation and the Kilmaluag Formation is higher than between the

Table 2.3.1: The fauna of the Kilmaluag Formation (K, bold blue) and five other Middle to Late Jurassic localities: Forest Marble Formation at Kirtlington (FM, purple); the Yanliao Biota (Y, green); the Itat Formation (I, red); the Morrison Formation (M, orange) and the Alcobaça Formation at Guimarota (G, pink). List compiled from multiple sources, see in text. Also: Evans and Milner, 1994; Kermack et al., 1998; Martin and Krebs, 2000; Sigogneau-Russell, 2003; Averianov et al., 2005, 2016; Butler and Hooker; 2005; Foster and Heckert, 2011; Sullivan et al., 2014; Rougier et al., 2015; Xu et al., 2017; Meng et al., 2017; Chure et al., 2006.

			K	F M	Y	I	M	G
Chondrichthyes	Hybodontiformes							
		Acrodus caledonicus	x					
		Asteracanthus		x				x
		Hybodus sp.	x	x		x		x
		Lissodus		x				
		Polyacrodus sp. nov						x
		Hybodont indet.	x	x				x
	Batoidea							
		Batoidea indet.		x				x
Actinopterygii	Acipenseriformes							
		Liaosteus hongi			x			
		Ptycholepididae indet.			x			
		Acipenseriformes indet.				x		
	Amiiformes							
		Caturus						x
		Caturidae indet.						x
		Ophiopsis sp.					x	
		Sinamiidae indet.				x	x	
		Amioidea indet.		x			x	
	Palaeonisciformes							
		Hulettia hawesi					x	
	Leptolepiformes							
		Leptolepis sp.					x	
	Ionoscopiformes							
		Ionoscopidae incertae sedis						x
	Macrosemiiformes							
		Macrosemiidae incertae sedis						x
	Pachycormiformes							
		Pachycormidae indet.						x
	Palaeonisciformes							
		Morrolepis schaefferi					x	

			Paleoniscidae indet.				x	
	Pycnodontiformes							
			Coelodus/Proscinetes sp.					x
			Macromesodon sp.					x
			Pycnodontoidea indet.		x		x	
	Semionotiformes							
			Lepidotes	x	x			x
			Semionotidae indet				x	
Dipnoi								
			Ferganoceratodus sp.			x		
			Potamoceratodus sp.				x	
	Ceratodontiformes							
			Ceratodus felchi				x	
			C. fossanovum				x	
			C. frazieri				x	
			C. guentheri				x	
			C. robustus				x	
Sarcopterygii	Coelacanthiformes							
			?coelacanth	x				
Lissamphibia	Anura	Discoglossidae						
			Eodisciglossus oxoniensis		x			
			Eodiscoglossus sp.			x		
			Discoglossidae indet.					x
		Pelobatidae						
			Unnamed pelobatid				x	
		Rhinophrynidae						
			Rhadinosteus parvus				x	
		Incertae sedis						
			Comobatrachus aenigmatis				x	
			Ennaebatrachus hechti				x	
			Eobatrachus agilis				x	
	Caudata	Albanerpetonidae						
			Cf. *Celtidens*					x
			Albanerpeton		x			
			Anoualerpeton priscus		x			
		Urodela						
			Beiyanerpeton jianpingensis			x		
			Chunerpeton tianyensis			x		
			Iridotriton hechti				x	
			Jeholotriton paradoxus			x		
			Kiyatriton krasnolutskii				x	
			Liaoxitriton daohugouensis			x		

			Pangerpeton sinensis				x			
			Urupia monstrosa					x		
		Incertae sedis								
			Comonexturoides marshi						x	
			Marmorerpeton kermacki	x	x					
			Marmorerpeton sp.							x
			Unnamed salamander	x	x	x	x	x		
Sauropsida	Testudinata									
			Dinochelys whitei						x	
			Dorsetochelys buzzops						x	
			Eileanchelys waldmani	x						
			Glyptops plicatulus						x	
			Uluops uluops						x	
			Cryptodira: cf.							
			Pleurosternidae		x					
			Pleurosternidae indet.							x
			Platychelidae indet.							x
	Lepidosauromorpha									
			Marmoretta sp.	x	x					
	Rhynchocephalia									
			Eilenodon robustus						x	
			Opisthias rarus						x	
			Theratairus antiquus						x	
			Sphenodontia indet.		x					
	Squamata	Anguimorpha								
			Dorsetisaurus pollicidens							x
			Dorsetiosaurus sp.						x	
			Unnamed dorsetisaur						x	
			Parviraptor gilmorei						x	
			Parviraptor sp.	x						x
			Taxon nov.	x						
			Unnamed Anguinomorpha		x					
		Booidea								
			Unnamed booiid						x	
		Paramacellodidae								
			Becklesius hoffstetteri							x
			Cf. *Paramacellodus* sp.	x					x	x
		Scincoidea								
			Saurillodon sp.		x				x	
			Schilleria utahensis						x	
			Saurillodon proformis							x

		S. henkeli						x
		S. cf. *obtusis*						x
		Unnamed ‘Scincomorpha’		x		x	x	x
	Scleroglossa							
		‘Yabeinosaurus’ youngi			x			
		Unnamed scleroglossan			x			
	Incertae sedis							
		Gekkotan incertae sedis.		x				
		Unnamed lizard	x				x	
Archosauromorpha	Choristodera							
		Cteniogenys antiquus					x	
		Cteniogenys sp.	x	x				
		Choristodera indet.				x		
	Crocodilomorpha							
		Amphicotylus lucasii					x	
		Eutretauranosuchus delfsi					x	
		“Fruitachampsa callisoni”					x	
		Goniopholis felix					x	
		G. gilmorei					x	
		G. lucasii					x	
		G. stovalli					x	
		G. stovalli					x	
		Goniolophis cf. *simus*						x
		Hallopus vistor					x	
		Lisboasaurus estesi						x
		Macelognathus vagans					x	
		Cf. *Nannosuchus*		x				
		Oplosuchus kayi					x	
		Goniopholidae indet.	x			x	x	
		Atopasauridae indet.	x	x				
		Unnamed crocodylomorpha	x				x	
		Goniopholidae indet.	x			x	x	
	Dinosauria							
		Dinosauria indet.	x					
	Ornithiscia							
		Camptosaurus dispar					x	
		C. amplus					x	
		Drinker nisti					x	
		Dryosaurus altus					x	
		Echinodon sp.					x	
		Fruitadens				x		

	“Fabrisauridae” [cf. *Alocodon*]	x			
	Gargoyleosaurus parkpinorum			x	
	Hesperosaurus mjosi			x	
	Mymoorapelta maysi			x	
	Othnielia rex			x	
	Othnielosaurus sp.			x	
	Phyllodon henkeli				x
	Stegosaurus armatus			x	
	S. longispinus			x	
	S. stenops			x	
	S. ungulatus			x	
	Tianyulong confuciusi		x		
	Iguanadontia indet.				x
	Ornithopoda indet.		x		
	Stegosauria indet.		x		
Sauropoda					
	Amphicoelias altus			x	
	A. fragillimus			x	
	Apatosaurus ajax			x	
	A. excelsus			x	
	A. louisae			x	
	Barosaurus lentus			x	
	Brachiosaurus altithorax			x	
	Camarasaurus supremus			x	
	C. grandis			x	
	C. lentus			x	
	C. lewisi			x	
	Diplodocus longus			x	
	D. carnegii			x	
	D. hayi			x	
	D. lacustris			x	
	Dyslocosaurus polyonychius			x	
	Dystrophaeus viaemalae			x	
	Dystylosaurus edwini			x	
	Haplocanthosaurus priscus			x	
	H. delfsi			x	
	Seismosaurus hallorum			x	
	Supersaurus vivianae			x	
	Suuwassea emilieae			x	
	Unnamed cetiosaurid			x	

	Neosauropoda indet. (not *Cetiosaurus*)	x			
	Mamenchisauridae indet.			x	
	Brachiosauridae indet.				x
	Sauropoda indet.	x			
Theropoda					
	Allosaurus fragilis				x
	A. jimmadensi				x
	Anchiornis huxleyi			x	
	Cf. *Archaeopteryx* sp.				x
	?Aviatyrannis jurassica				x
	Aurornis xui			x	
	Ceratosaurus nasicornis				x
	C. magnicornis				x
	C. dentisulcatus				x
	Coelurus fragilis				x
	Compsognathus sp.				x
	Elaphrosaurus sp.				x
	Eosinopteryx			x	
	Epidendrosaurus ningchengensis			x	
	Epidexipteryx hui (= *Scansoriopteryx heilmanni*)			x	
	Kileskus aristotocus			x	
	Koparion douglassi				x
	Ornitholestes hermanni				x
	Paronychodon sp.				x
	Pedopenna daohouensis			x	
	Cf. *Richardoestesia* sp.				x
	Saurophaganax maximus				x
	Stokesosaurus clevelandi				x
	Stokesosaurus sp.				x
	Tanycolagreus topwilsoni				x
	Torvosaurus tanneri				x
	Xiaotingia shengi			x	
	?Allosauroidea indet.				x
	Carnosauria indet.		x		
	Ceratosauria indet.				x
	“Coelurosauria” indet.		x		
	Dromaeosaurinae indet.				x x
	Tyrannosauridae indet.				x
	Veloceraptorinae indet.				x

			Unnamed troodontid					x	x
			Unnamed maniraptorans					x	
			Theropoda indet.	x					
		Pterosauria							
			Archaeoistiodactylus linglongtaensis						
			(?*Darwinopterus*)			x			
			Changchengopterus pani			x			
			Darwinopterus modularis			x			
			D. linglongtaensis			x			
			D. robustodens			x			
			Dendrorhynchoides mutoudengensis			x			
			Dermodactylus montanus					x	
			Fenghuangopterus lii			x			
			Jeholopterus ningchengensis			x			
			Jianchangnathus robustus			x			
			Jianchangopterus zhaoianus			x			
			Kepodactylus imperatus					x	
			Kunpengopterus sinensis			x			
			Laopteryx priscus					x	
			Mesadactylus ornithosphyos					x	
			Pterorhynchus wellnhoferi			x			
			Qinglongopterus guoi			x			
			Rhamphorhynchus						x
			Wukongopterus lii			x			
			Rhamphorhynchoidea indet.	x			x		x
			Pterodactyloidea indet.	x					x
Synapsida	Mammaliamorpha								
			Stereognathus ooliticus	x	x				
			Tritylodontidae indet.				x		
	Mammaliaformes								
			Mammalia indet.	x	x				
		Australosphenida							
			Pseudotribos robustus						
		Cladotheria							
			Amblotherium gracilis					x	
			A. minimum					x	
			Amblotherium sp.					x	
			Amphibetulimus krasnolutskii				x		
			Anthracolestes sergeii				x		
			Araeodon intermissus					x	

	Archaeotrigon brevimaxillus					x	
	A. distagmus					x	
	Comotherium richi					x	
	Drescheratherium acutum						x
	Dryolestes leiriensis						x
	Dryolestes priscus					x	
	Euthlastus cordiformis					x	
	Fruitafossor windscheffeli					x	
	Foxraptor atrox					x	
	Guimarotodus inflatus						x
	Henkelotherium guimarotae						x
	Krebsotherium lusitanicum						x
	Laolestes eminens					x	
	L. goodrichi					x	
	L. oweni					x	
	L. sp.					x	
	Nanolestes drescherae						x
	Palaeoxonodon ooliticus	x	x				
	Paurodon valens					x	
	Tathiodon agilis					x	
	Unnamed paurodontid					x	
Docodonta							
	Agilodocodon scansorius			x			
	Borealestes serendipitus	x	x				
	Borealestes mussettae		x				
	Borealestes sp.	x	x				
	Castorocauda lutrasimilus			x			
	Docodon victor					x	
	D. apoxys					x	
	Docofossor brachydactylus			x			
	Haldanodon exspectatus						x
	Hutegotherium yaomingi				x		
	Itatodon tataronovi				x		
	Krusatodon kirtlingtonensis		x				
	Krusatodon sp.	x	x				
	Simpsonodon oxfordensis (=*'Cyrtlatherium'*)		x				
	Simpsonodon sibiricus				x		
Eutheria							
	Juramaia sinensis			x			
Eutriconodonta							

	Aploconodon comoensis						x
	Comodon gidleyi						x
	Liaotherium gracile				x		
	Manchurodon simplicidens				x		
	Phascolotherium sp.	x					
	Priacodon ferox						x
	P. robustus						x
	P. lulli						x
	P. grandaevus						x
	P. fruitaensis						x
	Triconolestes curvicuspis						x
	Trioracodon bisulcus						x
	Volaticotherium antiquum				x		
	Amphilestidae indet.					x	
	Eutriconodonta indet.					x	x
Haramiyida							
	Arboroharamiya jenkinsi				x		
	Eleutherodon oxfordensis			x			
	Kirtlingtonia catenata			x			
	Maiopatagium furculiferum				x		
	Megaconus mammaliaformis				x		
	Millsodon oxfordensis			x			
	Sineleutherus issedonicus					x	
	Qishou jizantang				x		
Morganucodonta							
	Wareolestes rex	x		x			
Multituberculata							
	Bathmochoffatia hapax						x
	Ctenacodon laticepts						x
	C. scindens						x
	C. serratus						x
	“Ctenacodon” brentbaatar						x
	Ctenacodon. sp.						x
	Glirodon grandis						x
	Guimarotodon leiriensis						x
	Hahnotherium antiquum			x			
	Henkelodon naias						x
	Kermackodon multicuspis			x			
	Kielanodon hopsoni						x
	Kuehnodon dietrichi						x
	K. guimarotensis						x
	K. simpsoni						x
	K. dryas						x

	K. uniradiculatus		x
	Meketibolodon robustus		x
	Meketichoffatia krausei		x
	Paulchoffatia sp.		x
	Plesiochoffatia thoas		x
	P. peparenthos		x
	P. staphylos		x
	Proalbionbaatar plagiocyrtus		x
	Psalodon fortis	x	
	P. marshi	x	
	P. potens	x	
	Psalodon. sp.	x	
	Pseudobolodon oreas		x
	P. krebsi		x
	Xenachoffatia oinopion		x
	Zofiabaatar pulcher	x	
	Unnamed multituberculate	x	
Tinodontidae			
	Tinodon bellus	x	

Kilmaluag and Forest Marble Formations (47%, Table 2.3.2). The Itat Formation has one haramiyidan taxon (*Sineleutherus* [Averianov et al, 2011])—differentiating it from the Kilmaluag Formation—to date there are fewer haramiyidans than present in the Forest Marble Formation, and neither the Kilmaluag nor Itat formations have yielded multituberculates.

One of the most exceptional assemblages for comparison with the Kilmaluag Formation is the Yanliao Biota of northeastern China. Taking its name from the Yanliao area which contains extensive exposures of Middle to Late Jurassic fossiliferous strata, the term Yanliao Biota is used here following Xu et al. (2016, 2017) to include the Juilongshan/Haifenggou Formation and Tiaojishan/Lanqi Formation, as well as the 'Douhugou Biota' (Sullivan et al 2014). The strata yielding the Douhugou (including sites at Linglongta, Wubaiding, Mutoudeng, Guancaishan, Nanshimen, Daxishan, Daxigou and the Youlugou) are likely to correlate with the Tiaojishan/Lanqi Formation, and possibly the youngest part of the Juilongshan/Haifenggou Formation (Sullivan et al., 2014; Xu et al., 2017). Some confusion persists over exact correlations between different outcrops in the Yanliao area. Radiometric dates have provided a wide age range of 146-188 Ma, but a more conservative range is 157 ± 3 Ma (Xu et al., 2017), making it Bathonian to Oxfordian

(Figure 2.3.1). Biostratigraphical correlations support this Middle-Late Jurassic age (Sullivan et al., 2014; Xu et al., 2017).

Table 2.3.2: Similarity index for vertebrate faunas in Jurassic Formations, showing percentage similarity with the Kilmaluag Formation (Jaccard index). K = Kilmaluag Formation FM = Forest Marble Formation at Kirtlington; Y = the Yanliao Biota; I = the Itat Formation; M = the Morrison Formation; and G = the Alcobaça Formation at Guimarota.

	Hybodontiformes	Batoidea	Actinopterygia -Semionotiformes	Other Actinopterygia	Dipnoi*	Coelacanthiformes	Lissamphibia incertae sedis*	Other Lissamphibia*	Testudinata	Lepidosauromorpha*	Rhynchocephalia	Squamata	Choristodera	Crocodilomorpha*	Sauropoda	Theropoda	Other Dinosauria	Pterosauria	Therapsida (Mammaliamorpha)	**OVERALL**
K/FM	43	0	0	50	0	0	50	0	50	50	0	50	50	38	0	33	0	0	35	**44**
K/Y	0	0	0	0	0	0	33	0	0	0	0	40	0	0	0	13	0	13	42	**43**
K/I	25	0	0	0	0	0	33	0	0	0	0	25	50	29	33	50	0	33	47	**46**
K/M	0	0	0	50	0	0	50	0	20	0	0	27	0	11	4	6	0	33	14	**16**
K/G	43	0	0	50	0	0	33	0	33	0	0	27	0	29	0	0	33	40	19	**29**

The Yanliao Biota comes from a series of sedimentary and volcanic cycles, but despite there being multiple formations over such a large geographic area, the fossil-bearing strata are somewhat similar. These mostly comprise laminated tuffaceous mudstones and shales, yielding exceptionally complete skeletons with soft tissue preservation—resulting in recognition of the sites yielding the Yanliao Biota as a globally significant lagerstätte (Xu et al., 2017). The palaeoenvironment varied laterally, but overall represents a freshwater ecosystem similar in many ways to that preserved in the Kilmaluag Formation, but lacustrine rather than lagoonal, with a humid, warm climate and highly aquiferous soil (Xu et al., 2017).

Overall the vertebrate fauna of the Yanliao Biota have a 43% diversity similarity index at order level to the Kilmaluag Formation (Table 2.3.2). The strongest similarities are

between the mammaliaform (42%) and squamate (40%) faunas. Looking specifically at the mammaliaform taxa, there is a similar pattern of mammal groups represented as in the Kilmaluag, Forest Marble, and Itat Formations, with multiple docodontans, one or more eutriconodontans, and at least one cladotherian mammal (Table 2.3.1). Like the Forest Marble and Itat Formations, but unlike the Kilmaluag Formation, the Yanliao Biota includes haramiyidans. Unlike the other formations discussed so far, the Yanliao includes an australosphenidan (*Pseudotribos robustus*, Luo et al., 2007). The genera represented are exceptionally ecologically diverse, with specialised swimming (*Castorocauda*, Ji et al., 2006), digging (*Docofossor* , Luo et al., 2015) and gliding (*Maiopatagium*, Meng et al., [2017]) forms. However, this ecomorphological diversity may be the result of the completeness of the skeletal material known for these animals—their counterparts in other localities globally are often represented by more fragmentary, often dentomandibular material, which provides limited information about ecomorphology (see below for further discussion).

The Morrison Formation in North America also yields globally significant Jurassic mammal material. Historically it was one of the first fossil-bearing localities to be exploited in the world with collecting being carried out there since 1877 (Weishampel et al, 2004), and a great deal of attention has been given to the archosaur material. This rock unit extends across an enormous area of the west and Central North America—with significant outcrops in Arizona, Montana, Wyoming, Utah, and Oklahoma—and north into Canada (Turner et al., 2004). The Morrison Formation is between 155-148 Ma (Kowallis et al., 1998), and it largely comprises terrestrial deposits, with a huge range of lithologies including aeolian, fluvial and floodplain sandstones, floodplain/lacustrine mudstones and coal, and wetland and lacustrine carbonates (see Turner et al., 2004 for comprehensive geological overview).

The lowest similarity is found between the Kilmaluag Formation and the Morrison Formation in our overview, with only 16% overall (Table 2.3.2). The greatest similarity is between the orders of semionotiformes (50%), and lissamphibians of uncertain taxonomic placement (50%). There are around 45 species of Mesozoic mammal known from the Morrison Formation, including eutriconodontans, docodonts, multituberculates and cladotherians (Chure et al., 2006) (Table 2.3.1). Docodonts were among the first taxa to be found and described (Marsh, 1880) and subsequently five species of the genus *Docodon* were erected (Marsh 1887; Simpson 1929; and Rougier et al. 2014). These have since been

synonymised under *D. victor* and *D. apoxys* (Chure et al., 2016; Schultz et al., 2018), making Docodonta the least speciose mammaliaform order in the Morrison Formation, and less diverse for docodonts than the other localities discussed herein. However, in overall mammaliaform diversity, it is by far the more diverse of the Jurassic sites known globally to date and cladotherian mammals are the most diverse, with 11 genera described (Chure et al., 2006).

The mammals of the Morrison Formation are mostly represented by dentition and some by dentomandibular material, only *Fruitafossor* is known from a more complete skeleton with postcrania (Luo and Wible, 2005). The peg-like teeth and large front limbs suggest a fossorial insect-eating specialist, similar in ecology to modern xenarthrans (Luo and Wible, 2005). As with other Jurassic mammal-bearing formations, the lack of postcrania limit the ecological inferences that can be made, but the specialisations in *Fruitafossor* suggests that ecomorphological diversification among mammals in the Jurassic was not limited to Asian taxa. Like the Kilmaluag Formation, but unlike the Yanliao Biota, and Forest Marble and Itat formations, there are currently no haramiyidans known from the Morrison.

The final site in this comparison that has yielded globally significant Jurassic mammal material is the Alcobaça Formation in Portugal, namely from the Guimarota Coal Mine. The Alcobaça Formation is Kimmeridgian in age (Figure 2.3.1), and vertebrate bearing beds of Guimarota Coal Mine are approximately 20 m in thickness, comprising a layer of limestone between two coal seams (Schudack, 2000). These seams are composed of alternating marls, and represent a shallow lagoon environment with fluctuating water levels, resulting in changes in salinity that are reflected in the evidence from ostracods and charophytes (Helmdach, 1971; Schudack, 2000).

There are similarities between the faunal assemblage of the Alcobaça Formation in the Guimarota Coal Mine and the assemblages of the Kilmaluag, Forest Marble, Itat and Morrison formations in the fish (*Hybodus* and *Lepidotes*) lissamphibian (*Marmorerpeton*) and some diapsid faunas (*Paramacellodus*, goniopholid crocodiliformes, and non-pterodactyloid and pterodactyloid pterosaurs) (Table 2.3.1). The composition of the dinosaur assemblage at Guimarota is also broadly similar to that of the contemporaneous Morrison Formation—comparisons with the British and Russian sites are hampered by poor

preservation of specimens at these sites, which cannot be identified to higher taxonomic levels.

Comparing the Guimarota vertebrate assemblage with the Kilmaluag Formation, they score an overall similarity index of 29%, the highest similarity being found between the semionotiforms (50%) and pterosaurs (40%), and somewhat less between turtles (33%) and lissamphibians of uncertain taxonomic placement (33%). Both formations have docodonts and cladotherian mammaliaforms, but as in the other comparisons above, Guimarota has multituberculates—in fact they represent the most speciose mammal group at this locality, with 12 genera (Martin and Krebs, 2000; Martin, 2001). Mammaliaform similiarity is only 19% between the Kilmaluag and Alcobaça formations. The lack of haramiyidans or eutriconodontans in the Alcobaça Formation in Guimarota Coal Mine distinguishes this mammal assemblage from the other Jurassic localities described here (Table 2.3.1). The Alcobaça Formation, Morrison Formation and the Yanliao Biota have no tritylodontids in their assemblage, unlike the Forest Marble, Itat and Kilmaluag formations.

2.4 Collection Methods and Potential Biases

The method of collection employed at sites of the Kilmaluag Formation since its discovery in 1971 produces a bias towards larger, more complete specimens visible at outcrop (Figure 2.1.3), in contrast with most of the other sites discussed here. At Kirtlington Cement Quarry, Forest Marble Formation matrix was processed using a process of wet sieving of sediment followed by drying and hand picking (Freeman E., 1979; Evans and Milner, 1994). The same method has been employed to process the Itat Formation at the Berezovsk coal mine (Averianov et al., 2016). Similarly, at Guimarota the coal lignite sediment was dissolved in an alkaline bath and screen washed (Martin, 2001)—although more complete specimens were found in lumps of lignite prior to this process (Martin 2005). The Morrison Formation crops out in multiple localities, and these have been both screenwashed and collected by eye (Foster and Lucas, 2006; Foster 2011).

The hard-weathering nature and poor reaction to acid of the limestone in the vertebrate-rich strata of the Kilmaluag Formation is less compatible with bulk processing. This limits the volume of material collected from these outcrops, and introduces collection bias towards more readily visible material—such as bone associations, dentaries containing teeth, and single elements—that appear diagnostic at outcrop. Micro CT scans of collected specimens occasionally reveal isolated dental and skeletal fragments scattered throughout the limestone matrix. These commonly include tritylodontid teeth, salamander vertebrae and fish remains (pers. obs.). This suggests that if the Kilmaluag Formation could be bulk processed, it would yield similar diverse isolated microvertebrate remains to those of the Forest Marble Formation.

Collection in the Yanliao Biota localities is usually through concentrated excavation efforts, without screenwashing, and initial fossil finds often come from local farmers spotting fossil material during their work (Xu et al., 2016, 2017). This would suggest a similar collection bias may exist towards more complete material. But there is a substantially wider geographical area represented by the many outcrops of the Yanliao Biota compared to the geographically restricted Kilmaluag Formation, and this severely limits comparisons between these formations. Collection will be influenced by

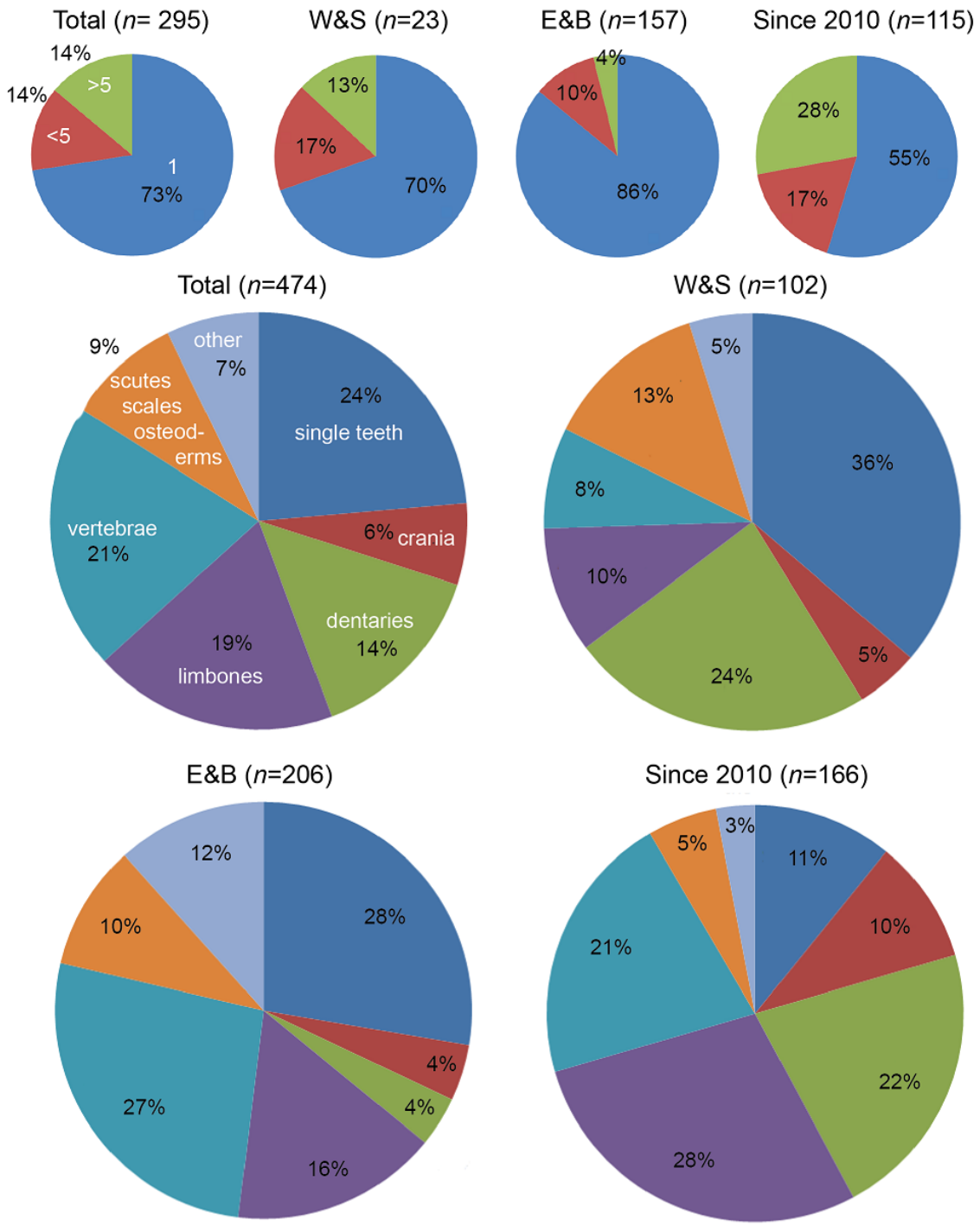

Figure 2.4.1: Collecting from the Kilmaluag Formation since 1971. Number of 'bones per find' along top row: numbers indicated in white text in first pie chart, percentages in black. Type of fossil find in bottom four pie charts: type of fossil in white in top left pie chart, percentages in black. Total = all finds since 1971 (W&S + E&B + Since 2010); W&S = Waldman and Savage (1971-1982); E&B = Evans and Barrett (2004 and 2006); Since 2010 = collections since 2010, carried out by NMS and Universities of Oxford and Birmingham. Sample sizes indicated by: *n*=.

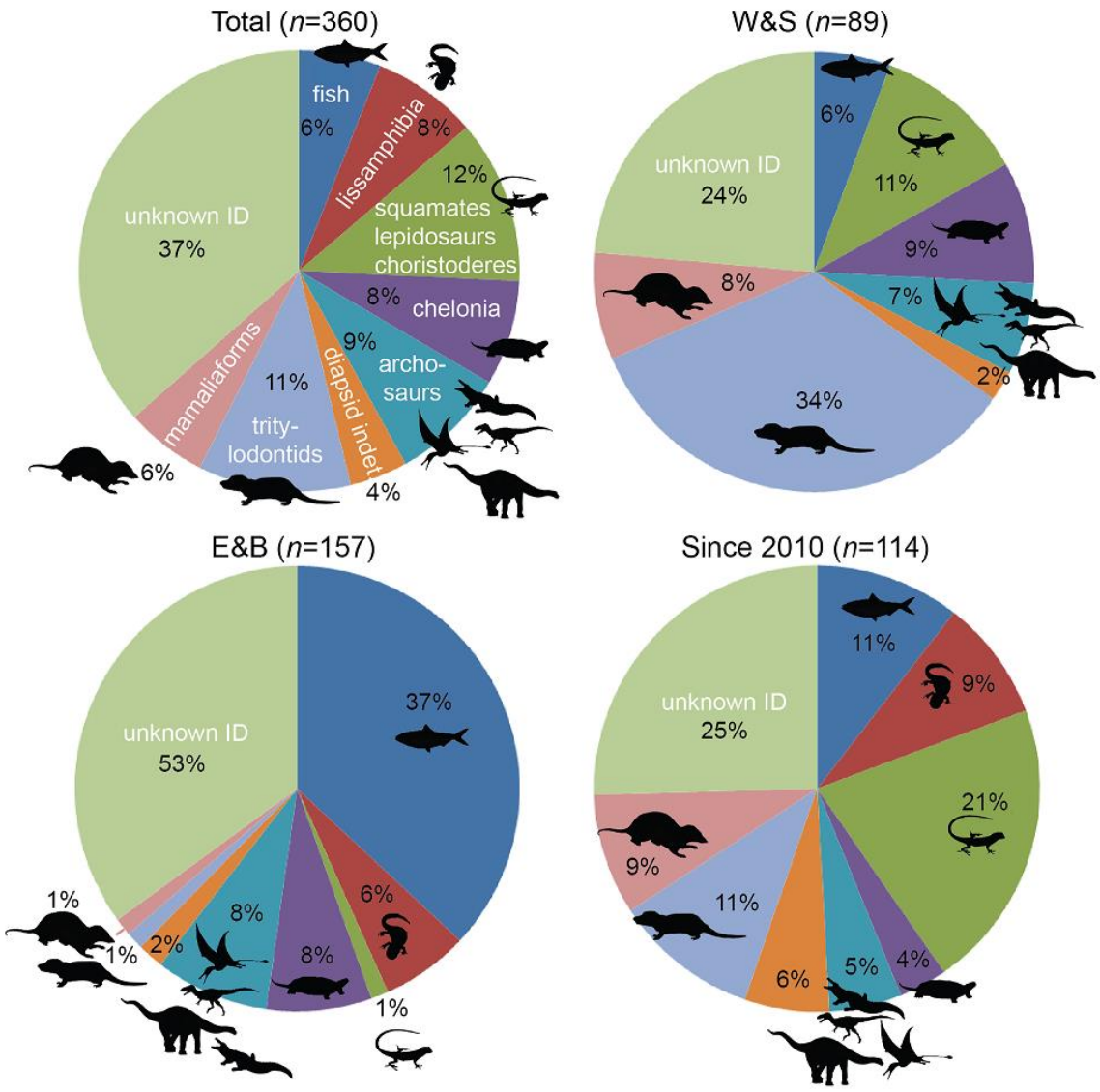

Figure 2.4.2: Collecting from different taxonomic groups in the Kilmaluag Formation since 1971. Taxonomic groups indicated in white in top left pie chart, percentages in black throughout. Total = all finds since 1971 (W&S + E&B + Since 2010); W&S = Waldman and Savage (1971-1982); E&B = Evans and Barrett (2004 and 2006); Since 2010 = collections since 2010, carried out by NMS and Universities of Oxford and Birmingham. Sample sizes indicated by: *n*=.

geographic range, and the largest assemblages in this comparison known from more extensive outcrops (the Yanliao Biota and the Morrison Formation, see Table 2.3.1).

There have been three periods of collecting at the outcrops of Kilmaluag Formation along the Strathaird Peninsula: from 1971 to 1982 collecting was carried out over the course of seven field trips by Dr Michael Waldman and Professor Robert Savage (W&S) and their team; in 2004 and 2006 collecting was carried out by Professor Susan Evans and Professor Paul Barrett (E&B) and their team; and collecting has been carried out since 2010

by Dr Stig Walsh from National Museums Scotland, Professor Roger Benson from the University of Oxford, and since 2016 also myself and Professor Richard Butler of the University of Birmingham (since 2010). Looking at an overview of the collections made from the Kilmaluag Formation since its discovery (Figures 2.4.1 and 2.4.2), 28% of total finds comprise more than a single bone/tooth, while 14% are associations of more than five bones (Figure 2.4.1). The bias towards associated skeletons is most notable in the recent collecting practices, with 28% of specimens collected since 2010 comprising more than five bones in association.

There are clear differences not only in the number of bones/teeth per specimen collected by each collecting team, but also in the skeletal elements, and the taxonomic groups represented. W&S collected mostly single teeth and dentaries (60% of all finds), as well as a large number of turtle, fish and crocodile scutes, scales and osteoderms (13%) (Figure 2.4.1). The collecting by E&B also contained significant numbers of single teeth (28%) and also vertebrae (27%). The most marked difference in collections is in the more recent work: since 2010 most of the specimens collected have comprised/included limb bones (28%), dentaries (22%) and vertebrae (21%), a total of 71% of all finds. These percentages reflect the larger number of single dentaries on one hand, and associated skeletons on the other.

In terms of representation of taxonomic groups, tritylodontids represent the most commonly collected group by W&S (34%, mainly single postcanine teeth), whereas E&B collected a large number of fish (37%, mostly shark teeth) (Figure 2.4.2). The greatest volume of unidentified material was collected by E&B (35%)—predominantly bone fragments that cannot be assigned taxonomically. Collecting since 2010 has been somewhat more balanced between taxonomic groups, with 21% comprising small diapsids such as squamates, lepidosaurs and choristoderes, and lissamphibians, mammaliaforms, and mammaliamorphs (tritylodontids) at about 10% representation each. Although 25% of collected specimens since 2010 are categorised as ‘unknown ID’, unlike in previous collecting many of these possess diagnostic characters, and merely await CT scanning to facilitate identification. This means the percentages discussed here will change in the coming years.

2.5 Discussion

The huge geographic range of the Morrison Formation and the many formations of the Yanliao Biota limit comparability with much smaller outcrops like the Itat and Kilmaluag formations, the Guimarota Coal Mine or Kirtlington Cement Quarry. The thickness of different sequences will also play a role in their productivity, and affect comparability. However, the broadly similar faunal diversity represented by the fossils from these small sites is testament to their richness and significance. The Kilmaluag Formation was initially considered to comprise a much less diverse fauna than the closely contemporaneous Forest Marble Formation site, Kirtlington Cement Quarry, with only occasional mammal or salamander material (Evans et al., 2006). More recent work (2010 onwards) indicates this is not the case, with multiple specimens from these taxonomic groups published, currently under study, and awaiting detailed study. Direct comparison of the Forest Marble Formation and Kilmaluag Formation suggests a strikingly similar faunal composition and diversity at these more or less contemporaneous Middle Jurassic British localities (Table 2.3.1 and 2.3.2).

Looking at the mammals and close relatives across all of these localities, the earlier branches of mammaliaforms such as the morganucodontans, docodonts and haramiyidans appear proportionally more common in the older strata (Itat, Forest Marble and Kilmaluag formations), whereas crown groups such as multituberculates and cladotherian mammals are much more diverse later in the Jurassic (in the Alcobaça Formation at Guimarota, and the in the Morrison Formation) (Figure 2.3.1, Table 2.3.1). There are no tritylodontids collected from the Alcobaça Formation in the Guimarota Coal Mine, the Morrison Formation or the Yanliao Biota, which are the three youngest assemblages discussed here.

The mammaliamorph tritylodontids are considered a close sister-group to mammaliaforms (Rowe, 1993; Luo et al., 2002; Ruta et al., 2013). They appeared in the Late Triassic and persisted alongside mammaliaforms and crown mammals into the Early Cretaceous (Hennig, 1922; Matsuoka et al., 2016; Chapter 3.1), with an almost global distribution in the Early-Middle Jurassic. They are often represented only by isolated teeth and cranial material, but complete skeletons including perinates have been recovered from the Early Jurassic Kayenta Formation of North America (Kermack, 1982; Hoffman and Rowe, 2018). *Dinnebitodon* (Sues, 1986) is also known from the Early Jurassic Kayenta

Formation, while *Bienotherium* (Young, 1940; Luo and Wu, 1994), *Dianzhongia* (Cui, 1981) *Lufengia* (Chow and Hu, 1959; Hopson and Kitching, 1972) *Oligokyphus* (Luo and Sun, 1994) and *Yunnannodon* (Cui, 1976) are known from the Early Jurassic of China. *Polistodon* is known from the Dashanpu Formation of China, partly contemporaneous with the Yanliao Biota (He and Cai, 1984), and *Yuanotherium* (Hu, Meng and Clark, 2009) is known from the Late Jurassic of China.

These distribution patterns have interesting implications for tritylodontid biogeography. The presence of tritylodontids in Early, Middle and Late Jurassic sediments in China suggests they were present in Asia throughout the time-period represented by the Yanliao Biota in China, despite not being found there. They were also present on the North American continent prior to the Morrison Formation deposition, but there is no evidence for them persisting there from the Middle Jurassic onward. Their absence in the Guimarota Coal Mine or other European Formations from the Late Jurassic onwards suggests they may have been absent from this region at that time. Their presence in Late Jurassic sediments in Asia, and the Early Cretaceous of Japan (Matsuoka, et al., 2016) suggests these regions may represent their last refugia, and that they became rare and/or extinct in other parts of the world by this time. These areas may represent their core distribution. However, this is based on a scant fossil record, and so remains speculative.

Another explanation for the absence of tritylodontids in the Alcobaça Formation in Guimarota Coal Mine, the Morrison Formation, and in the Yanliao Biota, could be ecological, and may be related to the pattern seen for the multituberculates in these formations. Tritylodontids are thought to have been mostly herbivorous, with specialised postcanine teeth, a diastema and procumbent incisors, giving them a superficial resemblance to modern rodents. Preliminary research on isotope ratios in tritylodontid teeth supports a predominantly herbivorous diet (Kalthoff et al., 2018). A similar resemblance to rodents is also seen in the crown mammal group, the multituberculates, and competitive exclusion caused by the rise of rodents has been suggested as a cause for the disappearance of Multituberculata as a group in the Eocene (Krause, 1986; Kielan-Jaworowska et al., 2004; Wood, 2010). Multituberculates may have competitively replaced tritylodontids in the Late Jurassic to Early Cretaceous: this theory is tentatively supported by the pattern seen in the assemblages discussed here. Although there are no multituberculates currently known in the Yanliao Biota, there are haramiyidans, which also exhibit ‘rodent-like’

adaptations to a more herbivorous/omnivorous diet (Grossnickle and Polly, 2013; Zhou et al., 2013), potentially putting them in dietary ecological completion with tritylodontids.

Collecting from the Kilmaluag Formation is influenced by a bias towards larger specimens that appear diagnostic at outcrop. But when the faunal composition is compared to faunas from elsewhere, particularly the screen-washed matrix of the Forest Marble, it is clear that persistent collecting is yielding almost as diverse an assemblage of mammals as might be expected through other collection methods (Table 2.3.1). Although the outcrops are geographically restricted, the assemblage of the Kilmaluag Formation is of similar diversity to other internationally important Middle and Upper Jurassic assemblages (Table 2.3.1). What's more, the more complete material preserved in the limestone of the Kilmaluag Formation promises to provide significant scientific information about new and previously known taxa, through minimally deformed preservation of cranial and postcranial material. Taken together, this makes the Kilmaluag Formation one of the most important sites in the world for understanding Middle Jurassic ecosystems, as well as the anatomy and evolution of multiple major lineages of vertebrates in the Mesozoic.

Chapter 3: Mammaliaforms and Tritylodontids of the Kilmaluag Formation

There is one mammaliamorph, and there are at least five mammaliaforms—a morganucodontan, two docodontans, a eutriconodontan and a cladotherian mammal—now known from fossils from the Kilmaluag Formation (Panciroli et al., 2018d; Chapter 2). Although collecting has taken place since the 1970s, only in the last decade has the amazing diversity of the site begun to emerge.

In order to fully document this diversity and the completeness of the fossil material found in the Kilmaluag Formation, I update and describe previously collected material, and new material collected since 2010. This provides a comprehensive overview of the exceptional fossil material from this locality, and its bearing on our understanding of the phylogenetics and anatomical evolution of Middle Jurassic mammals.

3.1 Tritylodontidae: *Stereognathus ooliticus*[1]

Tritylodontids are advanced cynodont mammaliamorphs that fall outside the clade Mammaliaformes, but their close relationship to mammals is now generally accepted (Rowe, 1993; Luo et al., 2002; Ruta et al., 2013). Superficially, tritylodontids would have appeared rodent-like: enlarged procumbent incisors replaced the absent canine teeth, they possessed a diastema, and their postcanine teeth were highly specialized for herbivory. Tritylodontids ranged in size from genera such as *Bocatherium* at <5 cm skull length (Clark and Hopson, 1985) to larger genera with >22 cm skull lengths, such as *Kayentatherium* (Kermack, 1982). They were the last surviving family of non-mammaliaform cynodonts, appearing in the fossil record in the Late Triassic (Hennig, 1922; Fedak et al., 2015), living alongside early mammals and other mammaliaforms throughout the Jurassic, and persisting into the Early Cretaceous (Maisch et al., 2004; Hu et al., 2009; Matsuoka et al., 2016). Although they shared many cranial and postcranial features with early mammaliaforms, they retained a quadrate-articular jaw joint, lacked a dentary-squamosal contact, and they had a large angular process and a large coronoid process on the dentary (Kemp, 2005). Their size range and specializations for herbivory are among the characteristics that distinguish them from many of the early mammals they lived alongside (Kemp, 2005).

Tritylodontidae currently includes over seventeen genera (with at least five more genera debated or synonymised) and have been described from Africa (Owen, 1884; Fourie, 1963), Antarctica (Lewis, 1986; Hammer and Smith, 2008), Asia (Young, 1940, 1982; Chow and Hu, 1959; Cui, 1976, 1981; He and Cai, 1984; Luo and Sun, 1994; Matsuoka and Setoguchi, 2000; Maisch et al., 2004; Watabe et al., 2007; Lopatin and Agadjanian, 2008; Hu et al., 2009; Matsuoka et al., 2016; Velazco et al., 2017), Europe (Charlesworth, 1855; Owen, 1857; Hennig, 1922; Waldman and Savage, 1972; Ensom, 1977, 1994), and North America (Kermack, 1982; Sues, 1985, 1986; Sues and Jenkins, 2006; Fedak et al., 2015), including Mexico (Clark and Hopson, 1985). All are considered herbivorous (Kühne, 1956; Sues, 1986), except *Yuanotherium minor*, which was described as having dental characteristics that suggest that it may have been omnivorous (Hu et al., 2009).

[1] The content of Chapter 3.1. was originally published as Panciroli, E., Walsh, S., Fraser, N., Brusatte, S. L., and Corfe, I. 2017c. A reassessment of the postcanine dentition and systematics of the tritylodontid *Stereognathus* (Cynodontia, Tritylodontidae, Mammaliamorpha), from the Middle Jurassic of the UK. *Journal of Vertebrate Paleontology*, 37: 1351448.

Stereognathus was the first tritylodontid genus named and identified (Charlesworth, 1855). Since that time, material from across the British Isles has been assigned to *Stereognathus*, and its name appears regularly on faunal lists. However, the anatomy and taxonomy of this genus remain poorly understood. Two species have been described: the type species *S. ooliticus* Charlesworth, 1855, is currently represented by hundreds of cusp fragments and at least forty-eight somewhat more complete postcanine teeth, two incisors, one edentulous fragment of maxilla, and the holotype comprising three postcanines in a fragment of maxilla. All of this material comes from sites in England (for overview, see Evans and Milner, 1994). A second species, *S. hebridicus*, was named by Waldman and Savage (1972) from the Isle of Skye in Scotland. Fossils assigned to this species currently include forty-one postcanines, many of them fragmentary and/or badly worn, with two in excellent condition and described herein. Although a few isolated limb bones have been collected from British sites and assigned to Tritylodontidae—notably a single femur from the Stonesfield Slate (Simpson, 1928; Kühne, 1956)—the identification as *Stereognathus* remains unconfirmed. These specimens are therefore considered to be outside the scope of this study.

Surprisingly, given the long history and amount of fossil material, *Stereognathus* has yet to be comprehensively described. There is currently a lack of clarity on its diagnosis, systematics, anatomical features, and variability. This is becoming a pressing issue as new tritylodontid specimens continue to be discovered around the world (e.g., Matsuoka et al., 2016; Velazco et al., 2017) yet cannot easily be compared with *Stereognathus*. Lack of detailed descriptions of some genera has repercussions for phylogenetic analyses, including incorrect character scoring for *Stereognathus*. Without the establishment of a firm description and diagnosis for *Stereognathus*, character scores remain unclear. Finally, recent field work on the Isle of Skye is discovering new *Stereognathus* specimens at a steady pace. This material has raised questions regarding their taxonomy, given that the original diagnosis of *S. hebridicus* was based only on a proposed size difference from *S. ooliticus*.

Here, I provide a reassessment of the anatomy of the postcanine dentition of *Stereognathus*, based upon all available material from the UK. I redescribe the holotype of *S. ooliticus* and synonymise *S. hebridicus* with *S. ooliticus*, based on close examination of *S. hebridicus* material. This includes the holotype and paratypes, alongside new and

exceptionally well-preserved postcanines from the Isle of Skye. I test whether specimens assigned to *S. hebridicus* from Skye are indeed statistically significantly larger than the English specimens, as stated in the original diagnosis of *S. hebridicus*. I discuss anatomical and size variation within the genus and provide a comprehensive anatomical description of *Stereognathus*, identifying previously unrecognized morphology. I also run a phylogenetic analysis using new scorings based on these data and discuss the implications of incomplete data on our understanding of tritylodontid phylogeny.

3.1 i) Materials and Methods

Localities

Stereognathus material in the British Isles has so far exclusively been found in Bathonian (Middle Jurassic) limestones and mudstones in two regions: southern England and the Isle of Skye in Scotland. These localities are similar geologically: they generally represent coastally placed, mostly brackish lagoonal environments prone to drying out and subject to marine transgressions caused by subsidence and sea-level change. Some sites have more freshwater influx.

The oldest microvertebrate site to yield *Stereognathus* material is Hornsleasow Quarry, part of the Chipping Norton Limestone Formation: it is early Bathonian and is a Site of Special Scientific Interest (SSSI) because it preserves a complete succession of Sharp's Hill Beds (Metcalf et al., 1992). Material comes from a productive clay lens, likely formed in a fresh to brackish water small pond, within close proximity to the coast (Metcalf et al., 1992). Finds include crocodylian teeth and osteoderms, turtle plates, and multiple fragmentary remains of small reptiles. There are also rarer pterosaur teeth and some small theropod and ornithischian dinosaur teeth, as well as a few larger remains such as *Cetiosaurus* teeth and bones and *Megalosaurus* teeth (Evans and Milner, 1994). Mammals and tritylodontids are present but appear less abundant than at other Bathonian microvertebrate localities, except the Taynton Limestone Formation (Evans and Milner, 1994; EP, pers. obs.).

The Stonesfield Slate is the informal, but still commonly used name for what is now the Taynton Limestone Formation in Oxfordshire. It is middle Bathonian and comprises

layers of thin oolite between fine-grained calcareous sandstones (Sellwood and McKerrow, 1974). This estuarine assemblage contains an abundance of invertebrates and fish, alongside crocodylians and marine reptiles. Terrestrial material is less common.

The Kilmaluag Formation on the Isle of Skye is Late Bathonian in age, although exact biostratigraphical correlations with English sites have proven difficult (Barron et al., 2012). For a comprehensive overview of the Kilmaluag Formation see Chapter 2. Kirtlington Cement Quarry is also a Late Bathonian locality that has been especially productive for microvertebrates, yielding a similar assemblage to Hornsleasow (see above), but with many more mammal species and specimens recovered in more complete condition (Evans and Milner, 1994), including tritylodontid material. For a geological overview, see Chapter 2.3 and 2.2. Westcliff in Dorset, also known as Watton Cliff, is also a late Bathonian locality. It was an offshore bank in which terrestrial debris collected (Holloway, 1983).

Woodeaton has yielded material of both middle and late Bathonian age, with vertebrate material similar in composition to the other British Bathonian microvertebrate locations (Evans and Milner, 1994; Parraga et al., 2016). Tritylodontid material has been recovered from this location from middle and late Bathonian horizons and is morphologically indistinguishable from that recovered from the other British sites (EP, pers. obs.). This material is currently being described by researchers at NHMUK (Parraga et al., 2016).

Tritylodontid material has also been identified in unprocessed samples from Tarlton Clay Pit, Leigh Delamere, and Swyre (all Bathonian, part of the Forest Marble), but it is very fragmentary, comprising only a few single isolated cusps.

Material

I studied material assigned to *Stereognathus ooliticus* and S. *hebridicus*, as well as *Stereognathus* sp. and unspecified Tritylodontidae, from the aforementioned British localities (above).

Stereognathus ooliticus material from BGS comprises the holotype BGS GSM113834, a fragment of maxilla with three postcanines collected from the Taynton Limestone Formation (Stonesfield Slate) in Oxfordshire, England. From DORCM specimens G11048 and G10828, postcanines from the Forest Marble. From GLRCM specimens, GLRCM MLR 20–22, GLRCM MLR 20–38, GLRCM 10174, GLRCM 2104,

GLRCM 2105_4, GLRCM 2105_6, GLRCM G50137, GLRCM G50236, GLRCM G50505, GLRCM G50506, GLRCM G50507, GLRCM G50508, GLRCM G50647, GLRCM G50705, GLRCM G50907, GLRCM G51108, GLRCM G51221, GLRCM G51222, GLRCM G51223, GLRCM G51224, GLRCM G51243, GLRCM G51244, GLRCM G51245, GLRCM G51520, GLRCM G51521, GLRCM G51616, GLRCM G51823, GLRCM G51906, GLRCM G51907, GLRCM G52021, GLRCM G52022, GLRCM G52026, GLRCM G52027, GLRCM G52038, GLRCM G52127, GLRCM G52202, GLRCM G52204, GLRCM G52205, GLRCM G52304, GLRCM G52641, GLRCM G52643, GLRCM G52820, GLRCM G52861, GLRCM G53402, GLRCM G53403, GLRCM G53404, GLRCM G53405, GLRCM G53406, GLRCM G53407, GLRCM G53408, GLRCM G53409, GLRCM G53410, GLRCM G53411, GLRCM G53412, GLRCM G53413, GLRCM G53414, GLRCM G53415, GLRCM G53416, GLRCM G53417, GLRCM G53418, GLRCM G53419, GLRCM G53420, GLRCM G53421, GLRCM G53422, GLRCM G53423, GLRCM G53424, GLRCM G53425, GLRCM G53426, GLRCM G53427, GLRCM G53428, GLRCM G53429, GLRCM G53430, GLRCM G53431, GLRCM G53432, GLRCM G53433, GLRCM G53434, GLRCM G53435, GLRCM G53804, GLRCM G53806, GLRCM G53807, GLRCM G53809, GLRCM G53811, GLRCM G53812, GLRCM G54017, GLRCM G54018, GLRCM G54610, GLRCM G54633, GLRCM G54634, GLRCM G54635, GLRCM G54701, GLRCM G54702, GLRCM G54703, GLRCM G54810, GLRCM G54811, GLRCM G55225, GLRCM G55226, GLRCM G55227, GLRCM G55534, GLRCM G55810, GLRCM G56416, GLRCM G56424, GLRCM G56425, GLRCM G56426, GLRCM G56433, GLRCM G510202, GLRCM G510203, GLRCM G510204, GLRCM G510205, GLRCM G510206, GLRCM G510207, GLRCM G510208, GLRCM G510209, GLRCM G510210, GLRCM G510211, and GLRCM, G75710, all postcanines from Hornsleasow, mostly single cusps.

At the NHMUK, the following postcanine fragments are identified as *S. ooliticus*: NHMUK PV M.36503, NHMUK PV M.36510, NHMUK PV M.36534, NHMUK PV M.36537, and NHMUK R.8720, and the following postcanine fragments are identified as Tritylodontidae—I identify them as *Stereognathus ooliticus*: NHMUK PV M.36534, NHMUK PV M.36539, NHMUK PV M.36506, NHMUK PV M.36543, NHMUK PV M.46103, NHMUK PV M.46266, NHMUK PV M.46261, NHMUK PV M.45265,

NHMUK PV M.46268, NHMUK PV M.46270, NHMUK PV M.46271, NHMUK PV M.46273, NHMUK PV M.46274, NHMUK PV M.46272, NHMUK PV M.46374, NHMUK PV M.46375, NHMUK PV M.46277, NHMUK PV M.46373, NHMUK PV M.46382, NHMUK PV M.46383, NHMUK PV M.46384, NHMUK PV M.46386, NHMUK PV M.46403, and NHMUK PV M.46415. The following are also identified as Tritylodontidae, but I do not identify them as such: NHMUK PV M.46255 and NHMUK PV M.46263. All of this material is from Kirtlington Cement Quarry, Oxfordshire, England, except NHMUK R.8720, which is from Westcliff. At the OUMNH, specimen J.21790 is an edentulous fragment of *S. ooliticus* maxilla from the Taynton Limestone Formation (Stonesfield Slate) and the following postcanines (mostly fragmentary) are *Stereognathus* sp. from Kirtlington Cement Quarry, but I consider them all to be *S. ooliticus*: OUMNH J.79435, OUMNH J.79439, OUMNH J.79447, OUMNH J.79448, OUMNH J.79459, OUMNH J.79466, OUMNH J.79469, OUMNH J.79470, OUMNH J.79471, OUMNH J.79477, OUMNH J.79478, OUMNH J.79480, OUMNH J.79484, OUMNH J.79492, and OUMNH J.21790.

The BRSUG material comprises *Stereognathus hebridicus* postcanine material: holotype postcanine BRSUG 20572; paratypes BRSUG 20573, BRSUG 20574, and BRSUG 20575; and more fragmentary specimens BRSUG 29000–29002 and BRSUG 28996–28999 (these include four to five postcanines grouped together per specimen number). All of this material was collected in the 1970s and 1980s near Elgol, from the Kilmaluag Formation, Middle Jurassic, Isle of Skye.

The NMS material comprises dental remains of *Stereognathus hebridicus*: NMS G.1992.47.120 (comprising two specimens in same matrix) and NMS G.2017.17.6, collected in the 1980s, and NMS G.2017.17.1, NMS G.2017.17.2, NMS G.2017.17.3, NMS G.2017.17.4, and NMS G.2017.17.5, collected between 2013 and 2016 during field work at various sites in the Kilmaluag Formation on the coast north of Elgol (Middle Jurassic, Isle of Skye). This includes some of the most intact postcanine material yet found, figured here for the first time.

Measurements were taken with digital calipers where possible. For specimens still in matrix, measurements were taken from digitally reconstructed micro-computed tomography (microCT) scans in Mimics 19.0. All microCT scans were digitally reconstructed and image processed using Mimics 19.0 at the National Museum of Scotland. Specimens were also

observed using conventional microscopy and morphological features recorded qualitatively based on previous literature and my observations. Maximum length and width were taken. To produce a large enough sample for statistical analysis, where minimal portions of a tooth were missing or worn, a conservative estimate of the original size was made, based on the proportions of more complete specimens.

Specimen NMS G.1992.47.120 was prepared by coating in paraloid B72 then using 10% acetic acid to remove the surrounding limestone matrix. When the tooth became too fragile to continue this process, microCT data were obtained using the microCT scanner built in-house at the University of Edinburgh, School of Geosciences Experimental Geoscience Facility. The scanner comprises a Feinfocus 10–160 kV dual-transmission/reflection source, MICOS UPR-160-AIR ultra-high-precision air-bearing table, PerkinElmer XRD0822 amorphous silicon X-ray flat-panel detector and terbium-doped gadolinium oxysulfide scintillator. An 0.8 mm aluminium plate limited beam hardening, and data were acquired using a reflection source with a peak energy of 120 kV and 10W target power. Data acquisition software was written in-house, and scans were reconstructed using Octopus 8.7 software. The holotype of *S. ooliticus* BGS GSM113834 was also scanned in-house at Edinburgh, using a 1.6 mm aluminium plate. Historic specimens from BRSUG were mechanically prepared in the 1970s and 1980s. The *S. hebridicus* holotype 20572 and paratypes 20573, 20574, and 20575 were microCT-scanned at the University of Bristol using a Nikon XTH225ST scanner with a 225 kV rotating target with a peak energy of 140 kV.

Terminology

I use cusp terminology modified from Watabe et al. (2007) with additions of the PIA (posterior interlocking area) and AIA (anterior interlocking area) from Lopatin and Agadjanian (2008) (Figure 3.1.1). I follow the convention of referring to tritylodontid molars as ‘postcanines,’ despite the absence of canines in tritylodontids. I use the cusp formula as begun by Simpson (1928), specifying buccal, medial, and lingual numbers of cusps, e.g., 2–2-2 in *Stereognathus*, i.e., two cusps in each longitudinal row. Postcanine can be abbreviated to PC (uppers) or pc (lowers); likewise to indicate buccal, medial, and lingual, I use uppercase for cusp terminology in the upper postcanines (B, M, and L), and

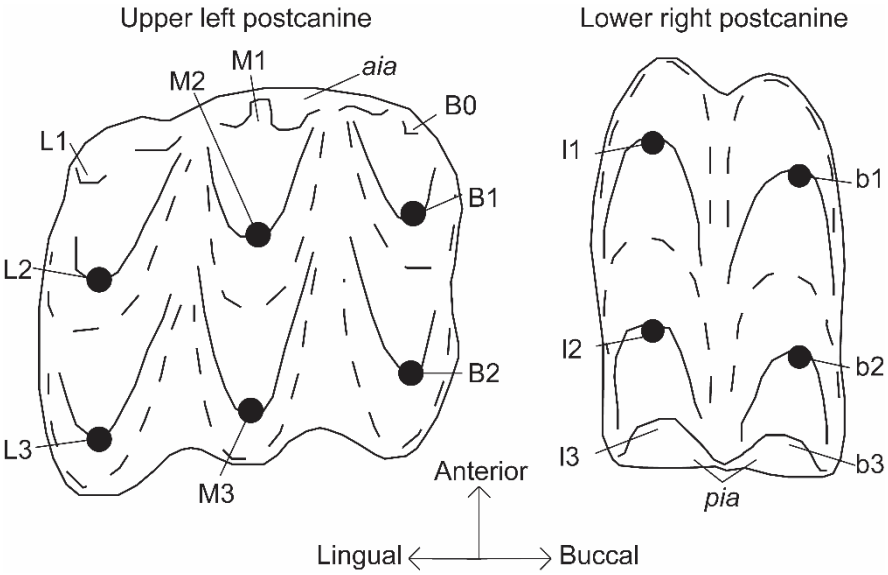

Figure 3.1.1: Postcanine cusp terminology for *Stereognathus* used herein (modified from Watabe et al., 2007). The PIA (posterior interlocking area) and AIA (anterior interlocking area) are present on both teeth, but the PIA is not visible in occlusal view on upper postcanines and the AIA is not visible in occlusal view on lower postcanines, because they are located on the underside of the tooth.

lowercase for lower cusps (b, m, and l). There is debate over the homology of cusps between more basal tritylodontids (such as *Oligokyphus*, which is considered the most basal tritylodontid) and derived tritylodontids (such as *Stereognathus*, which have a reduced cusp number). Based on *Oligokyphus* being the most basal genus (Clark and Hopson, 1985; Setoguchi et al., 1999), it appears that cusp reduction in later tritylodontids may have taken place at the anterior of the upper postcanine and posterior of the lower. This is suggested by the presence of vestigial cusps at these loci. Therefore, the posteriormost upper medial and lingual cusps are M3 and L3, and lower, the anteriormost cusps are b1, m1, and l1. Previous authors have considered the posteriormost buccal cusp in the upper molar as B2, not B3. Although I adhere to this convention, the homology of these cusps requires further study. In-depth discussions of which cusps are present, absent, or vestigial from the ancestral condition are considered to be outside the scope of this study. For more information, see discussions in Watabe et al. (2007) and Matsuoka et al. (2016).

Phylogenetic Analysis

Trees were analysed using TNT version 1.5 (Goloboff et al., 2008), and the character matrix of 35 characters and 17 taxa is based on that of Velazco et al. (2017), with *Stereognathus* rescored to reflect my findings (Appendices 1, 2). The New Technology search was used, selecting ratchet, sectorial search, tree drift, and tree fusing. The character states were unordered, and *Oligokyphus* was used as the outgroup because it is considered the most basal tritylodontid (Clark and Hopson, 1985; Setoguchi et al., 1999).

3.1 ii) Description

SYSTEMATIC PALAEONTOLOGY

SYNAPSIDA Osborn, 1903

CYNODONTIA Owen, 1861

MAMMALIAMORPHA Rowe, 1988

TRITYLODONTIDAE Cope, 1884

STEREOGNATHUS Charlesworth, 1855

STEREOGNATHUS OOLITICUS Charlesworth, 1855 (Figs. 3.2–3.7)

Stereognathus hebridicus Waldman and Savage, 1972:120–122; fig. 1 (original description).

Holotype: BGS GSM113834, fragment of left maxilla with three postcanines and four empty postcanine sockets. Collected from the Stonesfield Slate (now Taynton Limestone Formation), Oxfordshire (see Localities above).

Revised Diagnosis: Postcanines are quadrate in shape, rhomboidal in occlusal view, with cusp formula PC 2–2-2/pc 2–2. Cusps are subequal in size, with cusps longitudinally displaced anteroposteriorly. Intercuspal grooves are deep and ‘V’-shaped, and medial ridges of the cusps meet in the intercuspal groove subequally in unworn teeth. In upper postcanines, the ridges of L/M3 and B2 embrace the base of cusps L/M2 and B1. There are cuspules posterior and lingual to cusp L2, and sometimes B1. In the upper postcanines, vestigial cusps are found anterior to each longitudinal row of cusps, forming part of the AIA. The AIA extends across the anterior edge of the tooth buccolingually in the upper

postcanines, and the PIA forms a buccolingual projection on the posterior edge of the tooth. Upper postcanines have six to seven roots.

In lower postcanines, the AIA forms a buccolingual projection and the PIA comprises two embayments, the latter ridged inside and containing vestigial cusps l/b3. The PIA is framed by the posterobuccal and posterolingual terminations of the b2 and l2 cusp ridges and separated medially by the medial posterior projection of the meeting of the b2 and l2 cusp medial ridges in the intercuspal groove. The AIA and PIA of each tooth interlock with the adjacent teeth in the postcanine row. The anterior of the tooth is ‘M’-shaped in occlusal view, formed by the convex anterior faces of b/l1. In the lower postcanines the ridges of l/b1 embrace the base of cusps l/b2. Lower postcanines have a single root, retaining the quadrate shape of the crown and are straight-sided but indented buccolingually on the anterior face 1–2 mm ventrally to the base of the crown.

The maxilla is reduced and somewhat cylindrical in cross-section; it is more convex buccally and lingually but flattens dorsally. There is a dorsal ridge running anteroposteriorly along the distal edge of the maxilla, and there are no laminas extending into the secondary palate or jugal.

Referred Specimens: GLRCM MLR 20–22, GLRCM MLR 20–38, GLRCM 10174, GLRCM TEMP2104, GLRCM TEMP2105_4, GLRCM TEMP2105_6, GLRCM G50137, GLRCM G50236, GLRCM G50505, GLRCM G50506, GLRCM G50507, GLRCM G50508, GLRCM G50647, GLRCM G50705, GLRCM G50907, GLRCM G51108, GLRCM G51221, GLRCM G51222, GLRCM G51223, GLRCM G51224, GLRCM G51243, GLRCM G51244, GLRCM G51245, GLRCM G51520, GLRCM G51521, GLRCM G51616, GLRCM G51823, GLRCM G51906, GLRCM G51907, GLRCM G52021, GLRCM G52022, GLRCM G52026, GLRCM G52027, GLRCM G52038, GLRCM G52127, GLRCM G52202, GLRCM G52204, GLRCM G52205, GLRCM G52304, GLRCM G52641, GLRCM G52643, GLRCM G52820, GLRCM G52861, GLRCM G53402, GLRCM G53403, GLRCM G53404, GLRCM G53405, GLRCM G53406, GLRCM G53407, GLRCM G53408, GLRCM G53409, GLRCM G53410, GLRCM G53411, GLRCM G53412, GLRCM G53413, GLRCM G53414, GLRCM G53415, GLRCM G53416, GLRCM G53417, GLRCM G53418, GLRCM G53419, GLRCM G53420, GLRCM G53421, GLRCM G53422, GLRCM G53423, GLRCM

G53424, GLRCM G53425, GLRCM G53426, GLRCM G53427, GLRCM G53428, GLRCM G53429, GLRCM G53430, GLRCM G53431, GLRCM G53432, GLRCM G53433, GLRCM G53434, GLRCM G53435, GLRCM G53804, GLRCM G53806, GLRCM G53807, GLRCM G53809, GLRCM G53811, GLRCM G53812, GLRCM G54017, GLRCM G54018, GLRCM G54610, GLRCM G54633, GLRCM G54634, GLRCM G54635, GLRCM G54701, GLRCM G54702, GLRCM G54703, GLRCM G54810, GLRCM G54811, GLRCM G55225, GLRCM G55226, GLRCM G55227, GLRCM G55534, GLRCM G55810, GLRCM G56416, GLRCM G56424, GLRCM G56425, GLRCM G56426, GLRCM G56433, GLRCM G510202, GLRCM G510203, GLRCM G510204, GLRCM G510205, GLRCM G510206, GLRCM G510207, GLRCM G510208, GLRCM G510209, GLRCM G510210, GLRCM G510211, GLRCM G75710, NHMUK PV M.36503, NHMUK PV M.36510, NHMUK PV M.36534, NHMUK PV M.36537, NHMUK R.8720, NHMUK PV M.36534, NHMUK PV M.36539, NHMUK PV M.36506, NHMUK PV M.36543, NHMUK PV M.46103, NHMUK PV M.46266, NHMUK PV M.46261, NHMUK PV M.45265, NHMUK PV M.46268, NHMUK PV M.46270, NHMUK PV M.46271, NHMUK PV M.46273, NHMUK PV M.46274, NHMUK PV M.46272, NHMUK PV M.46374, NHMUK PV M.46375, NHMUK PV M.46277, NHMUK PV M.46373, NHMUK PV M.46382, NHMUK PV M.46383, NHMUK PV M.46384, NHMUK PV M.46386, NHMUK PV M.46403, NHMUK PV M.46415, NHMUK PV M.46255 NHMUK PV M.46263, OUMNH J.21790, OUMNH J.79435, OUMNH J.79439, OUMNH J.79447, OUMNH J.79448, OUMNH J.79459, OUMNH J.79466, OUMNH J.79469, OUMNH J.79470, OUMNH J.79471, OUMNH J.79477, OUMNH J.79478, OUMNH J.79480, OUMNH J.79484, OUMNH J.79492, and OUMNH J.21790.

Synonymized Specimens: The following specimens, all from the isle of Skye and some previously referred to *S. hebridicus*, are considered to belong to *S. ooliticus*: BRSUG 20572, BRSUG 20573, BRSUG 20574, BRSUG 20575, BRSUG 29000–29002, and BRSUG 28996–28999; and NMS G.1992.47.120 (comprising two specimens in same matrix), NMS G.2017.17.1, NMS G.2017.17.2, NMS G.2017.17.3, NMS G.2017.17.4, NMS G.2017.17.5, and NMS G.2017.17.6.

Holotype *S. ooliticus*

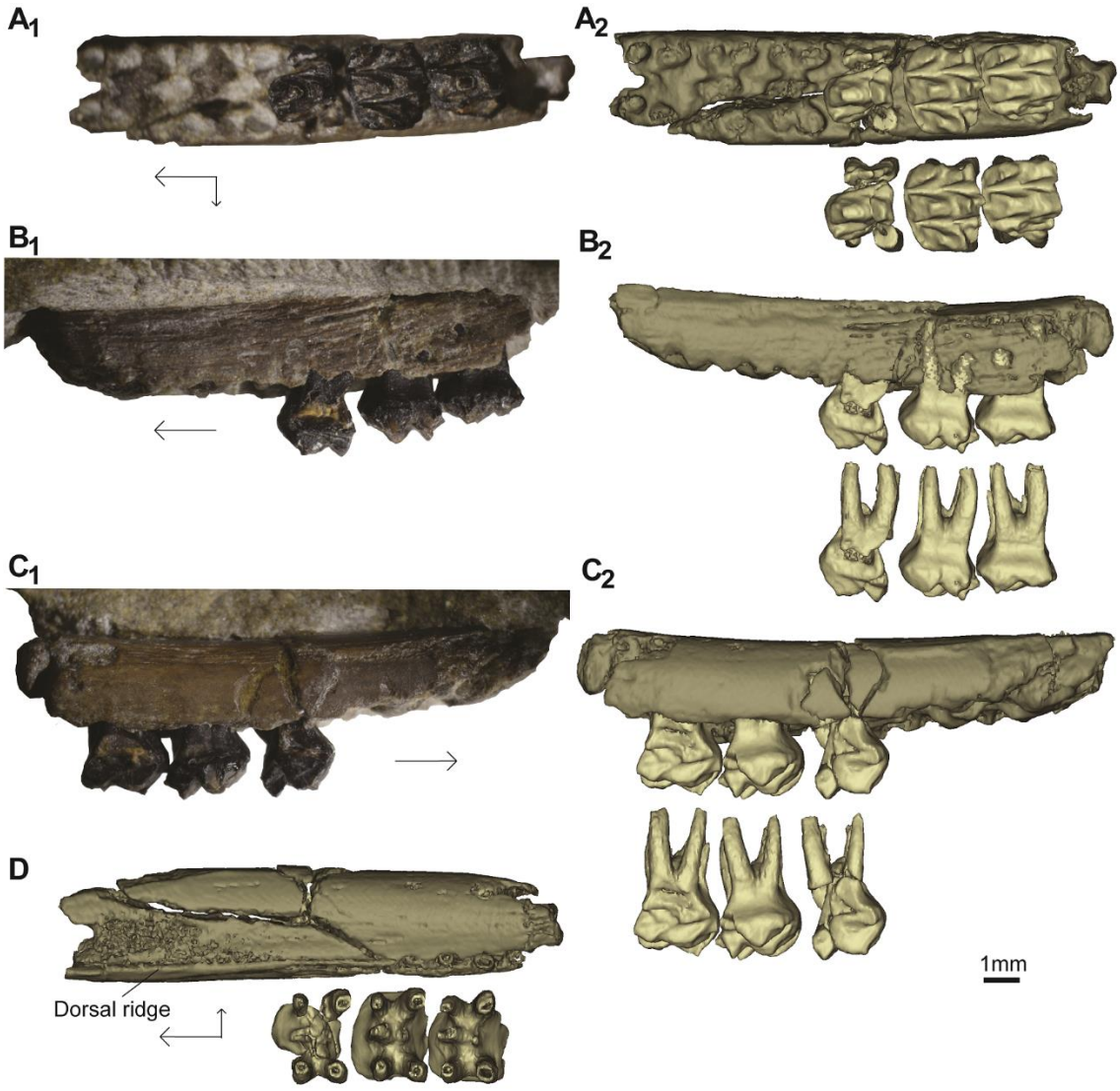

Figure 3.1.2: *Stereognathus ooliticus*, BGS GSM113834, holotype. A1, occlusal view; A2, occlusal view digital reconstruction, with teeth segmented from jaw; B1, buccal view; B2, buccal view digital reconstruction, with teeth segmented from jaw; C1, lingual view; C2, lingual view digital reconstruction, with teeth segmented from jaw; D, dorsal view of maxilla. Anterior direction indicated by longer black arrow, lingual by shorter arrow.

The holotype of *S. ooliticus*, BGS GSM113834, is a fragment of left maxilla 20.3 mm long, between 3.15 and 3.48 mm deep dorsoventrally, and between 3.9 and 4.8 mm wide buccolingually, although some damage to the buccal side means the original width was slightly greater (Figure 3.1.2). It was originally thought to be a dentary (Charlesworth, 1855; Owen, 1857), then re-identified as a right maxilla (Simpson, 1928), and then correctly identified as a left maxilla (Clark and Hopson, 1985). The abrasion of the buccal maxilla surface has exposed portions of the postcanine roots. The lingual side is less

Table 3.1.1: Measurements of British *Stereognathus* material. Measurements where slight breakages or wear made measurement uncertain (estimated measurements referred to in text) are in italics, and underlined where breakage was more significant.

Specimen No.	Species	Locality	Description	Length (mm)	Width (mm)	Width/ Length
BRSUG 20572	*hebridicus*		Holotype upper	5.1	5.4	1.06
BRSUG 20573	*hebridicus*	Kilmaluag	Paratype upper	4.8	5.4	1.13
BRSUG 20574	*hebridicus*	Kilmaluag	Paratype lower right	5.1	3.2	0.63
BRSUG 20575	*hebridicus*	Kilmaluag	Paratype lower right	5.8	3.8	0.66
BRSUG 29000	*hebridicus*	Kilmaluag, Skye	Fragmentary: upper left molar	NA	4.7	-
			Fragmentary:: lower molar	*3.1*	*2.3*	0.74
			Fragmentary: cusps	NA	3.5	-
BRSUG 29002	*hebridicus*	Kilmaluag	Upper right	3.6	NA	-
BRSUG 28996_A	*hebridicus*	Kilmaluag	Upper right	4.5	4.9	1.09
BRSUG 28996_B	*hebridicus*	Kilmaluag	Upper left	4.2	5.2	1.24
BRSUG 28996_C	*hebridicus*	Kilmaluag	Upper right	4.4	5.5	1.25
BRSUG 28996_D	*hebridicus*	Kilmaluag	Upper right	2.3	2.6	1.13
BRSUG 28996_E	*hebridicus*	Kilmaluag	Upper right	*4.3*	*5.1*	1.19
BRSUG 28997_A	*hebridicus*	Kilmaluag	Upper	*3.2*	3.7	1.16
BRSUG 28997_B	*hebridicus*	Kilmaluag	Upper	4.1	5.0	1.22
BRSUG 28997_C	*hebridicus*	Kilmaluag	Upper	*4.2*	*5.0*	1.19
BRSUG 28997_D	*hebridicus*	Kilmaluag	Upper	4.9	5.5	1.12
BRSUG 28997_E	*hebridicus*	Kilmaluag	Upper	2.6	2.6	1.00
BRSUG 28997_F	*hebridicus*	Kilmaluag	Upper	3.6	4.2	1.17
BRSUG 28997_G	*hebridicus*	Kilmaluag	Upper	4.0	4.8	1.20
BRSUG 28998_A	*hebridicus*	Kilmaluag	Lower	5.5	3.6	0.65
BRSUG 28998_B	*hebridicus*	Kilmaluag	Lower	5.6	3.5	0.63
BRSUG 28998_C	*hebridicus*	Kilmaluag	Lower	*4.9*	3.4	0.69
BRSUG 28998_D	*hebridicus*	Kilmaluag	Lower	5.2	3.2	0.62
BRSUG 28998_E	*hebridicus*	Kilmaluag	Lower	5.2	3.3	0.63
BRSUG 28998_F	*hebridicus*	Kilmaluag	Upper	4.6	5.0	1.09
BRSUG 28999_A	*hebridicus*	Kilmaluag	Lower	5.2	3.3	0.63
BRSUG 28999_B	*hebridicus*	Kilmaluag	Lower	5.1	3.2	0.63
BRSUG 28999_C	*hebridicus*	Kilmaluag	Lower	3.9	2.6	0.67
BRSUG 28999_D	*hebridicus*	Kilmaluag	Lower	2.6	1.8	0.69
BRSUG 28999_E	*hebridicus*	Kilmaluag	Upper fragment	2.7	NA	-
NMS G.1992.47.120	*hebridicus*	Kilmaluag	Lower	5.7	3.6	0.63
NMS G.2017.17.1	*hebridicus*	Kilmaluag	Lower	4.2	NA	
NMS G.2017.17.2	*hebridicus*	Kilmaluag	Upper	3.8	4.3	1.13
NMS G.2017.17.3	*hebridicus*	Kilmaluag	Lower	*5.5*	3.8	0.69

NMS G.2017.17.4	*hebridicus*	Kilmaluag	Upper fragmented	*3.2*	*4.5*	1.41
NMS G.2017.17.5	*hebridicus*	Kilmaluag	lower	NA	3.6	
NMS G.2017.17.6	*hebridicus*	Kilmaluag	Lower	5.7	4.1	0.72
BGS GSM113834	*ooliticus*	Stonesfield	Jaw fragment with 3PCs: anterior	*3.1*	NA	-
	ooliticus	Stonesfield	middle	3.4	3.6	1.06
	ooliticus	Stonesfield	posterior	3.5	*3.5*	1.00
GLRCM -G75710-ulm	*ooliticus*	Hornsleasow	Upper	4.5	4.5	1.02
GLRCM _MLR_20-22	*ooliticus*	Hornsleasow	Upper	4.2	*3.4*	0.79
GLRCM _MLR_20-38	*ooliticus*	Hornsleasow	Upper	*4.1*	*4.0*	0.97
GLRCM _H174	*ooliticus*	Hornsleasow	Lower	5.8	3.6	0.62
GLRCM TEMP2105_4	*ooliticus*	Hornsleasow	Lower	*4.3*	3.7	0.86
GLRCM TEMP2105_6	*ooliticus*	Hornsleasow	Lower	*3.9*	2.9	0.74
OUMNH J.79435	*ooliticus*	Kirtlington	Upper	3.1	NA	-
OUMNH J.79439	*ooliticus*	Kirtlington	Lower	3.2	NA	-
OUMNH J.79480	*ooliticus*	Kirtlington	Upper	3.2	3.8	1.19
DORCM G 11048	*ooliticus*	Forest Marble	Lower	5.3	3.2	0.60
DORCM G10828-lrm	*ooliticus*	Forest Marble	Lower	5.4	3.3	0.61

damaged, and convex. The maxilla fragment sits in the original matrix, mechanically prepared out of the rock except for the dorsal surface. Digital reconstructions reveal the shallow depth of the maxilla dorsoventrally, and the lack of laminae extending upwards onto the facial part of the skull, laterally under the jugal, or medially to partially form the secondary bony palate (see Clark and Hopson, 1985:399) (Figure 3.1.2). A ridge projects anteroposteriorly along the distal edge of the dorsal side of the maxilla, but it is broken and missing below the posteriormost postcanines.

There are three empty postcanine alveoli, followed by three postcanines, and then a final, posteriormost empty alveolus. This indicates at least seven teeth in the tooth row. The postcanine cusp formula is 2–2-2. The upper postcanines are quadrate when viewed occlusally, with the medial cusp row slightly offset posteriorly from the level of the lingual one and the lingual cusp row slightly further offset posteriorly from the medial one, making the crown rhomboidal. All the postcanines are wider buccolingually than they are long anteroposteriorly. The cusps are arranged in three anteroposterior rows of two cusps each. All are broken and missing cusps. In each tooth (where cusps are intact), the anterior ridges of cusps L/M3 and B2 embrace the bases of cusps L/M2 and B1.

The anteriormost postcanine measures 5.7 mm from the tip of the broken M3 to the tip of the roots. The broken and incomplete crown of the postcanine measures 3.1 mm in length (anteroposteriorly), and what remains of the postcanine buccolingually is only 1.6 mm in width. It is the least complete postcanine in the row: only the midline cusps M2 and M3 remain, and both are heavily worn and broken (Figure 3.1.3). The tip of the cusp of M2 is broken, revealing enamel and dentine layers. The tip and posterior slope of M3 is broken; the posterior slope is broken, with the missing portion of the posterior slope leaving a large gap between this and the subsequent tooth. The anterior of the postcanine is worn and broken, missing the M1 and AIA. Only a small portion of the intercuspal grooves remains between M2/M3 and the missing buccal and lingual cusp rows. The microCT scans reveal that most of the roots of this postcanine are intact, although the crown is separated from the roots. The crown is also cracked between cusps M2 and M3.

The middle of the three postcanines is the most complete, possessing all cusps except L3, and with complete roots. It measures 5.1 mm from the tip of M3 to the tip of the roots, and the crown is 3.4 mm in length (anteroposteriorly) and 3.6 mm in width (buccolingually). All of the cusps are worn and/or damaged, and all are missing most of their enamel. This is the only tooth in which the vestigial cusp L1 is present and visible (Figure 3.1.3). Vestigial cusps B0, M1, and L1 have been incorporated into the AIA, but much of the AIA is missing. There is a small cuspule posterior to, and displaced lingually from, the L2 cusp (Figure 3.1.3E). The corresponding part of the B1 cusp is missing. Comparison with the figure of this tooth by Owen (1857: fig. 5) indicates considerable damage since it was originally discovered and figured (discussed below).

The posteriormost postcanine measures 5.5 mm from the tip of the B1 (most complete cusp, but still broken at the tip) to the tip of the roots, and the crown is approximately 3.5 mm in length (anteroposterior) and 3.1 mm in width (buccolingual)—enough remains to estimate a pre-broken width of at least 3.5 mm. This postcanine is less complete than the middle postcanine: it is missing both lingual cusps but retains the remaining cusps, although they are damaged. The tips of all cusps are broken, with B1 being the most intact, although missing enamel. The AIA and PIA are both worn, but vestigial cusps M1 and B0 remain visible, connected by the AIA ridge.

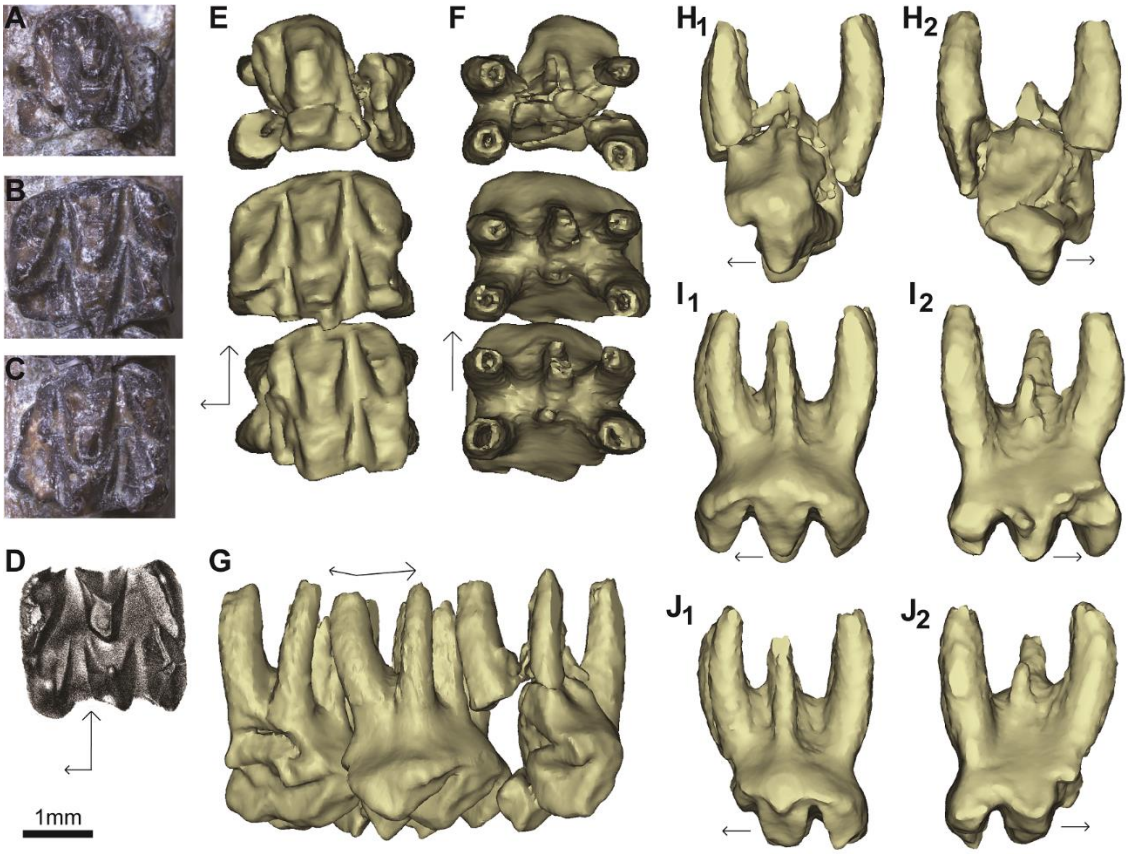

Figure 3.1.3: *Stereognathus ooliticus*, BGS GSM113834, holotype, postcanines only. Digitally reconstructed from microCT scans and segmented from the jaw. A, occlusal view of anterior-most postcanine; B, occlusal view of middle postcanine; C, occlusal view of posterior-most postcanine; D, original drawing by Owen (1857); E, occlusal view digital reconstruction; F, dorsal view digital reconstruction; G, anterolingual view digital reconstruction; H1, anterior view of anterior-most postcanine digital reconstruction; H2, posterior view of anterior-most postcanine digital reconstruction; I1, anterior view of middle postcanine digital reconstruction; I2, posterior view of middle postcanine digital reconstruction; J1, anterior view of posterior-most postcanine digital reconstruction; J2, posterior view of posterior-most postcanine digital reconstruction. Anterior direction indicated by longer black arrow, lingual by shorter arrow.

The roots of the anterior and middle postcanines in BGS GSM113834 comprise six branches, which are arranged in three anteroposterior rows of two branches each (Figure 3.1.3). The buccal and lingual roots are larger, and thicker along their lengths, whereas the medial roots are thinner, shorter, and taper more steeply. In the posteriormost postcanine, there are three roots in the medial row (Figure 3.1.3F), giving a total of seven roots. In all postcanines, the four larger roots are more or less the same width for most of their length (although the posterior two are slightly wider than the anterior two) and taper at the tips. The pulp cavity is hollow in all of the roots.

The AIA and PIA on all three postcanines in the holotype are badly worn, but some features remain visible. The PIA projects posteriorly, with a ridge running buccolingually along the edge of the tooth. This fits into the AIA of the next postcanine posteriorly in the tooth row, as seen between the middle and posteriormost postcanines. The AIA is also ridged buccolingually along the edge of the tooth, with vestigial cusps L1, M1, and B0 incorporated into the ridge. This is more clearly seen in the middle and posterior postcanines in the micro CT scan (Figure 3.1.3).

It is worth noting that the holotype of *S. ooliticus* is in a less complete state than when first discovered and later described by Owen (1857) (Figure 3.1.3D). Over 150 years of handling has resulted in considerable damage to the postcanine teeth. Looking especially at the most complete, middle tooth in the row: the anterolingual edge is now missing and the L3 has also gone missing since Owen's original drawing was made. The M3 is missing the tip of the cusp and posterolingual edge, and the B3 is damaged buccally and posteriorly, with sections of the tooth missing entirely. The remaining portions of the tooth appear somewhat worn at the edges since Owen's drawing was made. This makes comparisons with new material somewhat problematic.

Holotype *S. hebridicus*

The holotype of *S. hebridicus*, BRSUG 20572, is a large postcanine (Table 3.1.1) with the cusp formula 2–2-2 (arranged in three anteroposterior rows of two cusps) in a small fragment of jaw (Figure 3.1.4). It was originally described as an upper left postcanine but has since been identified as an upper right postcanine (Clark and Hopson, 1985). It is 7 mm from the tip of the M2 to the tip of the roots, and the crown is approximately 5.1 mm in length (anteroposterior) and 5.4 mm in width (buccolingual). The morphology of this specimen agrees with that of *S. ooliticus*.

There is a small cuspule posterior to L2 and offset lingually (Figure 3.1.4A). A root from the next tooth posteriorly in the tooth row remains intact in the fragment of jaw. It is positioned underneath the PIA, midway between the two widely spaced posterior roots. There were originally six roots: the two posteriormost roots are still present, encased in a small amount of maxilla material (Figure 3.1.4), but their tips are broken. The two larger anterior roots and the smaller anteromedial roots are broken where they meet the tooth base, but the hole for their pulp cavity is still visible.

Paratypes *S. hebridicus*

The badly damaged upper right postcanine, BRSUG 20573, originally referred to *S. hebridicus*, is missing much of the lingual cusps and M2, and the tips of the remaining cusps (Figure 3.1.5A–E). The crown measures 4.8 mm in length (anteroposterior) and 5.4 mm in width (buccolingual). The morphology is congruent with the holotype of *S. ooliticus*. Vestigial cusps M1 and B0 are still visible, incorporated into what remains of the AIA ridge. The PIA projects strongly posteriorly, with distinct indentations and ridges along its length, and a pit in the midline to receive the M1 of the next postcanine in the tooth row. Cusp B1 lacks a posterior cuspule, whereas L2 is broken in the region where one would be found, if present. The bases of only five of the roots remain, because the posteromedial part of the tooth is damaged (Figure 3.1.5F).

The specimen BRSUG 20574 is a lower left postcanine originally referred to *S. hebridicus*, but with morphology consistent with the lower postcanines of *S. ooliticus*. The crown measures 5.1 mm in length (anteroposterior) and 3.2 mm in width (buccolingual). The buccal side of the postcanine, including cusps, is well preserved, but the lingual side is damaged, with some enamel missing and both cusps broken (Figure 3.1.6A–E). The anterior side of each cusp is convex. The lingual ridge extending from cusp b1 terminates at the base of b2 ventrally to the cusp apex. This feature cannot be compared with the lingual side due to damage.

The AIA is a ridged buccolingual shelf and projects 1 mm anteriorly from the crown. This area is ‘M’-shaped in occlusal view. The posterior edge of the postcanine is almost straight and is slanted due to the anteroposterior cusp rows being offset, giving the tooth a rhomboidal appearance. There is no cingulid, but the buccal edge of the tooth forms an anteroposterior ridge that is termed here a pseudo-cingulid (Figure 3.1.6E). Beneath the crown the tooth pinches inwards before the single, quadrangular root extends straight ventrally. This root is broken, extending only 1– 2 mm ventrally below the posterior half of the crown. Some fragments of root and matrix are embedded in the hollow of the tooth.

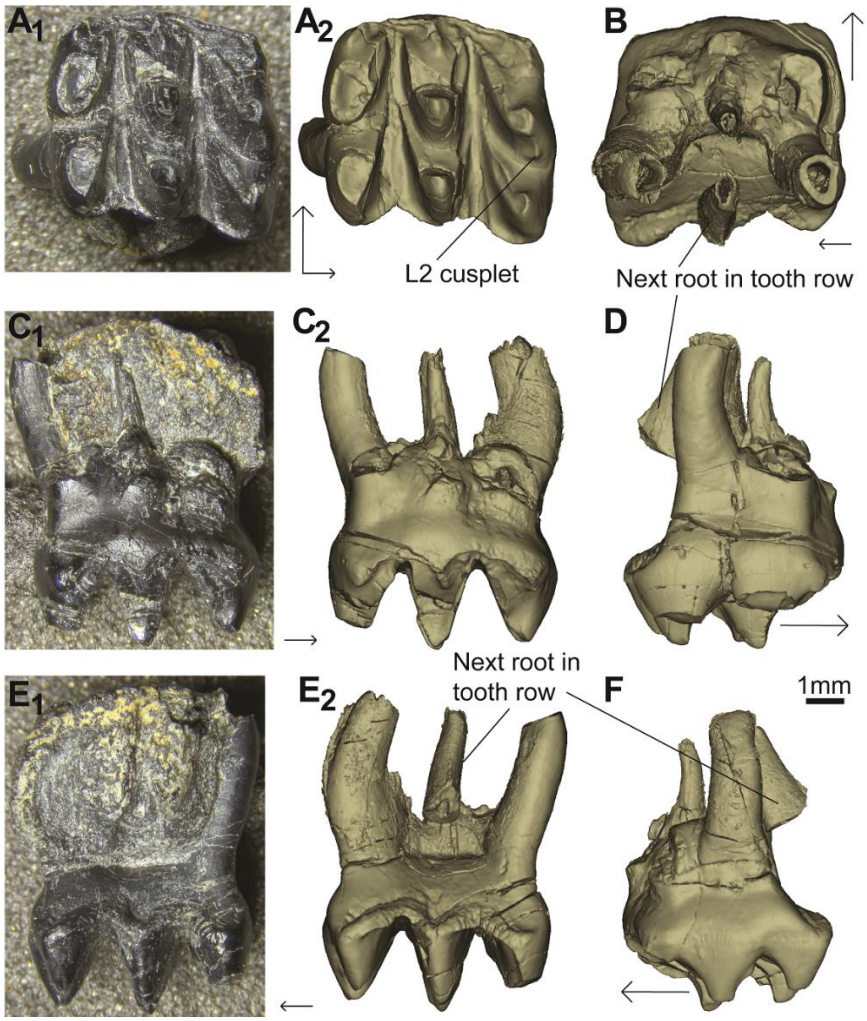

Figure 3.1.4: *Stereognathus hebridicus*, BRSUG 20572, holotype. A1, occlusal view; A2, occlusal view digital reconstruction; B, dorsal view digital reconstruction; C1, anterior view; C2, anterior view digital reconstruction; D, buccal view digital reconstruction; E1, posterior view; E2, posterior view digital reconstruction; F, lingual view digital reconstruction. Anterior direction indicated by longer black arrow, lingual by shorter arrow.

The lower left postcanine BRSUG 20575 is in poor condition, missing portions of enamel, all of the cusp tips, and the entire l2 cusp and portion of the tooth (Figure 3.1.6F–J). It was originally referred to *S. hebridicus* but has morphology congruent with the lower postcanines of *S. ooliticus*. The crown measures 5.8 mm in length (anteroposterior) and 3.8 mm in width (buccolingual). The PIA is missing on the lingual side and damaged on the buccal side, but what remains retains a similar shape to that of the paratype BRSUG 20574. Specimen BRSUG 20575 has a strong pseudo-cingulid running anteroposteriorly on the buccal side of the postcanine. The quadrangular root is broken, extending only up to 2 mm,

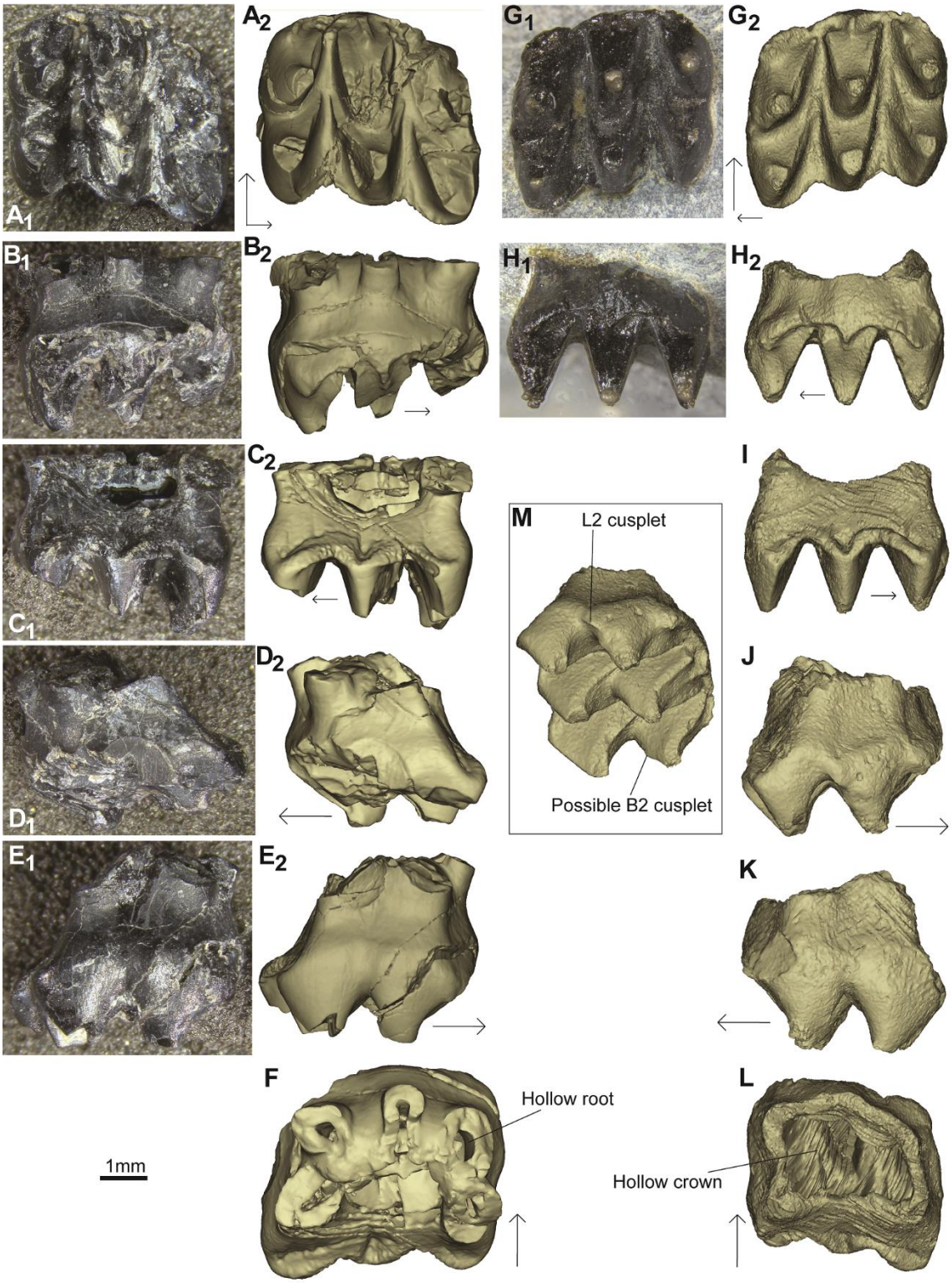

and the postcanine is hollow inside. There is a buccolingual indentation on the anterior face of the root, just less than 2 mm ventrally to the base of the crown.

New Material from Skye

NMS G.2017.17.2 is an upper left postcanine that I refer to *S. ooliticus*. It is currently the most intact upper postcanine of *Stereognathus* to be described, retaining most of the enamel, almost wholly intact cusps, and intact AIA and PIA (Figure 3.1.5G–M). The morphology is as for *S. ooliticus*: the crown has a cusp formula of 2–2-2; deep 'V'-shaped intercuspal grooves; longitudinal cusp rows offset anteroposteriorly; the tooth is quadrangular in occlusal view; and it is wider than it is long. The crown measures 3.8 mm in length (anteroposterior) and 4.3 mm in width (buccolingual).

Specimen NMS G.2017.17.2 has indents along the PIA and AIA for interlocking with the preceding and succeeding postcanines in the tooth row. The AIA is almost unworn and exhibits multiple cuspules and crenulations along the ridge, and in the position of the vestigial cusps (Figure 3.1.5G, M). This specimen also has distinct cuspules posterior to L2 and B1, displaced lingually and buccally, respectively.

NMS G.1992.47.120 is a lower right postcanine that I refer to *S. ooliticus*. It is currently one of the most intact lower pcs of *Stereognathus* to be described, being almost completely intact apart from the root, retaining all cusps, and with enamel still present (Figure 3.1.7). The crown measures 5.7 mm in length (anteroposterior) and 3.6 mm in width (buccolingual). As in *S. ooliticus*: cusp formula 2–2; deep 'V'-shaped intercuspal groove; tooth is quadrangular in shape in occlusal view; has equal-sized cusps; it is longer than it is wide; and the ridges running from b1 and l1 embrace the bases of cusps b2 and l2. The anterior of each cusp is convex; the posterior of the postcanine is almost straight, slanting slightly because the longitudinal cusps are offset anteroposteriorly. The buccal side of the postcanine is straighter than the lingual side in occlusal view, and the buccal edge of the crown has a pseudo-cingulid, as in *S. ooliticus* lower postcanines and *S. hebridicus* paratypes BRSUG 20574 and BRSUG 20575.

Figure 3.1.5 (previous page): *Stereognathus hebridicus*, BRSUG 20573, paratype, upper postcanines, and new specimen NMS G.2017.17.2, both reconstructed digitally from micro CT scans. A–F, BRSUG 20573: A1, occlusal view; A2, occlusal view digital reconstruction; B1, anterior view; B2, anterior view digital reconstruction; C1, posterior view; C2, posterior view digital reconstruction; D1, lingual view; D2, lingual view digital reconstruction; E1, buccal view; E2, buccal view digital reconstruction; F, dorsal view. G–M, NMS G.2017.17.2: G1, occlusal view; G2, occlusal view digital reconstruction; H1, anterior view; H2, anterior view digital reconstruction; I, posterior view digital reconstruction; J, lingual view digital reconstruction; K, buccal view digital reconstruction; L, dorsal view digital reconstruction; M, ventrolingual view digital reconstruction. Anterior direction indicated by longer black arrow, lingual by shorter arrow.

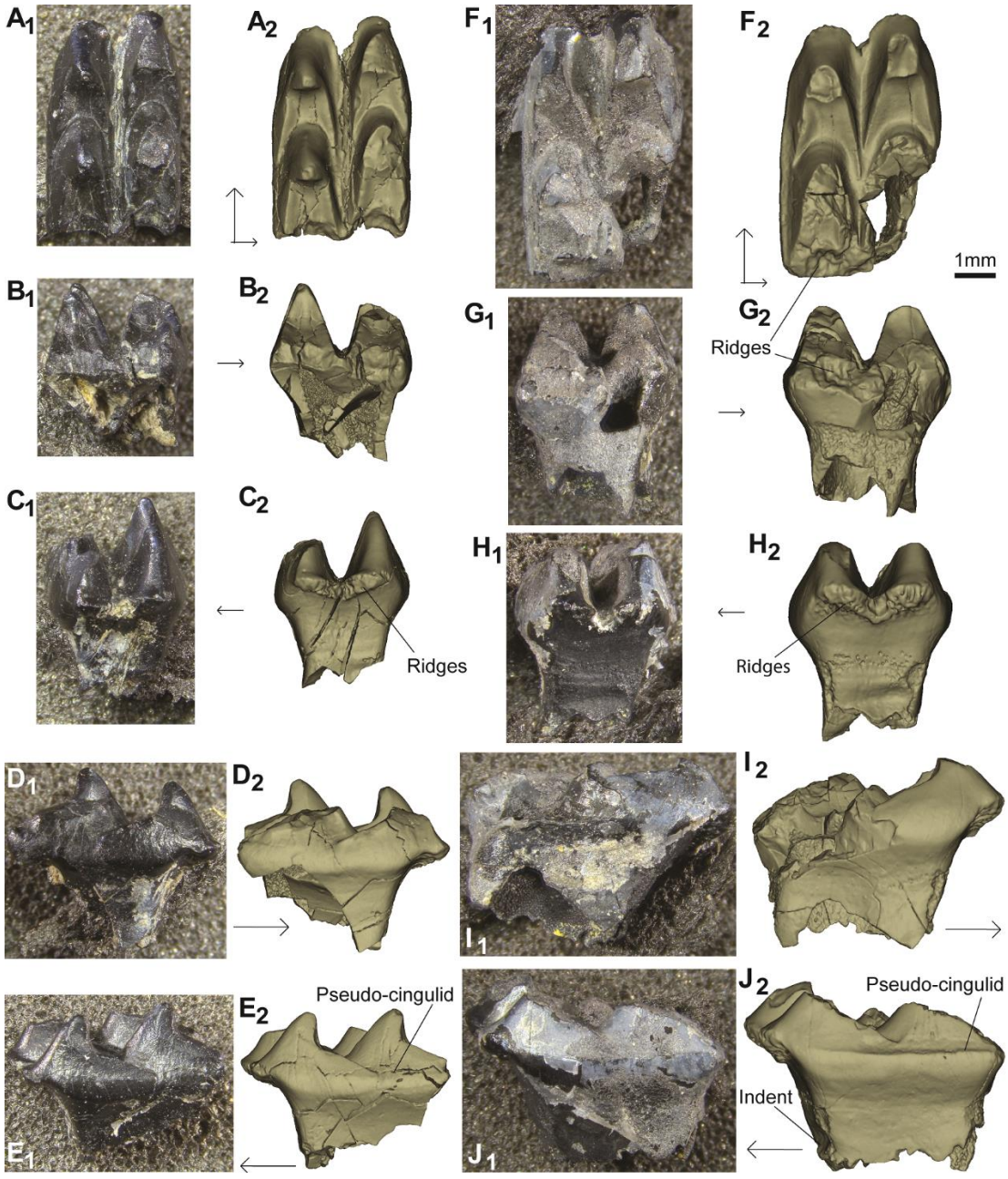

Figure 3.1.6: *Stereognathus hebridicus*, BRSUG 20574 and BRSUG 20575, paratypes, lower postcanines. A–E, BRSUG 20574: A1, occlusal view; A2, occlusal view digital reconstruction; B1, posterior view; B2, posterior view digital reconstruction; C1, anterior view; C2, anterior view digital reconstruction; D1, lingual view; D2, lingual view digital reconstruction; E1, buccal view; E2, buccal view digital reconstruction. F–J, BRSUG 20575: F1, occlusal view; F2, occlusal view digital reconstruction; G1, posterior view; G2, posterior view digital reconstruction; H1, anterior view; H2, anterior view digital reconstruction; I1, lingual view; I2, lingual view digital reconstruction; J1, buccal view; J2, buccal view digital reconstruction. Anterior direction indicated by longer black arrow, lingual by shorter arrow.

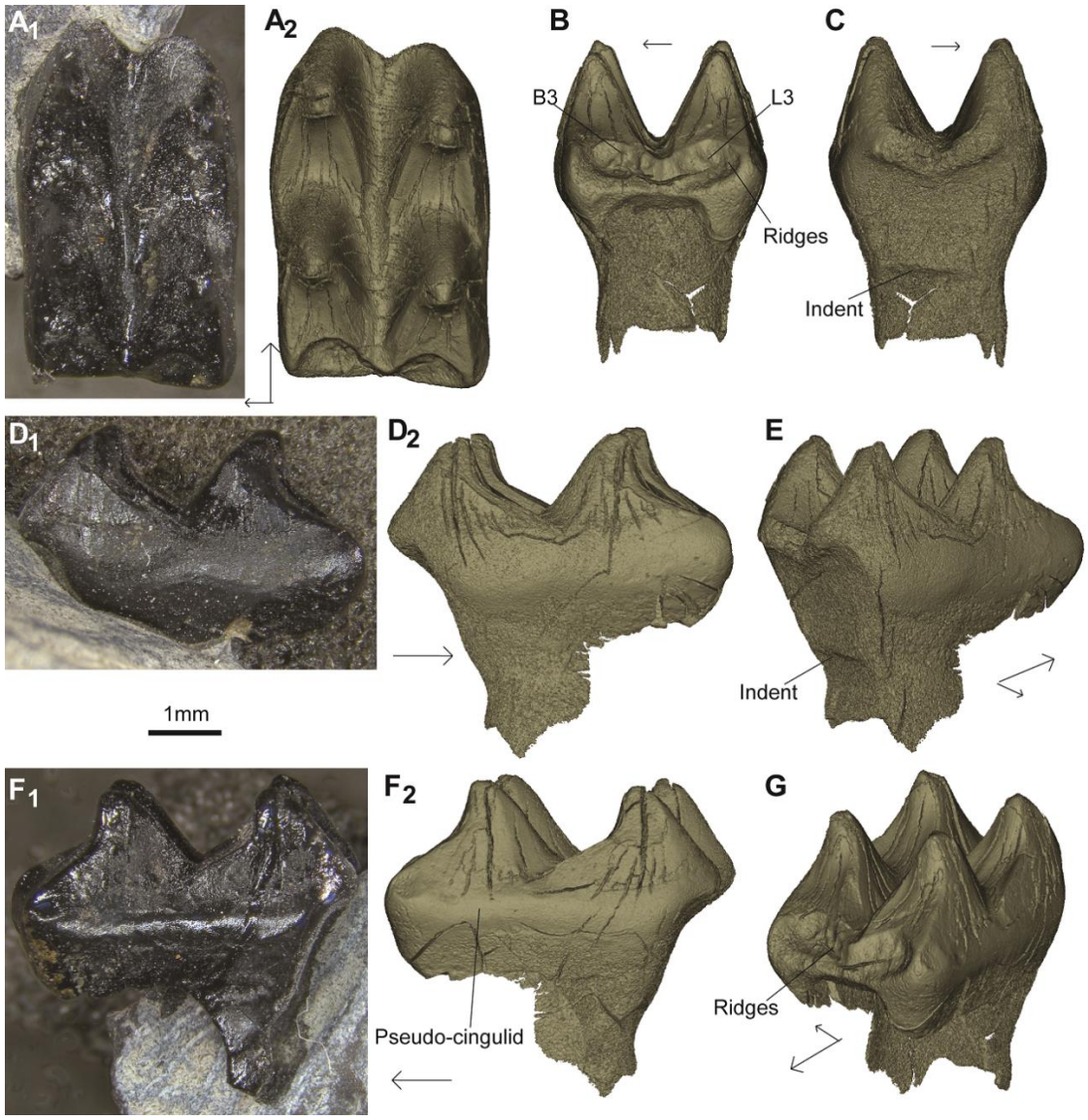

Figure 3.1.7: New specimen NMS G.1992.47.120, a lower postcanine, reconstructed digitally from micro CT scans. A1, occlusal view; A2, occlusal view digital reconstruction; B, posterior view digital reconstruction; C, anterior view digital reconstruction; D1, lingual view; D2, lingual view digital reconstruction; E, anterolingual view digital reconstruction; F1, buccal view; F2, buccal view digital reconstruction; G, posterobuccal view digital reconstruction. Anterior direction indicated by longer black arrow, lingual by shorter arrow.

The PIA on NMS G.1992.47.120 is deep and well defined, divided almost into two by the point where the medial ridges of the l2 and b2 meet in the intercuspal groove and project posteriorly. The embayments of the PIA are pitted and ridged, containing vestigial cusps b3 and l3 (Figure 3.1.7B and G). The AIA is most clearly seen in Figure 3.1.7E; the

anterior edges of b1 and l1 are convex, creating an ‘M’-shaped appearance in occlusal view, and project anteriorly to create a shelf that provides the point of contact with the PIA of the preceding tooth.

3.1 iii) Results

The sizes of postcanine tooth specimens attributed to *S. ooliticus* and *S. hebridicus* fall along a range I interpret as ontogenetic variation (Table 3.1.1; Figures 3.1.8 and 3.1.9). The lower postcanines for each species have a similar size distribution (Table 3.1.2), with most specimens between 5.1 and 5.5 mm in length and between 3.1 and 4 mm in width.

The upper postcanines do not share the same distribution for each putative species, according to my samples. Those attributed to *S. ooliticus* have modes of 3.1–3.5 mm in length and 3.6–4.0 mm in width, and those attributed to *S. hebridicus* have modes of 4.1–4.5 mm in length and 5.1–5.5 mm in width. The distribution of *S. hebridicus* upper postcanines—unlike the lowers of either putative species or the uppers of *S. ooliticus*—are bimodal for both length and width. They have two peaks in distribution: in length 3.1–3.5 mm and 4.1–4.5 mm, and in width 2.6–3 mm and 5.1–5.5 mm.

Table 3.1.2: The dataset used for analysis, including estimated measurements.

	S. ooliticus				*S. hebridicus*			
	Uppers		Lowers		Uppers		Lowers	
	length	width	length	width	length	width	length	width
Mean	3.59	3.80	4.94	3.33	3.91	4.63	4.89	3.25
sample size	9.00	5.00	5.00	5.00	19.00	15.00	16.00	15.00
sample range	1.37	1.20	1.95	0.75	2.81	2.90	3.20	2.27
s2	0.10	0.23	0.69	0.10	0.62	0.95	0.91	0.36
s	0.32	0.48	0.83	0.31	0.79	0.97	0.95	0.60

The mean of individual measurements is similar between both species, except for the width of the uppers, which is 3.8 mm in *S. ooliticus* and 4.6 mm in *S. hebridicus* (Table 3.1.2). The sample of *S. hebridicus* specimens is two to three times larger than for *S.*

ooliticus (Table 3.1.2). The largest range in the sample is among *S. hebridicus* lower postcanine lengths, and the smallest range is in *S. ooliticus* lower postcanine widths.

To test whether there was a difference in size between the two putative species, I carried out Mann-Whitney U tests on the length, width, and width/length ratio of upper and lower postcanines for *S. ooliticus* and *S. hebridicus*. The null hypothesis was that

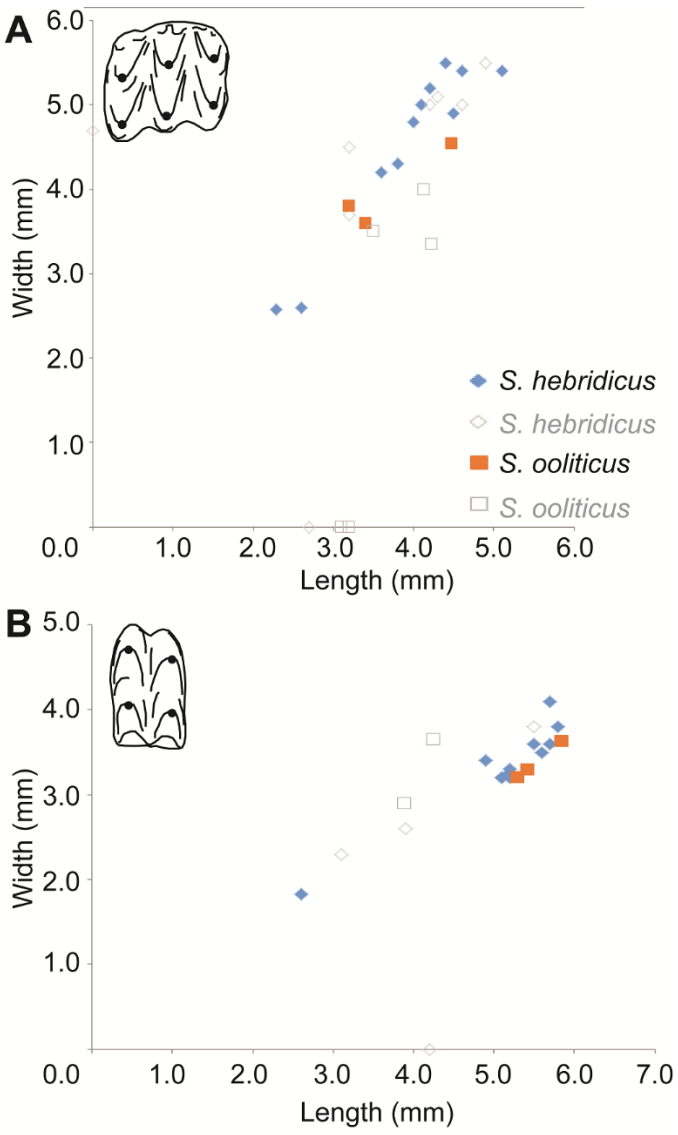

Figure 3.1.8: Scatterplots of postcanine measurements of *Stereognathus*. A, upper postcanines; B, lower postcanines. Key for B, as in A. Solid symbols denote complete specimens; open symbols denote incomplete specimens (orange square *S. ooliticus*; blue diamond *S. hebridicus*). Measurements in Table 3.1.1.

there was no difference in the median size of each species. I rejected the null hypothesis in only two instances: when comparing the widths of the upper postcanines and comparing the width/length ratios of the upper postcanines (which depend, in part, on widths), including incomplete specimens for which measurements were estimated. For all other measurements (lower postcanine width, length, and width/length ratio, and upper

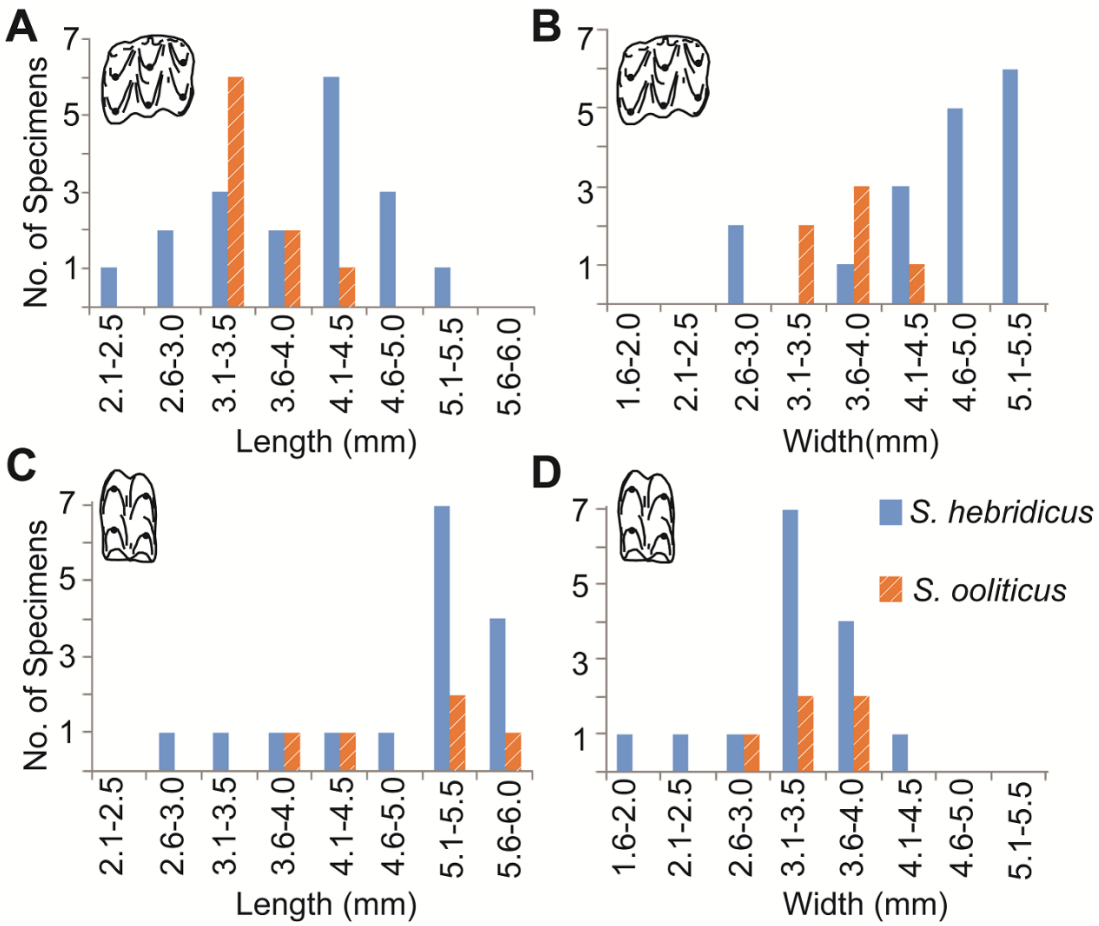

Figure 3.1.9: Distributions of dimensions of *Stereognathus* postcanine specimens. A, upper postcanine length; B, upper postcanine width; C, lower postcanine length; D, lower postcanine width. Orange striped bars *S. ooliticus*; blue bars *S. hebridicus*.

postcanine length), and when estimated lengths were removed from the data set, there was no statistically significant difference between samples.

When estimated measurements were included, *S. hebridicus* appeared to have wider upper postcanines than *S. ooliticus*. However, when estimates were excluded, there was no statistically significant difference between the putative species; therefore, I argue that this

statistical result is most likely artefactual and stems from conservatively estimated measurements used to achieve larger sample sizes for analysis. There was no corresponding significant difference found in the lengths of the upper postcanines when estimated measurements were included. When estimated measurements were included, there was also no corresponding difference in the sizes of the lower postcanines, with which the uppers must occlude.

I therefore conclude that the measurement differences in upper postcanine width and upper postcanine length/width ratio between the English and Scottish teeth are an artefact of estimating measurements, and not evidence that they belong to two distinct species.

3.1 iv) Discussion

Synonymizing *S. ooliticus* and *S. hebridicus*

Recognition of the size and morphological variability within *Stereognathus* allows for a systematic reassessment of *S. hebridicus*. I find no clear diagnostic differences between *S. hebridicus* and *S. ooliticus*, either in size or morphology. I therefore synonymise *S. hebridicus* with *S. ooliticus*.

The original diagnosis for *S. hebridicus* stated that this second species was '1.6 times' larger in size than the type species, *S. ooliticus* (Waldman and Savage, 1972:122). This size difference was determined on the basis of four isolated postcanines of *S. hebridicus* from Skye, of which only two were upper postcanines that could be compared with the *S. ooliticus* holotype. No other characters distinguishing *S. hebridicus* from *S. ooliticus* were identified, as the authors awaited 'full preparation of the material' from Skye before clarifying the diagnosis and anatomy of *S. hebridicus* (Waldman and Savage, 1972:122). However, the complete description and taxonomic assessment were never carried out. A comprehensive study of specimens assigned to *Stereognathus* more generally—both *S. hebridicus* and *S. ooliticus*—has not previously been undertaken.

Re-examination of all available *Stereognathus* postcanine material in the British Isles indicates that although the holotype postcanine of *S. hebridicus* is indeed larger than the holotype of *S. ooliticus*, when all *Stereognathus* postcanine tooth specimens are analysed together, it appears that all material—including both English and Scottish specimens—

comprise a spectrum of size with no discernible clustering between large and small morphs (Figure 3.1.8). Results of the Mann-Whitney U test found no statistically significant difference in measurements, except upper postcanine width and upper postcanine width/length ratio when estimated measurements of incomplete postcanines were included (Table 3.1.2). There is no corresponding difference in lower postcanine length, width, or width/ length ratio in the data including estimates, and no statistical difference at all when estimated measurements are not included. A correspondence between upper and lower postcanine size distributions would be expected, because uppers and lowers of drastically different sizes could not easily occlude with one another. I suggest that the evidence from the lower postcanines and the length of the upper postcanines of specimens attributed to each *Stereognathus* species indicates that size is not a diagnostic feature separating a purportedly larger species (*S. hebridicus*) from a smaller one (*S. ooliticus*). The spectrum of variation is probably best explained by ontogenetic variation, coupled with drawbacks in estimating measurements.

The mechanism for tooth replacement in tritylodontids is a 'conveyor belt' system in which teeth are added at the posterior end of the tooth row and lost at the anterior end at the diastema (Kühne, 1956; Matsuoka and Setoguchi, 2000). As a result, isolated tritylodontid postcanines are relatively abundant in the fossil record where tritylodontids occur in the British Isles (although they are mostly fragmentary). The advantage of this is the possibility of recovering postcanines from many ontogenetic stages, revealing information on the size range of these cynodonts. My measurements (Table 3.1.1; Figure 3.1.8 and 3.1.9) reflect this range of ontogenetic size variation.

Although some tritylodontids are possibly sexually dimorphic (Kühne, 1956; Hopson and Kitching, 1972; Matsuoka et al., 2016), I do not see any clear clustering between possible male and female morphs in these data. However, this may be due to sample size, and such clustering could possibly become apparent if a larger sample was available to us. At the very least, the size of my sample is adequate to show that there is no clear size distinction between the English and Scottish material. For that reason, coupled with the fact that there are no discrete character diagnostic differences among them, I refer them to a single species, which is *S. ooliticus* by priority.

In terms of discrete characters, there is no strong evidence to support *S. hebridicus* as a distinct species from *S. ooliticus*, either in the upper or in the lower postcanine

morphology. Assessing potential species-level apomorphies in all known specimens has proven difficult due to the fragmentary nature of the fossils; many features were missing due to damage or wear. This also meant that comparisons of specific characters between fossil localities cannot easily be made. However, where features are present, it appears that there is some variability, but it is not of the variety in which English specimens have one condition and Scottish specimens another. Specimens previously assigned to the two different species share characters, whereas others assigned to the same species do not. Preservation and tooth wear plays a greater role in interpretation than often acknowledged. The often damaged and fragmentary nature of the fossil record for this genus is reflected in my data, because many features could not be observed even in the most complete specimens. Moreover, my study has also revealed some new variable features. For example, the cuspules posterior to L2 and B2 in *Stereognathus* have not previously been identified but are present in material from multiple localities.

Despite the lack of morphological evidence for there being two distinct species, I cannot definitively rule out that these geographically separated populations—the more northern Scottish vs. the more southern English faunas— had not undergone some degree of biological speciation that is not reflected in my tooth-based morphological comparisons. However, this is not supported by the current fossil evidence. Future discoveries may shed further light on this.

To date, very little morphological description has been carried out for lower postcanines of *Stereognathus*, and no formal diagnostic characters have been identified (some features, such as the interlocking areas, were described but not used diagnostically; e.g., in Ensom, 1994). Here I have formally identified several morphological characters of the lower postcanines, which are present in both English and Scottish specimens: the projection of the AIA; the PIA comprising two embayments, pitted inside; the PIA framed by the termination of the b2 and l2 cusp ridges buccally and lingually, and separated medially by the posterior projection of the meeting of the b2 and l2 cusp medial ridges in the intercuspal groove; the ‘M’-shaped anterior of the postcanine in occlusal view; and a single root that retains the quadrate shape of the crown and is indented buccolingually on the anterior face (Figure 3.1.6, and 3.1.7). Whether the pseudo-cingulid, identified in more complete lower postcanine material is a diagnostic morphological character, or whether it develops as a result of wear during occlusion, is uncertain given the incompleteness of

Stereognathus material. Further investigation may reveal more about the pattern of occlusion in Tritylodontidae, particularly in more derived taxa.

Comparisons

All *Stereognathus* possess the sharp corners and quadrangular shape in both upper and lower postcanines originally described in *S. ooliticus* (Owen, 1857). *Stereognathus* shares this feature with *Polistodon* (He and Cai, 1984), *Xenocretosuchus* (Tatarinov and Mashenko, 1999), and *Montirictus* (Matsuoka et al., 2016). This is in contrast to the rounder shape of all other tritylodontid genera.

Upper and lower molar cusps in *Stereognathus* are more or less equal in size (damage and wear permitting), which is also the case in *Xenocretosuchus*, *Polistodon*, and *Montirictus*, but unlike in *Oligokyphus*, *Kayentatherium*, *Lufengia*, *Dinnebitodon*, *Yuanotherium*, *Bienotherium*, *Nuurtherium*, or *Shartegodon*, in which cusp size is variable. A faint pseudo-cingulid visible on the buccal edge of the crown of the lower postcanines has also been described for *Polistodon* (He and Cai, 1984).

Stereognathus and the recently described genus *Montirictus* from Japan (Matsuoka et al., 2016) share a great number of similarities, suggesting a close relationship between these genera. *Montirictus* upper postcanines also possess three rows of two cusps, and well-developed anterior and posterior interlocking areas. Matsuoka et al. (2016) described the vestigial cusps as absent in larger individuals and considered the vestigial M1 cusp to be a separate feature from the AIA protrusions, located instead on the crescentic anterior cusp face of the M2. I consider the vestigial cusp M1 to be present in *Montirictus*, incorporated as part of the AIA ridge as in *Stereognathus*. The teeth of *Montirictus* are quadrangular in shape like in *Stereognathus*. Both genera have ‘V’-shaped intercuspal grooves that meet subequally (nearly equally), a character they share with *Xenocretosuchus* (Tatarinov and Mashenko, 1999; Lopatin and Agadjanian, 2008) and *Polistodon* (He and Cai, 1984) and which is often modified or removed by wear.

Stereognathus had at least seven upper postcanines in the tooth row. Tritylodontids possessed between five (*Yunannodon*, *Bocatherium*) and 13 (*Polistodon*) upper postcanines (the functional tooth count in *Polistodon* was not reported and is now difficult to determine because the holotype is glued in occlusion, with bones of the dentary and jugal obscuring the rear of the tooth row). The posteriormost postcanine was not yet, if ever, fully erupted

(He and Cai, 1984). Non-functional posteriormost postcanines, and heavily worn and presumably soon-to-be-lost anteriormost postcanines, are present in various specimens due to the 'conveyor belt' mode of tooth replacement, in which teeth move anteriorly, with the oldest teeth falling out at the diastema and new replacement teeth being added at the back of the tooth row. This makes exact tooth count an unreliable character to compare among tritylodontids, because differences observed between specimens could be the result of capturing different moments in the tooth replacement process rather than a diagnostic difference in tooth count between two individuals or species. Upper tooth count can also be variable between different sides of the same animal (Young, 1982; He and Cai, 1984; Clark and Hopson, 1985; Matsuoka and Setoguchi, 2000; Watabe et al., 2007); the same is true for lowers. If there is a close relationship between *Stereognathus* and *Polistodon* (Watabe et al., 2007), it suggests the potential for a higher tooth count in the upper tooth row of *Stereognathus*, as recorded for *Polistodon* (He and Cai, 1984). More material is needed to address this issue.

The upper postcanines of *Stereognathus* have a cusp formula of 2–2-2. This differs from *Tritylodon* (Owen, 1884), *Oligokyphus* (Hennig, 1922), *Bienotherium* (Young, 1940), *Lufengia* (Chow and Hu, 1959), *Yunnanodon* (Cui, 1976), *Dianzhongia* (Cui, 1981), *Bienotheroides* (Young, 1982), *Kayentatherium* (Kermack, 1982; Sues, 1986), *Dinnebitodon* (Sues, 1986), *Yuanotherium* (Hu et al., 2009), *Shartegodon* (Velazco et al., 2017), and *Nuurtherium* (Velazco et al., 2017), which all have a higher number of cusps in one or more rows.

The width/length ratio has been used diagnostically by other authors; I found that this ratio for the lower postcanines of *Stereognathus* varied from 0.60 to 0.86 and that for uppers between 0.79 and 1.41 (Table 3.1.1). These measurements for tritylodontids are open to error because many specimens are missing enamel and have varying degrees of tooth wear. However, the ratio remains useful between genera.

Previous authors have identified only five roots in *Stereognathus*, and this result has been repeated by subsequent authors, particularly in character analysis. I show here, based on microCT data, that this root count is incorrect. This indicates that it may be necessary to microCT scan and recount the root numbers in some other tritylodontid specimens. The roots of *Stereognathus* upper postcanines instead vary in number between six and seven, potentially connected with their position in the tooth row (with more roots in posterior

postcanines). *Montirictus* also has six roots, but the roots of *Montirictus* compress inwards more tightly below the crown and orient outwards again ventrally. According to Cui and Sun (1987), *Bienotherium*, *Lufengia*, *Yunnanodon*, and *Bienotheroides* all have five roots, *Nuurtherium* also has five roots, and *Shartegodon* has four (Velazco et al., 2017). Cui and Sun (1987) observed that *Lufengia* has some fusion or dental laminae between the roots as in *Oligokyphus* (Kühne, 1956). *Oligokyphus* is described as having five roots connected transversely in two rows by dental laminae (Kühne, 1956). Such laminae are mostly absent in *Stereognathus*, although the medial roots are sometimes joined anteroposteriorly into a row (see posteriormost postcanine in BGS GSM113834, Figure 3.1.3F). The extent of this joining appears to be variable.

In BRSUG 20572, there is a large root in situ between the posterior roots of the postcanine, which by morphology and position belongs to the next tooth in the tooth row (absent) (Figure 3.1.4). However, the medial placement of this larger postcanine root does not follow the morphology of medial roots in the tooth row seen in the holotype BGS GSM113834. Because complete and well-preserved material is so rare, this unusual placement may have been more widespread in *Stereognathus*; it may be a post-depositional artefact or the result of the conveyor belt movement of the postcanines along the tooth row. This conveyor belt movement has been observed in other specimens of Tritylodontidae to produce an increasing curvature of the roots underneath the preceding postcanine, notably in the lower postcanines (Cui and Sun, 1987; Matsuoka et al., 2000).

The lower postcanines of *Stereognathus* have a cusp formula of 2–2, which differs from those of *Oligokyphus* (Kühne, 1956) and possibly *Tritylodon* (Fourie, 1963), which have the formula 3–3. The 2–2-2/2–2PC/pc cusp formula is shared with *Polistodon* (He and Cai, 1984), *Bocatherium* (Clark and Hopson, 1985), *Xenocretosuchus* (Tatarinov and Matschenko, 1999), *Montirictus* (Matsuoka et al., 2016), *Shartegodon* (Velazco et al., 2017), and *Nuurtherium* (Velazco et al., 2017). Although *Bienotherium* and *Kayentatherium* share the 2–2 cusp formula in the lower postcanines, the anterior cusps of both genera are larger than the posterior cusps (Young, 1947; Kermack, 1982), whereas in *Stereognathus*, *Xenocretosuchus*, *Montirictus*, *Shartegodon*, and *Nuurtherium* the cusps are equal. The lower postcanines of *Stereognathus* most closely resemble those of *Xenocretosuchus* and *Montirictus* in morphology, and they also bear close resemblance to the recently described *Shartegodon* and *Nuurtherium* (Velazco et al., 2017). They are all

quadrangular and rhomboidal in appearance, and *Stereognathus* and *Xenocretosuchus* possess vestigial (l3) and (b3) cuspules within the AIA and PIA (Tatarinov and Mashenko, 1999). The interlocking areas in *Stereognathus* are especially similar to those described in *Xenocretosuchus kolossovi* (Lopatin and Agadjanian, 2008), because the two taxa share the same ridges of chaotic enamel inside the embayments where the next tooth in the row 'locks' into place. This is also described for *Montirictus* (Matsuoka et al., 2016). These vestigial cusps are not mentioned in *Shartegodon* or *Nuurtherium*; however, I suggest that they may be present in *Shartegodon* (Velazco et al., 2017: fig. 9).

The roots of the lower postcanines of *Stereognathus* show a similar morphology to those of *Xenocretosuchus*, *Montirictus*, *Shartegodon*, and *Nuurtherium* in being box-like and extending straight downwards from the crown. Although in *Stereognathus* the ventral-most section of a postcanine has not yet been recovered, the specimens I examined shared the concave ridge 2–3 mm ventrally below the AIA as present in *Montirictus* (Matsuoka et al., 2016:fig. 3, parts B3, B4, C3. This feature is pronounced in *Montirictus*: the anterior face of the root is directed posteroventrally at an angle into this concavity, before bulging anteriorly below the concavity. The root also bifurcates below the line of concavity, with the anteriormost root half curving posteriorly at the ventral tip (Matsuoka et al., 2016). In *Shartegodon* (and possibly *Nuurtherium*), the root also curves as in *Montirictus*, but there is no bifurcation in the ventral part of the tooth, and the ridge identified for *Stereognathus* and *Montirictus* is not evident (Velazco et al., 2017:fig. 10). This 's'-shaped (referred to as 'c-shaped' in Velazco et al., 2017:14) curving is similar to that seen in other tritylodontid postcanines, but more pronounced and angular in appearance in *Montirictus* and *Shartegodon*, echoing the shape of the tooth crown. The lower postcanines DORCM G10828 from the Forest Marble, and GLRCM TEMP6036 from Hornsleasow, retain the most complete postcanine *Stereognathus* roots. They follow a *Montirictus*/*Shartegodon*-like pattern, but are not complete, and therefore I cannot confirm the ventral-most morphology of the root. The same is true for as yet undescribed material recently recovered from Woodeaton. More complete lower postcanine material is required.

Stereognathus lower postcanines resemble *Xenocretosuchus* (Lopatin and Agadjanian, 2008), *Montirictus* (Matsuoka et al., 2016), *Shartegodon* (Velazco et al., 2017), and *Nuurtherium* (Velazco et al., 2017) in having the buccal cusp row slightly posteriorly offset from the lingual row, and in the morphology of the PIA: forming two embayments

separated by the l2/b2 medial ridges meeting in the intercuspal groove and projecting posteriorly. In *Xenocretosuchus*, the ridges extending from the cusps into the intercuspal grooves were described as connecting in one intercuspal groove, but not the other (Lopatin and Agadjanian, 2008). However, this intercuspal groove is often modified by wear, and therefore this is not reliably diagnostic in either genus.

Phylogenetic Analysis

Many previous character analyses of Tritylodontidae place *Stereognathus* in a clade that includes *Bocatherium*, *Polistodon*, *Xenocretosuchus*, and *Montirictus* (Watabe et al., 2007). Most studies agree that *Oligokyphus* is the most basal member of Tritylodontidae and consider *Stereognathus*, *Bocatherium*, *Bientheroides*, *Xenocretosuchus*, and *Montirictus* to be 'advanced' tritylodontids (Clark and Hopson, 1985; Sues, 1986; Setoguchi et al., 1999; Watabe et al., 2007). However, only dental remains and two incomplete maxillae have been found and described for *Stereognathus*.

Clark and Hopson (1985) placed *Stereognathus* in a clade with *Bocatherium* and *Bienotheroides* based on the absence of facial, palatine, and zygomatic processes. Some characters were applied to *Stereognathus* 'by inference' (Clark and Hopson, 1985:399), based on resemblances between the holotype of *S. ooliticus* and more complete material for *Bocatherium* and *Bienotheroides*. They describe a 'prominent groove on the maxilla' of *S. ooliticus* as an indication that it possessed an infraorbital foramen at the junction of the premaxilla, the jugal, and the lacrimal. This groove is not clear either by direct observation or in microCT scan reconstruction, so I cannot confirm that *Stereognathus* possessed this character. *Stereognathus*, *Bocatherium*, *Bienotheroides*, *Dinnebitodon*, and *Yuanotherium* all share a uniquely reduced and cylindrical maxilla (referring to the

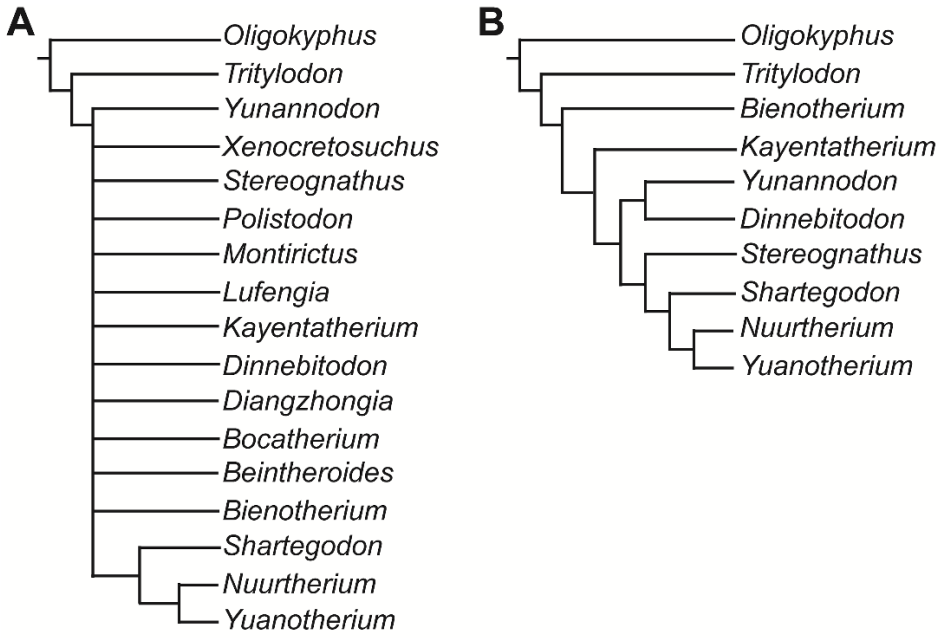

Figure 3.1.10: Trees generated by our phylogenetic analysis of tritylodontid taxa, using updated character codings for *Stereognathus*. A, strict consensus of the five parsimonious trees of 71 steps; B, the agreement subtree of 10 taxa.

convexity of the buccal and lingual sides, although in cross-section the maxilla of *Stereognathus* is somewhat rectangular), lacking laminal extensions into the face (Clark and Hopson, 1985:399). This highly derived character, along with the reduction to only two principal cusps per longitudinal row in the upper postcanines, supports grouping these tritylodontids into a clade.

The cladistic analysis by Watabe et al. (2007) used 17 taxa and 11 characters, six of which are dental. Watabe et al. (2007) scored the vestigial cusps as absent in *Stereognathus*, which I see from my reassessment is not the case. They also scored five cranial characters based on Clark and Hopson (1985), most of which were inferred (see above discussion). Their data were compiled second hand from multiple sources, concluding that these data were not sufficient at that time to satisfactorily resolve the polytomies among Tritylodontidae, namely, between *Stereognathus*, *Montirictus*, *Polistodon*, *Xenocretosuchus*, and *Bocatherium*, and between *Kayentatherium*, *Lufengia*, and *Diangzongia*. They suggested that additional characters are required to do so.

The most recent character analysis was carried out by Velazco et al. (2017), using 35 characters (22 skeletal and 13 dental). *Stereognathus* was scored on 15 of these characters:

nine dental and six skeletal. The tree presented in their paper (Velazco et al., 2017:fig. 16) was not the strict consensus tree of four most parsimonious trees of 68 steps as stated (elsewhere it is stated that there were two parsimonious trees [Velazco et al., 2017:28], but there were four). Unfortunately, there is also an error in their character matrix in the appendix for their paper. I obtained the correct matrix from Morphobank and reran the tree analysis using their methods to obtain their strict consensus tree. This places all tritylodontids in an unresolved polytomy, with the exception of *Oligokyphus* (outgroup) and *Tritylodon* as most basal, and a separate clade containing *Nuurtherium*, *Shartegodon*, and *Yuanotherium* in an unresolved polytomy.

Our reanalysis of *Stereognathus* clarifies certain characters, such as root count, and finds no support for other characters, such as a post-incisive snout constriction. I reran the Velazco et al. (2017) analysis with *Stereognathus* rescored (Appendices 1, 2). Five of the six skeletal characters I rescored as unknown (characters 1, 2, 7, 8, and 14). These characters were previously scored based on Clark and Hopson (1985), as mentioned previously, regarding inferences about the facial, palatine, and zygomatic processes for which I find no support. I retained the reduction of the maxilla as highly reduced (character 12), and the absence of a lateral extension of the maxilla (character 16), and added absence of the palatine contributing to the PC4 alveolus (character 14). The dental characters I retained were the cusp formula of upper postcanines as 2–2-2, the absence of M0 and L0, the large L3 cusp, and uncertainty over whether the lower postcanine bifurcates or is single-rooted (characters 24, 26, 27, 30, and 34). I rescored characters 25, 28, 29, 31, 32, 33, and 35. These are (respectively) the presence of the B0 cusp, the presence of a small M1 cusp and a small L1 cusp, six or seven roots in the upper postcanines, the presence of an anterior median root, the generalized lower cusp formula of 2–2, and the long single root in the lower postcanine with a curve in the ventralmost portion (‘s’-shaped).

Following Velazco et al. (2017) with updated characters for *Stereognathus* yields five parsimonious trees of 71 steps, and a strict consensus tree that is almost identical to the original, but with the polytomy between *Nuurtherium*, *Shartegodon*, and *Yuanotherium* resolved, finding *Shartegodon* and *Yuanotherium* more closely related to one another than to *Nuurtherium* (Figure 3.1.10A). In this matrix, six taxa have >50% missing data and three >60% (*Yunnanodon* 62.9%, *Montirictus* 65.7%, and *Xenocretosuchus* 77.2%). *Stereognathus* has 60% missing data. Removing *Montirictus* and *Xenocretosuchus* yields

three parsimonious trees of 70 steps and results in a strict consensus tree identical to that found by Velazco et al., but with the addition of a clade formed by *Polistodon* and *Bocatherium*. *Stereognathus* remains part of the polytomy with most other tritylodontids.

Eliminating taxa with the most missing entries can alter the relationships among taxa, without clarifying them (Wilkinson, 2003). In order to avoid this, I ran an agreement subtree on the whole data set with *Stereognathus* rescored, to identify the largest subset of taxa in all of the parsimonious trees that are identically related (Goloboff et al., 2008). This resulted in a tree with 10 taxa, including *Stereognathus*, placing it as the nearest outgroup to *Shartegodon*, *Nuurtherium*, and *Yuanotherium* (Figure 3.1.10B). Other than the addition of new taxa, this tree topology differs little from Clark and Hopson's (1985), despite including more characters and taxa.

In light of the difficulties coding only one of these tritylodontid taxa—*Stereognathus*—based on the previous literature, it seems that phylogenetic analyses of tritylodontids will remain problematic and cannot be further resolved until comprehensive re-descriptions (to confirm or re-describe characters as necessary) of existing material are available. I also suggest that there may be more intraspecies variation in cusp shape and morphology than previously recognized—often confounded by poor preservation and degree of tooth wear—and that this variation may have occasionally been erroneously interpreted as apomorphic. I therefore consider phylogenetic analysis to be preliminary until more detailed, up-to-date information is available for the many poorly described or figured taxa, and particularly for taxa that were unresolved in my analysis, such as *Polistodon*, *Lufengia*, *Beinotheroides*, *Diangzhongia*, and *Bocatherium*. As is often the case, more complete material for other taxa, including *Stereognathus*, *Xenocretosuchus*, and *Montirictus*, would almost certainly improve the resolution of future phylogenetic analysis.

3.2 Morganucodontidae: *Wareolestes rex*[2]

Morganucodontans are a diverse clade of proximate stem group mammals known from the Late Triassic until at least the Middle Jurassic, and possibly as late as the Early Cretaceous (Butler and Sigogneau-Russell, 2012). They were among the most abundant early mammaliaforms, and became globally distributed by the Early Jurassic, with fossils known from the USA (Jenkins et al., 1983), India (Datta and Das 1996), South Africa (Crompton, 1964), Greenland (Jenkins et al., 1994), China (Kermack et al.,1973; Young 1978; Luo and Wu, 1994), Russia (Gambaryan and Averianov, 2001) and across Europe (UK: Kermack et al., 1973; Freeman, E., 1979; Clemens, 2011; Switzerland: Clemens, 1980; France: Sigogneau-Russell, 1983; Evans and Milner, 1994; Debuysschere et al., 2015).

Morganucodontans provide important information on the evolutionary assembly of mammalian anatomy as they possess derived mammalian characters, including diphyodont replacement of the antemolar teeth (incisors, canines, premolars) (Crompton, 1974; Luo et al., 2004). Diphyodont replacement was argued for the second molar of *Megazostrodon* (Gow, 1986) but this has subsequently been debated (Luo et al., 2004). Like crown group mammals, morganucodontans also exhibited precise molar occlusion. However, full occlusion was achieved through enamel wear rather than precise occlusion upon tooth eruption (Mills, 1971; Crompton, 1974; Crompton and Luo, 1993; Luo et al., 2004). Alongside these mammalian synapomorphies, morganucodontans also retained plesiomorphic character states, such as the linear, mesiodistal alignment of the main cusps of postcanine teeth, retention of a post-dentary trough, and an anteriorly positioned angular process of the dentary (Kielan-Jaworowska et al., 2004).

Morganucodonta (Kermack et al., 1973) includes two families: Morganucodontidae and Megazostrodontidae (Stucky and McKenna, 1993; Kielan-Jaworowska et al., 2004). Megazostrodontidae was erected to include *Megazostrodon* and *Dinnetherium*, and is diagnosed by the reduction of the angular process, flaring of the ridge of the dentary condyle, and the well-developed labial cingulum on the upper molars, with the labial

[2] Chapter 3.2 was originally published as: Panciroli, E., Benson, R.B.J., and Walsh, S. 2017a. The dentary of *Wareolestes rex* (Megazostrodontidae): a new specimen from Scotland and implications for morganucodontan tooth replacement. *Papers in Palaeontology*, 3: 373–386.

cingulum tending to differentiate into posterior and anterior lobes (Gow, 1986; Kielan-Jaworowska et al., 2004). Following the initial description of Megazostrodontidae, *Brachyzostrodon* (Late Triassic, France and Greenland; Sigogneau-Russell, 1983), *Indozostrodon* (Early Jurassic, India; Datta and Das, 1996, 2001) and *Wareolestes* (Middle Jurassic, England; Freeman, E., 1979) were referred to Megazostrodontidae by these subsequent authors. It should be noted that *Indozostrodon* may be a junior synonym of *Indotherium* (Prasad et al., 2006), which was assigned to Morganucodontidae by Prasad and Manhas (2002); more complete material is required to resolve this.

Wareolestes rex was erected as a new genus and species by E. Freeman (1979) for a single well preserved molar tooth discovered at Kirtlington cement quarry, an exposure of the Middle Jurassic Forest Marble Formation in Oxfordshire, UK, which has yielded multiple representatives of early mammaliaform groups (Freeman, E., 1976, 1979; Kermack et al., 1998; Sigogneau-Russell, 1998, 2003; Butler and Hooker, 2005). Until now, *Wareolestes* has been known only from the type molar, NHMUK PV M36525, and some referred molar fragments (see below; Freeman, E., 1979; Butler and Sigogneau-Russell, 2016).

In 2015, field work in the Middle Jurassic Kilmaluag Formation of the Isle of Skye, Scotland recovered a dentary with multiple erupted and non-erupted teeth that I attribute to *Wareolestes rex*. This is the first occurrence of this genus in Scotland. The specimen was found at a coastal locality, with the buccal side of the jaw exposed and therefore slightly abraded. Nevertheless, it retains evidence of at least three replacement teeth and three permanent molars. The new specimen therefore provides crucial evidence for the mode of dental replacement in megazostrodontids. It also adds to our knowledge of the anatomy of *Wareolestes*: it clarifies the previously disputed position of the holotype for this genus (Hahn et al., 1991; Butler and Sigogneau-Russell, 2016), and adds a new feature that I consider to be an autapomorphy: the presence of a labial cingulid. Finally, it adds to a growing list of mammaliaforms known from the Bathonian (Middle Jurassic) Kilmaluag Formation of Scotland (Waldman and Savage, 1972; Savage, 1984; Evans and Milner, 1994; Close et al., 2016), allowing comparisons with the well sampled Middle Jurassic mammaliaform assemblage of England.

3.2 i) Materials and Methods

The specimen comes from the Straithaird Peninsula north of Elgol and approximately 1 km south of Cladach a'Ghlinne (see Close et al., 2016). It was found in a fallen boulder, below the tide line. Although not in situ, it can be identified as having come from the Kilmaluag Formation, part of the Middle Jurassic Great Estuarine Group of the Hebrides Basin. See Chapter 2.1 for geological overview. The specimen reported here was found in an argillaceous micritic limestone.

The new specimen NMS G.2016.34.1 was scanned at 95 kV and 225 µA using a Nikon XT H 225 ST micro CT scanner at the University of Cambridge Biotomography Centre (http://www.cbc.zoo.cam.ac.uk/) with an isotropic voxel size of 13.4 µm, 1998 slices at export. The density of the metamorphosed limestone matrix limited the contrast and resultion of the scan. The fossil was segmented from the matrix using Mimics 19.0 (Materialise, Leuven, Belgium; http://www.materialise.com/en/medical/software/ mimics). The specimen was also examined directly using a Meiji Techno RZ3361 microscope. The holotype was scanned on the same micro-CT equipment at 75 kV and 80 µA, with an isotropic voxel size of 3 µm, 866 slices at export. It was also digitally reconstructed using Mimics 19.0. A 3D digital model of NMS G.2016.34.1 in .stl format, and microCT tomographs, are available in Panciroli et al., (2017c).

Terminology

I follow the dental cusp terminology of Crompton (1974; Figure 3.2.1). Morganucodontans possess three main cusps, a/A, b/B and c/C, aligned anteroposteriorly in a triconodont pattern. There is also a distal cingulid cusp d/ D, aligned with the three main cusps, and a series of cingulid cusps which can include mesial cusp e/E and midline cusp g/G (= the kühnecone; Parrington, 1967) not aligned with the main a–d cusp row. Cusps are referred to in lower case for lower molars, and upper case for the upper molars. The terms labial and buccal are used synonymously.

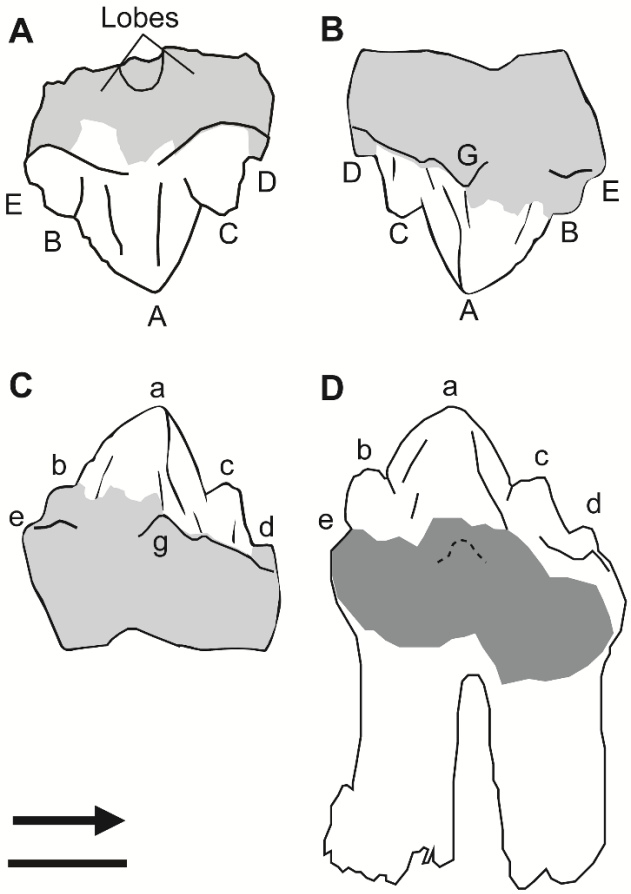

Figure 3.2.1: Megazostrodontidae cusp terminology. A, holotype *Wareolestes rex* NHMUK PV M36525 as an upper molar, lingual view. B, holotype *Wareolestes* NHMUK PV M36525 as an upper molar, labial view. C, holotype NHMUK PV M36525 as a lower molar as originally described, lingual view. D, segmented tooth from new specimen NMS G.2016.34.1 in labial view. Light shading indicates loss of enamel, dark shading missing portion of tooth. Arrow indicates anterior direction. Scale bar represents 1 mm.

3.2 ii) Description

SYSTEMATIC PALAEONTOLOGY

MORGANUCODONTA Kermack et al., 1973

MEGAZOSTRODONTIDAE Gow, 1986

WAREOLESTES Freeman, E., 1979

WAREOLESTES REX Freeman, E., 1979.

Holotype: NHMUK PV M36525; right or left, lower or upper molar from Kirtlington Mammal Bed, Forest Marble Formation (Bathonian, Middle Jurassic), Kirtlington Cement Works Quarry, Oxfordshire, England. A 3D digital model of this specimen in .stl format, and microCT tomographs, are available in the Dryad Digital Repository (Panciroli et al., 2017c).

Referred material: NHMUK PV M46240, NHMUK PV M46248, NHMUK PV M46775, all isolated molars from the Late Bathonian of Kirtlington, Oxfordshire, UK; plus NMS G.2016.34.1 from the Bathonian Kilmaluag Formation of the Isle of Skye, Scotland. The presence of an unerupted molar m3 indicates that NMS G.2016.34.1 represents a sub-adult. Re-identified specimens previously referred to *Wareolestes* include NHMUK PV M46563 (re-identified as *Gobiconodon* sp. indet. (Butler and Sigogneau-Russell, 2016)) and NHMUK PV M46811 (now the holotype of *Cherwellia leei* (Butler and Sigogneau-Russell, 2016)) both from the Late Bathonian of Kirtlington, Oxfordshire, UK.

Previous diagnosis: *Wareolestes rex* is a megazostrodontid morganucodontan (sensu Kielan-Jaworowska et al., 2004) with dental morphology that is congruent with other members of Morganucodonta: three principal cusps arranged anteroposteriorly along the tooth row (cusps a/A, b/B, and c/C). Megazostrodontidae is diagnosed by a reduced angular process, flared ridge of the dentary peduncle, the division of the upper labial cingulum into anterior and posterior lobes, and the presence of well-developed labial cingular cusps in the upper molars. *Wareolestes* shares with some morganucodontans a central cusp a/A larger than the other cusps (as in *Morganucodon*) and a wrinkled enamel surface (as in *Brachyzostrodon*) (Kielan-Jaworowska et al. 2004). Autapomorphies of *Wareolestes* are the placement of cusp g buccolingually in line with cusp a, and a poorly defined labial cingulum.

Revised diagnosis: In addition to the above, a new autapomorphy of *Wareolestes rex* is the presence of a labial cingulid in the lower molars, with cusp g buccolingually in line with cusp a, and a poorly defined lingual cingulid. The dental formula is ?.1.5.3/?.1.5.3.

Description

NMS G.2016.34.1 is a partial left dentary, missing its anterior portion from c/p1 anteriorly (Figures 3.2.2, and 3.2.3). The dentary condyle and coronoid process are also missing posteriorly. Portions of several erupted and unerupted teeth are present, and are

described below. The specimen is partially embedded in matrix, so description of the lingual surface is based on digital reconstructions from micro-CT scans.

The dentary, as preserved, measures 22.3 mm anteroposteriorly, with a maximum buccolingual width of 1.82 mm, measured at the level where m2 abuts m3. However, the dentary is crushed just posterior to this, and it is possible that it was slightly wider ventral to m3. It is 3.23 mm in dorsoventral depth from the ventral surface of the dentary to the alveolar margin at m2.

I identify the preserved tooth portions as being a partial, unerupted p2 and roots of dp2, unerupted p4 and m3, an erupted m1 (damaged), and an erupted m2 (damaged lingually). There is also a fragment of an unerupted p5. Empty alveoli for c, p1 and p3 are present. Based on this information, I estimate a dental formula of ?.1.5.3/?.1.5.3. Both *Megazostrodon* and *Dinnetherium* have five molars (Gow, 1986; Kielan-Jaworowska et al., 2004), but there is no indication of a fourth or fifth molar in NMS G.2016.34.1 (Figure 3.3.3), nor is there space in the dentary for further molars to form posterior to m3. I assume there was one canine in NMS G.2016.34.1, and a partial alveolus remains at the preserved anterior end of the dentary, however I am unable to determine incisor count because the anteriormost portion of the specimen is missing.

Identification of premolars and molars in NMS G.2016.34.1 was based on the replacement pattern evidenced by the position of replacement teeth within the dentary (see below). A distinct change in morphology between the posteriormost premolar and anteriormost molar has been observed in other morganucodontans (Kielan-Jaworowska et al., 2004). Compared to m1, the posteriormost premolar (p5) of *Megazostrodon rudnerae* has a taller cusp a (dorsoventrally) and less well developed cusps b and c, and m1 has a more prominent cingulid and taller cingular cusps than p5 (Crompton, 1974). Only a small portion of p5 is preserved in NMS G.2016.34.1, however, this preserved portion appears to be the anterior projection of a cingulid, indicating a molarized morphology for p5 in *Wareolestes rex* (Figure 3.3.4B). The morphology of the preserved portion of p5 is

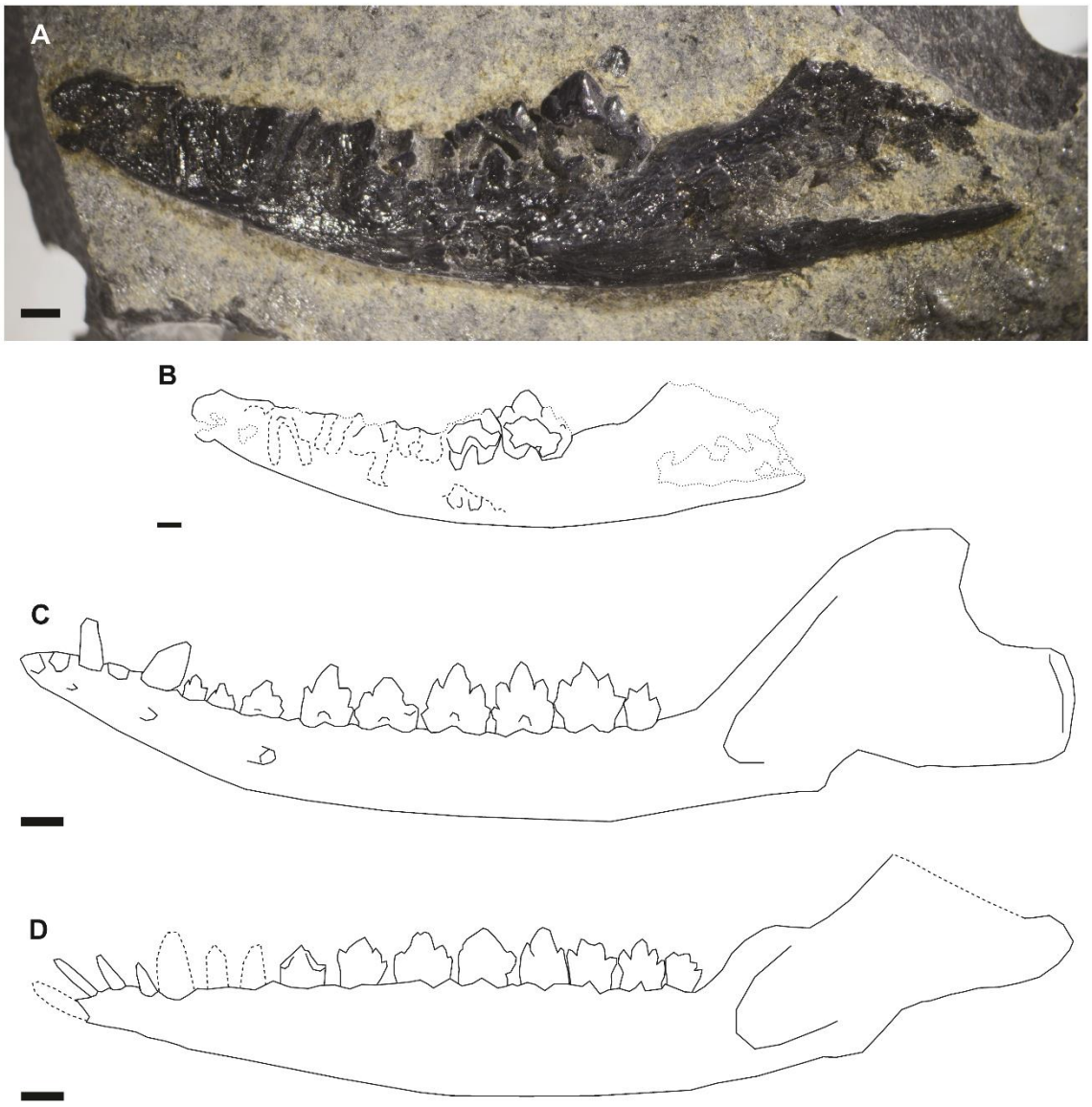

Figure 3.2.2: New specimen of *Wareolestes rex*, NMS G.2016.34.1 with comparative material. A, buccal view of *Wareolestes rex*, NMS G.2016.34. B, line drawing of *Wareolestes rex*, NMS G.2016.34, reduced in size for comparison with corresponding portions of C and D. C, line drawing of buccal view of *Dinnetherium nezorum*. D, line drawing of buccal view of *Megazostrodon rudnerae*. Sources: C, composite drawing from Gow (1986) and Kielan-Jaworowska et al. (2004); D, composite drawing from Jenkins et al. (1983) and Kielan-Jaworowska et al. (2004). Scale bar represents 1 mm.

not congruent with a remnant of root, as it is not hollow along its length (unlike a root), nor does it resemble the sharp anterior portion of the p4 crown. Therefore, I identify it as the

anterior projection of the cingulid, and suggest that p5 in *Wareolestes* is somewhat molarized.

The morphology of p4 is distinctly different from the molars, having a proportionally taller cusp a compared to cusps b and c. Although its roots are absent, the preserved ventral portion of p4 and the morphology of its alveolus indicate that it was double-rooted.

The premolar I identify as dp2/p2 in NMS G.2016.34.1 is double rooted, while the alveoli anterior to dp2/p2 are single rooted (Figure 3.2.4A). In *Megazostrodon rudnerae* the first two premolars are single rooted, and the posterior three double rooted (Gow, 1986). If this was the pattern in *Wareolestes*, it would suggest a premolar count of six; more than any other morganucodontan. Although it is possible that the premolar count may be higher than any other genus, it is more likely that *Wareolestes* has a different root pattern than *Megazostrodon*. I therefore suggest the anteriormost alveoli to be those of c and p1, and identify the anteriormost double rooted premolar present in NMS G.2016.34.1 as dp2/p2.

The remnants of dp2 include the lingual half of its double roots, and a small portion of the crown where it meets the roots. Ventral to this, between the root remnants, is the cusp a tip of a replacement tooth p2 (Figure 3.2.3). This forms a hollow cone, and the rest of p2 has either not formed or has been lost.

The dentary is fractured just anterior to the inferred position of the angular process. Although the angular process itself is not preserved, the mandibular body ventral margin anterior to the angular process is preserved. This surface is uniformly convex anteroposteriorly, albeit slightly, as in the intact dentaries of *Megazostrodon* and *Dinnetherium* (Jenkins et al., 1983; Gow 1986; Kielan-Jaworowska et al., 2004). There is no sign of the sigmoidal curvature typically associated with the ventral projection of an angular process, as seen in *Morganucodon*, *Hadrocodium* and other taxa with well-developed angular processes (Kermack et al., 1973; Crompton and Luo, 1993; Luo et al., 2001). I suggest that *Wareolestes* possessed a reduced angular process, termed a 'pseudangular' by Jenkins et al. (1983). Due to lack of preservation, it is not possible to assess if the angle of *Wareolestes* would have been slightly inflected, as in *Hadrocodium* (Luo et al., 2001).

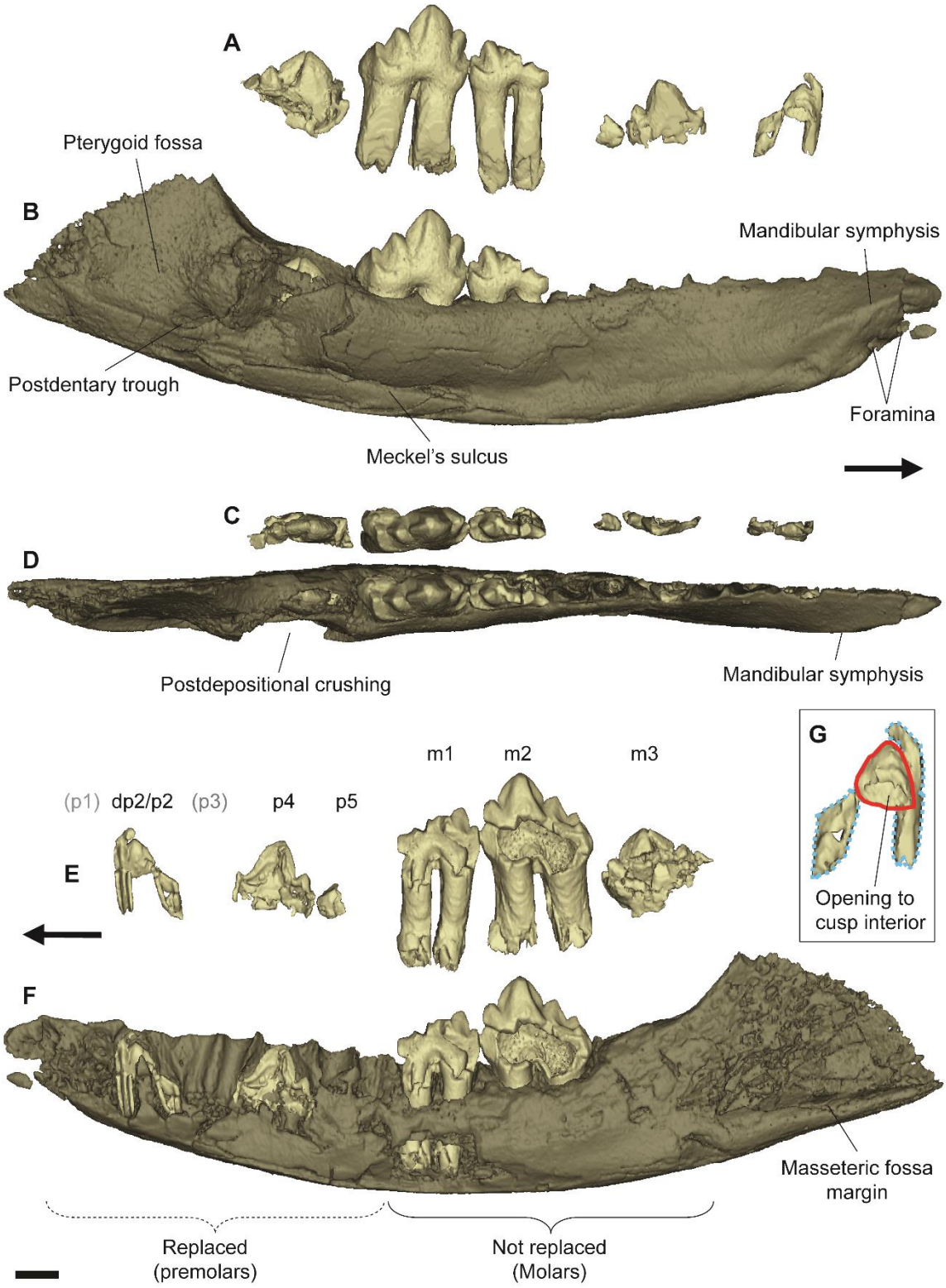

The ventral margin of the masseteric fossa is visible buccally on the posteroventral portion of the dentary, and there is some buccolingual crushing and abrasion of this feature

(Figure 3.2.3). The dentary is crushed ventral to m3, but the preserved morphology suggests it was buccolingually widest at this point of the jaw, as in *Megazostrodon* (Gow, 1986). The Meckel's sulcus is present on the ventrolingual surface of the dentary. The sulcus extends from the crushed section of dentary ventral to m3, to the base of p5. Examination of the X-ray CT data indicates that the Meckel's sulcus is crushed transversely, causing the lingual surface of the dentary to collapse buccally towards the mandibular canal, an internal neurovascular canal inside the mandibular body.

The ventral surface of the dentary is more strongly convex anteroposteriorly than in either *Megazostrodon* or *Dinnetherium*, but is closest in curvature to the latter (Figure 3.3.2; Gow, 1986; Kielan-Jaworowska et al., 2004). This curvature is consistent with the presence of a reduced angular process (as in *Dinnetherium*), and is accentuated by the dorsal curvature of the anterior portion of the dentary, particularly anterior to p5. This curvature is unlike the straighter morphology seen in most other morganucodontans, or in closely related groups such as Docodonta, but resembles some eutriconodontans such as *Phascolotherium*, and later eutherians such as *Kennalestes* (Kielan-Jaworowska et al., 2004). This similarity is probably functional, resulting from convergent evolution; I do not infer a close relationship between these taxa and *Wareolestes*.

The coronoid crest rises posterodorsally from just posterior to the unerupted m3. The dentary is broken posteriorly, so the coronoid process is missing. It is likely that *Megazostrodon* possessed a coronoid facet that articulated with the coronoid bone just posterior to the ultimate molar. However, this facet is not evident in NMS G.2016.34.1 due to crushing on the lingual surface of the dentary. Despite crushing, the postdentary trough is clearly visible, as in other morganucodontans, and other stem mammals with the

Figure 3.2.3 (previous page): Segmentation and digital reconstruction of the new specimen of *Wareolestes rex* G.2016.34.1 from micro-CT scan data. A, lingual view of dentition. B, lingual view of dentary. C, occlusal view of dentition. D, occlusal view of dentary. E, buccal view of dentition. F, buccal view of dentary with replacement pattern in *Wareolestes* underneath. G, dp2/p2 enlarged, showing deciduous premolar outlined in dotted line (blue), replacement premolar cusp a in solid line (red). Abbreviations: p, premolar, dp, deciduous premolar; m, molar. Arrows indicate anterior direction. Scale bar represents 1 mm.

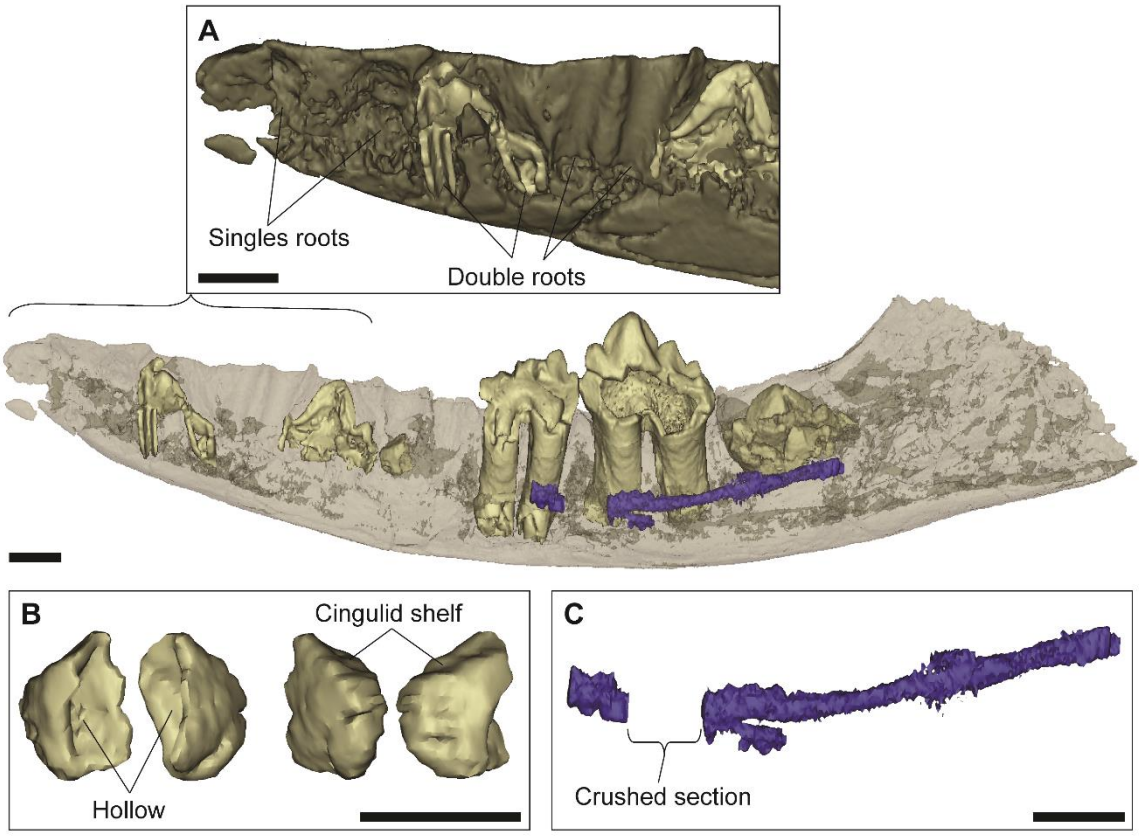

Figure 3.2.4: Detail of features of NMS G.2016.34.1. A, buccal view of the anterior of the dentary showing the single root alveoli followed by double root (see text). B, molarized morphology of the remnant of cingulid in p5. C, segmented pathway of the mandibular nerve within the dentary. Scale bars represent 1 mm.

primitive character of retaining post-dentary bones (Kielan-Jaworowska et al., 2004; Luo, 2011; Meng et al., 2015). It is smaller than in *Morganucodon*, closer in morphology to *Dinnetherium* (Kielan-Jaworowska et al., 2004). Ventral to m3, just ventral to mid-height on the buccal surface of the dentary, abrasion has revealed two small windows into the mandibular canal for the nerves and vessels in the interior of the dentary. This has been digitally reconstructed along some of the length of the dentary (Figure 3.2.4) although crushing and abrasion prevent full reconstruction of this feature.

Anterior to p5 the dentary flares lingually, forming the mandibular symphysis. However, because the dentary is broken anterior to the remnants of the alveoli of c/p1, few morphological details of the symphysis are evident. Foramina are visible anteriorly on the

Table 3.2.1: Measurements of new specimen and comparative data from Morganucodontidae. For partial teeth of *Wareolestes rex,* estimates were made conservatively.

Taxon	Dentition	Specimen No.	Max length (mm)	Max width (mm)	Reference
Megazostrodontidae					
Wareolestes rex	Lower m2	NMS G.2016.34.1.	1.97 (estimate)	1.18 (estimate)	
Wareolestes rex	Lower m3	NMS G.2016.34.1.	2.67	1.30 (estimate)	
Wareolestes rex	Lower m4	NMS G.2016.34.1.	2.35 (estimate)	1.0 (estimate)	
Wareolestes rex	molar	NHMUK PV M36525	2.31	1.24	E. Freeman (1979)
Brachyzostrodon coupatezi	lower molars	Multiple	1.75-2.15	0.75-1.21	Hahn *et al.* (1991)
Brachyzostrodon maior	lower molars		2.7	1.2	Hahn *et al.* (1991)
Morganucodontidae					
Paceyodon davidi	lower molars	multiple	3.3	1.6	Clemens (2011)
Morganucodon watsoni	lower molars	multiple	0.70-1.65	0.45-0.80	Pacey (1978)
Morganucodon watsoni	upper molars	multiple	0.80-1.60	0.45-0.80	Pacey (1978)
Morganucodon oehleri	lower molars	Multiple	1.06-2.30	CUP 2320	Kermack *et al.* (1973)
Morganucodon oehleri	upper molars	Multiple	1.40-2.30	CUP 2321	Kermack *et al.* (1973)
Hallautherium schalchi	lower molars	Multiple	1.08-1.39	0.44-0.66	Clemens (1980)
Helvetiodon schutzi	upper molar		2.85	1.09	Clemens (1980)
Incertae sedis					
Bridetherium dorsi	lower molars	Multiple	0.85-1.90	0.48-1.15	Clemens (2011)
Bridetherium dorsi	upper molars	Multiple	1.02-1.70	0.55-0.96	Clemens (2011)

ventrolingual surface of the symphysis, immediately posterior to its broken anterior portion, around the level of dp2/p2. There are at least two foramina, positioned approximately below c and pm1. The most completely preserved molar tooth is m2. As in the holotype molar, NHMUK PV M36525, the central cusp a of m2 in NMS G.2016.34.1 is higher dorsoventrally than cusps b and c. Cusp a also has distinct dorsoventral ridges on the posterior and anterior surfaces, with corresponding troughs, and there is an expanded labial cingulid that curves around the posterior edge of the tooth. The cingulid bears a prominent cusp d, and the cingulid continues onto the labial and lingual surfaces of the tooth. Damage

to the buccal side of m2 in NMS G.2016.34.1 means the highest cingular cusp g is not preserved. In the holotype (NHMUK PV M36525), cusp g is directly lingual to cusp a, unlike in *Morganucodon*, *Megazostrodon* and upper molars of *Brachyzostrodon* (Freeman, E., 1979; Hahn et al., 1991). The double roots of m2 are deep in NMS G.2016.34.1, extending close to the ventral surface of the dentary, and are not clubbed at their ventralmost point.

The other molar teeth of NMS G.2016.34.1 are less complete, and show morphologies that are congruent with that of m3. Cusps c and d are still present on m1, but a and b are missing, as is the lingual cingulid. The ridge extending from cusp d forms the posterior cingulid, which curves onto the lingual side of the tooth. The roots of m1 do not diverge as they extend ventrally, unlike in m3. Instead, they converge at their ventral ends, and they are slightly longer than in m2. Also, the lingual surface of m1 appears slightly flatter than that of m3.

Cusps a, b, c and d are visible in m3, despite the tooth being somewhat fractured. This tooth is longer anteroposteriorly than either m1 or m2 (Table 3.2.1). The distinct dorsoventral ridges and embayments seen in m2 and the holotype of *Wareolestes rex* are also visible in m3. There is no root present in m3.

3.2 iii) Discussion

Referral of NMS G.2016.34.1 to *Wareolestes rex*

NMS G.2016.34.1 is undoubtedly a morganucodontan: it retains the anteroposterior linear arrangement of the molar cusps that distinguishes morganucodontans from kuehneotheriids. Furthermore, like all other morganucodontans, it retains the postdentary trough and has diphyodont tooth replacement in the preserved premolar positions. This can clearly be seen by the presence or inferred presence of replacement teeth (Crompton and Luo, 1993; Luo et al., 2004; Kielan-Jaworowska et al., 2004; see below).

Wareolestes was placed in Megazostrodontidae by Hahn et al. (1991) and subsequently by Kielan-Jaworowska et al. (2004). I refer NMS G.2016.34.1 to Megazonstrodontidae because I infer that it had an apomorphic reduced angular process (the ‘pseudangular’) as seen in *Megazostrodon* (Crompton 1974) and *Dinnetherium*

(Jenkins et al. 1983). It is not possible to state whether it also shares the flaring of the dentary peduncle, as this is not preserved in NMS G.2016.34.1, nor the lobed upper molars and well developed cingular cusps, as no upper molars were recovered with NMS G.2016.34.1. However, as I consider this specimen to be referable to *Wareolestes* (see below), these features may be inferred to have been present based on their presence in other megazostrodontids.

NMS G.2016.34.1 is referred to *Wareolestes* based on the following apomorphies shared with the holotype: a substantial cusp d positioned directly distal to cusp c on a labial cingulid that curves around the posterior of the tooth and continues onto the lingual surface. Like the holotype, it also has wrinkled enamel on cusp a, a feature shared with *Brachyzostrodon* and *Helvetiodon*, but that distinguishes it from *Megazostrodon*. I also consider the overall structure and appearance of the tooth to be highly consistent with the holotype of *Wareolestes* (see above and Figure 3.2.5). As in the holotype molar, cusp a is proportionally longer anteroposteriorly than in *Morganucodon*, and has distinct dorsoventral ridges on its posterior and anterior surfaces, with corresponding troughs, producing shallow 'embayments' (Freeman, E., 1979, p. 160). Kielan-Jaworowska et al. (2004, p. 182) noted that the holotype tooth of *Wareolestes rex* is 'one-and-a-half times [the size of] most morganucodont teeth.' The m2 of NMS G.2016.34.1 is larger than the holotype (see Table 3.2.1 and Figure 3.2.6) and close in size to *Brachyzostrodon maior* and *Helvetiodon schutzi* (Table 3.2.1; Figure 3.3.6; it is slightly anteroposteriorly shorter and buccolingually wider than the m3 teeth of those taxa). The m1 and m3 are also large (though smaller than the holotype). The largest morganucodontid currently known is *Paceyodon davidi* (Clemens, 2011), the known molar of which is approximately 20% larger than m3 in NMS G.2016.34.1.

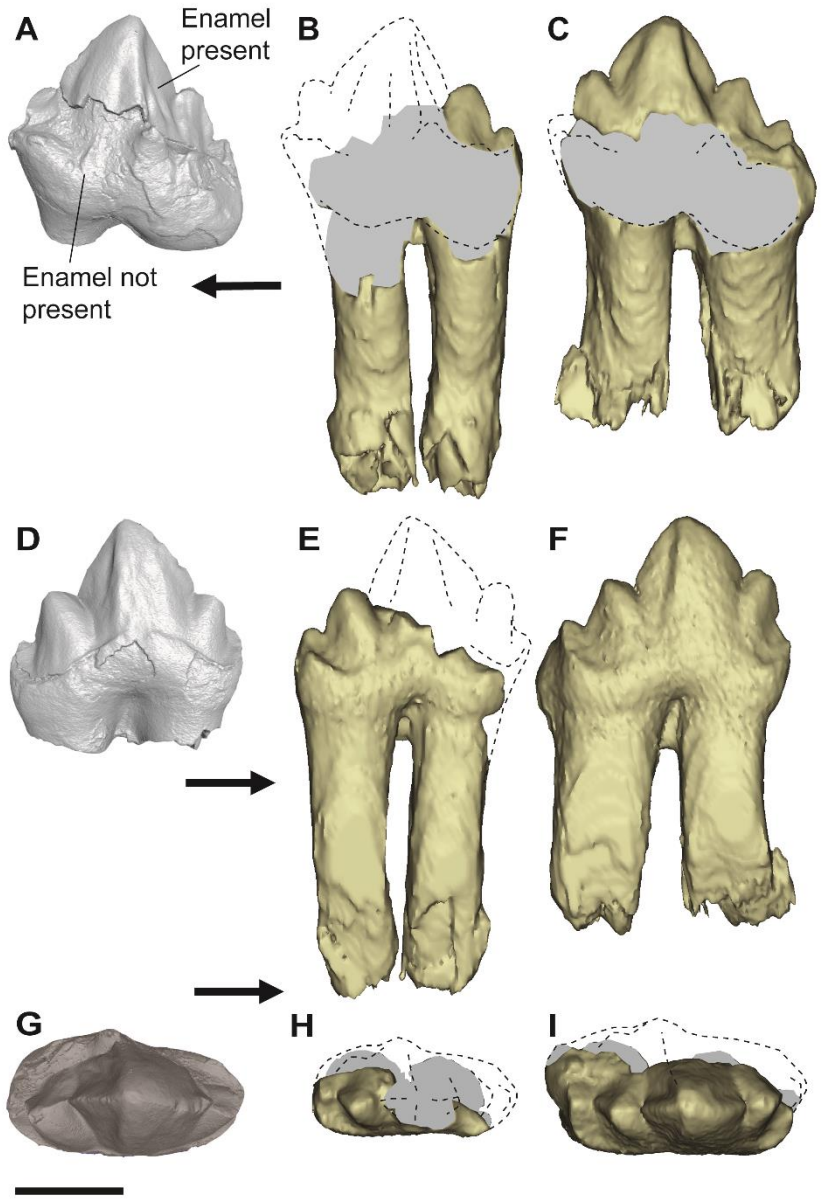

Figure 3.2.5: Comparison of the reconstructed CT scan of the holotype *Wareolestes rex* NHMUK PV M36525 as a lower molar, with m1 and m2 from NMS G.2016.34.1. A, buccal view of NHMUK PV M36525. B, buccal view of m1 NMS G.2016.34.1. C, buccal view of m2 NMS G.2016.34.1. D, lingual view of NHMUK PV M36525. E, lingual view of m1 NMS G.2016.34.1. F, lingual view of m2 NMS G.2016.34.1. G, occlusal view of NHMUK PV M36525. H, occlusal view of m1 NMS G.2016.34.1. I, occlusal view of m2 NMS G.2016.34.1. Grey areas indicate broken portions of tooth. Dotted lines indicate reconstructed features based on comparisons. Arrows indicate anterior direction. Scale bar represents 1 mm.

The holotype of *Wareolestes rex* has an enlarged cusp g and subequal cusps b and c, distinguishing it from the megazostrodontid *Dinnetherium*, in which cusp g is not enlarged,

and cusps b and c are approximately equal in height. While cusp g is missing in NMS G.2016.34.1, it shares the slight elevation of cusp b compared to cusp c. Finally, it differs from *Indozostrodon* in having a larger cusp a; this cusp is smaller, positioned more posteriorly and twinned with cusp c in *Indozostrodon*.

A previously cited difference between *Morganucodon* and *Megazostodon* is the manner of occlusion of the molar cusps. In *Morganucodon* it was thought that cusp a occludes between cusps A and B on the opposing upper molar, known as offset shearing (Crompton and Jenkins, 1968; Mills, 1971). In *Megazostrodon* cusp a was described as occluding between cusp B of the opposing upper molar, and cusp C of the preceding upper molar, called embrasure shearing (Crompton, 1974). However, recent preliminary work suggests that in *Morganucodon* at least, shearing patterns may be more variable along the tooth row than previously understood (Jäger et al. 2016).

Positions of isolated *Wareolestes* teeth within the tooth row

NMS G.2016.34.1 provides information about the positions of previously reported, isolated teeth of *Wareolestes* within the tooth row, and their taxonomic identifications. Since the initial description of *Wareolestes*, there has been disagreement about whether the holotype is an upper or lower molar (Hahn et al., 1991; Kielan-Jaworowska et al., 2004). The holotype of *Wareolestes rex* NHMUK PV M36525 was described as a lower molar by E. Freeman (1979), but Hahn et al. (1991) and Butler and Sigogneau-Russell (2016) suggested that it may be an upper molar, due to the presence of what appears to be a labial cingulum with ‘well developed labial cingular cusps’ (Kielan-Jaworowska et al., 2004, p. 179). Both of these features have been considered diagnostic for megazostrodontid upper molars, alongside partitioning of the labial cingulum into anterior and posterior lobes (Kielan-Jaworowska et al., 2004). If NHMUK PV M36525 represents an upper molar, then the surface considered to be the buccal side by E. Freeman (1979) would actually be the lingual side (Butler and Sigogneau-Russell, 2016; Figure 3.2.1).

Thanks to the in-situ placement of molars within the dentary in NMS G.2016.34.1, I can clarify the absence of a continuous lingual cingulid in the lower molars of *Wareolestes rex*. Unfortunately, the labial portion of the cingulid is not preserved in any of the molars of NMS G.2016.34.1. The specimen therefore provides no information on the morphology of the labial cingulid in *Wareolestes*. I cannot therefore, compare these cingular structures

with those of the holotype to evaluate the status of the holotype (NHMUK PV M36525) as an upper or lower molar based on the cingulum/cingulid. Nevertheless, I have re-examined the anatomy of NHMUK PV M36525 using microCT scanning (Figure 3.2.5). The resulting 3D models show that, due to the absence of enamel in the region of the 'labial' cingulum/cingulid (Figure 3.2.5A) there is no conclusive evidence for a continuous labial cingulum/cingulid, nor what can be described as 'well developed' labial cingular/cingulid cusps in the remaining dentine. The cingular cusps appear less well developed in NHMUK PV M36525 than they are in the upper molars of *Megazostrodon* (Crompton, 1974) or *Brachyzostrodon* (Hahn et al., 1991) based on the remaining dentine, and more closely resemble the size of the lingual cusps in lower molars of *Brachyzostrodon maior* (Hahn et al., 1991, fig. 2). Therefore, the preserved cingular morphology of NHMUK PV M36525 does not provide strong evidence of its identity as an upper molar.

Butler and Sigogneau-Russell (2016) referred a megazostrodontid molar from Kirtlington, NHMUK PV M46775, to *Wareolestes* sp. indet., identifying it as an upper. They suggested that the dorsoventrally longer cusps of this specimen, compared to the holotype NHMUK PV M36525, may indicate that this represents a distinct species of *Wareolestes*. I suggest that NHMUK PV M46775 may be an upper molar of *Wareolestes rex*. This is based on the presence of a prominent cingulid both labially and lingually, more developed 'labial' cusps than those in the holotype NHMUK PV M36525, and proportionally dorsoventrally longer cusps (see below) than the holotype. Consistent with this, Butler and Sigogneau-Russell (2016) suggested that *Wareolestes* upper molars were transversely wider than the lowers. The morphological difference between NHMUK PV M46775 and the holotype further supports my identification of the holotype as a lower left molar.

The m2 of NMS G.2016.34.1 strongly resembles the holotype specimen of *Wareolestes rex*, NHMUK PV M36525 (Figure 3.2.5). The m2 has similar proportions of cusps c and d and the posterior cingulid where it extends onto the lingual side of the tooth. The m2 of NMS G.2016.34.1 has a more expanded posterior cingulid than the cingulids on m1 or the holotype molar NHMUK PV M36525. The unerupted m3 crown in NMS G.2016.34.1 shows that it had an enlarged posterior portion of the cingulid, also similar to that of m3 but distinct from m1 and the holotype molar. This provides strong evidence of variation along the tooth row and suggests that the holotype molar, NHMUK PV M36525,

probably represents an m1 lower molar. The lingual cingulid in both NHMUK PV M36525 and m1 and m2 in NMS G.2016.34.1 tapers out directly below cusp a. Gow (1986) described the lower molars in *Megazostrodon* as having dorsoventrally taller cusps than the uppers; the molar cusp heights are proportionally similar between NMS G.2016.34.1 and NHMUK PV M36525 (Figure 3.2.5), consistent with the identification of NHMUK PV M36525 as a lower molar.

There are some small differences between NHMUK PV M36525 and the new specimen NMS G.2016.34.1, but most are the result of missing portions of enamel in the former, and the missing labial portion of the latter (Figure 3.2.6). For example, NMS G.2016.34.1 at first appears buccolingually narrower and the lingual molar surface slightly flatter. However, as already identified from differences between m1, m2 and m3 in NMS G.2016.34.1, there is variability in tooth morphology along the tooth row. Debuysschere et al. (2015) also noted variability in dental characters among Morganucodonta, such as features of the cingulum, related to position in the tooth row. They recommended that such characters should be treated with caution. What remains of the molars in NMS G.2016.34.1 supports this assertion. The paucity of megazostrodontid material, lack of enamel on the *Wareolestes* holotype, damage to the specimens, and intraspecific variation in cusp height and cingulum protrusion, suggests caution in treating these differences as anything other than intraspecific variation, and further supports my identification of NMS G.2016.34.1 as *Wareolestes rex*.

Brachyzostrodon lacks a distinguishable cusp g on the lower molars (Hahn et al., 1991; Crompton and Luo, 1993; Kielan-Jaworowska et al., 2004). The distinct wrinkling of enamel in *Wareolestes* and *Brachyozostrodon* could suggest a close relationship between these genera. However, I consider it unlikely that *Wareolestes* did not possess a cusp g on the lower molars, based on the strong morphological similarity between the holotype (above) (which possesses a cusp g in the apomorphic position buccal to cusp a) and the lower molars in NMS G.2016.34.1.

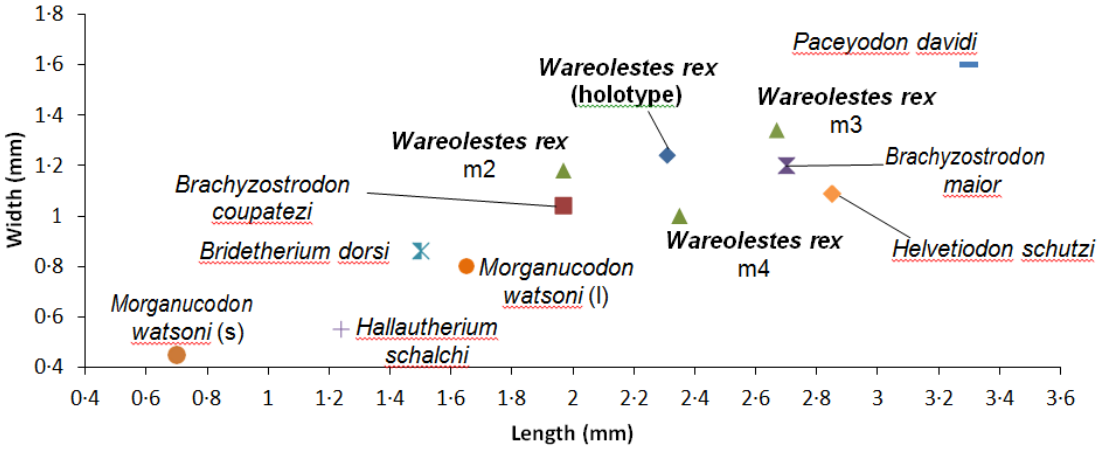

Figure 3.2.6: Lower molar measurements for new specimen and comparative material (see Table 3.2.1). Mean measurement from multiple specimens used for *Brachyzostrodon coupatezi*, *Bridetherium* and *Hallautherium*. Includes largest (l) and smallest (s) measurements for *Morganucodon watsoni* from Pacey (1978).

Pattern of dental replacement in Megazostrodontidae

NMS G.2016.34.1 provides information on the pattern of dental replacement in Megazostrondontidae, thanks to the presence of unerupted and partially erupted premolar and molar teeth, alongside fully developed teeth with complete roots for which no replacement tooth is present (Figure 3.2.3). Modes of dental replacement are important for understanding the origins of key aspects of mammalian oral processing. The precise occlusion between upper and lower teeth seen in morganucodontans, while still honed by wear after eruption, is closer to the more precise occlusion of the derived mammalian dentition (Kielan-Jaworowska et al., 2004; Luo et al., 2004). Critically, it is likely that such occlusion is only possible when rates of tooth replacement are reduced (i.e. diphyodont or single tooth generations).

It is considered beyond doubt that *Morganucodon* exhibited diphyodont replacement of antemolar teeth (incisors, canines, premolars) (Mills, 1971; Parrington, 1971; Crompton and Luo, 1993; Luo et al., 2004). Morganucodontans are considered to be the most early diverging mammaliaforms possessing this pattern of dental replacement (Mills, 1971; Parrington, 1973; Luo et al., 2004; Kielan-Jaworowska et al., 2004). This is in contrast to the more stemward mammaliaform *Sinoconodon*, which replaced its premolars once, but replaced the canine at least three times and replaced incisors in an alternating sequence, as

in many non-mammalian cynodonts (Crompton and Luo, 1993; Zhang et al., 1998). There is evidence for the resorption of anterior postcanines in mature individuals of *Morganucodon*, *Eozostrodon* and *Dinnetherium*, without replacement (Mills, 1971; Parrington, 1971; Crompton and Luo, 1993). This is a plesiomorphic cynodont characteristic also seen in early diverging taxa such as *Sinoconodon* (Crompton and Luo, 1993). There is no evidence to indicate such resorption in NMS G.2016.34.1. Gow (1986) argued that *Megazostrodon*, a morganucodontan, also replaced its anteriormost molars. There is clear evidence that, among morganucodontans, the molars in more posterior positions are never replaced, erupting as the individual reaches maturity as in most modern mammals (Parrington, 1971; Crompton and Parker, 1978; Luo et al., 2004; O'Meara and Asher, 2016). The wear facet patterns on many hundreds fragmentary mandibles of *Morganucodon watsoni* show no evidence of replacement in the posterior molars (Parrington, 1971; Young, 1982; Crompton and Luo, 1993); with molars frequently heavily worn in larger and older individuals, suggesting that they had not been replaced (Parrington, 1971). A similar observation has been made in four dentaries of *Megazostrodon* (Crompton, 1974; Gow, 1986) and eight dentaries of *Dinnetherium* (Jenkins et al., 1983). Gow (1986) suggested that *Megazostrodon* may have replaced its m2 due to this molar being less worn than m1 or m3 in two specimens from the Early Jurassic Elliot Formation, South Africa. However, Luo et al. (2004) considered the sample size too small to be definitive.

Our observations are consistent with the proposition that *Wareolestes*, a megazostrodontid morganucodontan, did not replace its molar teeth. I find no evidence for replacement for m1, m2 or m3 in NMS G.2016.34.1, despite the presence of replacement teeth more anteriorly along the tooth row. The m1 and m2 of this specimen have deep and well-developed roots that have not been even partially resorbed, and no portions of any replacement teeth are present at these loci. In contrast, the alveolus of p5 does not contain well developed roots or fragments thereof, suggesting that the preserved portion of p5 was an unerupted replacement tooth (Figure 3.2.3). In support of this hypothesis, I note that the preserved portion of p5 is located within the body of the jaw, roughly level with the emerging p4, indicating that this tooth was developing and erupting from the dentary at approximately the same time as p4.

NMS G.2016.34.1 provides evidence for specifically diphyodont replacement of the premolar teeth in *Wareolestes*, consistent with observations of *Morganucodon* (Young,

1982; Crompton and Luo, 1993). Premolar dp2/p2 comprises the roots of an erupted ‘milk tooth’ with the replacement premolar forming beneath. The alveoli for the deciduous premolars are clearly visible in the dentary, and the p4 remains within the dentary just ventral to the alveolar border.

Nevertheless, the pattern of dental replacement seen in *Wareolestes* is not identical to that described for *Morganucodon*. In both *Morganucodon*, and the more stemward mammaliaform *Sinoconodon*, premolar replacement occurs in a sequence from anterior to posterior (‘anteroposterior replacement’; Crompton and Luo, 1993; Zhang et al., 1998). However, in NMS G.2016.34.1 both preserved replacement premolars (p2, p4), and the preserved portion of p5, are located at approximately equal height within the dentary, indicating that anteroposterior replacement did not occur, or was only weakly manifested. Interestingly, p3 is represented only by an empty alveolus, and it is possible that the absence of a replacement p3 within the body of the dentary indicates a different timing of replacement at this locus. If correct, then this suggests possible alternate replacement of premolars in *Wareolestes*. Anteroposterior replacement of premolars is considered a derived character for Mammaliaformes (Rowe, 1988; McKenna and Bell, 1997). However, some stem therians and eutherian mammals developed alternating premolar replacement (Luo et al., 2004). Due to damage to the buccal side of the dentary, I do not consider there to be conclusive evidence for the sequence of premolar replacement in *Wareolestes*. As the anterior portion of the dentary is missing, NMS G.2016.34.1 also does not provide evidence on the replacement patterns of incisors or canines in *Wareolestes*.

3.3 Docodonta: *Borealestes serendipitus*

3.3a The Mandible and Dentition of *Borealestes*[3]

Docodonta are an extinct clade of mammaliaforms that fall outside the mammalian crown group, and are therefore important for understanding the morphological evolution of mammals as a whole (Simpson, 1929; Lillegraven and Krusat, 1991). Lillegraven and Krusat (1991) were the first to recognize that Docodonta have many autapomorphic features, and that they are a separate clade from Morganucodonta. They further posited that docodonts were more basal (stem-ward) than *Sinoconodon* and *Morganucodon* among 'mammals' (= Mammaliaformes of current terminology). However, in recent decades more complete cranial and skeletal material has led to the consensus that the Docodonta clade is closer to crown-group mammals than to *Sinoconodon* and Morganucodonta (Wible and Hopson, 1993; Luo, 1994; Luo et al., 2002; Martin, 2005). In some recent phylogenetic assessments of Mesozoic mammaliaforms, docodonts are more basal than Kuehneotheria (Gill, 2004) and haramiyidans (e.g., Luo et al., 2015a; 2017). It has been suggested that docodonts are more closely related to Late Triassic mammaliaforms such as *Tikitherium*, *Woutersia*, and *Delsatia*, but these hypothesized relationships are currently based on the isolated molars of these taxa, and are tentative at the best (Sigogneau-Russell and Hahn, 1995; Datta, 2005; Luo and Martin, 2007; Averianov et al., 2010).

All docodonts share a highly distinctive dental morphology, and they were one of the first mammaliaform clades to emerge across Eurasia in the Middle Jurassic (Lopatin and Averianov, 2005; Waldman and Savage, 1972; Luo and Martin, 2007). They are particularly abundant in fossil deposits of the Middle–Late Jurassic (Hu et al., 2006; Luo, 2007; Averianov et al., 2010; Martin et al., 2010; Meng et al., 2015; Rougier et al., 2015).

The postdentary elements—homologs to the mammalian middle ear—remain attached to the dentary in docodonts, a plesiomorphic characteristic in stem mammaliaforms (Lillegraven and Krusat, 1991; Ji et al., 2006; Luo, 2011; Meng et al., 2015). Nevertheless, docodonts are unique among Mesozoic clades in possessing distinctively complex molar

[3] Chapter 3.3a has been accepted for publication (25th April, 2019) as: Panciroli, E., Benson, R.B.J. and Luo, Z.-X. *in press*. The mandible and dentition of *Borealestes serendipitus* (Docodonta) from the Middle Jurassic of Skye, Scotland. *Journal of Vertebrate Paleontology*.

cusps and crests. It is generally accepted that docodont molars are capable of versatile shearing and crushing functions not seen in other Mesozoic mammaliaforms (Jenkins, 1969; Gingerich, 1973; Butler, 1997; Schultz et al., 2017). This may have contributed to their unusually diverse ecological specialisations. Docodonts are now known to have had very divergent locomotor morphologies, including semi-aquatic, fossorial, and arboreal specialisations, as revealed by well-preserved postcranial skeletons (Ji et al.,2006; Luo et al., 2015b; Meng et al., 2015).

Borealestes from the United Kingdom (Waldman and Savage, 1972; Sigogneau-Russell, 2003) is among the geologically oldest docodonts, being Bathonian in age. *Castorocauda* and *Agilodocodon* from China are also possibly from the latest Bathonian (Meng et al., 2015; Xu et al., 2017). The youngest record for Docodonta is *Sibirotherium* from the Lower Cretaceous of Russia (Maschenko et al., 2002). Docodonta were most diverse in the Middle Jurassic, and had a Laurasian distribution—this is with the possible exception of *Gondtherium* from Toarcian sediments in India (Prasad and Manhas, 2001, 2007). However, due to a paucity of material and poor preservation, the docodont affinities of *Gondtherium* are currently unresolved (Kielan-Jawarowska et al., 2004; Averianov et al., 2010).

The holotype of *Borealestes serendipitus* was discovered in the Kilmaluag Formation (Bathonian) of the Isle of Skye in the 1970s, and was the first Mesozoic mammal to be found in Scotland (Waldman and Savage, 1972). The holotype comprises a fragment of dentary, and three other dentary fragments were reported at the same time and referred to *B. serendipitus* by preliminary identification. These additional specimens are described here for the first time. A partial mammal skeleton of uncertain affinity was also collected from the Kilmalaug Formation in early 1970s. We can now confirm the identity of this specimen as *Borealestes serendipitus* herein, on the basis of its almost complete dentary, along with associated upper molars, and incisors. The characteristics of these parts of the fossil are described here (the rest of the skeleton is currently under study by E.P.; Panciroli et al., 2018b, in press).

Isolated molars of *B. serendipitus* were later recovered from the Forest Marble Formation in Kirtlington (Sigogneau-Russell, 2003) and Watton Cliff (Evans, 1992) in England, all Bathonian (Middle Jurassic) in age. A second species, *B. mussettae*, was later erected based on molars from Kirtlington (Sigogneau-Russell, 2003). Multiple specimens

from Kirtlington have been referred to *B. serendipitus* and *B. mussettae*, but not all specimens have been fully described.

Additional specimens of *Borealestes serendipitus* have been recovered during recent field work on the Isle of Skye, along with several other Mesozoic mammaliaforms, including the cladotherian mammal *Palaeoxondon ooliticus* and the morganucodontan *Wareolestes rex* (Close et al., 2016; Panciroli et al., 2017b, 2018a, b, in press). Material found during field work in 2016 includes another dentary of *Borealestes* (NMS G.2018.27.1, found by E.P.).

We re-examine previously collected material and combine it with newly collected specimens. We provide a full description of the dental and mandibular morphology of *Borealestes serendipitus*. This includes: the complete lower dentition and dental formula; postdentary trough and its related structures; Meckel's groove; efflected angular process; dentary peduncle; and nerve and blood vessel channels within the dentary. Based on this body of new information we provide a revised and expanded diagnosis for the genus *Borealestes*, and distinguishing features of *B. serendipitus* and *B. mussettae*. We have also reviewed the material for *Borealestes* in light of this diagnosis, and updated the referred specimen lists accordingly. We find evidence for ontogenetic changes in mandibular structures, as recently described in *Docodon* (Schultz et al., 2017). The more complete documentation of the dental and mandibular morphology of *Borealestes* provides new characters for an updated phylogenetic analysis of all docodonts including *Borealestes*.

3.3a i) Materials and Methods

Most of the micro-computed tomographic data (micro-CT) were obtained at the University of Bristol using a Nikon XTH225ST scanner with a 225kV rotating target with a peak energy of 140 kV. Resolution varies between specimens: BRSUG 20570, BRSUG20571, BRSUG29007, and NMS G.1992.47.121.4 are 6.77 µm; and NMS G.1992.47.121.3 is 12.77 µm. Synchrotron data for NMS G.2018.27.1 and NMS G.1992.47.121.1 were obtained at the European Synchrotron Radiation facility (ESRF), Grenoble, France. The resolution for NMS G.2018.27.1 is 6.35 µm. For NMS G.1992.47.121.1 the scan resolution was 6.15 µm, which was subsequently resampled to

12.3 µm. All microCT and synchrotron scans were digitally reconstructed and image processed using Mimics 19.0 at the National Museum of Scotland, Edinburgh. Specimens were also observed using conventional microscopy. All digital reconstructions can be found in the online depository at www.morphosource.org.

Measurements were taken from digitally reconstructed microCT scans in Mimics 19.0. It is unclear in previous studies how molar measurements were taken, so in order to standardise our measurements, we measured as follows (Figure 3.3a.1): for lower molar length we measured across the length of the tooth anteroposteriorly from cusps d to b, and cusps df to e; for upper molar length we measured the longest length on the labial part of the molar, and the longest on the lingual wing of the molar. For lower molar width we measured mediolaterally across cusp c, and across cusp g at right angles (in occlusal view) to the length measurement from cusp d to cusp b. For width of upper molars we measured across cusp X to midway anteroposteriorly along the buccal edge of the molar. Premolar and canine tooth measurements were taken anteroposteriorly from most anterior to most posterior edge of the crown, and mediolateral width was taken across the cusp of the tooth at the base of the crown. Although the latter width was not always the widest due to slight bulging of the cingulid in the premolars, measuring in this way provides a more consistent measurement and the difference was usually ≤ 0.1 mm. See Appendix 3 for usage of our dental terminology for docodonts.

We analyzed the character matrix used by Meng et al. (2015) including updated and rescored character states for *Borealestes serendipitus* and *Borealestes mussettae*. This data matrix has 23 taxa (24 with *B. mussettae*) scored for 48 characters of the dentary (47 in the original matrix, with one additional character), and upper and lower dentition. Of these taxa, fourteen are docodonts and nine are other mammaliaforms, including *Gondtherium*, a disputed docodont (Averianov et al., 2010), which is now found to fall outside of Docodonta (Meng et al., 2015).

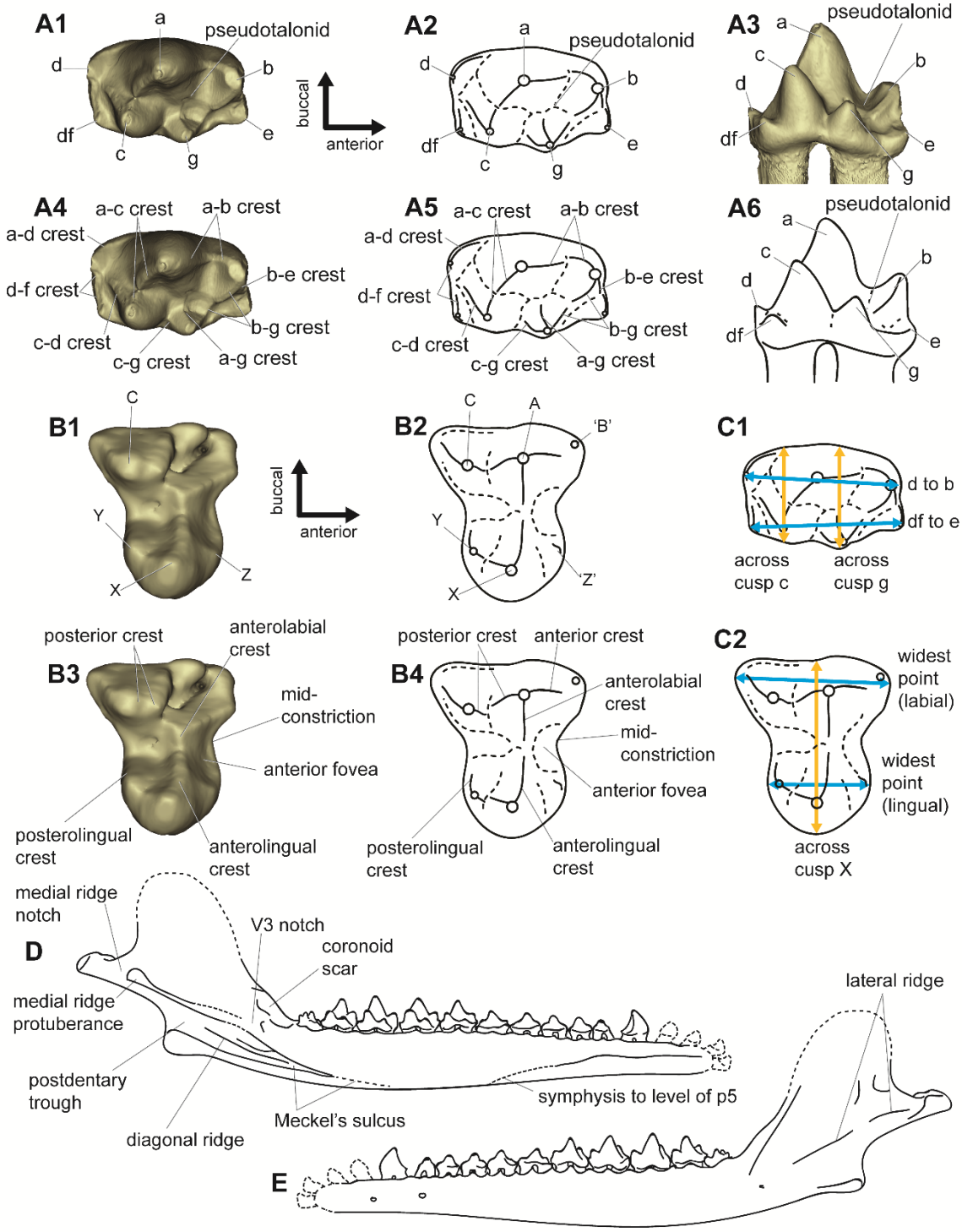

Some character states for the other taxa in the matrices provided in Meng et al. (2015) differed between the character listing, NEXUS and PAUP sections of their supplementary materials. Therefore, we re-assessed all of these character states for this analysis (Appendices 8-13).

We analyzed these data as for Meng et al. (2015), using PAUP* 4.0. A branch-and-bound tree search was conducted using parsimony with characters unordered and equally-weighted. One most parsimonious tree of 117 steps was retained. Our time-scaled phylogeny was created in R using the strap package. First and last appearance data (FADLAD) were taken from fossilworks.org, except for *Borealestes* species, where stratigraphic dates of formations were used from Holloway (1983) and Barron et al. (2012). The stratigraphic ages of the Chinese docodonts *Docofossor*, *Castorocauda*, and *Agilodocondon* were adopted from Xu et al. (2017).

Terminology

We follow Luo and Martin (2007) in the designation of cusps with letters, and using abbreviated crest designations according to their connections to cusps, combined with topographic descriptors to specify their locations on the tooth (Figure 3.3a.1). This nomenclature is based on a combination of alphabetical nomenclature from Butler (1997), and descriptive definitions from Sigogneau-Russell (2003), supplemented by Kielan-Jaworowska et al. (2004) and Pfretzschner et al. (2005). In addition, we provide a table of descriptive definitions as used by previous authors in Appendix 3. We preferentially use 'buccal' throughout the descriptive text, but retain the use of 'labial' for some terminology to provide ease of comparison with previous publications.

3.3a ii) Description

SYSTEMATIC PALEONTOLOGY

MAMMALIAFORMES Rowe, 1988 (emended)

DOCODONTA Kretzoi, 1946

Figure 3.3a.1 (previous page): Terminology of molar and mandibular morphologies of *Borealestes*. **A**, lower molar cusp terminology (left molar): **A1**, occlusal; **A2**, occlusal diagrammatic; **A3,** lingual view. Lower molar crest terminology: **A4**, occlusal; **A5**, occlusal diagrammatic; **A6**, lingual view. **B**, upper molar cusp terminology (right molar): **B1**, occlusal; **B2**, occlusal diagrammatic. Upper molar crest terminology: **B3**, occlusal; **B4**, occlusal diagrammatic. **C**, molar measurements (measurements listed in Table 3.3a.1): **C1**, lower molar measurements; **C2**, upper molar measurements. Figures based on lower m3 of holotype BRSUG 20570, and upper M3 of NMS G.1992.47.121.1. **D**, restoration of complete mandible in medial view; **E**, restoration of mandible in buccal view. **D** and **E** based on composite of specimens herein, incisors (dashed) based on *Agilodocodon.* Not to scale.

DOCODONTIDAE Simpson, 1929

BOREALESTES Waldman and Savage, 1972

Revised Diagnosis: Dental formula 4.1.?5.4/ 4.1.5.6. Upper molars of *Borealestes*: buccolingually wide and mesiodistally short; upper molars 'figure 8' shape, with anteroposteriorly constricted waist; two main buccal cusps, A and C, plus a small cusp B in the buccomesial corner; lingual half of the upper molar has main anterior lingual cusp X; cusp X larger and more prominent than smaller posterior lingual cusp Y; labial cusps connected by a ridge/ridges anteroposteriorly; transverse ridge extends between the main anterior labial cusp A and the main lingual cusp X. Lower molars: elongated anteroposteriorly, with labial row of higher cusps arranged in anterioposterior alignment with largest cusp a, and lingual row of smaller cusps with distinctive anterior cusp g and larger posterior cusp c; lower molars have cusps b–a–c in a triangular arrangement. Docodonts differs from other mammaliaforms but similar to pseudotribosphenids in possessing an anterior 'pseudotalonid basin'—anterior to the 'trigonid'—formed by cusps a, b, and g. Docodonts possess the plesiomorphic mammaliaform trait of attachment of postdentary elements to the dentary. *Borealestes* has an efflected angular process (sensu Simpson, 1929) and an enlarged medial ridge protuberance (sensu Schultz et al., 2017), both are docodont autapomorphies. *Borealestes* possesses enlarged and pointed upper and lower canines that are two-rooted, as in other docodonts.

Among docodonts, *Borealestes* most closely resembles *Krusatodon, Castorocauda,* and *Haldanodon* in lower molar morphology. These taxa share the derived feature of a larger cusp c than cusp g. It resembles *Castorocauda* and possibly also *Itatodon* in having a slightly recurved cusp c. *Borealestes* possesses an anterior 'cingulid' on the lower molars incorporating cusp e, similar to *Castorocauda* and *Docodon*. Cusp e is anteriorly projecting and forms part of the d–df-e interlock with the neighbouring molar, as in *Krusatodon* and *Simpsonodon*. On the premolars *Borealestes* has a distinct lingual cingulid and a posterior labial cingulid, as seen in most other docodontans. Unlike *Simpsonodon, Agilodocodon*, and *Docodon*, but like most other docodonts, *Borealestes* does not have dense creases and pits or other ornamentation on molar enamel surfaces. *Borealestes* species have a very distinctive a–c crest.

In upper molar morphology, *Borealestes* differs from all other docodonts except *Docodon* in having an anterior fovea: a concave area anterior to the anterolingual crest.

Borealestes differs from *Docodon* in having the anterior fovea positioned at the anteroposteriorly constricted waist of the upper molars. *Borealestes* differs from *Krusatodon*, *Agilodocodon*, *Simpsonodon*, *Docodon*, and *Haldanodon* in having transversely expanded and anteroposteriorly slightly compressed lingual wing of the upper molar, which is similar to *Docofossor* and *Dsungarodon*. The posterior upper molars are similar to *Haldanodon*, *Docofossor*, to some extent also to *Docodon*. *Borealestes* resembles *Docofossor* and *Dsungarodon* in having more reduced cusps Y and Z on the upper molars, and a larger cusp X.

BOREALESTES SERENDIPITUS Waldman and Savage, 1972

Holotype: BRSUG 20570, fragment of left dentary from the Kilmaluag Formation, Isle of Skye.

Referred Specimens: BRSUG 20571 fragment of left dentary; BRSUG 29007 fragment of right dentary; BRSUG 29008 three fragmentary molars in matrix, all from the Kilmaluag Formation, Isle of Skye. NMS G.1992.47.121.1, partial skeleton that includes upper molar rows and some incisors; NMS G.1992.47.121.3, almost complete right dentary detached from NMS G.1992.47.121.1; NMS G.2018.27.1, fragment of right dentary in matrix; NMS G.1992.47.121.4 (previously BRSUG 29006) anterior upper incisors, premaxilla, and nasal fragment—all from the Kilmaluag Formation, Isle of Skye.; OUMNH J.79474, OUMNH J.79475, and OUMNH 79498, all isolated lower molars, all from the Forest Marble Formation of Kirtlington, Oxfordshire. Lower molars NHMUK PV M46039, NHMUK PV M46521, NHMUK PV M46549, NHMUK PV M46610, NHMUK PV M46632, NHMUK PV M46728, NHMUK PV M46791, NHMUK PV M46841, NHMUK PV M46842, NHMUK PV M46845, NHMUK PV M46869, NHMUK PV M46389, NHMUK PV M46399, NHMUK PV M46401, NHMUK PV M46588, and upper molars NHMUK PV M46316, NHMUK PV M46396, and possibly NHMUK PV M46607 (uncertain), all from the Forest Marble Formation of Kirtlington, Oxfordshire. NHMUK PV M46058, NHMUK PV M44301, and probably NHMUK PV M46116, all lower molars from the Forest Marble Formation of Watton Cliff, Dorset. (The following specimens were referred to *B.* serendipitus, but are re-identified herein: OUMNH J.79446 re-identified as *Krusatodon* or *Simpsonodon*, OUMNH 79497 re-identified as *Simpsonodon*; OUMNH J.79514 re-identified as *Krusatodon*; NHMUK PV M46580 re-identified as *B. mussettae*; NHMUK PV

M46445 possibly *Krusatodon*; NHMUK PV M46066 not *B. serendipitus*, but identification uncertain. See Appendix 7 for details).

Revised Diagnosis: *Borealestes serendipitus* differs from all other docodonts and from *B. musettae* in that the primary cusp a has a rounded surface and as result an absence of the a–g crest on cusp a (present to variable extent on cusp g) and the absence of an a–d crest on cusp a (but a labially oriented a–d crest is present on cusp d). *B. serendipitus* has a stronger and more elevated b–g crest and c–d crest, than *B. mussettae*. Cusp e in *B. serendipitus* is positioned more lingually than in *B. mussettae*. *Borealestes serendipitus* differs from *B. mussettae* in having a distinct anterolabial and anterolingual crest between cusps A and X in the upper molars, and in that cusp Z is reduced. The anterior fovea is more distinct than in *B. mussettae*.

Description

Upper Tooth Row: NMS G.1992.47.121.4 is a rostral skull fragment consisting of the premaxillae and a part of one nasal of *Borealestes serendipitus*. This component belongs to the same partial skeleton as the upper molars (below), NMS G.1992.47.121.1 (currently under study by E.P.). This skull component became separated from the rest of the skeleton in the 1980s, after collection of this fossil in the field in the early 1970s. It was accessioned to the University of Bristol (as BRSUG 29006), but was subsequently relocated to National Museums Scotland where the rest of the skeleton is held.

The premaxilla of NMS G.1992.47.121.4 has the right I1 and I2 and a partial root of I3, the left I2 root, and the complete left I3 and I4 (Figure 3.3a.2). Combining the information from the right and the left incisors, we determine that *B. serendipitus* possesses four upper incisors. It has a single-rooted I1 with a leaf shaped crown, which has a convex external (buccal) surface and a concave internal (lingual) surface with a lingual cingulum (Figure 3.3a.2A1, C1, C2). The roots of I2 to I4 are deeply bifurcated, diverging at their tips. This bifurcation is similar to that seen in *Agilodocodon* (Meng et al., 2015:fig. s2) and *Haldanodon* (Krusat, 1980). The crowns of I2 to I4 are caniniform in lateral outline: they

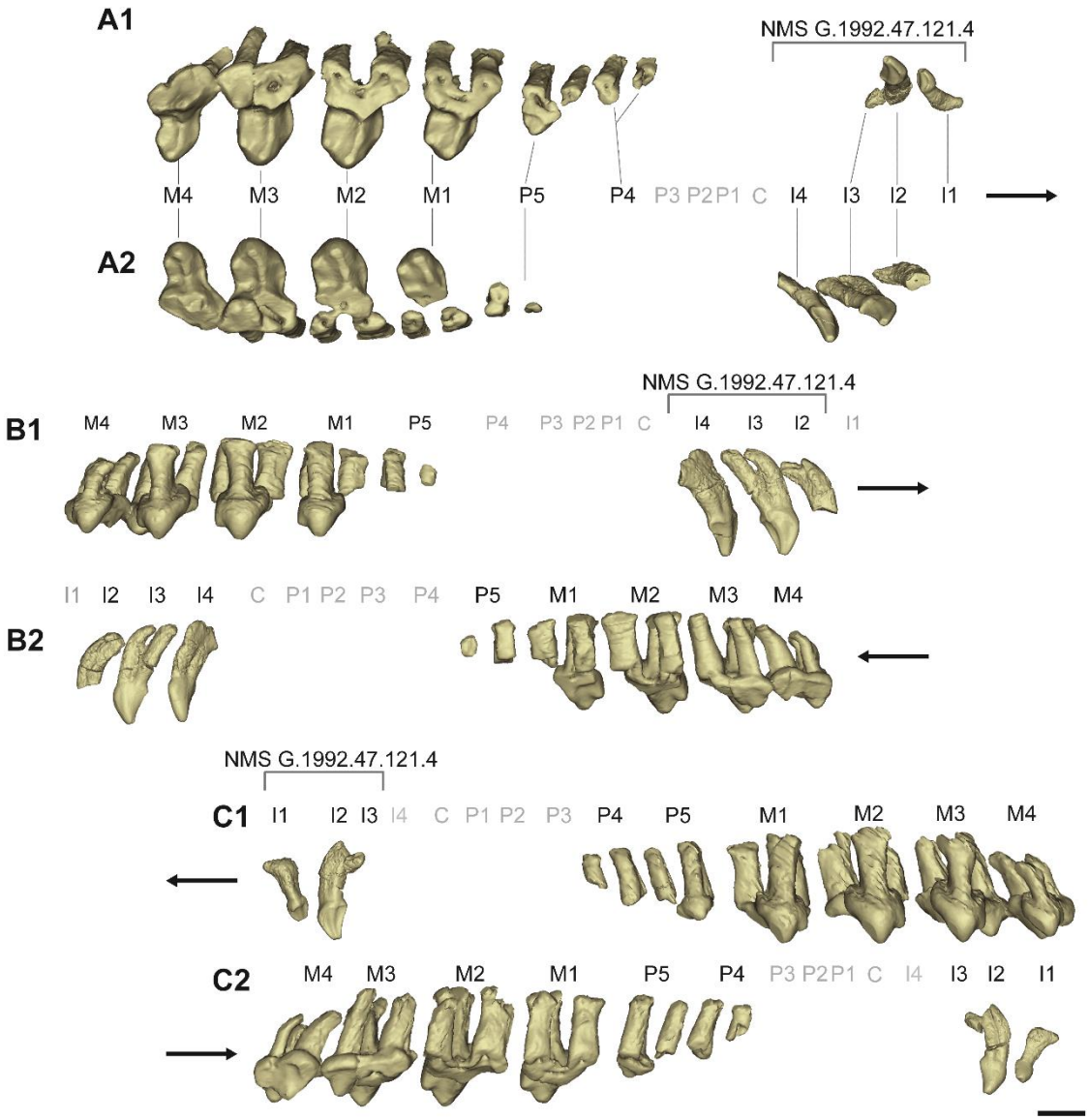

Figure 3.3a.2: *Borealestes serendipitus* upper dentition. Composite upper tooth row from NMS G.1992.47.121.1 (molars and premolars), and from NMS G.1992.47.121.4 (incisors). **A1**, right tooth row occlusal view; **A2**, left tooth row occlusal view; **B1**, left tooth row lingual view; **B2**, left tooth row buccal view; **C1,** right tooth row lingual view; **C2**, right tooth row buccal view. Digital reconstructions from micro-CT scans. Letters in gray indicate tooth positions represented by empty alveoli of lost teeth. Arrows in bold indicate anterior direction. Scale bars equal 1 mm.

are recurved, and the anterior edge of the tooth is convex and smooth. The buccal aspect of I2–I4 is gently convex and the lingual aspect is broadly concave with a ridge running from the apex of the crown to the base. There is a weak lingual cingulum with a small cuspule on

the posteriormost edge, which connects to the incisor apex via a curved low ridge. This overall morphology of upper incisors of *Borealestes* is similar to *Agilodocodon.*

The upper molars and premolars preserved with the partial skeleton of *Borealestes serendipitus* NMS G.1992.47.121.1 include: roots of right P4 and P5, and almost complete M1 to M4 (Figure 3.3a.2A1); and the partial roots of left P5, and almost complete M1 to M4 (Figure 3.3a.2A2) (for tooth measurements see Table 3.3a.1). The premolar-molar boundary in *Borealestes* (as for docodonts as a whole) can be clearly defined as two roots for the ultimate premolars and three roots for the first molar, which we also observe here.

The molars are transversely wide and have a figure-of-eight shaped outline in occlusal view. This occurs due to the anteroposterior mid-point constriction of the molar, which creates a distinct lingual wing (Figure 3.3a.2A1, A2). The lingual wing comprises a large cusp X, a smaller, more posterior cusp Y, and a much smaller cusp Z positioned on the anterior cingular margin of the tooth. The labial portions of the molar crown on right M1–3 and on left M1–3 are missing due to wear after exposure in the field. The buccodistal corner of M3 on both sides is preserved, and the M4s are well preserved. Although the left and right M3s are missing cusp A, the broad base of this cusp indicates that it is larger than cusp C, and both are positioned in anteroposterior alignment (Figure 3.3a.2A1, A2). A transverse crest connects cusps A and X. This crest is nearly continuous and is made up of the anterolabial and anterolingual crests. The transverse crest leading from cusp Y is not distinct, and only extends to the midpoint constriction of the crown. This crest does not extend further buccally and has no connection to the rounded cusp C or the buccodistal cingulum.

M4 is reduced, especially mesiodistally, and as such it is smaller than M3. M4 has a much reduced cusp C. Cusps A and C are joined by a short A–C crest, and both cusps are more lingually positioned, than on the preceding molars.

We infer that in all upper molars, there is an anterior crest running from cusp A to the position of an indistinct ‘cusp B’, as best seen in the right M3 (Figure 3.3a.2A1). This feature is incomplete in some upper molars where this region is broken/abraded. The upper molars have a buccal cingulum, which takes the form of a thin line, rather than a fully formed crest. The buccal margin is indented by an ectoflexus. The buccal cingulum is also present in what remains of both M3.

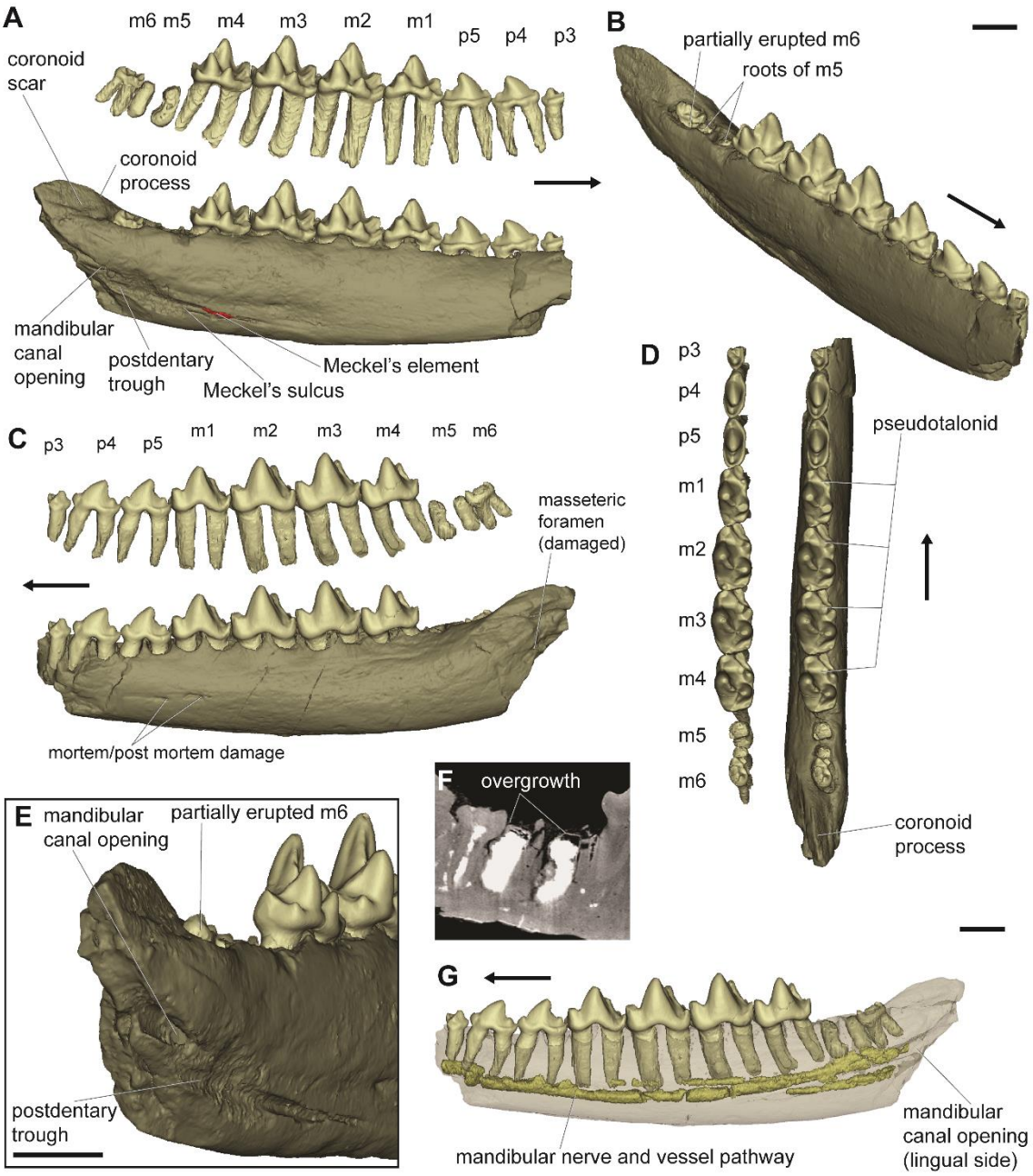

Figure 3.3a.3: *Borealestes serendipitus* BRSUG 20570 (holotype), partial left dentary. **A**, lingual, **B**, anterolingual, **C**, buccal, and **D**, occlusal views of the dentary and dentition. **E**, posterolingual view showing the opening for mandibular canal and relationship to postdentary trough. **F**, micro CT scan slice showing the possible overgrowth of m5 roots suggesting pre-mortem tooth loss. **G**, buccal view of dentary semi-transparent with segmented mandibular nerve and vessel pathway inside the dentary. Digital reconstructions from micro-CT scans. Arrows in bold indicate anterior direction. Scale bar same for **A**–**D** and **G**. Scale bars equal 1.

There is a distinct occlusal basin at the point of mid constriction, formed between cusps C and Y, and posterior to A–X crest, on all upper molars. This is functionally

analogous to the trigon basin of the tribosphenic upper molars. This is a general feature shared by most docodonts, with the exception of *Docofossor* (Luo et al., 2015b). There is a distinctly concave region anterior to the anterolabial and anterolingual crest (connecting cusps A–X), near the buccolingual mid-point of the crown. This is formed partly because of the mid-point constriction of the tooth and partly by the saddle-shape of the anterolabial and anterolingual crests. We have named this area the anterior fovea of the upper molars (Figure 3.3a.1B, 2, 7C–E). The anterior fovea is present in *Borealestes* and *Docodon*, but in *Docodon* the fovea is positioned more lingually on the anterior face of cusp X. We interpret the buccolingual midpoint position of the anterior fovea as a diagnostic feature of *Borealestes*.

A minor difference between M4 and more anterior molars is that the posterior half of M4 is more reduced such that the A–X crest almost becomes the transverse midline across the tooth crown (Figure 3.3a.2A1, A2). The M4 crown bears strong resemblance to the upper molars of *Haldanodon* by this placement of this crest, and by the mid-point constriction.

The molar crowns bulge outwards from the roots at their bases where they meet the alveolar margin (Figure 3.3a.2B1, C1). There are three roots per molar, and they are straight except for M4. The roots of M4 curve anteriorly, suggesting that during the eruption of this tooth, the tooth rotated, causing the bending of the roots. M4 roots are slightly shorter that the other molar roots. All of the upper molar roots widen towards their base in the maxillary alveolar margin. Roots of upper molars, especially the lingual root and posterior root, tend to have slightly inflated root-tips, indicating ontogenetic cessation of root growth.

Lower Tooth Row: The morphology of five dentaries including the holotype BRSUG 20570 confirm the diagnosis and morphology of *Borealestes serendipitus* (see Table 3.3a.1 for tooth measurements). The holotype comprises part of the left dentary containing the posterior root of p3, intact p4 and p5, and fully erupted m1 to m4 (Figure 3.3a.3). Although the crown of m5 is lost, the roots are in place within the dentary, and a hidden (but almost erupted) m6 is present (Figure 3.3a.3). Only a thin wall of bone separates the anterior alveolus of m6 and the posterior alveolus of m5. There is sign of bone regrowth just below the rim of the m5 alveolus (Figure 3.3a.3F), suggesting possible (traumatic) pre-mortem

loss of this molar. BRSUG 20571 is a fractured section of left dentary (Figure 3.3a.4A–E). It is broken anteriorly at the position of m1, and posteriorly behind the coronoid scar and depression that represents the entrance of the mandibular nerve (V3 notch). The roots of m1, roots and base of the crown of m2, the almost complete crown of m3, most of m4, and almost complete m5 remain in the dentary. The ultimate molar (m5) is much reduced in crown size, and the two roots are fused along much of their length, typical of the ultimate lower molars of docodonts. Only m3 has a preserved cusp a, m2–5 retain cusp b, and m3–5 cusp d. Most other cusps are broken or missing, but the preserved parts of these teeth show the clear morphology of *B. serendipitus*, including the distinct a–c crest, and the b–g crest with an absence of the a–g crest on cusp a.

BRSUG 29007 is an incomplete portion of right dentary (Figure 3.3a.4F–H). It is broken anteriorly at m1, and posteriorly just posterior to the coronoid scar. It has been extensively worn, although it is unclear whether this occurred as a result of pre-depositional transport, or during field exposure. Due to this wear, molars are identified by size (see Table 3.3a.1, and Appendix 4) and remaining morphological features. The posterior root of m1, the roots of m2, m3 to m4, and the roots of m5 and m6, are all present. The crowns of m3–4 are heavily worn, but the presence of a large cusp a lacking an a–g crest and possessing a strong a–c crest can still be distinguished on m4. The presence of these features helps to establish the specimen's identity as *Borealestes serendipitus*.

NMS G.2018.27.1 (Figure 3.3a.5) is an almost complete right dentary, still embedded in a small block of limestone matrix (Figure 3.3a.5B). The specimen has not been prepared, and only the posteriormost molars protrude from the surface of the block (Figure 3.3a.5A). The rest of the dentary is revealed through digital reconstruction of synchrotron CT scan data. The roots of i2 and i3 remain inside the alveoli, although the incisor crowns are missing, the canine is complete and double-rooted, p1, p2, and p5 are missing but their positions are represented by their alveoli. The posterior root of p3 remains inside the alveolus. The crown of p4 is present, although fractured in the mid-length of the tooth. Of the molars, m1 to m4 are present, and m5 crown is missing but its roots remain in the alveolus. The m3 crown is fractured and displaced, but still identifiable, while m4 is missing cusp a. The molars are otherwise intact, and possess a strong a–c crest and b–e crest, with the a–g crest absent on rounded cusp a: all are diagnostic features of *Borealestes serendipitus.*

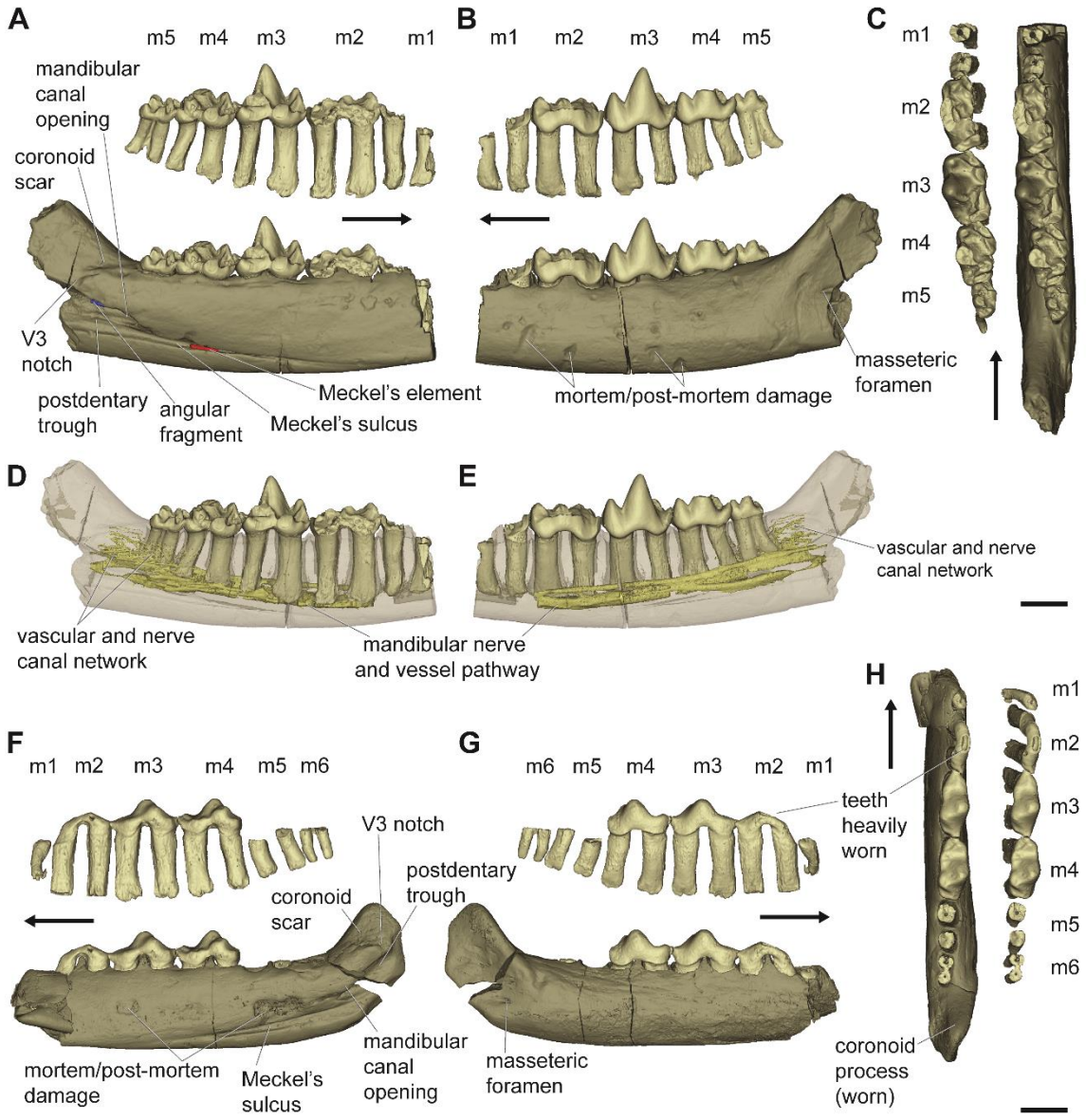

Figure 3.3a.4: *Borealestes serendipitus* BRSUG 20571 (partial left dentary), and BRSUG 29007 (partial right dentary). A, lingual, B, buccal, and C, occlusal views of the dentary and dentition of BRSUG 20571. D, lingual and E, buccal views of the dentary semi-transparent with segmented mandibular nerve and vessel pathway inside the dentary of BRSUG 20571. F, lingual, G, buccal, and H, occlusal views of the dentary and dentition BRSUG 29007. Digital reconstructions from micro-CT scans. Arrows in bold indicate anterior direction. Same scale throughout. Scale bars equal 1 mm.

NMS G.1992.47.121.3 is an almost complete right mandible (Figure 3.3a.6). It belongs to a partial skeleton, NMS G.1992.47.121.1 (currently under study by EP). It is complete except for the apex of the coronoid process and buccal surface of the incisor region. The incisors are missing, but exposed incisor alveoli indicate that the specimen had

four incisors, consistent with the count of incisor alveoli in NMS G.2018.27.1 (above). The roots of the canine remain in their alveoli, and the roots and some of the crown of p1 remain. The crowns of the rest of the remaining teeth are well-preserved, except for the missing tips of cusp a of m3 and m4. The molar morphology matches that of the holotype of *Borealestes serendipitus*, with distinct a–c and b–g crests, and an absent a–g crest on the rounded cusp a.

Dentary Morphology: The dentary of *Borealestes serendipitus* is gracile, as exemplified by NMS G.2018.27.1 and NMS G.1992.47.121.3 (Figure 3.3a.5, 6), similar to *Agilodocodon* (Meng et al., 2015). The most complete dentary, NMS G.1992.47.121.3, measures 23.3 mm in length from the alveolus of first incisor to the dentary condyle, which represents the complete length of the mandible. The body of the mandible of NMS G.1992.47.121.3 is between 0.9–1.2 mm in buccolingual width, and is 2.2 mm in dorsoventral depth below m3.

The mandibular symphysis of *Borealestes serendipitus* is vertically shallow, but anteroposteriorly long, and is indicated by a slightly rugose area on the medial surface of the dentary (Figure 3.3a.5C, 6A). The symphysis begins anteriorly in the incisor region, and continues posteriorly ventral to the canine and posteriorly to below p4–p5. The posterior extension of symphysis is similar to that of *Docodon* (Schultz et al., 2017).

There are three mental foramina on the buccal surface of the dentary, below i3–4, c, and p1, as seen in NMS G. 2018.27.1, NMS G.1992.47.121.3 (Figure 3.3a.5C, 6A). In BRSUG 20570 there are also two small nutritive foramina ventral to p5 and to m1, at around midheight dorsoventrally on the buccal surface of the dentary (Figure 3.3a.3C).

A very small nutritive foramen is present in the masseteric fossa, as seen in BRSUG 20570, BRSUG 20571, BRSUG 29007 and NMS G.1992.47.121.3 (Figure 3.3a.3C, 4B, G, 6B). Its position is low and it is not connected to the masseteric foramen, nor is the masseteric foramen large, unlike in zatherians such as *Peramus* (Davis, 2012). This appears to be a unique feature of *Borealestes*, as the same foramen is not present in the well preserved mandibles of *Docodon* (Rougier et al., 2015) or other docodonts (Meng et al., 2015).

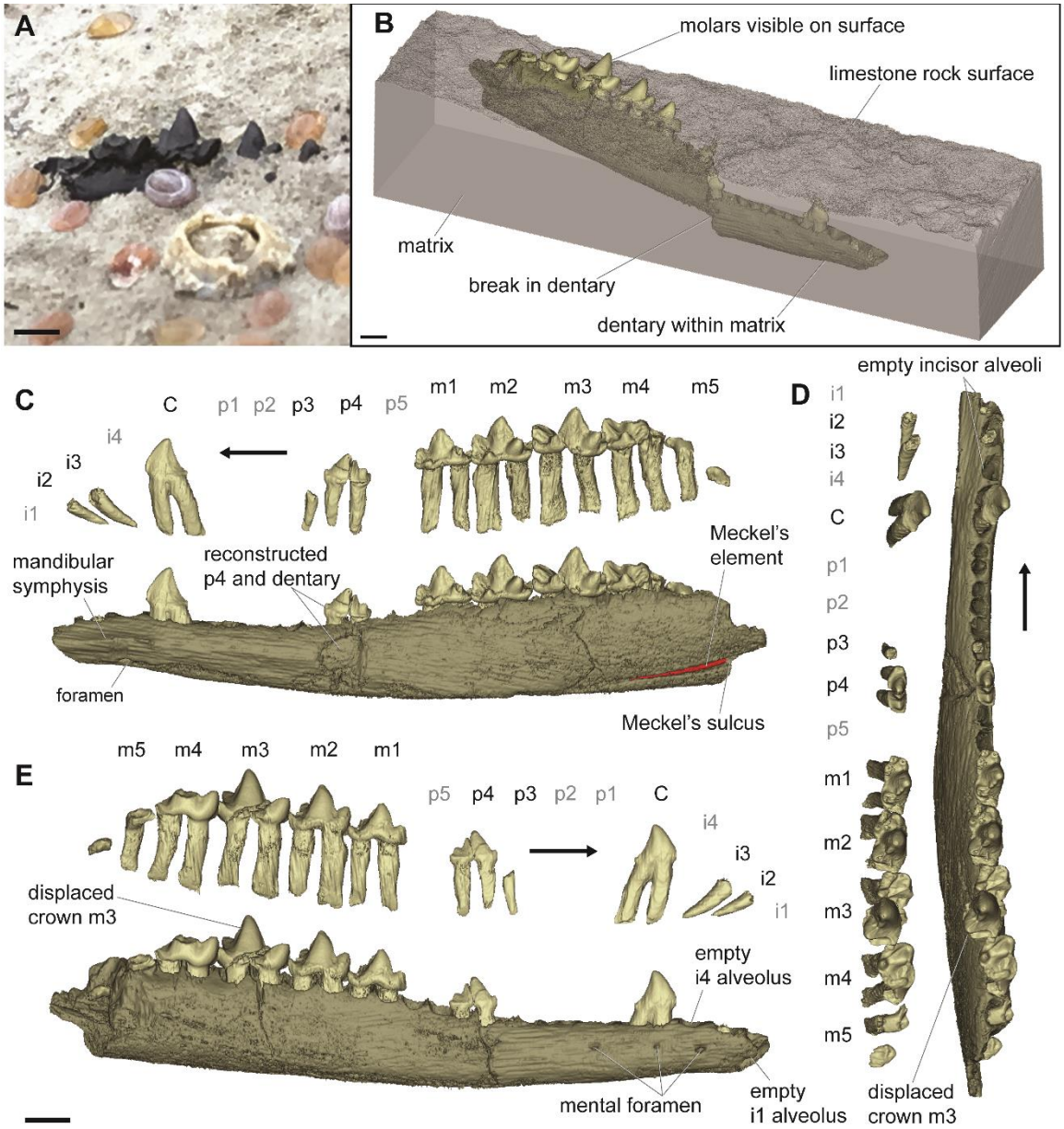

Figure 3.3a.5: *Borealestes serendipitus* NMS G.2018.27.1, partial right dentary. **A**, the jaw of NMS G.2018.27.1 as found in situ; **B**, digital reconstruction of dentary in matrix, showing original breakage at p4. Dentary reconstructed from micro CT scans and anterior and posterior portions re-aligned: **C**, lingual, **D**, occlusal, and **E,** buccal views of dentary and dentition. Letters in gray indicate tooth positions represented by empty alveoli of lost teeth. Arrows in bold indicate anterior direction. Same scale for **C**–**E**. Scale bars equal 1 mm.

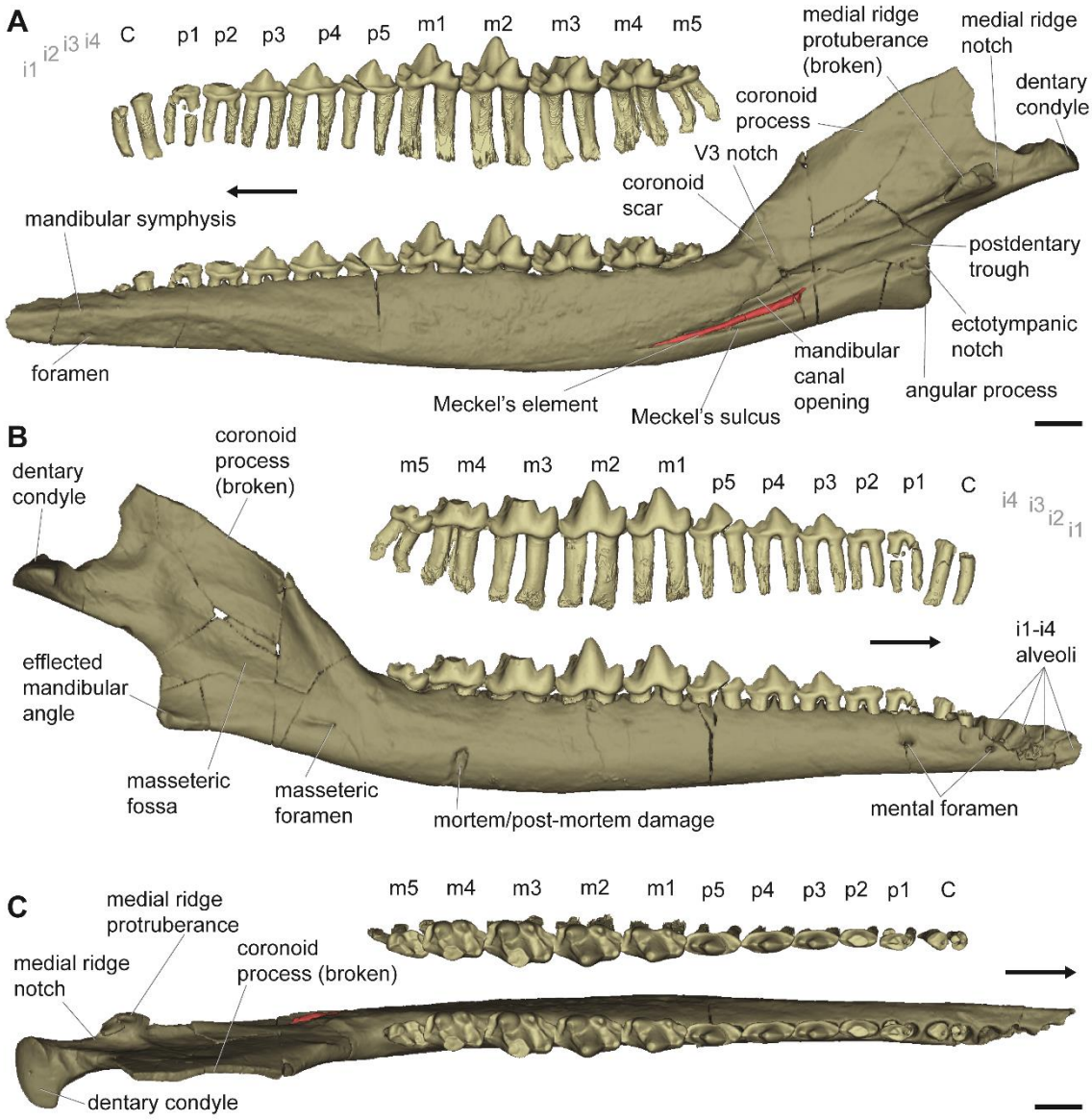

Figure 3.3a.6: *Borealestes serendipitus* NMS G.1992.47.121.3, almost complete right dentary. **A**, lingual, **B**, buccal, and **C**, occlusal views of dentary and dentition. Digital reconstructions from micro CT scans. Arrows in bold indicate anterior direction. Scale same throughout. Scale bars equal 1 mm.

The V-3 notch is located above the postdentary trough, posterior to the coronoid scar (Figure 3.3a.4F, 6A). The postdentary trough is dorsoventrally deep and clearly defined. Within the postdentary trough, there is a well-defined diagonal ridge (sensu Kermack et al., 1973) as in *Morganucodon* (Figure 3.3a.6A). The diagonal ridge is much better developed in *Borealestes* here than in *Docodon* (Schultz et al., 2017). There is an angular concavity or

notch, for receiving the hook-like reflected lamina of the angular bone, or the ectoympanic 'hook' as in *Castorocauda* and *Agilodocodon* (Ji et al., 2006; Meng et al., 2015).

The dorsal half of the trough is connected anteriorly to the mandibular canal. The mandibular canal is located ventral to the coronoid scar (Figure 3.3a.3A, 4A, F, 6A). The canal opening is connected to the postdentary trough in a deep groove defined by the diagonal ridge, best seen in NMS G.1992.47.121.3 (Figure 3.3a.6A). In well-preserved specimens, the mandibular canal can be traced inside the dentary, extending along the length of the mandibular body at the base of the tooth roots, on the buccal side of the root tips (Figure 3.3a.3G, 4D, E). In BRSUG 20571, a fine vascular network can also be traced posterior to and around the base of m5. This vascular network is near the position of the crypt for m6 in the (likely older) holotype of *Borealestes serendipitus*, BRSUG 20570. We hypothesise this may represent vascularization of the bone prior to the initial formation of the m6 tooth bud.

In BRSUG 29007, the alveolus of m6 is positioned anterior to the anterior margin of the coronoid process. In the growth series of *Docodon* (Schultz et al., 2017:fig 2), the ultimate molar in the juvenile mandible erupts medial to the coronoid process; but in successively older mandibles, the last molar shifts in relative position so that it is anterior to the coronoid process. Based on the shifting placement of the ultimate lower molar(s) in *Docodon*, the placement of the ultimate lower molar directly anterior to the coronoid process of the mandible in BRSUG29007 indicates that this individual of *B. serendipitus* was a fully grown adult.

The Meckel's sulcus is connected to the anterior end of the postdentary trough, and the sulcus starts from below the diagonal ridge and extends anteriorly to below the m4. Further anteriorly, it extends only 1 mm into the medial surface of the dentary. A faint line continues beyond this to the ventral surface of the dentary below m2.

The entrance to the mandibular canal is located dorsal to the Meckel's sulcus. The anteriormost extent of Meckel's sulcus varies between specimens, representing ontogenetic change in morphology (see Discussion). In BRSUG20570 the Meckel's sulcus extends from a point ventral to the mandibular canal opening and ends ventral to m3, stopping short of the ventral surface of the dentary. In BRSUG 29007 the Meckel's sulcus extends to a point ventral to m4, where it is reduced to a faint external groove. In NMS G.2018.27.1 the

sulcus is open and reaches anteriorly until a point ventral to m4. In all cases, the sulcus does not continue internally beyond the anteriormost point on the surface of the dentary.

Fragments of Meckel's element remain in the sulcus of all specimens except BRSUG 29007 (Figure 3.3a.3A, 4A, 5C, 6A). This is equivalent to the ossified Meckel's cartilage as identified for several extinct clades of crown group mammals (Luo, 2011; Meng et al., 2011). This element was identified as the prearticular in older literature (Kermack et al., 1973; Allin, 1975). As both the prearticular and the Meckel's element are anterior extensions of the articular (= malleus), these are synonymous terms for the homologous structure (Luo et al., 2017). The Meckel's sulcus ends anteriorly below m3, but continues as a faint external groove to meet the ventral surface of the dentary below m1 (Figure 3.3a.3A). A fragment of the postdentary complex remains in the post dentary trough in BRSUG 20571.

The anterior margin of the masseteric fossa along the coronoid process is distinct. There is an efflected angle of the angular process. The dentary condyle is a mediolaterally broad, projecting posteriorly on the dentary peduncle. In posterior view, the dentary condyle has a spindle shaped outline (Appendix 6). In lateral view, there is a low ridge extending from the dentary condyle along the dentary peduncle anteroventrally into the masseteric fossa (Figure 3.3a.6B). This is the lateral ridge, which is interpreted as the demarcation of the superficial masseter below and the deep masseter above (sensu Schultz et al., 2017). The peduncle sits above the line of the tooth row. What remains of the coronoid process is gracile, as is the whole dentary.

There is a strongly projecting medial ridge that overhangs the postdentary trough on the lingual side of the mandible (Figure 3.3a.6A). The ridge has a large protuberance, which appears to be curved dorsally, but close examination of the CT scan data shows this to be the result of a fracture along the flat shelf of the medial ridge, which has subsequently been glued into the incorrect anatomical position (pers. obs.) (Figure 3.3a.6A and Appendix 6). Therefore we interpret the apparent dorsally curved morphology is an artefact of post-mortem distortion.

The medial ridge ends at the protuberance, and there is a distinct and broad notch between the protuberance and the dentary peduncle, which is termed the medial ridge notch (Figure 3.3a.6A). This notch is present in *Docodon* (Schultz et al., 2017), but it appears to

be more pronounced in *Borealestes.* The medial ridge lessens at the V3 notch, just posterior to the coronoid scar (Figure 3.3a.6A).

BOREALESTES MUSSETTAE Sigogneau-Russell, 2003

Borealestes mussetti Sigogneau-Russell, 2003; Averianov, 2004:3 (emended gender).

Holotype: NHMUK PV M46495 right lower molar from the Forest Marble Formation at Kirtlington, Oxfordshire.

Referred Specimens: NHMUK PV M46224, NHMUK PV M46239, NHMUK PV M46001, NHMUK PV M46066, NHMUK PV M46836, NHMUK PV M46319, NHMUK PV M46809, and NHMUK PV M46835, all lower molars, and NHMUK PV M46394, NHMUK PV M46448, NHMUK PV M46580, and NHMUK PV M46871, all upper molars from the Forest Marble Formation at Kirtlington, Oxfordshire. NHMUK PV M46001 lower molar from Watton Cliff, Dorset. (NHMUK PV M46401, NHMUK PV M46389, NHMUK PV M46588 were previously referred to *B. mussettae*, but are re-identified as *B. serendipitus* herein). NHMUK PV M46404 and NHMUK PV M46204 were referred to *B. mussettae,* but lack clear diagnostic features below the level of order. Previously assigned to *B.mussettae*, but unavailable for confirmation NHMUK PV M46796.

Revised Diagnosis: Diagnosis for the genus *Borealestes* as for *B. serendipitus* (above). *B. mussettae* (Figure 3.3a.7B, D, E) differs from *B. serendipitus* in lower molar morphology in that the a–g crest is present on both cusp g and cusp a, and in having a strong a–d crest on cusp a—both features are absent on cusp a in *B. serendipitus*. Cusp g is slightly more developed in *B. mussettae*, and cusps g and c are placed further apart mesiodistally than in *B. serendipitus*. *Borealestes mussettae* has an anterior lingual cingulid that passes below cusp g to the midway along the molar mesiodistally. The df cusp is more developed in *B. mussettae* than in *B. serendipitus,* and is distinct from the d cusp. Cusp e is positioned in alignment with the anteroposterior axis of the molar, whereas cusp e is lingual of the anteroposterior axis on molars of *B. serendipitus* (Figure 3.3a.7).

Although *B. mussettae* resembles *B. serendipitus* in most features of upper molars, *B. mussettae* is distinctive in having a more rounded cusp A so that there is no anterior crest and no anterolabial crest on cusp A. *B. mussettae* is also distinguishable from *B. serendipitus* in having a short anterolingual crest on cusp X, with a cuspule on the crest.

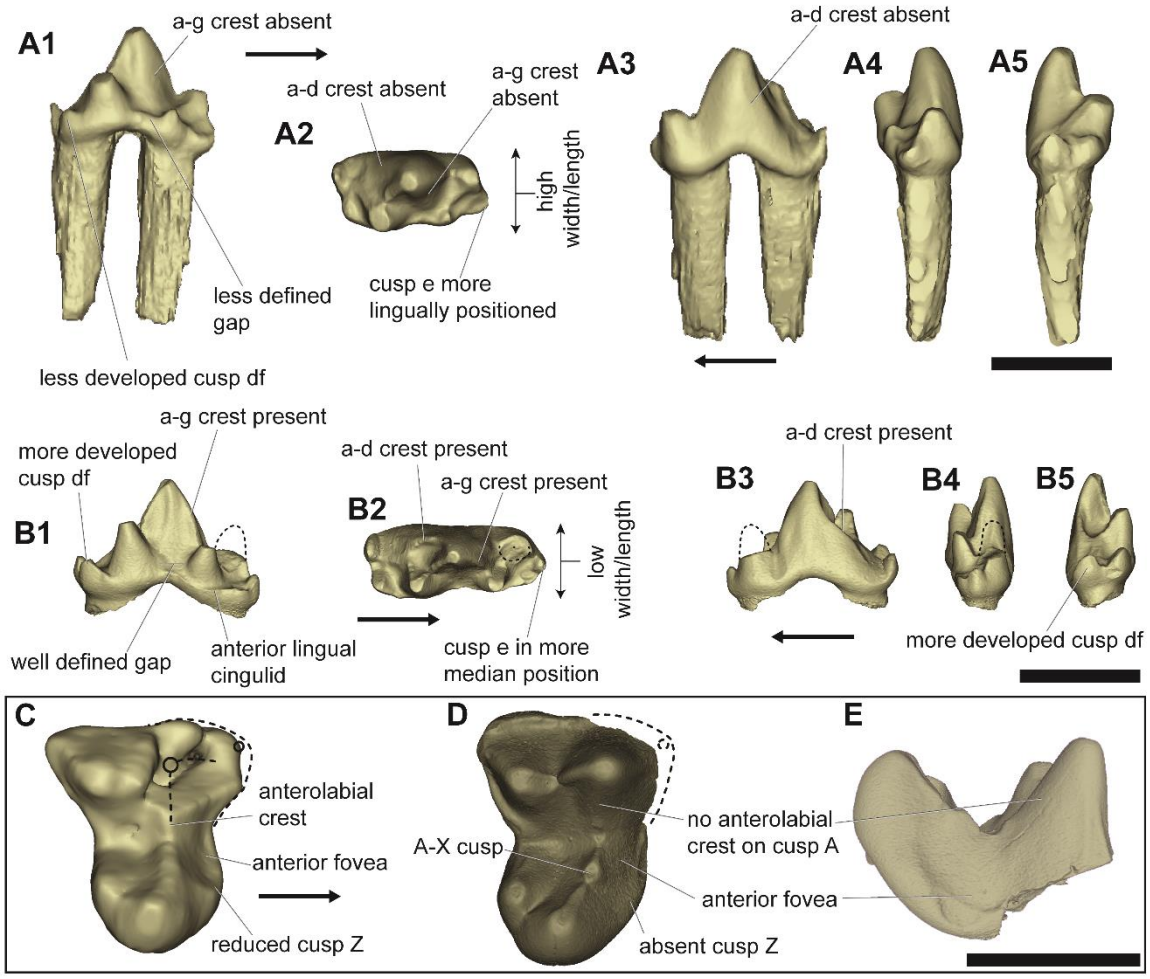

Figure 3.3a.7: Distinguishing characters of *Borealestes serendipitus* and *B. mussettae.* **A**, and **B**, lower molar characters. **A**, *Borealestes serendipitus* based on m1 of holotype BRSUG 20570: **A1**, lingual, **A2**, occlusal, **A3**, buccal, **A4**, anterior, and **A5,** posterior views of molar. All **B**, *B. mussettae* based on holotype NHMUK PV M46495, but crack through cusp a is repaired, and molar mirrored to facilitate comparison: **B1**, lingual, **B2**, occlusal, **B3**, buccal, **B4**, anterior, and **B5**, posterior views of molar. **C**, **D**, and **E,** distinctive upper molar characters for each species of *Borealestes*: **C**, M3 of *B. serendipitus*, NMS G.1992.47.121.1; **D**, *B. mussettae*, NHMUK PV M46871; **E**, *B. mussettae*, NHMUK PV M46871 in anterior view. **D** and **E** mirrored to facilitate comparison. Digital reconstructions from micro-CT scans. Dotted lines indicate missing portions of tooth. Arrows in bold indicate anterior direction. Same scale for **A**–**B**, and same scale for **C**–**E**. Scale bars equal 1 mm.

Cusp Z is reduced to absent relative to *B. mussettae*. The anterior fovea is less distinct in *B. mussettae* than in *B. serendipitus* (Figure 3.3a.7D, E).

Table 3.3a.1: Measurements of *Borealestes* lower dentition. Measurements in italics are from broken specimens. Dashes indicate missing teeth or tooth portions prevented measurement from being taken. See Figure 3.3a.1 for measurement methodology.

	All in mm		c	pm 1	pm 2	pm 3	pm 4	pm 5	m1/M 1	m2/M 2	m3/M 3	m4/M 4	m5/M 5	m6
BRSUG 20570	Length	d to b	-	0.97	1	1.2	0.97	1	1.2	1.32	1.32	1.2	-	0.61
		df to e	-	0.97	1	1.19	0.97	1	1.19	1.33	1.29	1.17	-	0.55
	Width	cross c	-	-	-	-	0.45	0.45	0.65	0.79	0.8	0.74	-	0.36
		cross g	-	-	-	-	0.45	0.45	0.57	0.76	0.84	0.82	-	0.37
BRSUG 20571	Length	d to b	-	-	-	-	-	-	-	1.66	1.67	1.37	0.81	-
		df to e	-	-	-	-	-	-	-	1.6	1.6	1.37	0.78	-
	Width	cross c	-	-	-	-	-	-	-	-	*0.94*	0.73	0.42	-
		cross g	-	-	-	-	-	-	-	-	0.99	0.86	0.56	-
BRSUG 29007	Length	d to b	-	-	-	-	-	-	-	-	*1.37*	*1.35*	-	-
		df to e	-	-	-	-	-	-	-	-	*1.42*	*1.36*	-	-
	Width	cross c	-	-	-	-	-	-	-	-	*0.66*	*0.67*	-	-
		cross g	-	-	-	-	-	-	-	-	*0.59*	*0.64*	-	-
NMS G.1992.47.121.3	Length	d to b	-	-	0.84	1.04	1.15	1.25	1.38	1.47	1.5	1.33	0.93	-
		df to e	-	-	0.84	1.04	1.15	1.25	1.35	1.41	1.49	1.31	0.85	-
	Width	cross c	-	*0.36*	0.39	0.42	0.46	0.48	0.79	0.89	0.97	0.78	0.43	-
		cross g	-	*0.36*	0.39	0.42	0.46	0.48	0.69	0.83	0.92	0.83	0.57	-
NMS G.2018.27.1	Length	d to b	0.9	-	-	-	1.1	-	1.25	1.34	*1.35*	*1.5*	-	-
		df to e	0.9	-	-	-	1.1	-	1.22	1.33	*1.31*	-	-	-
	Width	cross c	0.41	-	-	-	0.5	-	0.63	0.83	0.87	0.86	-	-
		cross g	0.41	-	-	-	0.5	-	0.56	0.76	*0.84*	-	-	-
NHMUK PV M46495 (*B. mussettae*)	Length	d to b	-	-	-	-	-	-	1.51	-	-	-	-	-
		df to e	-	-	-	-	-	-	1.57	-	-	-	-	-
	Width	cross c	-	-	-	-	-	-	0.67	-	-	-	-	-
		cross g	-	-	-	-	-	-	0.58	-	-	-	-	-
NMS G.1992.47.121.1 (*B. serendipitus*)	Right tooth row	Length	buccal	-	-	-	-	-	-	-	1.6	1.17	-	-
			lingual	-	-	-	-	-	0.81	0.98	0.95	0.7	-	-
		Width		-	-	-	-	-	*1.4*	1.6	1.67	1.41	-	-
	Left tooth row	Length	buccal	-	-	-	-	-	-	-	1.42	1.18	-	-
			lingual	-	-	-	-	-	0.77	0.9	0.93	0.7	-	-
		Width		-	-	-	-	-	1.77	1.63	1.39	1.77	-	-

Description

The holotype of *B. mussettae*, NHMUK PV M46495, is a lower right molar. Its crown is fractured between cusps a and c on the original specimen, as illustrated by Sigogneau-Russell (2003:fig 2). Here this fracture is digitally restored after segmentation of CT scans (Figure 3.3a.7B). Cusp b is missing, but the crown is otherwise intact. The overall morphology of the tooth is more mesiodistally elongate and buccolingually compressed, than in *B. serendipitus*. For molar measurements see Table 3.3a.1 and Appendix 4.

Because cusp b is missing, it is not clear how strong the b–g crest is in this specimen. However, it is clear that the b–g crest is notched in the depression between these cusps. There is a strong c–d crest on cusp c, although it is less distinctive on cusp d. The c–d crest is posteriorly oriented as in *B. serendipitus*. The a–c crest and the a–d crest are both distinctive, and there is a less distinct a–g crest. The a–g and a–c crests create a mesiodistally flat lingual surface on cusp a, with a faint ridge running from the tip of cusp a to the base dorsoventrally (Figure 3.3a.8B1).

Cusp g and cusp c are placed further apart in the holotype of *B. mussettae* than in *B. serendipitus*, leaving a small gap at the base of cusp a that is less distinct to absent in *B. serendipitus*, especially in more posterior molars (Figure 3.3a.2, 7). However, if we are correct that the holotype represents an m1, this gap may not be a feature of the whole tooth row, as we observe a similar larger gap in the m1 of *B. serendipitus* (Figure 3.3a.3). Further material is required to resolve this. The anterior lingual cingulid extends posteriorly from cusp e around the base of cusp g to the midpoint of tooth, and terminates ventral to cusp a. Unlike *B. serendipitus*, cusp df is very distinct in *B. mussettae*, projecting further posteriorly and dorsally. The divergent cusps c and g, and the buccolingually compressed crown, are key features of *B. mussettae* distinguishing it from *B. serendipitus*.

3.3a iii) Phylogenetic Analysis

Our analysis includes updated scores for previously missing characters for *Borealestes serendipitus*, described here for the first time. This phylogenetic analysis recovered a single most parsimonious tree of 117 steps (Figure 3.3a.8). The topology is

almost the same as for Meng et al. (2015), with the following differences: *Morganucodon*, *Megazostrodon*, and *Dinnetherium* no longer form a clade, but instead form successive outgroups to the rest of the taxa in the analysis; *Simpsonodon* has become a sister taxon to the clade comprising (*Tashkumyrodon* + (*Dsungarodon* + *Castorocauda*)), (*Borealestes* + (*Haldanodon* + (*Docodon* + *Docofossor*)). *Itatodon* has

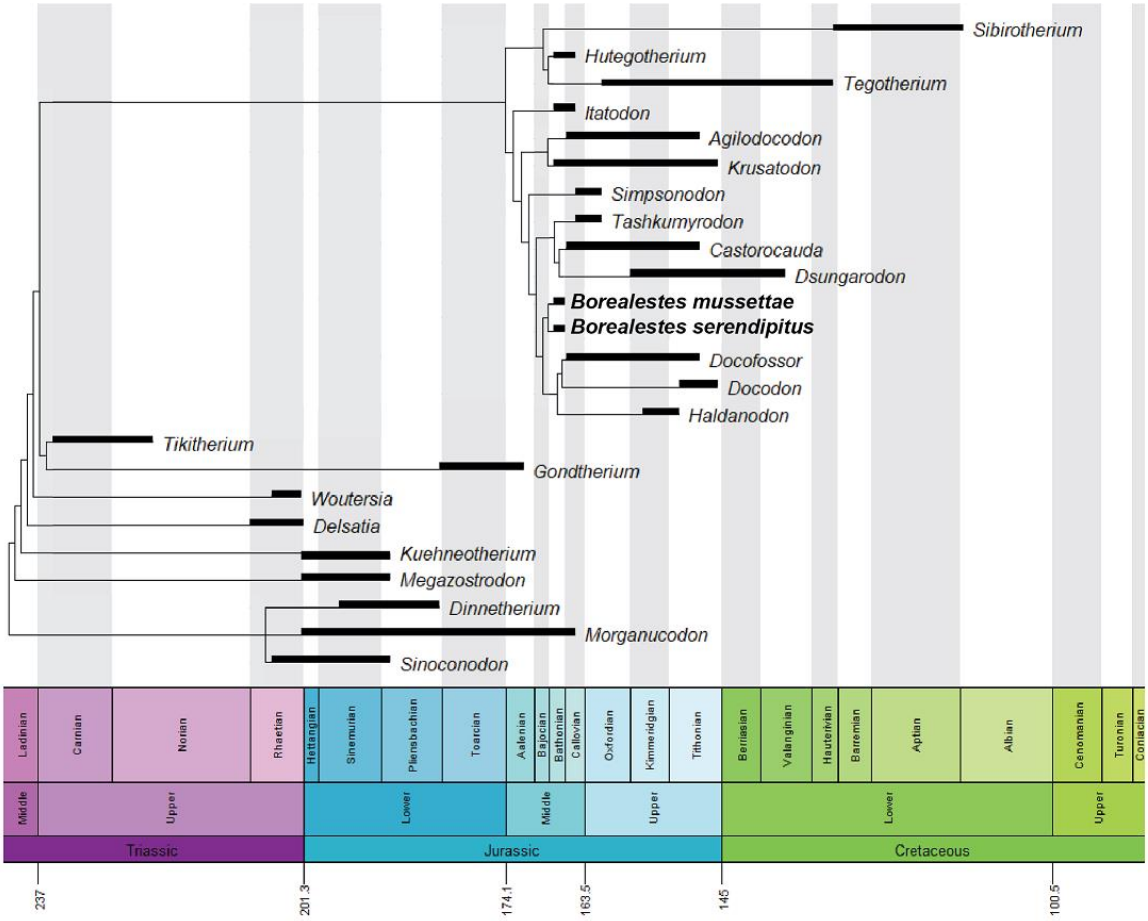

Figure 3.3a.8: Phylogeny of Docodonta, with tree topology based on updated phylogenetic analysis. Results of parsimony branch-and-bound analysis of docodonts and outgroups, resulting in tree of 117 steps. First-to-last appearances are represented by black box for each taxon (for sources of FAD/LADs see Methods). Nodes uniting taxa do not imply divergence times.

become an outgroup to the clade comprising (*Krusatodon* + *Agilodocodon*), *Simpsonodon*, (*Tashkumyrodon* + (*Dsungarodon* + *Castorocauda*), (*Borealestes* + (*Haldanodon* + (*Docodon* + *Docofossor*) (Figure 3.3a.8). Including *B. mussettae* in the analysis did not alter the tree topology. *B. serendipitus* and *B. mussettae* are united in the genus *Borealestes*,

and *Borealestes* is found as the sister taxon of the clade comprising *Haldanodon*, *Docofossor* and *Docodon*.

Characters recovered as autapomorphies of *Borealestes* in this analysis are: character 1, the obtuse angle of the angular process; character 4, the convergence of the Meckel's groove with the ventral margin of the mandible; character 18, cusp c is much larger than cingular cusp g in the lower molars; and 48, the presence of an anterior fovea in the buccolingual midpoint of the upper molar (also present in *Docodon*; Schultz et al., 2017).

Characters recovered as autapomorphies of *Borealestes serendipitus* are: character 22, the c–d crest is present and angled; and character 32, the cusp e cingulid being limited to the mesial part of the tooth; character. Characters recovered as apomorphies of *Borealestes mussettae* (lower molar characters only) are: Character 8, the absence of the anterolabial connecting crest on the upper molars; character 19, the pseudo-talonid being bound by the b–e crest; character 20, the presence of an a–g crest with a v-notch; character 21, the weakly developed b–g crest; character 27, presence of an a–d crest connected with a v-notch; character 42, a labially shifted cusp e; and character 44, the broad angle formed by cusps g–a–c (> 80º). The results of our PAUP analysis are available in Appendix 12.

3.3a iv) Discussion

Diagnostic Features of *Borealestes*

The new specimens collected from the Kilmaluag Formation on the Isle of Skye, combined with the specimens collected previously, allow us to clarify the diagnoses for *Borealestes serendipitus* and *B. mussettae*. We can confirm that the dental formula for *Borealestes serendipitus* is 4.1.?5.4/ 4.1.5.6. The estimated number of upper premolars will hopefully be clarified by better preserved fossils in the future. Previously referred specimens have been checked in light of this new diagnosis, and the specimen lists herein are up to date.

Borealestes resembles *Krusatodon, Castorocauda* and *Haldanodon* in possessing a very large cusp a, and larger cusp c than cusp g. Like most docodonts—except *Simpsonodon, Krusatodon, Agilodocodon,* and *Docodon—Borealestes* does not have pits or ornamentation in molar tooth enamel. The key features that distinguish *Borealestes* from

other docodonts include: (1) a distinctly pronounced a–c crest; (2) the obtuse angle of the angular process; (3) the convergence of the Meckel's groove with the ventral margin of the mandible; (4) cusp c being much larger than cusp g; (5) the c–d crest being present and angled; and (6) the presence of an anterior fovea in the buccolingual midpoint of the upper molars. However, it should be noted that the angular process and Meckel's groove are not known for *B. mussettae*, and so although these are returned as apomorphies in this analysis, further material is necessary to confirm features (2) and (3) for both taxa.

The differences between *B. serendipitus* and *B. mussettae* are summarised in Figure 3.3a.8. The species *B. serendipitus* differs from *B. mussettae* in: (1) the pseudo-talonid being bound by the b–g crest; (2) the better developed b–g crest; (3) the angle formed by cusps g–a–c being < 80º; (4) the presence of the anterolabial and anterolingual crest (the A–X crest) on the upper molars; (5) the reduction/absence of cusp Z; and (6) absence of a–g crest on cusp a. The a–d crest and df cusp are better developed, and cusps c and g placed anteroposteriorly further apart in *B. mussettae* than in *B. serendipitus*. Our re-examination of *Borealestes mussettae* shows that it is valid species, and sufficiently different from *B. serendipitus* (further details in Discussion).

Tooth-row Size Gradient

The molars of *B. serendipitus* increase in size along the tooth row from m1–m3, then decrease from m3 posteriorly (Table 3.3a.1; Appendix 4). In all docodonts for which the relatively complete tooth rows are known the ultimate molar is smaller than the penultimate molars and the ultimate upper molar is also less symmetrical than preceding molars. The decreasing size from m2–3 through to m5–6 documented in *Borealestes* is similar to the tooth size gradient known for *Haldanodon* (Krusat, 1980; Luo and Martin, 2007), *Docodon* (Jenkins, 1969; Schultz et al., 2017), *Castorocauda* (Ji et al., 2006) and *Agilodocodon* (Meng et al., 2015). However, *Borealestes* shows the steepest gradient for decreasing size toward the posterior molars, of all docodonts. For example, both *Borealestes* and *Docodon* have six molars, but the decreasing trend of m3 to m6 is more pronounced in *Borealestes* (Table 3.3a.1; Appendix 4).

The large sample of specimens of *Borealestes serendipitus* allows a quantitative comparison of *B. serendipitus* to *B. mussettae*. The initial diagnosis and description of *B. mussettae* suggested that *B. mussettae* was larger than *B. serendipitus* (Sigogneau-Russell,

2003). Our measurements do not support this, and show instead that specimens of *B. mussettae* are of similar size to *B. serendipitus* (Table 3.3a.1; Appendix 4). The width/length ratio of the type specimen of *B. mussettae* NHMUK PV M46495—a lower molar—is similar to p5 in *B. serendipitus*, but we suggest from the morphology that this specimen represents an m1, suggesting that *B. mussettae* has a buccolingually narrower molar row than *B. serendipitus*.

An alternative hypothesis is that NHMUK PV M46495 could represent a deciduous p5 in *B. serendipitus*. The sharply cusped crown, divergent orientation of cusps c and g (Figure 3.3a.7), and the lack of roots in the preserved tooth of *B. mussettae* type specimen could be consistent with the hypothesis that the type specimen is a deciduous dp5. However, the assessment of isolated deciduous premolars without the context of contiguous toothrow can be a complex issue (Averianov, 2004), which can only be resolved reliably when well preserved tooth row is available (Schultz et al., 2017). Much of the material currently referred to *B. mussettae* is fragmentary. More complete specimens of *B. mussettae*, or more juvenile material from *B. serendipitus*, would help resolve this.

Ontogenetic Changes in *Borealestes*

Most of the specimens of *B. serendipitus* found so far have not developed m6 (the ultimate molar) except for the holotype BRSUG 20570 (Figure 3.3a.3). A recent detailed analysis of *Docodon victor* shows that its ultimate molar did not erupt until late in adulthood, only in very mature individuals (Schultz et al., 2017). Our observations that *B. serendipitus* also shows a late eruption of m6 suggest this condition of delayed eruption of the ultimate molar may be widespread among docodonts. A corollary of this observation is that the holotype of *Borealestes serendipitus* BRSUG 20570 is the most mature individual of the species currently known.

Other changes in mandibular morphology of *D. victor*, as seen in successively older adult specimens, include a posterior shift in the Meckel's sulcus, a posterior shift in the anterior border of the coronoid process, and a medial-to-anterior shift of the ultimate molar placement relative to the coronoid process (Schultz et al., 2017). The morphology of BRSUG 20570 also conforms to this, further supporting our interpretation that there is some ontogenetic variation in the sample of mandibles of *B. serendipitus* from the Isle of

Skye, and that the type specimen BRSUG 20570, and possibly also BRSUG 29007, are the most mature individuals.

Of the other specimens described here, BRSUG 20571 is likely to represent the ontogenetically youngest individual, with the Meckel's sulcus meeting the ventral edge of the mandible below m1 (Figure 3.3a.4A–E). In NMS G.2018.27.1 (Figure 3.3a.5) and NMS G.1992.47.121.3 (Figure 3.3a.6) the anterior end of the Meckel's sulcus has become shorter and ends below m3 and m4, becoming a faint line on the exterior of mandible anterior to this. Although this posteriorly receding Meckel's sulcus is best documented in *Docodon* (Schultz et al., 2017) it was also previously shown for *Haldanodon* (Nowotny et al., 2001; Martin et al., 2010). This supports the hypothesis that a similar pattern of ontogenetic variation in mandibular morphology may be widespread throughout Docodonta.

Phylogeny of *Borealestes* and Docodonts

Our phylogenetic analysis with updated characters for the upper and lower dentition and dentary of *B. serendipitus* and *B. mussettae* returned similar results to previous analyses of Docodonta (Figure 3.3a.8; see Meng et al., 2015). Our analysis continues to support Docodonta as a clade, with *Tikitherium*, *Woutersia*, and *Delsatia* as their putative near relatives (Sigogneau-Russell and Hahn, 1995; Ji et al., 2006; Luo and Martin, 2007). *Borealestes* was found to form a clade with *Haldanodon, Docodon and Docofossor*, as recovered by previous authors (Martin and Averianov, 2004; Pfretzschner et al., 2005; Ji et al., 2006; Luo and Martin, 2007; Averianov et al., 2010; Meng et al., 2015). As noted in the description of molars, the posterior upper molar(s) of *Borealestes* bears strong resemblance to the molars of *Haldanodon*, also somewhat similar to those of *Docodon* (although to a lesser extent). These taxa share a relatively strong A–X crest, in perpendicular arrangement to the A–C crest on the upper molars.

The broad agreement of many studies is that there is strong support for the close relationship of *Borealestes* to *Haldanodon, Docodon,* and *Docofossor*. However, Sigogneau-Russell (2003) suggested a sister-group relationship between *Borealestes* + (*Simpsonodon* and *Krusatodon*), based on the morphology of the lower molars. This was an older study, prior to the discoveries of many more docodont taxa. Inclusion of additional taxa has changed the phylogeny. Also the earlier analysis was a manual and ad hoc cladistic phylogeny, not a parsimony analysis with comprehensive coverage of taxa and characters.

Another analysis that returned an alternative placement for *Borealestes* species was Hu et al. (2006). Their analysis of 24 lower molar characters included 13 docodont genera with *Morganucodon* as an outgroup. They found both *Borealestes* species at the base of the docodont tree. Their closest relationship to *Borealestes* was with *Docodon*—and as the outgroup to a clade formed by all other docodonts. Several taxa in this phylogeny are in an unresolved polytomy (Hu et al., 2006:fig 5). The small size of their character list may have contributed to this result, and this earlier study is before our addition of many more characters of *Borealestes* from the new specimens.

Some authors have proposed Docodonta be split into two families: Tegotheriidae (*Tegotherium, Sibirotherium, Hutegotherium,* and *Krusatodon*) and Simpsonodontidae (*Simpsonodon* and *Dsungarodon*), with basal docodonts represented by *Borealestes, Haldanodon* and *Docodon* (Maschenko et al., 2002; Martin and Averianov, 2004; Averianov et al., 2010). This was based on an analysis of 37 molar and dentary characters scored for 18 taxa, 13 of them docodonts. In the resulting tree, *Borealestes,* plus *Haldanodon* and *Docodon* were placed in an unresolved polytomy with *Castorocauda, Tashkumyrodon,* and a clade formed by the rest of Docodonta except *Itatodon,* which formed the outgroup to all other docodonts (Averianov et al., 2010:fig. 6). They considered *Castorocauda, Tashkumyrodon* and *Acuoduolodon* to be Docodonta incertae sedis (*Acuoduolodon sunae* has since been suggested to be a junior synonym of *Dsungarodon zoui* [Martin et al., 2010]).

Our analysis does not fully support the dichotomous relationships of families Tegotheriidae and Simpsonodontidae as hypothesized by Averianov et al. (2010). Although there is support for Tegotheriidae comprising *Tegotherium, Sibirotherium* and *Hutegotherium,* we find *Krusatodon* as the sister taxon to *Agilodocodon* outside of this clade (Figure 3.3a.8). We also find *Simpsonodon* as an outgroup to two clades formed by *Tashkumyrodon* + (*Dsungarodon and Castorocauda*), and the clade of *Borealestes* + (*Haldanodon* + (*Docodon and Docofossor*)), which has been corroborated by multiple previous analyses. 'Simpsonodontidae' has, therefore, become paraphyletic in our analysis.

All of these studies are based on molar, or molar plus dentary, morphological characters, without postcrania. This is due to the lack of postcranial material for many docodontans. The addition of postcrania from multiple docodontans to a phylogenetic analysis would undoubtedly help further resolve and stabilize docodont relationships.

3.3b Cranial and Postcranial Morphology of *Borealestes*

3.3b i) Materials and Methods

NMS G.1992.47.121.1, a partial skeleton of *Borealestes serendipitus*, was mechanically prepared by Sarah Finney at the University of Cambridge between 1994-1996 using a sodium bicarbonate airbrasive. It was then consolidated with 2% Paraloid B72. Some portions of the skeleton are detached from the limestone block (it is unclear when this occurred) and are stored separately. These separate elements are: NMS G.1992.47.121.2, the left petrosal (Panciroli et al., 2018b; Chapter 3.3.2); NMS G.1992.47.121.3, the right dentary (Panciroli et al, in press; Chapter 3.3a); NMS G.1992.47.121.4, the premaxilla and nasal fragment; NMS G.1992.47.121.5 a metatarsal; NMS G.1992.47.121.6, right clavicle; NMS G.1992.47.121.7, a carpal/tarsal element; NMS G.1992.47.121.8, a chevron; NMS G.1992.47.121.9, ?cranial fragment; NMS G.1992.47.121.10, carpal/tarsal element; NMS G.1992.47.121.11, fragment of ischium; and NMS G.1992.47.121.12, fragment of rib.

NMS G.1992.47.121.1 was scanned at the European Synchrotron Radiation Facility (ESRF) in Grenoble. The whole limestone block was scanned at 13 µm then subsampled to 26 µm, and a small sub-section, containing the palate and other cranial components, was scanned to 6.15 µm and subsequently resampled to 12.3 µm.

Micro-computed tomographic data for NMS G.1992.47.121.2, NMS G.1992.47.121.5, NMS G.1992.47.121.6, NMS G.1992.47.121.7, NMS G.1992.47.121.8, NMS G.1992.47.121.9, NMS G.1992.47.121.10, NMS G.1992.47.121.11, and NMS G.1992.47.121.12 were obtained at the University of Edinburgh, School of Geosciences Experimental Geoscience Facility, using their in-house built µCT scanner (built by Ian Butler). The scanner comprises a Feinfocus 10-160kV dual transmission/reflection source, MICOS UPR-160-AIR ultra-high precision air-bearing table, Perkin Elmer XRD0822 amorphous silicon x-ray flat panel detector and terbium doped gadolinium oxy-sulfide scintillator. The scan resolution is 8.9 µm. Data acquisition software was written in-house, and scans were reconstructed using Octopus 8.7 software.

Micro-computed tomographic data for NMS G.1992.47.121.3 and NMS G.1992.47.121.4 were obtained at the University of Bristol using a Nikon XTH225ST scanner with a 225kV rotating target with a peak energy of kV140. The scan resolution is 12.77µm.

All microCT and synchrotron scan data were digitally reconstructed and image processed using Mimics 19.0 at NMS. Where possible (i.e. when they were not covered completely by sediment), specimens were also observed using conventional microscopy at NMS. Measurements were taken using the measurement tools in Mimics 19.0, and corroborated with manual measurements using fine callipers or a microscope where possible.

3.3b ii) Description

NMS G.1992.47.121.1, or 'Block A', is an imperfect parallelepiped block of blue-grey limestone, measuring approximately 183 mm in length, 105 mm in width, and between 148 mm and 340 mm in thickness (Figure 3.3b.1). (Block A was substantially larger when collected—~240 mm in length, ~170 mm in width and ~50 mm in depth—and was reduced by curators at NMS when it became clear the block required reduction to obtain successful scans at high resolution for study. All offcuts were retained). The surface is undulating, with several hairline cracks visible in the prepared upper surface, also visible in synchrotron scan data. Skeletal elements are scattered on the surface of the block—including the palate and elements of the skull, left ilium and left radius. Synchrotron scans revealed other parts of the skeleton within the block. The surface bones sit on 'platforms' of rock, the result of acid and mechanical preparation, when the surrounding rock was removed. At least seven such platforms no longer contain fossil material, and likely indicate the original positions of bones that have been removed or detached during handling, such as the petrosal NMS G.1992.47.121.2 (Panciroli et al., 2018b; Chapter 3.3c) and the dentary (NMS G.1992.47.121.3 (Panciroli et al., 2019; Chapter 3.3a).

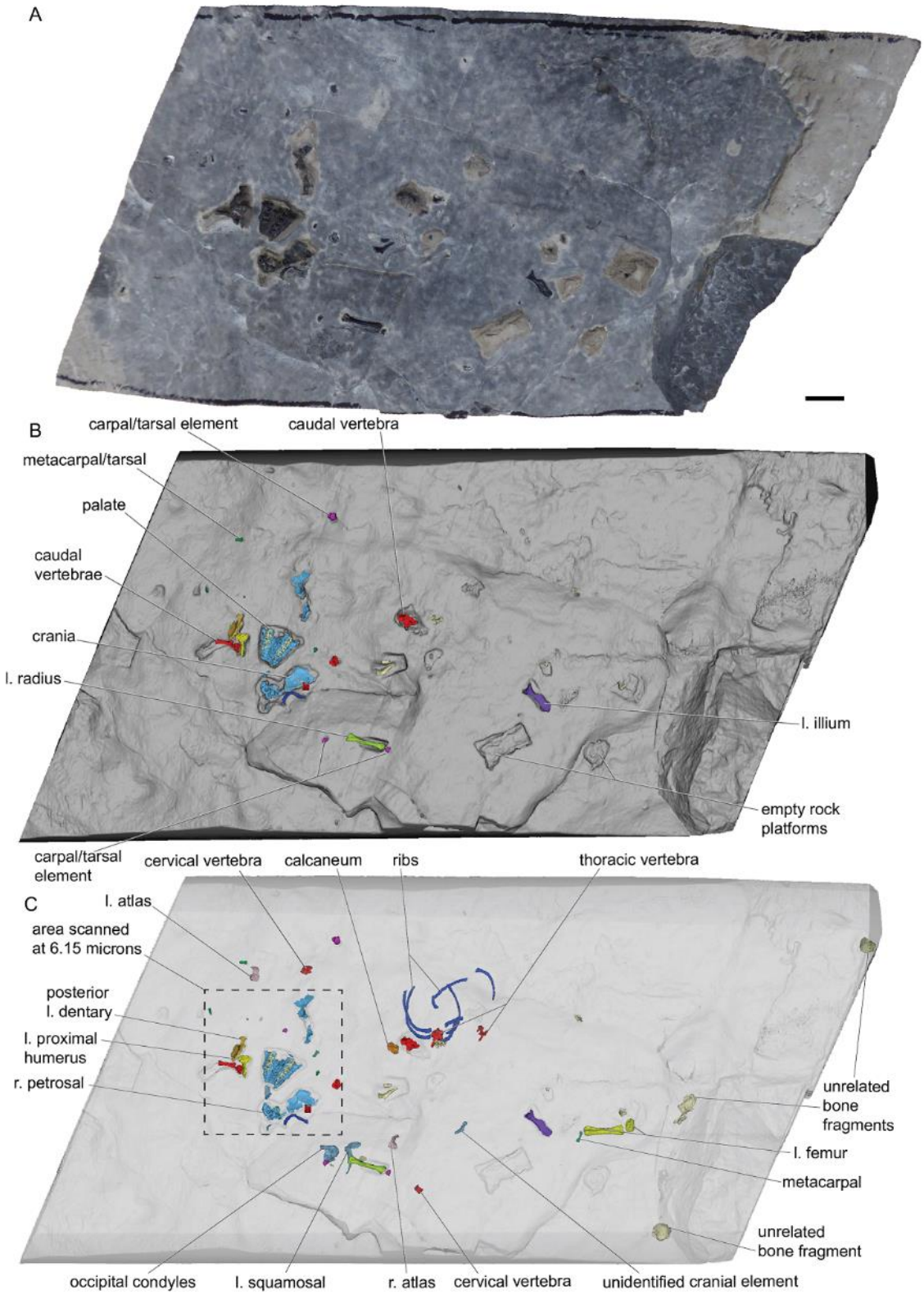
A
B
carpal/tarsal element
caudal vertebra
metacarpal/tarsal
palate
caudal vertebrae
crania
l. radius
l. illium
empty rock platforms
carpal/tarsal element
cervical vertebra
calcaneum
ribs
thoracic vertebra
C
l. atlas
area scanned at 6.15 microns
posterior l. dentary
l. proximal humerus
r. petrosal
unrelated bone fragments
l. femur
metacarpal
unrelated bone fragment
occipital condyles
l. squamosal
r. atlas
cervical vertebra
unidentified cranial element

Crania

Dentary and isolated lower dentition

The right dentary, NMS G.1992.47.121.3, is nearly complete, while only the posteriormost portion of the left dentary remains as part of skeletal block NMS G.1992.47.121.1 (Figures 3.3b.1 and 3.3b.2). For a complete description of the right dentary and lower dentition see Chapter 3.3a (Panciroli et al., 2019).

Although the incisors are missing from NMS G.1992.47.121.3, a single incisor and ventral tip of an incisor root are present in the skeletal block NMS G.1992.47.121.1, separated from the dentary and located in the matrix underneath the nasals (Figure 3.3b.2B). The complete incisor is a right incisor with a large buccal bulge and slightly recurved cusp. A ridge runs from the tip of the cusp to the base of the crown, where there is a slight cuspule along the rim of the base of the crown. The single root is wide, tapering ventrally. The alveoli on the preserved right dentary indicate that the anterior incisors were strongly procumbent, especially i1. This is consistent with the incisor morphology described in Chapter 3.3a (Panciroli et al., 2019) and also seen in other docodontans such as *Agilodocodon* (Meng et al., 2015).

Also separated from the rest of the skeleton, the damaged remnants of a premolar or molar is located near a posterior portion of the left dentary (Figure 3.3b.2A2). The tip of the main cusp is missing and the tooth is damaged lingually and buccally. The remains of the posterior root are present, but fragmented. It is not possible to give a more exact identification due to the poor preservation.

The posteriormost portion of the left dentary is preserved on the surface of the block, NMS G.1992.47.121.1, beside the fragment of a humerus and two caudal vertebrae (Figures 3.3b.1 and 3.3b.2). It comprises the anterior edge and central portion of the coronoid process, the dentary peduncle, and the medial ridge (Figure 3.3b.3A). Dorsoventrally, the dentary fragment extends from the dorsal portion of the postdentary trough to approximately halfway up the coronoid process. The morphology of this element conforms to that of the right dentary, see Chapter 3.3a for full description.

Figure 3.3b.1 (previous page): NMS G.1992.47.121.1, *Borealestes serendipitus*, also known as ‘Block A’. A, photograph of Block A; B, digital rendering of Block A from synchrotron scans; C, digital rendering of Block A from synchrotron scans with matrix semi-transparent, showing skeletal elements within the block. Scale bar equals 10 mm.

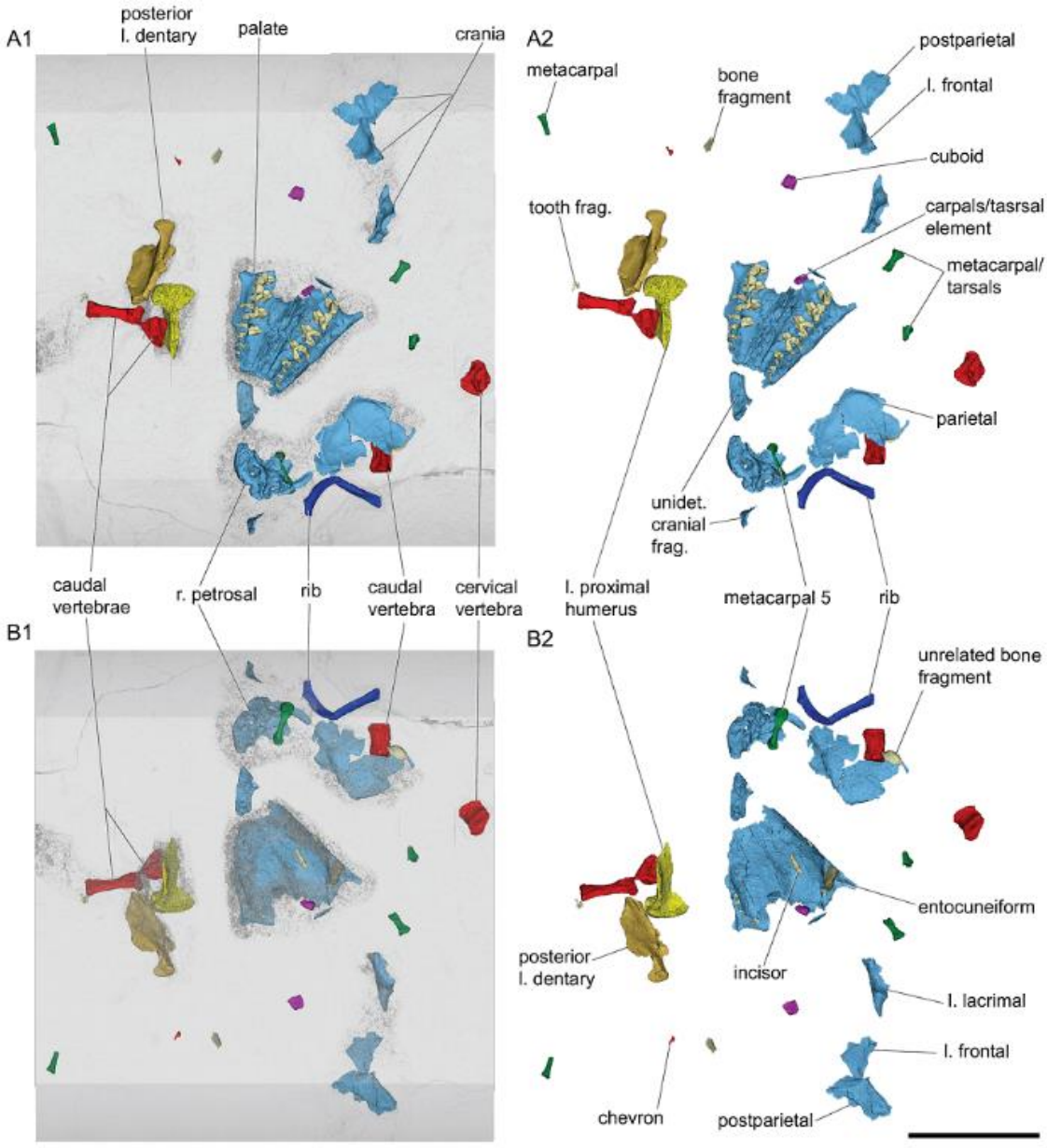

Figure 3.3b.2: Digital rendering of area of NMS G.1992.47.121.1 scanned at 6.15 microns (see Figure 3.3b.1). A1, elements with semi-transparent matrix; A2, elements from A1 without matrix; B1, elements from A1 viewed from underside of block, with matrix semi-transparent; B2, elements from B1 with matrix removed. Scale bar equals 10 mm.

Premaxilla

The left and right premaxillae, NMS G.1992.47.121.4, are near-complete, but have been dislodged from the main block surface and are slightly crushed. The left premaxilla is displaced anteriorly in relation to the right premaxilla. The left premaxilla is also more complete, and holds alveoli for I2, I3 and I4 (Figure 3.3b.3B) (identification of incisors is

possible due to presence of the intranarial process on the right premaxilla, and the position of the anterior premaxillary foramin in relation to I1 and I2. Incisors I3-4 are intact and approximately in life-position, and the root of I2 is in place, but its crown is broken off at the alveolar margin and missing. The posterior margin of the I4 alveolus is missing. In the right premaxilla, the alveoli for I1-3 are present, although the lateral margin of the premaxilla is more fragmented. The I3 alveolus is crushed, and I3 is not present, but I1-2 are both present and approximately in position, with some displacement. The I1 is single-rooted, but its root is bulbous dorsally inside the premaxilla. The I2 root is partially divided with a groove along the length of the root on both the buccal side and the lingual side (a figure of 8 in cross-section). I3 and I4 are two-rooted. For detailed description of the incisor morphology see Chapter 3.3a (Panciroli et al., 2019).

The margins of the incisive foramen are intact (Figure 3.3b.3B5). The anterior edges of the foramen lie mediolaterally parallel to the posterior margin of the I2 alveoli. There is a small projection of the premaxilla, jutting posteriorly into the incisive foramen where the premaxillae contact each other anteriorly, creating a heart-shaped anterior margin to the foramen (Figure 3.3b.3B6). Anterior to the incisive foramen are the ventral premaxillary foramen, adjacent to I2. There are also two much smaller foramen medial to the I3 alveoli (Figure 3.3b.B5).

On the ventral palatal plate of the premaxilla there are depressions between the alveoli and medial to the toothrow, which are for the receipt of the lower incisor tips when the mouth is closed. The posterior margin of the premaxillae for contact with the maxilla is not preserved. The anteriormost tips of the premaxillae are also preserved, although in poor condition. There is a stump or base of the internarial process on the right premaxilla—this makes identification of the right I1 certain. In the interior of the premaxilla there is a canal connecting from the anterior premaxillary foramen to the ventral maxillary foramen. The anterior opening of this canal is exposed on the broken

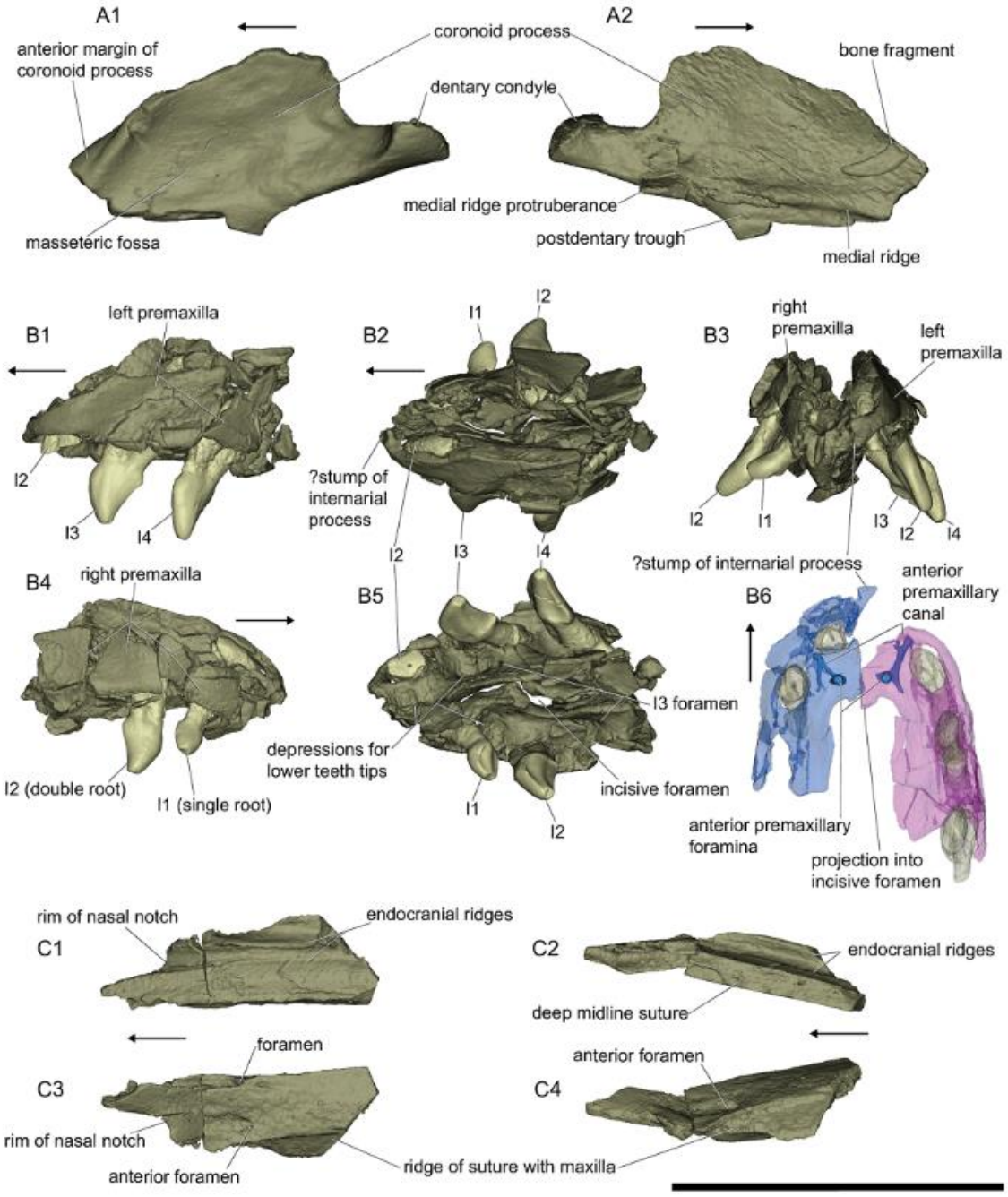

Figure 3.3b.3: Cranial elements from Block A. A, NMS G.1992.47.121.1 posterior left dentary; A1, lateral view, A2, medial view. B-C, NMS G.1992.47.121.4 premaxillae with incisors, and anterior nasal fragment. B1, left lateral view; B2, dorsal view; B3, anterior view; B4, right lateral view; B5, ventral view; B6, semi-transparent digital rendering of reconstructed premaxillae and incisors, showing path of premaxillary canal; C1 ventral view; C2, medial view; C3, dorsal view; C4, left lateral view. Scale bar equals 5 mm.

anterior surface of the left premaxilla (Figures 3.3b.3B3 and 3.3b.B6). Posteriorly this canal is traced to the ventral premaxillary foramen, to which the canal is connected from inside the premaxilla (Figure 3.3b.3B6). This canal splits into branches in the interior of the right premaxilla. These canals cannot be traced as extensively in the right premaxilla due to poor preservation, but part of this incomplete canal is present in the right premaxilla, and is connecting the ventral premaxillary foramen laterally toward the interdental gap between I1 and I2 (Figure 3.3b.3B6).

The lateral surfaces of the premaxillae are more or less vertical from the alveolar margins, with some slight lateral bulging around each incisor root—although fragmentation of the bone make the extent of these bulges uncertain. The dorso-ventral depth of the premaxilla increases posteriorly, from ~0.5 mm anterior to I2, to ~2.4 mm at the alveolus of I4.

On the endocranial surface of the premaxillae, a groove runs from the endocranial openings of each of the ventral premaxillary foramen, meeting in the midline across the sutures. This creates a canal between the endocranial openings of the ventral premaxillary foramen.

Maxilla and palatine

The anterior portions of both maxillae are missing, but they are complete from P4/P5 posteriorly (Figure 3.3b.4). The facial part of the anterior maxilla is not complete, and the premolar-bearing margin of the maxilla is missing, so the exact count of the premolars is not known. But five upper premolars can be reconstructed based on the lower premolar number on the complete mandible of the specimen (right dentary NMS G.1992.47.121.3, see above). The palatal processes of both maxillae are fragmented; the right maxilla is more complete. Both maxillae have preserved the cheek teeth in life-position—the right P4 to M4, and left P5 to M4. The crowns of these teeth, especially the premolars, have been abraded. This ventral surface of the palatal plate of the maxillae, which contain the teeth, was uppermost on the matrix when the fossil was found. The abrasion of the tooth crowns occurred post mortem. The worn surfaces of the teeth are not due to dental occlusion, but due to abrasion in sedimentary processes. For detail of the upper premolar and molar morphology, see Chapter 3.3a (Panciroli et al., 2019).

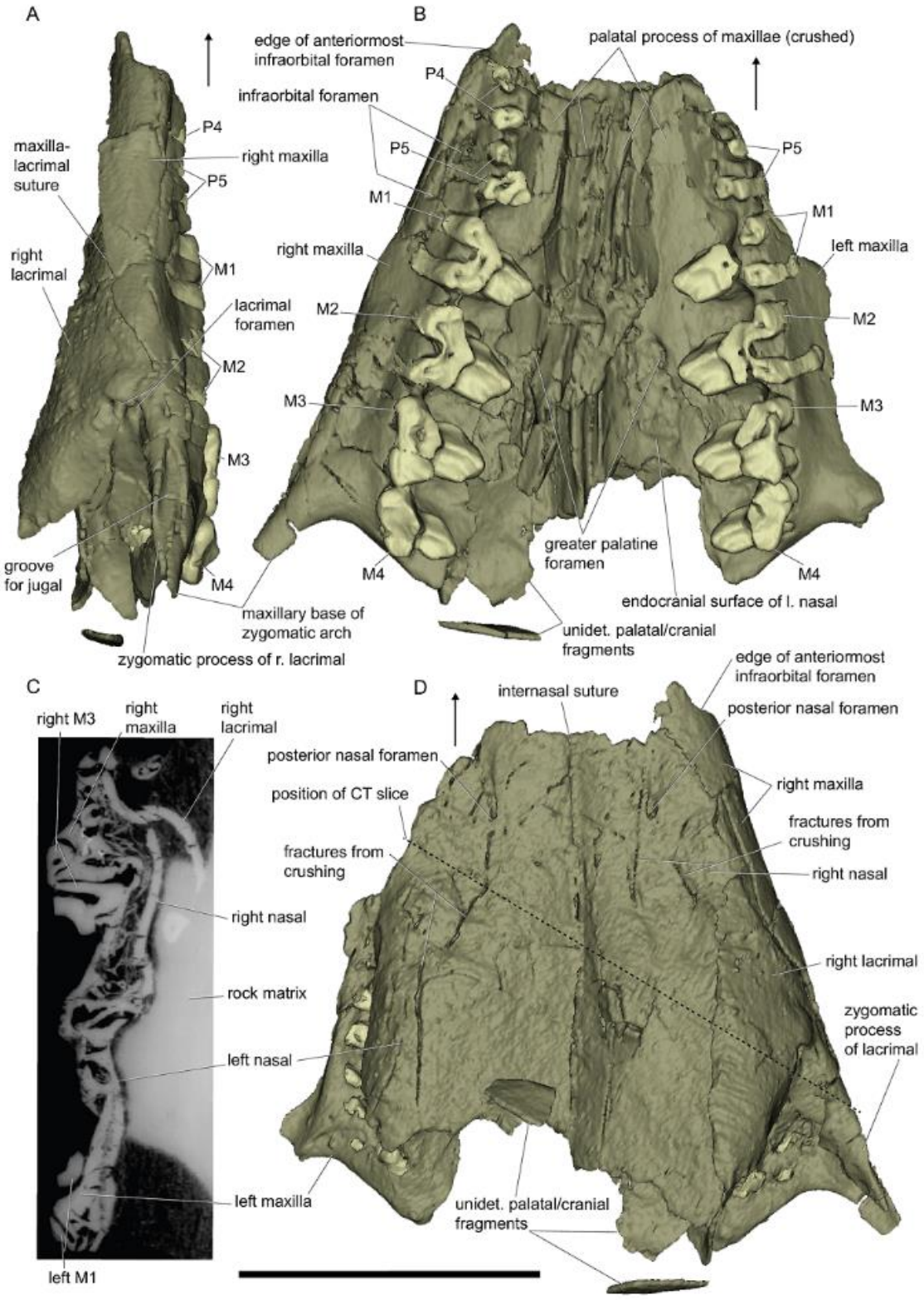

Figure 3.3b.4: The palatal segment of NMS G.1992.47.121.1. A, right lateral view; B, ventral view; C, synchrotron slice showing cross-section of palate; D, dorsal view. Scale bar equals 5 mm.

The palatal process of the maxillae continue posteriorly until approximately the M2/3. Crushing and displacement of the medial portion of the palatal process of the maxillae makes this area difficult to interpret. The greater palatine foramen is preserved medial to M2, and the palatal process of the maxillary bone appears to project posteriorly into the palatal process of the palatine bone along the midline suture (Figure 3.3b.4B). This projection has a low ventral anteroposterior ridge. An alternative interpretation is that the palatal process of a maxilla ends at M2/3, and the "projection" aforementioned may be the palatal process of the palatine. The posteriormost portion of the palatal process of the maxillary bone is not preserved in the left maxilla.

The posterior part of the maxilla holds the ultimate molar and its roots. The contact of the maxilla with the palatine appears smooth. The contact between the maxilla and palatal process of the palatine appears to have been close to the lingual edge of the molar row, but as the maxilla is broken here, this interpretation has some uncertainty. A fragment of right palatine indicates that the suture may have been as little as 0.4 mm from the lingual margin of the alveolus of the ultimate molar. The maxillary base of the zygomatic arch is better preserved in the right maxilla, and does not appear to posteriorly project beyond the maxilla-palatine suture posterior to the ultimate molar (Figure 3.3b.4).

The suture of the maxilla-lacrimal slopes posteroventrally from a point dorsal to M2, to P4, overlapping the ventralmost portion of the lacrimal (Figure 3.3b.4A). Although the lateral wall of the maxilla is somewhat compressed (a post-mortem distortion) it is clearly laterally convex. The lateral portion of the left maxilla is not preserved.

The lateral surface of the maxilla shows three anterior foramen of the infraorbital canal. These foramen are dorsal to the roots of the P5/M1 junction, P4/P5 junction, and P3/P4 junction of the right maxilla (Figure 3.3b.4B). Because the external aspect of the maxilla is dorsoventrally compressed, the two more posterior foramina appear relatively small in comparison to the very large infraorbital foramina in the maxilla in *Docodon* (Schultz et al. 2017), *Haldanodon* (Lillegraven and Krusat, 1991) and *Docofossor* (Luo et al., 2015). Only the rounded posterior edge of the anteriormost infraorbital foramen is preserved. In *Borealestes* these infraorbital foramen are located more anteriorly in relation to the tooth row than in *Docodon*: in *Docodon* two infraorbital foramen are located dorsal to the M1/M2 junction and roots of P4 on the lateral side of the maxilla (Schultz et al.,

2017:fig. 9). In *Haldanodon* three foramen are located above the roots of the penultimate and ultimate premolars, and the M1 (T. Martin, pers. com.).

Crushing makes it impossible to reconstruct most of the endocranial surface and internal structure of the maxilla (Figure 3.3b.4C). However the groove on the posterior endocranial surface of the maxilla for the lacrimal is well preserved on both maxillae. Compression has also distorted the shape of the palatal surface of the maxilla, tilting the tooth row mediodorsally.

Nasals

Three fragments of nasal are preserved: the right and left from just anterior to the anteriormost projection of the lacrimal, to just anterior to the suture with the frontal (the latter suture line is not preserved) (Figure 3.3b.4D). There is also an anterior fragment of the left nasal (Figure 3.3b.3C).

The anterior fragment of the left nasal is separated from the rest of the skeleton and is attached to the premaxillae by a small portion of matrix and paraloid, as part of NMS G.1992.47.121.4. It is 0.5 mm in length, and includes an anterior foramen on the exterior dorsal surface (Figure 3.3b.3C3-4). There is a dorsoventrally deep midline suture where it would have met the right anterior frontal (Figure 3.3b.3C2). The rim of the anterior nasal notch indicates the notch was wide and terminated 1.6 mm anterior to the anterior nasal foramen. The nasal is narrow anteriorly, widening and extending under the maxilla posterolaterally. A ridge is present on the lateral side of the nasal, where it sat under the anterior of the maxilla (Figure 3.3b.3C3-4), and presumably under the septomaxilla, although the latter is not preserved. Endocranially, strong ridges run anteroposteriorly along the length of this section of the nasal. These ridges are not seen in the larger posterior portions of nasal.

The posterior nasal portions are much wider than the anterior portion, and their midline suture is dorsoventrally deep and forms a projecting ridge endocranially (Figure 3.3b.4C). The nasals appear to slightly overlap the lacrimals at the suture between these elements. As indicated by the fractures along their length, crushing has distorted the original shape of the nasals, making them appear flatter than they may have been in life.

The posterior nasal foramen is present, positioned mediolaterally halfway across each nasal on the anterior portion of the preserved bone (Figure 3.3b.4D). These foramina

open directly into the endocranial space of the nasals. Crushing prevents the identification or reconstruction of endocranial structures of the nasals.

Lacrimals

Both lacrimals are preserved in NMS G.1992.47.121.1, the right lacrimal is in natural articulation with the maxilla (Figure 3.3b.4), and the left lacrimal is located on the surface of the block, posterior to the maxillae (Figures 3.3b.2 and 3.3b.5). The right lacrimal is more complete than the left (Figure 3.3b.5B).

The zygomatic process of the lacrimal is long and slender. It extends to the line of the posterior edge of the ultimate molar, and sits in a dorsal groove of the maxilla, where they form the anterior base of the zygomatic arch (Figure 3.3b.4 and 3.3b.5). It has a distinct lateral groove to receive the jugal. The orbital flange of the lacrimal extends posteriorly at least as far as the end of the zygomatic process, but the suture with the frontal is not preserved.

The dorsal and ventral lacrimal foramina are large (Figures 3.3b.4A and 3.3b.5A and B). The lacrimal is laterally convex, and endocranially the surface is domed, with two dorsoventral ridges: one on the orbital flange of the lacrimal, posterior to the lacrimal foramen; the second anteriorly, on the facial extension of the lacrimal (Figure 3.3b.5A4 and B4). On the lateral exterior surface of the lacrimal, the ridge that receives the jugal posteriorly runs along the length of the lacrimal anteriorly, where it marks the edge of the maxilla (Figure 3.3b.5A2 and B2). Ventral to this groove, the lacrimal sits underneath the lateral surface of the maxilla. The anteriormost portion of the facial extension of the lacrimal is not preserved on either side, and it is unclear how far it extends, or how it meets the nasal and maxilla anteriorly.

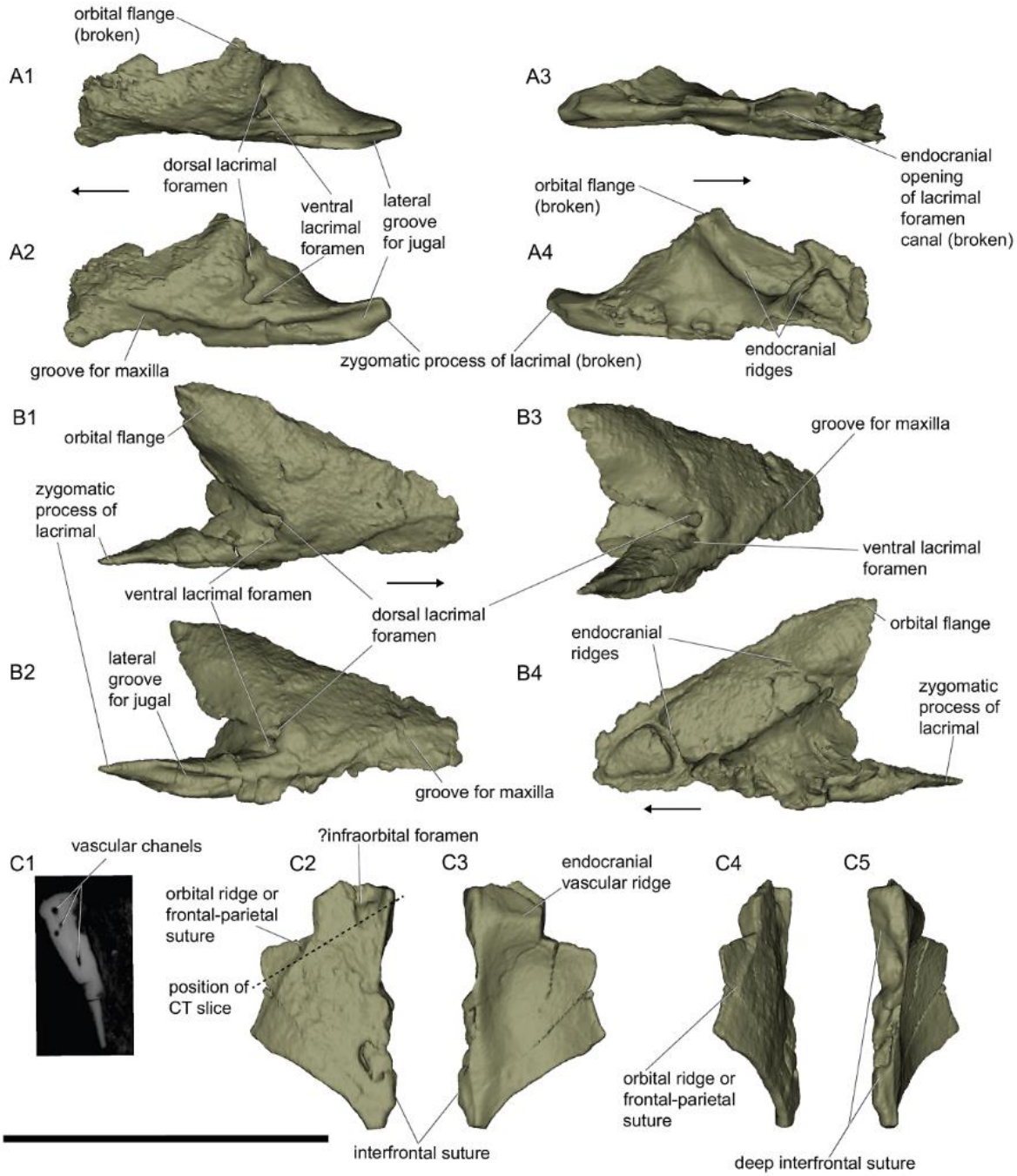

Figure 3.3b.5: The left lacrimal and left frontal of NMS G.1992.47.121.1. A1, dorsal view of left lacrimal; A2, left lateral view; A3, ventral view; A4, medial view; B1, dorsal view of right lacrimal; B2, right lateral view; B3, right posterolateral view; B4, medial view (see also Figure 3.3b.4); C1, synchrotron slice showing cross section of left frontal; C2, dorsal view; C3, ventral view; C4, left lateral view; C5, medial view. For right lacrimal see Figure 3.3b.4. Scale bar equals 5 mm.

Frontal

A fragment of frontal is located beside the postparietal on the surface of the block of limestone (Figures 3.3b.2 and 3.3b.5C). The fragment is from the dorsomedial portion of the left frontal. The interfrontal suture is partly preserved. Although somewhat damaged along its edge, it is clearly vascularised internally (Figure 3.3b.5C1), and thickens anteriorly. This thickening is due to a transverse ridge on the endocranial surface, which likely marks the anterior margin of the olfactory bulb (Figure 3.3b.5C3). A posterior equivalent, which would mark the delineation between the cranial cavity and the olfactory bulb, is not preserved.

The posterior of the frontal bone, where it meets the interparietal, is not preserved, nor is the lateral wall. The remnants of an anteroposterior indentation and ridge on the external surface of the frontal, sloping posteroventrally, is interpreted as either an orbital ridge, or as marking the extent of the anterior overlap of the parietal bone (see below) (Figures 3.3b.5C2 and 3.3b.C4). As the anteriormost portion of the parietal is not preserved, it is not possible to confirm this.

Anteriorly, a possible foramen could correspond to the infraorbital foramen of *Haldanodon* (Lillegraven and Krusat, 1991) (Figure 3.3b.5C2). However, this area is damaged and the anterior portion missing so this identification is not certain.

Parietal

The left parietal is the largest preserved portion of the cranium, with most of it present including the medial interparietal suture, the parietal-postparietal suture, and multiple lateral fragments (Figure 3.3b.6). The posterior of the cranium formed by the parietal is transversely wide, with a small sagittal crest at the dorsoventrally deep suture between the left and right parietals. Where the interparietal suture meets the postparietal suture, the parietal contributes to a dorsal projection of the sagittal crest. The parietal is overlapped by the postparietal along the posterior margin, forming a slight nuchal crest running posterolaterally (Figure 3.3b.6B and D).

The walls of the parietal are thin, except along the interparietal suture. There is a thickening on the lateral side of the parietal in the temporal area. This corresponds to a bulge on the endocranial surface, possibly the rim of the indentation of the meninges of

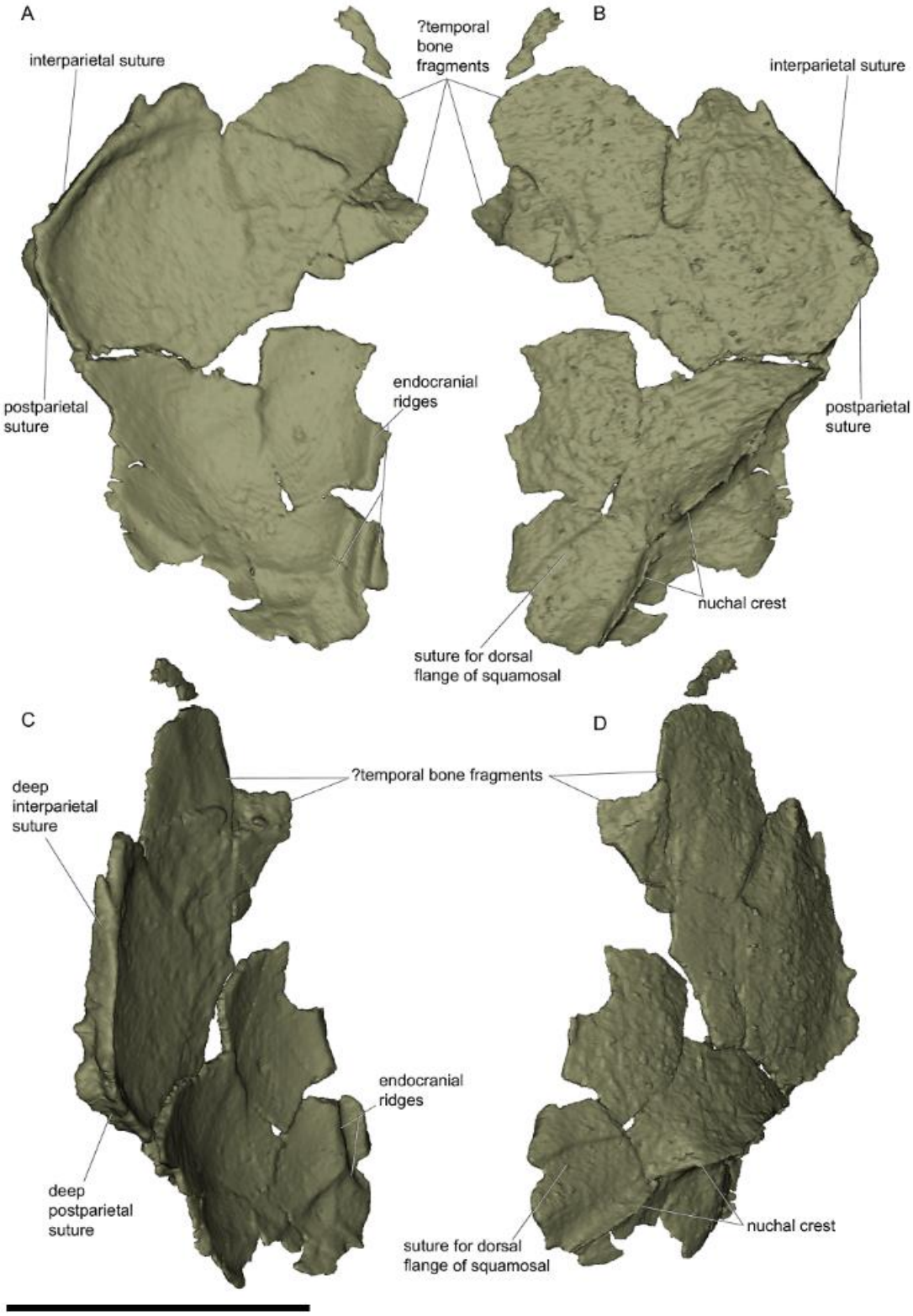

Figure 3.3b.6: The left parietal of NMS G.1992.47.121.1. A, endocranial/ventral view; B, dorsal view; C, medial view; D, left lateral view. Scale bar equals 5 mm.

the left lobe of the brain (Figure 3.3b.6A and C). On the exterior posterolateral wall of the parietal, a ridge running parallel to the nuchal crest probably marks the overlapped edge of the dorsal flange of the squamosal (Figure 3.3b.6B and D).

The identity of an indentation on the anterior dorsolateral surface of the parietal (Figure 3.3b.6B and D) is uncertain. Crushing and flattening of the bone here makes interpretation difficult and hinders reconstruction, but there are three possibilities: 1) it represents post depositional damage; 2) it marks the posterodorsal overlap of the temporal bone; or 3) it resulted from the bite of a predator or scavenger. I consider the third possibility to be the least likely, and favour the second interpretation, which would suggest that the bone located anteroventrally below this indentation could be a fragment of the temporal region.

Postparietal

The postparietal is approximately triangular in shape along the dorsal edge where it meets the parietals (Figure 3.3b.7). It slopes posteroventrally towards the supraoccipital (not preserved). The posteroventral edge of the postparietal is not preserved.

A small projection of the postparietal inserts between the parietals posterior to the interparietal suture, and this forms the dorsalmost projection of the sagittal crest. Laterally in both directions, the postparietal overlaps the posterior edge of the parietals, contributing to a nuchal crest.

There is a gentle bulge along the midline of the postparietal, forming a midline ridge (Figure 3.3b.7A). There are a series of foramen along the exterior dorsal side of the postparietal. The postparietal is well vascularised, including along the length of the medial ridge (Figure 3.3b.7A3). The endocranial surface of the postparietal is unclear—close greyvalues in the synchrotron scan data between this section of the fragment and the matrix it sits upon make digital segmentation problematic. However, there is an endocranial swelling that mirrors the exterior medial ridge of the postparietal. Posteroventrally the postparietal thins, but the suture with the posteriormost portion of the cranium is missing.

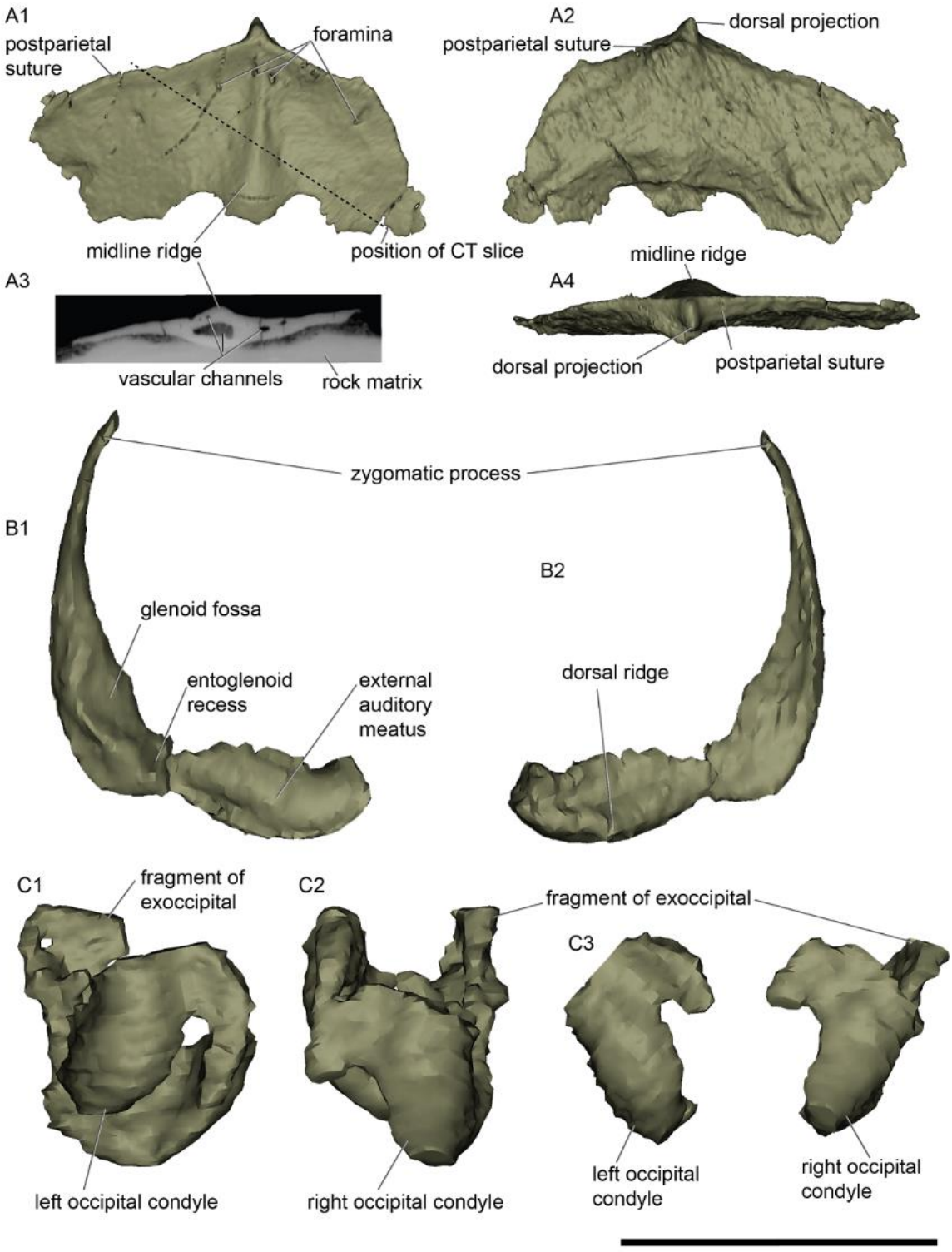

Figure 3.3b.7: The postparietal, squamosal and occipital condyles of NMS G.1992.47.121.1. A1, posterodorsal view of postparietal; A2, anterior/endocranial view; A3, synchrotron slice showing cross section of postparietal; A4, anteroventral view; B the left squamosal, reconstructed (originally in two misaligned pieces), B1, ventral view of squamosal; B2, dorsal view of squamosal; C1-C2, the occipital condyles; C3, reconstruction of occipital condyles. Scale bar equals 5 mm.

Petrosals

See Chapter 3.3c for a complete description of the petrosals of *Borealestes* (Panciroli et al., 2018b). Both petrosals are preserved: the right petrosal is more complete, and still attached to the matrix as part of NMS G.1992.47.121.1. The left petrosal NMS G.1992.47.121.2 is less complete, and is separate from the rest of the skeleton.

Squamosal

The right squamosal is preserved in NMS G.1992.47.121.1, located beside the occipital condyles, separated from the rest of the skull, and below the surface of the block (Figure 3.3b.1 and 3.3b.7B). There is a wide glenoid fossa for articulation with the dentary condyle; the squamosal glenoid is a shallow and concave structure with a slightly raised postglenoid ridge, and the glenoid appears to have an oval outline in ventral view. The squamosal also shows a long and slender zygomatic process. The squamosal glenoid and zygoma in *Borealestes* are similar to those of *Haldanodon* (Lillegraven and Krusat, 1991; Ruf et al., 2013). The posteromedial portion of the squamosal (= the cranial moiety of the squamosal) posterior to the glenoid fossa is broken and displaced. But on the cranial moiety there is the beginning of a strong dorsal ridge (Figure 3.3b.7B2)—possibly this ridge would join dorsally with the strong nuchal crest on the lateral aspect of the parietal (Figure 3.3b.6B and D), which is the case in the preserved skull of *Haldanodon* (Lillegraven and Krusat, 1991. The external auditory meatus is preserved on the ventral side of the dorsal flange of the squamosal, extending from just posterior to the glenoid fossa medially to a depression called the entoglenoid recess (sensu Ruf et al., 2013: fig. 2—this is the same as the ventromedial squamosal recess of Lillegraven and Krusat, 1991).

By comparison to the more complete basicranium with intact squamosal and petrosal of *Haldanodon* (Lillegraven and Krusat, 1991), for which there is a more recent reconstruction (Ruf et al., 2013), we interpret that the squamosal projects quite far laterally, making the skull widest at this point and giving the skull an overall triangular shape.

Occipital condyle and exoccipital

The exoccipital and occipital condyles are separated from the skull, and are preserved within the matrix of Block A beside the right squamosal (Figure 3.3b.1 and 3.3b.7C). Whether they contacted at the midline dorsomedially, ventral to the postparietal,

is uncertain—there may have been a slight gap and contact only with the supraoccipital (Figure 3.3b.7C3). On the preserved part of exoccipital, the interior of the bone appears to be hollow. In *Haldanodon*, the basicranium developed extensive pneumaticity, and the hollow spaces related to pneumaticity expand from the petrosal into the exoccipital (Ruf et al., 2013: fig. 4: condylar plexus). The hollowed interior of the exoccipital, especially the occipital condyle of *Borealestes*, appears to be similar. Based on this, it is interpreted here that the exoccipital bone has similar pneumatic interior structure as in docodonts as a whole. The occipital condyles project from the base of the skull and are oval in shape. The jugular process of the right exoccipital is preserved on the ventral side, although there is damage to the ventral aspect of the exoccipitals. The basioccipital is not preserved.

Postcrania

Axial Skeleton

Atlas arches

Both half neural arches of the atlas (C1) are preserved in NMS G.1992.47.121.1, located on opposite sides of the palate and majority of cranial elements (Figure 3.3b.1). They are intact (Figure 3.3b.8A and B), with dorsoventrally tall dorsal arches that are convex laterally, and a small ventrolateral projection, resembling closely the morphology of the half arches of the atlas in *Morganucodon* (‘*Eozostrodon* ‘, Jenkins and Parrington, 1976). The articular areas for the occipital condyle and atlas are both preserved, the former being slightly larger than the latter, and both oval in shape and slightly concave. There is a strong medially directed projection where the two articular areas meet. The centrum of the atlas (C1) is not preserved in this specimen of *Borealestes*, consistent with the fact that the half neural arches are not fused at the dorsal midline. Because the dentition of NMS G.1992.47.121.1 shows no sign of any tooth replacement and indicates it is an adult individual, the lack of fusion of components of the atlas is an adult character of the vertebrae, at least for *Borealestes*. This is a plesiomorphic feature of cynodonts (Jenkins and Parrington, 1976; Rowe, 1988).

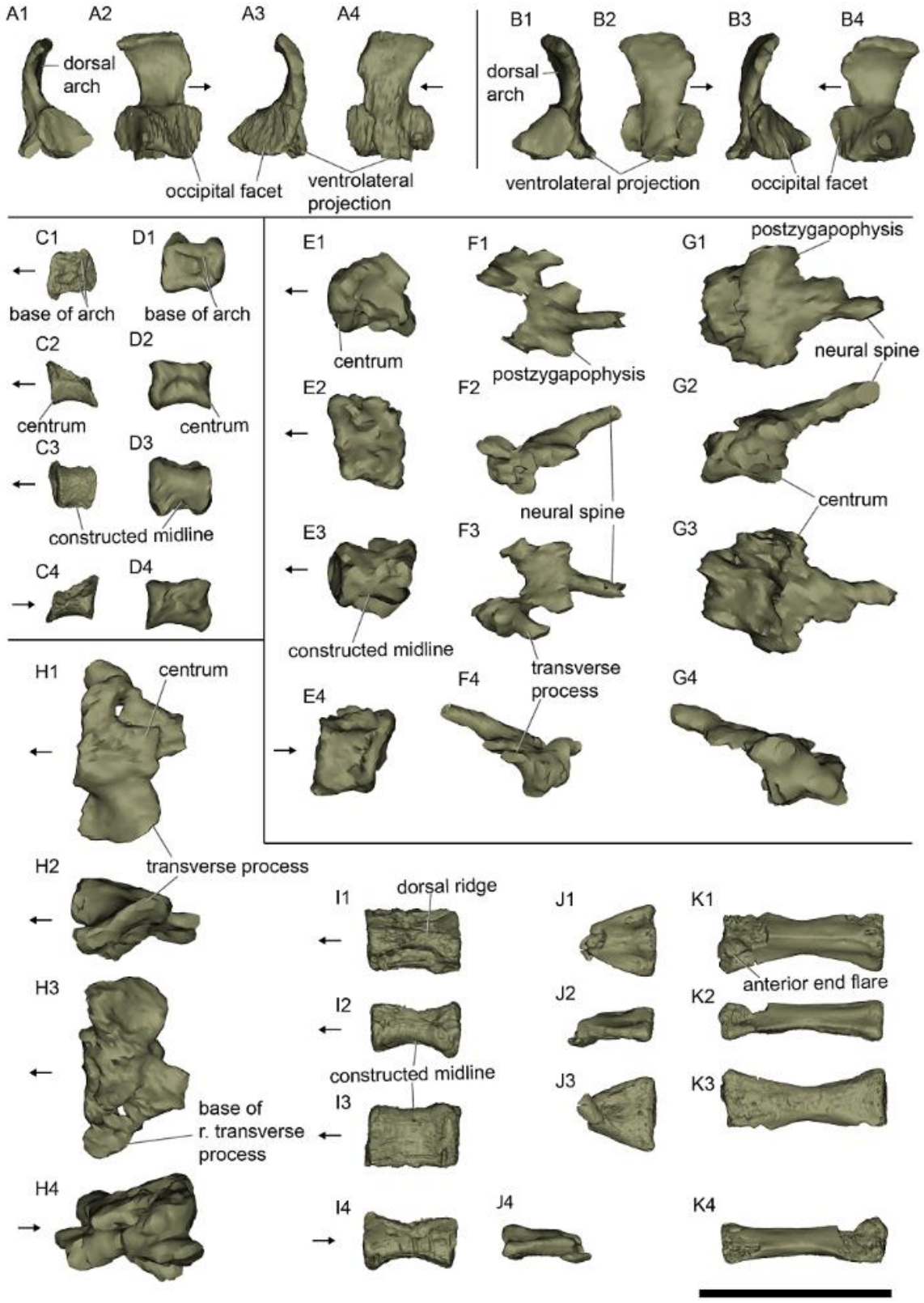
A1
A2
A3
A4
dorsal arch
occipital facet
ventrolateral projection
B1
B2
B3
B4
dorsal arch
ventrolateral projection
occipital facet
C1
D1
base of arch
base of arch
C2
D2
centrum
centrum
C3
D3
constructed midline
C4
D4
E1
centrum
E2
E3
constructed midline
E4
F1
postzygapophysis
F2
neural spine
F3
transverse process
F4
G1
postzygapophysis
neural spine
G2
centrum
G3
G4
H1
centrum
H2
transverse process
H3
base of r. transverse process
H4
I1
dorsal ridge
I2
constructed midline
I3
I4
J1
J2
J3
J4
K1
anterior end flare
K2
K3
K4

Vertebrae

There are two cervical, three thoracic, and four caudal vertebrae preserved in NMS G.1992.47.121.1 (Figure 3.3b.8C-J). The cervical and caudal vertebrae are most completely preserved. In addition, there are two chevrons, one almost complete and the second a smaller, worn fragment (Figure 3.3b.9A-B).

Post-Axial Cervical Vertebrae

The post-axial cervical vertebrae of *Borealestes* are represented by two centra. Both are small and lack transverse processes (Figure 3.3b.8C-D). The exact position of these vertebral centra in the cervical vertebral column is uncertain. Of the two cervical centra, one is noticeably smaller than the other. I suggest that the smaller centrum may belong to a vertebra in C2-3 positions (Figure 3.3b.8C), while the larger is more likely to belong to C3-4 positions (Figure 3.3b.8D). The body or centrum is amphicoelous, oval when viewed anteroposteriorly. The bases of the neural arch can be discerned on both vertebrae, but the arch and the dorsal portion of the vertebrae are not preserved. Both vertebrae are slightly distorted, but it is clear they are only slightly longer anteroposteriorly than they are wide mediolaterally. The middle part of the centrum is bilaterally constricted on both.

Thoracic vertebrae

The three thoracic vertebrae represented in NMS G.1992.47.121.1 comprise one distorted and poorly preserved centrum lacking processes or arch (Figure 3.3b.8E), one neural spine with transverse processes, but no centrum (Figure 3.3b.8F), and a dorsoventrally compressed almost complete vertebra, with centrum, arches and neural spine (Figure 3.3b.8G). The three thoracic vertebrae are located at some distance from each other in the limestone block (Figure 3.3b.1). Their exact position in the vertebral column is not certain.

The centrum is badly distorted in both vertebrae preserving a centrum (Figure 3.3b.8E and G), making the original shape difficult to discern. It appears to be

Figure 3.3b.8 (previous page): Atlas arches and vertebrae of NMS G.1992.47.121.1. A1-4, left atlas arch ; A1, posterior view; A2, medial view; A3, anterior view; A4, left lateral view; B1-4, right atlas arch; B1, posterior view; B2, right lateral view; B3, anterior view; B4, medial view; C-D, cervical vertebrae; E-G, thoracic vertebrae; H-K, caudal vertebrae. In C-K numbers correspond to: 1, dorsal view; 2, right lateral view; 3, ventral view; 4, left lateral view. Scale bar equals 5 mm.

anteroposteriorly shorter than it is mediolaterally wide or dorsoventrally tall. As with the cervical vertebrae, it is amphicoelous and constricted at the middle part of the centrum, and shows a distinct rim around the edge of the centrum.

The neural spine of the thoracic vertebra is long and slants diagonally posteriorly from the neural arch (Figure 3.3b.8F and G). The postzygapophyses are at the base of the neural arch, and on the right side of one vertebra the articular facet for the rib is preserved, posterolateral to the base of the prezygapophysis (which is not present) (Figure 3.3b.8F). The neural canal is preserved in the largest of the vertebrae, but it is compressed.

Caudal vertebrae

There are four caudal vertebrae preserved in NMS G.1992.47.121.1, one proximal (Figure 3.3b.8H), one more distal (Figure 3.3b.8I), and two distalmost along the tail length (Figure 3.3b.8J and K). The most proximal vertebrae is incomplete, comprising the left transverse process, a portion of the centrum, and the base of the incomplete right transverse process. The centrum is compressed dorsoventrally, and lacks the dorsal and ventralmost portions, including the base of the neural arch. The size and structure of this vertebra suggests it is from the base of the tail, ca3-7. The preserved transverse process projects quite far laterally, similar to that seen in *Castorocauda* (Ji et al., 2006).

The next vertebra preserved in the caudal series is mid-way along the tail, likely between ca8- 12 (Figure 3.3b.8I). It is amphicoelous and strongly constricted at the midline, especially dorsoventrally. It is longer anteroposteriorly than it is wide mediolaterally, presenting a rectangular profile in dorsal and ventral view. There is no neural canal. The ventral side is smooth and convex, while the dorsal side of the vertebra has a strong ridge running anteroposteriorly, flanked by deep indentations laterally. There are no complete preserved transverse processes or zygapophyses, although there appears to be the base of possible zygapophysis on the dorsal surface of the vertebra at the posterior and anterior ends.

The two distalmost caudal vertebrae comprise one posterior end of a vertebra (Figure 3.3b.8J) and a second almost complete vertebra (Figure 3.3b.8K), probably from somewhere between ca14-18. They are positioned together on the surface of the limestone block, beside the fragments of the left dentary and left humerus (Figures 3.3b.1 and 3.3b.2). The almost complete caudal vertebra is much longer anteroposteriorly than it is wide

mediolaterally. It is damaged on the right anterior side, and what is preserved on the left includes a distinct ridge, projecting dorsolaterally. There is no corresponding projection on the poster end of the vertebra. The less complete vertebra matches the morphology of the posterior portion of the more complete vertebra, and was therefore likely to have originally been of similar proportions and shape.

Both of the posteriormost caudal vertebrae have a smooth ventral surface, and a ridge along the dorsal surface. Unlike in the ca8-12 vertebrae, this ridge comprises most of the body of the vertebrae, with no lateral indentations. The vertebrae flare mediolaterally at the anterior and posterior ends, forming mediolaterally wide articulation surfaces with the next vertebra. Unlike the other vertebrae described here for *Borealestes,* there is no concavity on the centrum.

Chevrons

The two chevrons preserved are very different in size, the larger coming from a more anterior position and the smaller from a distal position on the tail (Figure 3.3b.9A-B). The smaller chevron is part of the main limestone block, NMS G.1992.47.121.1, and is positioned near the main portion of the skull (Figure 3.3b.2). The larger chevron, NMS G.1992.47.121.8, was dislodged from the main block.

NMS G.1992.47.121.8 is almost intact, and is diamond shaped when viewed dorsally or ventrally (Figure 3.3b.9A1 and A3). It flares laterally at the midline, and these flares project dorsally to their position between the caudal vertebrae, and enclose a dorsal canal along the anteroposterior length of the chevron. There is a protuberance at the elongated anterior end of the chevron (Figure 3.3b.9A3-4), but damage makes it unclear if the same protuberance was present on the posterior end.

The smaller chevron, part of NMS G.1992.47.121.1, comprises only a small projection and the central body of the chevron (Figure 3.3b.9B). Although superficially resembling a claw, the flared main body of the bone is mediolaterally broad, making it incongruent with ungual morphology. The small size suggests it was a distal chevron from near the tip of the tail.

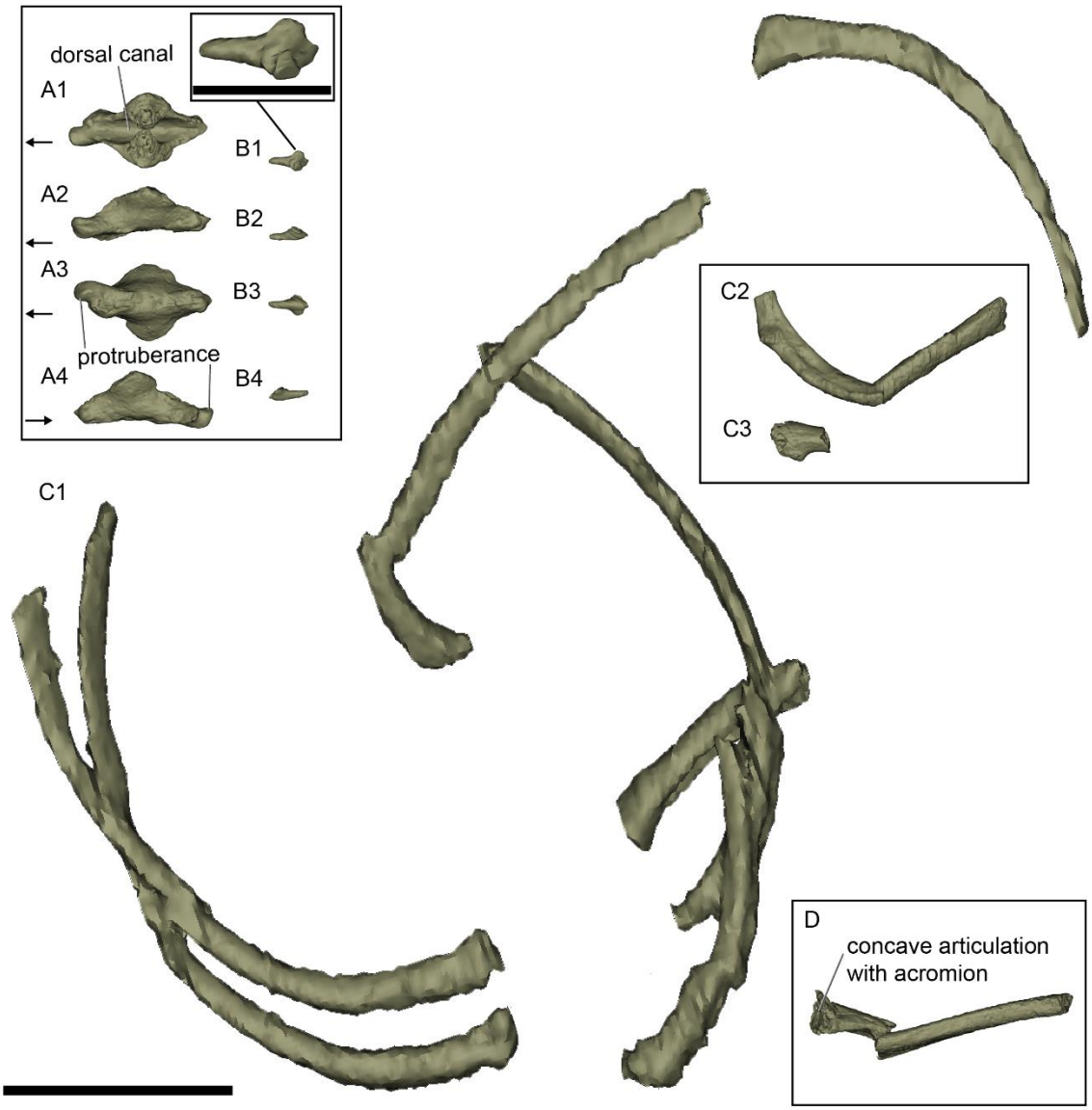

Figure 3.3b.9: Chevrons, ribs and clavicle of Block A. A, larger chevron NMS G.1992.47.121.8; B, smaller chevron part of NMS G.1992.47.121.1 (numbers correspond to: 1, dorsal view; 2, right lateral view; 3, ventral view; 4, left lateral view); C, ribs as preserved in NMS G.1992.47.121.1; C2, rib preserved near cranial elements in NMS G.1992.47.121.1; C3, rib fragment NMS G.1992.47.121.12; D, right clavicle NMS G.1992.47.121.6. Scale bar equals 5 mm.

Ribs and clavicle

The total number of ribs in *Borealestes* is not known, but there are eight preserved in NMS G.1992.47.121.1 (Figure 3.3b.9C1 and C2), and a further rib fragment has been separated from the rest of the skeleton, NMS G.1992.47.121.12 (Figure 3.3b.C3).

A portion of the right clavicle, NMS G.1992.47.121.6, is separated from the main limestone block (Figure 3.3b.9D). The lateral end is slightly concave, and would have articulated with the acromion on the scapulacoracoid (not present). The medial end of the clavicle that would articulated with the interclavicle is missing.

Humerus

Only a fragment of the left proximal humerus is present in NMS G.1992.47.121.1, located beside the fragment of posterior left dentary (Figures 3.3b.1 and 3.3b.2). The deltopectoral crest is preserved in the upper surface of the matrix, together with part of the greater turbercle (Figures 3.3b.1, 3.3b.2 and 3.3b.10A). The abraded broken surface of this fragment of humerus suggests the bone may have been complete on the surface of the limestone, but was either broken or abraded prior to collection.

The deltopectoral crest is large, with deep fossae for muscle insertion (Figure 3.3b.10A). What remains of the greater tubercle and humeral head indicate a relatively large head, but there is too little preserved to indicate further details of its morphology. However, what is preserved appears to be intermediate between the gracile morphology of the humerus in *Agilodocodon* (Meng et al., 2015) and the more robust morphology of *Haldanodon* (Martin 2005).

Radius

The left radius of *Borealestes* is preserved on the surface of the limestone block in specimen NMS G.1992.47.121.1 (Figure 3.3b.1). It is complete with only some minor damage to the distal end (Figure 3.3b.10B). There is a relatively wide, cup-shaped and projecting articular fovea, strongly sloping medially in dorsal view.

The radius is somewhat sigmoidal along its length, allowing it to sit alongside the ulna (which is not preserved). The distal end of the radius is somewhat expanded, but does not appear to be transversely wider than the proximal end, although the missing styloid process makes this interpretation uncertain. A ridge runs along the distal half of the length of the shaft on the dorsal side, somewhat laterally positioned. This blends smoothly into a groove on the lateral side of the distal radius. This groove would run to the styloid process, but this process is broken and missing. Medially, a much smaller groove is visible on the mediodorsal surface of the distal end of the radius.

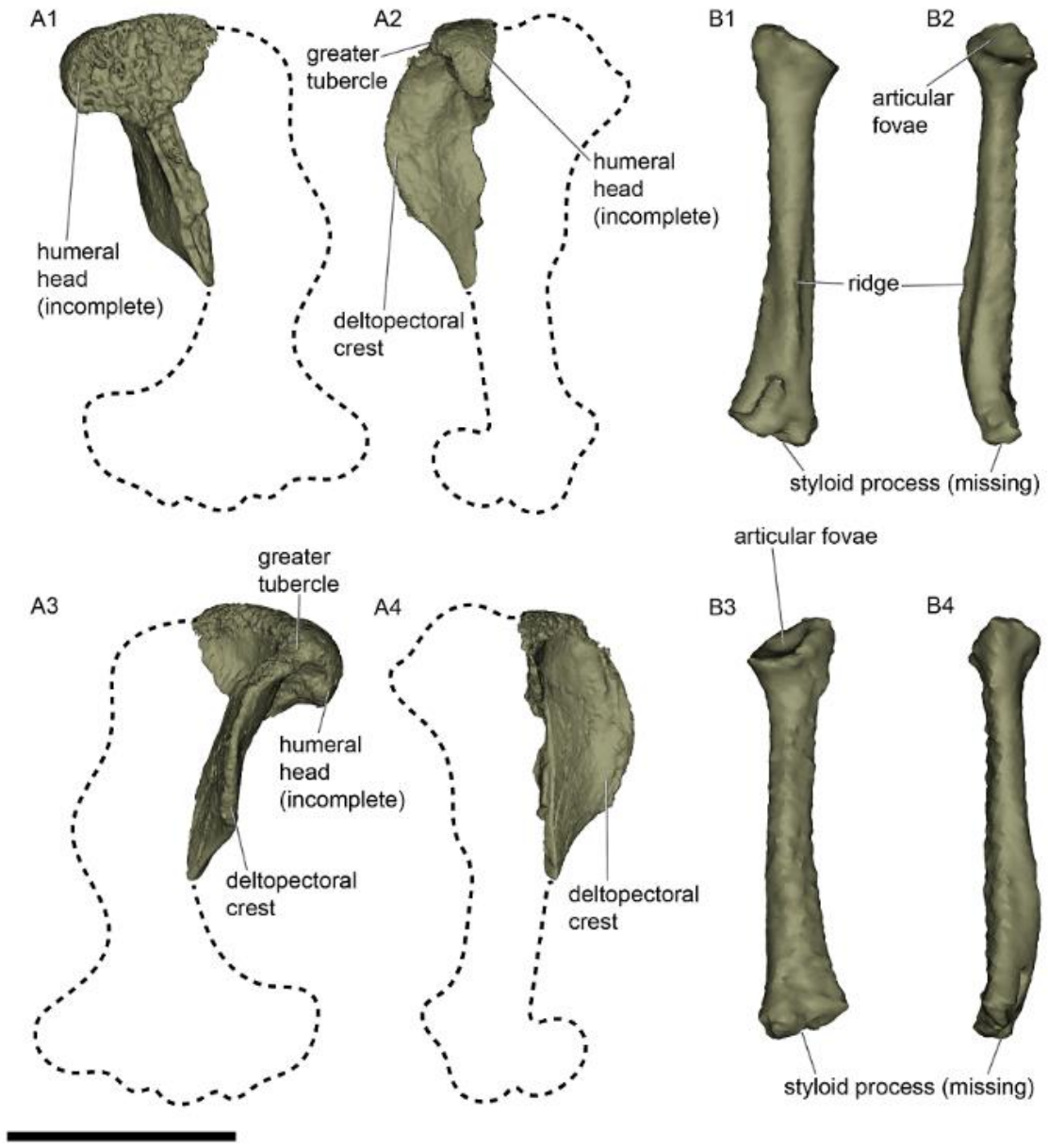

Figure 3.3b.10: The humerus and radius of NMS G.1992.47.121.1. A1-4, left humerus; A1, posterior view; A2, lateral view; A3, anterior view; A4, medial view; B1-4, left radius; B1, anterior view; B2, medial view; B3, posterior view; lateral view. Scale bar equals 5 mm.

Ilium

The right ilium of *Borealestes* is preserved on the surface of the limestone block NMS G.1992.47.121.1, and is almost complete (Figure 3.3b.1). The element is long and elongate, and the iliac blade is flattened laterally, but convex medially (Figure 3.3b.11A).

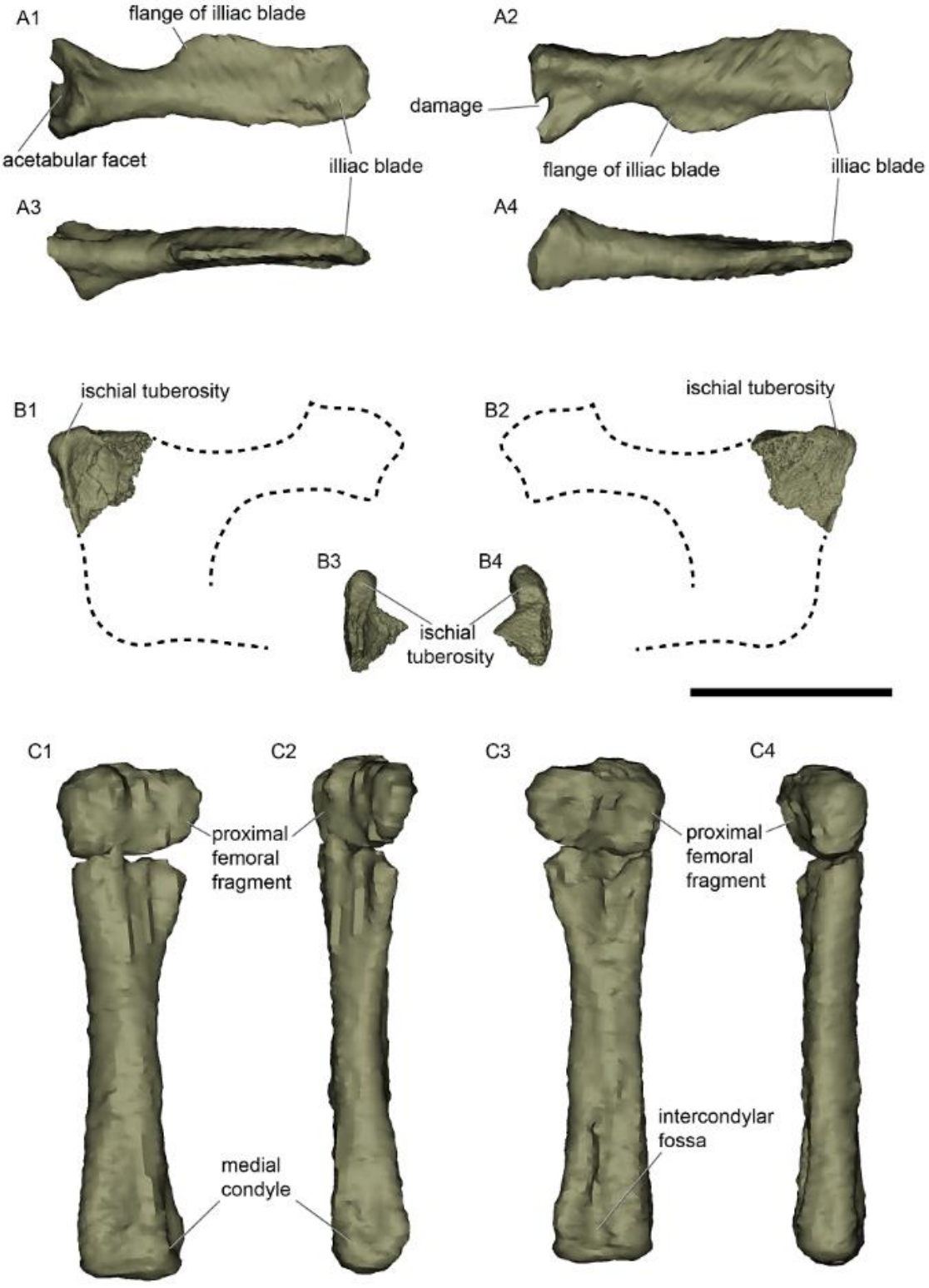

There is a thin flange on the dorsal edge of the iliac blade, projecting dorsally from midway along the ilium and narrowing slightly anteriorly. The ventral edge of the anterior end of the iliac blade is also mediolaterally thin, and has no discernible bulging along the

rim. There is no discernible rugose ilio-sacral contact on the medial side of the ilium, but some ghosting in the original tomographic slices makes it unclear.

The acetabular facet is large, triangular when viewed posteriorly, and slightly convex. The surface is slightly angled anterodorsally. The articulation with the ischium is damaged—a notch has been removed from the bone, most likely during collection or preparation of the specimen. The articulation with the ischium and pubis are evidently narrow, forming a shallow acetabular facet for the femoral head.

Ischium

The bone fragment NMS G.1992.47.121.11 is identified as the dorsal corner of the right ischial blade, the only part of the ischium preserved in this specimen of *Borealestes* (Figure 3.3b.11B). There is a strong ischial tuberosity, with a concave lateral surface of the ischium. The dorsal edge of the ischium appears wide and flattened, sloping medioventrally.

Femur

An incomplete left femur is preserved in this specimen of *Borealestes*, located at the opposite end of the limestone block from the rest of the skeleton, near the right ilium (Figure 3.3b.1). The distal portion of the femur is well preserved extending from below the third trochanter (trochanter not preserved) (Figure 3.3b.11C). A fragment of the proximal portion of the femur is preserved near the broken and crushed end of the distal portion, and has been placed in approximate position in the reconstruction, but it does not preserve the proximal morphology.

The preserved morphology of the distal femur is slender and gracile, similar to *Agilodocodon* (Meng et al., 2015). The intercondylar fossa is distinct, and there is a noticeable medial condyle, but the lateral condyle is less distinct and neither condyles flare, indicating the distal end of the femur was not transversely broad. The preserved diaphysis

Figure 3.3b.11 (previous page): The ilium, ischium and femur of NMS G.1992.47.121.1. A1-4, the right ilium; A1, right lateral view; A2, medial view; A3, dorsal view; A4, ventral view; B1-4, right ischial fragment; B1, right lateral view; B2, medial view; B3, dorsal view; B4, ventral view; C1-4, left femur; C, anterior view; C2, medial view; C3, posterior view; C4, lateral view. Scale bar equals 5 mm.

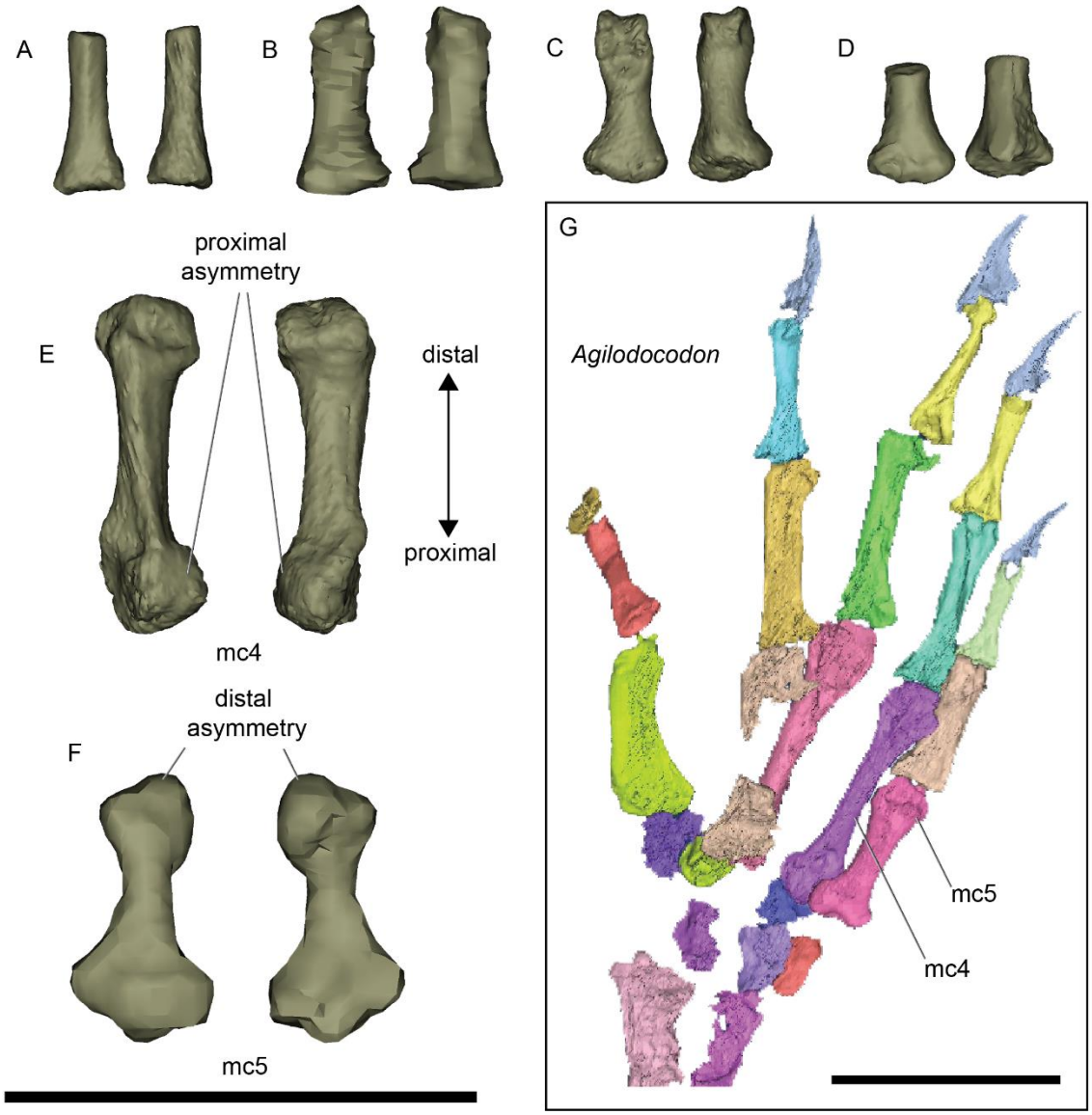

Figure 3.3b.12: Manus and unidentified elements of Block A. A-D, intermediate metacarpals or metatarsals part of NMS G.1992.47.121.1; E-F part of NMS G.1992.47.121.1; G, manus of *Agilodocodon* for comparison (from Meng et al., 2015:fig. S6. Scale bars equal 5 mm.

of the femur is slender, similar to those of *Agilodocodon*, and other mammaliaforms such as *Morganucodon* and *Megazostrodon* (Jenkins and Parrington, 1976).

Manus and Pes

There are seven metacarpal/tarsals, and seven carpal/tarsal elements present in NMS G.1992.47.121.1 (and associated dislodged material). Most are preserved in the main block containing the partial skeleton, but three other autopodial elements are preserved separately,

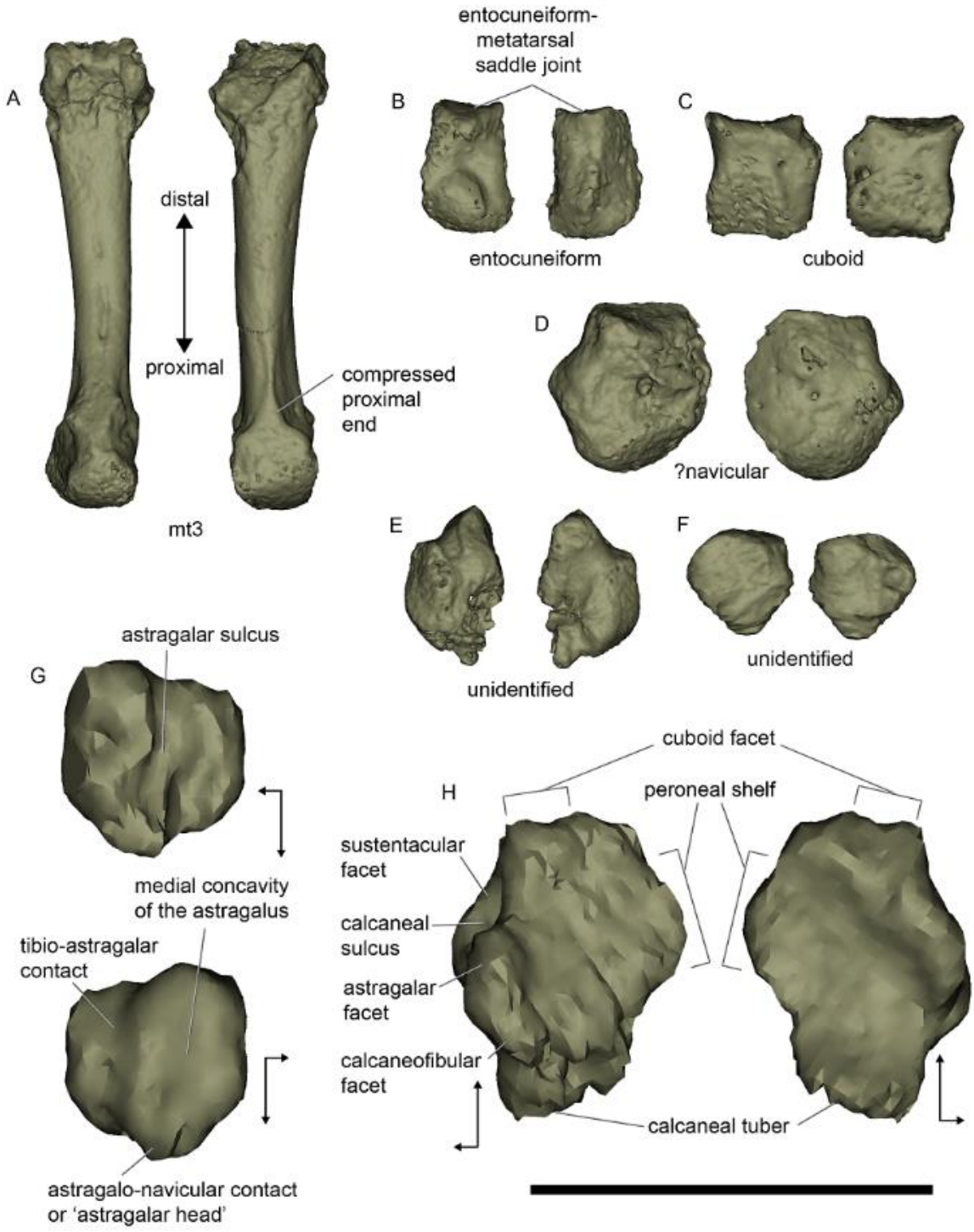

Figure 3.3b.13: Pes and unidentified elements of Block A. A, metatarsal III NMS G.1992.47.121.5; B-H part of NMS G.1992.47.121.1. In G-H long arrows indicate distal, short arrows indicate medial. Scale bar equals 5 mm.

NMS G.1992.47.121.5, NMS G.1992.47.121.7 and NMS G.1992.47.121.10 (Figure 3.3b.12-13). None of these elements are in articulation, and most are not in close association, hindering identification.

One metatarsal can be positively identified: NMS G.1992.47.121.5 is separated from the skeletal block and represents mt3 (Figure 3.3b.13A), recognisable from the compacted morphology of the proximal joint, and size (compared to other elements, and to those of *Agilodocodo*n). Two metacarpals are also preserved: mc4 is identified by the distinctive proximal asymmetry (Figure 3.3b.12E), and mc5 has distinctive distal asymmetry (Figure 3.3b.12F). All of these elements are identified by their resemblance to the corresponding elements in *Agilodocodon* (Meng et al., 2015) (Figure 3.3b.12G). There are no features that allow for further identification of the remaining four autopodial elements, but their shorter length, with broader proximal end suggest they are intermediate metacarpals or metatarsals.

The right calcaneus is well preserved in NMS G.1992.47.121.1, and is located near the ribs on the main skeleton block, below the surface (Figure 3.3b.1). It is short and curved ventrally, with a small calcaneal tuber (Figure 3.3b.13H). The calcaneal tuber appears to have an uneven surface, perhaps due to lack of full ossification. The morphogy of the calcaneus shows plesiomorphic features of the most early diverging mammaliaforms such as *Morganucodon* (Zhou et al, 2013), and other docodonts for which the calcaneus is known, such as *Agilodocodon* (Meng et al., 2015) and *Docofossor* (Luo et al., 2015). In *Borealestes* the calcaneus is slightly less elongate than in *Agilodocodon*, being more similar to the morphology of *Morganucodon.* For ecomorphological analysis of the calcaneus, see Chapter 4.4.

Two of the carpal/tarsal elements remain unidentified (Figure 3.3b.13E [NMS G.1992.47.121.10] and F), but the remaining elements are identified as an entocuneiform (Figure 3.3b.13B), a cuboid (Figure 3.3b.13C), a probable navicular NMS G.1992.47.121.7 (Figure 3.3b.13D) and an astragalus (Figure 3.3b.13G). The left entocuneiform has a well formed entocuneiform-metatarsal saddle joint, facilitating movement of metatarsal 1. The cuboid also has a wide distal cuboid-metatarsal facet. The astragalus was positioned deep within the limestone block, and the resolution of the synchrotron scan means surface detail is limited. However the tibio-astragalar trochlea and post-astragalar shelf are identifiable. They are less developed than in *Docofossor*, and like the rest of the pedal and manual

elements there is no sign of the anatomical specialisations for a fossorial lifestyle as seen in *Docofossor*.

3.3b iii) Discussion

Cranium

Anterior cranial elements

For a complete description of the right dentary and lower dentition with comparisons to other taxa see Chapter 3.3a (Panciroli et al., 2019). Most features of the anterior bones of the skull are similar to those seen in other docodontans, but particularly the long, gracile rostrum of *Agilodocodon* (Meng et al., 2015) (Figures 3.3b.13-15). The anterior incisors of *Borealestes* are strongly procumbent, especially i1 as seen in *Agilodocodon*. This characteristic was argued in *Agilodocodon* to suggest a possible adaptation for exudativory, with this procumbent morphology resembling that seen in New World monkeys that gnaw on bark to eat sap (Meng et al., 2015:765). This would have been a plausible feeding mode for an arboreal docodontan, but close comparison between extant exudativores and *Agilodocodon* does not support this idea, as the docodontan does not have features such as restricted labial enamel, broad lower incisor girth, toothcombs and 'short-tusked' canines (Wible and Burrows, 2016). The morphology of the docodontan procumbent incisors more closely resembles extant insectivorous mammals, such as macroscelideans, and this is also supported by the molar morphology.

For detailed discussion and comparisons of upper incisor morphology see Chapter 3.3a (Panciroli et al., 2019). It is unclear if the premaxilla formed the posterior margin of I4 as in *Haldanodon*, or whether it was formed by the maxilla (Figure 3.3b.3B). In *Morgaucodon* the premaxilla meets the palatine between I3 and I4 (Kermack et al., 1981). At the anterior end of the right premaxilla I identify a possible stump of the internarial process, or the median process of the premaxillary bone, as identified in *Haldanodon* (Lillegraven and Krusat, 1991:59). This is a plesiomorphic feature retained in mammaliaforms, seen in all docodonts and also described in multituberculates (Miao, 1988).

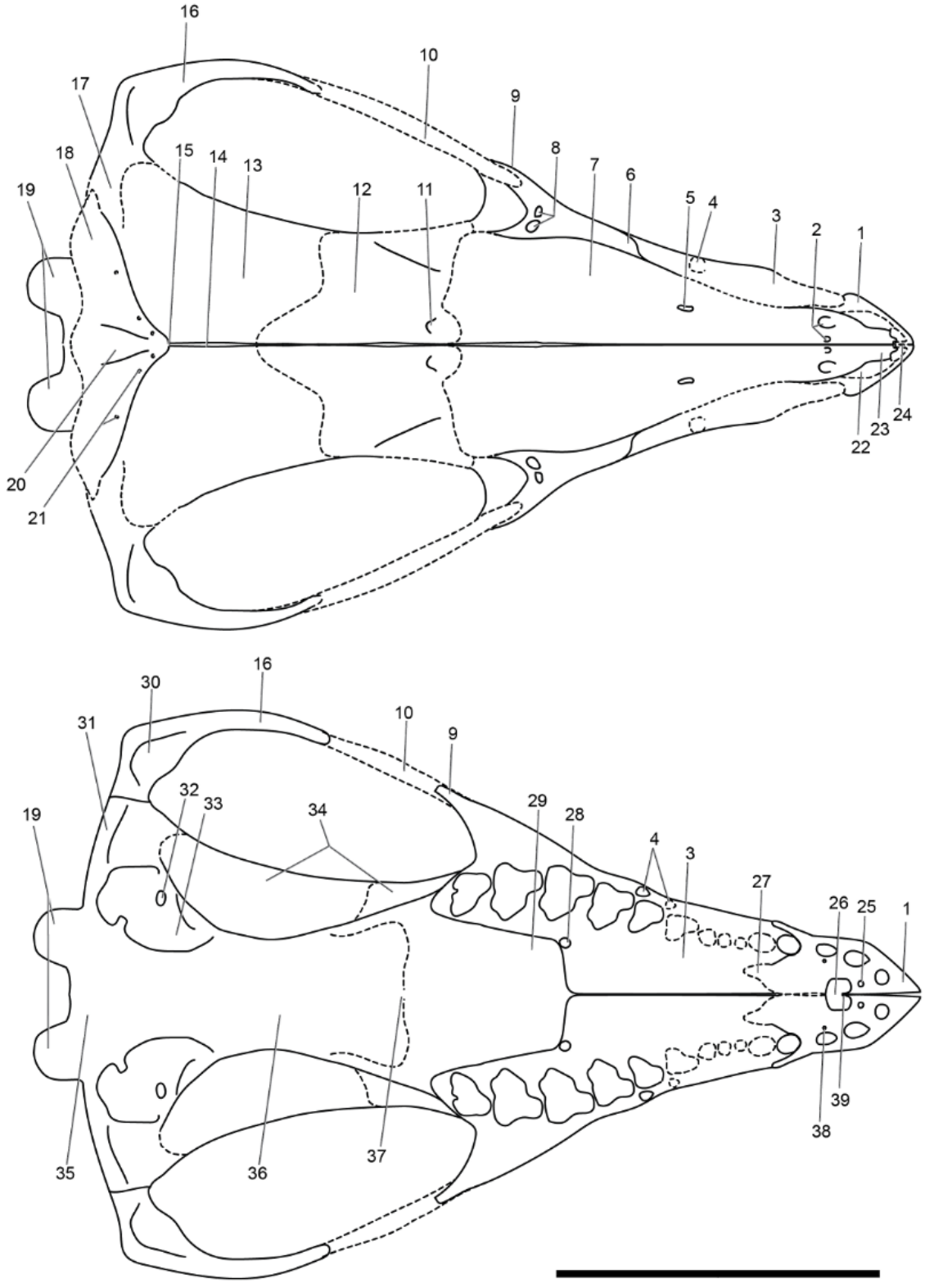
16
17
18
19
15
14
13
12
11
10
9
8
7
6
5
4
3
2
1
20
21
22
23
24
16
30
31
10
9
32
33
34
29
28
4
3
27
26
25
1
19
35
36
37
38
39

The vascular canals connecting the anterior premaxillary foramen anteriorly and laterally are likely to be for the greater palatine nerve and artery, and similar vascular channels have been traced in pre-mammalian cynodonts (Benoit et al., 2017). Some features observed in other docodontans such as *Haldanodon*, that are not preserved in this specimen of *Borealestes*, include a bulging canine root in the maxilla, the position of the infraorbital foramen just posterior to the canine, presence and position of the septomaxilla, and the "posterior salient" of the premaxillary bone (Lillegraven and Krusat, 1991: 46). I have reconstructed the missing portions of the skull of *Borealestes* (Figures 3.3b.13-15) based on the morphology of these features in other docodontans, notably *Agilodocodon*.

The greater palatine foramen marks the edge of the palatal process of the maxilla, medial to M2, and the palatal process of the maxillary bone may project posteriorly into the palatal process of the palatine bone along the midline suture, but this is unclear due to damage to the specimen (Figure 3.3b.4B). Such a projection is not seen in *Morganucodon* nor *Haldanodon*, so it may be that this projection is a fragment of the palatine bone. The position of the greater palatine foramen in *Borealestes* differs from *Haldanodon*. In both taxa it is positioned medial and slightly anterior to M2, and there is no greater palatine groove (unlike in *Morganucodon*). But in *Haldanodon* the foramen is oblong, positioned closer to the midline suture, and on the edge of the palatine process of the maxilla. It is not clear whether the posterior rim of the grater palatine foramen in *Borealestes* is formed by the palatine process of the palatine (as in *Haldanodon*), but the foramen is more rounded, and positioned closer to the toothrow (Figures 3.3b.4 and 3.3b.14).

Figure 3.3b.14 (previous page): Reconstruction of the skull of *Borealestes serendipitus* in dorsal (above) and ventral (below) views. 1 Premaxilla; 2 Anterior nasal foramina; 3 maxilla; 4 Infraorbital foramen; 5 Posterior nasal foramen; 6 lacrimal; 7 nasal; 8 Lacrimal foramen; 9 Zygomatic process of lacrimal; 10 jugal; 11 Infraorbital foramen; 12 Frontal; 13 parietal; 14 Interparietal suture; 15 Sagittal crest; 16 squamosal; 17 Dorsal flange of squamosal; 18 postparietal; 19 Occipital condyles; 20 Midline ridge of postparietal; 21 postparietal foramina; 22 septomaxilla; 23 Anterior projection of nasal; 24 internarial bar; 25 Anterior premaxillary foramen; 26 Incisive foramen; 27 Palatal posterior salient of premaxilla; 28 Greater palatine foramen; 29 Palatal process (not known); 30 Glenoid fossa; 31 External auditory meatus; 32 Fenestra vestibuli; 33 Pars cochlearis; 34 Orbital area not unknown; 35 Basicranium not known; 36 Pterygoid and basicranium not known; 37 Primary palate not known; 38 I3 foramen; 39 Posterior projection of premaxilla into incisive foramen; 40 Coronoid process; 41 Nuchal crest; 42 Angular process of dentary; 43 Masseteric foramen; 44 Dentary; 45 Mental foramen; 46 Anterior premaxillary foramen. Scale bar equals 5 mm.

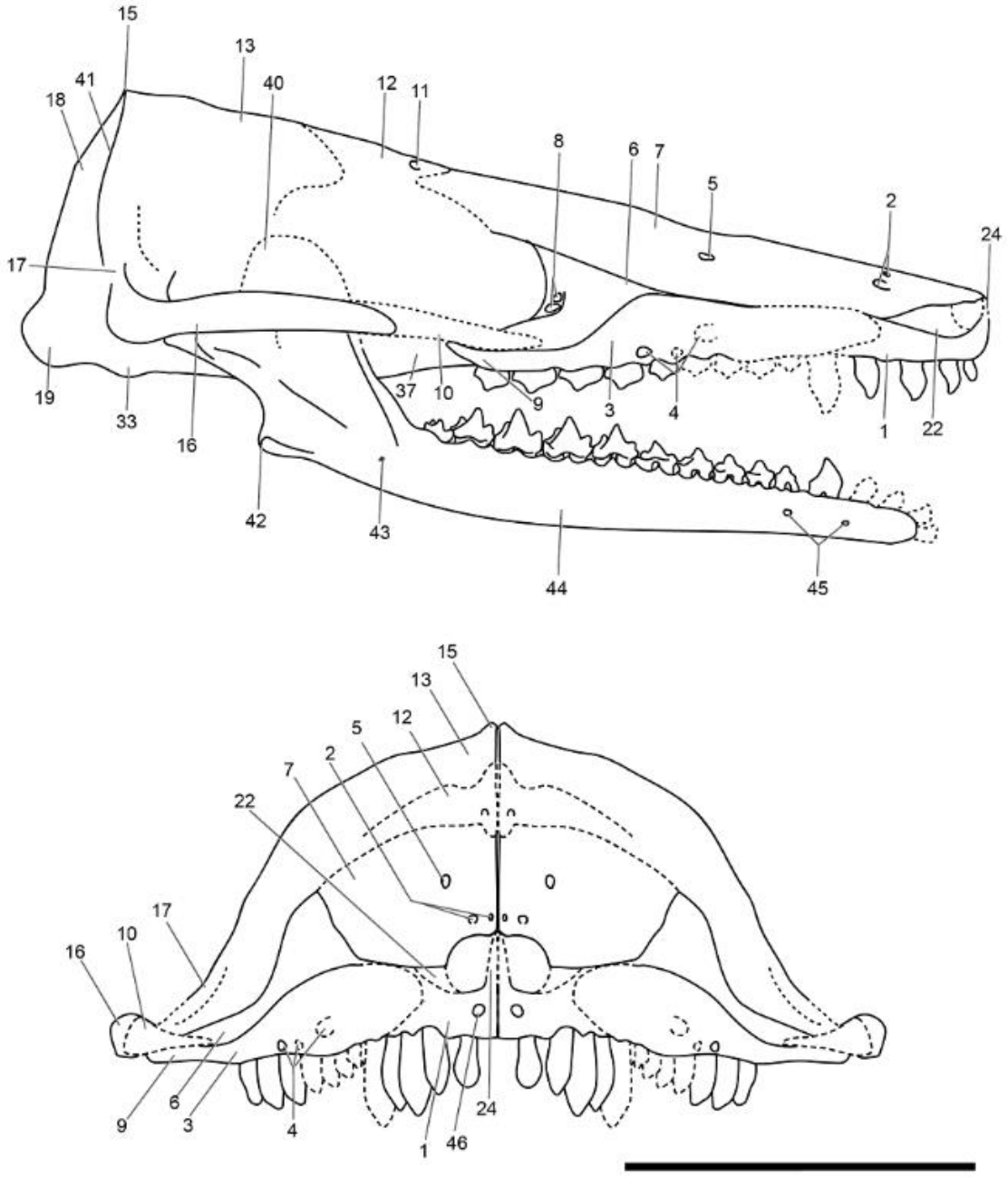

Figure 3.3b.15: Reconstruction of the skull of *Borealestes serendipitus* in right lateral (above) and anterior (below) views. Labels as for Figure 3.3b.13. Scale bar equals 5 mm.

It is unclear if the maxilla would have formed the posterior alveolar margin of i4. In *Haldanodon* the maxilla forms the posterior alveolar margin of i5 and holds all of i6, the posteriormost incisor alveolus in *Haldanodon* (Lillegraven and Krusat, 1991:p46).

The posteriorly mediolaterally broad nasals more closely resemble *Haldanodon* in their width (Lillegraven and Krusat, 1991:p46), than the slightly narrower skull of

Agilodocodon (Meng et al., 2015), or the greater extension of the maxillae and lacrimals dorsally as seen in *Morganucodon* (Lillegraven and Krusat, 1991). This accentuates the triangular dorsal profile of the skull, exaggerated further by the wide zygomatic arches (see below). The posterior nasal foramina are positioned approximately in line with P4, which is more posteriorly positioned and fully enclosed by the nasal than in *Haldanodon*. As in *Haldanodon*, but unlike *Morganucodon*, the nasals extend posteriorly to lie at least in line with the base of the maxillary base of the zygomatic arch. Anteriorly the nasals resemble *Haldanodon*, with a long projection of the nasal medial to the anterior nasal foramen.

The lacrimal, and what remains of the frontal, resemble other docodontans and early diverging mammaliaforms such as *Morganucodon*.

Posterior cranial elements

The small sagittal crest along the unfused medial contact of the parietals of *Borealestes* is similar to that seen in other docodontans, but slightly less prominent than in *Haldanodon*, or the geologically older early diverging mammaliaform *Morganucodon*. The nuchal crest is also similar to other docodontans, notably *Haldanodon*. Both of these features are seen variably in other mammal groups, usually associated with muscular attachment, and/or sexual dimorphism. However the interparietal described in *Haldanodon* is positioned posteriorly between the parietals and the dorsal edge of the postparietal (Lillegraven and Krusat, 1991:77). In *Borealestes*, the postparietal sits against the parietal directly, and a small dorsal projection slots into the parietal suture to contribute to the small sagittal crest (Figures 3.3b.7 and 3.3b.13). The bulge along the midline of the postparietal and the foramina present on the dorsal lateral surface, indicating high vascularisation of this bone, and conforms with the form of the postparietal in *Haldanodon*.

The complete description and morphology of the petrosals of *Borealestes* can be found in Chapter 3.3.2 (Panciroli et al., 2018b). The portion of squamosal preserved includes the auditory meatus and the glenoid fossa, and suggests a gracile squamosal and jugal more like *Agilodocodon* (Meng et al., 2015) than the more robust squamosal and jugal of *Haldanodon* (Lillegraven and Krusat, 1991). Like *Haldanodon* however, the squamosal appears to project quite far laterally, giving the skull a triangular outline from above (Figures 3.3b.13 and 3.3b.14).

The morphology of the occipital condyles in *Borealestes* resembles *Haldanodon*, and is little changed from other early mammaliaforms such as *Eozostrodon*, and *Megazostrodon* (Jenkins and Parrington, 1976). The dorsal flange of the squamosal is not preserved in *Borealestes*, but the indentation on the posterolateral side of the parietal suggests it was present and extended approximately a third of the way up the parietal dorsally (Figure 3.3b.6), more similar to *Morganucodon* than *Haldanodon*.

The crushing and flattening of the anterior dorsolateral surface of the parietal bone makes it unclear if the indentation there has resulted from pre- or post-depositional damage, or represents a ridge marking the posterodorsal overlap of the temporal bone. If it was the latter, this would suggest the bone located anteroventral to it was a fragment of the temporal region. However the indentation would suggest a strong finger-like projection of the temporal, which is unlike that seen in other docodontans.

Postcranium

Axial Skeleton

The atlas neural arches of *Borealestes* form part of the atlas-axis complex. This complex is little changed from earlier cynodonts, such as the tritylodontids *Oligokyphus* and *Kayentatherium* (Kühne, 1956; Jenkins and Parrington, 1976; Sues and Jenkins, 2006). Although the atlar centrum is not preserved and the components of the atlas are not fused in the specimen NMS G.1992.47.121.1, the preserved half of the arches suggest the atlas would have resembled other early mammaliaforms and cynodonts.

The vertebrae preserved in this specimen of *Borealestes* suggest a similar morphology to other docodontans in the cervical and thoracic vertebrae, and to those of non-mammaliaform cynodonts (Sues and Jenkins, 2006).

In the caudal series of *Agilodocodon* there is a clear change in morphology from ca7 to ca8: the transverse process is reduced and the more posteriorly positioned vertebrae are more elongated. From this comparison to the associated caudals of *Agilodocodon* (Meng et al., 2015), the proximal caudal in *Borealestes* NMS G.1992.47.121.1 is most likely from a position anterior to ca8, as the transverse processes of this caudal project quite far laterally, similar to the proximal caudals of *Agilodocodon*. The projection is similar to that seen in

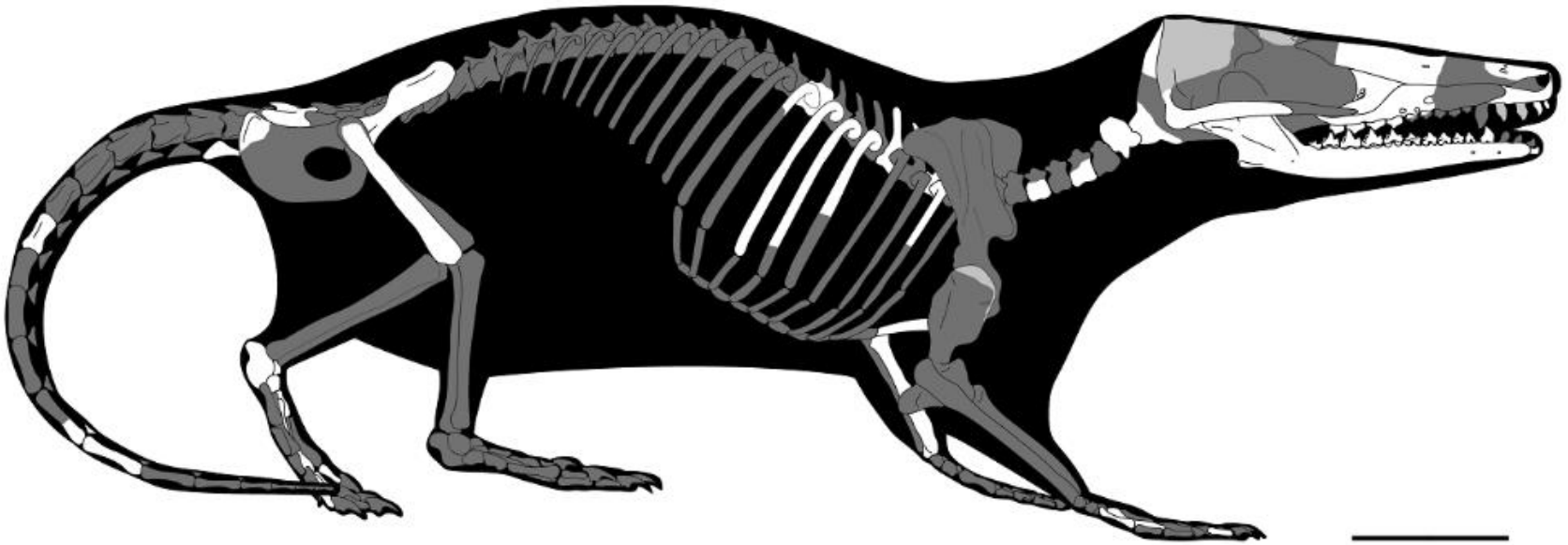

Figure 3.3b.16: Skeletal reconstruction of *Borealestes serendipitus*. White bones present in Block A (including dislodged fragments), dark grey bones not present in Block A, and pale grey bones present on left side of skeleton and mirrored for reconstruction. Scale bar equals 5 mm.

Castorocauda (Ji et al., 2006), whereas in *Agilodocodon* the proximal caudal vertebrae are narrower and less flattened. But the well-developed zygapophyses in *Agilodocodon* suggest a thinner more mobile tail than other docodontans, or other mammaliaforms such as *Megaconus* (Meng et al., 2015:Supplementary Materials). The single preserved proximal caudal of *Borealestes* appears intermediate between the morphologies of the proximal caudals of *Castorocauda* and *Agilodocodon* (Figure 3.3b.8H). The remaining tail bones are similar to those in *Castorocauda,* which are essentially little changed from earlier mammaliaforms and even some tritylodontids such as *Oligokyphus* (Kühne, 1956). This suggests a sturdy but mobile tail for *Borealestes*—as supported by the presence of large chevrons which would have increased the dorsoventral depth and robustness of the tail—which may have assisted in locomotion in water (as is *Castorocauda*). However, the isolated caudal vertebrae do not offer enough information to infer ecology in *Borealestes*.

No material from the posterior thoracic or lumbar regions is preserved in *Borealestes*. The reduction or loss of the lumbar ribs in mammaliaforms is variable among groups, even within subclades of mammaliaforms (Chen et al., 2017) For most docodonts for which the lumbar region is known, lumbar ribs of reduced size are retained. The exception is *Agilodocodon*, which has no lumbar ribs on the last four lumbar vertebrae, and shows a more distinctive thoraco-lumbar transition than in *Castorocauda* (Meng et al., 2015). This can be interpreted to correspond to an increased range of movement in the posterior vertebral column. The ribs of *Borealestes* are preserved, and they resemble the morphology of most docodontans, such as *Agilodocon* and *Docofossor*, and show no signs of the flattened, reinforced specialisation for a semi-aquatic lifestyle seen in *Castorcauda* (Ji et al., 2006; Meng et al., 2016).

Appendicular skeleton

The very fragmentary portion of the proximal humerus limits comparisons with other taxa. Nevertheless, the preserved deltopectoral crest is flared and appears to be intermediate between the gracile morphology of the arboreal *Agilodocodon* (Meng et al., 2015) and the more robust morphology of *Haldanodon* (Martin 2005) and *Docofossor* (Luo et al., 2015). The prominent deltopectoral crest suggests the attachment of strong muscles

(e.g. insertion of the pectoralis, and deltoid muscles, and possibly also origins of the brachialis muscle, Gambaryan et al., 2015), suggeting strength in the forelimb. In *Haldanodon* the humerus is more robust than the femur. The shaft of the humerus is not preserved in NMS G.1992.47.121.1, meaning that although *Borealestes* has quite a slender, elongate femur it is not possible to compare these two proximal limb bones directly. However the radius is more gracile than in *Haldanodon*, again suggesting a less robust morphology overall for *Borealestes*.

What remains of the ilium and ischium is similar to that seen in other docodonts, but with a slightly more developed iliac blade than in *Agilodocon*, suggesting more muscle attachment in this area.

The proportions of the manus can provide useful ecomorphological inferences among mammals, but unfortunately only disarticulated scattered proximal and distal manus and pes elements are preserved in NMS G.1992.47.121.1. These elements resemblance those in *Agilodocodon* (Meng et al., 2015), and are far less robust in morphology than seen in the specialist digger *Docofossor* (which is also brachydactylous), or in *Haldanodon* (Martin, 2005).

The *Borealestes* calcaneus is slightly less elongate than in *Agilodocodon*, being closer to the morphology of *Morganucodon*, which is surprisingly less elongate than earlier tritylodontids such as *Oligokyphus* (Kühne, 1956). For a description and ecomorphological analysis of the calcaneus and astragalus, see Chapter 4.4. The tibio-astragalar trochlea and post-astragalar shelf are less developed than in *Docofossor* (Luo et al., 2015), and like the rest of the pedal and manual elements there is no sign in *Borealestes* of the anatomical specialisations for a fossorial lifestyle as seen in *Docofossor*.

3.3c Morphology of the Petrosal and Stapes of *Borealestes*[4]

There were previously five docodonts for which reasonably complete cranial material is known: *Docodon*, *Haldanodon*, *Castorocauda*, *Agilodocodon* and *Docofossor*. Only the petrosal of *Haldanodon* has been recovered and described so far (Lillegraven and Krusat, 1991; Ruf et al., 2013). Here I describe the petrosals of *Borealestes*, expanding the information on the cranial morphology of docodonts.

Borealestes is the oldest docodont for which cranial material is known, and can thus shed light on the comparative morphology of the petrosal of docodonts as a whole. I used high-resolution micro-computed tomography (µCT) and digital reconstruction to explore the petrosal anatomy, and to generate an endocast of the inner ear of *Borealestes*. I compare these with the petrosal and inner ear of *Haldanodon*, and other key Mesozoic mammals for which the petrosals are known. This comparison provides important new information on the characteristics of the inner ear of a primitive docodont, and the evolutionary transformation from the simpler inner ear in early mammals in general (Luo et al., 1995), to the complex inner ear morphology (including coiled cochlea) of stem therians and crown Theria (Luo, 2001; Ruf et al., 2009, 2013; Luo et al., 2011; Luo et al., 2016; Schultz et al., 2017b).

3.3c i) Materials and Methods

The left petrosal of *Borealestes*, specimen NMS G.1992.47.121.2 is in the collections at the National Museum of Scotland (NMS) in Edinburgh, Scotland. It is part of the skeleton of *Borealestes* NMS G.1992.47.121.1 (which includes the right petrosal) recovered in 1972 by M. Waldman and R. J. G. Savage from the Jurassic limestone beds near Elgol, Isle of Skye. The exact location where the skeleton was recovered is yet to be determined (currently under investigation by EP). For a geological overview of the Kilmaluag comprises see Chapter 2.

[4] Chapter 3.3c was originally published as: Panciroli, E., Luo, Z.-X. and Schultz, J.A. 2018b. Morphology of the petrosal and stapes of *Borealestes* (Mammaliaformes, Docodonta) from the Middle Jurassic of Skye, Scotland. *Papers in Palaeontology*, 5: 139-156.

NMS G.1992.47.121.1 is a fragmentary skeleton to which the left petrosal NMS G.1992.47.121.2 belongs, but from which it is now detached. The right petrosal is still part of the rock block of NMS G.1992.47.121.1. The skeleton has not yet been described, and is not identified to species level, but I confirm it belongs to the genus *Borealestes*. The left petrosal, along with several other bone fragments, was dislodged from the complete skeleton historically during handling, allowing them to be scanned and described separately. The right petrosal remained in situ with the skeleton. Micro-computed tomographic data (µCT) of NMS G.1992.47.121.2 were obtained using the micro-CT scanner built in-house at the University of Edinburgh, School of Geosciences Experimental Geoscience Facility. The scanner comprises a Feinfocus 10–160 kV dual transmission/reflection source, MICOS UPR-160-AIR ultra-high precision air-bearing table, Perkin Elmer XRD0822 amorphous silicon x-ray flat panel detector and terbium doped gadolinium oxy-sulfide scintillator. The scan resolution is 8.9 lm. Data acquisition software was written in-house by Dr Ian Butler, and scans were reconstructed using Octopus 8.7 software (https://octopusimaging.eu/). Phase-contrast synchrotron data from NMS G.1992.47.121.1 were obtained at the European Synchrotron Radiation Facility (ESRF), Grenoble, France. This produced data with a scan resolution of 6.15 µ, which was subsequently resampled to 12.3 µ.

These data were then digitally reconstructed and image processed using Mimics 19.0 at the National Museum of Scotland (https://www.materialise.com/en/medical/software/mimics). Digital reconstructions are available in the Dryad Digital Repository (Panciroli et al., 2018c). Raw data are part of a dataset comprising the fragmentary skeleton NMS G.1992.47.121.1.

3.3c ii) Description

Petrosals

NMS G.1992.47.121.2 (Figures 3.3c.1B–E, 3.3c.2) is the separated left petrosal of *Borealestes*. The lateral trough, the mastoid region and the associated structures are not preserved in this petrosal. The pars cochlearis is also incomplete, missing the anteromedial portion (Figures 3.3c.1D–E, 3.3c.2F). Nonetheless, the promontorium, or ventral eminence

of the pars cochlearis, is relatively well preserved and shows many surface features (Figure 3.3c.2C–E). The right petrosal (Figures 3.3c.1F– G, 3.3c.3–6) is considerably better preserved in the lateral trough, the cavum epiptericum, the prootic groove structure, and in the paroccipital and mastoid regions. All of these structures are consistent with those identified in the petrosals of the docodont *Haldanodon* (Ruf et al., 2013). In the following, each of the petrosal structures are described by referring to both petrosals.

A bony ridge is visible on the anterolateral aspect of the promontorium (Figures 3.3c.2E, and 3.3c.5A). This promontorium ridge is better preserved on the right petrosal than the left. The main part of the promontorium bulges anteromedially and ventrally, best shown in the left petrosal (Figure 3.3c.2). On the right petrosal, a piece of promontorium is broken but has been digitally restored (Figure 3.3c.5). The bone is better preserved in the apical region of the pars cochlearis of the right petrosal (Figure 3.3c.5). However, an area of the endocranial surface is missing on the internal surface of the anterior pars cochlearis of the right petrosal. The entire apical region is broken off on the left (Figure 3.3c.2). These breakages help to expose the tiny foramina of the circum-promontorium plexus on the interior surface of the cochlear canal (Figures 3.3c.2F, and 3.3c.3C).

The crista interfenestralis is present, separating the fenestra vestibuli from the perilymphatic foramen and connecting the promontorium with the more posteriorly located mastoid region in complete petrosals, as in other Mesozoic mammals (Rougier et al., 1996; Ruf et al., 2009, 2013; Luo et al., 2012). The crista interfenestralis is intact in the right petrosal (Figures 3.3c.5A, and 3.3c.6), but on the left petrosal (Figure 3.3c.2) it is fractured and collapsed into the hollowed inner ear space of the petrosal. Despite this, it can still be recognized without question, and has been digitally restored to its original position (Figure 3.3c.2C–F).

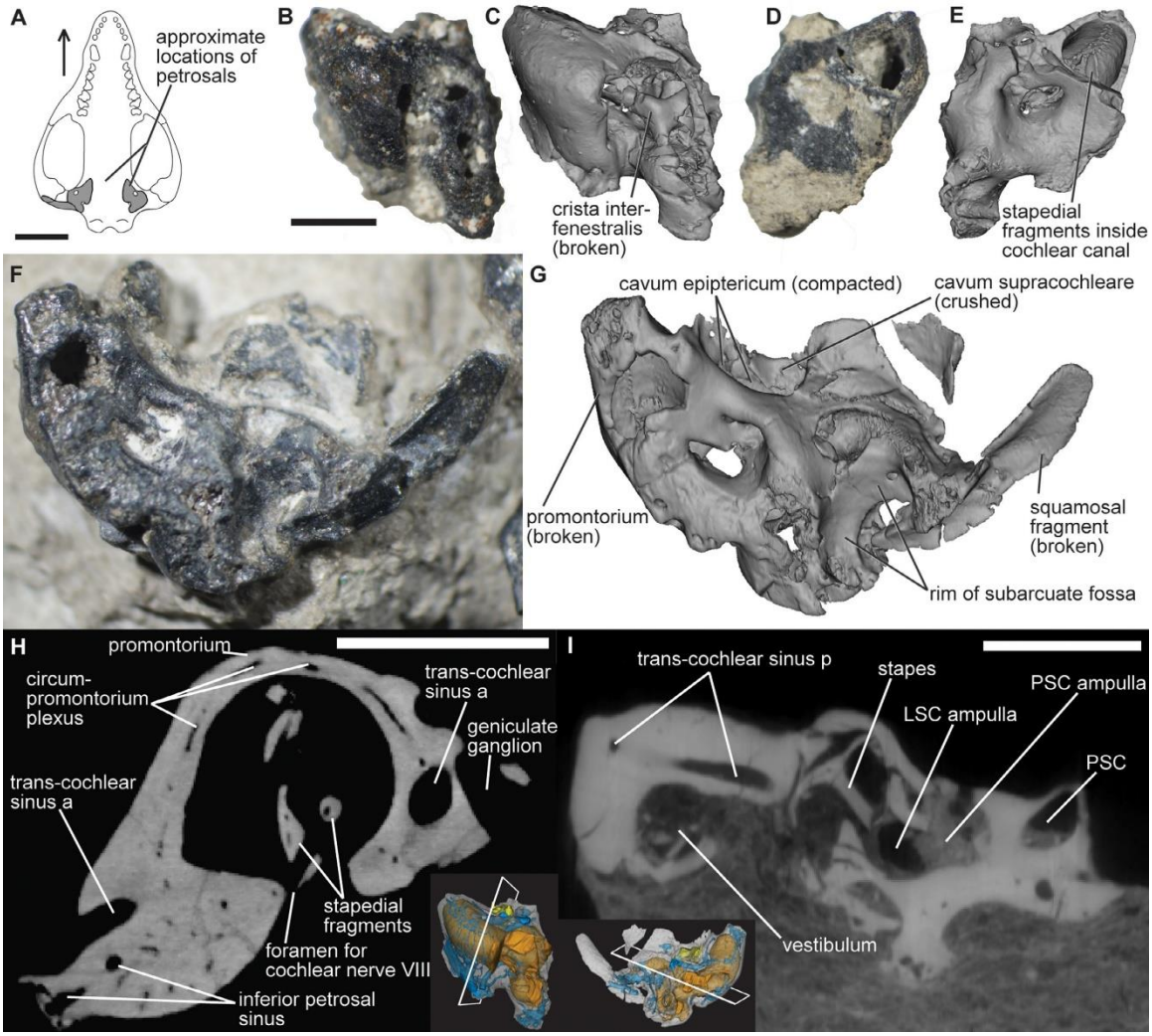

Figure 3.3c.1: Petrosals of the docodont *Borealestes*. Photos and digital reconstructions from CT and synchrotron scans. A, approximate positions of preserved petrosals in schematic skull outline of docodont (simplified from *Haldanodon*, partly based on Ruf et al. 2013). B–E, left petrosal NMS G.1992.47.121.2: B, photo of left petrosal in ventral view; C, digital reconstruction in ventral view showing crushing and dislocated fragments inside petrosal; D, photo of left petrosal in endocranial view; E, digital reconstruction of the endocranial view showing fragments inside petrosal. F–G, right petrosal NMS G.1992.47.121.1: F, photo of right petrosal in endocranial view; G, digital reconstruction of right petrosal in endocranial view with main features labelled for orientation. H–I, lCT-scan slices with main features labelled and approximate position of slice picture shown in inset: H, left petrosal NMS G.1992.47.121.2; I, right petrosal NMS G.1992.47.121.1. Abbreviations: a, anterior; LSC, lateral semi-circular canal; p, posterior; PSC, posterior semi-circular canal. Scale bar in 1A represents 5 mm, all other scale bars represent 1 mm (scale bar in B also refers to C–G).

The left petrosal shows several posterior openings of the inferior petrosal sinus canal, anteromedial to the perilymphatic sulcus (and also anterior to the jugular notch) on the posteromedial corner of the promontorium (Figure 3.3c.2). Of these, the first opening is

large, and anteromedially located. This opening is connected to the inferior petrosal sinus, enclosed in a thick bony canal along the medial edge of the pars cochlearis. This is termed the opening of the inferior petrosal sinus. A second, smaller opening is located lateral to the first opening, and this tiny foramen is also connected to a small tributary channel networked with the inferior petrosal sinus (Figure 3.3c.2). These surface foramina can be traced to the inferior petrosal sinus in the medial (or inferior) part of pars cochlearis, as in the petrosals of the docodont *Haldanodon* and other Mesozoic mammals (Wible, 1990; Rougier et al., 1992, 1996; Ladevèze and de Muizon, 2007, 2010; Luo et al. 2012; Ruf et al., 2013). The bony canal of the large inferior petrosal sinus is only preserved partially on the left petrosal, and both its anterior part (near the apex of pars cochlearis) and its posterior section are broken (Figure 3.3c.2). The broken posterior part of the inferior petrosal sinus canal is connected to a trans-cochlear sinus channel (described below). Of the three openings connected to inferior petrosal sinus, the posteriormost opening is also the opening of the posterior trans-cochlear sinus. The interpretation of how the inferior petrosal sinus is connected to the trans-cochlear sinus channel is based on the left petrosal, as the medial edge of the pars cochlearis where the inferior petrosal sinus would be located has been eroded in the right petrosal.

In both the left and right petrosals, I have visualized and identified two vascular channels that traverse the pars cochlearis through the bone, respectively called the anterior trans-cochlear sinus, and the posterior trans-cochlear sinus (Figures 3.3c.2, 3.3c.3, and 3.3c.7). The anterior trans-cochlear sinus channel is confluent with the posterior end of the inferior petrosal sinus (Figure 3.3c.2A, B), but the posterior trans-cochlear sinus has its own opening on the posteromedial corner of the promontorium (Figure 3.3c.2A, D–E). In the right petrosal, because the media edge containing the canal of the inferior petrosal sinus has been eroded and lost, the two openings of the anterior trans-cochlear sinus and the posterior trans-cochlear sinus appear well separated (Figure 3.3c.3).

The bony floor of the lateral trough is only partly preserved in the left petrosal (NMS G.1992.47.121.2) but is more complete in the right petrosal (NMS G.1992.47.121.1). The lateral flange is preserved as a broken edge on the right petrosal,

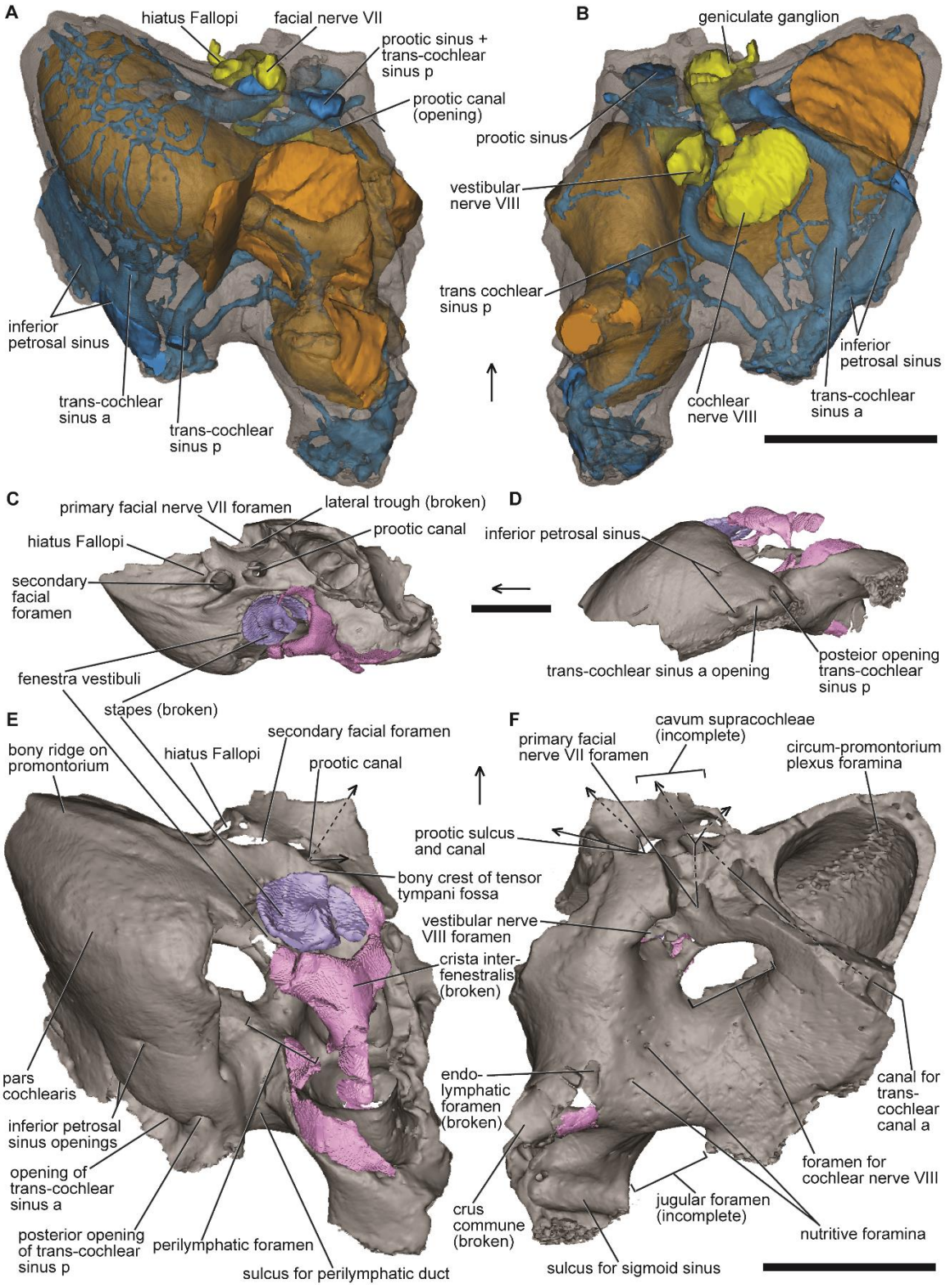

and is altogether lost in the left petrosal (Figures 3.3c.2, 3.3c.5, and 3.3c.6). The following structures can be identified in the posterior part of lateral trough: the hiatus Fallopii for the

greater petrosal nerve; the secondary facial nerve foramen (on the lateral wall of cavum supracochleare); and a large opening for the confluent prootic canal and the tympanic opening of the posterior trans-cochlear sinus channel (Figures 3.3c.2, and 3.3c.3). I also interpret a shallow depression area anterior to the fenestra vestibule, and near the opening of the hiatus Fallopii, as the fossa for the tensor tympani along the posterior rim of the lateral trough. The depression I have interpreted as the tensor tympani fossa is similar in location to the tensor tympani fossa identified in the petrosals of Cretaceous multituberculates, and in the Cretaceous triconodontid from the Cloverly Formation (Wible and Hopson, 1993, fig. 5.3; see also Wible and Hopson, 1995, figs 7, 8). Posteromedially, a bony ridge separates the prootic canal, secondary facial foramen and hiatus Fallopii from the fenestra vestibuli, forming part of the latter's anterior rim. The secondary facial foramen is anterior to the prootic canal opening.

The crista interfenestralis is crushed and displaced dorsally in the left petrosal NMS G.1992.47.121.2, distorting the original shape and proportions of the fenestra vestibuli and the perilymphatic foramen (Figures 3.3c.1C, and 3.3c.2E). Although the crista interfenestralis is better preserved in the right petrosal, the promontorial roof in this region is broken. The lateral periphery of the fenestra vestibuli is also broken. The preservational defects have distorted the shape of the fenestra vestibuli. The preserved shape of stapedial foot plate (described below) can give a reliable approximation to the shape of the fenestra vestibuli. I digitally repositioned the fragments of the crista interfenestralis of specimen NMS G.1992.47.121.2, to partially restore the periphery of the fenestra vestibuli. Based on the restoration, I interpret the fenestra vestibuli as being more or less round in circumference, as reflected in the shape of the stapedial footplate

Figure 3.3c.2 (previous page): Left petrosal of the docodont *Borealestes* NMS G.1992.47.121.2. Digital reconstructions from CT scan. A–B, semi-translucent views of interior structures of the left petrosal in: A, ventral; B, endocranial view; blue = vascular structures; yellow = nerves; brown = inner ear endocast. C–F, exterior surface structure with repositioned stapes (lilac), and periphery of fenestra vestibuli and crista interfenestralis (pink): C, dorso-lateral view (tilted); D, medial view (tilted); E, ventral (external) view; F, dorsal (endocranial) view. Arrows indicate anterior direction. Abbreviations: a, anterior; p, posterior. All scale bars represent 1 mm.

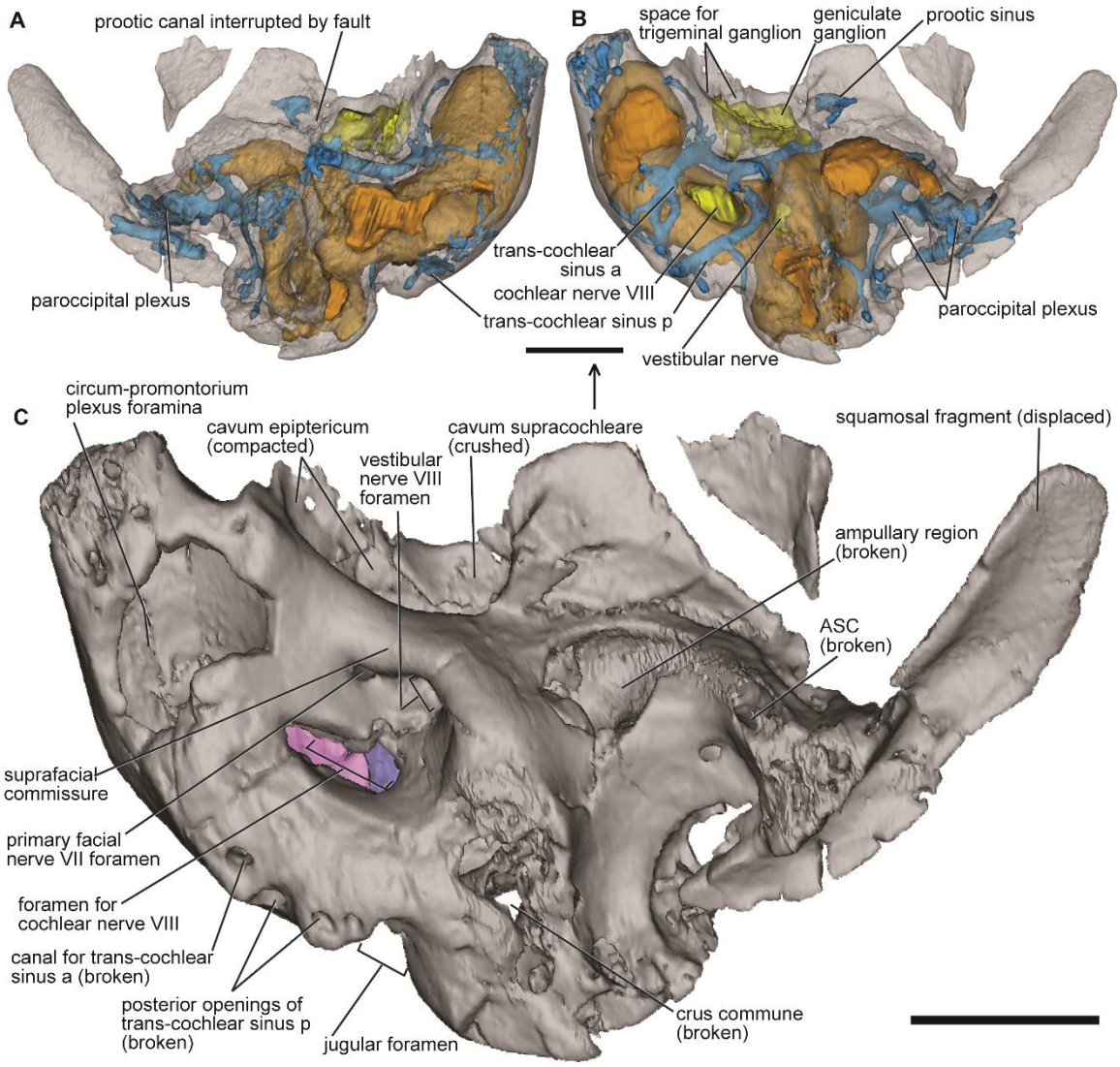

Figure 3.3c.3: Right petrosal of the docodont *Borealestes* NMS G.1992.47.121.1. Digital reconstructions from synchrotron scan. A–B, semi- translucent views of interior structures of the right petrosal in: A, ventral; B, endocranial view; blue = vascular structures; yellow = nerves; brown = inner ear endocast. C, major exterior structures preserved on the endocranial aspect of the right petrosal. More detailed identification shown in stereo paired images in Figure 4. Arrows indicates anterior direction. Abbreviations: a, anterior; p, posterior. Scale bars represent 1 mm.

(Figures 3.3c.2, 3.3c.5, and 3.3c.8). Both the fenestra vestibuli and the perilymphatic foramen are large, relative to the size of the promontorium. The fenestra vestibuli is positioned posterolaterally to the promontorium, and the perilymphatic foramen is posterior to the promontorium.

A perilymphatic sulcus for the perilymphatic duct (aquaeductus cochleae) is present in both petrosals. This sulcus connects the perilymphatic foramen and the margin of the jugular foramen (Figures 3.3.2E, 3.3c.5, and 3.3c.6). This is similar to other stem mammals and several Mesozoic clades of crown mammals (Kermack et al., 1981; Crompton and Luo, 1993; Wible and Hopson, 1993; Lillegraven and Hahn, 1993; Wible and Hopson, 1995; Rougier et al., 1996; Luo et al., 2001). The jugular foramen is only represented by its margin on the petrosal; the medial periphery of this foramen is not preserved in this specimen.

In the endocranial aspect of the digital reconstruction, the osseous cochlear canal is visible in both petrosals because the anterior part of the pars cochlearis is broken, although less severely in the right, than in the left petrosal (Figures 3.3c.1D–G, 3.3c.2, and 3.3c.3). Minute foramina for blood vessels and sinuses are visible on the interior surface of the cochlear canal (Figures 3.3c.2F, and 3.3c.3C), which I interpret to be connected to the circum-promontorium sinus plexus (sensu Kermack et al., 1981) inside the bone covering the pars cochlearis (visible in the endocast, see endocast section below). I can trace this network of small vessels (Figures 3.3c.2A, and 3.3c.7A, B, E, F). Additional small nutritive foramina connected to these small vessels are also visible on the endocranial surface of the petrosal (Figure 3.3c.2F).

The internal auditory meatus is well preserved in both petrosals. The primary foramen for the facial nerve (VII) to enter the internal auditory meatus can clearly be identified, and can be traced to the incomplete cavum supra-cochleare that houses the geniculate ganglion (Figures 3.3c.2F, 3.3c.3C, and 3.3c.4) (Rougier et al., 1992, 1996; Ruf et al., 2013). The foramen for the cochlear nerve (VIII), and laterally to that the foramen for the vestibular nerve (VIII), are present. This structure is only partly preserved and can be clearly recognized in the left petrosal (NMS G.1992.47.121.2) (Figure 3.3c.2C–F). In the right petrosal (NMS G.1992.47.121.1), a fault-line has cut through this region, where the bone is also crushed laterally (Figure 3.3c.4, dashed line). The hollowed open space of the cavum supracochleare, as seen on the left, is crushed on the right petrosal. The large secondary facial nerve foramen is preserved in a similar position on both petrosals. This foramen is the exit of the facial nerve from the cavum supracochleare. On the left petrosal, the bone of the suprafacial commissure is broken, so

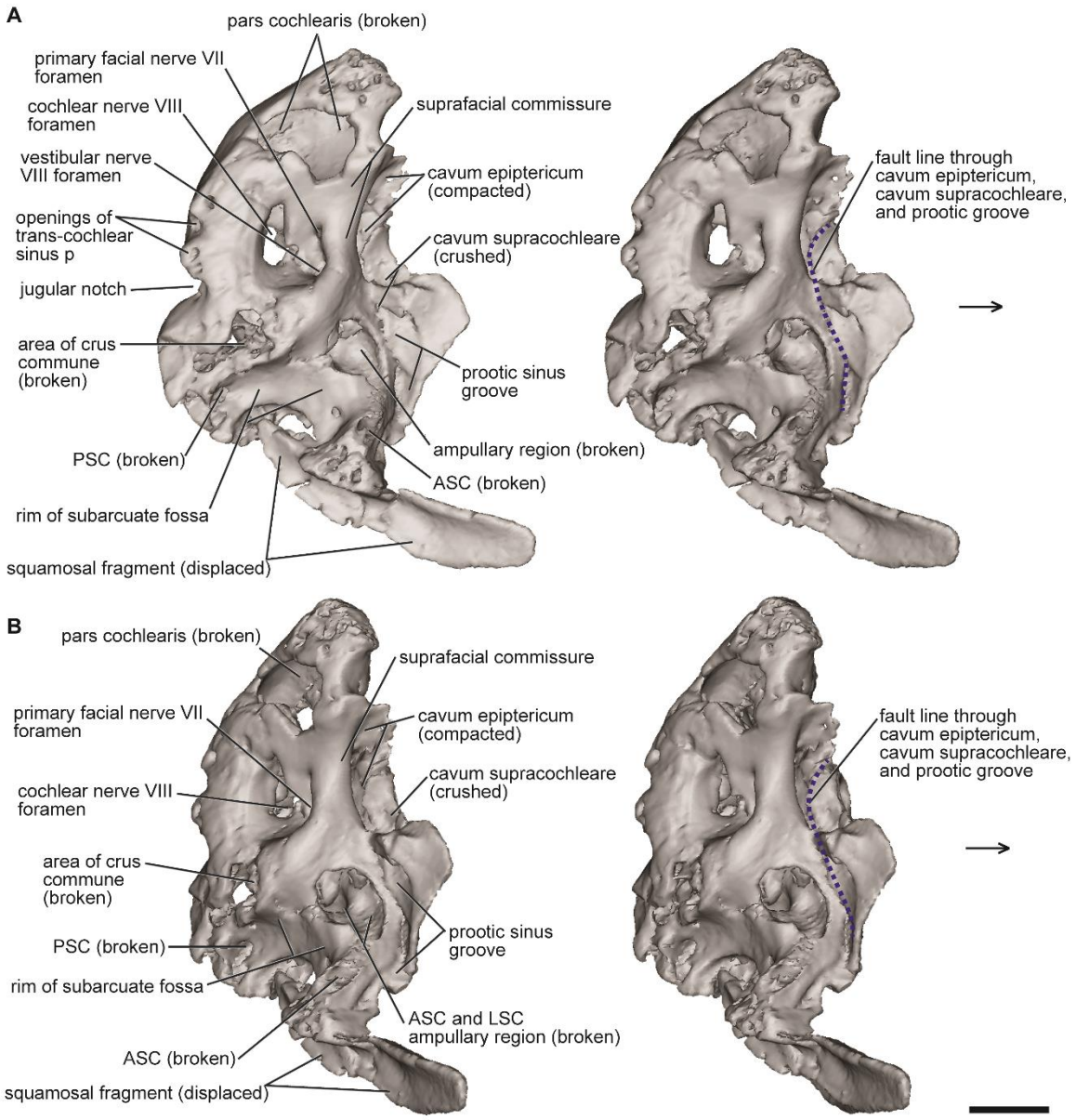

Figure 3.3c.4: Stereo pairs of right petrosal of the docodont *Borealestes* NMS G.1992.47.121.1. Endocranial view from digital reconstructions of synchrotron scans. Exterior structures preserved on the endocranial (internal) aspect of the right petrosal. A, dorsal view (stereo pair). B, dorsolateral view (stereo pair). The petrosal has a major fracture (fault) indicated by dashed line that cuts through the bone, along the prootic sinus groove, and then the cavum supracochleare that contained the geniculate ganglion. Further anteriorly, distortion by the same fault compacted the cavum epiptericum for the trigeminal ganglion, compressing this structure into a narrow space. Arrows indicate anterior direction. Abbreviations: ASC, anterior semi-circular canal; LSC, lateral semi-circular canal; p, posterior; PSC, posterior semi-circular canal. Scale bar represents 1 mm.

the entire path of the facial nerve can be traced from the internal auditory meatus to the cavum supracochleare, and further from the cavum through to the secondary facial foramen.

In the left petrosal the prootic sinus groove continues as a prootic canal, perforating the petrosal just posterior to the cavum supracochleare. In the right petrosal, the bone in the area where the prootic groove would join the space of cavum supracochleare is distorted by crushing and displacement along the fault line that cuts through the prootic groove and the cavum supracochleare. As a result of this distortion, the relationship of these two structures is obscured in the right petrosal. Largely based on the location of the prootic canal opening on the external (tympanic) aspect of the left petrosal, I interpret the prootic sinus as traversing through the cavum supracochleare in a similar manner in the right petrosal (Wible and Hopson, 1995). In the reconstructed dorsal-to-ventral sequence, the prootic sinus vein diverges from the sigmoid sinus at the top the subarcuate fossa. It then follows the prootic sinus groove along the lateral margin of the subarcuate fossa (Figure 3.3c.4), and enters the petrosal near the cavum epiptericum (Figure 3.3c.2). Inside the petrosal, the prootic sinus joins the lateral end of the posterior trans-cochlear sinus, before it enters the tympanic cavity through the prootic canal opening (Figures 3.3c.2, and 3.3c7A–B). Distally, the prootic sinus connects with the lateral head vein (Wible and Hopson, 1995).

The cavum epiptericum, a bony space formed by the petrosal that houses the trigeminal ganglion of cranial nerve V, is preserved on the right petrosal (Figures 3.3c.3, and 3.3c.4), but completely lost to damage on the left petrosal. Medially, the cavum epiptericum is separated from the internal auditory meatus by a saddle-shape structure known as the suprafacial commissure (Figures 3.3c.3C, and 3.3c.4). Posteriorly, the cavum epiptericum is separated by a sliver of bone from the cavum supracochleare, but both the cavum epiptericum and the cavum supracochleare are in the same broader depression formed by the petrosal. This pattern is similar to features on the endocranial aspect of the petrosal in *Haldanodon* (Lillegraven and Krusat, 1991) and *Morganucodon* (Kermack et al., 1981; Graybeal et al., 1989). This differs slightly from the petrosal of the Jurassic triconodontid *Priacodon*, in which the semilunar recess (related to the cavum epiptericum) is a large concave structure, in close proximity to the endocranial opening of

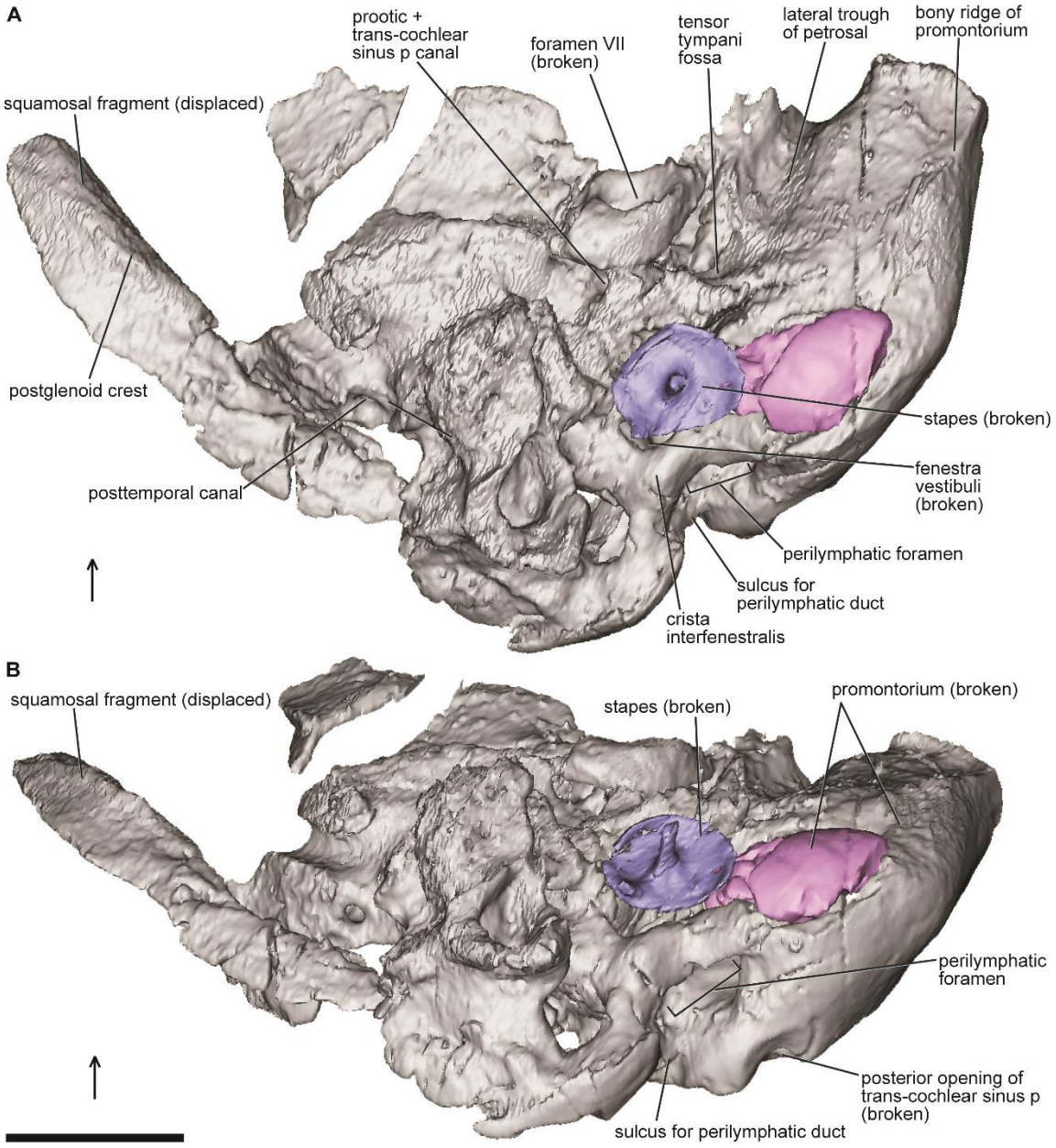

Figure 3.3c.5: Right petrosal of the docodont *Borealestes* NMS G.1992.47.121.1. Digital reconstructions of ventral view from synchrotron scan. External surface structures with the stapes restored to the fenestra vestibuli, and displaced promonotium fragments repositioned. A, ventrolateral view; B, ventromedial view. For full structural identifications see Figure 6. The petrosal is associated with a broken and displaced strip of the squamosal. Arrows indicate anterior direction. Abbreviation: p, posterior. Scale bars represent 1 mm.

the prootic canal (Rougier et al., 1996, fig. 1). The cavum supracochleare for the geniculate ganglion is present in *Priacodon*, but the bony floor of this space is interpreted as absent

(Rougier et al., 1996, p. 9), a feature that also differs from the structure of *Borealestes* (Figures 3.3c.3, and 3.3c.4).

The paroccipital region of the petrosal is relatively well preserved in the right petrosal, NMS G.1992.47.121.1 (Figures 3.3c.5, and 3.3c.6). The anterior part of the paroccipital region is elevated from the rest of the petrosal. Its most notable structure is the Y-shaped crest of the crista parotica. I interpret the presence of a fossa incudis: a shallow depressed area accommodating the incus, which serves as the contact point of the incus and the petrosal. On the lateral side of the anterior paroccipital process, there is a broad depression representing part of the entoglenoid recess between the petrosal and the cranial moiety of the squamosal (Figures 3.3c.5, and 3.3c.6). The posterior paroccipital process is excavated by a large and deep paroccipital pneumatic recess (sensu Ruf et al., 2013). The stylomastoid notch, which is the exit of the facial nerve from the tympanic region, is located medially to the base of the posterior paroccipital process (Figure 3.3c.6). The stapedial muscle fossa is a deep pit located posterior to the fenestra vestibuli and anteromedial to the posterior paroccipital process. The mastoid pneumatic recess is a deep excavation into the paroccipital-mastoid region of the petrosal, and is located medial to the stapedial muscle fossa and posterolateral to the perilymphatic foramen (Figures 3.3c.5, and 3.3c.6). These petrosal structures of *Borealestes* are identical to those in the petrosal of the docodont *Haldanodon*, as described by Ruf et al. (2013), with the four deeply excavated structures of the petrosal (paroccipital pneumatic recess, the stapedial fossa, the mastoid pneumatic recess, and the entoglenoid recess (partly on petrosal)) all strikingly similar between these two taxa.

The right petrosal (NMS G.1992.47.121.1) also preserves the bony channels and grooves for the arterial system from the superior ramus of the stapedial artery from the tympanic cavity and the arteria diploetica magna from the occiput (Wible, 1990; Rougier et al., 1992; Wible and Hopson, 1995). The pterygo-paroccipital foramen is located anterior to the crista parotica (Figure 3.3c.6). The foramen is represented by an open notch because the lateral border of this foramen is broken in this petrosal of *Borealestes*. By contrast, in the more complete petrosal of *Haldanodon*, the pterygoparoccipital foramen is fully encircled. This foramen is the passage for the superior ramus of the stapedial artery extant mammals and stem mammaliaforms (Wible, 1990; Rougier et al.,

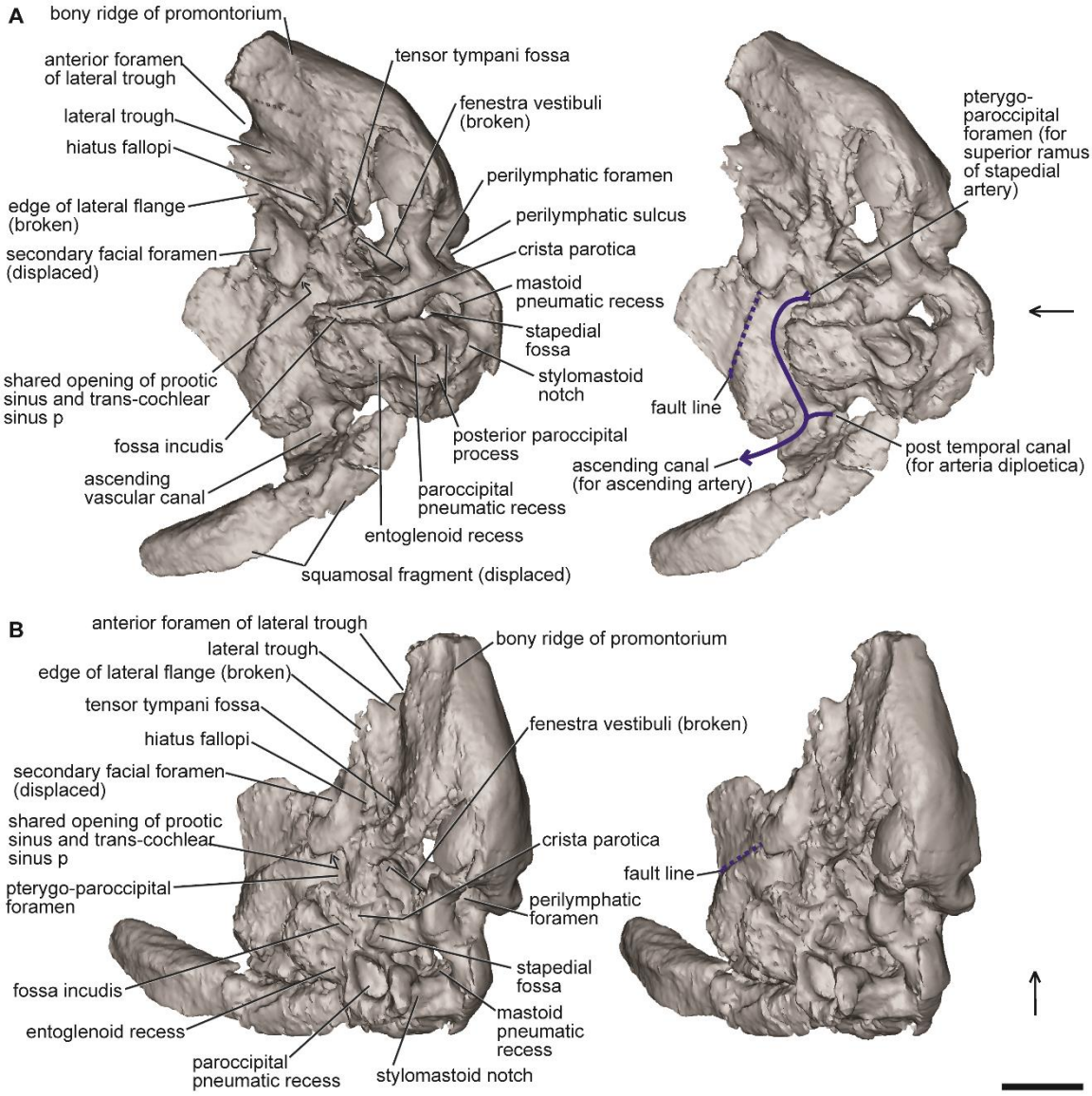

Figure 3.3c.6: Stereo pairs of the right petrosal of the docodont *Borealestes* NMS G.1992.47.121.1. Ventral view from digital reconstructions from synchrotron scans. Exterior structures preserved on the ventral aspect of the right petrosal. A, ventrolateral view (stereo pair); B, ventral view (stereo pair). The petrosal has a major fracture (fault) indicated by dashed-line that cuts through the bone along the prootic groove and its canal, and then through the cavum supracochleare that contained the geniculate ganglion. This has distorted the cavum supracochleare and dislocated the opening of the secondary facial foramen. Further anteriorly the same fault compacted the cavum epiptericum for the trigeminal ganglion, and compressed this structure. The lateral flange of the petrosal is broken, and only shown in its remaining and broken edge. The associated and incomplete strip of squamosal is displaced. A piece of petrosal anterior lamina, and the broken piece of the promontorium are omitted from these renderings. The solid lines with arrows indicate the interpreted courses of superior ramus of stapedial artery (via pterygo-paroccipital foramen), the arteria diploetica magna (via the post-temporal canal) and the ascending vessel of temporal region from the confluence of these two vessels. Arrows indicate anterior direction. Abbreviation: p, posterior. Scale bar represents 1 mm.

1992; Wible and Hopson, 1995). Dorsal of this foramen, the superior stapedial ramus follows an open groove lateral to the anterior paroccipital process and joins the arteria diploetica magna that enters through the post-temporal canal (partially preserved in right petrosal) (Figure 3.3c.6). The superior ramus of the stapedial artery and the arteria diploetica magna would be confluent with each other to form the ascending artery housed by the ascending vascular canal on the lateral side of petrosal that is also a part of the temporal skull surface. In the petrosal of *Haldanodon* (Lillegraven and Krusat, 1991; Ruf et al., 2013) these structures are not fully exposed, or not fully segmented from the micro-CT scans. The bony structures related to this vasculature, as revealed by CT scanning of the petrosal of *Borealestes*, are generally similar to those reconstructed for *Morganucodon*, and other Mesozoic mammals (Wible, 1990; Rougier et al., 1992; Wible and Hopson, 1995; Luo et al., 2012).

Endocast of the inner ear

Both petrosals were crushed post mortem, with the right petrosal being more complete. In both cases the inner ear endocasts are somewhat distorted. The approximate position of the fenestra vestibuli and perilymphatic foramen are identifiable despite this. Although the apex of the cochlear canal is absent in specimen NMS G.1992.47.121.2, it is clear that the canal is curved (Figures 3.3c.2A–B, and 3.3c.7A–D), and this is confirmed by the more complete cochlear canal of the right petrosal (Figures 3.3c.3A–B, and 3.3c.7E–H). The degree of curvature/coiling is similar to that of *Haldanodon* (Ruf et al., 2013), which can be traced in the right petrosal of *Borealestes*.

Vascular channels in pars cochlearis

The high quality of my scans (at a resolution of 12.3 and 8.9 µm) permits the reconstruction of some vascular channels and networks of small blood vessels in the bone of the pars cochlearis (Figure 3.3c.7). Some of these networks of tiny vessels can be

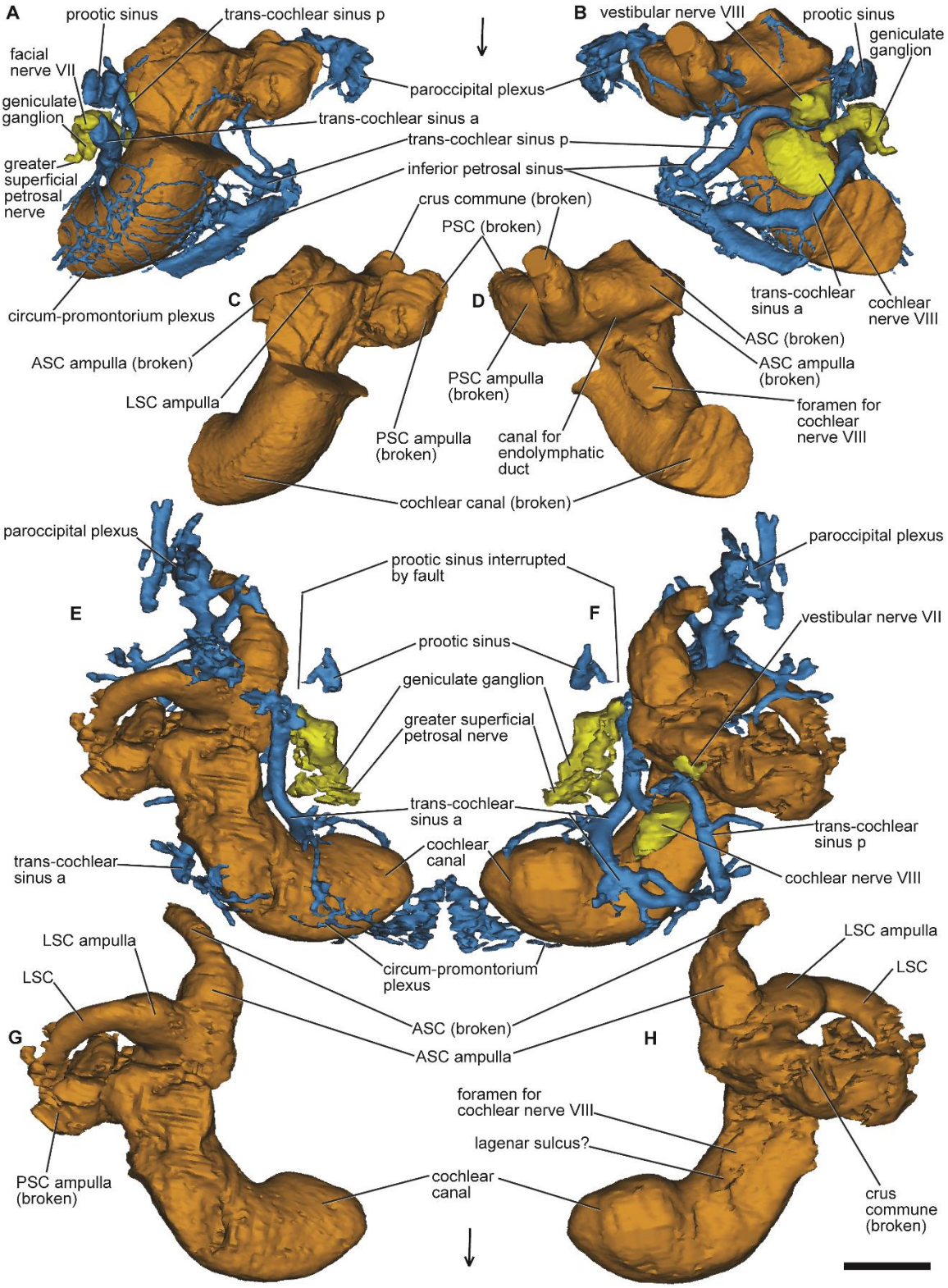

directly traced and shown to be connected to the structures inside the bony labyrinth (Figures 3.3c.2, 3.3c.3A–B, and 3.3c.7).

A noteworthy feature of these is the circum-promontorial sinus plexus (sensu Kermack et al., 1981) a network of tiny vessels (probably venous in nature) embedded in the pars cochlearis on the ventromedial side of the cochlear canal. This vascular network connects to the inferior petrosal sinus along the medial side of the promontorium (pars cochlearis) (Figures 3.3c.2A, B; 3.3c.3A, B; 3.3c.7A, B, E, F). I also identify two relatively large vascular channels that traverse the bone of the pars cochlearis. I interpret these as probably venous in nature due to their full connections to other sinuses or veins (Figures 3.3c.2, 3.3c.3, and 3.3c.7). I have here termed these two major channels the anterior and posterior trans-cochlear sinuses (Figures 3.3c.2, 3.3c.3, and 3.3c.7).

The anterior trans-cochlear sinus (a) connects medially with the inferior petrosal sinus. From there it traverses through the bone of the pars cochlearis and enters laterally into the space of the cavum supracochleare (Figures 3.3c.2, and 3.3c.3), the space that houses the geniculate ganglion of the facial nerve. Inside the pars cochlearis the course of anterior trans-cochlear sinus curves anteriorly around the bony internal auditory meatus. The opening for the secondary foramen of the facial nerve (VII) is very large in both left and right petrosals. This foramen could accommodate the passage of additional structure, such as the anterior trans-cochlear sinus. I therefore offer a speculative interpretation that the anterior trans-cochlear sinus exits through the enlarged secondary facial foramen, along with the facial nerve.

The posterior trans-cochlear sinus (p) starts in the posteromedial corner of the promontorium near the jugular notch, originating from a single large foramen in the left petrosal (Figure 3.3c.2), or in two foramina as in the right petrosal (Figure 3.3c.3). The bony course of this sinus is positioned more posteriorly than, and away from, the anterior trans-cochlear sinus. It curves around the main opening of the internal auditory meatus, and

Figure 3.3c.7 (previous page): Endocasts of interior structures of petrosals in *Borealestes*. A–D, left petrosal NMS G.1992.47.121.2: A, ventral view of the preserved inner ear endocast, with blood vessels and nerves; B, endocranial view the inner ear, with blood vessels and nerves; C, inner ear in ventral view (as preserved, incomplete), without vessels or nerves; D, inner ear in endocranial view (as preserved, incomplete) without vessels and nerves. E–H are of right petrosal NMS G.1992.47.121.1: E, ventral view of the preserved inner ear endocast, with blood vessels and nerves; F, endocranial view the inner ear, with blood vessels and nerves; G, inner ear in ventral view (as preserved, incomplete), without vessels or nerves; H, inner ear in endocranial view (as preserved, incomplete) without vessels and nerves. Blue = vascular structures, yellow = nerves. Abbreviations: a, anterior; ASC, anterior semi-circular canal; LSC, lateral semi-circular canal; p, posterior; PSC, posterior semi-circular canal. Arrows indicate anterior direction. All scale bars represent 1 mm.

between the cochlear nerve foramen and the vestibular nerve foramen (Figures 3.3c.2, 3.3c.3, and 3.3c.7). The posterior trans-cochlear sinus is confluent with the prootic canal, suggesting that this sinus is connected to the prootic vein, before the prootic vein exits the petrosal into the tympanic region at the prootic canal opening (Figure 3.3c.2).

The anterior and posterior trans-cochlear sinuses are connected below the facial nerve geniculate ganglion in the cavum supracochleare, as shown in the right petrosal (Figures 3.3c.3B, and 3.3c.7F). However, this confluence is not observed in the left petrosal, where anterior trans-cochlear sinus and posterior trans-cochlear sinus remain separate below the geniculate ganglion. This feature may be bilaterally variable, or the asymmetry may be an artefact of preservation.

I also recognize a network of small vessels in the paroccipital region of the petrosal, just underneath the entoglenoid recess. This corresponds to the squamosal plexus (Ruf et al., 2013, fig. 4). Altogether, these venous features demonstrate a high degree of vascularization of the cochlea and surrounding osteological structures of the pars cochlearis, as initially observed in *Haldanodon* (Ruf et al., 2013).

The internal auditory meatus on the endocranial aspect of the petrosals is relatively shallow, somewhat similar to that in the petrosal of *Morganucodon* (Kermack et al., 1981). The floor is divided by a low crest (crista falciformis) into a ventral depression for the large foramen of the cochlear nerve, and a dorsal depression for the primary facial nerve foramen and the foramen for the vestibular nerve (Figures 3.3c.2F, and 3.3c.3C). The bony floor of the cochlear nerve foramen is preserved as a large and long slit in the right petrosal (Figures 3.3c.1G, 3.3c.3, and 3.3c.4) but this foramen appears to be broken widely open on the left petrosal (Figure 3.3c.2). The sulcus for the lagenar nerve as found in inner ear endocast in *Haldanodon* (Ruf et al., 2013, fig. 6) corresponds in position to part of the wide opening outline of the cochlear foramen in *Borealestes*. In the endocast of the right petrosal there is a suggestion of a possible lagenar nerve sulcus, but it cannot be conclusively identified in both petrosals of *Borealestes* due to lack of preservation.

Due to breakage of the anterior part of the pars cochlearis in the left petrosal (NMS G.1992.47.121.2), the anterior part of the internal auditory meatus that would encircle the primary facial nerve foramen is incomplete in this specimen. Fortuitously, this helps to expose the entrance of the facial nerve (VII) into the petrosal, and the facial nerve's conduit leading to the space for the geniculate ganglion can be clearly identified (Figure 3.3c.2F). In

my digital reconstruction, the vestibular nerve (VIII) appears to be close to the primary facial nerve and the geniculate ganglion (Figure 3.3c.7B). This is because the primary facial nerve foramen is in close proximity to the foramen of the vestibular nerve (Figures 3.3c.2F, and 3.3c.3C), and both are situated together in dorsal depression in the floor of the internal auditory meatus. In the petrosals of other mammaliaforms described so far, the passages of the vestibular nerve (VIII) and the facial nerve (VII) are clearly more widely separated (Kermack et al., 1981; Graybeal et al., 1989; Ruf et al., 2013; also pers. obs. on *Sinoconodon* and *Hadrocodium*).

Stapes

Among the bone fragments displaced into the interior of both petrosals (Figure 3.3c.1H, I), I recovered parts of the left and right stapes (Figure 3.3c.8). I identify a posterior and anterior stapedial crura, and crural fragments (Figure 3.3c.8). In the left petrosal, the stapedial footplate is fractured into three pieces which, I estimate, together constitute about 70% of the entire footplate (Figure 3.3c.8A–H). The reconstructed footplate has a nearly circular outline and is overall convex proximally toward the inner ear space. The lateral (external) aspect of the footplate is slightly concave, with curved edges around the periphery. The stapedial footplate recovered from the right petrosal (Figure 3.3c.8I–P) is more complete and confirms the position of the crura and the round shape of the footplate. The morphology of the bullate footplate resembles the stapes of *Haldanodon* (sensu Sánchez-Villagra and Nummela, 2001; Ruf et al., 2013).

Both stapes show a central protruding bony knob preserved on the concave side (the lateral surface) of the footplate, which represents the base of the anterior crus (Figure 3.3c.8). I recovered additional separated pieces of bone that can be identified as fragments of the stapedial crura; the crural fragment coloured orange in Figure 3.3c.8C

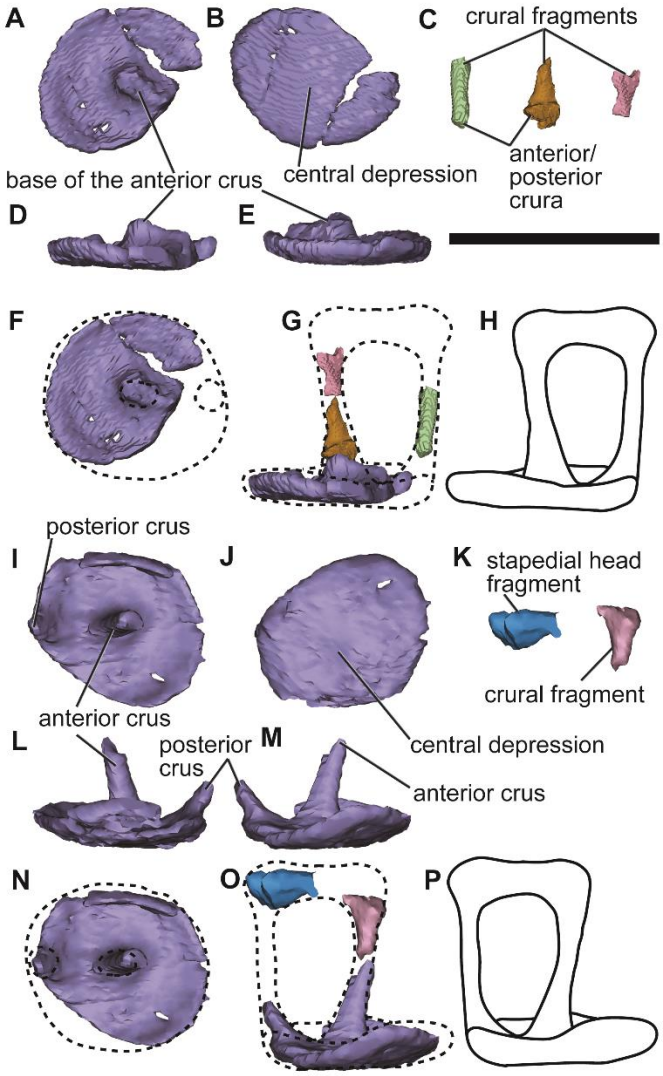

Figure 3.3c.8: Stapes of the docodont *Borealestes*. A–G, preserved parts of the left stapes NMS G.1992.47.121.2: A, left stapedial footplate (fractured and incomplete) in external view (from the inner ear space); B, left stapedial footplate (fractured and incomplete) in the internal view (toward the inner ear space); C, fragments of crura associated with the left stapedial footplate; D, approximately dorsal; and E, ventral side views of left stapedial footplate; F, interpretive reconstruction of external view of left stapedial footplate; G, interpretive reconstruction of crura from their fragments; H, interpretive reconstruction of side view of left stapes. I–O, preserved parts of the right stapes NMS G.1992.47.121.1: I, right stapedial footplate (incomplete) in external view (from the inner ear space); J, right stapedial plate (incomplete) in the internal view (toward the inner ear space); K, fragments of crura associated with the right stapedial foot- plate; L, approximately dorsal; and M, ventral side views of right stapedial footplate, showing the crural bases; N, interpretive reconstruction of the outline of right stapedial footplate in external view; O, interpretive association of crural fragments with their bases on footplate; P, interpretive reconstruction of side view of right stapes. All reconstructions based on remaining portions of stapes of NMS G.1992.47.121.1 and NMS G.1992.47.121.2, and the stapes of *Haldanodon* (Ruf et al. 2013). Scale bars represent 1 mm.

(the middle fragment of the three) is most likely to be the lateral portion of the anterior crus. The two other fragments may be parts of the anterior or the posterior crus (Figure 3.3c.8G). The right stapes even has longer parts of each crus preserved in anatomical position, which indicate a square outline of the stapedial head (Figure 3.3c.8I–P). In addition, I interpret the rather bulbous fragment (Figure 3.3c.8K, blue coloured left-hand fragment) recovered from the right petrosal as part of the stapedial head (Figure 3.3c.8O). The stapedial footplate has a length of approximately 0.8 mm, and width of approximately 0.6–0.7 mm (based on measurements of both stapedial footplates), giving it a stapedial ratio of 0.75–0.86. However, the exact ratio is not certain due to the broken periphery of the footplate.

3.3c iii) Discussion

The petrosal and endocast of *Borealestes* are morphologically similar to those of *Haldanodon*, but there are some key differences that separate the two genera. A bony ridge visible on the anterolateral aspect (Figures 3.3c.2E, 3.3c.4A, and 3.3c.6) corresponds to a similar bony ridge in the same position on the petrosal of *Haldanodon* (Ruf et al., 2013). The anterior part of the cochlear canal is clearly curved, and the apical region of the curved cochlear canal is slightly inflated, as can be determined in the right petrosal of *Borealestes* (Figure 3.3c.7E–H). Both of these features on the right inner ear endocast are consistent with the incomplete inner ear endocast on the left side. The degree of curvature/coiling and apical inflation appears similar to that of *Haldanodon* (Ruf et al., 2013).

In *Haldanodon*, the anterior rim of the fenestra vestibuli is separated from the tympanic openings of the prootic canal, the secondary facial foramen, and from the hiatus Fallopii (Ruf et al. 2013, fig. 2). In the same region of petrosal of *Borealestes*, the fenestra vestibuli is also separated from these structures. However, *Borealestes* has an elevated crest in continuation with the bony ridge of the promontorium on the left petrosal (the same region is damaged on the right petrosal). This crest separates the fenestra vestibuli and the prootic canal opening (Figure 3.3c.2C, E). Such a crest is not present in *Haldanodon* and therefore *Borealestes* is different in this feature.

The morphology of the stapedial footplate is bullate as in *Haldanodon* (sensu Sánchez-Villagra and Nummela, 2001; Ruf et al., 2013). In their description of the stapes of

Haldanodon exspectatus, Ruf et al. (2013) reconstructed the stapes as having parallel anterior and posterior crus, with a large stapedial foramen. This is consistent with cynodonts and stem mammals for which the stapes is known (Novacek and Wyss, 1986; Lillegraven and Krusat, 1991; Allin and Hopson, 1992; Crompton and Luo, 1993; Luo, 2007; Gaetano and Abdala, 2015; Schultz et al., 2018). The stapedial footplates of *Haldanodon* and *Borealestes* are now almost equally well known. In *Haldanodon*, the stapedial head is smaller than the stapedial footplate, the anterior crus is in central position, and the posterior crus is on the rim of the stapedial footplate. The rim of the stapedial footplate is slightly curved upward (bullate shape) and the stapedial footplate is basically round. Because *Borealestes* and *Haldanodon* are both docodonts, and phylogenetic analyses indicate they are closely related within a subclade of docodonts (Ji et al., 2006; Luo and Martin, 2007; Averianov et al., 2010; Ruf et al., 2013; Luo et al., 2015b; Schultz et al., 2018), my reconstruction of the stapes of *Borealestes* (augmented by information from that of *Haldanodon*) is justifiable on a phylogenetic basis (Figure 3.3c.8H, P).

New key features identified in both petrosals of *Borealestes* are the two vascular sinuses that traverse the pars cochlearis: trans-cochlear canal anterior (a) and trans-cochlear canal posterior (p) (Figures 3.3c.2A–B, 3.3c.3A–B, and 3.3c.7). These connect to the large channels of the inferior petrosal sinus; the venous vessels extending in an anteroposterior direction along the medial side of the pars cochlearis of the petrosal. Within the bone of the pars cochlearis, the trans-cochlear canals are also connected to the circum-promontorium plexus. The inferior petrosal sinus is a major vascular structure in petrosals among Mesozoic groups of crown mammals (Rougier et al., 1992; Rougier et al., 1996; Luo et al., 2012; Hughes et al. 2015). For crown therians, this feature is well documented in Cretaceous and Paleocene metatherians (Wible, 1990; Ladevèze and de Muizon, 2007, 2010). In the petrosals of *Borealestes*, the channel for the inferior petrosal sinus, the circum-promontorium plexus, and the two trans-cochlear vascular sinuses (Figures 3.3c.2A, B; 3.3c.3A, B; and 3.3c.7A, B, E, F), form a well-developed vascular network. This corroborates earlier observations that the petrosals of docodonts are highly vascularized, more so than that of *Morganucodon* (Kermack et al., 1981; Graybeal et al., 1989). In extant monotremes, the petrosal does not have the heavy vascularization in these regions, in contrast to *Haldanodon* and *Borealestes'* extensive vascularization throughout the petrosal (Kuhn and Zeller, 1987; Ruf et al., 2013).

The trans-cochlear sinuses in the petrosal of *Borealestes* are newly recognized anatomical features. Either these are unique features (autapomorphic) of *Borealestes*, or they could be derived features (apomorphic) of docodonts as a whole if their presence can be confirmed by re-scanning and re-segmenting the petrosal of *Haldanodon*, or petrosals of other docodonts. These two sinuses are also interesting in their connection to other vessels. The posterior trans-cochlear sinus connects from the endocranial opening of the prootic (venous) sinus through the pars cochlearis to the inferior petrosal sinus. This suggests that in *Borealestes* the prootic sinus was connected to the inferior petrosal sinus. The posterior trans-cochlear sinus is confluent with the prootic sinus, and then exits through the prootic canal passing through the lateral trough of the petrosal (see Wible and Hopson, 1995 and Rougier and Wible, 2006 for overviews of the prootic canal in cynodonts). This vascular channel connection is a new finding and has not been previously documented in other mammaliaforms. However, the lack of these trans-cochlear sinuses in other mammaliaforms could be due to the fact that the interior structures in the petrosals of other mammaliaform have not yet been examined by such high-resolution micro-CT scanning as in my study of *Borealestes*.

The preserved features on the anterior and posterior paroccipital processes and in the mastoid region in the right petrosal of *Borealestes* (Figures 3.3c.5, and 3.3c.6) are almost identical to the more complete homologues in *Haldanodon* (Ruf et al., 2013). The major excavated (presumably pneumatized) structures in these regions, and the degree of vascularization in the bone that form them, is similar in *Borealestes* and *Haldanodon* in the following: the entoglenoid recess (partly preserved); the well-developed paroccipital plexus; the prominent paroccipital pneumatic recess on the ventral aspect of the posterior paroccipital process; the depth of the stapedial muscle fossa; and the deep mastoid pneumatic recess. The pneumatization of the exterior surface structures in the paroccipital and mastoid regions of the petrosal, and high degree of vascularization in the bones forming these structures are unique and derived features of *Borealestes* and *Haldanodon*, and possibly of docodonts as a group.

The overall morphology of the inner ear of *Borealestes* is similar to that of *Haldanodon*, and implies similar hearing capabilities in these two genera of docodont. The vascularization in the petrosal of *Haldanodon*, the presence of a paroccipital pneumatic recess, and curvature of the cochlea were all considered to be evidence in support of a

fossorial lifestyle in that genus by Ruf et al. (2013). This was coupled with features such as vascularization in the rest of the basicranium, and thicker lateral and posterior semi-circular canals (Ruf et al., 2013). As these additional features are not preserved in *Borealestes*, I can only tentatively infer a similar lifestyle for these two taxa. The hypothesis about a fossorial lifestyle of *Borealestes* can be tested when the postcranial morphology is more fully revealed; the petrosals described here are part of a larger morphological study of a nearly complete specimen of the *Borealestes* skeleton NMS G.1992.47.121.1. The additional cranial material, coupled with postcranial elements, are expected to shed further light on the palaeobiology of *Borealestes* in the future.

3.3d Phylogenetic Analysis of *Borealestes serendipitus*

3.3d i) Methods

To assess the phylogenetic placement of *Borealestes serendipitus* in light of newly available cranial and postcranial characters, I used the matrix of Zhou et al. (2019), assembled for the analysis of a new docodontan specimen, *Microdocodon gracilis*. This dataset includes 126 taxa scored for 556 characters: 40 mandibular; 187 dental; 145 postcranial; 176 cranial characters and 8 soft-tissue characters. These characters are based on the matrix from Huttenlocker et al. (2018), with additional characters from Krause et al. (2014) and soft-tissue characters added by Zhou et al. (2019). *Borealestes* was scored for 275 characters (49%), which is comparable with three of the other five docodonts in this matrix, *Castorocauda* (42%), *Docofossor* (46%), and *Microdocodon* (53%), but less complete than *Haldanodon* (63%) or *Agilodocodon* (63%).

Analyses were carried out using most of the same methodology as Zhou et al. (2019), using PAUP Version 4 (Swofford, 2003), in order to facilitate comparison. A heuristic search was carried out using parsimony, with characters equally weighted, and unordered. Gaps were treated as missing, and multistate taxa interpreted as uncertain. Trees were obtained using stepwise addition with one tree held at each step, and the addition sequence set to random, with 10000 replicates. MaxTrees was set to 600 (auto-increased by 100), and the branch swapping algorithm was tree bisection reconnection (TBR), with a reconnection limit of 8 and steepest descent option in effect.

I carried out five analyses: 1) Zhou et al.'s (2019) original analysis (without *Borealestes*); 2) adding *Borealestes* characters scores to original data matrix; 3) adding *Borealestes* and amending characters scores for characters 32, 56, 67, and 312 for *Agilodocodon* and *Docofossor* where my interpretation differed from the previous authors' (Table 3.3d.1); 4) dataset without *Borealestes*, but with amended characters scores for *Agilodocodon* and *Docofossor*; 5) the complete dataset including *Borealestes*, but with *Borealestes* scores congruent with those scored for *Agilodocodon* and *Docofossor* by Zhou et al. (2019) (see Discussion below).

I used PAUP statistical tools to obtain the Consistency index (CI), Homoplasy index (HI), Retention index (RI) and Rescaled consistency index (RC) for all analyses.

3.3d ii) Results

Results of statistical tests on each of these analyses are in Table 3.3d.2. The topology of analyses 1 and 4 obtained broadly the same results as Zhou et al. (2019), except for the placement of *Castorocauda*, which was placed as the basalmost member of Docodonta, whereas *Haldanodon* was basalmost in the results reported by Zhou et al. (2019). There were multiple small shifts in placement throughout the tree, but no significant changes in overall topology (Figure 3.3d.1A). In analysis 2, *Haldanodon* was placed basalmost in Docodonta, and *Borealestes* was placed crownward of *Haldanodon*, *Castorocauda* and *Docofossor*, as the closest taxon to closely related taxa *Agilodocodon* and *Microdocodon* (Figure 3.3d.1B). Analysis 5 also obtained this topology for Docodonta.

Analysis 3, with *Borealestes* added to the matrix and scores for five characters for *Agilodocodon* and *Docofossor* amended based on differing interpretation, returned slightly different results from all other analyses. In analysis 3 two trees were returned from the initial heuristic search, both of 2838 steps. They differed in the placement of *Haldanodon*, *Castorocauda* and *Docofossor*, with one placing *Haldanodon* basalmost, and the other placing *Castorocauda* basalmost. I calculated a strict consensus tree from these two trees, which returned an unresolved polytomy for these three docodontan taxa.

3.3d iii) Discussion

Previous phylogenetic analyses using only dentomandibular characters, including my own in Chapter 3.3a (based on Meng et al., 2015), recovered very different tree topologies for Docodonta from the one recovered here using cranial and postcranial

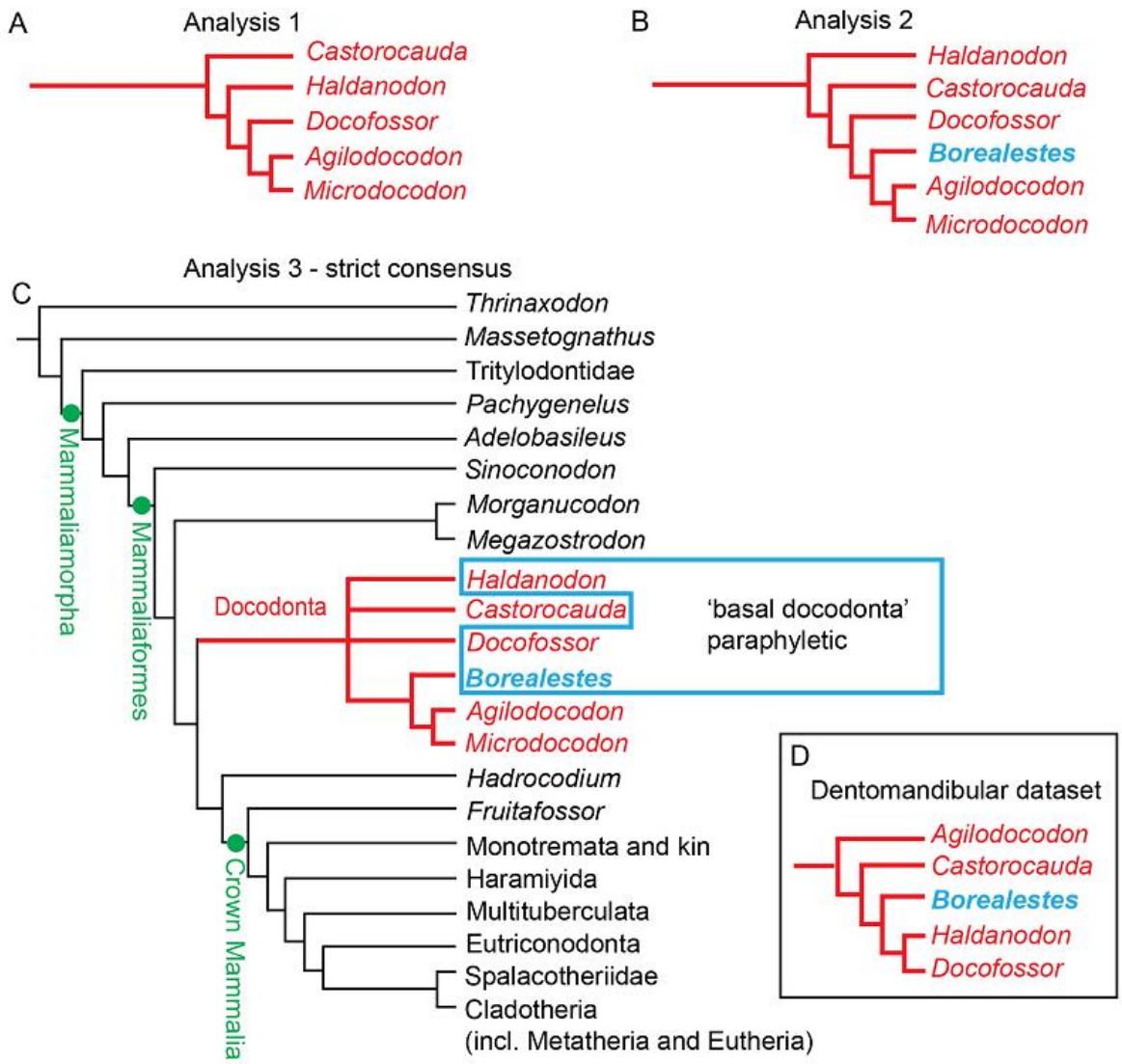

Figure 3.3d.1: Results of phylogenetic analysis using parsimony analysis, with characters equally weighted and unordered (for full methods see Chapter 3.3d i). A, result running original Zhou et al. (2019) character matrix; B, result after adding scores for *Borealestes* to data matrix; C, result with *Borealestes added* to data matrix and amended character scores for *Agilodocodon* and *Docofossor*; D, relationship of same taxa in dentomandibular dataset (see Chapter 3.3a).

characters. Here for example, *Borealestes* is recovered in a clade with *Agilodocodon* and *Microdocodon*, whereas most previous analyses have placed it in a 'basal docodontan' clade with *Haldanodon*, *Docodon* and *Docofossor* (Martin and Averianov, 2004; Pfretzschner et al., 2005; Ji et al., 2006; Luo and Martin, 2007; Averianov et al., 2010; Meng et al., 2015). In my dentomandibular analysis *Agilodocodon* was found as a sister-taxon to *Krusatodon*, removing *Krusatodon* from the clade 'Tegotheriidae' proposed by

previous authors (Maschenko et al., 2002; Martin and Averianov 2004; Averianov et al., 2010). *Castorocauda* was recovered as the closest taxon to *Dsungarodon* and *Tashkumyrodon* in my dentomandibular analysis. The relationships with *Krusatodon, Dsungarodon* and *Tashkumyrodon* cannot be tested here as they are not included in the expanded dataset of cranial and postcranial characters, but it is clear that incorporating cranial and postcranial characters has recovered a novel tree topology.

The ensemble consistency index (CI) for this dataset is low, with only around 32% of the data consistent with the cladogram in these analyses (Table 3.3d.2). This could suggest there are a large number of uninformative characters in this dataset, although including a higher number of taxa included a data matrix can also lower the CI (Kitching et al., 1998). The retention index (RI)—which should help address problems of homoplasy versus synapomorphy (Farris, 1989)—is much higher, at 0.798-0.799 (Table 3.3d.2).

The autapomorphies of *Borealestes* in this analysis (Figure 3.3d.2) are: character 19, the presence of a pterygoid muscle fossa on the medial ramus of the mandible; character 20, the presence of a pterygoid shelf (also present in *Docodon*, a taxon not in this analysis); character 58, the presence of a distal cingulid in addition to cusp c on the ultimate lower premolar; character 63, the absence of crenulation of cusps on the distal cingulid of the premolars; character 99, the lack of an a-g crest; character 102, the weak interlocking of the lower molars; character 178, the enlargement of upper incisor 2; character 179, having additional cuspules on the posterior upper incisors; character 206, a diastema behind the canine; character 248, the expanded helical surface of the distal end of the clavicle; character 319, the lack of distinct terminal swelling on the calcaneal tuber; character 341, the saddle-shaped contact between the entocuneiform and metatarsal 1; character 414, the presence of a stapedial artery sulcus on the petrosal.

Nine character changes occur at the base of the clade formed by *Borealestes*, *Agilodocodon* and *Microdocodon* in this analysis. Four of them are seen in all three taxa: possession of a crest on the anterior border of the coronoid process; the presence of a labial cingulid on the ultimate lower molar; the distinct cusp c on the ultimate lower

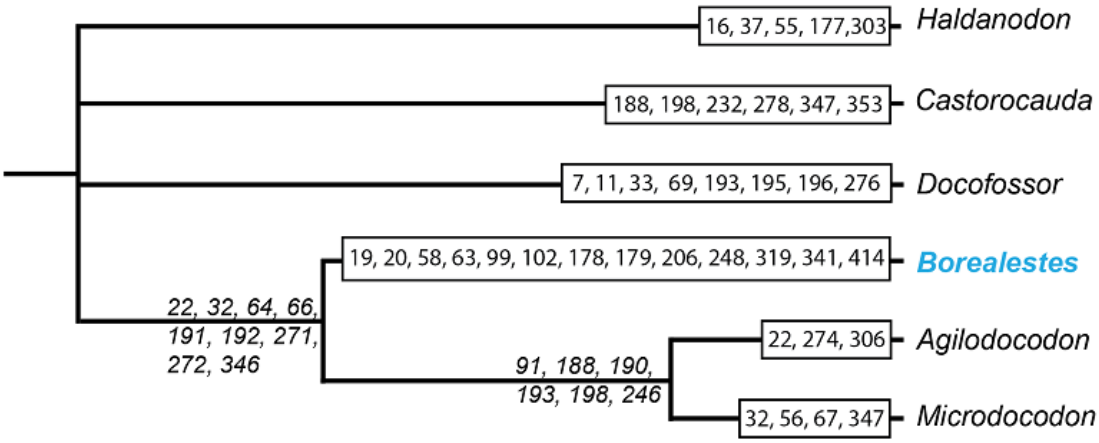

Figure 3.3d.2: Character changes for each node in Docodonta recovered in analysis 3. Characters in box change for that taxon, characters not in box change at base of that clade.

premolar; and having five or more lower premolars. Three characters are scored as missing data in *Borealestes* (they are not preserved in any known specimens of this taxon), but are recovered as synapomorphies for the clade: having five or more upper premolars; the weak entepicondyle and ectepicondyle of the humerus; and the presence of sigmoidal shelf for the supinator ridge extending from the ectepicondyle. A final two characters change or are unknown for *Microdocodon*: the high position of the dentary condyle relative to the level of the postcanine alveoli (this changes to be level with the alveoli in *Microdocodon*); and the presence of a ventrolateral tubercle on the proximal metatarsal V (this character is unknown in *Microdocodon*).

The characters amended in analysis 3 for *Agilodocodon* and *Docofossor* are outlined in Table 3.3d.1, and relate to characters of the lower premolars, height of the dentary condyle, and width of the base of the astragalar neck. It might be anticipated that changing these characters in *Agilodocodon* to be the same as *Borealestes* may create a closer relationship between these taxa, but looking across all analyses the altered scores have had no effect on the positions of these taxa, which are the same in analyses where those characters are not amended.

Recognising that interpretation of certain characters can cause differences between analyses, I ran multiple versions of this character dataset, using previous scores, scores amended based on my own interpretation, and scores for *Borealestes* that are congruent with the interpretations of previous authors rather than my own. These differing scores did

not substantially affect tree topology, and did not affect the placement of *Borealestes* at all. This means we can place high confidence in this tree topology for Docodonta. The lack of cranial and postcranial characters for so many docodontan taxa means dentomandibular datasets are still necessary, but comparing the difference between my dentomandibular and full skeletal dataset results suggest the incorporation of cranial and postcranial characters can have profound effects on the placement of particular taxa—particularly *Agilodocodon* in this case (Figure 3.3d.1C and D). The addition of *Microdocodon* to a dentomandibular datatset may produce interesting results, considering the sister-taxon relationship proposed by this analysis.

3.4 Cladotheria: *Palaeoxonodon ooliticus*[5]

The Middle Jurassic was a key period in the evolutionary history of mammals. Recent research suggests a global radiation of early mammals beginning in the Early Jurassic, and entailing large increases in diversity and phenotypic disparity (Luo, 2007; Close et al., 2016). This gave rise to docodontans, shuotheriids, australosphenidans, multituberculates, and cladotherians in the Early to Middle Jurassic (Luo et al., 2002; Kielan-Jaworowska et al., 2004). Continued fossil discoveries are critical to understanding this radiation. Furthermore, Cladotheria includes Theria, the clade comprising living marsupials and placentals and their stem lineages. Therefore, early cladotherian fossils provide information on the ancestral morphologies of the group, from which the more derived structures of extant therians evolved.

The early cladotherian *Palaeoxonodon* was originally reported based on isolated teeth from the Middle Jurassic of England (Freeman, E., 1976a, b, 1979; Sigogneau-Russell, 2003), and its detailed phylogenetic affinities remained uncertain. An almost complete dentary from the Isle of Skye, Scotland (NMS G. 2015.17.1), described by Close et al. (2016), revealed that the lower tooth row of *Palaeoxonodon* shows a gradient of variation in several dental characters that were used to delimit species in previous taxonomy. Based on these new observations, a previously erected *Palaeoxonodon* species, *Palaeoxonodon freemani*, and the genus *Kennetheridium* (Sigogneau-Russell, 2003), were both synonymised with the type species of *Palaeoxonodon*, *P. ooliticus*. This dentary also provided additional characters for a more informative phylogenetic analysis, supporting previous work that suggested *Palaeoxonodon* is the sister taxon to *Amphitherium* (Close et al., 2016; but see also Averianov et al. 2015 for an alternative hypothesis).

Here, I report two further specimens of *Palaeoxonodon* from the Isle of Skye. A newly discovered specimen, NMS G.2017.37.1, was found during fieldwork in 2017. Although it is not as complete as that found by Close et al. (2016), it includes the base of the coronoid process and adjacent regions of the dentary. These features were missing from previous specimens and allow additional characters to be scored for phylogenetic analysis.

[5] Chapter 3.4 was originally published as: Panciroli, E., Benson, R.B.J., and Butler, R.J. 2018a. New partial dentaries of *Palaeoxonodon ooliticus* (Mammalia, Amphitheriidae) from Scotland, and posterior dentary morphology in stem cladotherians. *Acta Paleontologica Polonica*, 63:197-206.

Another specimen, NMS G.1992.47.123, was recovered during fieldwork by Michael Waldman and Robert J.G. Savage in 1973. It had previously been mentioned as an undescribed pantotherian by Clemens (1986) and Evans et al. (2006). The discovery of this specimen pre-dates all other known specimens of *Palaoxonodon*, including the holotype of *P. ooliticus* (Freeman, 1976a). However, for reasons unknown, it was never described. After being transferred posthumously from the late RJG Savage of the University of Bristol to the National Museum of Scotland, it was rediscovered by EP in the collections at NMS in 2016.

3.4 i) Materials and Methods

The two specimens described here are both in the collections at the NMS: NMS G.1992.47.123 and NMS G.2017.37.1. Both were collected from the Kilmaluag Formation of the Great Estuarine Group (Bathonian, Middle Jurassic) of the Strathaird Peninsula, north of Elgol, Isle of Skye, Scotland. NMS G.2017.37.1 was collected at Cladach a' Ghlinne, whereas NMS G.1992.47.123 was collected approximately 0.8 km south of Cladach a' Ghlinne along the coastline. See Chapter 2.1 for overview of the geology of the Kilmaluag Formation.

Micro-CTscan data were obtained for NMS G.1992.47.123 using the micro-CT scanner built in-house at the University of Edinburgh, School of Geosciences Experimental Geoscience Facility. The scanner comprises a Feinfocus 10-160kV dual transmission/reflection source, Perkin Elmer XRD0822 amorphous silicon x-ray flat panel detection, and terbium doped gadolinium oxy-sulfide scintillator. Data acquisition software was written in-house, and scans were re-constructed using Octopus 8.7 software. The scan resolution for this scan is 20 μm. NMS G.2017.37.1 micro-CT scan data were obtained at Cambridge Biotomography Centre (http:// www.cbc.zoo.cam.ac.uk/) using a Nikon Metrology XT H 225 ST micro-CT scanner. The scan resolution for this scan is 7.64 μm. All micro-CT scans were digitally reconstructed, image processed, and measured using Mimics 19.0 at the National Museum of Scotland. Digital reconstructions are available in SOM (Supplementary Online Material available at http://app.pan.pl/SOM/app63-Panciroli_etal_SOM.pdf).

Lower molar terminology follows that of Sigogneau-Russell (2003) with the following amendments: the talonid cusp is renamed the hypoconid, and the crest running from the hypoconid to the metaconid is the oblique cristid (as in Davis, 2011); the paraconal sulcus is renamed the hypoflexid (as in Close et al., 2016); cusp e is not present in *Palaeoxonodon*.

Phylogenetic analysis was carried out using TNT 1.5, with settings as in Close et al. (2016): all analyses were carried out by first using the new technology search with default command settings, and stipulating that the shortest tree was to be found 10 times. This was followed by TBR branch swapping on the recovered most parsimonious trees (MPTs), and then calculating a strict consensus. Jackknife resampling statistics were calculated using 1000 replicates, and values are displayed as absolute frequencies. Bremer support values were obtained by TBR branch swapping on the MPTs, incrementally increasing suboptimal trees from one to eight steps (see SOM for TNT script and amended data matrix).

3.4 ii) Description

SYSTEMATIC PALAEONTOLOGY

MAMMALIA Linnaeus, 1758

CLADOTHERIA McKenna, 1975

AMPHITHERIIDAE Owen, 1846

PALAEOXONODON Freeman, 1976b

PALAEOXONODON OOLITICUS Freeman, 1976b

Type species: *Palaeoxonodon ooliticus* Freeman, 1976b Figure 1; Forest Marble Formation, Bathonian, Kirtlington, Oxfordshire, England, UK.
Holotype: NHMUK PV M36508, right lower molar (Freeman, 1976b: pl. 17: 1–4).
Type locality: Kirtlington, Oxfordshire, England, UK.
Type horizon: Forest Marble Formation, Bathonian (Mammal Bed).
Stratigraphic and geographic range: Middle to Late Bathonian, England and Scotland.
Material: NMS G. 2015.17.10, partial left dentary referred to this species by Close et al. (2016); NMS G.1992.47.123 and NMS G.2017.37.1, two partial left dentaries, described

here; from the Kilmaluag Formation (Bathonian), Isle of Skye, Scotland, UK. Specimens originally referred to *Palaeoxonodon freemani*, *Palaeoxonodon* sp., *Kennetheridium leesi*, and *Kennetheridium* sp. (Close et al., 2016). Right lower molars: NHMUK PV MJ.59, MJ.196, ?MJ.242, M36507 (Freeman, E., 1979: pl. 17: 1–4, but now lost), MJ.197, MJ.213, MJ.388, MJ.530, MJ.569, MJ.593, MJ.715, ?M44303, MJ.702, MJ.290, MJ.117, MJ.379, ?MJ.430, MJ.514, MJ.428, MJ.515, MJ.532, MJ.801; left lower molars: NHMUK PV ?MJ.200, MJ.236, MJ.619, MJ.639, MJ.849, ?MJ.220, ?MJ.350, ?MJ.618, MJ.626, MJ.628, MJ.657, MJ.701, MJ.727, MJ.825, MJ.827, MJ.837, ?M51823, MJ.802, MJ.53, MJ.746, MJ.289, ?MJ.518, MJ.824, MJ.214, MJ.846); right upper molars: NHMUK PV MJ.146, MJ.524, MJ.749, MJ.754, MJ.792, M36512, MJ.99, MJ.238, MJ.241, MJ.458, MJ.817, M36532. More questionably, Sigogneau-Russell (2003), also referred right upper molars: NHMUK PV MJ.44, MJ.231, MJ.669, M34994, MJ.32, MJ.506, MJ.508, MJ.512bis, MJ.742, MJ.743, MJ.788; and left upper molars NHMUK PV MJ.137, MJ.392, MJ.436, MJ.636, M36504, M36530, M36526, MJ.25, MJ.294, MJ.627. All from the Forest Marble Formation (Bathonian), Kirtlington, Oxfordshire, England, UK.

Emended diagnosis (modified from Close et al. 2016): Tribosphenic cladotherian mammal differing from dryolestoids in possessing an elongate lower molar talonid with hypoconid placed buccal to the midline of the crown, well-developed upper molar metacone, and winglike parastylar region. Differs from all other non-zatherian cladotherians in possession of a mesiolingual lower molar cingulid. Differs from *Amphitherium* in possession of five molars instead of six or seven, the more lingual position of the hypoconid, and presence of an entocristid partially enclosing an incipiently basined talonid (sensu Sigogneau-Russell, 2003). Differs from *Nanolestes* in possessing less cuspidate upper molars with weaker development of cusp B, and relatively taller and less procumbent lower molar paraconid. Differs from *Arguimus* in the presence of a more fully triangulated trigonid of m1 with a larger paraconid, more spirelike lower molar cusps, absence of a distinct cusp e, and larger metaconid on ultimate molar. Resembles *Amphitherium* and *Nanolestes* but differs from zatherians in the absence of a distinct cusp e

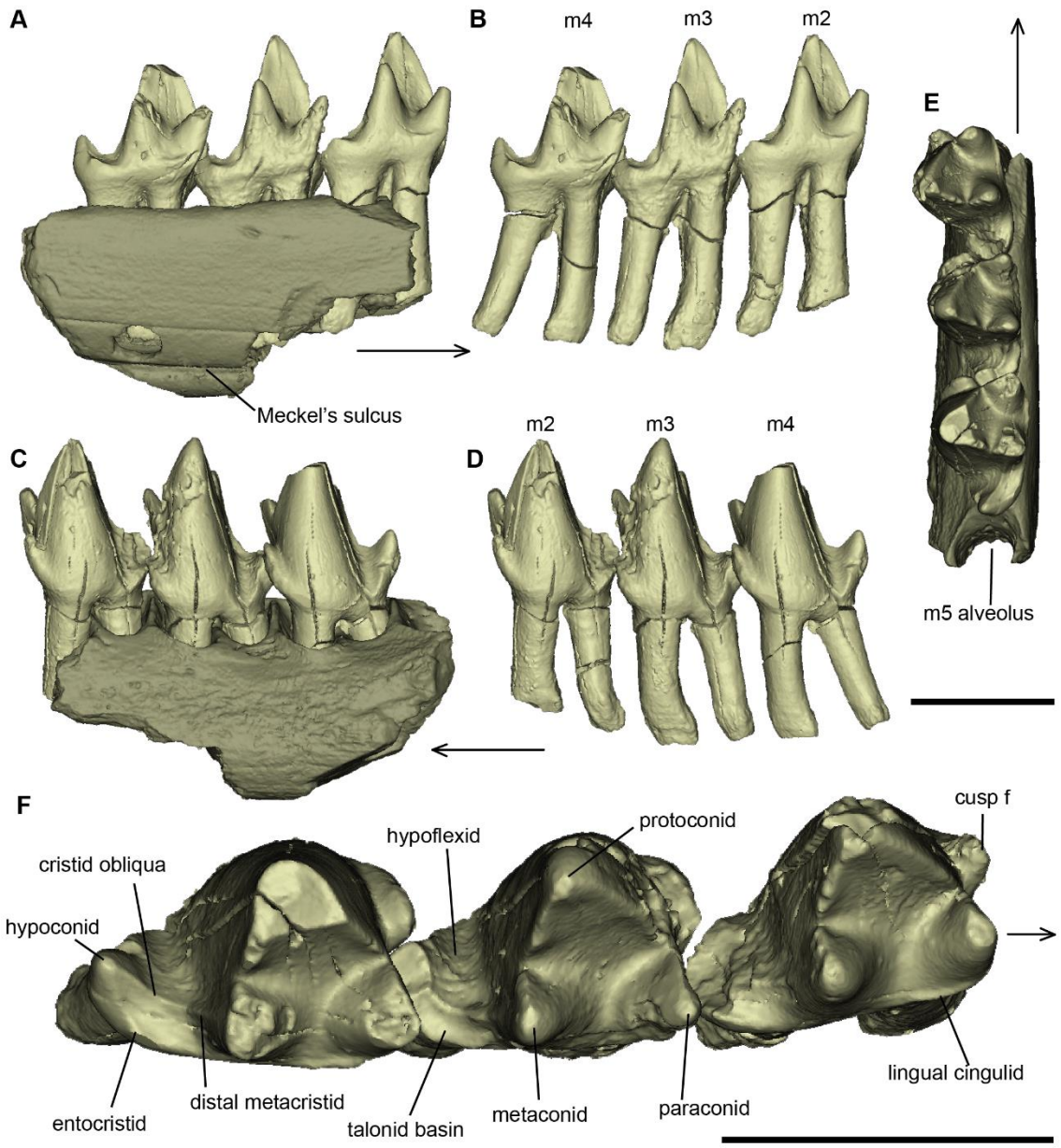

Figure 3.4.1: Amphitheriid mammalian *Palaeoxonodon ooliticus* Freeman, 1976b (NMS G.1992.47.123) from the Kilmaluag Formation, Bathonian. In lingual (A), buccal (B), and occlusal (C) views; partial left dentary (A1–C1); dentition only (A2–C2). Arrows indicate anterior direction.

on lower molars, absence of hypoconulid, and buccally positioned metacone. Relatively slender dentary unlike dryolestids, with a deep masseteric fossa and coronoid scar as in other amphitheriids. The masseteric fossa intrudes slightly into the body of the dentary below the ultimate molar, unlike all other early cladotherians. The posterior opening of the mandibular canal, the mandibular foramen, is offset from the Meckel's sulcus, unlike

Amphitherium or *Peramus*. The posteriormost mental foramen is positioned in the canine/incisor region of the dentary.

New Material

NMS G.1992.47.123 is a fragment of left dentary containing m2, m3, and m4 in position, with roots, and the anterior part of the alveolus for m5 (Figure 3.4.1). The molar crowns were broken and detached from their roots, and the latter remained inside the dentary fragment. The crowns have been restored to their original positions digitally to facilitate description and comparison. The dentary fragment measures 2.5 mm in anteroposterior length, 0.62 mm in width at the widest point, and the dentary dorsoventral depth below m3 is 1.3 mm (for tooth measurements see Table 3.4.1).

All three crowns of NMS G.1992.47.123 are well preserved, except for the following damage: the protoconid, metaconid, and paraconid cusp tips of m4 are missing; the hypoconid tip and tip of cusp f of m3 are missing; and the hypoconid and buccal apical portion of the protoconid are missing from m2 (Figure 3.4.1). The surface of the paraconid of m3 is damaged, missing enamel on the lingual surface of the paraconid, metaconid, and cingulid, and some of the anterobuccal enamel surface is also missing apically on the protoconid. The oblique cristid of m3 is well preserved, revealing a distinct incipient talonid basin in occlusal view (Figure 3.4.1C), defined lingually by the entocristid. The incipient talonid basin of m4 is well preserved, with a clear entocristid on the lingual edge.

NMS G.2017.37.1 is a fragment of left dentary 7.2 mm long with an approximate dorsoventral depth of 1.6 mm below m3 (Figure 3.4.2) (for tooth measurements see Table 3.4.1). The teeth m3 and m4 are preserved in position. Most of m2 is also preserved in position, but was fragmented prior to discovery. A fragment of the m1 root is also present. The alveolus for m5 is present but empty (Figure 3.4.2B1). The cusp tips are missing from both m3 and m4, but the protoconid, paraconid, and metaconid positions are clear on both molars, as are the hypoflexid, hypoconid, and incipient talonid basin, defined lingually by the entocristid. None of these features are easily identified in m2, in which the hypoconid and hypoflexid are missing, and only the base of the anterior half of the crown is present.

Table 3.4.1. Dental measurements (in mm) for *Palaeoxonodon ooliticus* E. Freeman (1976b) NMS G.1992.47.123 and NMS G.2017.37.1. Measurements follow Sigogneau-Russell (2003) and Close et al. (2016).

Specimen	Tooth	Total length	Total width	Total crown height	Trigonid		Talonid		Proto-conid height
					length	angle	length	cusp to meta-cristid	
NMS G.1992.47.123	m2	0.88	0.62	0.91	0.63	60°	0.25	0.19	0.21
	m3	0.88	0.60	0.98	0.61	49°	0.27	0.11	0.31
	m4	0.89	0.64		0.61	50°	0.27	0.12	
NMS G.2017.37.1	m3	1.00	0.78		0.75	47°	0.25	0.15	
	m4	0.89	0.84		0.60	58°	0.40	0.15	

Multiple fractures are present on the dentary, but the general osteology is evident. The Meckel's sulcus is preserved on the lingual surface of the dentary, extending anteriorly from a point just ventral to the mandibular foramen, up to the fractured region ventral to m2 (Figure 3.4.2C1). The mandibular foramen is present posteriorly on the lingual surface of the dentary, posteroventral to the empty alveolus for m5 and offset from the Meckel's sulcus. The pterygoid shelf is unclear from the preserved morphology.

The masseteric fossa, located posteriorly on the buccal surface of the dentary, is deep and is defined by ridges anterodorsally and ventrally. A masseteric foramen is located anteroventrally within the masseteric fossa. The anterior margin of the masseteric fossa is well-developed and extends anteriorly, ventral to the alveolus for m5. It extends just slightly into the body of the mandible ventral to m5 (Figure 3.4.2A1, B1).

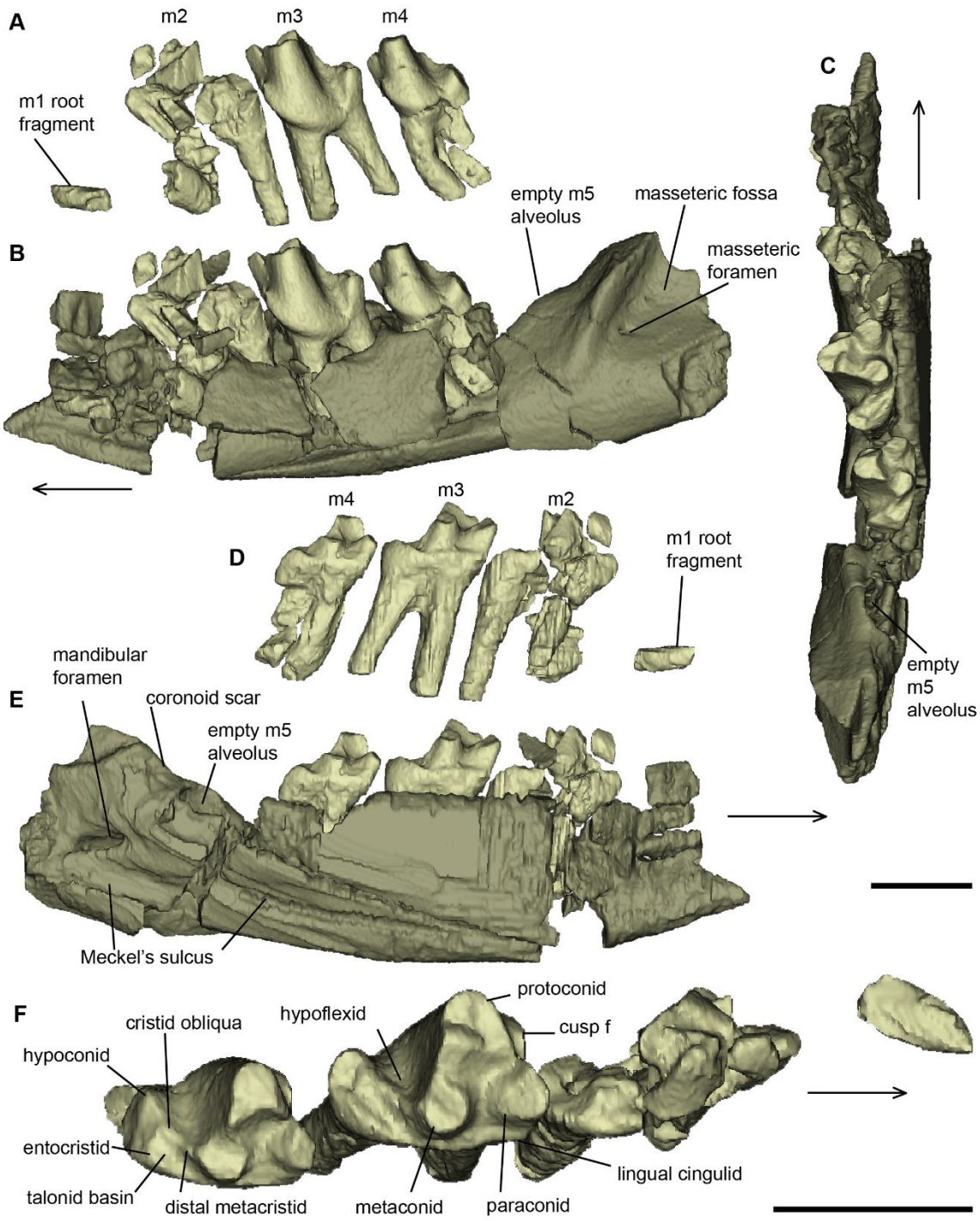

Figure 3.4.2: Amphitheriid mammalian *Palaeoxonodon ooliticus* Freeman, 1976b (NMS G.2017.37.1) from the Kilmaluag Formation, Bathonian. In lingual (A), buccal (B), and occlusal (C) views; partial left dentary (A1–C1), dentition only (A2–C2). Arrows indicate anterior direction.

3.4 iii) Results

Phylogenetic analysis

I reran the phylogenetic analysis of Close et al. (2016), which was based on the matrix of Zhou et al. (2013), updating scores for characters of the posterior portion of the dentary present in NMS G.2017.37.1. These included the position of the mandibular foramen, the morphology of the anterior margin of the masseteric fossa, the presence of the masseteric foramen, and the presence of a coronoid scar (see Appendix 18 for newly scored characters). I also re-evaluated and amended six characters present in NMS G. 2015.17.1 that were either not scored by, or that I interpreted differently from, Close et al. (2016). These include confirming the absence of Crompton's groove, the absence of a premolar or precanine diastema, confirming the presence of the hypoconid, and the morphology of the postcanine roots. Additionally, I re-evaluated and re-scored six characters present in *Amphitherium*, *Peramus*, and *Arguimus* (see Appendix 18 for justification for rescoring, and Zhou et al. 2013 for full character list).

The phylogenetic analysis recovered 5376 most parsimonious trees. Despite the additional character scores, I found no change in the relationships between *Palaeoxonodon*, *Amphitherium*, and *Peramus* from previous analyses, with *Palaeoxonodon* and *Amphitherium* placed in a sister-group relationship. These relationships have weak Bremer support values of 1, and this clade (Amphitheriidae) forms an unresolved polytomy with *Nanolestes*, *Arguimus*, and the clade including *Kielantherium* + *Aegialodon* + Theria, as in Close et al. (2016).

Five autapomorphies were recovered for *Palaeoxonodon* by my phylogenetic analysis, the first three of which were already identified by Close et al. (2016), and the last two of which are identified for the first time here: (i) the posterior-most mental foramen being positioned in the canine/incisor region of the dentary (more anteriorly than in *Amphitherium* or *Peramus*); (ii) the absence of a mesiolingual cingular cuspule e; and (iii) an absent/weak ectoflexus in the second upper molar; (iv) the slight extension of the masseteric fossa onto the body of the mandible; and (v) the position of the mandibular foramen offset from the Meckel's sulcus. *Palaeoxonodon* and *Amphitherium* share

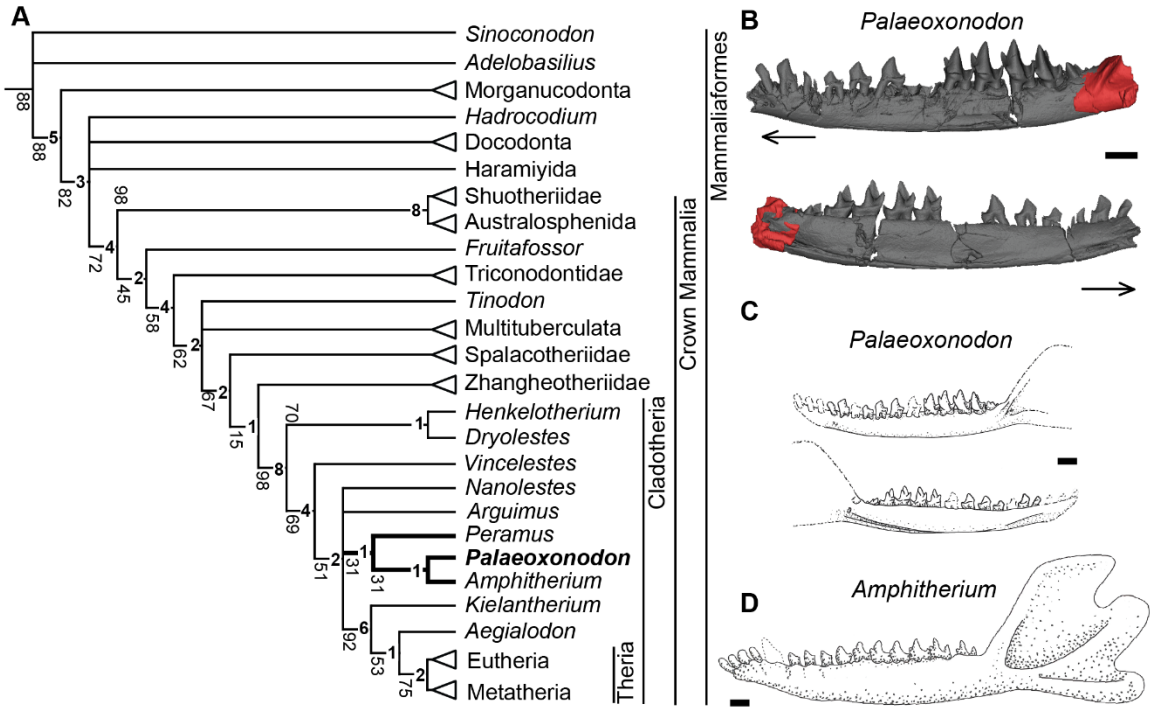

Figure 3.4.3: Parsimony analysis and reconstructions of dentary of *Palaeoxonodon ooliticus* (B, C), with *Amphitherium* (D) for comparison. A. Equally weighted parsimony analysis with additional mandibular characters for the early cladotherian *Palaeoxonodon ooliticus*, and rescored and updated matrix from Close et al. 2016 (adapted from Zhou et al. 2013). Jackknife resampling statistics and Bremer values (bold) are shown adjacent to individual nodes. B. Composite of NMS G. 2015.17.1 (grey) and coronoid of NMS G.2017.37.1 (red) in buccal (B1) and lingual (B2) views (arrows indicate anterior direction). Data for NMS G. 2015.17.1 from Close et al. (2016). C. Reconstruction of jaw in buccal (C1) and lingual (C2) views. D. Reconstruction based on composite created by EP from NHMUK PV M.36822 and OUMNH J.20075 in buccal view. Scale bars 1 mm.

synapomorphic characters in the presence of a narrow labial stylar shelf of the penultimate upper molar, and the more labial position of the metacone relative to the paracone. *Palaeoxonodon*, *Amphitherium*, and *Peramus* share the following synapomorphies: the convergence of the Meckel's sulcus with the ventral border of the mandible; and possessing open rooted postcanines.

3.4 iv) Discussion

Most previous cladistic analyses support a sister group relationship between *Palaeoxonodon* and *Amphitherium* (Prothero, 1981; Close et al., 2016; but see Averianov et al., 2015 for an alternative view). In these previous analyses this was based on (i) the large talonid (accounting for one-third of molar length), (ii) possessing a buccally positioned principal hypoconid, (iii) roots that are mostly equal in diameter along their length except for a slight narrowing distally, and (iv) the possession of five premolars with (v) moderately well-developed lingual cingulids.

Close et al. (2016) identified the variably present cuspule on the oblique cristid (mesoconid) in their specimen NMS G. 2015.17.1 as a feature shared with the holotype NHMUK PV M36508 (and two other specimens according to Sigogneau-Russell 2003: NHMUK PV MJ530 and NHMUK PV MJ618) from the Forest Marble Formation. The mesoconid is not present in either of the new specimens, NMS G.1992.47.123 or NMS G.2017.37.1. Therefore I support the interpretation of this character as variable among specimens of *Palaeoxonodon*.

Close et al. (2016) also suggested that the different dental characters used to erect the species *P. freemani* and *Kennetheridium leesi* on the basis of isolated teeth (Sigogneau-Russell, 2003) are the morphological differences between tooth positions in the same tooth row of their specimen, relegating the latter two taxa to junior subjective synonyms of *P. ooliticus*. This character variation includes differences in talonid length, prominence of the cingulid, size of the paraconid, and height and cusp sharpness of the trigonid, among different molars in the same individual. Similarly, some of this variation is visible in NMS G.1992.47.123: for example the paraconid is much smaller in m3 and m4 than in m2, and slopes at a shallower angle in m2; and the cingulid is more prominent in m2 than m3 or m4. I can add that the entocristid is more prominent in m2, and that the protoconid is broader both anteroposteriorly and buccolingually in m4. This adds to the evidence for variation along the tooth row, and emphasises the need for caution in erecting new species based on isolated teeth.

A posterior portion of the dentary including the base of the coronoid process, masseteric fossa, and mandibular foramen are preserved in NMS G.2017.37.1 and have not previously been preserved in any other specimen of *Palaeoxonodon*. The preserved

morphology suggests a sloping coronoid process, as in other early cladotherians. Strong masseteric ridges and a deep masseteric fossa are also present, as in other early cladotherians including other amphitheriids such as *Amphitherium* (Butler and Clemens, 2001), other peramurids, dryolestids, and paurodontids (Martin, 1999; Kielan-Jaworowska et al., 2004; Davis, 2012). Unlike paurodontids, the dentary is relatively slender. The preserved morphology of NMS G.2017.37.1 suggests that a pterygoid shelf may have been present on the lingual surface of the dentary; however, its extent is not clear from this specimen. The pterygoid shelf is strongly protruding in many other early cladotherians (Martin, 1999; Kielan-Jaworowska et al., 2004). The anterior position of the posteriormost mental foramen, in the canine/ incisor region of the dentary, is recovered here as an autapomorphy of *Palaeoxonodon*. While there is a possibility that a more posterior foramen may have been present in the fractured portion of the dentary below p1 in NMS G. 2015.17.1, I find no evidence for this at present, pending the recovery of new specimens.

Close et al. (2016) identified a possible coronoid scar in NMS G. 2015.17.1, which can be confirmed in NMS G.2017.37.1. This is absent in *Peramus* according to previous analyses (Clemens and Mills, 1971; Davis, 2012), but was coded as present by Zhou et al. (2013). I have rescored this character as absent in *Peramus* in my analysis. The coronoid scar is present in *Amphitherium* (Butler and Clemens, 2001) and many other early cladotherians, including the zatherian *Nanolestes* (Martin, 2002). However, it is absent in another zatherian, *Arguimus* (Lopatin and Averianov, 2006). Close at al. (2016) also inferred a lower incisor count of four based on comparison to *Amphitherium*. Although this feature cannot be verified using NMS G.1992.47.123 or NMS G.2017.37.1, I consider it likely to have been present, as this character state is common among early Cladotheria. As such, I have used it in my reconstruction (Figure 3.4.3C).

The presence of a Meckel's sulcus is common among stem mammals. In NMS G.2017.37.1, the mandibular foramen is preserved, indicating that *Palaeoxonodon* had a Meckel's sulcus that was offset from the foramen, a feature not shared with either *Amphitherium* (Butler and Clemens, 2001) or *Peramus* (Clemens and Mills, 1971; Davis, 2012). The mandibular foramen in *Palaeoxonodon* also does not appear to be confluent with the pterygoid shelf, unlike in *Amphitherium* and *Peramus*, although damage to this part of the dentary in NMS G.2017.37.1 makes this interpretation uncertain. The position of the mandibular foramen ventral to the alveolar plane, seen in *Palaeoxonodon* and

Amphitherium, is also shared with other early cladotherians, and the possible basal metatherian *Sinodelphys*. The clade comprising *Palaeoxonodon* + *Amphitherium* + *Peramus* is in a polytomy with *Nanolestes*, the clade comprising *Kielantherium* + *Aegialodon* + Theria, and *Arguimus*. *Arguimus* shares few dentary character states with *Palaeoxonodon*. *Arguimus* has no Meckel's sulcus (the absence of Meckel's sulcus is an autapomorphy of *Arguimus*; see Lopatin and Averianov 2006) and no coronoid scar. *Vincelestes* also has no Meckel's sulcus or coronoid scar (Bonaparte and Rougier 1987). While other analyses have recovered the relationship of *Vincelestes* as closer to Theria than either *Peramus* or *Amphitherium* (Kielan-Jaworowska et al., 2004; Bonaparte, 2008), my results, like those of Close et al. (2016) and Zhou et al. (2013) place *Vincelestes* as a sister group to the polytomy comprising *Palaeoxonodon* + *Amphitherium* + *Peramus*, *Nanolestes*, *Arguimus*, and *Kielantherium* + *Aegialodon* + Theria.

The phylogenetic affinities of *Palaeoxonodon* have been contested due to the presence of an 'incipient basin' (Sigogneau-Russell, 1999, 2003) on the talonid, referred to as the incipient talonid basin herein, and the variable presence of a cuspule on the oblique cristid. In an alternative hypothesis, Averianov et al. (2015) recovered a close relationship between *Amphibetulimus* and *Palaeoxonodon*, placing them in a clade with *Nanolestes*. This clade was found to be phylogenetically distinct from, and crownward to, *Amphitherium* (Averianov et al., 2015). Support for this relationship with *Nanolestes*, rather than with *Amphitherium* and *Peramus* was based on the absence of a 'retromolar space', the proportional size of the stylocone relative to the metacone in the upper molars, and absence of a coronoid scar. I now confirm the coronoid scar is in fact present in *Palaeoxonodon*. The analysis by Averianov et al. (2015) also included *Mozomus*, which was found to form a polytomy with Zatheria (including *Peramus* and *Arguimus*), and the clade comprising *Palaeoxonodon* + *Nanolestes* + *Amphibetulimus*. Neither *Mozomus* nor *Amphibetulimus* were included in my analysis and so I did not test the relationships between these taxa and other early cladotherians.

Characters of the talonid basin have previously been used to argue for a close affinity between *Palaeoxonodon* and *Peramus*, to the exclusion of *Amphitherium* (Freeman, E., 1976b, 1979; Kielan-Jaworowska et al., 2004). However, the presence of plesiomorphies such as the principal talonid cusp (hypoconid) with no embrasure for occlusal contact with the metacone of the upper molar may suggest *Palaeoxonodon* is more stemward than

Peramus, and indeed several authors have suggested that *Palaeoxonodon* and the morphologically similar *Amphitherium* are sister-taxa, occuring stemward of *Peramus* (Sigogneau-Russell, 2003; Davis 2011, 2012). Close et al., (2016) suggested that the 'incipient' talonid basin of *Palaeoxonodon* and the talonid basin of *Peramus* could either be homoplastic, or a synapomorphy of the clade *Palaeoxonodon* + *Amphitherium* + *Peramus*, and this currently cannot be resolved. I agree with Close et al. (2016) that the phylogenetic analyses carried out in their paper and herein cannot resolve this unambiguously.

Palaeoxonodon is the only taxon in my analysis in which the mandibular foramen is located in the pterygoid fossa and offset from the Meckel's sulcus. In *Amphitherium*, the foramen is aligned with the posterior end of the Meckel's sulcus, as it is for the most closely related taxa among early Cladotheria (Butler and Clemens, 2001; Kielan-Jaworowska et al., 2004). This is a condition seen in crown Marsupialia and some basal metatherians, such as *Didelphodon* (Fox and Naylor, 1986; Wilson et al., 2016), but not in more crownward Metatheria. However, there is some damage to the posterolingual portion of the dentary in NMS G.2017.37.1. More complete, undamaged specimens may shed further light on the placement of the mandibular foramen. The very slight extension of the anterior crest of the masseteric fossa into the body of the dentary is not shared with any other taxon in this analysis, except the extant *Oryctolagus* (European rabbit). However the more extreme extension of the anterior crest of the masseteric fossa, where it extends below the ultimate pre-molar or first molar, is commonly seen in multituberculates (e.g., Gambaryan and Kielan-Jaworowska, 1995). This may suggest *Palaeoxonodon* had a more extensively developed superficial masseteric muscle than other early cladotherians. Without knowing the position and morphology of the condylar process, which is crucial for determining the in-lever for the dentary (Gill et al., 2014), it is difficult to make informed inferences about the biomechanics of mastication in this genus. Ideally this requires more complete mandibles that are amenable for muscle reconstruction, as shown in other studies (Lautenschlager et al., 2017) (however, see Chapter 4.3 for estimated bite force based on reconstructions).

The presence of a masseteric foramen (also referred to as the labial mandibular foramen), located in the masseteric fossa on the buccal side of the dentary, is a newly identified feature in *Palaeoxonodon*. A deep masseteric fossa with a distinct masseteric foramen is a feature shared with peramurans, but is also present in numerous taxa across

different lineages, including other zatherians, triconodontids, and basal metatherians and eutherians (Davis, 2012). In *Palaeoxonodon* the foramen is not as large as in some specimens of *Peramus*, but it quickly merges with the mandibular canal inside the dentary, posteroventrally to the position of m5. The morphology of this foramen in *Palaeoxonodon* is similar to that described by Davis (2012) for the specimens of *Peramus* that lack an enlarged masseteric foramen: the mandibular canal is enlarged mesial to the masseteric fossa, and is separated by only a thin wall of bone (Davis, 2012: 813–814). Davis suggests the variability in the size of the masseteric foramen in specimens of *Peramus* may be attributed to post-depositional crushing and infill. Until further specimens of *Palaeoxondon* are found possessing the posterior portion of the dentary, it is not possible to say if the size of this feature similarly varies in this taxon.

3.6 Conclusions

The new fossil material being found and described from the Kilmaluag Formation is providing valuable new information about multiple taxa and the families they belong to. The completeness of the material from taxa previously known from only scattered fragments permits clarification of many previously unknown morphological features. Their addition to phylogenetic analyses has clarified phylogenetic relationships, and informed our understanding of their anatomical evolution, with implications for broader patterns of mammal macroevolution.

Stereognathus

Reevaluating the British collections of *Stereognathus*, I provide strong evidence to suggest that *S. hebridicus* is a junior subjective synonym of *S. ooliticus*. The former species was based on size, without a comprehensive description of morphology. My analysis indicates that the holotype, paratypes, and subsequently discovered *S. hebridicus* material fall along an ontogenetic size spectrum, overlapping the size range of *S. ooliticus*. There is no statistically significant difference in size distribution between postcanines attributed to these two putative species.

Morphological analysis finds that many characters within *Stereognathus* are variable within the genus, as well as appearing variable due to cusp wear through occlusion and post-mortem damage. Despite this, I outline several important features of *Stereognathus*, including cusp formula 2–2-2/2–2PC/pc; subequal cusps with medial ridges of the cusps meeting in the intercuspal groove subequally; cuspules posterior and distal to cusps L2 and B1 in upper postcanines; vestigial cusps incorporated into the AIA and PIA; a buccolingual indent on the anterior face of the lower postcanine root, 1–2 mm ventral to the base of the crown; and the maxilla reduced and somewhat cylindrical in cross-section, with no lamina extending into the secondary bony palate or jugal.

Despite the need for considerable further studies redescribing existing species and identifying additional characters for phylogenetic analysis, Tritylodontidae remains one of the most successful and long-lived cynodont groups, far outlasting other non-mammaliamorph cynodonts by persisting into the Early Cretaceous.

Although it is tempting to draw conclusions from the fragmentary remains for many tritylodontids, including *Stereognathus*, it is important to recognize the limitations of the current fossil evidence. Cusp wear can alter tritylodontid postcanines and lead to the erection of genera and species that may not stand the test of time and confuse later research. For tritylodontids, it may be better to err on the side of caution and focus on comprehensive re-evaluations of what, in many cases, are still poorly described collections. Upon these sturdier foundations new examinations of this fascinating, yet understudied, group can be built.

Wareolestes

The megazostrodontid morganucodontan *Wareolestes rex* was erected for a single molar tooth from Kirtlington in England (Freeman, E., 1979), and until now only four isolated molariform teeth had been referred to *W. rex*. The new specimen NMS G.2016.34.1, a left dentary, extends the known distribution of this genus to the Kilmaluag Formation of the Isle of Skye, Scotland, and adds to the faunal list for this locality.

Through morphological comparison, the molars remaining in the dentary provide strong evidence supporting the original identification of holotype specimen of *W. rex* as a lower left m1. NMS G.2016.34.1 indicates an apomorphic labial cingulid in *Wareolestes rex*, previously incorrectly identified as lingual cingulid.

Replacement teeth within the dentary indicate a diphyodont replacement of the premolariform dentition. This supports previous evidence for such tooth replacement patterns in other morganucodontans, including *Morganucodon*, *Megazostrodon* and *Dinnetherium*. I find no evidence for replacement in m2, as suggested for *Megazostrodon* (Gow, 1986).

Due to abrasion on the buccal portion of the dentary and loss of p1 and p3, I cannot clearly identify the sequence of dental replacement along the tooth row of NMS G.2016.34.1. However, the absence of a replacement p3 within the body of the dentary suggests possible alternating premolar replacement in *Wareolestes*, a character seen in some stem therians and eutherian mammals. Hopefully further finds may clarify this.

Palaeoxonodon

Newly described specimens of *Palaeoxonodon ooliticus* from the Isle of Skye add valuable new information for morphological comparison, and new data for phylogenetic analysis. The additional features of the masseteric fossa, and the position of the mandibular foramen identified in NMS G.2017.37.1, while not altering the phylogenetic relationships between *Palaeoxonodon* and its nearest relatives among cladotherians, are new autapomorphies for this genus. They provide additional character scores for future analysis, reducing the amount of missing information for this taxon.

The 're-discovery' of NMS G.1992.47.123 provides a cautionary tale for palaeontologists who delay in the publication of specimens. By not pursuing identification and description of this specimen, an opportunity was missed to name a second Mesozoic mammal from Scotland, an important taxon for understanding the morphology of early Cladotheria. This more complete specimen would also have provided a holotype with some variation in the tooth row, perhaps preventing the erection of taxa that are now suggested to be junior synonyms. This is an informative lesson from the palaeontological history of Mesozoic mammals. NMS G.1992.47.123 also contributes to the description of diverse Scottish Mesozoic mammal specimens that have, until now, remained undescribed, and therefore unrecognised scientifically.

Although a relatively large number of upper teeth and lower dentitions from *Palaeoxonodon* are now known, they have not yet been found in association, and postcrania have yet to be identified. This provides a goal for further discoveries in the diverse microvertebrate beds of the Isle of Skye in the coming years.

Borealestes

For the first time since its discovery, the diagnosis for *Borealestes serendipitus* has been outlined in detail and clarified in light of the wealth of fossil material from the Kilmaluag Formation. There are clear diagnostic differences between *Borealestes serendipitus* and the sister taxon, *Borealestes mussettae*: namely the well-developed b-g crest and absence of a-g crest in the lower molars of *B. serendipitus*, and reduction of cusp Z and presence of A-X crest in the upper molars of *B. serendipitus*. *B. mussettae* lacks these features and appears to have a more anteroposteriorly elongate tooth morphology. The range of ontogenetic stages represented by the Kilmaluag Formation material for *B.*

serendipitus supports the same ontogenetic changes in the dentary seen in *Docodon*, the late eruption of an m6 and posterior shift in the anterior border of the coronoid process in more mature individuals.

The cranial and postcranial morphology of *Borealestes* as revealed by NMS G.1992.47.121.1 provide unprecedented information on a docodontan taxon from early in the clade's evolutionary history. The gracile morphology bears many resemblances to the arboreal to scansorial *Agilodocodon* from China (Middle Jurassic), but also to the more robust, semi-aquatic and/or semi-fossorial *Haldanodon* from the Alcobaça Formation of Portugal (Late Jurassic).

The high-resolution of my computed tomography and synchrotron scans has made it possible to characterise the details of the vascularised structures of the petrosal of *Borealestes*, and provide the first endocranial view of a docodont petrosal. This has led to the identification of two previously unknown structures: the anterior and posterior trans-cochlear sinuses. This has also made it feasible to develop an overall reconstruction of the vascular and innervation structure in the petrosal. Despite post mortem crushing and the displacement of fragments of the petrosal and stapes inside the cochlear canal, I have been able to digitally reconstruct broken fragments of the petrosal and stapes. This reveals a more or less circular fenestra vestibuli and stapedial footplate, with a bullate morphology, as in *Haldanodon*. There are broad similarities in the morphology of the petrosal of *Borealestes* to that of *Haldanodon*, from which I tentatively suggest a similar ecology for these two docodonts.

The results of a phylogenetic analysis using only dentomandibular characters from multiple docodontans differs from an analysis incorporating cranial, postcranial and soft tissue characters from fewer docodontans, but multiple other mammaliaform groups. The dentomandibular analysis returned similar results to previous analyses: *Borealestes* was found to form a clade with *Haldanodon, Docodon and Docofossor*, the so-called 'basal docodontans'. It does not support two other previously proposed clades 'Tegotheriidae' or 'Simpsonodontidae'. The expanded cranial, postcranial and soft tissue dataset supports the affinity between *Borealestes* and *Agilodocodon* suggested through anatomical observation, particularly of the gracile features shared by these taxa, but does not support the 'basal docodontan' clade.

While the analysis using only dentomandibular data only did not find a close relationship between *Borealestes* and *Agilodocodon*, it is the dental characters in the expanded data matrix that unite these taxa in a clade with *Microdocodon* in the broader phylogenetic analysis incorporating crania and postcrania. In the cranial, postcranial and soft analysis the topographical relationships between *Borealestes* and *Haldanodon*, *Docofossor* and *Castorocauda*, while they have shifted somewhat, are still similarly placed relative to one another as in the dentomandibular-only analysis. This suggests that the inclusion of postcranial characters has had a profound effect on the placement of *Agilodocodon* specifically, rather than on *Borealestes*. It also highlights the limited utility of an expanded character dataset when so few docodontans are known from more than dentomandibular material.

Chapter 4: Biomechanics and Ecomorphology of Mammaliaforms of the Kilmaluag Formation

4.1 Body Mass Estimates

Body mass plays an important role in multiple physiological, biomechanical and ecological factors in vertebrate animals. For example, it is widely known that body mass affects the energetics of locomotion (Taylor et al., 1970; Garland, 1983), limb postures and safety factors of limb bones (Biewener, 1989a and b, 1990), and specific functional characters of the skeleton (Grand, 1990), population density (Damuth, 1981, 1987) and home range (Lindstedt et al 1986), basal metabolic rate (Kleiber, 1935; Hayssen and Lacy, 1985), life span (Western, 1979) and even gestation length in placental mammals (Western, 1979).

Scaling relationships between these factors are the subject of many publications, with research testing ecological rules. Examples include Cope's Rule (body mass tends to increase in lineages of animals over time) (Rensch, 1948), Foster's Rule (body mass increases or decreases depending on availability of resources e.g. Island/Insular Dwarfism) (Foster, 1964), Bergmann's Rule (body mass correlated with latitude) (Blackburn et al., 2008), or Kleiber's Rule (metabolic rate scales to the one-third power of the animal's mass) (Kleiber, 1932).

For paleobiological studies of mammals and their near relatives, body size is often treated as a proxy for morphological disparity to characterise patterns of evolutionary trends in mammals (Alroy, 1999; Smith et al., 2010b), and mode of macroevolution (Slater, 2013). The distribution of body mass of mammals is a key attribute of mammalian ecological communities (Smith and Lyons, 2011) as body mass and diet are interrelated in mammals (Price and Hopkins, 2015).

However, exploration of body mass scaling relationships have shown that scaling of body size can be dependent on phylogeny, and is often influenced by the specific anatomy of a group. For example the long bones of primates are proportionally longer than those of other mammal groups, and so scaling relationships must be adjusted when dealing with them (Alexander et al., 1979). With this in mind, scaling relationships for fossil taxa must

be established based on relevant modern analogues. Another important consideration is that scaling relationships between size and body mass are linked to metabolic rate (Foster, 2009). Metabolic rate in most groups of stem mammals is likely to be lower than in modern mammals (e.g. O'Meara and Asher 2016; Newham et al., 2018).

One final drawback in attempts to estimate body mass in fossil taxa is the incomplete nature of the fossil record. Scaling relationships that use skull length (e.g. Gingerich and Smith, 1984; Luo et al., 2001) are often not applicable to Mesozoic mammals, which are usually represented by dentition and dentary material. In cases where more extensive skull material exists, it is seldom complete, and often distorted and fragmentary, making reconstruction and measurement difficult. For this reason relationships that use single bones that are more likely to survive in the fossil record (such as the dentary) have greater utility.

Two calculations frequently used to calculate body mass in Mesozoic mammals are those proposed by Foster (2009), and Campione and Evans, (2012). Foster (2009) used mandibular length and known body mass in extant marsupial mammals to formulate a regression calculation for body mass which was then applied to the Mesozoic mammals of the Morrison Formation. Extant marsupials have a lower metabolism than extant placental mammals (Byers, 1999), making them more comparable to Mesozoic mammals. Extant marsupial molar morphology and tooth row length/composition (e.g. number of postcanine teeth) also bears closer resemblance to Mesozoic mammals than those of extant placental mammals Foster, 2009). These factors make marsupials a more suitable analogue for stem mammaliaforms when using regression.

Regression calculations using femur length have been used in body mass estimates for docodont fossils including *Castorocauda lutrasimilis* (Ji et al., 2006), *Agilodocodon scansorius* (Meng et al., 2015) and *Docofossor brachydactylus* (Luo, 2015) (Table 1). The regression calculation of Campione and Evans, (2012) used femur and other limb bone lengths in a dataset of extant mammals and non-avian reptiles to test methods of limb-scaling body mass regression, and the influence of gait and posture on regression calculations. They found significantly strong correlations using femur length and circumference, and humerus length and circumference, to calculate body mass across mammal groups. This suggests a conserved relationship between these variables that can reasonably be applied to fossil mammaliaform taxa. Only a partial humerus is preserved in

NMS G.1992.47.121.1, *Borealestes*, and femur length has commonly been applied to other docodonts, so I have chosen the femur length scaling relationship as a second method to obtain body mass estimates for the Kilmaluag Formation mammal taxa.

4.1 i) Methods

To estimate the body mass of mammaliaform taxa from the Kilmaluag Formation, measurements were taken of the maximum mandible length and maximum femur length for all available taxa (see Table 1 for taxa, specimen numbers, and measurements). Where fossils were damaged or incomplete, conservative estimates were made, completing missing components of the bone based on comparisons with the morphology of closely related taxa.

The following body mass regression calculations were then used:

1) Ln (body-mass [g]) = 2.9677 x Ln (mandible-length [mm]) – 5.6712 (Foster, 2009)

2) Log_{10}BodyMass = 2.993 x Log_{10}FemurLength-2.341 (Campione and Evans, 2012)

Calculations were carried out in Microsoft Excel 2013. Additional body mass estimates were taken from Foster (2009), Meng et al. (2015) and Luo (2015) to provide comparisons.

4.1 ii) Results

Results for both calculations are presented in Table 4.1.1 and Figure 4.1.1. Using mandibular length in the regression calculation of Foster (2009), the body mass for *Borealestes serendipitus* NMS G.1992.47.121.3 was calculated at 40g, *Krusatodon kirtlingtonensis* NMS G.1992.47.122.1 was calculated at 93g, *Wareolestes rex* NMS G.2016.34.1 was calculated at 100g, and *Palaeoxonodon ooliticus* NMS G. 2015.17.1 was calculated at 13g. The dentaries of *Wareolestes rex* NMS G.2016.34.1 and *Palaeoxonodon ooliticus* NMS G. 2015.17.1 are both incomplete, and so length was estimated based on reconstructions informed by the morphology of closely related taxa: *Morganucodon* (for *Wareolestes*) and *Amphitherium* (for *Palaeoxonodon*).

Table 4.1.1: Body mass estimates for Kilmaluag Formation mammaliaform taxa, and other docodontans. Values in italics are based on conservative estimates, where fossil material is incomplete or damaged.

Kilmaluag Formation taxa	Specimen no	Mandibular length (mm)	Femoral length (mm)	Foster (2009)	Campione and Evans (2012)
Borealestes serendipitus	NMS G.1992.47.121.1/3	23.3	*12.82-14*	40g	*9-12 g*
Krusatodon kirtlingtonensis	NMS G.1992.47.122.1	31.1	*18.0822*	93g	*26g*
Wareolestes rex	NMS G.2016.34.1	*32*	-	*100g*	-
Palaeoxondon ooliticus	NMS G. 2015.17.1	*16*	-	*13g*	-
Other taxa					
Docofossor brachydactylus	BMNH131735 (Luo et al., 2015)	17	12.5	16g	9g
Docodon	YPM 11826 (Foster, 2009)	35.8	-	140.7g	-
Agilodocodon scansorius	BMNH001138 (Meng et al., 2015)	23	13	37.8g	10g
Castorocauda lutrasimilis	JZMP04117 (Ji et al., 2006)	49	-	357 g	-

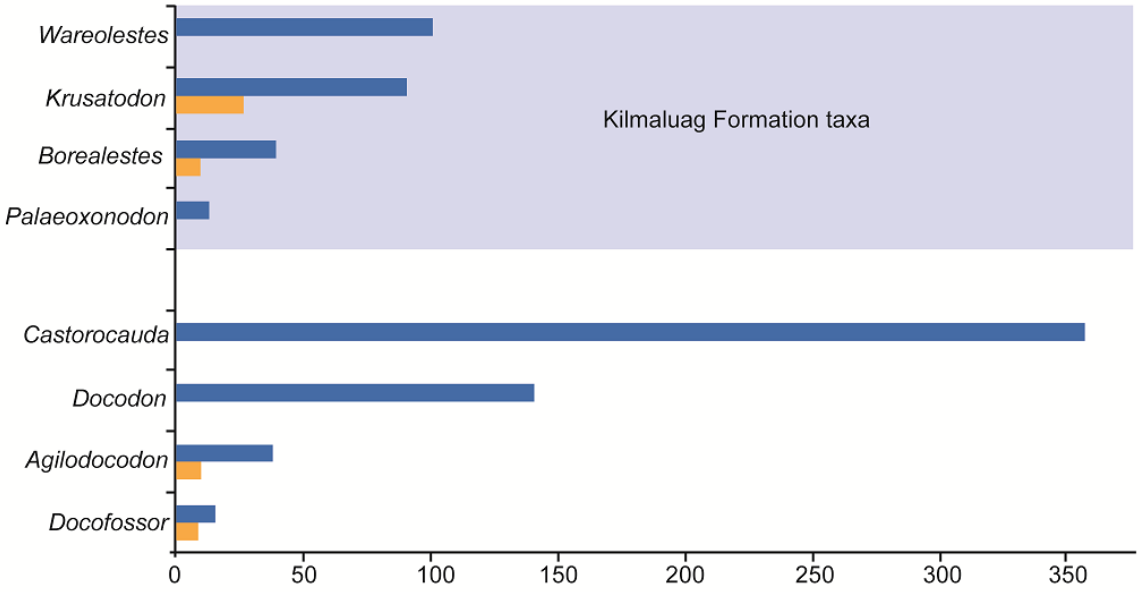

Figure 4.1.1: Body mass estimates for the Kilmaluag Formation mammaliaform taxa. Blue bar = estimate based on dentary length; orange bar = estimate based on femur length.

Using the calculation of Campione and Evans (2012) which utilised femoral length, the body mass for *Borealestes serendipitus* NMS G.1992.47.121.1 was calculated at 9g, and *Krusatodon kirtlingtonensis* NMS.1992.47.122.1 was calculated at 26g. The femur in these specimens is damaged, so both calculations are based on estimated total length: the femur of NMS G.1992.47.121.1 is missing the proximal end, and so a measurement range is given to account for this unknown morphology; the proximal femur of NMS.1992.47.122.1 is fragmented, so measurement is based on reconstruction of displaced fragments. No femoral material is currently known for *Wareolestes rex* or *Palaeoxonodon ooliticus*.

4.1 iii) Discussion

The body mass estimates provided here for the mammaliaform taxa of the Kilmaluag Formation suggest a range of size from 9g to 100g (Table 4.1.1). This is similar to that found for the Morrison Formation with estimates ranging from the smallest, *Fruitafossor* at 6 g, to the largest taxon, the docodontan *Docodon* at 141 g (Foster, 2009). The pattern of body mass distribution in the Morrison Formation resembles many modern ecosystems in the relatively higher abundance of smaller body mass taxa (<50 g) versus larger taxa (125-150 g), but the Morrison Formation taxa had a peak diversity at a lower body mass that most modern small mammal faunas (Foster, 2009). Although overall abundance has not yet been examined quantitatively in the taxa found in the Kilmaluag Formation, docodonts appear to be the most abundant mammaliaform fossils based on collecting (pers. obs; see also Chapter 2.2 and 2.3). This would be similar to the pattern seen for mammaliaform body mass and abundance distribution in the Morrison Formation (Foster, 2007).

The estimates for *Borealestes serendipitus* (NMS G.1992.47.121.1 and NMS G.1992.47.121.3, both are parts of the same individual) were substantially different using the two calculations presented here. It is estimated to be 9-12 g based on femoral length, or to be 40 g based on the mandible. The lower estimates are similar to the size range of the extant shrew genera, *Sorex* and *Neomys*, and the small marsupial planigale, *Planigale* (Hayssen and Lacy, 1985). The higher estimates are similar to extant hopping mice species, *Notomys*, or murids such as the least chipmunk *Tamius minimus* (Garland, 1983; Hayssen and Lacy, 1985). These ranges of estimates for *Borealestes* are similar to the range of body

masses estimated for *Agilodocodon* using the same two methods (Meng et al, 2015) (Table 4.1.1). The docodontan taxa of the Kilmaluag show a body size range between the very low body mass estimate for *Docofossor* of 9-16 g (Luo et al., 2015), and the much larger *Docodon*, with a body mass estimate of 140.7 g (Foster, 2009).

The highest body mass estimate for any docodont in the literature is for *Castorocauda lutrasimilus* which has been suggested to be up to 800 g in body mass (Ji et al., 2006). Using skull length and the regression calculation of Gingerich and Smith (1984; see also Luo et al., 2001), Ji et al. (2006) arrived at a lower body mass estimate of 518 g. However, using mandibular length in this analysis, the lower estimate falls to 357 g. Although lower than previous calculations, this is still a substantially larger body mass estimate than those for other docodontan taxa, including those in the Kilmaluag Formation.

The calculations for the other docodontan, *Krusatodon*, based on NMS G.1992.47.122.1 (currently under separate study) range from 26-93 g, suggesting this taxon was between the size of the marsupial dunnart, *Sminthopsis*, and the slightly larger eastern chipmunk, *Tamias striatus* (Hayssen and Lacy, 1985). As with *Borealestes*, the femur measurement gives a smaller body mass estimate than the mandibular measurement.

Meng et al. (2015:SM p.11) suggested that docodontans possess relatively shorter femora relative to body mass than other mammaliaforms and extant taxa, which could explain the consistent and large difference between the results of these two body mass estimation methods across all known docodontans so far. Therefore this analysis might suggest *Krusatodon* has either a longer hind limb, or shorter rostrum, than most other docodontan taxa. Further analysis of NMS G.1992.47.122.1 should help clarify the morphology of this taxon. Ultimately the most reliable body mass estimations come from integrating multiple measurements from the skeleton, as found by Campione and Evans (2012). The lack of complete fossil material for many taxa makes this difficult to test for docodontans.

Wareolestes rex NMS G.2016.34.1 and *Palaeoxonodon ooliticus* NMS G. 2015.17.1 are only represented by incomplete mandibular material. Their body mass estimates are therefore less robust than those of the other two Kilmaluag Formation taxa. However, it is clear from observation that *Wareolestes* is a substantially larger and more robust taxon, particularly as the dentary NMS G.2016.34.1 belongs to a sub-adult specimen (Panciroli et al., 2017a; Chapter 3.2). It has been suggested by previous authors that the dental

morphology of *Wareolestes rex* indicates a more carnivorous ecology for this taxon (Freeman, E., 1979). The body mass estimate for *Wareolestes* of 100 g is about the same as an extant black rat, *Rattus rattus*—significantly larger than any other mammal currently known from the Kilmaluag Formation—and coupled with bite force analysis (See Chapter 4.2) lends some support to this hypothesis. In contrast, *Palaeoxonodon* is clearly a small taxon, based on measurements of the preserved dentary (Close et al., 2016; Panciroli et al., 2018a; Chapter 3.4), and therefore less likely to be carnivorous. This is also supported by results of bite force analysis (Chapter 4.2).

4.2 Jaw Biomechanics and Bite Force Analysis

Bite force analysis using engineering principles provides useful information for inferring dietary ecology (Aguirre et al., 2002). The relationship between the material properties of food—such as intractability, or 'hardness'—and the functional morphology of the feeding apparatus, especially the jaws, is well established for small insectivorous mammals (e.g. Freeman, P.W., 1979; Strait, 1993; Dumont, 1995, 1999; Aguirre et al., 2003; Santana et al., 2011). Such studies provide extant analogues for their Mesozoic counterparts (e.g. Gill et al., 2014).

Analyses of bite force can be carried out in vivo for extant animals (Aguirre et al., 2002; Freeman and Lemen, 2008), or using an extant dataset including skull and mandibular measurements to infer dietary ecology in fossil taxa (Therrien et al., 2015). Ideally biomechanical analyses of jaw function require the morphology of the skull to obtain data such as masseter/pterygoid musculature attachment area, and the cross-section and length of muscles (Turnball, 1970; Davis et al., 2010; Santana et al., 2011). In some exemplary cases where fossil skulls are relatively well preserved, these muscles can be inferred for Mesozoic mammals and incorporated into the biomechanical analyses of early mammals (e.g., Lautenschlager et al., 2017). However, most fossil material of Mesozoic mammals are limited to teeth and jaws, and rarely includes sufficient cranial material for such analyses.

Nevertheless, the dentary alone can provide enough information on the functional morphology of a taxon to infer diet and feeding behaviour (Therrien, 2005). Engineering principles have been applied to Mesozoic mammals, for example using beam-analysis and finite element analysis (FEA) (Gill et al, 2014; Brannick and Wilson, 2018; Lautenschlager et al., 2018), geometric morphometrics (Grossnickle and Polly, 2013), and other measures of mechanical advantage (Grossnickle, 2017).

It is a complex task to test the relationship of dietary specialisation, feeding behaviour, and morphological characters of the jaws (Ross et al., 2012; Ross and Iriarte-Diaz, 2014). However, it is feasible to correlate the masticatory movement of the jaw with musculo-skeletal features (Grossnickle 2017; Bhullar et al. 2019), and to estimate the correlation of structural traits of the mandible to the biting force magnitude (Therrien et al.

2016). Such estimates can then be applied to fossils of extinct taxa (Brannick and Wilson, 2018).

The horizontal ramus of the dentary (mandibular body) can be treated as a simplified beam with an elliptical cross-section, and beam theory can be used to calculate cross-sectional properties (Therrien, 2005). This is based on the assumption that the cross-sections of the dentary can be approximated as an ellipse that behaves as a homogeneous unit without dissipation of stress, and that it is principally loaded in bending during feeding. In this approach, the dentary is modelled as a cantilever, with the articular condyle as the fulcrum (Figure 4.2.1). This makes it possible to estimate resistance to mediolateral, dorsoventral and overall relative bending forces, giving an indication of the efficiency of the dentary to transfer the in-force of the adductor musculature to the bite at any given point in the dentary (Therrien, 2005; Gill et al 2014).

Studies of extant mammals have found increased bite force in small mammals correlates with the increased hardness of their food items (e.g. Aguirre et al., 2002, 2003). In the case of insectivores, intractability is often measured in terms of exoskeletal or cuticle thickness, and the force required to pierce and chew it (Evans and Sanson, 2005). For example, generally speaking coleopteran cuticles require more force and energy to fracture than the relatively thinner cuticles of lepidopterans (Evans and Sanson, 2005). These relationships, applied to fossil mammal taxa and their prey items, permit inferences to be made about dietary preference.

4.2 i) Methods

I used four mammal taxa represented by fossil dentaries found in the Kilmaluag Formation, Isle of Skye, Scotland: *Palaeoxonodon ooliticus* NMS G. 2015.17.1 (Close et al., 2016), *Wareolestes rex* NMS G.2016.34.1 (Panciroli et al., 2017b), *Borealestes serendipitus* NMS G.1992.47.121.3 (Panciroli et al., in review) and *Krusatodon kirtlingtonensis* NMS G.1992.47.122.1 (unpublished, under study by EP). Positions for measurement along the dentary were selected at interdental gaps (Figure 4.2.1), after Therrien (2005) and subsequently other authors (e.g. Gill et al. 2014; Brannick and Wilson, 2018). Where applicable, dentition within the dentary is incorporated into the calculation, as

the removal of dentition can alter measured strain values during analysis ('closed-section' versus 'open-section' models, see Daegling et al., 1992).

A hollow beam model was used for *Borealestes serendipitus* NMS G.1992.47.121.3, as this model has been shown by sensitivity analysis to be accurate in determining bending strength (Therrien et al., 2016). However, not all of the specimens from the Kilmaluag Formation have suitable CT slices in the correct orientation to accurately calculate cortical bone distribution for hollow beam analysis, so the solid beam model was used for all taxa, in order to permit comparison between taxa. Solid beam models do not account for variations in internal structure such as differences in trabecular (cancellous) bone density, density of cortical bone, the presence of the mandibular canal, or for the presence of alveoli for tooth-roots along the length of the mandibular body. However the advantage of the solid beam model is that only the external dimensions of the dentary are required, making it possible to apply it to taxa where CT scan slice data are not available. The solid beam model may not provide as accurate absolute values for bite force (measured in Newtons), but a previous sensitivity analysis (Therrien et al., 2016) has determined that the relative values along the length of the dentary body and between taxa are consistent between the solid beam models (mandibular canal filled in as cortical bone) and the hollow beam models (the mandibular canal left open) (Therrien, 2016). This assumption holds for the cross-sections at inter-dental positions (Figure 4.2.1).

For the hollow model of NMS G.1992.47.121.3, CT slices at the interdental gaps starting from posterior to the canine, and ending posterior to the ultimate molar, were exported from Mimics 19.0 as .tiff images (Figure 4.2.1C-D). These slices were prepared in Fiji/ImageJ by removing any tooth emergent above the rim of the alveolus, and removing any trabecular bone or mineral infill inside the dentary, leaving only cortical bone and tooth within the alveolus. The images were converted to 32-bit greyscale and the maximum and minimum threshold values and scale determined. Second moment of

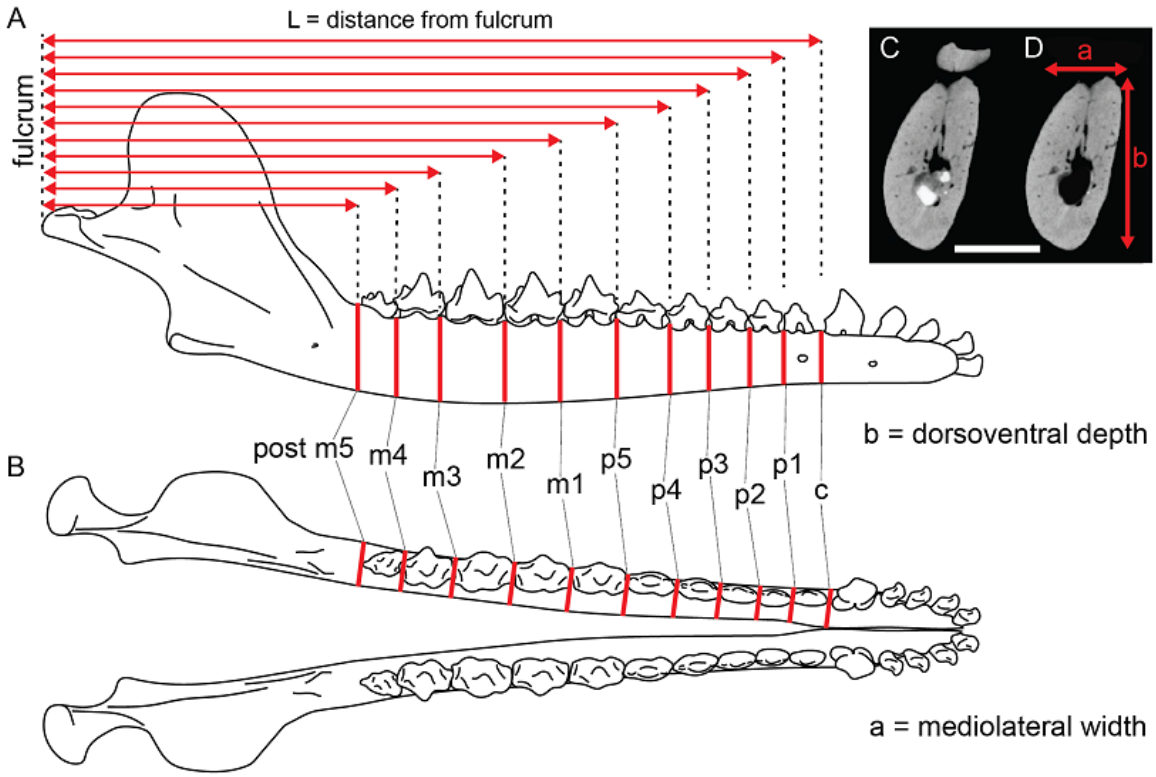

Figure 4.2.1: Methodology for data collection. A, measurements of dorsoventral depth *b*; B, measurements of mediolateral width *a*; C, example of CT slice used for moment calculation in Image J (from position posterior to m3 on *Borealestes* NMS G.1992.47.121.3); D, CT slice from C prepared for calculation. Red lines indicate measurements. See text for more details of methodology. Dentary from Panciroli et al. (in review), Section 3.3.1).

area calculations were made using MomentMacroJ v1.4 (http://www.hopkinsmedicine.org) and are in mm^4.

Solid model measurements for all taxa were taken in Fuji/ImageJ from .tiff images of digital reconstructions (produced using Mimics 19.0) with known scale. All digital reconstruction and measurement was done at NMS.

To calculate bending force in the dorsoventral and mediolateral axes, the position of the fulcrum—the articular condyle—must be known. Two specimens lacked a preserved articular condyle, *Wareolestes rex* NMS G.2016.34.1 and *Palaeoxonodon ooliticus* NMS G. 2015.17.1. For these specimens the distance from each interdental position was calculated by measuring to the posteriormost preserved portion of the dentary, and an estimated distance from that point to the approximate condyle position was added: this value was 10 mm for NMS G.2016.34.1, and 4.5 mm for NMS G. 2015.17.1. These estimates were based

on the morphology of closely related taxa, *Morganucodon* (for *Wareolestes*) and *Amphitherium* (for *Palaeoxonodon*). Results for these taxa must therefore be treated with caution until further material permits confirmation and refinement of these calculations. Although beam analysis was carried out on *Wareolestes rex*, NMS G.2016.34.1, damage to the buccal surface of the dentary means these results must also be treated with caution, particularly for the anterior of the dentary.

Second moment of area, **I**, is a measure of the distribution of bone around the neutral axis (here assumed to be the centre of the mandible). Two values are obtained: **Ix** = distribution of bone around mediolateral axis, b, and **Iy** = distribution of bone around dorsoventral axis, a. This is done using the formulae:

$$Ix = \pi b a^3/4$$
$$Iy = \pi a b^3/4$$

The second moment of area in each axis can be used to calculate the polar moment of inertia, **J**, which predicts a structure's ability to resist torsion. **J** is calculated as:

$$J = Ix + Iy$$

The second moment of area can be used to calculate the section modulus, **Z** (**Zx** and **Zy**), which is a measure of bending strength around the mediolateral (x) or dorsoventral (y) axis. The formula for **Z** is:

$$Zx = Ix/a$$
$$Zy = Iy/b$$

If values of **Z** are known, this can be coupled with each interdental position's distance from the fulcrum, **L**, and the maximum force that can be resisted in each axis can be calculated:

Dorsoventral bending force = Log Zx/L
Mediolateral bending force = Log Zy/L

Log accounts for size in solid models, but is omitted in the hollow model as it is not necessary—size has already been accounted for in the hollow model calculation. These can be used to compare variation in the relative and axis-specific maximum bending force that can be applied along the length of the dentary in different taxa. This is important as resistance to dorsoventral loads is related to bite force upon prey items, whereas mediolateral force relates to resisting transverse or torsional stresses produced by food/prey items, usually through struggling or other similar movement (Therrien, 2005).

4.2 ii) Results

Results of these analyses show that the hollow model has much higher resistance to dorsoventral than to mediolateral bending for *Borealestes serendipitus* (Figure 4.2.2A-B) (details in Table 4.2.1, Figures 4.2.2-4). This difference increases posteriorly along the mandibular body below the tooth row. The same pattern is seen in the resistance to torsion, or the polar moment of inertia (J) (Figure 4.2.2C). Comparing the hollow and solid model for *Borealestes* NMS G.1992.47.121.3, the pattern is similar for resistance to bending and torsion, although the hollow model finds a lower value for m4 relative to m3, which is not seen in the solid model (Figures 4.2.2-3).

For the solid models (Figure 4.2.3), looking only at the two docodonts there is a clear pattern of greater resistance to bending and torsion in *Krusatodon* NMS G.1992.47.122.1 than in *Borealestes*, evidenced by the higher maximum dorsoventral and mediolateral maximum bending force values, and polar moment of inertia (Figure 4.2.3). This difference increases along the dentary posteriorly, with a peak at the p5-m1 loci. This pattern reverses for relative bending force (Zx/Zy), with both taxa being similar in profile, but *Borealestes* having slightly higher values. In both taxa values increase along the tooth row posteriorly.

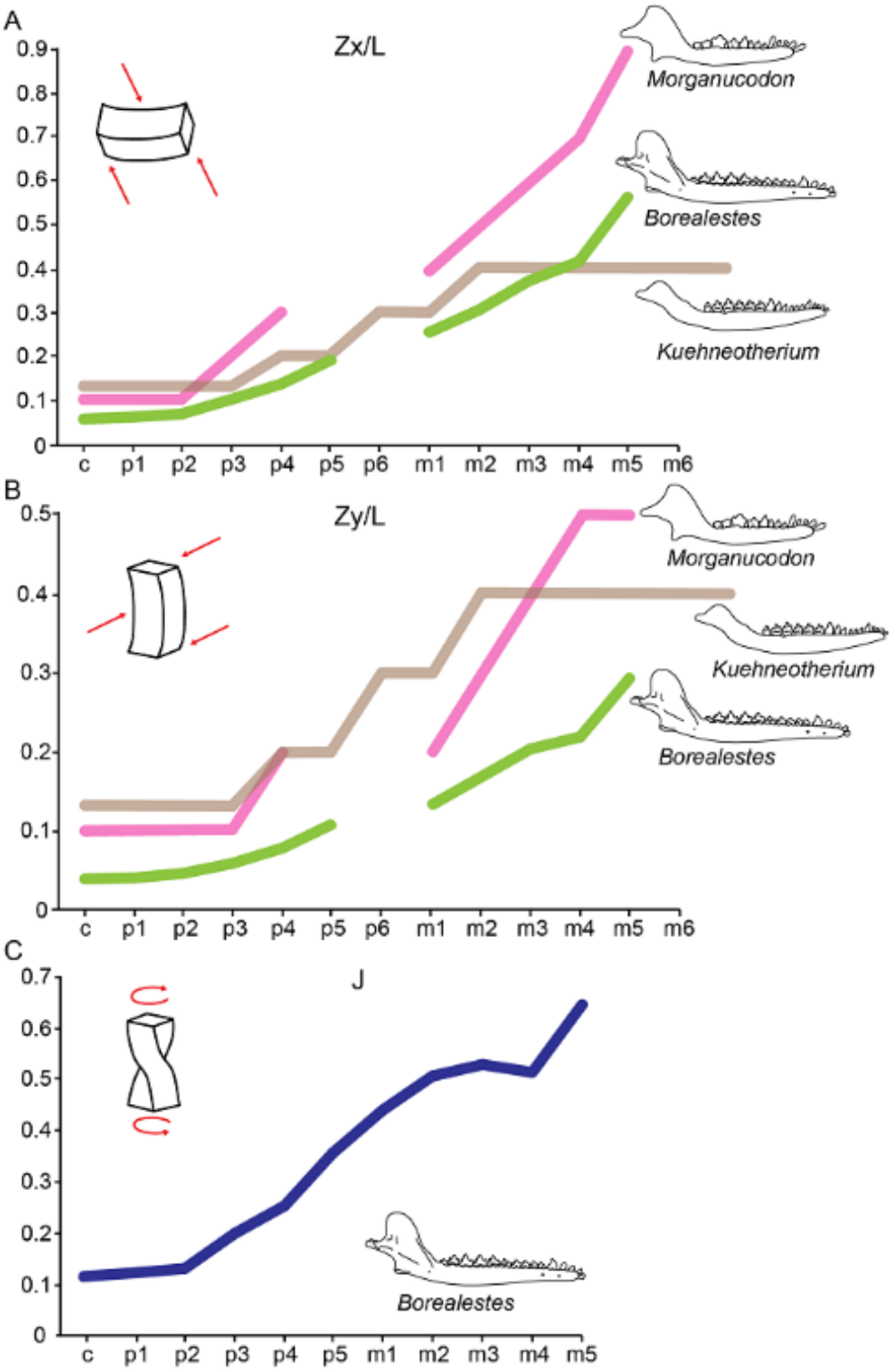

The four mammaliaform taxa included in the solid model analysis showed differences in their resistance to bending forces and torsion along the tooth row (see Figure 4.2.4). *Palaeoxonodon* NMS G. 2015.17.1 shows consistently lower values for most of the

tooth row than the other taxa, particularly in the anterior of the dentary, but it shares similar values to *Borealestes* in the premolars for resistance to bending forces in each axis. *Palaeoxonodon* showed a higher resistance to mediolateral maximum bending forces than *Borealestes* at the canine, with a similar value to *Krusatodon* at that locus (Figure 4.2.4B). When relative bending resistance is measured, *Palaeoxonodon* NMS G. 2015.17.1 has similar values to *Krusatodon* and *Wareolestes* for the molar teeth.

The resistance to bending and polar moment of inertia for *Wareolestes* NMS G.2016.34.1 was markedly higher than all of the other taxa in the posterior, molar row of the dentary, and similar to *Krusatodon* in the premolars (Figure 4.2.4). There is low resistance to mediolateral bending force or torsion at the canine in all taxa, although in *Wareolestes* NMS G.2016.34.1 the value is not known as the canine is not preserved.

4.2 iii) Discussion

Borealestes has different values relative to *Krusatodon* for resistance to bending and torsion in the mandibular body below the tooth row (Figure 4.2.3). This suggests that these taxa must differ in bite force. By inference they fed on different food resources of worms and insects, despite being closely related phylogenetically, and part of the same assemblage. Both the hollow and solid models for *Borealestes* show a pattern of steady increase in resistance to bending and torsion posteriorly along the dentary. This resembles the pattern seen in *Morganucodon* (Figure 4.2.2) (Gill et al., 2014). The different pattern in *Krusatodon*, with a peak of resistance in both axes around m1 (Figure 4.2.3) which indicates the focused biting of prey items at this locus, more closely resembles the pattern in *Kuehneotherium* (Gill et al., 2014).

Figure 4.2.2 (previous page): Results of hollow model moment calculations for *Borealestes* NMS G.1992.47.121.3, with *Morganucodon* and *Kuehneotherium* for comparison (data from Gill et al., 2014 and P. Gill pers. com). A, the dorsoventral maximum bending force values; B, the mediolateral maximum bending force values; C, the torsion values. Tooth row position on the x-axis, maximum force (in Newtons) on the y-axis. Dentary drawings by EP based on Gill et al., 2014). Gaps indicate different premolar counts in different taxa.

Table 4.2.1: Results of bite force and torsion analysis on Kilmaluag mammaliaform fauna. Italics indicate estimated values due to missing or incomplete material.

Tooth position	*Borealestes* NMS G.1992.47.121.3 hollow model			*Borealestes* NMS G.1992.47.121.3 solid model			*Krusatodon* NMS G.1992.47.122.1 solid model			*Wareolestes* NMS G.2016.34.1 solid model			*Palaeoxonodon* NMS G. 2015.17.1 solid model		
	Zx/L	**Zy/L**	**J**	**Log Zx/L**	**Log Zy/L**	**J**	**Log Zx/L**	**Log Zy/L**	**J**	**Log Zx/L**	**Log Zy/L**	**J**	**Log Zx/L**	**Log Zy/L**	**J**
c	0.006	0.004	0.118	0.039	0.027	1.370	0.060	0.050	3.686	-	-		*0.040*	*0.050*	1.056
p1	0.006	0.004	0.124	0.043	0.027	1.417	0.107	0.078	6.905	*0.215*	*0.103*	10.899	*0.038*	*0.038*	0.869
p2	0.007	0.005	0.132	0.043	0.027	1.331	0.128	0.087	7.799	*0.233*	*0.102*	10.284	*0.043*	*0.036*	0.898
p3	0.010	0.006	0.198	0.053	0.031	1.694	0.237	0.149	15.275	*0.294*	*0.113*	11.630	*0.046*	*0.031*	0.850
p4	0.014	0.008	0.253	0.074	0.040	2.211	0.310	0.182	19.204	*0.295*	*0.102*	9.740	*0.058*	*0.037*	1.021
p5	0.019	0.011	0.356	0.099	0.050	2.853	-	-		*0.328*	*0.123*	9.299	*0.076*	*0.046*	1.285
m1	0.025	0.013	0.439	0.116	0.055	3.046	0.353	0.225	21.546	*1.054*	*0.616*	38.902	*0.068*	*0.036*	0.928
m2	0.031	0.017	0.506	0.138	0.068	3.318	0.318	0.194	16.533	*1.706*	*0.906*	44.555	*0.082*	*0.045*	1.051
m3	0.037	0.020	0.528	0.157	0.076	3.252	0.364	0.222	16.547	*2.434*	*1.178*	45.991	*0.109*	*0.071*	1.386
m4	0.041	0.022	0.516	0.189	0.093	3.587	0.518	0.319	22.470	-	-		*0.121*	*0.082*	1.586
m5	0.056	0.029	0.644	0.230	0.111	3.964	-	-		-	-		*0.118*	*0.073*	1.266

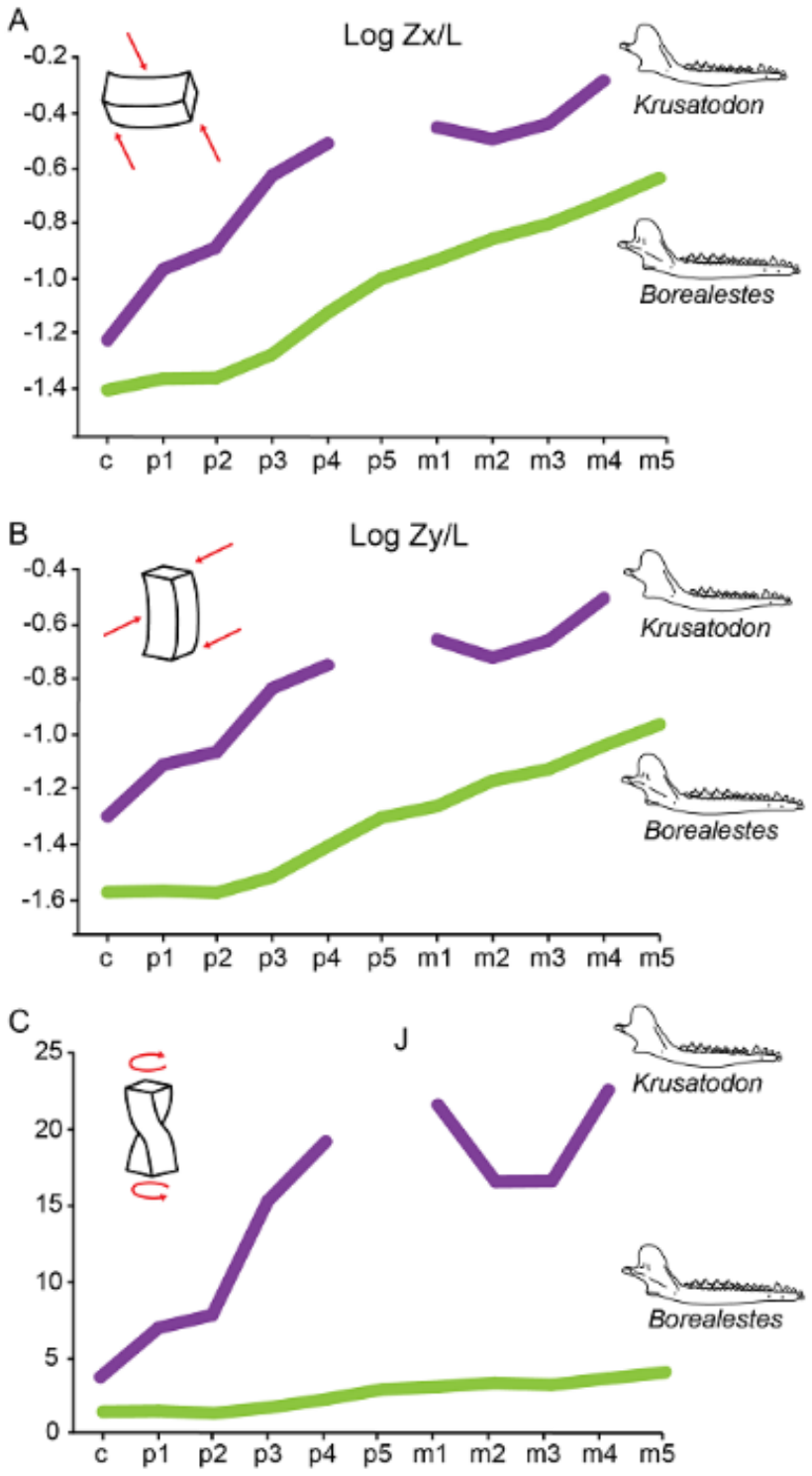

Figure 4.2.3: Results of solid model moment calculations for docodonts *Borealestes* NMS G.1992.47.121.3 and *Krusatodon* NMS G.1992.47.122.1. A, dorsoventral maximum bending force values; B, the mediolateral maximum bending force values; C, the torsion values. Tooth row position on the x-axis, maximum relative force on the y-axis. Gaps indicate different premolar counts in different taxa.

Maximum bending forces and polar moment of inertia values for *Krusatodon* suggest this taxon had a dentary more resistant to both dorsoventral and mediolateral bending than *Borealestes* (and *Palaeoxonodon*), with this resistance increasing along the dentary posteriorly (Figure 4.2.3-4). The different patterns of resistance to bending and polar moment of inertia found by Gill et al. (2014) for *Kuehneotherium* and *Morganucodon*—coupled with finite element analysis and textural analysis of microwear—was used as evidence for niche-partitioning in the diets of these two Late Triassic to Early Jurassic taxa. The same reasoning suggests that *Krusatodon* was able to process harder food items than *Borealestes*. *Kuehneotherium* and *Morganucodon* are not closely related, although phylogenetic placement for *Kuehneotherium* remains unstable due to the paucity of skeletal material. On the other hand *Borealestes* and *Krusatodon* are both docodontans, possibly closely related in a clade within Docodonta (See Sections 3.3a and 3.3d), and so these results suggest detectable niche-partitioning between two phylogenetically closely related taxa with similar morphologies.

The general trend of increased resistance to bending along the length of the dentary posteriorly in all taxa is expected, as the decreasing distance to the fulcrum reduces the out-lever. The low resistance to bending forces or torsion at the canine in all of these taxa suggests none of them could withstand the forces exerted by significant struggling in prey items, as would be associated with a hyper-carnivorous meat-eating diet (Therrien et al., 2016). The resistance to bending forces and torsion for *Wareolestes* NMS G.2016.34.1 is higher along most of the dentary than the other taxa, and is especially high in the molar dentition (Figure 4.2.4). A strong bite that is resistant to torsion is consistent with interpretations for a more carnivorous ecology for this taxon than the others, based on molar morphology. High values for bending and torsion along the molar row may suggest capability to process especially hard carapaces of insects, or

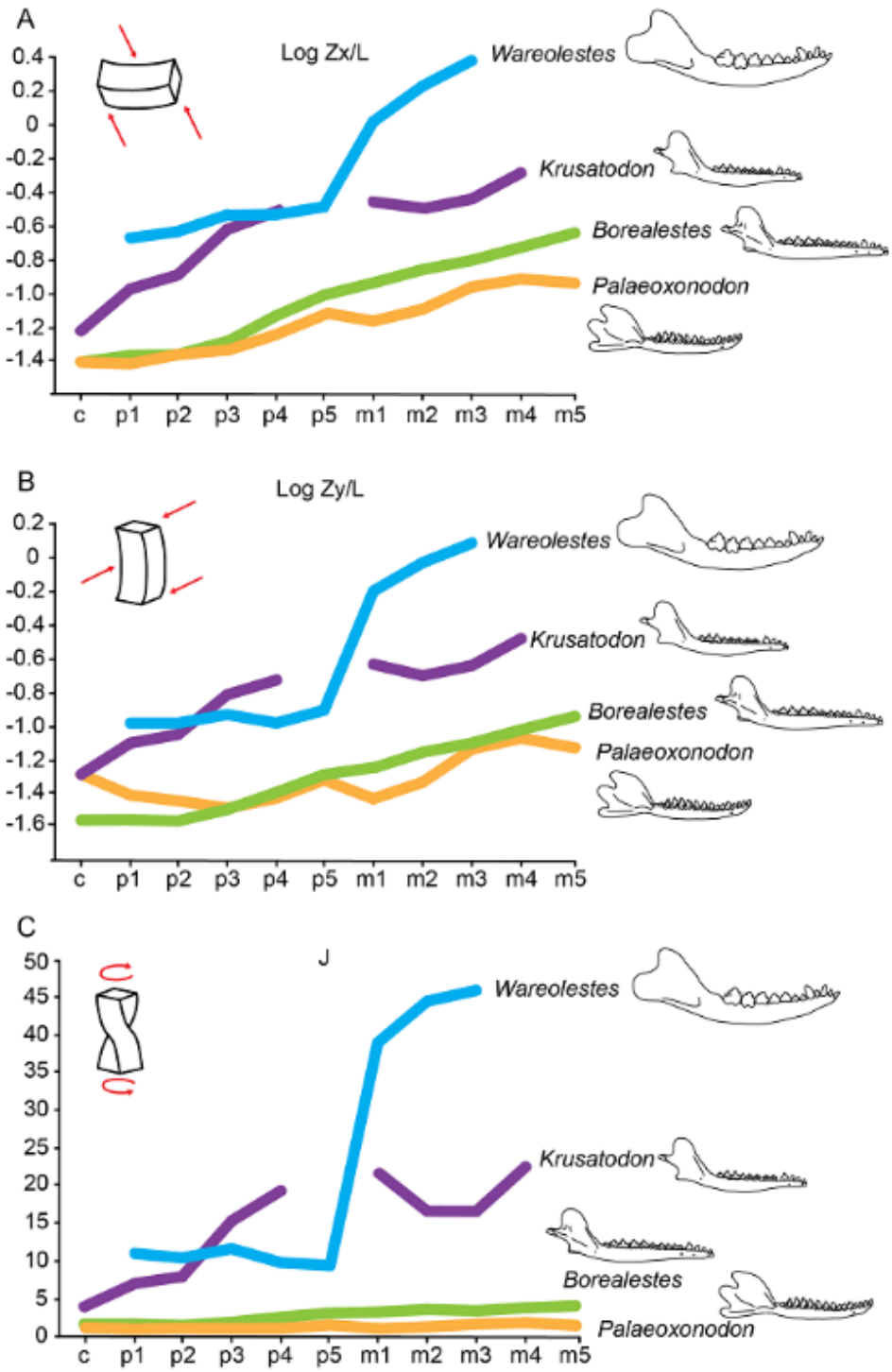

Figure 4.2.4: Results of solid model moment calculations for four taxa from the Kilmaluag Formation: *Borealestes* NMS G.1992.47.121.3, *Krusatodon* NMS G.1992.47.122.1 *Palaeoxonodon ooliticus* NMS G. 2015.17.1, and *Wareolestes rex* NMS G.2016.34.1. A, dorsoventral maximum bending force values; B, the mediolateral maximum bending force values; C, the torsion values. Tooth row position on the x-axis, maximum relative force on the y-axis. Dentary drawing by EP from specimens, with missing morphology reconstruction based on closely related taxa (see Methods for additional information). Gaps indicate different premolar counts in different taxa.

even crush small bones—potentially those of other microvertebrate animals, although without absolute values for bite force (due to the use of the solid model versus hollow model) this cannot be explored quantitatively. A similar pattern of increased dorsoventral and mediolateral buttressing is seen in modern carnivorous mammals, such as hyaenids, that process a high percentage of harder food (Therrien, 2005) and in Late Cretaceous stagodontids also inferred to be hard-object feeders (Brannick and Wilson, 2018). The larger body size calculated for *Wareolestes* (Chapter 4.1) is consistent with this interpretation. However, the canine area is absent in this specimen, so bite force at this key locus in carnivorous taxa cannot be determined. The specimen of *Wareolestes*, NMS G.2016.34.1, represents a sub-adult, as evidenced by the presence of replacement adult teeth within the dentary below their deciduous precursor positions (Panciroli et al., 2017b; Chapter 3.2). This means that the bite force and body mass for an adult of this taxon remains unknown. The damage to the buccal surface of the dentary in this specimen also means these results should be interpreted with caution.

The mammal taxa included in this analysis, all found in the Kilmaluag Formation except for *Kuehneotherium* and *Morganucodon*, are likely to have been insectivorous based on their dental cusp morphology. The only insect remains found so far from the Kilmaluag Formation were recently collected from the shaley exposures on the Trotternish Peninsula on the northern tip of Skye, and are currently awaiting study. These include multiple small (2-5 mm length) elytra of beetles, that are moderately well preserved (pers. obs. EP). The only other insect fossils known from Skye are from earlier Sandstone deposits of the Great Estuarine Group: they are Trichoptera (caddisfly) from the genus *Conchindusia* (pers. com. A. Ross, 2018).

The diverse insect assemblage of the Early Jurassic deposits of Strawberry Bank in Yorkshire provides an example of the thriving insect community that could have populated the Kilmaluag Formation. The Strawberry Bank lagerstätte contains: Blattodea (cockroaches); Coleoptera (beetles); Diptera (flies); Hemiptera (bugs); Dermaptera (earwigs); Mecoptera (scorpionflies); Neuroptera (lacewings); Odonta (dragonflies and damselflies); and Orthoptera (grasshoppers, locusts and crickets) (Williams et al., 2015). This provides a broad range of potential food sources for small vertebrate insectivores

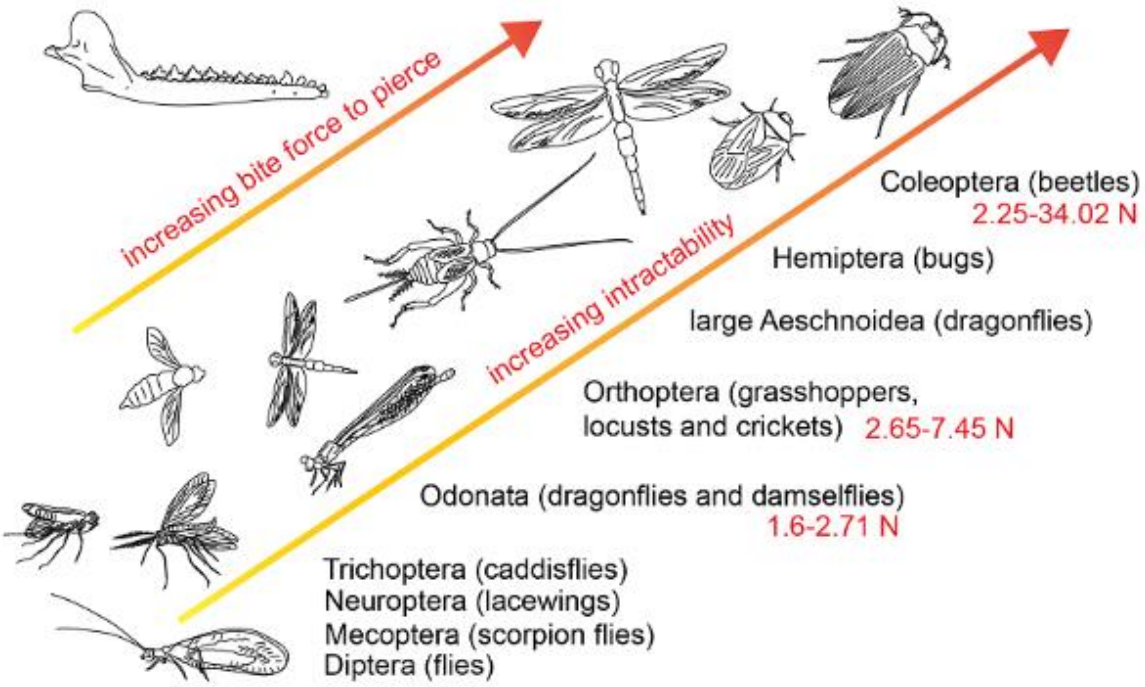

Figure 4.2.5: The relationship between insect cuticle intractability and mammal jaw bite force. Based on data from Freeman (1981) and Aguirre et al. (2003). Insects drawings by EP based on fossil taxa.

including mammals. Previous studies have established maximum forces (usually in Newtons, N) required to pierce different insect cuticles (Table 4.2.2) (Aguirre et al., 2003). These values can be used alongside other 'hardness' scales (e.g. Freeman, 1981) to permit the generalised ranking of known Jurassic insect groups by 'hardness', or intractability, from the softer insect food items (e.g. lacewings, scorpion flies) to the hardest (beetles) (Freeman, 1981) (Table 4.2.2, Figure 4.2.5). Many studies do not distinguish between different material properties and the integrated mechanical performance of insect cuticles, referring to 'hardness' without defining it in mechanical terms, and using terminology interchangeably. Evans and Sanson (2005) suggest hardness is only a surface property (ability to withstand indentation), and define what they consider the more important material properties that must be considered in relation to insect cuticles: strength (resistance to applied load without failure or plastic deformation), toughness (resistance to crack propagation), stiffness (resistance to deformation) and plasticity (ability to undergo irreversible deformation in response to applied force) (Gordon, 1991). For this reason, rankings of insect 'hardness' must be treated with caution, as a thin-walled but strong and

tough cuticle may be equivalent—or even more resistant—to stress than a thicker but weaker cuticle wall.

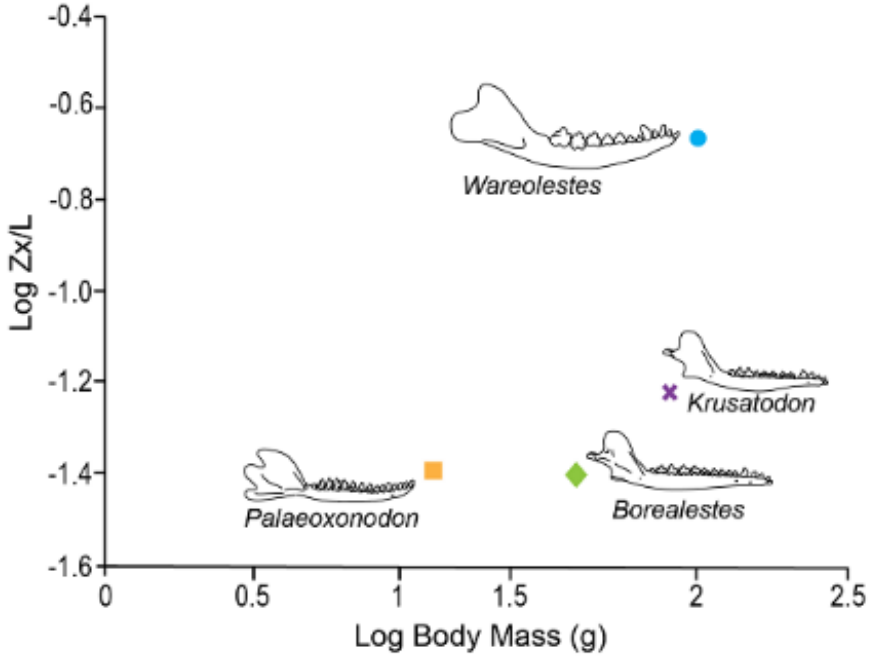

Figure 4.2.6: Body mass and bite force scaling in the Kilmaluag Formation mammal taxa. Bite force values at canine locus except *Wareolestes*, for which pc1 locus was used because canine is absent in specimen NMS G.2016.34.1.

Measuring intractability of insect exoskeletons does not account for the whole story of the relationship between food item properties and jaw biomechanics and bite force of insectivorous mammal taxa. The internal organs of insect prey items present another biomechanical challenge for insectivores (Evans and Sanson, 2005). Prey length must also be taken into account, as the structural strength of insects increases with size and mass (Aguirre et al., 2003). This is because as insects increase in dimensions and mass, their external and internal structures must deal with increased loading (Evans and Sanson, 2005). Therefore Mesozoic mammal mastication patterns must be considered, as well as tooth complexity for processing food items. Docodonts present an unusual independent origin for complex tooth cusps, capable of versatile shearing and crushing not seen in other stem group mammaliaforms (Jenkins, 1969; Gingerich, 1973; Butler, 1997; Luo, 2007; Schultz et al., 2017). New fossil discoveries in recent decades of docodontans also revealed a wider

range of features of the teeth (Luo and Martin, 2007: figs 3 and 4). This complexity may contribute to the range of ecological specialisation seen within this clade, including in my new results from biomechanical analysis of *Borealestes* and *Krusatodon*.

Bite force and chewing frequency also both scale with body mass (Druzinsky, 1993). My results support the relationship between body mass and bite force, with the largest taxon, *Wareolestes*, inferred to have the highest dorsoventral bite force (Figure 4.2.6). Plotting dorsoventral bending maximum force against body mass suggests *Borealestes* had a weaker bite for its size than *Krusatodon* or *Palaeoxonodon*. This further supports the argument for niche partitioning among these contemporaneous Jurassic mammal taxa.

Dental microwear analysis would help further establish possible prey items for these taxa, as patterns of microwear on the enamel surface has been shown to correspond to diet (e.g. Silcox and Teaford, 2002; Gill et al., 2014). Finite element analysis of the dentary would also help to further explore the dietary ecology of the Kilmaluag Formation mammal fauna, as has been carried out for other Mesozoic taxa (Gill et al., 2014). However, such analyses are constrained by the completeness of the cranial material found at this locality, which is usually crushed and/or fragmentary (pers. obs. EP). Another point to note is that the fossil mammal material found in the Kilmaluag Formation does not necessarily represent a true integrated fauna, as some material may have been washed into the freshwater bodies by watercourses, or during heavy rainfall (see Chapter 2).

4.3 Morphometric Analysis of the Calcaneum and Astragalus of *Borealestes*

Specialisations for different locomotor modes are correlated with differences in skeletal osteology, as a result of changing musculature and biomechanics (Hildebrand and Goslow, 2001). Locomotor mode is related to an animal's ecological strategy, and this correlation between form and function, known as ecomorphology can be quantified and analysed (e.g. Van Valkenburgh, 1987; Polly, 2007, 2010; Samuels et al 2013). By quantitatively analysing the morphology of extant taxa for which locomotor mode is known, and combined morphometric analyses of both extant and extinct mammal species, inferences can be made about ecomorphology of extinct mammal species. There have been many studies of postcranial ecomorphology in mammals, including primates (e.g. Strasser, 1992), carnivores (e.g. Van Valkenburgh, 1987), marsupials (e.g. Argot, 2002; Bassarova et al., 2009), artiodactyls (Janis et al., 2002), and rodents (e.g. Szalay, 1985; Samuels and Van Valkenburgh, 2008). However, many of these are phylogenetically restricted, limiting inferences beyond that group or clade.

A caveat when using skeletal morphology to infer locomotion or habitat preference is that the morphology does not respond to the locomotion itself, but to the strain or loading applied to the bone during movement. Therefore, similar movements may result in convergent morphologies: for example semi-aquatic and semi-fossorial lifestyles often result in similar morphologies as a result of pushing against water or soil respectively, and these can be hard to distinguish in multivariate analyses (Van Valkenburgh, 1985; Panciroli et al., 2017a).

Taking body mass into account is crucial for any analysis of locomotion and morphology. Loading on the skeleton occurs not only by locomotion, but through supporting body mass (Szalay 1994). Larger body mass results in distinctive morphological specializations for particular locomotor behaviours due to allometric constraints on the skeleton (Bertram and Biewener, 1990). Mesozoic mammals were relatively small in body size (see Kielan-Jaworowska, Cifelli and Luo, 2004 for overview) with the notable exception of Cretaceous goboconodotonid *Repenomamus* (Hu et al., 2005). This makes studies of larger-bodied extant animals of limited utility in the study of Mesozoic mammal

ecomorphology. Among small mammal taxa different parts of the skeleton scale differently with changes in size, but overall there is less influence of allometry on the skeletal morphology (Biewener, 1990). Increases in body mass in rodents for example, can be compensated for by altering muscle mechanical advantage and limb posture without strong skeletal allometry (Samuels and Van Valkenburgh, 2008).

Although some studies have used morphology to infer locomotion exclusively in smaller extant mammals (≤5 kg) such as rodents (Szalay, 1985; Vianey-Liaud, Hautier and Marivaux, 2015; Ginot et al, 2016) many of these focus on certain groups within a clade, and have often been predominantly descriptive rather than quantitative. There have been studies of locomotion in fossil rodents (Candela and Picasso, 2008; Samuels and Van Valkenburgh, 2008; Vianey-Liaud, Hautier and Marivaux, 2015) and small carnivorans (Schultz and Guralnick, 2007; Smith and Smith, 2010), but again, these studies tended to focus on specific clades of placentals, and are restricted in phylogenetic scope, limiting their application for Mesozoic mammals.

Recently several studies have used manual digit ray proportions to infer ecology in Mesozoic mammals (Bi et al., 2014; Meng et al., 2015, 2017), based on studies that have established correlations between intrinsic proportions of the manual and pedal digit ray lengths and locomotor mode in euarchontan and marsupial mammals (Argot, 2001; Weisbecker and Wharton, 2006; Kirk et al., 2008). The Jurassic haramiyidan *Arboroharamiya jenkinsi* was included in an analysis of the phalangeal indices of 26 extant mammal taxa and 6 fossil taxa, inferring an arboreal locomotion for this taxon (Zheng et al., 2013). The same data were later utilised to infer a scansorial/arboreal locomotor mode for *Shenshou lui* (Bi et al 2014). A larger study using manual and pedal digit ray proportions by Meng et al (2017) used 161 extant taxa in to infer ecology in 9 fossil taxa, including the docodontan *Agilodocodon scansorius*. They found some support for the scansorial/arboreal locomotor mode inferred previously for this taxon.

The largest postcranial ecomorphological analysis for application on Mesozoic mammal taxa carried out to date is Chen and Wilson (2015), who utilised a phylogenetically diverse dataset of 107 extant species from across the extant mammal family tree, representing eight locomotor modes, most of them ≤5 kg in body mass. They used 45 linear measurements of the postcrania to generate 56 ratios that reflect functionality in different parts of the postcranial skeleton (converting measurements to osteological

indices helps account for size differences between taxa). These indices were then analysed in canonical variate analyses (CVA), and used to infer locomotor modes for ten fossil taxa. However, for the docodontan *Haldanodon exspectatus* the Chen and Wilson (2015) study could not clearly resolve between an arboreal or semifossorial locomotor mode for this taxon (Chen and Wilson, 2015).

The results from Chen and Wilson (2015) support the assertion that the signal for locomotor mode is difficult to detect in small bodied mammals. However, they successfully assigned 90% of extant mammal taxa to the correct locomotor mode. They found reducing the number of locomotor modes included in the analysis improved prediction of locomotor mode targeted in the study. A drawback of this study in terms of wider application for Mesozoic taxa is the use of multiple osteological indices. While analyses of the whole postcrania (qualitative and quantitative) always provide the most reliable results regarding ecomorphology, for most Mesozoic mammals for which postcranial material is known, it is either incomplete or distorted post mortem. This missing data for the skeletal element measurements in incomplete fossils cause ambiguity when such taxa are combined into an extant mammal dataset.

In the skeleton of *Borealestes serendipitus* NMS G.1992.47.121.1, the only appendicular elements preserved intact are the left illium, left radius, and isolated pedal and manus elements, including the calcaneum and astragalus. Fragments of a single humerus, ischium, and femur are partially preserved, and the rest of the appendicular skeleton is missing. This limits the multivariate ecomorphological analyses that can be carried out on this specimen.

4.3 i) Evolution of the Mammalian Tarsus

I have chosen to focus on the calcaneum and the astragalus of *Borealestes serendipitus* NMS G.1992.47.121.1 to infer locomotor mode for this taxon. These are robust bones often preserved in the fossil record. The biomechanics of the hind limb provide forward propulsion through the in-lever of the calcaneal tuber at the ankle for therians. The morphology of the ankle (especially the calcaneum) has been shown to

correlate well with locomotion and stance in extant mammal taxa, particularly the degree of flexion and inversion-eversion of the foot (Taylor, 1970; Polly, 2008). The morphology of the ankle (and the hind limb as a whole) is less influenced by secondary ecological factors such as prey capture and feeding that often mask the locomotor specialization of the forelimb (Polly, 2007; Martín-Serra, Figuerido, & Palmqvist, 2014; Schutz & Guralnick, 2007; Samuels, Meachen, & Sakai, 2013).

The general condition for extant mammals is that main foot flexion is at the crurotarsal joint, with some inversion, eversion and flexion movement within the tarsus itself depending on locomotor mode of the taxon (Szalay, 1993, 1984). Two of the main changes from the therapsid-like to mammalian pedal morphology were the superpositioning of the talus and calcaneum, and the loss of articulation between the fibula and tarsus (Jenkinds 1970b; Szalay, 1993; Isidro and Vazquez, 2006). However, this morphology is not seen in all modern mammals, monotremes being the notable exception. Early mammals were predominantly plantigrade (Kielan-Jaworowska et al., 2004; Kielan-Jaworowska and Hurum, 2006). A digitigrade stance in mammals is usually associated with a cursorial or graviportal locomotor mode, and with increases in body mass (Kubo et al., 2019).

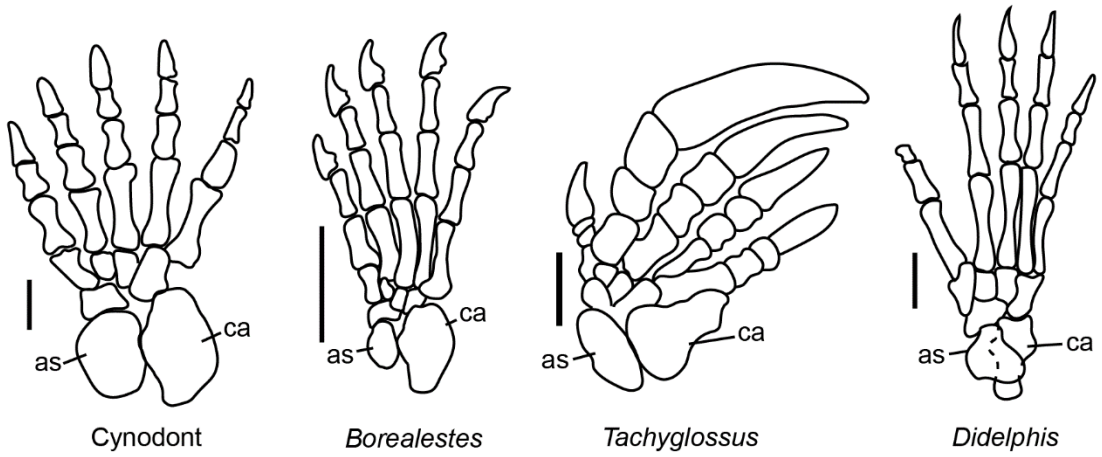

Figure 4.3.1: The simplified pes of a non-mammalian cynodont, *Borealestes* and two crown mammals. The superpositioning of the astragalus is indicated by a broken line. The 'Manda cynodont' and *Didelphis* are adapted from Chen et al., (2017), *Tachyglossus* from Szalay (1993), and reconstruction of *Borealestes* based on *Agilodocodon* in Meng et al. (2015).

Using derived extant mammals to study Mesozoic mammal calcaneal morphology has limitations, especially for stem mammaliaform groups such as docodontans. The calcaneum

of docodontans (e.g. Meng et al., 2015) is little changed morphologically from derived cynodonts such as tritylodontids (Kühne, 1956; Jenkins, 1971; Szalay, 1994) (Figure 4.3.1 and 4.3.2), and morganucodontans (Jenkins and Parrington, 1976; Szalay, 1994) (Figure 4.3.2).

On the calcaneum of *Borealestes* (Figures 4.3.1, and 4.3.2) there is a well-defined calcaneal tuber, and well-defined articulating surfaces on the calcaneum for the contact of the astragalus, and for the cuboid. The peroneal part of the calcaneum is broad and shelf-like. These features are similar to those already known from *Agilodocodon* (Meng et al., 2015: fig. S8 in their Supplementary Materials). The calcaneal features of *Borealestes* (and *Agilodocodon*) are early diverging mammaliaform characters, as seen in other early mammaliaforms such as the morganucodontans *Morganucodon* and *Megazostrodon* (Jenkins and Parrington, 1976; Szalay, 1994) and the haramiyidan *Megaconus* (Zhou et al., 2013).

The sustentacular facet of *Borealestes* faces medially and is almost certainly the vertically oriented contact of the calcaneum and the astragalus, as in *Morganucodon* and the tritylodontid *Oligokyphus* (Jenkins and Parrington, 1976; Szalay, 1994; Chen et al., 2017). In contrast, the sustentacular facet is re-oriented and extends partly underneath the astragalus in some stem therians (Chen and Luo 2012), or fully as in crown therians (Jenkins, 1970b; Szalay 1994). Because the astragalus and calcaneum are intact in *Borealestes*, and the sustentacular structures are not exposed in *Agilodocodon* (Meng et al., 2015: SM fig. S7), the calcaneum of *Borealestes* provides useful new information on this feature. The calcaneum has a facet that can be interpreted as the calcaneofibular articulation. The latter is later lost in crown therian mammals, probably separately in metatherians and eutherians (Szalay, 1993, 1994; Luo et al., 2003).

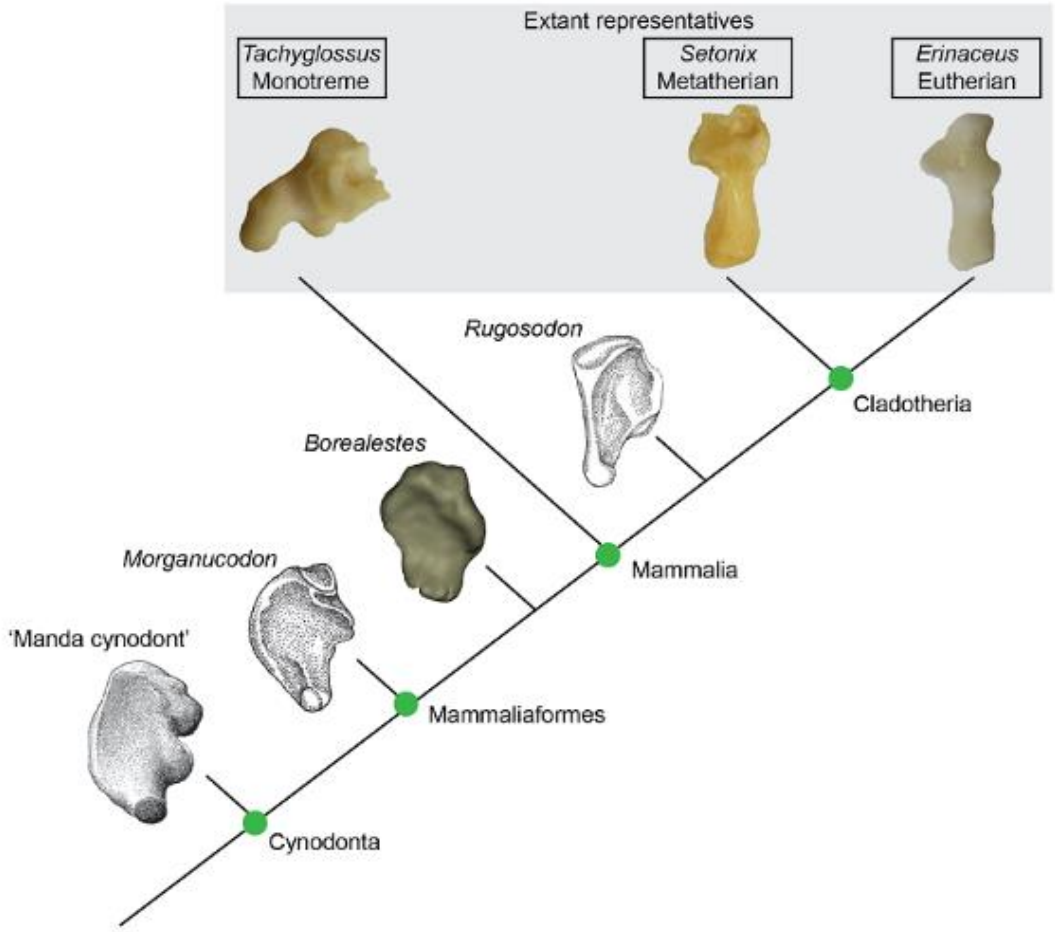

Figure 4.3.2: The evolution of the mammal calcaneum. *Morganucodon* and *Rugosodon* calcanea adapted from Luo et al. (2016).

The calcaneum and the astragalus are not preserved in original articulation in NMS G.1992.47.121.1. Based on the above anatomical interpretation of the calcaneum visualized in 3D, and on comparison to the in situ preservation of these bones in *Agilodocodon* (Meng et al., 2015: fig. S8), we interpret that there is no superposition of the astragalus over the calcaneum. This is also consistent with the lack of superpositional relationship of these bones in the intact ankle of eleutherodontid haramiyidans (Meng et al., 2017: fig. 3 and extended data figures S7). The superpostional relationship is not to the same extent seen in the crown mammalian groups such as multituberculates (Krause and Jenkins, 1983; Kielan-Jaworowska and Gambaryan, 1994; Yuan et al., 2013), the stem therian group spalacotherioids (Chen and Luo, 2012; Luo et al., 2016), or crown therians (Szalay, 1993, 1994).

In analyses of the comparative morphology and evolution of pedal anatomy, monotremes are important as a defining group, along with therians. But the morphologies of pedal bones of monotremes are highly-transformed, not only in comparison to extant therians, but also in comparison to the early diverging mammaliaforms (Lessertisseur and Saban, 1967; Szalay, 1994; Hurum et al., 2006; Luo et al., 2015). Although monotremes were once were cited by some authors as an example of a basal morphology for mammals (Lewis, 1963; Isidro and Vazquez, 2006), the majority of workers consider monotreme pedal structure and function as specialized and derived in its own right (e.g., Lessertisseur and Saban, 1967; Jenkins, 1970a; Pridmore, 1985; Szalay, 1994; Gambaryan et al., 2002; Gambaryan and Kuznetsov, 2013). While some authors have gone as far as describing monotreme posture as 'reptilian' (e.g. Eaton, 1962), thorough analysis of monotremes shows their movement to be similar to nonspecialised therian mammals (Jenkins, 1970a) with some highly derived monotreme-specific pedal movement (Pridmore 1985; Gambaryan and Kuznetsov 2013). Differing interpretations of some calcaneal characters in *Tachyglossus* and *Zaglossus* have led to disagreement in the literature about their pedal function. For example, there has been a critical difference in interpreting the homology of the calcaneal tuber and the peroneal process in the calcaneum of monotremes (Lewis, 1983, versus Szalay, 1993; in this study, Szalay's interpretation of the peroneal process and calcaneal tuber is followed). However, monotreme pedal morphology (as with many aspects of their anatomy and locomotor function) is derived—even more so in the echidnas, which have evolved from a platypus-like ancestor (Szalay, 1993, 1994)—limiting the value of comparisons with stem mammaliaforms for this part of the anatomy (although see below) (Figure 4.3.1 and 4.3.2).

Because the docodontan calcaneum is plesiomorphic for mammaliaforms as a whole, the ecomorphological signals that can be detected in derived extant therian calcanea provide limited comparison, considering the specialisation of montreme pedal structure. Nonetheless, certain biomechanical principles should still be applicable. The well-defined calcaneal tuber is an apomorphy of tritylodontids and mammaliaforms (Kühne, 1956; Szalay, 1994; Zhou et al., 2013; Luo et al., 2016)), and provides an attachment point for the tendon of the gastrocnemius and soleus muscles of the lower limb, and plantar flexor muscles of the tarsus (Ginot et al., 2016). The calcaneum therefore forms the base of the biomechanical fulcrum of the lower limb and pes, with the gastrocnemius and soleus

providing the in-level for plantar flexion of the tarsus (Szalay, 1993; Polly, 2010; Ginot et al., 2016; Panciroli, 2017a). Therefore the length of the calcaneum, and more specifically of the tuber in relation to the calcaneum as a whole, has an applicable functional significance that is likely applicable to Mesozoic mammals.

'Robustness' is commonly identified as a trait seen in the morphology of fossorial taxa, with robust limb bones reflecting heavy loading caused by compressive and torsional stress when digging (Stein 1993; Samuels and Van Valkenburgh, 2008). Similar morphology is seen in semi-aquatic taxa due to the increased area of insertion for musculature to provide the power stroke in water (Stein, 1988; Samuels and Van Valkenburgh, 2008). This robustness can be detected in the calcaneum (Chen and Wilson, 2015; Panciroli et al., 2017a).

Increased projection of the sustentaculum and broadness of the calcaneal body provides increased lateral movement against the rest of the ankle, particularly when the surface is flattened, and is usually correlated with an arboreal locomotor mode (Polly and Macleod, 2008; Ginot et al., 2016; Panciroi et al., 2017). A narrow calcaneal body with reduced lateral movement is seen in cursorial and saltatorial taxa, in which most movement of the hind limb is in the parasagittal plane (Ginot et al., 2016; Panciroli et al., 2017a). The morphology of the cuboid facet indicates the degree of lateral movement in the tarsus. In rodents, a flat or only slightly concave cuboid facet permits greater movement, whereas an anteroposteriorly concave cuboid facet restricts this movement, and is often seen in more cursorial taxa (Candela and Picasso, 2008). Cursorial and saltatorial mammals are likely to have elongate tubers in relation to a short calcaneal body (Chen and Wilson, 2015; Ginot et al., 2016).

While the calcaneum forms the lever, the astragalus forms the fulcrum of the ankle in its position at the base of the tibial shaft. The morphology of the astragalar trochlea is related to joint rotation, and the rotational angle of the tibia is determined by the angle of the astragalar head, and so astragalar morphology is related to foot posture, ecology and locomotion (Carrano, 1997). The trochlea tends to be asymmetrical in plantigrade mammals—which are more likely to be arboreal, scansorial or semi-aquatic—whereas the trochlea tends to be symmetrical in digitigrade mammals—more likely to be terrestrial or cursorial. Consistent with digitigrade cursorialist mammals is that mediolateral movement of the astragalus in more constrained relative to the tibia. The angle of the astragalar head

also varies between a mediolateral axis that is parallel in orientation to the trochlea in plantigrade taxa, or at an angle in more digitigrade animals (Carrano, 1997). The depth of the trochlea itself limits medio-lateral movement of the tibia in relation to the astragalus.

The tibio astragalar joint of the platypus, *Ornithorhynchus anatinus*, allows this semi-aquatic monotreme to abduct its feet relative to the limb, and provides a wide range of movement including eversion and hyperextension (Luo et al., 2015). This appears to resemble the morphology of docodont *Docofossor brachydactylus*, suggesting a similar posture and range of movement for this Jurassic fossorial taxon.

4.3 ii) Methods

The dataset comprised measurements from members of 81 extant taxa, mostly ≤5 kg (see below): 67 provided by Chen and Wilson (2015), and 14 additional taxa from the collections at National Museums Scotland (NMS) (Table 4.3.1). All 81 taxa plus *Borealestes* were used in the calcaneal analysis, while 79 were used in the astragalar analysis (the astragali of *Dactylopsila* and *Petauroides* were not available). Additional taxa from NMS were selected to provide examples of phylogenetically independent origins for locomotor modes, for example the addition of the fossorial eutherian talpid *Talpa europaea* and marsupial notoryctid *Notoryctes*.

My dataset includes representatives of 38 families from 14 orders, categorised into 8 locomotor groups, based on the literature (Figure 4.3.3, Table 4.3.1). I also ran my analyses with only 6 locomotor modes (removing semi-fossorial and gliding), and ran separate analyses including only taxa within the order Rodentia (29 taxa), Diprotodontia (10 taxa) and Carnivora (11 taxa). These were chosen because they were the best represented orders in my dataset. All extant monotremes reach body masses above the 5 kg limit, but as the only representative of this early diverging branch of Mammalia they were included in this analysis to provide important data on morphology that is phylogenetically distinct from the rest of the taxa analysed. Two other taxa can reach sizes above the 5 kg limit, *Leopardus* (=*Oncifelis*) and *Urocyon*

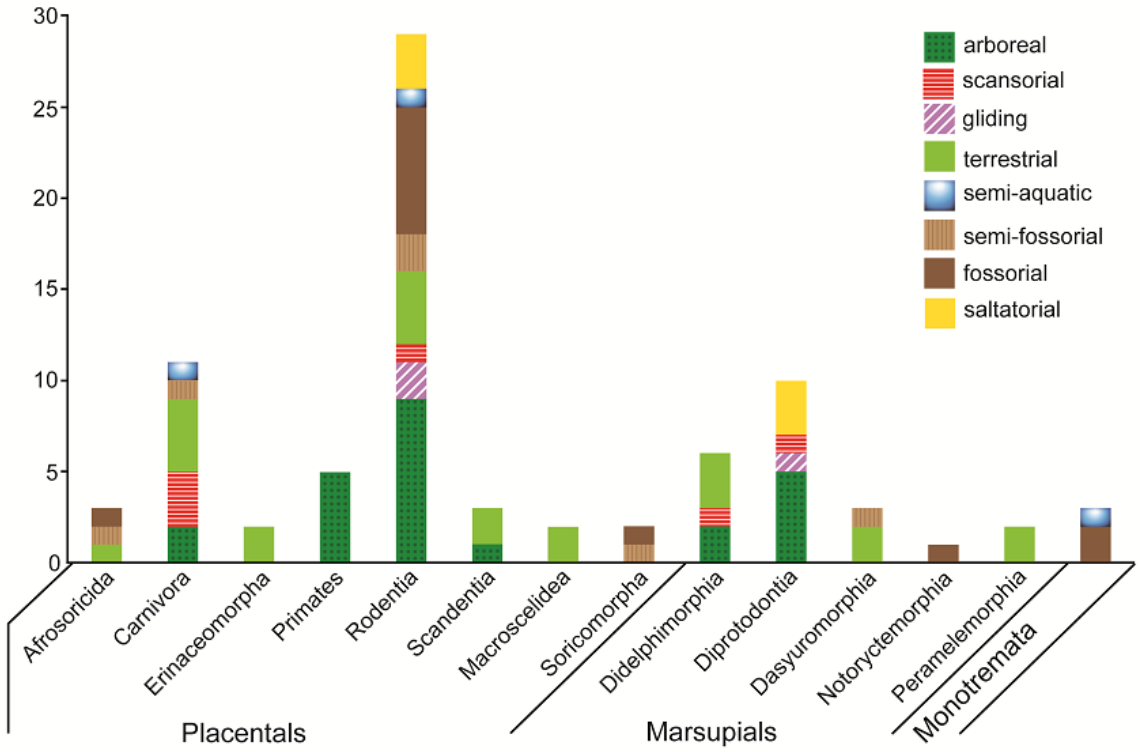

Figure 4.3.3: Distribution of taxa in this analysis by order and locomotor grouping.

Measurements (Figure 4.3.4) from Chen and Wilson (2015) were obtained using Mitutoyo Digimatic Digital Calipers (±0.05mm accuracy) where large enough, and for smaller elements digital photographs with scale were measured in ImageJ (Chen and Wilson, 2015:5). Additional measurements from collections at NMS were taken using the same methods: with digital calipers, or from digital photographs using ImageJ/Fuji for taxa too small to measure manually. Measurements were converted to ratios that have been found to be biomechanically informative by previous analyses (Chen and Wilson 2015; Ginot et al., 2016).

For analyses in R, the supertree by Bininda-Emonds et al. (2007) was adapted and pruned using the ape package (Paradis and Schliep, 2018). The following taxa were not present on this supertree, and so their closest relatives were substituted: *Rattus andamanensis* (substitute, *R. argentiventer*); *Sciurus aberti* (substitute, *S. griseus*); *Glis glis* (substitute, *Glirulus japonicus*); and *Zaglossus bartoni* (substitute, *Z. bruijni*).

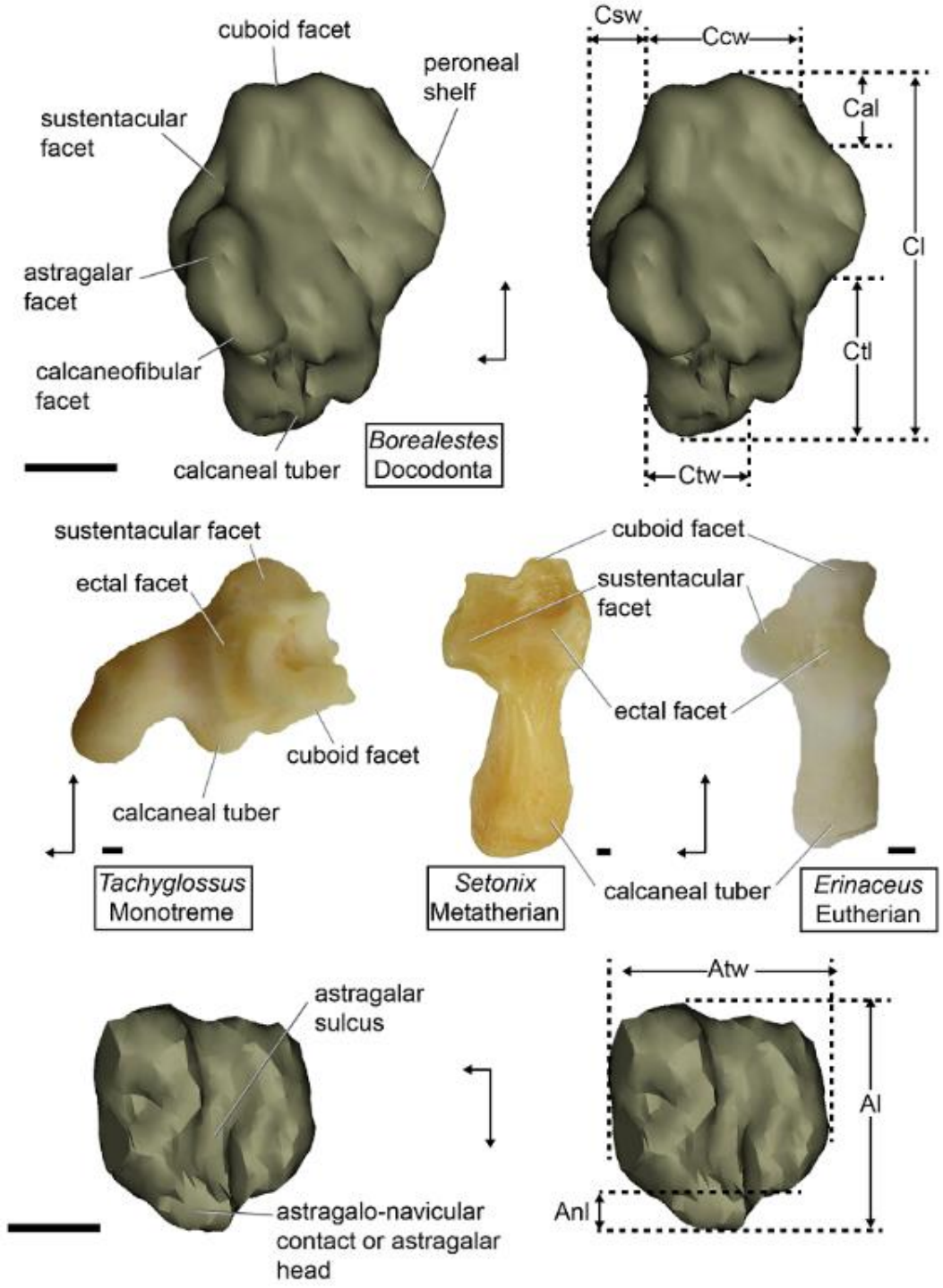

Figure 4.3.4: Measurements taken for this analysis, and examples of crown mammal calcanea.

Principal component analyses and statistical analyses were carried out in R (R core team, 2013) using the geomorph (Adams et al., 2018), moments (Komsta and Novomestky,

2015) packages. Each principal component was tested using a phylogenetically corrected ANOVA in the phytools (Revel, 2012) and paleotree (Bapst, 2012) packages, to determine the significance of the correlation with locomotor mode. A linear discriminant analysis (LDA) was run using the MASS package (Venables, 2002), to determine the ability of the data to correctly determine locomotor mode in extant taxa, and then to predict locomotor mode for *Borealestes serendipitus*. For R-scripts, see Appendix 19.

4.3 iii) Results

The results of the PCA are shown in Figures 4.3.5 and 4.3.6 and Tables 4.3.2-5 (for positions of all extant taxa in morphospace see Appendices 21-22).

Table 4.3.2: Distribution of principal component axes for PCA on complete dataset of calcaneal and astragalar ratios, with *F* and *P* values from a phylogenetically corrected ANOVA.

CALCANEA	**PC 1**	**PC 2**	**PC 3**	**PC 4**	**PC 5**	**PC 6**	**PC 7**
Standard deviation	1.671933	1.368166	1.19514	0.768237	0.498584	0.224945	0.122583
% Variance	0.399337	0.267411	0.204051	0.084313	0.035512	0.007229	0.002147
% Cumulative	0.399337	0.666749	0.8708	0.955112	0.990625	0.997853	1
F value	6.814974	2.055724	1.604339	1.382263	1.718868	1.74101	0.478179
P value	0.00030***	0.1524	0.2878	0.359	0.2431	0.2345	0.9007
ASTRAGALUS							
Standard deviation	1.209091	0.733552	-	-	-	-	-
% Variance	0.730951	0.269049	-	-	-	-	-
% Cumulative	0.730951	1	-	-	-	-	-
F value	1.928254	2.469629	-	-	-	-	-
P value	0.1871	0.086	-	-	-	-	-

The PCA on calcaneal ratios successfully captured variation in calcaneal morphology. The PC1 axis explained 40% of the variation, predominantly reflecting the dorsoventral length of the calcaneal tuber (longer on negative PC1,), versus the calcaneal head (longer on positive PC1), ratios Cal/Cl, Cal/Ctl, and Ctl/Cl (Fig 4.3.5, Table 4.3.2). The PC2 axis explained 27% of the variation, reflecting the mediolateral width of the sustentacular facet

(wider on negative PC2) and width of the cuboid facet (wider on positive PC2), ratios Csw/Ccw, Ctw/Ccw, and Ccw/Cl. Negative PC1 and PC2 scores capture a dorsoventrally long and mediolaterally wide calcaneal tuber.

Table 4.3.3: Results of LDA assigning extant taxa to locomotor mode using PCA results for calcanea. A = arboreal; F = fossorial; G = gliding; S = saltatorial; Sa = semi-aquatic; Sc = scansorial; Sf = semi-fossorial; T = terrestrial.

	A	F	G	S	Sa	Sc	Sf	T
A	17	1	3	0	2	1	3	5
F	1	7	0	0	0	1	0	1
G	0	0	0	0	0	0	0	0
S	0	2	0	4	0	0	0	1
Sa	0	0	0	0	1	0	0	0
Sc	0	0	0	0	0	0	0	0
Sf	0	0	0	0	0	0	2	3
T	6	2	0	2	0	4	1	12
% correct	**71**	**58**	**0**	**67**	**33**	**0**	**33**	**55**

Table 4.3.4: Results of LDA assigning extant taxa to locomotor mode using PCA results for astragali. A = arboreal; F = fossorial; G = gliding; S = saltatorial; Sa = semi-aquatic; Sc = scansorial; Sf = semi-fossorial; T = terrestrial.

	A	F	G	S	Sa	Sc	Sf	T
A	13	2	1	3	1	2	1	7
F	0	2	0	0	0	0	0	0
G	0	0	0	0	0	0	0	0
S	1	0	0	3	0	0	1	0
Sa	0	0	0	0	0	0	0	0
Sc	0	0	0	0	0	0	0	1
Sf	0	0	0	0	0	0	0	0
T	8	8	2	0	2	4	4	14
% correct	**59**	**17**	**0**	**50**	**0**	**0**	**0**	**64**

While the above calcaneal shape changes are captured in the analysis, only PC1 correlates significantly with locomotor mode according to the ANOVA (Table 4.3.2), and only arboreal versus fossorial and saltatorial, fossorial versus semi-aquatic, and saltatorial versus semi-aquatic were significantly distinguished. The LDA results for the calcaneal PCA reflect this poor correlation, with only the majority of arboreal (71%) and saltatorial (67%) extant taxa being correctly assigned to locomotor mode (Table 4.3.3). The overall success of the LDA was only 52% for the calcaneal PCA. The LDA using the PCA on calcaneal

ratios assigned *Borealestes* a semi-fossorial locomotor mode based on these data (Table 4.3.5).

Table 4.3.5: LDA locomotor assignments for *Borealestes* using different analyses. LM = locomotor mode: Sc = scansorial; Sf = semi-fossorial.

Analysis	LM
Calcaneal ratios – complete dataset, 8 locomotor modes	Sf
Calcaneal ratios – complete dataset, 6 locomotor modes	Sc
Astragalus – complete dataset	Sc

Reducing the number of locomotor modes to 6 reduced the accuracy of the LDA results for extant taxa in most locomotor modes, except terrestrial, which rose from 55% to 67%. The 6-locomotor mode LDA using the PCA on calcaneal ratios assigned *Borealestes* a scansorial locomotor mode.

The PCA on astragali also captured shape change in this pedal element. The PC1 axis captured 73% of the variation, reflecting change in the length of the astragalar head, with a longer head on positive PC1 (Figure 4.3.6, Table 4.3.22). The PC2 explained the remaining 27% of variation, capturing change in the astragalar body, with a longer body on negative PC2. However, there was no correlation in astragalar shape with locomotor mode in this analysis, with none of the PC axes significantly correlating with locomotor mode in the phylogenetically corrected ANOVA (Table 4.3.2). Results of the LDA on extant taxa only correctly assigned taxa to their known locomotor mode >50% of the time for terrestrial (63%) and arboreal (59%) taxa, with an overall success rate of just 24% (Table 4). This LDA using the PCA on astragalar ratios predicted a scansorial locomotor mode for *Borealestes*.

Carrying out PCA on calcaneal ratios using only taxa from single orders produced better results for the LDA, but did not significantly improve the results of the ANOVA (Appendix 23). For all three within-order analyses a higher proportion of the variation was capture by the PC1 axis (Rodentia 53%, Diprotodontia 55% and Carnivora 42%), but only PC1 in Rodentia correlated significantly with locomotor mode (*P* value 0.0066, see Appendix 23 for full results). The LDA on Rodentia and Diprotodontia assigned all extant taxa to their locomotor modes with ≥75% success except scansorial and gliding (both 50%)

and semi-fossorial (25%). The LDA on Carnivora assigned all extant taxa to their correct locomotor mode.

4.3 iv) Discussion

My results suggest that the quantifiable morphology of the calcaneum and astragalus of extant mammals does not statistically correlate with locomotor mode across multiple mammalian orders. My dataset includes 14 different orders, and although PC1 in the calcaneal analysis correlates for the four out of eight locomotor modes—those that result in the most derived morphology (salutatory, arboreal, semi-aquatic, fossorial) and therefore produce the most extreme morphological variation—it only successfully allocates just over half of extant taxa to their known locomotor mode in the LDA. For the astragalus, only a quarter were allocated correctly in the LDA. Even previous within-order PCA analyses of the calcaneum have found weak correlation with locomotor mode and a strong phylogenetic signal, due to morphological similarity within different clades within that order (e.g. Panciroli et al., 2017a). For example Ginot et al. (2016) used a dataset of linear measurements of calcanea and astragali within Rodentia, and although they were able to distinguish locomotor mode groups using a linear discriminant analysis, and there was some correlation with locomotor mode, their MANOVA found phylogeny significantly correlated with the morphological variation seen in their dataset.

Only including taxa from my dataset within a single order—in this case Rodentia, Carnivora, and Diprotodontia—did not significantly increase the statistical correlation with locomotor mode in my analysis. However, the LDA successfully allocated most taxa to their locomotor mode with ≥50% success, particularly fossorial taxa (86%), and correctly

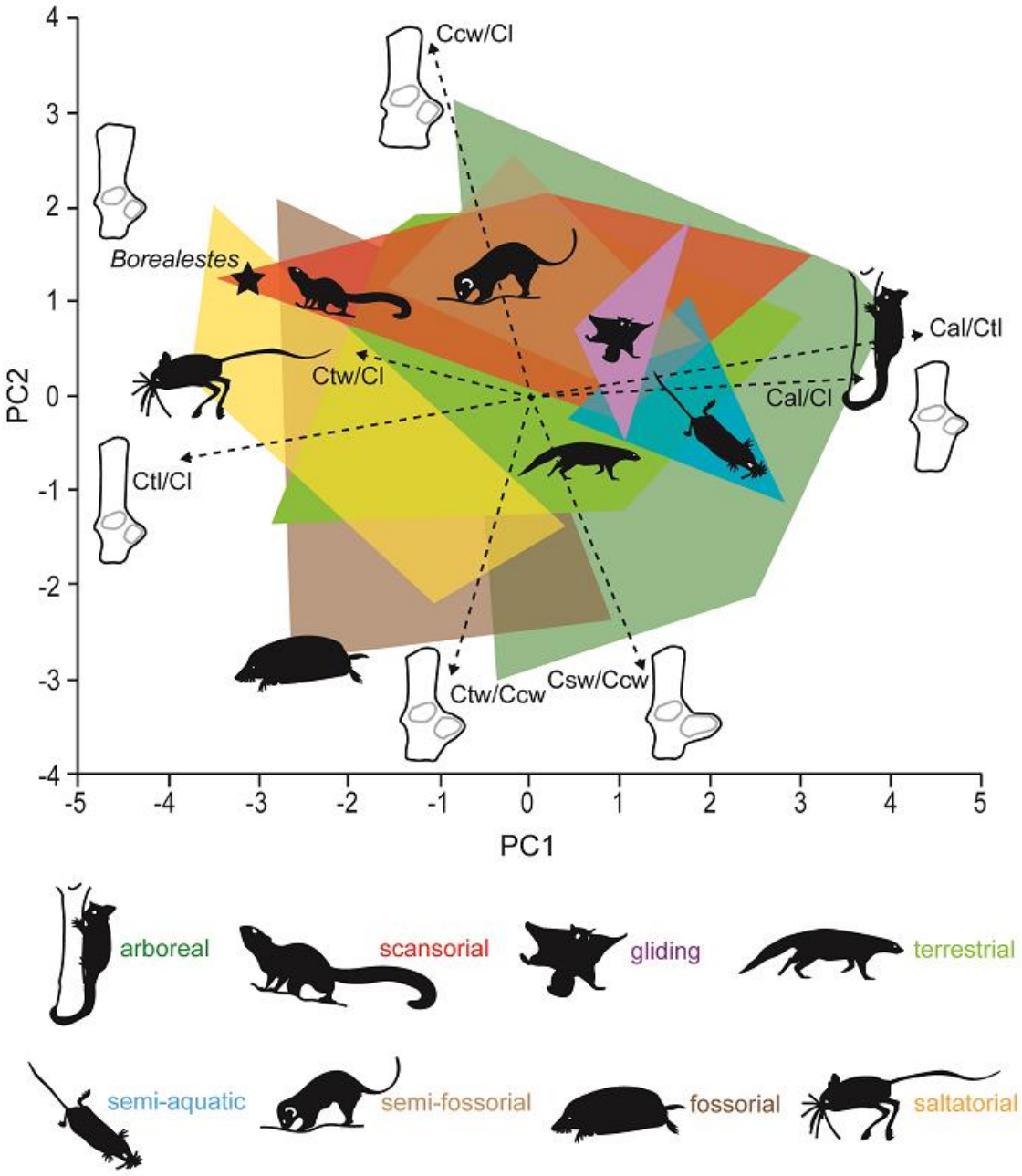

Figure 4.3.5: Results of PCA using calcaneal ratios.

assigned 100% of Carnivorans to their locomotor mode. Although the small size of these data subsets limits the statistical power of these analyses, these results support the suggestion that the signal for correlations between locomotor mode and morphology using calcaneal data in these small-bodied taxa cannot be significantly distinguished from the pattern anticipated by phylogeny. This does not limit their utility in assigning locomotor

mode, indeed the results suggest that linear discriminant analyses provide a robust method for determining locomotor mode in more closely related taxa, particularly for modes that result in more divergent morphology, such as fossoriality.

PCA of the calcaneum and astragalus in extant taxa does not provide a robust method to quantitatively infer locomotor mode for non-crown mammalian taxa, such as early diverging mammaliaforms like docodontans. It is possible that the wide phylogenetic range of taxa in this analysis is likely to have encompassed phylogenetically independent origins of different locomotor modes. It was hypothesised that the basal morphology of the docodontan calcaneum would limit inferences from an extant therian dataset. A broad phylogenetic range of extant taxa might have compensated for the basal morphology, ensuring that inferences were statistically robust across Mammalia. But this is also limited by the fact that monotremes have very specialized tarsal morphologies in their own right, relative to both extant therians and to early mammaliaforms. The basal morphology of the docodontan calcaneum cannot be fully explored in my analysis however, because the results for the extant taxa showed only weak correlation with locomotor mode, and therefore are not robust for application to fossil material.

It is somewhat surprising that the ratios used in this analysis do not reflect locomotor mode as strongly as anticipated, given that they were chosen based on their correlation with known biomechanical principles. The calcaneal tuber in particular, as the fulcrum of the foot, should reliably reflect locomotion due to its position as the in-lever for plantar flexion of the tarsus (Szalay, 1993; Polly, 2010; Ginot et al., 2016; Panciroli, 2017a). While this is a solid biomechanical principle, two factors obscure this relationship in these analyses: small body mass, and phylogeny. The ability of smaller mammals to compensate for changes in locomotion by altering stance and muscular mechanical advantage (Samuels and Van Valkenburgh, 2008) makes osteological signals for locomotor mode more difficult to detect than in larger-bodied taxa, even in derived extant taxa (Biewener, 1990; Bertram and Biewener 1990). The differences in overall calcaneal morphology between different taxonomic groups further obscures this signal. This is unsurprising for a dataset drawn from

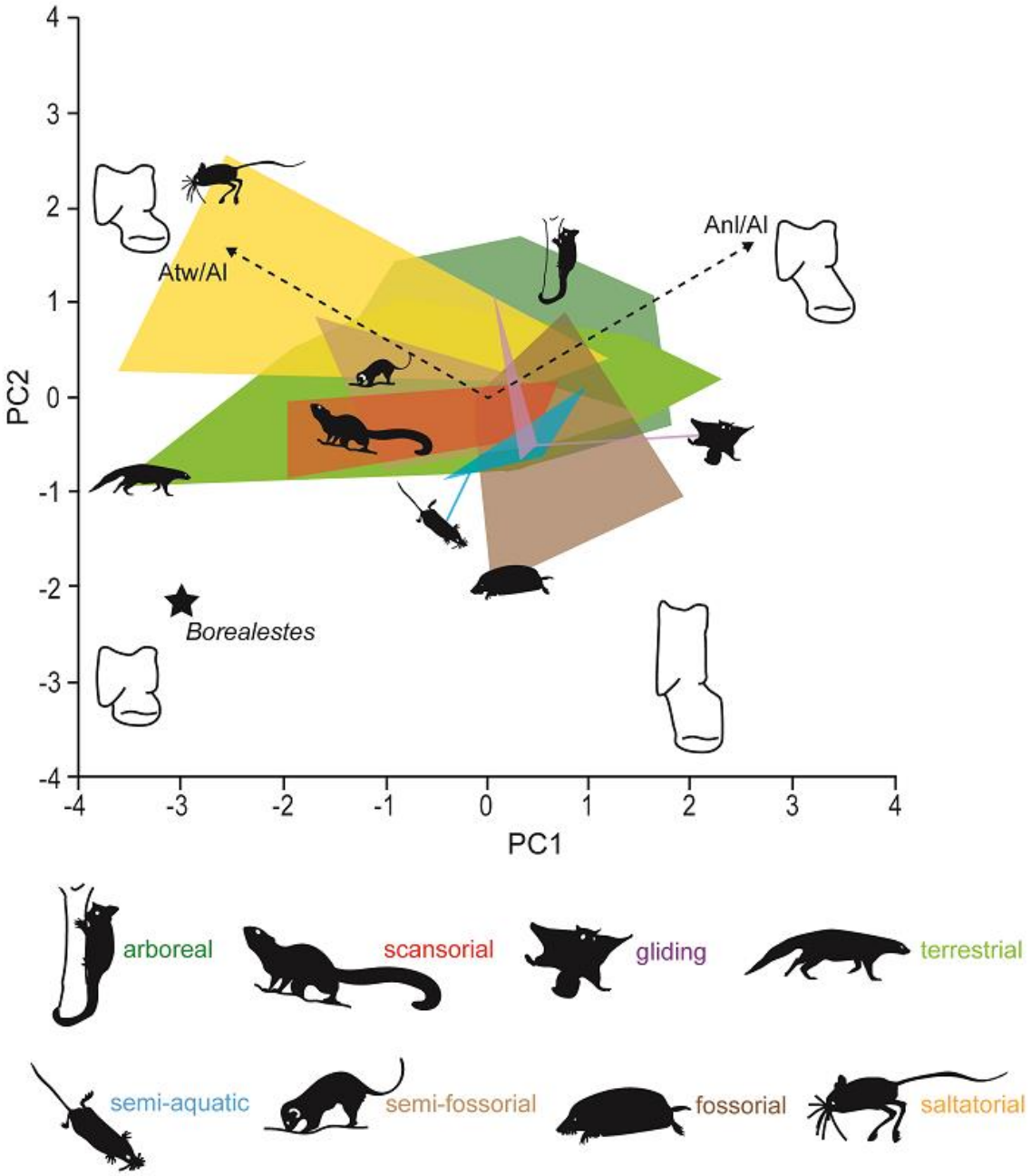

Figure 4.3.6: Results of PCA using astragalar ratios.

a non-independent distribution (Felsenstein, 1985). A more complete postcranial skeleton, providing multiple osteological indices for analysis beyond that afforded by the calcanea presented here, is likely to capture a stronger signal for locomotor mode than a single bone, especially for a taxon with a general, basal morphology (Chen and Wilson, 2015).

However, although the current quantitative analysis has proven unreliable for estimating the locomotor mode for *Borealestes*, this does not negate qualitative observational analysis of calcaneal and astragalar morphology. The most obvious observation is that the calcaneum and the astagalus of *Borealestes* is not indicatative of any derived locomotor mode. For example there is not as deep a tibio-astragalar trochlea on the astragalus as that seen in the fossorial docodontan *Docofossor* (Luo et al., 2015). A more complete discussion of the calcaneal morphology of NMS G.1992.47.121.1 and comparisons with other early diverging mammaliaforms can be found in Chapter 3.3b.

A potential approach to assessing ecomorphology in extinct taxa would be to use a dataset comprising other non-crown mammalian taxa—and even non-mammalian cynodonts—with postcranial morphology that indicates specialisation for particular locomotor modes. Using such a dataset, without extant taxa, could produce useful inferences for locomotor mode in more enigmatic and incomplete fossil material such as *Borealestes* NMS G.1992.47.121.1. However, the number of taxa preserving calcanea is very small, and without living taxa in the dataset for which locomotor mode and ecology is known definitely through observation, results from such an analysis would need to be viewed with caution.

4.4 Conclusions

By assessing the mammal assemblage of the Kilmaluag Formation as a whole, and then looking in more depth at certain taxa, it is possible to gain some understanding of the ecological interactions between the different taxa present. Putting aside the caveat that we are not yet certain all taxa collected to date are coeval (this question is currently being addressed by researchers from the University of Birmingham and National Museums Scotland, see Chapter 2) the presence of multiple small-bodied mammaliaforms—including two docodontans—in the same ecosystem provides an excellent opportunity to explore ecological interactions and ecomorphology. The results here support niche-partitioning in the diets of the Kilmaluag Formation mammal fauna.

Body Mass

Body mass among mammal occupying the same ecosystem is an important factor when considering the ecology of faunal assemblages as a whole. Estimates of body mass can be integrated with biomechanical analyses to build a more comprehensive picture of the ecology of individual taxa, and support assertions regarding the occupation of separate niche-space.

Results from the Kilmaluag Formation mammal assemblage indicate a spread of small mammal body size, ranging from the lower estimates for *Borealestes* and *Palaeoxonodon*, of around 9-13g, to the highest estimate for *Wareolestes* of 100g. These suggest a basis for probable partitioning of these taxa in their palaeoecological community, and could have implications for their life histories such as differences in growth-trajectory, longevity, and home-range. It is clear that the Kilmaluag Formation captures a diverse assemblage, worthy of dedicated future study.

Bite Force

These data suggest detectable differences in the bite force and resistance to torsion in four (presumed) contemporaneous mammaliaform taxa from the Kilmaluag Formation of Skye. This indicates niche partitioning between these taxa, with an ecological range from

more carnivorous taxa such as the large-bodied *Wareolestes*, to the weaker bite forces along the dentary length found for *Palaeoxonodon* and *Borealestes*.

The two most complete dentaries in this analysis, belonging to the closely related docodontan taxa *Krusatodon* and *Borealestes* show a different pattern of biomechanical resistance along the dentary length, despite being of similar size and dentary and tooth cusp morphology. This suggests a different dietary ecology allowed these taxa to exploit disparate food sources in their shared environment.

Despite caveats, it is clear that certain patterns of intractability in insects can be identified, and these can be placed alongside bite force analyses to suggest mammal-insect interactions in fossil ecosystems. Together, these factors indicate the complex biomechanical relationships that must be taken into account when inferring dietary ecology for Mesozoic taxa. While such analyses should be interpreted with caution—particularly for specimens that are damaged or incomplete—these results provide broad support to a diverse ecological model for contemporaneous mammaliaform taxa in the Bathonian freshwater environment of the Isle of Skye.

Principal Component Analysis of *Borealestes*

The results of a principal components analysis on the calcaneum and astragalus of *Borealestes serendipitus* NMS G.1992.47.121.1 suggest a scansorial or semi-fossorial locomotor mode for this taxon. However, only PC1 in the calcaneal data correlated significantly with locomotor modes in the extant therian taxa, and only for more specialised locomotor modes. The non-specialist, basal morphology of *Borealestes* calcaneum and astragalus cannot be meaningfully integrated into an analysis using crown therians with derived calcaneal morphology. Although the morphologies of the tarsus in extant monotremes are somewhat akin to that seen in early diverging mammaliaforms (for example there is less juxtaposition of the astragalus and calcaneum), it is still morphologically derived (for example the peroneal and calcaneal tuber characters). The small number of extant monotreme taxa also reduce their statistical significance for providing inferences in quantitative analyses.

Although principal component analyses of the calcaneum and astragalus does not provide a robust method for determining locomotor mode in the early diverging mammaliaform *Borealestes*, a dataset of multiple osteological measurements/ratios, or

2D/3D landmarks, is likely to provide more definitive results. While these data are not available for NMS G.1992.47.121.1 or other taxa collected to date, ongoing discoveries in the Kilmaluag Formation of the Isle of Skye will hopefully yield more complete postcranial material of *Borealestes* for such an analysis to be carried out in the future.

Chapter 5: Conclusions

My research questions (Chapter 1), fall broadly into two categories: diversity and phylogeny, and ecology and ecomorphology. Through detailed study of anatomy, character scoring for updated phylogenetic analyses, biomechanical analyses, and analyses of shape, I have addressed these questions, and present in this chapter a summary of my key findings.

Diversity and Phylogeny

Q1. Is the Kilmaluag Formation mammal assemblage is as diverse as geologically contemporaneous sites globally?

The Kilmaluag Formation mammal assemblage is of similar diversity to contemporaneous sites globally, as shown in Chapter 2. When compared to five other Middle-Late Jurassic microvertebrate-bearing localities (the Forest Marble, Itat, Morrison and Alcobaça Formations and the Yanliao Biota), the Kilmaluag Formation comprises a similar overall diversity. This includes fish, lissamphibians, testudines, lepidosaurs, squamates, archosaurs and synapsids. The composition of taxa is most similar to the Forest Marble and Itat Formations, and the Yanliao Biota. Although the Kilmaluag Formation is slightly less diverse at a generic level than most other sites, it is important to consider that the Scottish material cannot easily be bulk processed, crops out in a very geographically restricted range, and until recently has only been sporadically sampled. This will undoubtedly influence comparisons between it and other sites, which are almost all of greater geographic extent, and bulk sampled. Of the six sites, it has the lowest diversity of mammals at a generic level, but a similar diversity to the Forest Marble and higher diversity than the Itat Formation at a family level. The absence of Haramiyids and multituberculates (to date) is the main reason for the lower generic mammal diversity currently recorded from the Kilmaluag Formation.

Q2. Does the completeness of fossil mammal material from the Kilmaluag Formation influences the results of phylogenetic analyses for multiple taxa?

In Chapter 3, I added and rescored 36 characters for three taxa (12 characters for *Stereognathus*, 12 characters for *Palaeoxonodon*, and 12 characters for *Borealestes* in the dentomandibular character dataset), and for the first time scored *Borealestes serendipitus* in an expanded dataset of 556 dental, cranial, postcranial and soft-tissue characters. These additional characters did not shift the overall position of these taxa compared to previous studies, but they added an increased level of support for their relationships. The notable exception is the expanded dataset for *Borealestes*, which recovered *Borealestes* as a sister-taxon to the gracile Chinese docodont *Agilodocodon*, rather than as part of the 'basal docodontan' clade proposed by previous authors. However, the lack of cranial and postcranial characters for the majority of docodontan taxa, and the inclusion of many derived characters in this data matrix only applicable to crown Mammalia, make these results less reliable for Docodonta than those of the dentomandibular dataset.

Q3. As a basal docodontan, does* Borealestes *provide key anatomical information for resolving docodontan phylogenetic relationships?

The results of my phylogenetic analysis using the dentomandibular character dataset in Chapter 3 have reinforced the close relationship between 'basal docodontans' *Haldanodon*, *Docodon* and *Docofossor*. The analysis found limited support for 'Tegotheriidae' and no support for 'Simpsonodontidae', two clades proposed by previous authors. This clarifies the topography of Docodonta. Further cranial and postcranial material for multiple docodontans, integrated into a suitable phylogenetic analysis, would undoubtedly improve our understanding of this clade.

Ecology and Ecomorphology

Q4. Did niche partitioning take place among mammals in the ecosystem of the Kilmaluag Formation?

In Chapter 3 I showed that the Kilmaluag Formation mammal assemblage includes members from a wide body mass range (9-100 g) of small mammaliaforms. Body mass and diet are interrelated, and in my bite force analysis in Chapter 3 I found distinct differences in bending strength and torsion along the length of the dentary in four taxa from the Kilmaluag Formation mammal assemblage (*Borealestes*, *Krusatodon*, *Wareolestes* and

Palaeoxonodon). This indicates niche-partitioning, as each taxon exploits foodstuff of differing 'hardness'—most likely insect cuticles of varying intractability.

Q5. Can quantitative biomechanical analyses be used to explore the locomotion and ecology of fossil mammal taxa?

Although it is undoubtedly true that biomechanical analyses shed light on the locomotion of fossil taxa, my analysis of *Borealestes serendipitus* in Chapter 4 was hampered by: 1) a lack of skeletal elements that provide useful ecomorphological indicators in small mammals; and 2) the basal morphology of *Borealestes* limiting comparison with extant taxa. While comparative anatomy gives some indicators for ecology (see below), the results of a geometric morphometric analysis on the calcaneum and astragalus using linear measurements did not provide statistically meaningful locomotor inferences for extant taxa or for *Borealestes*. I suggest that linear measurements may not capture meaningful shape change correlated to locomotor mode in small mammals (<5 kg), which are not subject to the same effects of allometry due to their low body mass. Utilising 3D geometric morphometrics may provide better results. I also suggest that the calcaneum, used here because it was one of the few intact bones that might yield information on locomotor mode, is not informative for early diverging mammaliaforms, especially when compared to the radically different morphology of derived extant crown mammals.

Q6. As a basal docodontan, is the locomotor ecology of **Borealestes** *conserved (i.e. lacking derived specialisations)?*

Although biomechanical analyses were inconclusive, through observational comparisons with other docodontans it is clear that *Borealestes* does not show the derived ecomorphological specialisations seen in some of the other taxa in this clade. In Chapters 3 and 4 I demonstrated that *Borealestes* morphology is more gracile than the semi-fossorial/semi-aquatic *Haldanodon*, but more robust than the arboreal/scansorial *Agilodocodon*. There are no indications of the shortened robust limbs of the fossorial docodontan taxon, *Docofossor*, nor the flattened tail, recurved teeth or plated ribs of the semi-aquatic *Castorocauda*. This, together with the basal phylogenetic position of *Borealestes* found in phylogenetic analyses in Chapter 3, suggests *Borealestes* represents the basal docodontan morphology—or at most, a slightly more gracile basal docodontan.

Further material from this taxon, from the appendicular skeleton in particular, should add clarity to the picture of *Borealestes* locomotor mode and ecology.

The diverse mammal assemblage of the Kilmaluag Formation provides new data to explore evolutionary hypotheses. These fossils are from a key stage in mammal evolution, when the earliest branches of mammaliaform flourished alongside non-mammalian cynodonts and the first crown group mammals. The range of taxa from the Kilmaluag Formation is congruent with this pattern of taxonomic diversity. Clear patterns of niche-partitioning are evident among these coeval taxa, providing the first glimpse into the complexity of this ecosystem. Mammaliaforms were unexpectedly ecologically diverse in the Middle Jurassic, and Docodonta had exceptionally high ecomorphological diversity for such an early-diverging clade. This makes the exceptionally complete skeleton of the early docodontan *Borealestes serendipitus* an important specimen for understanding the emergence of ecological diversity in this clade of mammaliaforms. Comparative observations of the functional anatomy of *Borealestes* and suggest these early members of Docodonta were ecological generalists, with no apparent derived locomotor specialisations. Thanks to their complex molar morphology, docodontans were able to exploit multiple niche-spaces, which may have contributed to their capacity for later ecomorphological specialisation. While biomechanical analyses of the skeletal elements of *Borealestes* found to date produced inconclusive results, the results provide clear signposting for further research to understand their ecomorphology, and the emergence and success of this clade as a whole, especially in light of exciting new fossil material from Skye.

Acknowledgements

A huge debt of gratitude goes to supervisors Nick Fraser and Stig Walsh for supporting me on a day-to-day basis during this research, both academically and pastorally. Thanks to my supervisor Zhe-Xi Luo for his unsurpassed mammal expertise, advising and guiding me in this research and beyond. A special thank you goes to Roger Benson and Richard Butler for their ongoing support, collaboration, and many helpful discussions about this project and methodology. I'm grateful to the Palaeontographical Association for awarding me the Richard Owen Research Fund for this research. Thanks to the many collaborators involved in this research: Zhe-Xi Luo, Nick Fraser, Stig Walsh, Roger Benson, Richard Butler, Julia Schultz, Ian Corfe, Vincent Fernandez, and Stephen Brusatte. I am so lucky to have had the support of the Natural Sciences Department at National Museums Scotland, who welcomed me into the department and supported me. This research wouldn't be possible without Vincent Fernandez, who gave his expertise and time to obtain synchrotron scan data. I'm also indebted to Tom Davies at the University of Bristol for his time and expertise in acquiring initial CT scan data to get me kick-started, and to Ian Butler at the University of Edinburgh for CT scanning the separate skeletal fragments—and many other scans he's given his time and expertise to acquire, and for useful discussions. Thanks go to those who helped with the ESRF application, especially Ian Corfe, and also Stephen Brusatte, and Florian Fusseis. Others who helped me with their discussions include: Pam Gill, Elis Newham, Kai Jäger, Alexander Averianov, and Emily Rayfield. For providing access to material: Pip Brewer, Hilary Ketchum, David Rice, Jonathan Hanson, and Michael Day. Huge love goes to the fieldwork teams on Skye for their companionship and discussions each spring, which annually re-invigorated me. Thanks to the John Muir Trust and Scottish Natural Heritage for permission to carry out field work on Skye each year—this work enriched my thesis and provided new research material. The published articles included in this thesis were improved by the constructive comments of multiple reviewers. Thank you to my examiners Andrew Kitchener and Thomas Martin for the friendly grilling they gave me during my viva, and new ideas it sparked. Finally, and most crucially, I wouldn't have managed any of this without the unwavering love and support of my husband and best friend, Matt.

References

Adams, D.C., Collyer, M.L. and Kaliontzopoulou, A. 2018. Geomorph: Software for geometric morphometric analyses. R package version 3.0.6.

Adkins, R.M., Walton, A.H. and Honeycutt, R.L. 2003. Higher-level systematics of rodents and divergence time estimates based on two congruent nuclear genes. *Molecular phylogenetics and evolution*, 26:409–420.

Agnarsson, I., Kuntner, M. and May-Collado, L.J. 2010. Dogs, cats, and kin: a molecular species-level phylogeny of Carnivora. *Molecular phylogenetics and evolution*, 54:726–745.

Aguirre, L.F., Herrel, A., van Damme, R. and Matthysen, E. 2002. Ecomorphological analysis of trophic niche partitioning in a tropical savannah bat community. *Proceedings of the Royal Society B Biological Sciences*, 269:1271–1278.

Aguirre, L.F., Herrel, A., van Damme, R. and Matthysen, E. 2003. The implications of food hardness for diet in bats. *Functional Ecology*, 17:201–212.

Alexander, R.M., Jayes, A.S., Maloiy, G.M.O. and Wathuta, E.M. 1979. Allometry of the limb bones of mammals from shrews (*Sorex*) to elephant (*Loxodonta*). *Journal of Zoology*, 189:305–314.

Allin, E.F. 1975. Evolution of the mammalian middle ear. *Journal of Morphology*, 147:403–438.

Allin, E.F. and Hopson, J.A. 1992. Evolution of the auditory system in Synapsida ("mammal-like reptiles" and primitive mammals) as seen in the fossil record. P587–614. In Webster, D.B., Fay, R.R. and Popper, A.N. (eds). *The evolutionary biology of hearing*. Springer, 859 pp.

Alroy, J. 1999. The fossil record of North American mammals: evidence for a Paleocene evolutionary radiation. *Systematic Biology*, 48:107–118.

Andrews, J.E. 1985. The sedimentary facies of a late Bathonian regressive episode: the Kilmaluag and Skudiburgh Formations of the Great Estuarine Group, Inner Hebrides, Scotland. *Journal of the Geological Society of London*, 142:1119–1137.

Anquetin, J. 2009. A new stem turtle from the Middle Jurassic of Scotland: new insights into the evolution and palaeoecology of basal turtles. *Proceedings of the Royal Society B*, 276:879–886.

Anquetin, J. 2010. The anatomy of the basal turtle *Eileanchelys waldmani* from the Middle Jurassic of the Isle of Skye, Scotland. *Earth and Environmental Science Transactions of the Royal Society of Edinburgh*, 101:67–96.

Argot, C., 2002. Functional-adaptive anatomy of the forelimb in the Didelphidae, and the paleobiology of the Paleocene marsupials *Mayulestes ferox* and *Pucadelphys andinus*. *Journal of Morphology*, 247:51–79.

Averianov, A.O. 2004. Interpretation of the Early Cretaceous mammal *Peraiocynodon* (Docodonta) and taxonomy of some British Mesozoic docodonts. *Russian Journal of Theriology*, 3:1–4.

Averianov, A.O., and Lopatin, A.V. 2006. *Itatodon tatarinovi* (Tegotheriidae, Mammalia), a docodont from the Middle Jurassic of Western Siberia and phylogenetic analysis of Docodonta. *Paleontological Journal*, 40:668–677.

Averianov, A.O., Lopatin, A.V., Skutschas, P.P., Martynovich, N.V., Leshchinskiy, S.V., Krasnolutskii, S.A. and Fayngertz, A.V. 2005. Discovery of Middle Jurassic mammals from Siberia. *Acta Palaeontologica Polonica*, 50:789–797.

Averianov, A.O, Krasnolutskii, S.A. and Ivantson, S.V. 2010. New docodontans from the Middle Jurassic of Siberia and reanalysis of Docodonta interrelationships. *Proceedings of the Zoological Institute*, 314:121–148.

Averianov, A.O., Martin, T., Lopatin, A., and Krasnolutskii, S. 2015. Stem therian mammal *Amphibetulimus* from the Middle Jurassic of Siberia. *Paläontologische Zeitschrift*, 89:197–206.

Averianov, A.O., Martin, T., Skutschas, P.P., Danilov, I.G., Schultz, J., Schellhorn, R., Obraztsova, E., Lopatin, A., Sytchevskaya, E., Kuzmin, I. and Krasnolutskii, S. 2016. Middle Jurassic vertebrate assemblage of Berezovsk coal mine in western Siberia (Russia). *Global Geology*, 19:187–204.

Averianov, A., Martin, T., Lopatin, A., Skutschas, P., Schellhorn, R., Kolosov, P. and Vitenko, D. 2018. A high-latitude fauna of mid-Mesozoic mammals from Yakutia, Russia. *PloS one*, 13:p.e0199983.

Bapst, D.W. 2012. paleotree: an R package for paleontological and phylogenetic analyses of evolution. *Methods in Ecology and Evolution*, 3:803–807.

Barrett, P.M. 2006. A sauropod dinosaur tooth from the Middle Jurassic of Skye, Scotland. *Transactions of the Royal Society of Edinburgh*, 97:25–29.

Barron, A.J.M., Lott, G.K. and Riding, J.B. 2012. Stratigraphic Framework for the Middle Jurassic Strata of Great Britain and the Adjoining Continental Shelf: Research Report RR/11/06. British Geological Survey, Keyworth. 177 pp.

Bassarova, M., Janis, C.M. and Archer, M. 2009. The calcaneum–on the heels of marsupial locomotion. *Journal of Mammalian Evolution*, 16:1–23.

Benoit, J., Manger, P.R. and Rubidge, B.S. 2016. Palaeoneurological clues to the evolution of defining mammalian soft tissue traits. *Scientific reports*, 6:p.25604.

Benson, R.B., Mannion, P.D., Butler, R.J., Upchurch, P., Goswami, A. and Evans, S.E. 2013. Cretaceous tetrapod fossil record sampling and faunal turnover: implications for biogeography and the rise of modern clades. *Palaeogeography, Palaeoclimatology, Palaeoecology*, 372:88–107.

Benson, R.B., Campione, N.E., Carrano, M.T., Mannion, P.D., Sullivan, C., Upchurch, P. and Evans, D.C. 2014. Rates of dinosaur body mass evolution indicate 170 million years of sustained ecological innovation on the avian stem lineage. *PLoS Biology*, 12:p.e1001853.

Benton, M.J., Martill, D.M. and Taylor, M.A. 1995. The first Lower Jurassic dinosaur from Scotland: limb bone of the ceratosaur theropod from Skye. *Scottish Journal of Geology*, 31:177–182.

Bertram, J.E.A., Biewener, A.A. 1990 Differential scaling in the long bones in the terrestrial Carnivora and other mammals. *Journal of Morphology*, 220:157–169 doi:10.1002/jmor.1052040205

Bhullar, B.A.S., Manafzadeh, A.R., Miyamae, J.A., Hoffman, E.A., Brainerd, E.L., Musinsky, C. and Crompton, A.W. 2019. Rolling of the jaw is essential for mammalian chewing and tribosphenic molar function. *Nature*, 566, 528–532.

Bi, S.-D., Wang, Y.-Q., Guan, J., Sheng, X., Meng J. 2014. Three new Jurassic euharamiyidan species reinforce early divergence of mammals. *Nature*, 514:579–584.

Biewener, A.A. 1989a. Mammalian terrestrial locomotion and size. *Bioscience*, 39:776–783.

Biewener, A.A. 1989b Scaling body support in mammals: limb posture and muscle mechanics. Science, 245:45-48.

Biewener, A.A. 1990. Biomechanics of mammalian terrestrial locomotion. *Science*, 250:1097–1103.

Bininda-Emonds, O.R., Cardillo, M., Jones, K.E., MacPhee, R.D., Beck, R.M., Grenyer, R., Price, S.A., Vos, R.A., Gittleman, J.L. and Purvis, A. 2007. The delayed rise of present-day mammals. *Nature*, 446:507.

Blackburn, T.M., Gaston, K.J. and Loder, N. 1999. Geographic gradients in body size: a clarification of Bergmann's rule. *Diversity and distributions*, 5:165–174.

Bonaparte, J.F. 2008. On the phylogenetic relationships of *Vincelestes neuquenianus*. *Historical Biology*, 20:81–86.

Bonaparte, J.F. and Rougier, G.W. 1987. Mamíferos del Cretácico Inferior de Patagonia. IV Congresso Latinomericano de Paleontologia 1: 343–359.

Brannick AL and Wilson GP. 2018. New specimens of the Late Cretaceous Metatherian *Eodelphis* and the evolution of hard-object feeding in the Stagodontidae. *Journal of Mammalian Evolution*, https://doi.org/10.1007/s10914-018-9451-z.

Buckland, W. 1824. Notice on the *Megalosaurus* or the Great Fossil Lizard of Stonesfield. *Transactions of the Geological Society of London*, 2:390-396.

Butler, P.M. and Clemens, W.A. 2001. Dental morphology of the Jurassic holotherian mammal *Amphitherium*, with a discussion of the evolution of mammalian post-canine dental formulae. *Palaeontology*, 44:1–20.

Butler, P.M. and Hooker, J.J. 2005. New teeth of allotherian mammals from the English Bathonian, including the earliest multituberculates. *Acta Palaeontologica Polonica*, 50:185–207.

Butler, P.M and Sigogneau-Russell, D. 2016. Diversity of triconodonts in the Middle Jurassic of Great Britain. *Palaeontologia Polonica*, 67:35–65.

Byers, J.A. 1999. Play's the thing—marsupials at play. *Natural History*, 108:40–45.

Campione, N.E., and Evans, D.C. 2012. A universal scaling relationship between body mass and proximal limb bone dimensions in quadrupedal terrestrial tetrapods. *BMC Biology*, 10:60

Candela, A., Picasso, B. 2008. Functional anatomy of the limbs of Erethizontidae Rodentia, Caviomorpha): indicators of locomotor behavior in Miocene porcupines. *Journal of Morphology*, 269:552593.

Charlesworth, E. 1855. Notice on New Vertebrate Fossils. *Report of the British Association for the Advancement of Science*, 1854:80.

Chen, P.-J. and Hudson, J.D. 1991. The chonchostracan fauna of the Great Estuarine Group, Middle Jurassic, Scotland. *Palaeontology*, 34:515–545.

Chen, M. and Wilson, G.P. 2015. A multivariate approach to infer locomotor modes in Mesozoic mammals. *Paleobiology*, 41:1–33.

Chow, M. and Hu, C. 1959. A new tritylodontid from Lufeng, Yunnan.*Vertebrata PalAsiatica*, 3:7–10.

Christensen, P., Maisey, K. and Perry, D. H. 1984. Radio-tracking the numbat, *Myrmecobius fasciatus*, in the Perup Forest of western Australia. *Australia Wildlife Research*, 11:275–288.

Chure, D.J., Litwin, R., Hasiotis, S.T., Evanoff, E. and Carpenter, K. 2006. The fauna and flora of the Morrison Formation. *New Mexico Museum of Natural History and Science Bulletin*, 36:233–249.

Clark, N.D.L. 2018. Review of the Dinosaur Remains from the Middle Jurassic of Scotland, UK. *Geosciences*, 8.

Clark, J.M. and J.A. Hopson. 1985. Distinctive mammal-like reptile from Mexico and its bearing on the phylogeny of the Tritylodontidae. *Nature*, 315:398–400.

Clark, N.D.L., Ross, D.A., and Booth, P. 2005. Dinosaur tracks from the Kilmaluag Formation (Bathonian, Middle Jurassic) of Score Bay, Isle of Skye, Scotland, UK. *Ichnos*, 12:93–104.

Clemens, W.A. 1980. Rhaeto-Liassic mammals from Switzerland and West Germany. Zitteliana, 5:51–92.

Clemens, W.A. 1986. On Triassic and Jurassic mammals. P237–246 in Padian, K. (ed.) *The Beginning of the Age of Dinosaurs*. Cambridge University Press, Cambridge. 378 pp.

Clemens, W.A. 2011. New morganucodontans from an Early Jurassic fissure filling in Wales. *Palaeontology*, 54:1139–1156.

Clemens, W.A. and Mills, J.R.E. 1971. Review of *Peramus tenuirostris*. *Bulletin of the British Museum of Natural History, Geology*, 20:89–113.

Close, R.A., Friedman, M., Lloyd, G.T. and Benson, R.B. 2015. Evidence for a mid-Jurassic adaptive radiation in mammals. *Current Biology*, 25:2137-2142.

Close, R.A., Davis, B.M., Walsh, S., Woloniewicz, A.S., Friedman, M., and Benson, R.B.J. 2016. A lower jaw of *Palaeoxonodon* from the Middle Jurassic of the Isle of Skye, Scotland, sheds new light on the diversity of British stem therians. *Palaeontology*, 59:155–169.

Close, R., Benson, R., Alroy, J., Behrensmeyer, A., Benito, J., Carrano, M., Clearly, T., Dunne, E., Mannion, P., Uhen, M. and Butler, R. 2019. Diversity dynamics of Phanerozoic terrestrial tetrapods at the local-community scale. *Nature Ecology and Evolution*, 3:590.

Cohen, K.M., Finney, S.C., Gibbard, P.L. and Fan, J-X. 2018. The ICS International Chronostratigraphic Chart. *Episodes*, 36:199-204.

Conith, A.J., Imburgia, M.J., Crosby, A. J., and Dumont E.R. 2016. The functional significance of morphological changes in the dentitions of early mammals. *Journal of the Royal Society Interface*, 13:20160713.

Cooper, C.E. 2011. *Myrmecobius fasciatus* (Dasyuromorphia: Myrmecobiidae). *Mammalian Species*, 43:129–140.

Cope, E.D. 1884. The Tertiary Marsupialia. *American Naturalist*, 18:686– 697.

Cope, J.C.W., Dufl, K.L., Parsons, C.F., Torrens, H.S., Wimbledon, W.A. and Wright, J. 1980. A Correlation of Jurassic Rocks in the British Isles. Pt. 2: Middle and Upper Jurassic. Geological Society Special Report 15. 109 pp.

Crompton, A.W. 1964. A preliminary description of a new mammal from the Upper Triassic of South Africa. *Proceedings of the Zoological Society of London*, 142:441–452.

Crompton, A.W. 1974. The dentition and relationships of the southern African Triassic mammals, *Erythrotherium parringtoni* and *Megazostrodon rudnaerae*. *Bulletin of the British Museum of Natural History*, 24:397–437.

Crompton, A.W. and Jenkins, F.A. 1968. Molar occlusion in Late Triassic Mammals. *Biological Reviews*, 43:427–458.

Crompton, A.W. and Parker, P. 1978. Evolution of the mammalian masticatory apparatus. *American Scientist*, 66:192–201.

Crompton, A.W. and Luo, Z.-X. 1993. Relationships of the Liassic mammals *Sinoconodon*, *Morganucodon oehleri*, and *Dinnetherium*. P30–44. In Szalay, F. S., Novacek, M.J. and McKenna, M.C. (eds). *Mammal phylogeny: Mesozoic differentiation,*

multituberculates, monotremes, early therians and marsupials. Springer, New York. 249 pp.

Cui, G. 1976. *Yunnania*, a new tritylodont genus from Lufeng, Yunnan. *Vertebrata PalAsiatica*, 3:85–90.

Cui, G. 1981. A new genus of Tritylodontoidea. *Vertebrata PalAsiatica*, 19:5–10.

Cui, G. and Sun, A. 1987. Postcanine root system in Tritylodontids. *Vertebrata PalAsiatica*, 25:245–259.

Daegling, D.J., Ravosa, M.J., Johnson, K.R., and Hylander, W. 1992. Influence of teeth, alveoli, and periodontal ligaments on torsional rigidity in human mandibles. *American Journal of Physical Anthropology*, 89:59–72.

Damuth, J. 1981. Population density and body size in mammals. *Nature*, 290:699–700.

Damuth, J. 1987. Interspecific allometry of population density in mammals and other animals: the independence of body mass and population energy-use. *Biological Journal of the Linnean Society*, 31:193–246.

Datta, P. M. 2005. Earliest mammal with transversely expanded upper molar from the Late Triassic (Carnian) Tiki Formation, South Rewa Gondwana Basin, India. *Journal of Vertebrate Paleontology*, 25:200–207.

Datta, P.M. and Das, D.P. 1996. Discovery of the oldest fossil mammal from India. *Indian Minerals*, 50:217–222.

Datta, P.M. and Das D.P. 2001. *Indozostrodon simpsoni*, gen. et sp. nov., an Early Jurassic megazostrodontid mammal from India. *Journal of Vertebrate Paleontology*, 21, 528–534.

Davis, B.M. 2011. Evolution of the tribosphenic molar pattern in early mammals, with comments on the "dual-origin" hypothesis. *Journal of Mammalian Evolution*, 18: 227–244.

Davis, B.M. 2012. Micro-computed tomography reveals a diversity of peramuran mammals from the Purbeck Group (Berriasian) of England. *Palaeontology*, 55: 789–817.

Davis, J.L., Santana, S.E., Dumont. E,R. and Grosse, I.R. 2010. Predicting bite force in mammals: two-dimensional versus three-dimensional lever models. *Journal of Experimental Biology*, 213:1844–1851

Debuysschere, M., Gheerbrant, E. and Allain, R. 2015. Earliest known European mammals: a review of the Morganucodonta from Saint-Nicolas-de-Port (Upper Triassic, France). *Journal of Systematic Palaeontology*, 13:825–855.

Delciellos, A.C. and Vieira, M.V. 2006. Arboreal walking performance in seven didelphid marsupials as an aspect of their fundamental niche. *Austral Ecology*, 31:449–457.

Douady, C.J. and Douzery, E.J. 2003. Molecular estimation of eulipotyphlan divergence times and the evolution of "Insectivora". *Molecular phylogenetics and evolution*, 28:.285–296.

Druzinsky, R.E. 1993. The time allometry of mammalian chewing movements: chewing frequency scales with body mass in mammals. *Journal of Theoretical Biology*, 160:427–440.

Dumont, E.R. 1995. Enamel thickness and dietary adaptation among extant primates and chiropterans. *Journal of Mammalogy*, 76:1127–1136.

Dumont, E.R. 1999. The effect of food hardness on feeding behaviour in frugivorous bats (Phyllostomidae): an experimental study. *Journal of Zoology*, 248:219-229.

Eaton, T.H., 1962. Adaptive features of the fore limb in primitive tetrapods and mammals. *American Zoologist*, 2:157–160.

Eizirik, E., Murphy, W.J., Koepfli, K.P., Johnson, W.E., Dragoo, J.W., Wayne, R.K. and O'Brien, S.J. 2010. Pattern and timing of diversification of the mammalian order Carnivora inferred from multiple nuclear gene sequences. *Molecular Phylogenetics and Evolution*, 56:49–63.

Endo, H., Yonezawa, T., Rakotondraparany, F., Sasaki, M. and Hasegawa, M. 2006. The adaptational strategies of the hindlimb muscles in the Tenrecidae species including the aquatic web-footed tenrec (*Limnogale mergulus*). *Annals of Anatomy*, 188:383–390.

Ensom, P.C. 1977. A therapsid tooth from the Forest Marble (Middle Jurassic) of Dorset. *Proceedings of the Geologists' Association*, 88:201–205.

Ensom, P.C. 1994. A lower postcanine of *Stereognathus* sp. (Reptilia, Therapsida) from the Bathonian of southern England. *Proceedings of the Dorset Natural History and Archaeological Society*, 115:139–141.

Erickson, G.M., Catanese, J. III and Keaveny, T.M. 2002. Evolution of the biomechanical material properties of the femur. *The Anatomical Record*, 268:115–124.

Evans, S.E. 1991. A new lizard-like reptile (Diapsida: Lepidosauromorpha) from the Middle Jurassic of England. *Zoological Journal of the Linnean Society*, 103:391–412.

Evans, S.E. and Milner, A.R. 1994. Middle Jurassic microvertebrate assemblages from the British Isles. P303–321. In Fraser, N.C. and Sues, H.-D. (eds). *In the Shadow of the Dinosaurs: Early Mesozoic tetrapods*. Cambridge University Press, Cambridge. 429 pp.

Evans, S.E. and Waldman, M. 1996. Small reptiles and amphibians from the Middle Jurassic of Skye Scotland. P219-226. In Morales, M. (ed) *The Continental Jurassic*, Museum of Northern Arizona Bulletin 60. 588 pp.

Evans, S., Barrett, P., Hilton, J., Butler R.J., Jones, M.E.H., Liang, M.-M., Parrish, J.C., Rayfield, E.J., Sigogneau-Russell, D. and Underwood, C.J. 2006. The Middle Jurassic vertebrate assemblage of Skye, Scotland. P36–39. In: Barrett, P. and Evans, S. (eds). Proceedings of the Ninth Symposium on Mesozoic Terrestrial Ecosystems and Biota, Natural History Museum, London.

Famoso, N.A., Hopkins, S.S.B. and Davis, E.B. 2018. How do diet and body mass drive reproductive strategies in mammals? *Biological Journal of the Linnean Society*, 124:151–156.

Fedak, T.J., Sues, H.D. and Olsen P.E. 2015. First record of the tritylodontid cynodont *Oligokyphus* and cynodont postcranial bones from the McCoy Brook Formation of Nova Scotia, Canada. *Canadian Journal of Earth Sciences*, 52:244–249.

Felsenstein, J. 1985. Phylogenies and the comparative method. *The American Naturalist*, 125:1–15.

Foster, J.B. 1964. The evolution of mammals on islands. *Nature*. 202:234–235.

Foster, J. 2007. *Jurassic West—The Dinosaurs of Morrison Formation and Their World*. The Indianan University of Press, Bloomington and Indianapolis, Indiana. 389 pp.

Foster, J.R. 2009. Preliminary body mass estimates for mammalian genera of the Morrison Formation (Upper Jurassic, North America). *PaleoBios*, 28:114–122.

Foster, J.R. and Lucas, S.G. 2006. Paleontology and Geology of the Upper Jurassic Morrison Formation: Bulletin 36 (Vol. 36). New Mexico Museum of Natural History and Science.

Foster, J.R. and Heckert, A.B., 2011. Ichthyoliths and other microvertebrate remains from the Morrison Formation (Upper Jurassic) of northeastern Wyoming: a screen-washed sample indicates a significant aquatic component to the fauna. *Palaeogeography, Palaeoclimatology, Palaeoecology*, 305:264–279.

Fourie, S. 1963. A new tritylodontid from the Cave Sandstone of South Africa. *Nature* 4876:201.

Freeman, E. 1976a. A mammalian fossil from the Forest Marble (Middle Jurassic) of Dorset. *Proceedings of the Geologists' Association*, 87:231–235.

Freeman, E. 1976b. Mammal teeth from the Forest Marble (Middle Jurassic) of Oxfordshire, England. *Science*, 194:1053–1055.

Freeman, E. 1979. A Middle Jurassic mammal bed from Oxfordshire. *Palaeontology*, 22:135–166.

Freeman, P.W. 1979. Specialized insectivory: beetle-eating and moth-eating molossid bats. *Journal of Mammalogy*, 62:467–479.

Freeman, P.W. 1981. Correspondence of food habits and morphology in insectivorous bats. *Journal of Mammalogy*, 62:166–173.

Freeman, P.W. and Lemen, C.A. 2008. Measuring bite force in small mammals with a piezo-resistive sensor. *Journal of Mammology*, 89:513–517.

Freudenthal, M. and Martín-Suárez, E. 2013. Estimating body mass of fossil rodents. *Scripta Geologica*, 145:1-15.

Fox, R.C. and Naylor, B.G. 1986. A new species of Didelphodon Marsh (Marsupialia) from the Upper Cretaceous of Alberta, Canada: palaeobiology and phylogeny. *Neues Jahrbuch für Geologie und Paläontologie, Abhandlungen*, 172: 357–380.

Gabe, M., Gasc, J.P., Lessertisseur, J., Saban, R. and Starck, D. 1967. Mammifères: téguments et squelette (No. 591 GRA).

Gaetano, L.C. and Abdala, F. 2015. The stapes of gomphodont cynodonts: insights into the middle ear structure of non-mammaliaform cynodonts. *PLoS one*, 10:e0131174.

Gambaryan, P.P. and Kielan-Jaworowska, Z. 1995. Masticatory musculature of Asian taeniolabidoid multituberculate mammals. *Acta Palaeontologica Polonica*, 40: 45–80.

Gambaryan, P.P. and Averianov, A.O. 2001. Femur of a morganucodontid mammal from the Middle Jurassic of central Russia. *Acta Palaeontologica Polonica*, 46:99–112.

Gambaryan, P.P., Aristov, A.A., Dixon, J.M. and Zubtsova, G.Y. 2002. Peculiarities of the hind limb musculature in monotremes: an anatomical description and functional approach. *Russian Journal of Theriology*, 1:1–36.

Gambaryan, P.P. and Kuznetsov, A.N. 2013 An evolutionary perspective on the walking gait of the long-beaked echidna. *Journal of Zoology*, 290:58-67.

Gambaryan, P.P, Kuznetsov, A.N., Panyutina, A.A. and Gerasimov, S.V. 2015. Shoulder girdle and forelimb myology of extant Monotremata. *Russian Journal of Theriology*, 14:1–56.

Garland, T. 1983. The relation between maximal running speed and body mass in terrestrial mammals. *Journal of Zoology*, 199:157–170.

Gebo, D., and K. Rose. 1993. Skeletal morphology and locomotor adaptation in Prolimnocyonatavus, an early Eocene hyaenodontid creodont. *Journal of Vertebrate Paleontology*, 13:125–144.

Gill, P.G. 2004. *Kuehneotherium* from the Mesozoic fissure fillings of South Wales. Ph.D. dissertation, University of Bristol, Bristol, 285 pp.

Gill, P.G., Purnell, M.A., Crumpton, N., Brown, K.R., Gostling, N.J., Stampanoni, M. and, Rayfield, E.J. 2014. Dietary specialisations and diversity in feeding ecology in the earliest stem mammals. *Nature*, 512:303–305

Gingerich, P.D. 1973. Molar occlusion and function in the Jurassic mammal *Docodon*. *Journal of Mammalogy*, 254:1008–1013.

Gingerich, P.B. and Smith, B.H. 1984. Allometric scaling in the dentition of primates and insectivores. Pp 257-272. In WL Jungers (ed). *Size and Scaling in Primate Biology*. Plenum Press, New York.

Gingerich, P.D. 2003. Land-to-sea transition in early whales: evolution of Eocene Archaeoceti (Cetacea) in relation to skeletal proportions and locomotion of living semiaquatic mammals. *Paleobiology*, 29:429–454.

Ginot, S., Hautier, L., Marivaux, L. and Vianey-Liaud, M. 2016. Ecomorphological analysis of the astragalo-calcaneal complex in rodents and inferences of locomotor behaviours in extinct rodent species. *PeerJ*, 4:e2393.

Goloboff, P.A., Farris, J.S. and Nixon, K.C. 2008. TNT, a free program for phylogenetic analysis. *Cladistics*, 24:744–786.

Gordon, J.E. 1991. *The New Science of Strong Materials: Or Why You Don't Fall Through the Floor*, Second revised edition. Penguin, London. 288pp.

Gow, C.E. 1986. A new skull of *Megazostrodon* (Mammalia, Triconodonta) from the Elliot Formation (Lower Jurassic) of southern Africa. *Palaeontologia Africana*, 26:13–23.

Grand, T.I. 1990. The functional anatomy of body mass. P39-47. In Damuth, J.D. and MacFadden, B.J. (eds). *Body size in mammalian palaeobiology: estimation and biological implications*. Cambridge University Press, Cambridge. 397 pp.

Grant, T. and D. Fanning. 1989. The platypus: a unique mammal. New South Wales University Press, Kensington, Australia.

Graybeal, A., Rosowski, J.J., Keten, D.R. and Crompton, A.W. 1989. Inner-ear structure in *Morganucodon*, an early Jurassic mammal. *Zoological Journal of the Linnean Society*, 96:107–117.

Grossnickle, D.M. 2017. The evolutionary origin of jaw yaw in mammals. *Scientific Reports*, 7:45094.

Grossnickle, D.M. 2018 Macroevolutionary patterns and dietary adaptations in early cladotherian mammals. Dissertation: University of Chicago.

Grossnickle, D.M., and Polly, P.D. 2013. Mammal disparity decreases during the Cretaceous angiosperm radiation. *Proceedings of the Royal Society B: Biology Sciences*, 280:20132110.

Guy-Ohlson, D. 1989. Spore and pollen assemblage zonation of Swedish Bajocian and Bathonian sediments. P70-91. In Batten, D.J. and Keen, M.C. (eds). *Northwest European Micropalaeontology and Palynology*. British Micropalaeontological Society Series, Ellis Horwood Limited, Chichester. 266 pp.

Hahn, G., Sigogneau- Russell, D. and Godefroit, P. 1991. New data on *Brachyzostrodon* (Mammalia; Upper Triassic). *Geologica et Paleontologica*, 25:237–249.

Harris, JP. and Hudson, JD. 1980. Lithostratigraphy of the Great Estuarine Group (Middle Jurassic), Inner Hebrides. *Scottish Journal of Geology*, 16:231–250.

Hayssen, V. and Lacy, R.C. 1985. Basal metabolic rates in mammals: taxonomic differences in the allometry of BMR and body mass. *Comparative Biochemistry and Physiology Part A: Physiology*, 81:741–754.

He, X., and K. Cai. 1984. The tritylodont remains from Dashanpu, Zigong. Journal of Chengdu College of Geology (Special Paper on Dinosaurian Remains of Dashanpu, Zigong, Sichuan [II]):33–45.

Helmdach, F.F. 1971. Stratigraphy and ostracode-fauna from the coal mine Guimarota (Upper Jurassic). *Memórias dos Serviços Geológicos de Portugal, N.S.*, 17:43–88.

Hennig, E. 1922. Die Säugerzähne der württembergischen Rhät-Lias-Bonebeds. *Neues Jahrbuch für Mineralogie, Geologie und Paläontologie, Beilage-Band* 46:181–267

Hesselbo, S.P. and Coe, A.L. 2000. Jurassic sequences of the Hebrides Basin, Isle of Skye Scotland. P41–58. In Graham, J.R. and Ryan, A. (eds). Field Trip Guidebook, International Sedimentologists Association Meeting, Dublin.

Hildebrand, M. and Goslow, G.E. Jr. 2001. *Analysis of Vertebrate Structure, 5th Edition*. John Wiley, New York. 635 pp.

Hoffman, E.A. and Rowe, T.B., 2018. Jurassic stem-mammal perinates and the origin of mammalian reproduction and growth. *Nature*, 561:104.

Holloway, S. 1983. The shell-detrital calcirudites of the Forest Marble Formation (Bathonian) of South West England. Proceedings of the Geologists' Association 94:259–266.

Hopson, J. A., and A. W. Crompton. 1969. Origin of mammals. P15–72. In Dobzhansky, T., Hecht, M. K. and Steere, W. C. (eds). *Evolutionary Biology*, Volume 3. Appleton-Century-Crofts, New York.

Hopson, J.A., and Kitching, J.W. 1972. A revised classification of cynodonts (Reptilia; Therapsida). *Palaeontologia Africana*, 14:71–85.

Howell, A.B. 1930. Aquatic mammals. Charles C. Thomas, Springfield, Illinois.

Hu, Y., Meng, J., Wang, Y. and Li, C. 2005. Large Mesozoic mammals fed on young dinosaurs. *Nature*, 433:149.

Hu, Y., Meng, J. and Clark, J.M. 2009. A new tritylodontid from the Upper Jurassic of Xinjiang, China. *Acta Palaeontologica Polonica*, 54:385–391.

Hudson, J.D. 1962. The stratigraphy of the Great Estuarine Series (Middle Jurassic) of the Inner Hebrides. *Transactions of the Edinburgh Geological Society*, 19:139–165.

Hudson, J.D. 1980. Aspects of brackish-water facies and faunas from the Jurassic of north-west Scotland. *Proceedings of the Geologists' Association*, 91:99–105.

Hughes, E.M., Wible, J.R., Spaulding, M. and Luo, Z.-X. 2015. Mammalian petrosal from the Upper Jurassic Morrison Formation of Fruita, Colorado. *Annals of Carnegie Museum*, 83:1–17.

Isidro, A. and Vazquez, M.T. 2006. Phylogenetic and ontogenetic parallelisms on talo-calcaneal superposition. *The Foot*, 16:1–15.

Iwaniuk, A., and Pellis, S. 2000. The relative importance of body size, phylogeny, locomotion, and diet in the evolution of forelimb dexterity in fissiped carnivores (Carnivora). *Canadian Journal of Zoology*, 78:1110–1125.

Jaccard, P. 1912. The distribution of the flora of the alpine zone. *New Phytologist*, 11:37–50.

Jäger, K., Gill, P., Corfe, I.J. and Martin, T. 2016. 3D analysis of the chewing cycle and dental occlusion of *Morganucodon watsoni*. P160. In Farke, A., Mackenzie, A. and Miller- Camp, J. (eds). SVP 2016: Meeting Program & Abstracts. Society for Vertebrate Paleontology.

Janis, C.M. 1990. Correlation of cranial and dental variables with body size in ungulates and macropodids. P255–288. In Damuth, J. and MacFadden, B.J. (eds). *Body Size in Mammalian Paleobiology: Estimation and Biological Implications*. Cambridge University Press, New York. 397 pp.

Janis, C.M., Theodor, J.M., Boisvert, B. 2002. Locomotor evolution in camels revisited: a quantitative analysis of pedal anatomy and the acquisition of the pacing gait. *Journal of Vertebrate Paleontology*, 22:110–121.

Jenkins, F. A., Jr. 1969. Occlusion in *Docodon* (Mammalia, Docodonta). *Postilla*, 139:1–24.

Jenkins, F.A. 1970a. Limb movement in a monotreme (*Tachyglossus aculeatus*): a cineradiographic analysis. *Science*, 168:1473–1475.

Jenkins, F. A. Jr. 1970b. Cynodont postcranial anatomy and the "prototherian" level of mammalian organization. *Evolution*, 24:230–252.

Jenkins, F. A., Jr. 1971. The postcranial skeleton of African cynodonts. *Bulletin of the Peabody Museum of Natural History*, 36:1–216.

Jenkins, Jr., F.A. and Parrington, F.R. 1976. The postcranial skeletons of the Triassic mammals *Eozostrodon*, *Megazostrodon* and *Erythrotherium*. Philosophical Transactions of the Royal Society of London B Biological Sciences, 273:387–431.

Jenkins, F.A., Crompton, A.W. and Downs, W.R. 1983. Mesozoic mammals from Arizona: new evidence on mammalian evolution. *Science*, 222:1233–1235.

Jenkins, F.A., Shubin, N.H., Amaral, W.W., Gatesey, S.M., Schaff, C.R., Clemmensen, L.B., Downs, W.R., Davidson, A., Bonde, N. and Osbaek, F. 1994. Late Triassic continental vertebrates and depositional environments of the Fleming Fjord Formation, Jameson Land, East Greenland. *Meddelelser om Grønland*, 32:3–25.

Ji, Q., Luo, Z.-X., Yuan, C.-X. and Tabrum, A.R. 2006. A swimming mammaliaform from the Middle Jurassic and ecomorphological diversification of early mammals. *Science*, 311:1123–1127.

Jones, M.E., Rose, R.K. and Burnett, S. 2001. *Dasyurus maculatus*. P1-9. In Mammalian Species, No. 676, American Society of Mammalogists.

Judd, J.W. 1878. The secondary rocks of Scotland. Third paper. The strata of the western coasts and islands. *Quarterly Journal of the Geological Society of London*, 34:660–743.

Kalthoff, D.C., Schulz-Kornas, E., Corfe, I., Martin, T., McLoughlin, S. and Schultz, J.A. 2018. Food choice in Tritylodontidae (Cynodontia). Abstract 13th Mesozoic Terrestrial ecosystems, Bonn, Germany.

Kemp, T.S. 2005. The Origin and Evolution of Mammals. Oxford University Press, Oxford. 344 pp.

Kermack, K. A. 1988. British Mesozoic mammal sites. *Special Papers in Palaeontology*, 40:85–93.

Kermack, D.M. 1982. A new tritylodontid from the Kayenta Formation of Arizona. *Zoological Journal of the Linnean Society*, 76:1–17.

Kermack, K.A., Mussett, F. and Rigney, H.W. 1973. The lower jaw of *Morganucodon*. *Zoological Journal of the Linnean Society*, 53:87–175.

Kermack, K.A., Mussett, F. and Rigney, H.W. 1981. The skull of *Morganucodon*. *Zoological Journal of the Linnean Society*, 71:1–158.

Kermack, K.A., Lee, A.J., Lees, P.M. and Mussett, F. 1987. A new docodont from the Forest Marble. *Zoological Journal of the Linnean Society*, 89:1–39.

Kermack, K.A., Kermack, D.M., Lees, P.M. and Mills, J.R. 1998. New multituberculate-like teeth from the Middle Jurassic of England. *Acta Palaeontologica Polonica*, 43:581–606.

Kielan-Jaworowska, Z., Cifelli, R.L. and Luo, Z.-X. 2004. *Mammals from the Age of Dinosaurs: Origins, Evolution, and Structure*. Columbia University Press, New York. 630 pp.

Kielan-Jaworowska, Z. and Hurum, J.H. 2006. Limb posture in early mammals: sprawling or parasagittal. *Acta Palaeontologica Polonica*, 51.3.

Kindahl, M. 1949. The embryonic development of the hand and foot of *Eremitalpa* (*chrysochloris*) *granti* (Broom). *Acta Zoologica*, 30:133–152.

Kitching, I.J., Forey, P.L., Williams, D. and Humphries, C., 1998. Cladistics: the theory and practice of parsimony analysis. Oxford University Press, USA. 252 pp.

Kirk, E.C., Lemelin, P., Hamrick, M.W., Boyer, D.M. and Bloch, J.I. 2008. Intrinsic hand proportions of euarchontans and other mammals: implications for the locomotor behavior of plesiadapiforms. *Journal of human evolution*, 55:278–299.

Kleiber, M. 1932. Body size and metabolism. *Hilgardia*, 6:315–353.

Komsta, L., and Novomestky, F. 2015. moments: Moments, cumulants, skewness, kurtosis and related tests. https://cran.r-project.org/web/packages/moments/index.html

Körtner, G., and Geiser, F. 2000. Torpor and activity patterns in free-ranging sugar gliders *Petaurus breviceps* (Marsupialia). *Oecologia*, 123:350–357.

Kowallis, B.J., Christiansen, E.H., Deino, A.L., Peterson, F., Turner, C.E., Kunk, M.J. and Obradovich, J.D. 1998. The age of the Morrison Formation. *Modern Geology*, 22:235–260.

Krause, D.W. 1986. Competitive exclusion and taxonomic displacement in the fossil record; the case of rodents and multituberculates in North America. *Rocky Mountain Geology*, 24:95–117.

Krebs, B. 1991. Das Skelett von *Henkelotherium guimarotae* gen. et sp. nov. (Eupantotheria, Mammalia) aus dem Oberen Jura von Portugal. *Selbstverlag Fachbereich Geowissenschaften*, 133, FU Berlin.

Kretzoi, M. 1946. On Docodonta, a new order of Jurassic Mammals. *Anneles Historico-Naturales Musei Nationalis Hungarici*, 39:108–111.

Krusat, G. 1980. Contribuição para o conhecimento da fauna do Kimeridgiano da mina de lignito Guimarota (Leiria, Portugal). IV Parte. *Haldanodon exspectatus* Kühne & Krusat 1972 (Mammalia, Docodonta). *Memórias dos Serviços Geológicos de Portugal*, 27, 1–79.

Kubo, T., Sakamoto, M., Meade, A. and Venditti, C. 2019. Transitions between foot postures are associated with elevated rates of body size evolution in mammals. *Proceedings of the National Academy of Sciences*, p.201814329.

Kühne, W.G. 1956. The liassic therapsid *Oligokyphus*. British Museum (Natural History), London, 149 pp.

Kühne, W.G. and Krusat, G. 1972. Legalisierung des taxon *Haldanodon* (Mammalia, Docodonta). *Neues Jahrbuch für Geologie Monatshefte*, 300–302

Kuhn, H.J. and Zeller, U. 1987. The cavum epiptericum in monotremes and therian mammals. *Mammalia Depicta*, 13:51–70.

Lackey, J.A. 1996. *Chaetodipus fallax*. *Mammalian Species*, 517:1–6.

Ladevèze, S. and De Muizon, C. 2007. The auditory region of early Paleocene Pucadelphydae (Mammalia, Metatheria) from Tiupampa, Bolivia, with phylogenetic implications. *Palaeontology*, 50:1123–1154.

Ladevèze, S. 2010. Evidence of early evolution of Australidelphia (Metatheria, Mammalia) in South America: phylogenetic relationships of the metatherians from the Late Palaeocene of Itabora'ı (Brazil) based on teeth and petrosal bones. *Zoological Journal of the Linnean Society*, 159:746–784.

Larivière, S. 1999. *Mustela vison*. Mammalian Species, 608:1–9.

Lautenschlager, S., Gill, P., Luo, Z.-X., Fagen, M.J. and Rayfield, E.J. 2017. Morphological evolution of the mammalian jaw adductor complex. *Biological Reviews*, 92:1910–1940.

Lautenschlager, S., Gill, P., Luo, Z.-X., Fagan, M.J. and Rayfield, E.J. 2018. The role of miniaturisation in the evolution of the mammalian jaw. *Nature*, 561:533–537.

Lessertisseur, J. and Saban, R. 1967. Squelette appendiculaire. P709–1078. In: Grassé, P.-P. (ed). Traité de Zoologie. Tome XVI (Fascicle I). Mammiferes: Teguments et Skelettes. Masson, Paris.

Lewis, O.J. 1983. The evolutionary emergence and refinement of the mammalian pattern of foot architecture. *Journal of Anatomy*, 137:21–45.

Lewis, G.E. 1986. *Nearctylodon broomi*, the first Nearctic tritylodont. P295–303. In Hotton, N., Maclean, P.D., Roth, J.J. and Roth, E.C. (eds). *The Ecology and Biology of Mammal-like Reptiles*. Smithsonian Institution Press, Washington, D.C. 326 pp.

Lillegraven, J.A. and Hahn, G. 1993. Evolutionary analysis of the middle and inner ear of Late Jurassic multituberculates. *Journal of Mammalian Evolution*, 1:47–74.

Lillegraven, J.A. and Krusat, G. 1991. Cranio-mandibular anatomy of *Haldanodon exspectatus* (Docodonta; Mammalia) from the Late Jurassic of Portugal and its implications to the evolution of mammalian characters. *Contributions to Geology, University of Wyoming*, 28:39–138.

Lindstedt, S.L., Miller, B.J., and Buskirk, S.W. 1986. Home range, time and body size in mammals. *Ecology*, 67:413–418.

Linnaeus, C. 1758. Systema naturae per regna tria naturae: secundum classes, ordines, genera, species, cum characteribus, differentiis, synonymis, locis, 824 pp. Tenth edition. Laurentius Salvius, Stockholm.

Linzey, A.V. 1983. *Synaptomys cooperi*. Mammalian Species, 210:1–5.

Lopatin, A.V. and Averianov, A.O. 2005. A new docodont (Docodonta, Mammalia from the Middle Jurassic of Siberia. *Doklady Biological Sciences*, 405:434–436.

Lopatin, A.V. and Agadjanian, A.K. 2008. A tritylodont (Tritylodontidae, Synapsida) from the Mesozoic of Yakutia. *Doklady Biological Sciences*, 419:107–110.

Lopatin, A.V., Maschenko, E.N. and Leschchinskiy, S.V. 2009. Early Cretaceous mammals of Western Siberia: 2. Tegotheriidae. *Paleontological Journal*, 43:453–462.

Luo, Z.-X. 1994. Sister taxon relationships of mammals and the transformation of the diagnostic mammalian characters. P98–128. In Fraser, N. C. and Sues, H.-D. (eds). *In the Shadow of Dinosaurs: Early Mesozoic Tetrapods*. Cambridge University Press, Cambridge, U.K. 429 pp.

Luo, Z.-X. 2001. Inner ear and its bony housing in tritylodonts and implications for evolution of mammalian ear. *Bulletin of Museum of Comparative Zoology*, 156:81–97.

Luo, Z.-X. 2007. Transformation and diversification in early mammal evolution. *Nature*, 450:1011–1019.

Luo, Z.-X. 2011. Developmental patterns in Mesozoic evolution of mammal ears. *Annual Review of Ecology, Evolution and Systematics*, 42:355–380.

Luo, Z.X., 2015. Origin of the mammalian shoulder. P167-187. In *Great Transformations: Major Events in the History of Vertebrate Life.* The University of Chicago Press, Chicago, Illinois. 424 pp.

Luo, Z.-X. and Martin, T. 2007. Analysis of molar structure and phylogeny of docodontan genera. *Bulletin of Carnegie Museum of Natural History*, 39:27–47.

Luo, Z.-X., and Sun, A. 1994. *Oligokyphus* (Cynodontia: Tritylodontidae) from the Lower Lufeng Formation (Lower Jurassic) of Yunnan, China. *Journal of Vertebrate Paleontology*, 13:477–482.

Luo, Z.-X., and Sun, A. 2001. A new mammaliaform from the Early Jurassic of China and evolution of mammalian characteristics. *Science*, 292:1535–1540.

Luo, Z.-X. and Wu, X.-C. 1994. The small tetrapods of the lower Lufeng Formation, Yunnan, China. P251–270. In Fraser, N.C. and Sues, H. (eds). *In the Shadow of the Dinosaurs: early Mesozoic tetrapods*. Cambridge University Press, Cambridge. 429 pp.

Luo, Z.-X. and Wible, J.R. 2005. A Late Jurassic digging mammal and early mammalian diversification. *Science*, 308:103–107.

Luo, Z.-X., Crompton, A.W. and Lucas, S.G. 1995. Evolutionary origins of the mammalian promontorium and cochlea. *Journal of Vertebrate Paleontology*, 15:113–121.

Luo, Z.-X. Crompton, A.W. and Sun, A.-L. 2001. A new mammaliaform from the early Jurassic and evolution of mammalian characteristics. *Science*, 292:1535–1540.

Luo, Z.-X., Kielan-Jaworowska, Z. and Cifelli, R.L. 2002. In quest for a phylogeny of Mesozoic Mammals. *Acta Palaeontologica Polonica*, 47:1–78.

Luo, Z.-X., Ji, Q., Wible, J.R. and Yuan, C.X. 2003. An Early Cretaceous tribosphenic mammal and metatherian evolution. *Science*, 302:1934–1940.

Luo, Z.-X. Kielen-Jaworowska, Z. and Cifelli, R.L. 2004. Evolution of dental replacement in mammals. *Bulletin of the Carnegie Museum of Natural History*, 36:159–175.

Luo, Z-X., Ji, Q., Yuan, C-X. 2007. Convergent dental adaptations in pseudo-tribosphenic and tribosphenic mammals. *Nature Letters*, 450:93–97.

Luo, Z.-X., Ruf, I. and Martin, T. 2012. The petrosal and inner ear of the Late Jurassic cladotherian mammal *Dryolestes leiriensis* and implications for ear evolution in therian mammals. *Zoological Journal of the Linnean Society*, 166:433–463.

Luo, Z.-X., Schultz, J.A. and Martin, T. 2011. Fossil evidence on the evolution of inner ear cochlea in Jurassic mammals. *Proceedings of the Royal Society B*, 278:28–34.

Luo, Z.-X., Gatesay, S.M., Jenkins, F.A., Amaral, A.A. and Shubin, N.H. 2015a. Mandibular and dental characteristics of Late Triassic mammaliaform *Haramiyavia*

and their ramifications for basal mammal evolution. *Proceedings of the National Academy of Sciences*, 112:E7101–E7109.

Luo, Z.-X., Meng, Q.-J., Ji, Q., Liu, D., Zhang, Y.-G. and Neander, A. I. 2015b. Evolutionary development in basal mammaliaforms as revealed by a docodontan. Science, 347, 760–764.

Luo, Z.-X., Schultz, J.A. and Ekdale, E.G. 2016. Evolution of the middle and inner ears of mammaliaforms: the approach to mammals. P139–174. In Clack, J.A., Fay, R.R. and Popper, A.N. (eds). *Evolution of the vertebrate ear*. Springer International Publishing, 355 pp.

Luo, Z.-X. Meng, Q.-J., Liu, D., Y-G. Zhang, and Yuan, C.-X. 2016. Cruro-pedal structure of the paulchoffatiid multituberculate *Rugosodon eurasiaticus* and evolution of the multituberculate ankle. *Palaeontologia Polonica*, 67:149–169.

Luo, Z.-X., Q.-J., Meng, D. M. Grossnickle, D. Liu, Y.-G. Zhang, A. I. Neander, and Q. Ji. 2017. New evidence for mammaliaform ear evolution and feeding adaptation in a Jurassic ecosystem. *Nature*, 548:326–329.

Marsh, O.C. 1880. Notice on Jurassic mammals representing two new orders. *American Journal of Science*, 20:235–239

Marsh, O.C. 1887 American Jurassic Mammals. *American Journal of Science*, 33:326–348.

Marshall, P. 2003. Ichnofossils of the *Psilonichnus* Ichnofacies and their paleoecological and paleoenvironmental significance in the Scottish Middle Jurassic. *Ichnos*, 9:pp.95–108.

Martin, T. 1999. Dryolestidae (Dryolestoidea, Mammalia) aus dem Oberen Jura von Portugal. *Abhandlungen der senckenbergischen naturforschenden Gesellschaft*, 550:1–119.

Martin, T. 2001. Mammalian fauna of the Late Jurassic Guimarota ecosystem. *Publicación Electrónica de la Asociación Paleontológica Argentina*, 7.1.

Martin, T. 2002. New stem-lineage representatives of Zatheria (Mammalia) from the Late Jurassic of Portugal. *Journal of Vertebrate Paleontology*, 22:332–348.

Martin, T. 2005. Postcranial anatomy of *Haldanodon exspectatus* (Mammalia, Docodonta) from the Late Jurassic (Kimmeridgian) of Portugal and its bearing for mammalian evolution. *Zoological Journal of the Linnean Society*, 145:219–248.

Martin, T. 2018. Mesozoic mammals—early mammalian diversity and ecomorphological adaptations. P199–299. In Zachos, E. and Asher, R. (eds). *Handbook of Zoology: Mammalian Evolution, Diversity and Systematics*, DeGruyter, Berlin. 381 pp.

Martin, T. and Krebs, B. 2000. (eds). *Guimarota: A Jurassic Ecosystem*. Pfeil, Munich, 91–96 pp.

Martin, T., Nowotny, M. 2000. The docodont Haldanodon from the Guimarota mine. P91-96. In Martin, T. and Krebs, B. (eds). *Guimarota: A Jurassic Ecosystem*. Pfeil, Munich, 91–96 pp.

Martin, T. and Averianov, A.O. 2004. A new docodont (Mammalia) from the Middle Jurassic of Kyrgyzstan, central Asia. *Journal of Vertebrate Paleontology*, 24:195–201.

Martin, T. Averianov, A.O. and Pfretzschner, H.-U. 2010. Mammals from the Late Jurassic Qigu Formation in the Southern Junggar Basin, Xinjiang, Northwest China. *Palaeobiodiversity and Palaeoenvironment*, 90:295–319.

Martin, T., M. Nowotny, and M. Fischer. 2010. New data on tooth replacement in the Late Jurassic docodont mammal *Haldanodon exspectatus*. Society of Vertebrate Paleontology 70th Annual Meeting, Program and Abstracts:130A.

Martin-Silverstone, E.G. and Barrett, P.M. 2018. A three-dimensionally preserved Middle Jurassic monofenestratan pterosaur from the Isle of Skye, Scotland. Abstracts of the Palaeontological Association Annual Meeting, Bristol, UK.

Maschenko, E.N., Lopatin, A.V. and Voronkevich, A.V. 2002. A new genus of the tegotheriid docodonts (Docodonta, Tegotheriidae) from the Early Cretaceous of West Siberia. *Russian Journal of Theriology*, 1:75–81.

Matsuoka, H. and T. Setoguchi. 2000. Significance of Chinese tritylodonts (Synapsida, Cynodontia) for the systematic study of Japanese materials from the Lower Cretaceous Kuwajima Formation, Tetori Group of Shiramine Ishikawa, Japan. *Asian Paleoprimatology*, 1:161–176.

Matsuoka, H., Kusuhashi, N. and Corfe, I.J. 2016. A new Early Cretaceous tritylodontid (Synapsida, Cynodontia, Mammaliamorpha) from the Kuwajima Formation (Tetori Group) of Central Japan. *Journal of Vertebrate Paleontology*, 36:p.e1112289.

Maisch, M.W., Matzke, A.T. and Sun, G. 2004. A new tritylodontid from the Upper Jurassic Shishugou Formation of the Junggar Basin (Xingjiang, NW China). *Journal of Vertebrate Paleontology*, 24:649–656.

McKenna, M.C. 1975. Toward a phylogenetic classification of the Mammalia. P21–43. In Luckett, W.P. and Szalay, F.S. (eds). *Phylogeny of the primates*. Plenum Publishing Corporation, New York. 483 pp.

McKenna, M.C. and Bell, S.K. 1997. Classification of mammals above the species level. Columbia University Press, 640 pp.

Meachen-Samuels, J. 2010. Comparative scaling of humeral cross-sections of felids and canids using radiographic images. *Journal of Mammalian Evolution*, 17:193–209.

Mellere, D. and Steel, R.J. 1996. Tidal sedimentation in Inner Hebrides half grabens, Scotland: The Mid-Jurassic Bearreraig Sandstone Formation. P49–79. In DeBatist, M. and Jacobs, P. (eds). *Geology of Siliciclastic Shelf Seas*. Geological Society, London, Special Publications, 117 pp.

Meng, J., Y.-Q. Wang, and C. Li. 2011. Transitional mammalian middle ear from a new Cretaceous Jehol eutriconodont. *Nature*, 472:181–185.

Meng, Q.-J., Ji, Q., Zhang, Y.-G., Liu, D., Grossnickle, D.M. and Luo, Z.-X. 2015. An arboreal docodont from the Jurassic and mammaliaform ecological diversification. *Science*, 347:764–768.

Meng, Q.-J., Grossnickle, D.M., Liu, D., Zhang, Y.G., Neander, A.I., Ji, Q. and Luo, Z.X., 2017. New gliding mammaliaforms from the Jurassic. *Nature*, 548:291–296.

Meredith, R.W., Westerman, M. and Springer, M.S., 2009. A phylogeny of Diprotodontia (Marsupialia) based on sequences for five nuclear genes. *Molecular Phylogenetics and Evolution*, 51:554–571.

Meredith, R.W., Janecka, J.E., Gatesy, J., Ryder, O.A., Fisher, C.A., Teeling, E.C., Goodbla, A., Eizirik, E., Simão, T.L., Stadler, T. and Rabosky, D.L. 2011. Impacts of the Cretaceous Terrestrial Revolution and KPg extinction on mammal diversification. *Science*, 334:521–524.

Metcalf, S.J., Vaughan, R.F., Benton, M.J., Cole, J., Simms, M.J. and Dartnall, D.L. 1992. A new Bathonian (Middle Jurassic) microvertebrate site, within the Chipping Norton Limestone Formation at Hornsleasow Quarry, Gloucestershire. *Proceedings of the Geologists' Association*, 103:321–342.

Miao, D. 1988. Skull morphology of *Lambdopsalis bulla* (Mammalia, Multituberculata) and its implications to mammalian evolution. *Contributions to Geology, University of Wyoming, Special Papers 4*, 26:1–104.

Mills, J.R.E. 1971. The dentition of *Morganucodon*. P29–63. In Kermack, K.A. and Kermack, D.M. (eds). *Early mammals*. Academic Press. 203 pp.

Morton, N. 1987. Jurassic subsidence history in the Hebrides, NW Scotland. *Marine and Petroleum Geology*, 4:226–242.

Morton, N., and J.D. Hudson. 1995. Field guide to the Jurassic of the Isles of Raasay and Skye, Inner Hebrides, NW Scotland. P209–280. In Taylor, P.D. (ed). *Field Geology of the British Jurassic*. Geological Society, London.

Newham, E., Benson, R., Upchurch, P., and Goswami, A. 2014. Mesozoic mammaliaform diversity: the effect of sampling corrections on reconstructions of evolutionary dynamics. *Palaeogeography, Palaeoclimatology, Palaeoecology*, 412:32–44.

Newham, E., Gill, P., Brewer, P., Schneider, P., Gostling, N. and Corfe, I. 2018. Life history partitioning follows phylogeny amongst Middle Jurassic mammaliaforms. Abstracts of the 13th Symposium on Mesozoic Terrestrial Ecosystems, Bonn, Germany.

Novaceck, M.J. and Wyss, J. 1986. Origin and transformation of the mammalian stapes. *Contributions to Geology University of Wyoming Special Paper*, 3:35–53.

Nowak, R. 1999. *Walker's mammals of the world*, 6th Edition. Johns Hopkins University Press, Baltimore. 2015 pp.

Nowotny, M., T. Martin, and M.S. Fischer. 2001. Dental anatomy and tooth replacement of *Haldanodon exspectatus* (Docodonta, Mammalia) from the Upper Jura of Portugal. *Journal of Morphology*, 248:268.

Nunome, M., Yasuda, S.P., Sato, J.J., Vogel, P. and Suzuki, H. 2007. Phylogenetic relationships and divergence times among dormice (Rodentia, Gliridae) based on three nuclear genes. *Zoologica Scripta*, 36:537-546.

Nyakatura, J.A., Fischer, M.S. and Schmidt, M. 2008. Gait parameter adjustments of cotton-top tamarins (*Saguinus oedipus*, Callitrichidae) to locomotion on inclined arboreal substrates. *American Journal of Physical Anthropology*, 135:13–26.

O'leary, M.A., Bloch, J.I., Flynn, J.J., Gaudin, T.J., Giallombardo, A., Giannini, N.P., Goldberg, S.L., Kraatz, B.P., Luo, Z.X., Meng, J. and Ni, X., 2013. The placental mammal ancestor and the post–K-Pg radiation of placentals. *Science*, 339:662–667.

Olson, L.E., Sargis, E.J. and Martin, R.D. 2004. Phylogenetic relationships among treeshrews (Scandentia): a review and critique of the morphological evidence. *Journal of Mammalian Evolution*, 11:49–71.

O' Meara, R.N. and Asher, R.J. 2016. The evolution of growth patterns in mammalian versus nonmammalian cynodonts. *Paleobiology*, 42:439–464.

Opazo, J.C. 2005. A molecular timescale for caviomorph rodents (Mammalia, Hystricognathi). *Molecular phylogenetics and evolution*, 37:932–937.

Osborn, H.F. 1903. The reptilian subclasses Diapsida and Synapsida and the early history of the Diaptosauria. *Memoirs of the American Museum of Natural History*, 1:449–507.

Owen, R. 1846. *History of British Fossil Mammals and Birds*. John Van Voorst, London. 560 pp.

Owen, R. 1857. On the affinity of *Stereognathus ooliticus* (Charlesworth) a mammal from the Oolitic slate of Stonesfield. *Quarterly Journal of the Geological Society of London*, 13:1–11.

Owen, R. 1861. *Palaeontology, or a Systematic Summary of Extinct Animals and their Geological Relations*, 2nd edition. Adam and Black, Edinburgh. 163 pp.

Owen, R. 1884. On the skull and dentition of a Triassic mammal (*Tritylodon longaevus*) from South Africa. *Quarterly Journal of the Geological Society of London* 40:146–152.

Pacey, D. 1978. On a tetrapod assemblage from a Mesozoic fissure fill, South Wales. Unpublished PhD thesis, University College London. 273 pp.

Panciroli, E., Janis, C., Stockdale, M. and Martín-Serra, A. 2017a. Correlates between calcaneal morphology and locomotion in extant and extinct carnivorous mammals. *Journal of Morphology*, 278:1333–1353.

Panciroli, E., Benson, R.B.J. and Walsh, S. 2017b. The dentary of *Wareolestes rex* (Megazostrodontidae): a new specimen from Scotland and implications for morganucodontan tooth replacement. *Papers in Palaeontology*, 3:373–386.

Panciroli, E., Benson, R.B.J. and Walsh, S. 2017c. Data from: The dentary of *Wareolestes rex* (Megazostrodontidae): a new specimen from Scotland and implications for

morganucodontan tooth replacement. Dryad Digital Repository. https://doi.org/10.5061/dryad.5n36j

Panciroli, E., Walsh, S., Fraser, N., Brusatte, S.L. and Corfe, I. 2017d. A reassessment of the postcanine dentition and systematics of the tritylodontid *Stereognathus* (Cynodontia, Tritylodontidae, Mammaliamorpha), from the Middle Jurassic of the UK. *Journal of Vertebrate Paleontology*, 37:1351448.

Panciroli E., Benson, R.B.J. and Butler R.J. 2018a. New partial dentaries of *Palaeoxonodon ooliticus* (Mammalia, Amphitheriidae) from Scotland, and posterior dentary morphology in stem cladotherians. *Acta Paleontologica Polonica*, 63:197–206.

Panciroli, E., Schultz, J.A. and Luo, Z.-X. 2018b. Morphology of the petrosal and stapes of *Borealestes* (Mammaliaformes, Docodonta) from the Middle Jurassic of Skye, Scotland. *Papers in Palaeontology*, 5:139–156

Panciroli, E., Schultz, J.A. and Luo, Z.-X. 2018c. Data from: Morphology of the petrosal and stapes of *Borealestes* (Mammaliaformes, Docodonta) from the Middle Jurassic of Skye, Scotland. Dryad Digital Repository. https://doi.org/10.5061/dryad.07934k0

Panciroli, E.P., Benson, R.B.J., and Walsh, S. 2018d. The Mammal-Rich Freshwater Assemblage of the Middle Jurassic Kilmaluag Formation, Isle of Skye, Scotland. Abstracts of the 13th Symposium on Mesozoic Terrestrial Ecosystems, Bonn, Germany.

Panciroli, E., Benson, R.B.J. and Luo, Z.-X. 2019. The mandible and dentition of *Borealestes serendipitus* (Docodonta) from the Middle Jurassic of Skye, Scotland. *Journal of Vertebrate Paleontology*, 39, p.e1621884.

Parraga, J., Bernard, E., Brewer, P. and Ward, D.J. 2016. A diverse new late Bathonian microvertebrate microvertebrate assemblage from Woodeaton Quarry, Oxfordshire, UK. *Journal of Vertebrate Paleontology* (Program and Abstracts), 36:202.

Parrington, F.R. 1967. The origins of mammals. *Advancements in Science*, 24:165–173.

Parrington, F.R. 1971. On the upper Triassic mammals. *Philosophical Transactions of the Royal Society of London B*, 261:231–272.

Parrington, F.R. 1973. The dentitions of the earliest mammals. *Zoological Journal of the Linnean Society*, 52:85–95.

Pretzschner, H.-U., Martin, T., Maisch, M., Matze, A. and Sun, G. 2005. A new docodont from the Late Jurassic of the Junggar Basin of northwest China. *Acta Palaeontologica Polonica*, 50:799–808.

Price, S.A. and Hopkins, S.S.B. 2015. The macroevolutionary relationship between diet and body mass across mammals. *Biological Journal of the Linnean Society*, 115:173–184.

Pridmore, P.1985. Terrestrial locomotion in monotremes (Mammalia: Monotremata). *Journal of Zoology*, 205:53–73.

Polly, P.D. and Macleod, N. 2008. Locomotion in fossil Carnivora: An application of eigensurface analysis for morphometric comparison of 3D surfaces. *Palaeontologia Electronica*, 11:10–13.

Polly, P.D. 2007. Limbs in mammalian evolution. P245–268. In Hall, B.K. (ed). *Fins into limbs: Evolution, development, and transformation*. University of Chicago Press, Chicago, Illinois. 344 pp.

Polly, P.D. 2010. Tiptoeing through the trophics: Measuring digitigrady in Carnivora for palaeoenvironmental inference. P374–410. In Goswami, A. and Friscia, A. (eds). *Carnivoran evolution: New views of phylogeny, form and function*. Cambridge University Press, Cambridge. 523 pp.

Prasad, G.V.R. and Manhas, B.K. 2001. First docodont mammals of Laurasian affinities from India. *Current Science*, 81:1235–1238.

Prasad, G.R. and Manhas, B.K. 2002. Triconodont mammals from the Jurassic Kota Formation of India. *Geodiversitas*, 24:445–464.

Prasad, G.R. Verma, O. and Parmar, V. 2006. An overview of the Mesozoic mammalian fauna of India. P101–104. In Barrett, P.M. and Evans, S.E. (eds). *Ninth International Symposium on Mesozoic Terrestrial Ecosystems and Biota*. Natural History Museum Publications, London. 187 pp.

Prasad, G.R. 2007. A new docodont mammal from the Jurassic Kota Formation of India. *Palaeontologia Electronica*, 10:7A.

Prothero, D.R. 1981. New Jurassic mammals from the Como Bluff, Wyoming, and the interrelationships of non-tribosphenic theria. *Bulletin of the American Museum of Natural History*, 176:281–168.

R Core Team. 2013. R: A language and environment for statistical computing. R Foundation for Statistical Computing, Vienna, Austria.

Rees, J. and Underwood, C.J. 2005. Hybodont sharks from the Middle Jurassic of the Inner Hebrides, Scotland. *Earth and Environmental Science Transactions of the Royal Society of Edinburgh*, 96:351–363.

Rensch, B. 1948. Histological changes correlated with evolutionary changes of body size. *Evolution*, 2:218–230.

Riding, J.B. and Wright J.K. 1989. Palynostratigraphy of the Scalby Formation (Middle Jurassic) of the Cleveland Basin, north-east Yorkshire. *Proceedings of the Yorkshire Geological Society*, 47:349–354.

Riding, JB, Walton, W. and Shaw, D. 1991. Toarcian to Bathonian (Jurassic Palynology of the Inner Herides, Northwest Scotland. *Palynology*, 15:115–179.

Ross, F.C, Iriarte-Diaz, J. and Nunn, C.L. 2012. Innovative approaches to the relationship between diet and mandibular morphology in primates. *International Journal of Primatology*, 33:632–660.

Ross, C.F., and Iriarte-Diaz, J. 2014. What does feeding system morphology tell us about feeding? *Evolutionary Anthropology*, 23:105–120.

Rougier, G.W. and Wible, J.R. 2006. Major changes in the ear region and basicranium of early mammals. P269–311. In Carrano, M.T., Gaudin, T.J., Blob, R.W. and Wible, J.R. (eds). *Amniote paleobiology: Phylogenetic and functional perspectives on the evolution of mammals, birds, and reptiles*. University of Chicago Press, Chicago, Illinois. 448 pp.

Rougier, G.W. and Hopson, J.A. 1992. Reconstruction of the cranial vessels in the Early Cretaceous mammal *Vincelestes neuquenianus*: implications for the evolution of the mammalian cranial vascular system. *Journal of Vertebrate Paleontology*, 12:188–216.

Rougier, G.W. 1996. Basicranial anatomy of *Priacodon fruitaensis* (Triconodontidae Mammalia) from the Late Jurassic of Colorado, and a reappraisal of mammaliaform interrelationships. *American Museum Novitates*, 3183:1–38.

Rougier, G.W., Martinelli, A.G., Forasiepi, A.M., Novacek, M.J. 2007. New Jurassic mammals from Patagonia, Argentina: a reappraisal of australosphenidan morphology and interrelationship. *American Museum Novitates*, 3566:1–54

Rougier, G.W., Sheth, A.S., Carpenter, K., Appella-Guisafre, L. and Davis, B.M. 2015. A new species of *Docodon* (Mammaliaformes, Docodonta) from the Upper Jurassic Morrison Formation and a reassessment of selected craniodental characters in basal mammaliaforms. *Journal of Mammalian Evolution*, 22:1–16.

Rowe, T. 1988. Definition, diagnosis and origin of Mammalia. *Journal of Vertebrate Paleontology*, 8:241–264.

Rowe, T.B. 1993. Phylogenetic systematics and the early history of mammals. P129–145. In Szalay, F.S., Novacek, M.J., and McKenna, M.C. (eds). *Mammal Phylogeny: Mesozoic Differentiation, Multituberculates, Monotremes, Early Therians, and Marsupials*. Springer, New York. 249 pp.

Rowe, T., Rich, T.H., Vickers-Rich, P., Springer, M. and Woodburne, M.O. 2008. The oldest platypus and its bearing on divergence timing of the platypus and echidna clades. *Proceedings of the National Academy of Sciences*, 105:1238–1242.

Ruf, I., Luo, Z.-X., Wible, J.R. and Martin, T. 2009. Petrosal anatomy and inner ear structures of the Late Jurassic *Henkelotherium* (Mammalia, Cladotheria, Dryolestoidea): insight into the early evolution of the ear region in cladotherian mammal. *Journal of Anatomy*, 214:679–693.

Ruf, I., Luo, Z.-X. and Martin, T. 2013. Reinvestigation of the basicranium of *Haldanodon exspectatus* (Mammaliaformes, Docodonta). *Journal of Vertebrate Paleontology*, 33:382–400.

Ruta, M., Botha-Brink, J., Mitchell, A. and Benton, M.J. 2013. The radiation of cynodonts and the ground plan of mammalian morphological diversity. *Proceedings of the Royal Society B Biological Sciences*, 280:20131865.

Samuels, J.X. and Van Valkenburgh, B. 2008. Skeletal indicators of locomotor adaptations in living and extinct rodents. *Journal of Morphology*, 269:13871411.

Samuels, J.X., Meachen, J.A. and Sakai, S.A. 2013. Postcranial morphology and the locomotor habits of living and extinct carnivorans. *Journal of Morphology*, 274, 121–146.

Sanchez-Villagra, M.R. and Nummela, S. 2001. Bullate stapes in some phalangeriform marsupials. *Mammalian Biology*, 66:174–177.

Santana, S.E., Grosse, I.R. and Dumont, E.R. 2012. Dietary hardness, loading behavior, and the evolution of skull form in bats. *Evolution: International Journal of Organic Evolution*, 66:2587–2598.

Sargis, E.J. 2001. The grasping behaviour, locomotion and substrate use of the tree shrews *Tupaia minor* and *T. tana* (Mammalia, Scandentia). *Journal of Zoology*, 253:485–490.

Savage, R.J.G. 1984. Mid Jurassic mammals from Scotland. P211–213. In Reif, W.E. and Westphal, F. (eds). Third Symposium on Mesozoic Terrestrial Ecosystems, Attempto, Tübingen.

Schudack, M.E. 2000. Geological setting and dating of the Guimarota-beds. P21–26. In Martin, T. and Krebs, B (eds). *Guimarota A Jurassic Ecosystem*. Verlag, Munich, Germany. 156 pp.

Schultz, J.A., Bhullar, B.A.S. and Luo, Z.-X., 2017a. Re-examination of the Jurassic mammaliaform *Docodon victor* by computed tomography and occlusal functional analysis. *Journal of Mammalian Evolution*, 26:9–38.

Schultz, J.A., Zeller, U. and Luo, Z.-X. 2017b. Inner ear labyrinth anatomy of monotremes and implications for mammalian inner ear evolution. *Journal of Morphology*, 278:236–263.

Schultz, J.A., Ruf, I. and Martin, T. 2018. Oldest known multituberculate stapes suggests an asymmetric bicrural pattern as ancestral for Multituberculata. *Proceedings of the Royal Society B*, 285:20172779.

Schutz, H. and Guralnick, R.P. 2007. Locomotor mode in extant and extinct mustelid carnivorans. *Zoological Journal of Linnean Society London*, 150:895–914.

Seebeck, J.H. 2001. *Perameles gunnii*. P1–8. In *Mammalian Species*, No. 654. American Society of Mammalogists.

Setoguchi, T., Matsuda, M. and Matsuoka, H. 1999. New discovery of an Early Cretaceous tritylodontid (Reptilia, Therapsida) from Japan and the phylogenetic reconstruction of Tritylodontidae based on the dental characters. P117–124. In Wang, Y.Q. and Deng, T. (eds). *Proceedings of the Seventh Annual Meeting of the Chinese Society for Vertebrate Paleontology*. China Ocean Press, Beijing.

Sigogneau-Russell, D. 1983. A new therian mammal from the Rhaetic locality of Saint-Nicolar-de-Port (France). *Zoological Journal of the Linnean Society*, 78:175–186.

Sigogneau-Russell, D. 1998. Discovery of a Late Jurassic Chinese mammal in the upper Bathonian of England. *Comptes Rendus de L'Acad'emie des sciences-Series IIA*, 327:571–576.

Sigogneau-Russell, D. 1999. Réévaluation des Peramura (Mammalia, Cladotheria) sur la base de nouveaux spécimens du Crétacé inférieur d'Angleterre et du Maroc. *Geodiversitas* 21:93–127.

Sigogneau-Russell, D. 2003. Holotherian mammals from the Forest Marble (Middle Jurassic of England). *Geodiversitas*, 25:501–537.

Sigogneau-Russell, D. 2003. Docodonts from the British Mesozoic. *Acta Palaeontologica Polonica*, 48:357–374.

Sigogneau-Russell, D. and Hahn, R. 1995. Reassessment of the Late Triassic symmetrodont mammal *Woutersia*. *Acta Palaeontologica Polonica*, 40:245–260.

Simpson, G.G. 1928. *A Catalogue of the Mesozoic Mammalia in the Geological Department of the British Museum.* British Museum (Natural History), London. 215 pp.

Simpson, G.G. 1929. American Mesozoic Mammalia. *Memoirs of the Peabody Museum of Yale University*, 3:1–235.

Slater, G.J. 2013. Phylogenetic evidence for a shift in the mode of mammalian body size evolution at the Cretaceous-Paleogene boundary. *Methods in Ecology and Evolution*, 4:734–744.

Smith, A. 1995. Leadbeater's Possum. P224-226. In Strahan, R. (ed). *Mammals of Australia*. Washington D.C.: Smithsonian Institution Press. 756 pp.

Smith, T. and Smith, R. 2010. A new genus of "Miacid" carnivoran from the earliest Eocene of Europe and North America. *Acta Palaeontologica Polonica*, 55:761–764.

Smith, F.A. and Lyons, S.K. 2011. How big should a mammal be? A macroecological look at mammalian body size over space and time. *Proceedings of Royal Society of London, Series B. Biological Sciences*, 366:2364–2378.

Smith, F.A., Lyons, S.K., Ernest, S.K.M., Jones, K.E., Kaufman, D.M., Dayan, T., Marquet, P.A., Brown, J.H. and Haskell. J.P. 2003. Body mass of late Quaternary mammals. *Ecology*, 84:3402,

Smith, A.T., Xie, Y., Hoffmann, R.S., Lunde, D., MacKinnon, J., Wilson, D.E. and Wozencraft W.C. 2010a. *A guide to the mammals of China*. Princeton University Press, Princeton. 576 pp.

Smith, F.A., Boyer, A.G., Brown, J.H., Costa, D.P., Dayan, T., Ernest, S.M., Evans, A.R., Fortelius, M., Gittleman, J.L., Hamilton, M.J. and Harding, L.E. 2010b. The evolution of maximum body size of terrestrial mammals. *Science*, 330:1216–1219.

Strait, S.G. 1993. Molar morphology and food texture among small-bodied insectivorous mammals. *Journal of Mammalogy*, 74:391–402.

Stein, B. 1988. Morphology and allometry in several genera of semiaquatic rodents (*Ondatra*, *Nectomys*, and *Oryzomys*). *Journal of Mammalogy*, 69:500–511

Steppan, S.J., Adkins, R.M. and Anderson, J. 2004. Phylogeny and divergence-date estimates of rapid radiations in muroid rodents based on multiple nuclear genes. *Systematic biology*, 53:533–553.

Strasser E. 1992. Hindlimb proportions, allometry, and biomechanics in Old World monkeys (Primates, Cercopithecidae). *American Journal of Physical Anthropology*, 87:187213.

Stucky, R.K. and McKenna, M.C. 1993. *Mammalia*.P739–771. In Benton, M.J. (ed). *The Fossil Record 2*. Springer, Netherlands. 846 pp.

Sues, H.D. 1985. First record of the tritylodontid *Oligokyphus* (Synapsida) from the Jurassic of western North America. *Journal of Vertebrate Paleontology*, 5:328–335.

Sues, H.D. 1986. *Dinnebitodon amarali*, a new tritylodontid (Synapsida) from the Lower Jurassic of western North America. *Journal of Paleontology*, 60:758–762.

Sues, H.D., and Jenkins Jr., F.A. 2006. The postcranial skeleton of *Kayentatherium wellesi* from the Lower Jurassic Kayenta Formation of Arizona and the phylogenetic significance of postcranial features in tritylodontid cynodonts. P114–152. In Carrano, M.T. (ed). *Amniote Paleobiology: Perspectives on the Evolution of Mammals, Birds, and Reptiles*. The University of Chicago Press, Chicago, Illinois. 448 pp.

Sullivan, C., Wang, Y., Hone, D.W.E., Wang, Y., Xu, X. and Shang, F. 2014. The vertebrates of the Jurassic Daohugou biota of Northeastern China. *Journal of Vertebrate Paleontology*, 34:243–280.

Swofford, D.L. 2003. PAUP*. Phylogenetic Analysis Using Parsimony (*and Other Methods). Version 4. Sinauer Associates, Sunderland, Massachusetts.

Szalay, F.S. 1985. Rodent and lagomorph morphotype adaptations, origins, and relationships: some postcranial attributes analyzed. P83–132. In Luckett, W.P., Hartenberger, J.P. (eds). *Evolutionary Relationships among Rodents*. Heidelberg Springer, Berlin. 722 pp.

Szalay, F.S. 1993. Pedal evolution of mammals in the Mesozoic: tests for taxic relationships. P108–128. In Szalay, F. S., Novacek, M.J. and McKenna, M.C. (eds). *Mammal phylogeny: Mesozoic differentiation, multituberculates, monotremes, early therians and marsupials.* Springer, New York. 249 pp.

Szalay, F.S. 1984. Arboreality: is it homologous between metatherian and eutherian mammals? *Evolutionary Biology*, 18:215–258.

Szalay, F.S. 1994. Evolutionary History of the Marsupials and an Analysis of Osteological Characters. Cambridge University Press, Cambridge. 496 pp.

Tatarinov, L.P. 1994. On an unusual mammalian tooth from the Mongolian Jurassic. *Paleontologicheskii Zhurnal*, 2:97-105.

Tatarinov, L.P. and Mashenko, E.N. 1999. A find of an aberrant tritylodont (Reptilia, Cynodontia) in the Lower Cretaceous of the Kemerovo Region. *Paleontologicheskii Zhurnal*, 33:422–428.

Taylor, C.R., Schmidt-Nielson, K. and Raab, J.L. 1970. Scaling of energetic cost of running to body size in mammals. *American Journal of Physiology-Legacy Content*, 219:1104–1107.

Therrien F. 2005. Mandibular force profiles of extant carnivorans and implications for the feeding behaviour of extinct predators. *Journal of Zoology*, 267:249–270.

Therrien, F., Quinney, A., Tanaka, K. and Zelenitsky, D.A. 2016. Accuracy of mandibular force profiles for bite force estimation and feeding behaviour reconstruction in extant and extinct carnivorans. *Journal of Experimental Biology*, 291:3738–3749

Turner, C.E. and Peterson, F. 2004. Reconstruction of the Upper Jurassic Morrison Formation extinct ecosystem—a synthesis. *Sedimentary Geology*, 167:309–355.

University of Michigan. 2014. *Animal Diversity Web*. https://animaldiversity.org/

van Staaden, M.J. 1994. *Suricata suricatta*. *Mammalian Species*, 483:1–8.

Van Valkenburgh, B. 1985. Locomotor diversity within past and present guilds of large predatory mammals. *Paleobiology*, 11:406–428.

Van Valkenburgh, B. 1987. Skeletal indicators of locomotor behavior in living and extinct carnivores. *Journal of Vertebrate Paleontology*, 7:162–182.

Velazco, P.M., Buczek, A.J. and Novacek, M.J. 2017. Two new tritylodontids (Synapsida, Cynodontia, Mammaliamorpha) from the Upper Jurassic, Southwestern Mongolia. *American Museum Novitates*, 3874:1–36.

Venables, W.N. and Ripley, B.D. 2002. *Modern Applied Statistics with S*, 4th Edition. Springer, New York. 498 pp.

Vianey-Liaud, M., Hautier, L. and Marivaux, L. 2015. Morphological disparity of the postcranial skeleton in rodents and its implications for paleobiological inferences: the case of the extinct Theridomyidae (Rodentia, Mammalia). P539–588. In Cox, F.G., Hautier, L. (eds). *Evolution of the rodents: advances in phylogenetics, functional morphology and development*. Cambridge University Press, Cambridge. 624 pp.

Voss, R.S. and Jansa, S.A., 2009. Phylogenetic relationships and classification of didelphid marsupials, an extant radiation of New World metatherian mammals. *Bulletin of the American Museum of Natural History*, 322:1-177.

Wakefield, M.I. 1995. Ostracod biostratinomy at lagoonal shorelines: examples from the Great Estuarine Group, Middle Jurassic, Scotland. *Proceedings of the Geologists' Association*, 106:211-218.

Waldman, M. and Savage, R.J.G. 1972. The first Jurassic mammal from Scotland. *Journal of the Geological Society of London*, 128:119–125.

Waldman, M, and Evans, E.E. 1994. Lepidosauromorph reptiles for the Middle Jurassic of Skye. *Zoological Journal of the Linnean Society*, 112:135–150.

Walker, E. 1968. *Mammals of the World*, 6th Edition. Johns Hopkins University Press, Baltimore. 2015 pp.

Watabe, M., Tsubamoto, T. and Tsogtbaatar, K. 2007. A new tritylodontid synapsid from Mongolia. *Acta Palaeontologica Polonica*, 52:263–274.

Weisbecker, V. and Wharton, D.I. 2006. Evidence at hand: diversity, functional implications, and locomotor prediction in intrinsic hand proportions of diprotodontian marsupials. *Journal of Morphology*, 267:1469–1485.

Weishampel, D.B., Dodson, P. and Osmolska, H. 2004. *The Dinosauria*, 2nd edition. University of California Press, Berkeley. 861 pp.

Western D. 1979. Size, life history and ecology in mammals. *African Journal of Ecology*, 17:185–204.

Wible, J.R. 1990. Petrosals of Late Cretaceous marsupials from North America and a cladistics analysis of the petrosal in therian mammals. *Journal Vertebrate Paleontology*, 10:183– 205.

Wible, J.R. and Hopson, J.A. 1993. Basicranial evidence for early mammal phylogeny. P45–62. In Szalay, F.S., Novacek, M.J. and McKenna, M.C. (eds). *Mammal phylogeny: Mesozoic differentiation, multituberculates, monotremes, early therians and marsupials.* Springer, New York. 249 pp.

Wible, J.R. 1995. The homologies of the prootic canal in mammals and non-mammalian cynodonts. *Journal of Vertebrate Paleontology*, 15:331–356.

Wilkinson, M. 2003. Missing entries and multiple trees: instability, relationships, and support in parsimony analysis. *Journal of Vertebrate Paleontology*, 23:311–323.

Williams, M., Benton, M.J. and Ross, A. 2015. The Strawberry Bank Lagerstätte reveals insights into Early Jurassic Life. *Journal of the Geological Society*, 172:683–692.

Wills, S., Barrett, P.M. and Walker, A. 2014. New dinosaur and crocodylomorph material from the Middle Jurassic (Bathonian) Kilmaluag Formation, Skye, Scotland. *Scottish Journal of Geology*, 50:183–190.

Wilson, D. and Reeder, D. 2005. *Phalanger gymnotis*. P46. In Wilson, D. and Reeder, D. (eds). *Mammal Species of the World*, Volume 1, 3rd Edition. The Johns Hopkins University Press, Baltimore, Maryland. 2142 pp

Wilson, G.P., Ekdale, E.G., Hoganson, J.W., Calede, J.J. and Vander Linden, A. 2016. A large carnivorous mammal from the Late Cretaceous and the North American origin of marsupials. *Nature Communications*, 7:13734.

Wilson, G.P., Evans, A.R., Corfe, I.J., Smits, P.D., Fortelius, M. and Jernvall, J. 2012. Adaptive radiation of multituberculate mammals before the extinction of dinosaurs. *Nature*, 483:457–460.

Wood, T. 2010. The Extinction of the Multituberculates Outside North America: a Global Approach to Testing the Competition Model. PhD thesis, The Ohio State University, USA.

Yeates, D. 1992. Why remove autapomorphies? *Cladistics*, 8:387–389.

Yensen, E. and T. Tarifa. 2003. *Galictis cuja*. *Mammalian Species*, 728:1–8.

Young, C.C. 1940. Preliminary notes on the Mesozoic mammals of Lufeng, Yunnan, China. *Bulletin of the Geological Society of China*, 20:93–111.

Young, C.C. 1947. Mammal-like reptiles from Lufeng, Yunnan, China. *Proceedings of the Zoological Society of London*, 117:537–597.

Young, C.C. 1978. New material of *Eozostrodon*. *Vertebrata PalAsiatica*, 16:1–3.

Young, C.C. 1982. On a *Bienotherium*-like tritylodont from Szechuan, China. P10–13. In Yang, Z. (ed). *Selected works of Yang Zhongjian*. Science Press, Beijing. [Chinese].

Young, C.C. 1982. Two primitive mammals from Lufeng, China. In Yang, Z. (ed). *Selected works of Yang Zhongjian*. Science Press, Beijing. [Chinese].

Xu, X., Zhou, Z.H., Sullivan, C., Wang, Y. and Ren, D. 2016. An updated review of the Middle-Jurassic Yanliao Biota: Chronology, Taphonomy, Paleontology, and Paleoecology. *Acta Geologica Sinica* (English Edition), 90:1801–1840.

Xu, X., Zhou, Z., Sullivan, C. and Wang, Y. 2017. The Yanliao Biota: a trove of exceptionally preserved Middle-Late Jurassic terrestrial life forms. P131–167. In NC Fraser and H-D Sues (eds) *Terrestrial Conservation Lagerstätten*. Dunedin Academic Press, London. 356 pp.

Zhang, F., Crompton, A.W., Luo, Z.-X. and Schaff, C.R. 1998. Pattern of dental replacement of *Sinoconodon* and its implications for evolution of mammals. *Vertebrata PalAsiatica*, 36:197–217.

Zheng, X.-T., Bi, S.-D., Wang, X.-L. and Meng, J. 2013. A new arboreal haramiyid shows the diversity of crown mammals in the Jurassic period. *Nature*, 500:199–202.

Zhou, C.F., Wu, S., Martin, T. and Luo, Z.-X. 2013. A Jurassic mammaliaform and the earliest mammalian evolutionary adaptations. *Nature*, 500:163–167.

Zhou, C.F., Bhullar, B.-A.S., Neander, A.I., Martin, T. and Luo, Z.-X. 2019. New Jurassic Mammaliaform sheds light on early evolution of mammal-like hyoid bones. *Nature*, 365:276–279.

APPENDICES

APPENDIX 1. Description of characters in phylogenetic analysis.

Characters and scorings are from Velazco et al. (2017), except for *Stereognathus*, which was rescored based on our updated morphological description. Characters are unordered. *Oligokyphus* is the outgroup.

(1) Snout: longer than postcanine tooth-row length (0); shorter than postcanine tooth row length (1).

(2) Postincisive constriction of the snout: present (0); absent (1).

(3) Anterior margin of orbit: directly dorsal to the distal margin of PC1 (0); above the anteroposterior midpoint of PC2 (1).

(4) Lacrimal size: large (0); reduced (1).

(5) Lacrimal foramina: absent (0); one (1); two (2).

(6) Anterior contact of lacrimal: premaxilla (0); maxilla (1).

(7) Premaxilla posterior extension on secondary palate: anteriorly (0); between incisors and the mesial cheek teeth (1); near the most mesial teeth (2).

(8) Contact between premaxilla and palatine on palate: absent (0); present (1).

(9) Premaxilla-maxillary: contact follows the mesiolingual shape of PC1 (0); contact occurs in the snout (1).

(10) Interdigitations on the maxillopalatine suture: absent (0); present (1).

(11) Interdigitations on the premaxillopalatine suture: absent (0); present (1).

(12) Maxilla presence on the hard palate: large and occupies most of the area of the palate (0); highly reduced, pre- served as a narrow band forming the lingual margins of the postcanine teeth (1).

(13) Palatine contact: anteriorly and laterally, the palatine is bordered by the maxilla and premaxilla (0); bordered only by the maxilla (1).

(14) Palatine contribution to the PC4 alveolus: present (0); absent (1).

(15) Greater palatine foramina: three (0); two (1); one (2); absent (3).

(16) Lateral (facial and zygomatic) extension of maxilla: present (0); reduced or absent (1).

(17) Zygomatic process of the maxilla: constitutes the ventral aspect of the anterior root of the zygomatic arch (0); consti- tutes the dorsal aspect of the anterior root of the zygomatic arch (1).

(18) Jugal contribution to the medial and inferior orbital walls: present (0); absent (1).

(19) Foramina on jugal above PC2: three foramina present (0); absent (1).

(20) Coronoid process height: very tall (0); short (1).

(21) Coronoid process anterior margin shape: gently curved anterior margin (0); straight anterior margin (1).

(22) Angle of the alveolar line and the anterior margin of the coronoid process: <900 (0); >900 (1); 900 (2).

(23) Upper postcanine alveolar tooth rows: diverge posteriorly (0); parallel (1).

(24) Upper postcanine teeth generalize cusp formula: 2–2-2 (0); 2–3-2 (1); 2–3-3 (2); 2–3-4 (3); 2–4-3 (4); 2–4-4 (5); 3–3-3 (6); 3–4-4 (7).

(25) Upper cheek tooth B0 cusp: present (0); absent (1).

(26) Upper cheek tooth M0 cusp: present (0); absent (1).

(27) Upper cheek tooth L0 cusp: present (0); absent (1).

(28) Upper cheek tooth M1 cusp: large (0); small (1); absent (2).

(29) Upper cheek tooth L1 cusp: large (0); small (1); absent (2).

(30) Upper cheek tooth L3 cusp: large (0); small (1); absent (2).

(31) Upper postcanine roots: four (0); five (1); six (2); seven (3).

(32) Upper postcanine teeth anterior median root: absent (0); present (1).

(33) Lower postcanine teeth generalize cusp formula: 2–2 (0); 3– 3 (1).

(34) Lower postcanine root number: one (0); two (1).

(35) Lower postcanine root length and curvature: long with the distal 2/3 curved (0); long and curved throughout its entire length (1); short and slightly curved (2).

APPENDIX 2. Character matrix used for phylogenetic analysis.

Polymorphisms are as follows: A (0, 2); B (2, 6); C (1, 0); D (2, 3)

Taxon	10	20	30	35
Bienotherium	1100111011	-011200???	??02111010	21?11
Bienotheroides	1110102100	1101A1????	??0BC11110	10000
Bocatherium	1100102100	110111???0	0210111220	?????
Dianzhongia	11????20??	?????0????	??11111001	3????
Dinnebitodon	11????21??	?1???1????	??01111002	?????
Kayentatherium	1100112001	-0?1200110	0002111010	??0??
Lufengia	11????20??	?????0????	???2111000	10?12
Montirictus	??????????	??????????	???0111220	20011
Oligokyphus	0000210011	-011300111	1107000000	21111
Polistodon	11?101????	?????000?1	01?0111220	??0??
Stereognathus	??????????	?1?1?1????	???0011110	D10?0
Tritylodon	00???10011	-011200??0	0212111000	11???
Xenocretosuchus	??????????	??????????	???0111220	??0??
Yunnanodon	11????????	??????????	???1111002	10?12
Yuanotherium	??????2100	11??101???	???4000011	?????
Shartegodon	1100?02100	010010000?	??05100110	00000
Nuurtherium	?????????0	?1???????0	0003100010	10000

APPENDIX 3. Docodontan lower molar terminology

Terminology used in this paper	Butler (1997) & Pfretzschner et al. (2005)	Sigogneau-Russell (2003) & Kielan-Jaworowska et al. (2004)	Luo & Martin (2007)
cusp a	cusp a	main cusp	cusp a
cusp b	cusp b	mesiolabial cusp	cusp b
cusp c	cusp c	distolingual cusp	cusp c
cusp d	cusp d	distolabial talonid cusp	cusp d
cusp e	cusp e	cuspule	cusp e / mesiolingual cingulid cuspule
cusp df	cusp df	lingual talonid cusp	docodont cusp f / distolingual cingulid cuspule
cusp g	cusp g	mesiolingual cusp	cusp g
a-b crest			a-b crest / anterior crest
a-c crest			a-c crest / postero-oblique crest
a-d crest		posteromain crest	
a-g crest		anteromain crest	a-g crest / antero-oblique crest
b-g crest		anterobasal crest	
b-e crest		crescent	
c-d crest			c-d crest / Transtalonid crest
c-f crest		posterior crest	
d-f crest		cingulum	d-f crest / Distal-cingulid crest

APPENDIX 4. Tooth row gradients

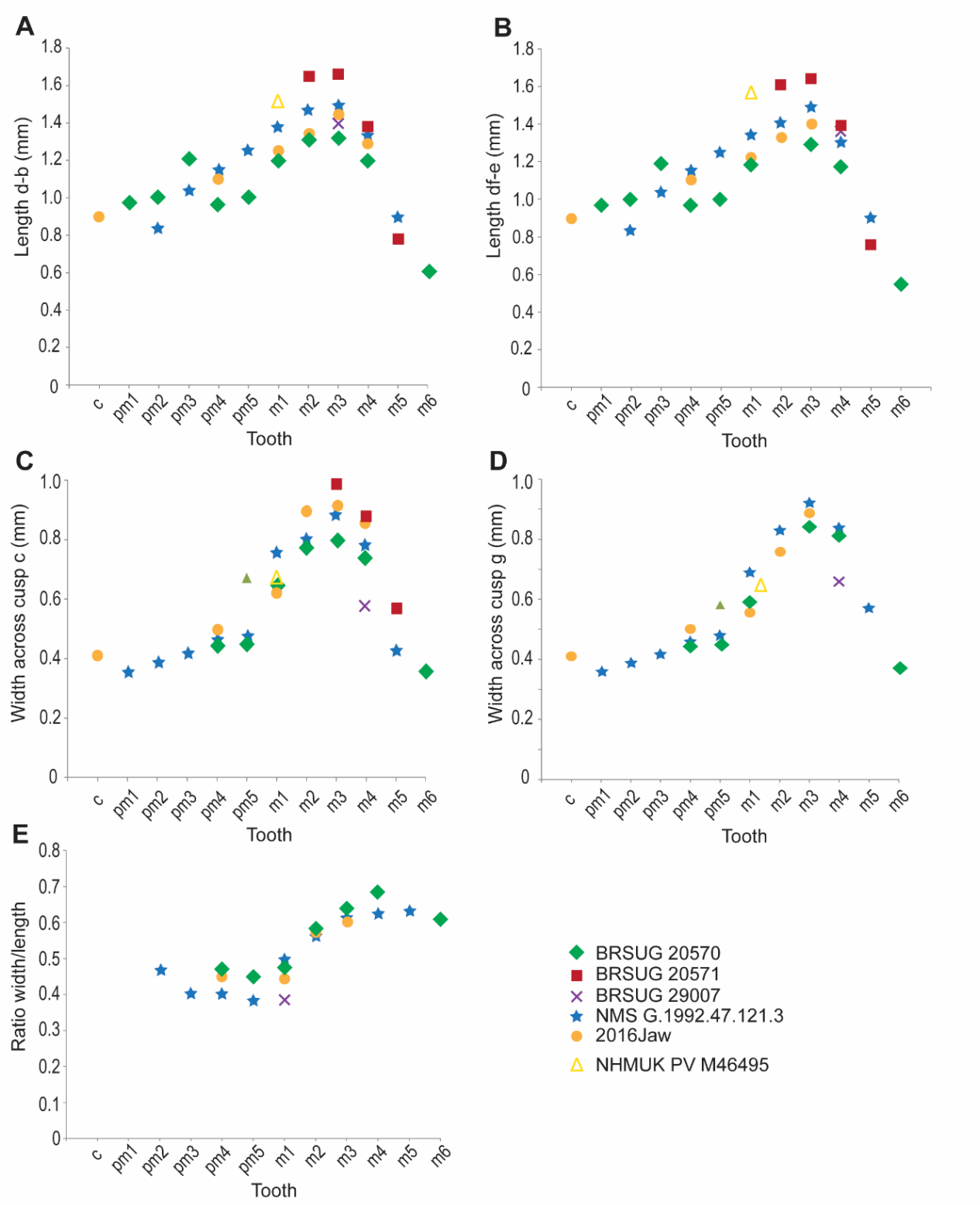

Size gradient and width to length ratio of toothrows of *Borealestes serendipitus* and *B. mussettae* holotype. A, length measured from cusp d to b; B, length measured from cusp

df to e; C, width measured across cusp c; D, width measured across cusp g; E, the ratio of width divided by length. All measurements in mm. For measurements see Table 1, and for measurement methodology see Figure 1 and text. [Intended for page width 183 mm]

APPENDIX 5. Comparative figure of *Borealestes serendipitus* tooth rows

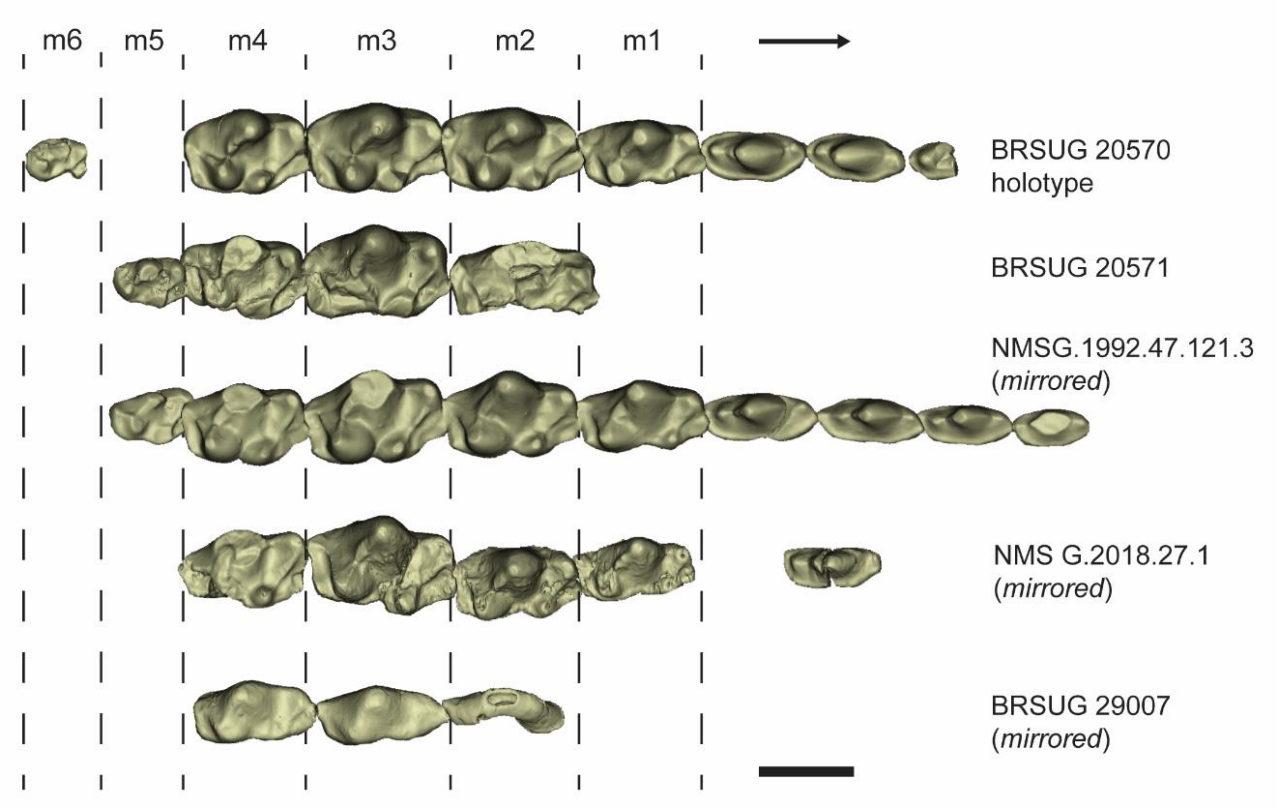

Comparison of multiple specimens of *Borealestes serendipitus.* Lower tooth rows in five specimens of *B. serendipitus*, some mirrored to permit easy comparison with the holotype material. NMS G.2018.27.1 m3 crown was displaced post-mortem and is here placed back to correct position to facilitate comparison. The unusually buccolingually narrow teeth of BRSUG 29007 are caused by post mortem erosion. Same scale throughout. All scale bars equal 1 mm.

APPENDIX 6. Dentary condyle of *Borealestes serendipitus* NMS G.1992.47.121.3

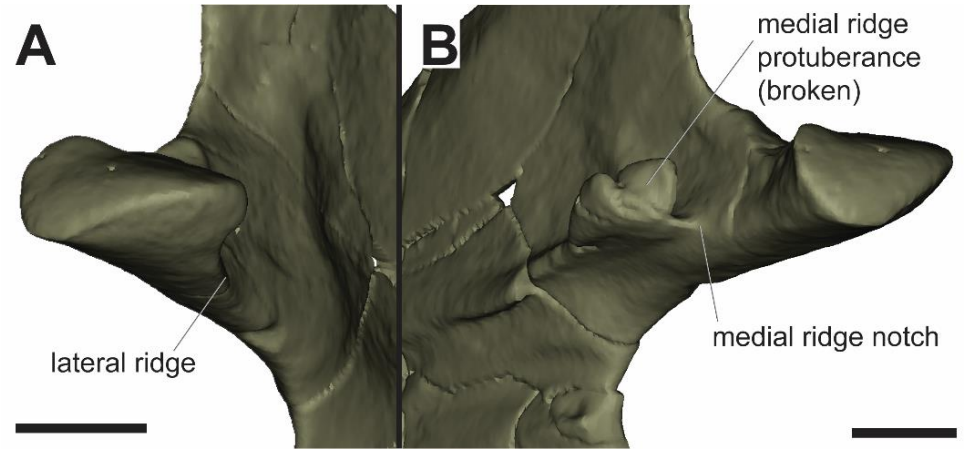

The dentary condyle of specimen NMS G.1992.47.121.3, *Borealestes serendipitus*, showing A, the spindle-shaped condyle, and *B*, the broken and displaced flange of the medial protuberance.

APPENDIX 7. Notes on *Borealestes* species

Specimens were re-examined in light of refined diagnosis for both species of the genus *Borealestes*. Justification for identifications given (see main text for details of diagnoses).

NHM PV specimen	*B. serendipitus*	*B. mussettae*	Docodonta	Notes on identification
M.44301	yes			The c and g cusp close together, no a-d or a-g crest.
M.46039	yes			Very worn, but lacks a-g or a-d crest.
M.46058	yes			Lacks a-d crest.
M.46116	uncertain			Heavily worn, ID uncertain but probably *B. serendipitus.*
M.46316	yes			No cusp on the A-X crest.
M.46396	yes			Strong A-X crest as expected for *B. serendipitus*.
M.46400			yes	The tooth doesn't match morphology of molar of *Borealestes*: too anteroposteriorly elongated, with large cingulid cusps B and C. Not *Borealestes*.
M.46445			yes	Cusp Y too large, indent too deep, A-X crest too distinct. This incomplete tooth is probably a labial wing of *Krusatodon* right upper molar.
M.46521	yes			No a-g and a-d crest (not even on cusp d). Posterior cingulid cuspules almost non-existent.
M.46549	yes			No a-d crest.
M.46580		yes		Cuspule on the A-X crest, and distinct cusp Y. No cusp Z.
M.46607			yes	Resembles M46400, but does not resemble *B. serendipitus.*
M.46610	yes			No a-g, no a-d, has all diagnostic morphology of *B. serendipitus*.
M.46632	probably			Very worn, but nothing contradicts an ID as *B. serendipitus.*
M.46728	probably			Not any major diagnostic features, but nothing contradicts an ID as *B. serendipitus.*
M.46791	yes			No a-g, or a-d. Has diagnostic morphology of lower molar *B. serendipitus*, with very small cusp g far from cusp c, indicating an m1.
M.46841	yes			No a-d or a-g crest.
M.46869	yes			Anteriorly very worn, no a-d crest or a-g crest.
M46246	no	unlikely	Probably	This was labelled as *Borealestes* cf. *mussettae,* but it almost certainly neither as it has none of the diagnostic features.
M46845	likely			Referred to 'Docodonta', but likely *B. serendipitus*, indicated by a very weak a-g crest.

M46842	yes			Referred to 'Docodonta', but likely *B. serendipitus*, no a-g crest.
M. 46001		yes		Has strong a-g crest and a-d crest.
M. 46066		yes		Has a-g crest.
M.46224		yes		Has a-g crest and well defined pseudotalonid by a-g and b-g crests.
M.46239		yes		Has a-g, a-c, and a-b crests. Longer length/width ratio.
M.46319		yes		Worn, but has a-d crest and wide space between cusps c and g.
M.46389	yes			No a-g crest, the tooth is bucco-labially wide.
M.46394		yes		The A-X crest weak to non-existent.
M.46399	yes			Strong c-d cusp and no a-d cusp.
M.46401	yes			No a-d crest.
M.46404	no	probably not	yes	Very fragmentary; the preserved part is probably the labial wing of upper molar. Could be *Krusatodon,* certainly not *B. serendipitus* as there is a cusp on the A-X crest—if it *is* an A-X crest.
M.46448		yes		Cusp on A-X crest and a more distinct cusp Y than in *B. serendipitus*.
M.46495		HOLOTYPE		See main text and figures.
M.46588	yes			No a-d crest, buccolingually wide.
M.46809		yes		Has a-g crest.
M.46835		yes		Worn and enamel broken, but seems to show an a-g crest; c and g cusps far apart, and the overall morphology buccolingually narrow.
M.46836		yes		Has strong a-g crest and a-d crest.
M.46871		yes		See main text and figures.
J.79446			yes	Has an a-g crest, not a tooth of *B. serendipitus*; cusps c and g close together and strong a-g and a-c crests, but not matching *B. mussettae.* Likely an anterior lower molar of *Krusatodon* or *Simpsonodon*.
J.79474	yes			No a-g crest, but all other features are diagnostic of *B. serendipitus*.
J.79475	yes			No a-g or a-d crest
J.79497			yes	Has an a-g crest, wrinkled enamel on posterior of molar, probably a tooth of *Simpsonodon*.
J.79498	maybe	maybe	maybe	Probably a premolar, not diagnostic features for ID.
J.79514			yes	Strong a-g crest and a-d crest, cusp a conical, very tall and pointed, strong lingual cingulid, large cusp b. Doesn't match *Borealestes*. No wrinkled enamel. Cusps c and g missing, but resembles *Krusatodon*.

APPENDIX 8. Data matrix used in this analysis

```
#NEXUS
Begin data;
Dimensions ntax=25 nchar=47;
Format datatype=standard symbols="01234" gap=-;
Matrix
Sinoconodon  00010000000000000?00???0000?000?0000000?00000 00
Morganucodon 000000000000000010000??0000?00000000000?1000000
Dinnetherium  100100000000000010000??0000?00000000000?1000000
Megazostrodon 100000000000000010000??0000?00000001000?2000000
Kuehneotherium 1001?000000000000?00???0000?00020001000?2010000
Delsatia ??????????????1021000??0000?00000001000?20100??
Woutersia ?????10000101012100 0??0000?00000001000?201000?
Gondtherium ?????110000020???????????0?????????????????????
Tikitherium ?????110000021???????????0?????????????????????1?
Haldanodon2111111112112110313111001110211111011114012011
Docodon 2111111112112111313111011102102101001114012011
Docofossor 211111111211211131311100101021021110?1114012011
Dsungarodon ?????111110121103112100110102101010012101111111
BorealestesS 11101111110121103011120010 1?1112111011103011111
BorealestesMUp ?????110?10121103022010010201111111011 0?1101??
Tashkumyrodon ??????????????103?32111010 20?01101101211111 1??
Castorocauda 211?1??????????10311210101020110201001210101 11?1
Itatodon  ???11??????????10413201?01020110101101210301 11?1
Simpsonodon ????111111011010411 21?10112011110110121030111 1?
Krusatodon ?????11?0101111031221201102110110110121030111 1?
Agilodocodon  2111111101 01111041221211112110110110121030111111
Tegotherium ???111111101111041220011102000010110221031 1111?
Hutegotherium ??111111011110412200111020000101102210311 1111?
Sibirotherium  ???111111011110312200101020000101102210311 1111
;
End;
```

APPENDIX 9. Characters scores for *B. serendipitus*

Characters were scored using the Meng et al (2015) matrix—see S5 for full character list. The following scores were added or changed.

Additional characters added:
48: Presence of an anterior fovea on the upper molars: (0) absent, (1) present and positioned at mid-line constriction of upper molar, (2) present and lingually offset from the midline of the upper molar.

This character is absent in all docodonts except *Docodon* (2) and *Borealestes* (1).

1-5: characters can now be scored thanks to new material

8 and 9: defined as mesio-lingual and mesio-labial crests (Meng et al 2015), but meaning anterolingual and anterolabial. Supplementary of Meng et al (2015) gave character states for character 9 as (0) and (2), this has been amended to (0) and (1).

18: cusp c re-scored, from (1) sub-equal to cusp g, to (0) much larger than cusp g.

19: the anterior border of the pseudo-talonid was scored as (1) present and bordered by the b-g crest. In Meng et al 2015 the score for this character differed between the character list (2), the matrix table (3), and the Nexus file (1).

20: a-g crest re-scored from (2) raised with v-notch, to (1) present or lower. Although there is no a-g crest on cusp a in *B. serendipitus*, there is a very a small portion of crest variably on cusp g, and so this cannot be scored as absent.

21: the b-g crest has been rescored from (0) absent or weakly developed, to (1) present.

27: the a-d crest was re-scored from (2) connected by a crest with a v-notch, to (1) incomplete. This is because the a-d crest is only present on the d cusp, where is runs labially below the a cusp, and is not present on the a cusp.

28: the alignment of the a-d cusp was re-scored from (0) present and straight to (?) not applicable, because it is not present on cusp a.

32: The mesio-lingual cingulid from cusp e was re-scored from (1) extending posteriorly below cusp g to (2) absent or limited to mesial part of the tooth. This cingulid does not extend below cusp g in *B. serendipitus*.

42: the placement of cusp e was re-scored from (1) cusp e labially shifted to (0) lingual position.

44: the degree of triangulation of cusps g-a-c was re-scored from (0) >80 degrees to (1) < 80 degrees.

47: the number of canine roots was scored in the matrix of Meng et al 2015 as (1), but listed in their character descriptions as (?). We can confirm it is (1).

APPENDIX 10. Characters scores for *B. mussettae*

Characters were scored using the Meng et al (2015) matrix – see S5 for full character list. The following scores were added or changed.

1 to 5: the dentary is not yet known for *B. mussettae*.

8: the transverse anterio lingual and anterolablial crest was scored as (0) absent, unlike *B. serendipitus*.

9: the transverse anterio lingual and anterolablial crest in the posterior molar was scored as (?) unknown, as we believe only the anterior upper molars are known for *B. mussettae*.

19: the anterior border of the pseudo-talonid was scored as (2) present and bordered by the b-e crest, unlike in *B.serendipitus*. This is because of the weaker b-g crest in *B. mussettae* and the subsequent slight shift in the position of the pseudotalonid.

20: unlike *B. serendipitus*, *B. mussettae* has (1) a raised a-g crest and it has a v-notch.

21: the b-g crest was scored (0) absent or weakly developed because it is poorly developed compared to *B. serendipitus*.

22: the c-d crest was scored as present with the c-d crest being straight, unlike the angle in *B. serendipitus*.

27: the a-d crest is (2) present and connected with a v-notch in *B. mussettae*.

32: The mesio-lingual cingulid from cusp e was scored as (1) extending posteriorly below cusp g, in contrast to *B. serendipitus*.

41: this was scored as (?) because the interlocking between lower molars is not yet known for *B. mussettae*.

42: the placement of cusp e was scored as (1) cusp e labially shifted to for this species, in contrast to *B. serendipitus*.

44: the degree of triangulation of cusps g-a-c was scored as (0) >80 degrees, in contrast to *B. serendipitus*.

46 and 47: the number of roots in the canine and upper molars is not yet known for *B. mussettae*.

APPENDIX 11. Cross-reference and scoring of other taxa in Meng et al (2015) matrix

Character lists in Meng et al (2015) differed between the NEXUS file, the matrix table provided for score verification, and the example scores in the character list. We compared these data matrices, and where scores differed we scored those characters based on our own observations of specimens, predominantly from the literature.

Sinoconodon
21: crest b-g (?) not applicable
32: changed to (?) not applicable

Morganucodon
3: changed to (0) facing medially

Dinnetherium
3: changed to parallel to ventral margin (through observation of specimen MCZ 20870)

Megazostrodon
3: changed to (0) convergent to ventral margin

Kuehneotherium
21: changed to (?) not applicable
32: changed to (2) limited to the mesial part of the tooth

Woutersia
9: changed to (0) absent

Gondtherium
9: changed to (0) absent

Tikitherium
9: changed to (0) absent
14: changed to (1) present

Haldanodon
17: changed to (3) distinctive and anteriorly positioned
34: changed to (1)

Docodon
17: changed to (3)
34: changed to (0)
37: changed to (0)

Docofossor
17: changed to (3)
31: changed to (0)

Dsungarodon

1 and 2: changed to (?), although *Acuodulodon* and *Dsungarodon* have been suggested to be synonymous by Martin et al 2010, we consider the material too poorly preserved to be certain, and the synonymisation relies too heavily on premolar characters, which are similar among some docodontans genera (and therefore may be similar in this case). We therefore choose not to use this interpretation for this analysis.
17: changed to (3)
31: changed to (0)

Borealestes
See S1 and S2 for new scores

Tashkumyrodon
17: changed to (3)
19: changed to (3)

Castorocauda
17: changed to (3)
19: changed to (1)

Itatodon
17: changed to (4)
19: changed to (3)
And extra character removed from end

Simpsonodon
17: changed to (4)
19: changed to (1)
22: changed to (?) not applicable due to enamel folding
31: changed to (1)
32: changed to (1)

Krusatodon
17: changed to (3)
23: changed to (0)
31: changed to (1)

Agilodocodon
17: changed to (4)
31: changed to (1)

Tegotherium
17: changed to (4)
21: changed to (0)

Hutegotherium
17: changed to (4)
21: changed to (0)

Sibirotherium

21: changed to (0)
23: changed to (0)

APPENDIX 12. PAUP analysis (*Borealestes*)

```
P A U P *
Version 4.0a (build 163) for 32-bit Microsoft Windows (built on Jul 23 2018 at 17:54:24)
Wed Sep 05 09:30:24 2018
paup> ToNEXUS fromFile='Mengetal2015matrixAMENDED_ALL5.9.18.txt';
Processing of file "F:\Manuscripts\Borealestes dentary\Phylogenetic
analysis\PAUP\Mengetal2015matrixAMENDED_ALL5.9.18.txt" begins...

Data matrix has 24 taxa, 48 characters
Valid character-state symbols: 01234
Missing data identified by '?'
Gaps identified by '-'
Processing of input file "Mengetal2015matrixAMENDED_ALL5.9.18.txt" completed.
Input data matrix:

                  1        2        3        4      4
Taxon          123456789012345678901234567890123456789012345678
-----------------------------------------------------------------
Sinoconodon     0001000000000000?00???0000?000?0000000?00000000
Morganucodon    0000000000000000010000??0000?00000000000?10000000
Dinnetherium    1001000000000000010000??0000?00000000000?10000000
Megazostrodon   1000000000000000010000??0000?00000001000?20000000
Kuehneotherium  1001?000000000000?00???0000?00020001000?20100000
Delsatia        ??????????????1021000??0000?00000001000?20100??0
Woutersia       ?????10000101021000??0000?00000001000?201000?0
Gondtherium     ?????110000020???????????0?????????????????????0
Tikitherium     ?????110000021???????????0?????????????????????1?0
Haldanodon      211111111211211031311100111021111110111140120110
Docodon         211111111211211131311110111021021010011140120112
Docofossor      21111111121121113131110010102102111O?11140120110
Dsungarodon     ?????111110121103112100110102101010012101111111O
BorealestesS    11101111110121103011120010 1?1112111011030111111
BorealestesMUp  ?????110?10121103022010010201111111011O?1101??1
Tashkumyrodon   ??????????????103?32111010 20?01101101211111112?0
Castorocauda    211?1??????????10311210101020110201001210101l1?10
Itatodon        ???11?????????10413201?01020110101101210301l1?10
Simpsonodon     ????111111011010411 21?10112011110110121030111l?0
Krusatodon      ??????11?0101111031221201102110110110121030111l?0
Agilodocodon    211111110101111041221211112110110110121030111110
Tegotherium     ???111111101111041220011102000010110221031111l?0
Hutegotherium   ???1111111011110412200111020000101102210311111?0
Sibirotherium   ???111111101111031220010102000010110221031111110

paup> BandB mulTrees=no;

Branch-and-bound search settings:
  Optimality criterion = parsimony
```

```
    Character-status summary:
      Of 48 total characters:
        All characters are of type 'unord'
        All characters have equal weight
        All characters are parsimony-informative
    Gaps are treated as "missing"
  Initial upper bound: unknown (compute heuristically)
  Addition sequence: furthest
  Initial 'Maxtrees' setting = 100
  Branches collapsed (creating polytomies) if maximum branch length is zero
  'MulTrees' option not in effect; only 1 tree will be saved
  No topological constraints in effect
  Trees are unrooted

Maxtrees reset to 200

Branch-and-bound search completed:
  Score of best tree found = 117
  Number of trees retained = 1
  Time used = 00:03:09 (CPU time = 00:02:45.5)

paup> ShowTrees / tOrder=right;

Note: No outgroup has been defined; tree is (arbitrarily) rooted at first taxon.

Tree 1 (rooted using default outgroup)

/---------------------------------------------------------------------------------- Sinoconodon
|
|    /----------------------------------------------------------------------------- Morganucodon
|    |
\----+    /------------------------------------------------------------------------ Dinnetherium
     |    |
     \----+    /------------------------------------------------------------------- Megazostrodon
          |    |
          \----+    /-------------------------------------------------------------- Kuehneotherium
               |    |
               \----+     /--------------------------------------------------------- Delsatia
                    |     |
                    \-----+    /---------------------------------------------------- Woutersia
                          |    |
                          \----+    /----------------------------------------------- Gondtherium
                               |    |
                               |    |    /------------------------------------------ Tikitherium
                               \----+    |
                                    |    |                              /---------- Sibirotherium
                                    |    |                              |
                                    \----+    /-----------------------------+    /----- Tegotherium
                                         |    |                              \----+
```

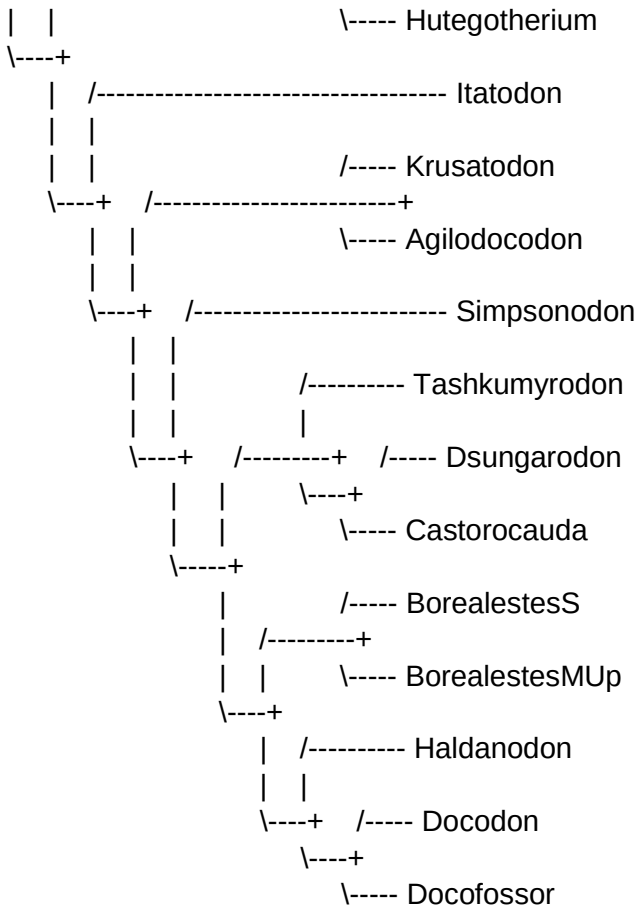


```
paup> DescribeTrees / xout=internal apoList;

Tree description:

  Unrooted tree(s) rooted using outgroup method

  Note: No outgroup has been defined; tree is (arbitrarily) rooted at first taxon.
  Optimality criterion = parsimony
    Character-status summary:
      Of 48 total characters:
        All characters are of type 'unord'
        All characters have equal weight
        All characters are parsimony-informative
    Gaps are treated as "missing"
    Character-state optimization: Accelerated transformation (ACCTRAN)

Tree 1 (rooted using default outgroup)

Reconstructed states for internal nodes:

                  1       2       3       4      4
Node          123456789012345678901234567890123456789012345678
--------------------------------------------------------------
```

25 21111111121121113131110011102102111001114012011 0
26 21111111121121103131110011102111111011114012011 0
27 11101111110121103011110010101111111011103011111 1
28 21111111110121103111110010101111111011103011111 0
29 21111111110121103112101010201101010012101111111 0
30 21111111110121103112111010201111011012101111111 0
31 21111111110121103112111010201111011012103011111 0
32 21111111110111104112111010201111011012103011111 0
33 21111111010111041221211102110110110121030111110
34 21111111110111041221110102011110110121030111110
35 21111111110111041220110102011010110121030111110
36 21111111110111041220011102000010110221031111110
37 21111111110111041220010102000010110221031111110
38 21111111110111041220010102000010110121030111110
39 21111110000021104122001010200001011012103011110
40 21111110000020104122001010200001011012103011110
41 21111100000010102100001000000000000010000201000 10
42 21111100000010102100001000000000000010000201001 0
43 10011000000000000100001000000000000010000201000 00
44 10010000000000001000001000000000000010000200000 00
45 10010000000000001000001000000000000000000100000 00
46 00010000000000001000001000000000000000000100000 00

Tree length = 117
Consistency index (CI) = 0.5812
Homoplasy index (HI) = 0.4188
Retention index (RI) = 0.8287
Rescaled consistency index (RC) = 0.4816

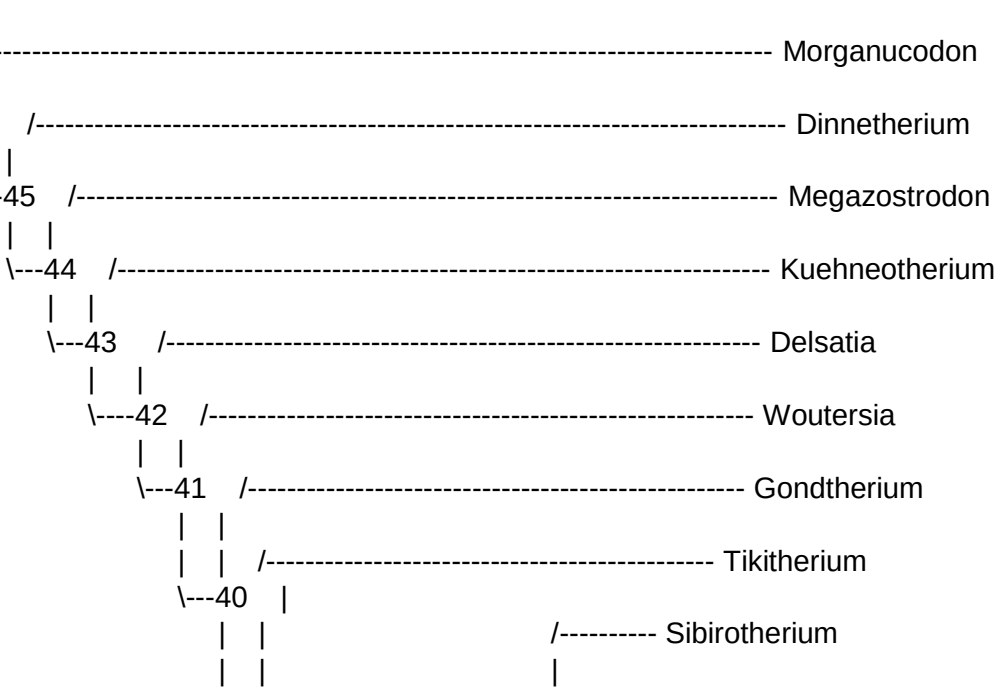

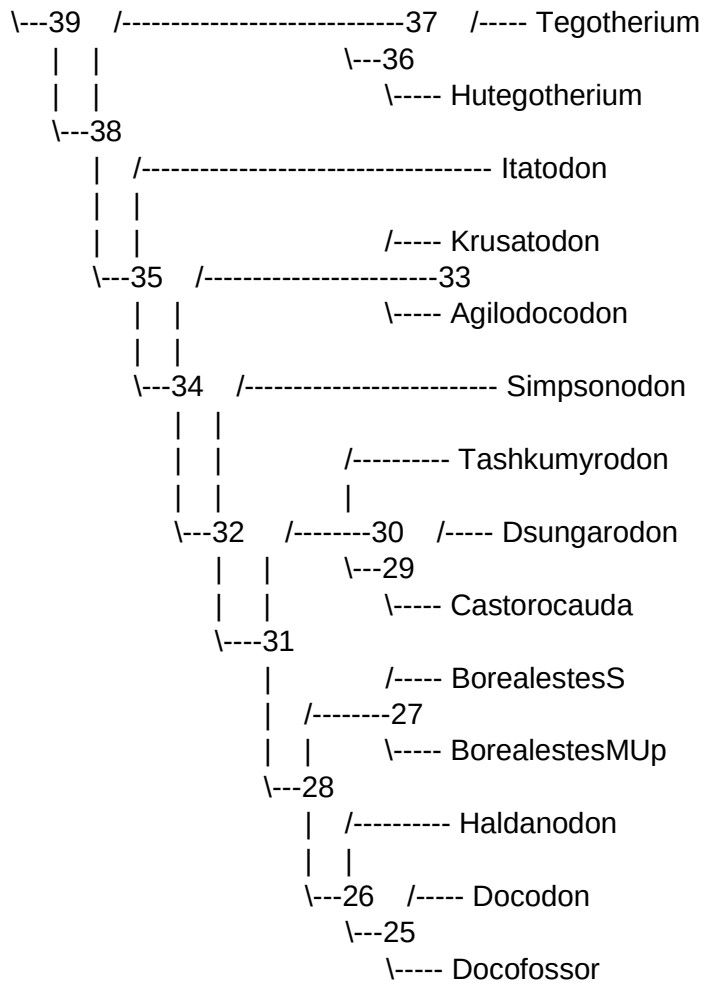

Apomorphy lists:

Branch	Character	Steps	CI	Change
node_46 <-> Sinoconodon	17	1	0.571	1 <=> 0
	41	1	0.800	1 <=> 0
node_46 --> Morganucodon	4	1	0.333	1 ==> 0
node_46 --> node_45	1	1	0.667	0 ==> 1
node_45 --> node_44	36	1	0.500	0 ==> 1
	41	1	0.800	1 ==> 2
node_44 --> Megazostrodon	4	1	0.333	1 ==> 0
node_44 --> node_43	5	1	1.000	0 --> 1
	17	1	0.571	1 --> 0
	18	1	0.500	0 --> 1
	43	1	1.000	0 ==> 1
node_43 --> Kuehneotherium	32	1	0.400	0 ==> 2
node_43 --> node_42	1	1	0.667	1 --> 2
	2	1	1.000	0 --> 1
	3	1	1.000	0 --> 1
	6	1	1.000	0 --> 1
	13	1	0.500	0 --> 1

	15	1	1.000	0 ==> 1
	17	1	0.571	0 --> 2
	47	1	1.000	0 --> 1
node_41 --> Woutersia	11	1	0.500	0 ==> 1
node_41 --> node_40	7	1	1.000	0 ==> 1
	13	1	0.500	1 --> 2
	17	1	0.571	2 --> 4
	19	1	0.500	0 --> 2
	20	1	0.667	0 --> 2
	25	1	1.000	0 --> 1
	27	1	0.500	0 --> 2
	32	1	0.400	0 --> 1
	34	1	0.500	0 --> 1
	35	1	0.500	0 --> 1
	36	1	0.500	1 --> 0
	37	1	0.667	0 --> 1
	38	1	1.000	0 --> 2
	39	1	1.000	0 --> 1
	41	1	0.800	2 --> 3
	44	1	0.667	0 --> 1
	45	1	0.500	0 --> 1
	46	1	1.000	0 --> 1
node_40 --> node_39	14	1	0.500	0 ==> 1
node_39 --> node_38	8	1	0.500	0 ==> 1
	9	1	0.500	0 --> 1
	10	1	1.000	0 ==> 1
	12	1	1.000	0 ==> 1
	13	1	0.500	2 --> 1
node_38 --> node_35	22	1	0.500	0 --> 1
	29	1	0.667	0 ==> 1
	30	1	0.333	0 --> 1
node_35 --> node_34	21	1	0.500	0 ==> 1
	31	1	0.333	0 ==> 1
node_34 --> node_32	19	1	0.500	2 ==> 1
node_32 --> node_31	13	1	0.500	1 ==> 2
	17	1	0.571	4 ==> 3
node_31 --> node_28	20	1	0.667	2 --> 1
	23	1	0.250	1 ==> 0
	27	1	0.500	2 --> 1
	33	1	1.000	0 ==> 1
	38	1	1.000	2 ==> 1
node_28 --> node_26	10	1	1.000	1 ==> 2
	11	1	0.500	0 ==> 1
	19	1	0.500	1 ==> 3
	26	1	0.250	0 --> 1
	29	1	0.667	1 ==> 2
	40	1	0.500	0 ==> 1
	41	1	0.800	3 ==> 4
	44	1	0.667	1 ==> 2

```
                    45          1   0.500  1 ==> 0
node_26 --> node_25       16          1   1.000  0 ==> 1
                    31          1   0.333  1 ==> 0
                    32          1   0.400  1 ==> 2
                    37          1   0.667  1 --> 0
node_25 --> Docodon       23          1   0.250  0 ==> 1
                    34          1   0.500  1 ==> 0
                    48          1   1.000  0 ==> 2
node_25 --> Docofossor    26          1   0.250  1 --> 0
node_28 --> node_27       1           1   0.667  2 --> 1
                    4           1   0.333  1 --> 0
                    18          1   0.500  1 ==> 0
                    48          1   1.000  0 ==> 1
node_27 --> BorealestesS  22          1   0.500  1 ==> 2
                    32          1   0.400  1 ==> 2
node_27 --> BorealestesMUp 8          1   0.500  1 ==> 0
                    19          1   0.500  1 ==> 2
                    20          1   0.667  1 --> 2
                    21          1   0.500  1 ==> 0
                    27          1   0.500  1 --> 2
                    42          1   0.250  0 ==> 1
                    44          1   0.667  1 ==> 0
node_31 --> node_30       41          1   0.800  3 ==> 1
                    42          1   0.250  0 --> 1
node_30 --> node_29       22          1   0.500  1 ==> 0
                    31          1   0.333  1 ==> 0
                    35          1   0.500  1 ==> 0
node_29 --> Dsungarodon   23          1   0.250  1 ==> 0
                    24          1   0.333  0 ==> 1
                    27          1   0.500  2 ==> 1
                    29          1   0.667  1 ==> 2
node_29 --> Castorocauda  32          1   0.400  1 ==> 2
                    42          1   0.250  1 --> 0
node_30 --> Tashkumyrodon 19          1   0.500  1 ==> 3
                    30          1   0.333  1 ==> 0
                    40          1   0.500  0 ==> 1
node_32 --> Simpsonodon   14          1   0.500  1 ==> 0
                    26          1   0.250  0 ==> 1
node_34 --> node_33       9           1   0.500  1 --> 0
                    22          1   0.500  1 ==> 2
                    24          1   0.333  0 ==> 1
                    28          1   1.000  0 ==> 1
                    30          1   0.333  1 --> 0
node_33 --> Krusatodon    17          1   0.571  4 ==> 3
                    23          1   0.250  1 ==> 0
node_33 --> Agilodocodon  26          1   0.250  0 ==> 1
node_35 --> Itatodon      19          1   0.500  2 ==> 3
node_38 --> node_37       37          1   0.667  1 --> 2
                    42          1   0.250  0 ==> 1
```

node_37 --> node_36 24 1 0.333 0 ==> 1
node_37 --> Sibirotherium 17 1 0.571 4 ==> 3

paup> SaveTrees file='F:\Manuscripts\Borealestes dentary\Phylogenetic analysis\PAUP\Tree.txt';

1 tree saved to file "F:\Manuscripts\Borealestes dentary\Phylogenetic analysis\PAUP\Tree.txt"

APPENDIX 13. Systematic character list for docodontans and outgroups (see Meng et al 2015)

Mandibular Features

1. Mandible --- Angular process shape:
(0) Pointed angle (two sides of the angular process forming an angle of 90 degrees and higher)
(1) Obtuse angle (two sides of the angular process forming an angle of less than 90 degrees)
(2) Rounded angular process

2. Angular process of the mandible with an efflected ventral crest:
(0) Absent
(1) Present

3. Mandible angular process – receiving structure for ectotympanic:
(0) Medially facing concavity for ectotympanic
(1) Posteriorly facing groove for ectotympanic

4. Meckel's groove to ventral margin of mandible:
(0) Convergent to the ventral margin
(1) Parallel to ventral margin

5. Replacement dental lamina (Crompton's) groove (visible along the lingual alveolar margin of last molars):
(0) Present
(1) Absent

Upper Molar Characteristics

6. Transversely widening of upper molars:
(0) Absent
(1) Present

7. Mesiolingual cusp X of upper molars: wear facets on the labial aspect of the cusp:
(0) Absent
(1) Wear facets present on the labial side of the lingual cusp

8. Transverse mesiolingual and mesiolabial crests between Cusp A and Cusp X on anterior molars:
(0) Absent
(1) Present and complete

9. (New). Transverse mesiolingual and mesiolabial crests between Cusp A and Cusp X on posterior molars:
(0) Absent

(1) Present and complete

10. Cusp Y (=upper distolingual cusp):
(0) Absent or indistinctive
(1) Present as a distinctive cusp
(2) Present, as crest aligned in anteroposterior line

11. Size and development of Cusp C (distolabial cusp) and its separation from Cusp A (mesiolingual cusp):
(0) Cusp C present and enlarged
(1) Reduced cusp C twinned with cusp A

12. Posterior transverse crest extending from the distolabial (C) to the posterior cingulum (modified according to comment by Averianov et al., 2010):
(0) Absent
(1) Present

13. Presence of Cusp E separated from cusp B on posterior upper molars.
(0) Present
(1) Cusp E present and in labiolingual alignment with cusp B
(2) Absent

14. Constricted waist between the labial part and the lingual part of the upper tooth.
(0) Absent
(1) Present

Lower Molar Characteristics

15. Cusp c on lingual cingulid and in alignment with mesiolingual cusp g (mesiolingual):
(0) Absent
(1) Present

16. The a-c v notch crest (posteromain crest of Sigogneau-Russell, 2003):
(0) Present
(1) Absent

17. Presence vs. absence and size of cusp g (mesiolingual):
(0) Absent
(1) Small
(2) Distinctive, opposite to primary cusp a
(3) Distinctive, anteriorly positioned (more anteriorly placed than primary cusp a)
(4) Anteriorly placed and hypertrophied (to the same size as, or larger than cusp c)

18 Cusp c to cusp g size ratio:

(0) Cusp c much larger than cingular cusp g (if the latter is present)
(1) Sub-equal to the mesiolingual cusp g

19. Development of pseudo-talonid:
(0) Absent
(1) Present and its anterior-border by b-g crest
(2) Present and its anterior-border by b-e crest
(3) Present buy cusp b is much taller than g so the pseudotalonid appears to be lingually open

20. Raised a-g crest:
(0) Absent
(1) Present or lower
(2) Raised, with v-notch

21. Crest b-g:
(0) Absent, or weakly developed
(1) Present

22. The c-d crest in the posterior basin – presence/absence and alignment:
(0) Absent
(1) Present, c-d crest or c-f-d crests straight
(2) Present, c-d crest angled

23. Crest extending from cusp c to cusp df or the cusp df position:
(0) Absent
(1) Present

24. Placement of cusp d (modified from Sigogneau-Russell 2003: character 7; Luo & Martin 2007 Character 16; assuming homology of the morganucodontan cusp d to docodontan cusp d):
(0) Labial position (in alignment with a-b crest, or nearly so)
(1) Median placement (nearly halfway along the transverse width of posterior crown)

25. Distal Cusp d-f (=cusp dd of Hu et al. 2007):
(0) Absent
(1) Present

26. Folding enamel (on either upper or lower) (Sigogneau-Russell, 2003: character 5; Luo & Martin 2007 Character 17, scored on the posterior face of lower cusp a or lingual face of upper cusps A-C):
(0) Absent or weakly developed
(1) Present

27. Connecting structure of cusps a and d (modified from Luo and Martin 2007 character 19; Hu et al. 2007, Character 14):

(0) Not connected
(1) Incomplete
(2) Connected by a crest with a v-notch

28. Alignment of posterior crest of cusp a toward cusp d (postero-main crest of Sigogneau-Russell 2003; as defined in Luo & Martin 2007 character 18):
(0) Present and straight
(1) Present and angled

29. The b-g Crest - Crest between the mesio-labial cusp and mesio-lingual cusps:
(0) Absent
(1) Present, low and broken (v-valley)
(2) Present and continuous

30. Size of cusp e:
(0) Present and distinctive
(1) Reduced

31. Mesiolingual cingulid (width would be related with presence/absence of cusp e):
(0) Narrow or absent
(1) Wide

32. Mesiolingual line-like cingulid extending from cuspule e or an equivalent position:
(0) Connected to cusp g
(1) Extending posteriorly to below the cusp g
(2) Absent or limited to the mesial part of the tooth

33. Size ratio of cusp b and cusp a:
(0) Large, well separated by a notch from cusp a
(1) Small, approximated to cusp a

34. Cusp b position:
(0) Close to cusp a
(1) Well-separated from cusp a by a deep notch

35. The “docodont cusp f” (Posterolingually positioned as defined by Martin and Averianov 2004: figs 3 and 5, and differing from mesiolabially positioned cusp f; Luo & Martin 2007 character 24):
(0) Absent
(1) Present

36. The “standard cuspule f” (mesiolabially positioned, as defined by Kielan-Jaworowska et al. 2004: fig. 5.9: ‘mesiolabial cusp’. We follow Luo &

Martin 2007 [character 25] in regarding this cusp to be different from cusp g in posterolingual position):
(0) Absent
(1) Present

37. The b-e crest:
(0) Absent
(1) Present and continuous from cusp b to the cingulid
(2) Present, as a part of the pseudotalonid rim

38. Anterior basin:
(0) No basin
(1) Small concavity
(2) Pseudotalonid basin

39. Distal basin:
(0) Absent
(1) Present

40. Width ratio of anterior basin vs. distal basin (modified from Hu et al. 2007 character 21, measured at the level of cusps/crests on occlusal surface):
(0) Posterior basin narrower than anterior basin (or anterior part of the tooth)
(1) Posterior basin wider than anterior basin

41. Interlock of lower molars:
(0) No interlock
(1) d-b-e interlock
(2) d – 'standard-f'-e interlock
(3) d-"f"-e interlock
(4) d-b overlap

42. Placement of lower cusp E:
(0) Lingual position (lingual to the median axis of the lower molar)
(1) Cusp e labially shifted

43. Cusp triangulation (cusp triangulation between the a-c crest and the a-b crest following Butler 1997; Sigogneau-Russell and Godefroite 1997; Luo & Martin 2007 character 28):
(0) Absent
(1) Present

44. Degree of triangulation of cusps g-a-c:
(0) Broad triangle (>80 degrees)
(1) Sharp-triangled (≤80 degrees)

45. Gibbousness of crown base overhanging the roots at crown–root junction (scored at the middle molar[s] if multiple molars are known):
(0) Absent
(1) Present

46. Number of upper molariform roots:
(0) Two
(1) Three

47. Number of lower canine roots:
(0) One
(1) Two

Additional character in this analysis -
48. Presence of an anterior fovea on the upper molars:
(0) absent
(1) present and positioned at mid-line constriction of upper molar
(2) present and lingually offset from the midline of the upper molar

APPENDIX 14. Data matrix used in phylogenetic analysis (*Borealestes* -based on Zhou et al., in review)

#NEXUS

Begin data;

Dimensions ntax=113 nchar=491;

Format datatype=standard interleave symbols="012345" gap=-;

Matrix

Thrinaxodon

00000000000000000000000000?0?0?0?01000???????0?000000000?????000????000
00?????0000?000???0??????????????????00?????????????????????????0??00??00
???????????????000000000000????00?0?0000001??0???????000000000000100000000
00000?0?000000?000000000000000000000000????000000??000000000000000000?000
0?000000000000000?000000000110000000??000000000?00????????0000??000??00
?0?00?000?0000010?1000000???0????0?0000?00??0?0?000000000000000000000000
000000000000000000000000000?000000000000000100000000000???

Massetognathus

00000100000000000100000000?0?0?0001000?????????200000000?????020????040
00?????0000?000?????????????????????00?????????????????????????03300??11
???????????????000000000000????00?0?0000001000?0?0?0?00000?0???0??0000000
0??0?0??????0?????00????000000000000????1000?0??00000???0??0???0?00????
???????????????????????????????????????0???0??00?00????????1000??000??00
?0?00?000?0000010010000000???0????0?0000?00??0?0?101000000000000010000000
000003000000000000000010000000?000000000?000000000000010???

Probainognathus

00000000000000000100000000?000?0001000?????????000000000?????000????000
00?????0000?000???0??????????????????00?????????????????????????0??00??00
???????????????000000000000????00?0?000000???0???????00000?????0??0100000
0??0?0?0????0?????00???????????0????0?????10???0??000?0???0??0???0?00????
???????????????????????????????????????0??00?00?????0??1000??000??00
?0?00?000?0000010011000000???0????0?0000?00??0?0?001000000?00000010000000
000000000000000000000010000000?000000000?000000000000101???

Tritylodontids

00000100000000000000000010?000?3000200?????????20?000000?????121????241
10?????0000?000?????????????????????00?0?0?????????????????????03300??23
???????????????2030000??2????0000?0?10??11200200001000100000000?0100000
1000000000000000000000000000(01)1000000????2000010?000000000000000000?0
000?00?000000000000000000000001??000?0?000000000?00?0???0?01111??10000
00?00000000?000001000000100???000000?0000000?0100?00210000000000000100000
000(01)0103010000000000002001000?1000000000000(01)00000100?0111???

Pachygenelus

00000000000001000000000000000000?20000100??????1?000100000?????100????000
00?????0000?000??000?????????????????00?????????????????????????0??00??00
???????????????3030000100000??0000?1?2000001??1??????000000?00??0??10???0
?000100?00?000?000000000000000010000001000210001????00?0000000?????00????
???00000000100?0?0?01111??1?00000
?0000?000?000001011000000???000000?0000010000?1?00210011000000010000000
010000010101010000001000000?1000000000000000000000????????

Adelobasileus

??0??????00

??????0000?000??000???00
??0??????????????
??0????????????????????
??00000?????????0221100?????00
00001?11??10100001001000??????000000000010000?10?????????0????????????0??
0?0?000?????????00??0200??????0001100???????????0?????????
Sinoconodon
000000100000000000000000011010000000100????01100011000?0000000???000
00020??01000000?1000???0000???0????00?000???0?????????0????????00000??00
?0?0?????000000000000000033112202000000?????????101000?0???0?01?????
?00100000000000000000000000010000000?????????????????000?00?0???00?????
??00000010000?0002211001000000
000010111010100000000001000?000000000000010001010102100110000000010000010
010100010100010000002000100020000000100000000010000102???
Morganucodon
000010100000000000000000002(01)0100000001000000000100011020000000100?0??1
1000020??2100000110000???0000???0????00?410???0?????????0????????0000100
1100?0??????000(01)0(01)000000000000(23)(12)000000001101???????????00(12)0000
00000??11?1?000??1???00?100?00000?000000000100000????2100010???00001000
0010?0000??000?000000000000000000000000???0???????0??00000010100(01)(01)
?000231111201000000001011101010001101001110?0100000000001000010100021002
10000000100000100101000101010100000002000100020000110011000000001000011
2???
Megazostrodon
000010000000000000000000002002001000010000000000000110200000000100?0??120
00020??2100000100000???0000???0????00?400???0?????????0????????000010011
00?0??????000101000000000000110000000001001???????????202?00?00000?0110100
0???????0??100000000?000000000100000??0??2100010?000000100000?000000?000
0?00?0000?00000?00??0???0?0?1?000000000000000?0010100???000231101201 0?00
000010111010000011?1001110??1000000000001000101?00210?21???0??001?000010
?1??000101010100000?2?0010?0200001?00???????00??0?????????
Haldanodon
000001100010001000100000002101001000110?000000010001102010101000?0??110
00020??21031200?0000???0000???0????00?1020000????????00????????032012111
00?0??????000001000000101122000000000001100??????????00200?????????????
??????????100101000?00?000001200001 0????2100??????000?00000?0???0?????
???0???000001020011?0002311003010000
000010121010 0?00110210111 0?0100000000001001101000????21000???00??000020
11?1000101010100000002000100201001110110000000000???2?????
Docofossor
00000100000000110?000000002101003000110?00?000010001102010100000?0??110
00020??21031200?0000???0000???0????00?1020000????????10????????032012111
00?0??????000101000000101122323110000001100??????????0200????????010?000
0?????????????????????????????000010010121000???0000?000000010110010010
0?0101101100000000000000000010000000100010 01????1?????????????????????
??
??????????????????????????????????????1000??????????????
Agilodocodon
000001100010001100000000002101002000110?000000010001102111201 0000?0??110

00000??21031200?0000???0000???0????00?1020000????????10????????032012111
00?0??????000101000000111000020011000011100?????????????020000?????1010?000
00??????1101001????0???0?00?0100011110001210000000000000?000001011000?010
0?0101101100000000000000000001000000110001001????1020011??0?231100?????00
00001?12????????1??2101110?0??0000000???100110100021021???1110010000?2?
?1???0???????10???????????0002??0??????1000?????????????????
Castorocauda
00?00110001???1?000000000021010010001l0?0???0?0100011020101000000?0??110
00020??21031200?0000???0000???0????????0?????????????????????????0?0???11
00?0??????000??100?????110000??0?10??01100???????????0200??????10001000
0?????????????????????????00001200001000002100000000000000000001011000?010
0?01?1101100000000000000?00?0??000000001100???010?????????????????????
??1110010000???
??????0??????10??000?2????0??2????1???11?00???????????????
Borealestes
000011100010001100110100002101012000110??????110301?0(12)1112010?00????1
1000020??2103020110000???01020??00???0000020?10111??????0????????0320121
1100?01?1?0???01110000???011?002?0?0001011010??????????020000?0????0????
??????????111?????????????????0??1???????????21000?????0?????????????????
100?01011?1100000000000000?001?10?0?0??????01??0?1020011??002311003????
00??0?1?1?1???????????0111???0?100???????1001101????????201???00100?0?
2???????????1110?00???1??????0012???11???110???0?1????????????
Hadrocodium
1??2?130010?402110000000002001002O0?010?000010100001100000000100?0??120
00020??01000000?0000???0000???0????00?000???0?????????0????????000010011
00?0??????000000000001000334443000000l101??????????0200?????????????
??????????????????????????????????0????????????????????????????????
??1000002010l?0002311123010000
00001?111010?1001102101011001000000000100?1010??????21?0??????1????020
12?1030101000100000012?2?10?02010121100l?00??000?2??1213???
Megaconus
00000?10000?001?000000000?220100?0002100????10??2?0111201??300121????240
11?????0??00?0120?????????????????????0?000?????????????????????044010013
?????????????32400??2??2??3333430O??2???12?03001100l?12000?00?0010111000
00000???11?0?0??????00?00000?00001000????21?0??0000???0?00000?200210?00?
0??0000?000000000???00?0??0???00?0?????001?0????1???????????????????
??00?????1???011??10000???
??????????????0????????????????????????????????????
Eleutherodon
??????????????????????????????????????0???????????1112???????1??????140
11?????0??0??0120?????????????????????0?000?????????????????????043010013
??01301?1?01?130?????????????????
??
??
??
??
Sineleutherus
??2??111201??300101????140
11?????0??0??0120?????????????????????0?000?????????????????????03?010013

??????????????2??????????????????????????01301?1?01?130??????????????????
??
??
??
??
Thomasia
??????????????????????????????????????1?????0??2??????10??310?01????14?
00?????0??0??0??????????????????????0?000??????????????????????0330???13
?????????????21?000???????3323??????3???1?1?400??001??300??????????????
??
??
??
??
Haramiyavia
0100110??00000????000000002?010?100021?0?????0???2?00?0?00??300121????140
00?????0??0??0120??????????????????????0?000??????????????????????033010023
??????????????2010000100100?133?1???000??121020000001?0?00????????????????
??
??
??
??????????????????00??????????????2????????????????????????????
Rugosodon
1112?10??00?302?10102120102224001000210??????0???2?00001?0????1221????241
00?????0??0??00?0??????????????????????0?000??????????????????????03300??23
??????????????2140000110 2??0144220010 3?1112204100010 0?020011111010?112110
000001101101100111100110010 0?000010110001 21?011000000?1?0010020110010001
210010001000012002000111000101100011100021 01?0??????????????????????????
??1????????????????
??????????????????0??
Kuehneodon
1112?10??000302110102120102224001000210 1?????0???2?0000120??311221????241
00?????0??0??00?0??????????????????????0?000??????????????????????03300??23
??????????????2140000110 2??1144320010 3?1112204100010 0?02001????????????????
??
??
??
??
Sinobaatar
1112?10??00130211010212010222400100021 00?????0???2?0000010??201221????241
00?????0??0??00?0??????????????????????0?000??????????????????????03300??23
??????????????2040000 2???2??024423001?0?1112000001011 2?0200?11?10100112110
000001101101100111100110010020000 10110001210(01)110000000111010020110010 0
012100100010000120020001110001011000111000210100001010110?000???????????
??1?????????2???00
??????????????????0??
Plagiaulacids
1112?10??00(01)3021101021201022400100021 01?????0???2?0000120??211221????2
4100?????0??0??00?0??????????????????????0?000??????????????????????03300??
23??????????????21400002???2??0244(23)300103?1112000001011200200?????0?????

??1?????????
??231111301
??000000101211101100211???11110?10?000000000100011111??????21?0??????????
0?000201001002000100?0000202?1122202000100(01)11010000?21?????????
Cimolodontans
1112?10??00130211010212010 22(12)40(01)(12)0002100?????0???2?0000000??201221
????241(01)0?????0??0??00?0?????????????????????0?000?????????????????????
03300???23?????????????3040000 2???2??1(23)44330120?11120?00010112202000101
10100112110000001101101100111001100100(12)0000(01)01100??2101110000000111
?100201100100012100100020211120020011110011011000111000210100001010(01)10
?00023111130100(12)00(01)00101211101100 21121(01)111(01)0010(01)(01)000000001(
01)00111032312121100111??211100000(12)0100100200010020000 2(01)211122202001
10012101000002111022 3???
Shuotherium
0010110??0000021??000?00?0????0?0001010???????1111100001 1??0?0013?200120
0?0100?1323021 0?01110000100???0????11?102002?0000?0??0000000?1001200??22
1100??0100111?????????????????3?????0??????????????????020?????????????????
??
??
??
??
Pseudotribos
0?10011000?0001???00??????2101010001110??0???01111 10000?1110?0013?200120
0?0100?1323021 0?0111000?100???0????11?102002?0000?0??0000000?1001200??22
1100??0100111?01?0??10010?00331 0000??01100???????????0200???????101??00?
?0010001?????????????0????0???12000000????211???00000?10?0000000?00??????
??????????????????????????????????????0???0????????????????????????????
??
??????????????0?????????????????2???1????????????????????????
Asfaltomylos
0012112110000021??00220000213101200 10????????11011?0????????0?13?2??13?
????13?02100000??111022141100011112??????????????????????????????01?0???22
11?1102??0000?????????????????????????0?????????????????02?????????????????
??
??
??
??
Ambondro
?????1???00????1????????0?????0???0?0?????????12131?0??110???0?13?2??13?
??0?13300120100??111022241120?11112??????????????????????????????01?0???22
11?1102010000?????????????????????0?????????????????02?????????????????
??
??
??
??
Ausktribosphenos
0010012010000021??002200002??101200101 0??????121310000 11011?0?13?2??13?
??02133001201 00?022102214122003212 3??????????????????????????03?0????22
21?1112111000?????????????????3????00?????????????????02?????????????????

??
??
??
??
Bishops
01?10120100?0021??00220000213101200l0?0???????12131000?1011?0?13?2??13?
??02133001201O0?122102214122003212З??????????????????????????03?0????22
21?1112111000?????????????03??0?00????????????????020??????????????????
??
??
??
??
Teinolophos
1100212010013021??0022000?21310120010?????????????0??????????3?2??13?
??1111200120010??222042231210?02?23??????????????????????????3?0????22
21?2113102000???02??????????????????
??
??
??
??
Steropodon
011001???0??00?1?????????????????????10?????????????0????????0?13?2??13?
??1111200120110?022204223121O?02?23??????????????????????????03?0????22
21?2113102000?????????????3??3????????????????????02??????????????????
??
??
??
??
Obdurodon
11?2?120100130211011220001213111211101O??????1013100??00????0?13?2??130
0?1111200120010?022204223121O?02?2320?10?????????????0???????03300??22
21?2113102000Ч?5????2??2??333443??0????1?????????????0200??????????????????
??21???1????11?????????????????????
??10000211011O?000231111????00
00001?111?1101001112101110??1000000000000?00?0????????1?0???????????030
12?10000?40?1100211?120201122?0012110011?0??00002????2????
Ornithorhynchus
11?2?10010013021101122000121311121110(02)10?????????????????????????13?2??1
????1?1??????2?010?022204223121O??2?2320?1?????????????????????????03300??
??????2?1?1?2???4?5?????2??2??334443??0????1????????????0????1111011111010
000001000100000010100000000000012000000100121111100001110000002201100210
000?000000010110000000001000110001101001l(01)0100002110010?000231111411
000000001011101101001112101110?110000000000000?00?0?32312121100111012101
003011010000240011002112120201122210012110011?0?100002111223000
Tachyglossus
11?2?10??001402110000000021311l??1?010?????????????????????????????????
??
?????????????4?5?????2??2??334443??????????????????????????1111011111010O0
000100010000001010000000000001200000010012111110100111000000220110021000

0?000000001011000000000100011000011010011(01)0100002110010?00023111141100
000000101110110100111210111 0?1100000000000 10?00?0?3231212110011101210100
3012110200240011?02112120211122210012110011?0?(12)00102111223000
Fruitafossor
11?0014000000021??1100001121010110 01?10?00000010?00100000?0??00??????100
0??????0??00000?0?????????????????00?00?????????????????????5400??0?
?????????????02?0??100100233320 00?001100?????????3001 0????????0100001
0???????0??000011000?00100000120001001001 21?????0000???00??0100?100?0?0
????????000000000000?0?0000???????????01??0????10???11?????????????????
??
?????????????00?????????????2?1?????????????????????????
Gobiconodon
11?1010??000102110122100112114001001010?000000110101000 10000?0100?0??120
00010??12100001 00?00???0000???0????00?110???1?????????0????????00100?211
01?0??????000203000010010111220000000 01010??????????20201??????01010?001
10000?10111211111110011100000111000 10000?2100210000100000001211 0?000?000
0?00?0001?000100000100000000??????????0?1000000112011 1?0002311113010000
00001?12112000001111001111102000000110001 11?1011???????1?1????12????0020
02110000110000010001120011112212101100 01?000001??0??0?00???
Repenomamus
11?1010??001102110122100112114001001010?000000110101000 10000?0100?0??120
00010??12100001 00?00???0000???0????00?110???1?????????0????????00100?211
01?0??????000203000010010111220000000 01010??????????02010001010101 0?001
10000110111211111110011100000111000 10000?2100210000100000001211 00000?000
0?000000110001000002000000000?0?00?1100011000000112011 1?0002311113010000
00001?12112000001111001111102000 0?0110001111101 1??????21?1????12?????020
02110000110000010001120011112212101100 01?000001010??0100???
Yanoconodon
11?1010??001102110122100 1?2214001000010?000000000001100000000?0100?0??110
00010??02000012 1?00???0000???0????00?000???1?????????0????????000012111
00?0??????000303000000000133334300010011 10??????????020000000001010?000
000001101112111111100111000001010100000012100210000000000000001100000?001
0?000000100001000001000000000000?000110002000000 1020?11??00????????????
????????????0?????????????????????????????????32312121???1101221010 0?0
0?????0??????110?????2????1022????????????0???????????????
Jeholodens
11?1010??00?10211012??001?2214001000010?000000010101100000000?0100?0??110
00010??02000012 1?00???0000???0????00?000???1?????????0????????000012111
00?0??????000101000010010?33223200000011 11??????????020000000?010102000
000001101112111111100111 00??0101010000001210021000000000000001100000?001
0?000000100001000001000000000000000010000000000102?011?0002311?130100??
0???10??1?????????????????????0??0?0?????????????????21????????1221??????
??????00?10??110???00?????1022???011??01??0??????1?????????
Trioracodon
11?10?0??0011021??122100102214001000010?00000?010101100001 00?0100?0??110
00110??11000001 21?00???0000???0????00?100???1?????????1????????000011211
00?0??????000?0300??000000123321000??01100???????????0200?????????????
??
??0?????????????02311????????

0??0?0??1010???0?????????????????0??0?0???1??10???????????0????????????0??
?????0????????1?????????????????0?????????????????????????
Amphilestes
11?11?0??001102???122??0??211400200001????????11010?10000000?0?00?0??12?
??010??1110000100?00???0000???0????00?????????????????????????00?0???12
01?0??????000??????????00??21??0000??????0???????????020?????????????????
??0?????????????
??
??
?????????????1???
Priacodon
11?1010??0011021??122100102214001000010?000000000101100101001?0100?0??110
00110??1100000121?00???0000???0????00?100???1?????????1???????000011211
00?0??????000??300??0?000012222100??01101?????????10200?????????????
??0??
??0?????0????1??00231111301??00
0000101?12100??0111100??1000??000???00??1100101????????2??0???????????020
?????000??????10???????(12)??1022?10???????????0??0??1?????????
Tinodon
1??11????001021??121?00???104?130?00?????????01010?00000?00?0?1201??12?
??0100011100001001?10000100???00??010?101????00???0???0????0?000210???22
11?0??????000??????????1???22??1??0?????????????????02???????????????
??
??
??
???
Akidolestes
1????10??00?20????122100102114011001110?00000?1101000000120?111302011200
?0100011000001301220?0100???00??020?101????000??0??0000000?00022012122
2100??000000010100??1001100001000000001110???????????0200?????0?0011?000
0010011011021111111001110111111011101000012111120100001 1?0000021001021001
000000001?00201001000111000010000121000021010?001020??1?????????????????
??
??????0??????100?0???2??????12????????0???0???????????????
Spalacotherium
1111010??000202?????2100102114011001110?00000?1101000000100?111312001200
?0100011000001301120?0100???00??020?101????000??0??0000000?00022012122
2100??0000000??????????10??000?0000000??10???????????0200?????????????
??1??????0???????
??
??
?????????????????0???
Zhangheotherium
11?0010??0002020??1221001?2114010101110?000001110100000 1?00?01131100120
0?0100011000001301110 0?0100???00??020?101????000??0??0000000?00022012122
2100??000000020200??1001002200000100001110??????????20200?11100000112110
0010011011021111111001110111111011101000012111220000000 1?11002100100?001
000000001030201001000111000010000020000021 01????1020111?00123111 12????11

01001?1?1?10???0??121011110020000000000001?0?11?1??????21??????1??????0??
????0??1????100???0???2????12??2?????????00?????????????????
Maotherium
11?0010??0002020??122100102114010101110?000001110100000001?00?01131100120
0?0100011000001301110?0100???00??020?101????000??0??0000000?00022012122
2100??000000020200??100100220000010000111?????????0200?11?0000011?110
00?00110110211?111100111011111011101000012111220000000?1?10021(01)?100?0
010000000?103020100????11100001000002(01)000021010?00102011?00123111112??
??1101001?1???10?100?11000111???2000000000001???11?????????????????12????
?0201??20?0???22??1000000???2????12?02?1???0??00??????1?????????
Dryolestes
11?1011100002020??11210?012113012001110?000010000011000 1?00?01130100130
0?0200000000000?0111000220??000??110?001????000??0??0001000?00022012122
1100?00100000100 00??000000110000000030111 0?????????20200?????????????
??
??1?????????????2311124001111
01001?1?10???????11211111??0??11000????110021??????????0?????????????
???????1???10?0?????????????????????????00??0?????????????
Henkelotherium
11?1011100002021??112101??2113012001110?00000?000001100?0?00?01130100130
0?0200000?00000?0111000220??000??110?001????000??0??0001000?00022012122
1100?00100000?0?????00?0?0110000000??0???0???????????02?0?????0??011?110
0??0???011021111?110?111011?1001110210001 21?022000000011100002110000?10?
????????1?????????????????????????0???0?1011???1020?11?00?2311124??11??
????????????????????????????0?01?000????1100????????????????????????????
???1????20001?0??1??????????20????????????????????????????
Amphitherium
11?1111100002021??11210?012103012001110?11?0?000000????01?00?0?13010013?
??0001001000000?00110000210?0000??11110?1????000??0??0001000?0002101??22
1111000000000??100?????0???000?0?00?????????????????02????????????????
??
??
??
??
Peramus
11?1111100002021??112101012103012001110?1100200002011000 0?00?01130100130
0?000100110000110011(01)0002110000(01)?01211201?0??010000??000100200001101
21221111000000000??2?????000000033 10?00??0???0???????????02?0???????????
??
??
??
??
Vincelestes
11?2?111000(01)2021??111101012113012001110?000010100000000000?00?011301001
300?000000000000100110000210??000?0120?101?0??010000??00010120000110001
221100?000000001030000001000333342000030??00???????????02?00111101001 1?1
10?1201?101?021101111001110101000 1110?000012101220000000111000021100 00?1
020?00?1001030201011000111010 0??0???210??0?001110020200 11?00123?112400?1

1101001011101001001 1(01)21111110020110000000011002111??????21?0??????????
?0101101000102010000001012000100020000100111000000??1?????????
Nanolestes
11?1011100002021??112?0??121030120011107??????00000?10000?00?0?13010013?
0?000100010000110011000021000?00?0121?101????0?0000??1012012000011012122
1111000000000 1?1?????0010?02??0?00??0???0???????????020?????????????????
??
??
??
??
Kielantherium
11?101110?002?21??111101?2????0130011?0???????00000?10000?00?0?13011013?
0?000110211000110111020151100 00(01)00120?102000?0100?0??100201110101?0121
22211100100000??????????0???12??0??0??????0???????????020?????????????????
??
??
??
??
Aegialodon
??1?01??13?
??000110211000 11?11102015110 0?11001????????????????????????????1???2122
21?1001000000??020?????????????????
??
??
??
??
Montanalestes
11?2?13100004021??111201032103013001110???????12020?10001000?0?13?2??13?
??0102101110001120120211511001110 02??????????????????????????0??0?2122
21?1001110000??????????????03??0?00????????????????02?????????????????
??
??
??
??1?????????
Prokennalestes
11?1113100001021??111201022103012001110?1(01)112?1202001000020?011302201
300?0201101110001120120211511001110022102020207010011001011010000012012 1
222121001110000????????0101?0033?0000?00?1?0???????????0200?????????????
??
??23111251111
110(12)00102?10?????13?1?111011????11001?????110?21?????????2??1??????????
???????????0????????????1????????????1????????????0?????????????
Murtoilestes
??00????????13022013?
???2021011100011?012021151100?1100?21020202 0?0?00110010110000000 12?12122
2121001?10000????????0??????????????????????????????????020?????????????????
??
??

??
??
Eomaia
11?1113100001021??111201022103012001110?10111112010010000020?01130220130
0?020?10111000112??202?151100111??2210202020?0100110010??000?00012012122
21210011??000001000000000003310010000?100???????????0200111?10100112110
01200?10110221011110021101112002210210001211122000000001?101102111000?012
2100021220302010130111110100000100210001200111?0?1?????2??0????1??51?11??
????????1?????????????????????????????11?????????????????????????0??
??????00??0??100?0???2???10??20???????02??1??????1?????????
Juramaia
1?12??11000?????????1201022?03011001110?10112012010011 00?020?01130230130
0?02?????110?0112?1??2?1511001????2211202020?0100110010110111101012012122
2121001?10000010?0?00100000331000000?100???????????02001?11101001??1??
0???????1102210??110?21?01????02210200????????????????????????????????
??
??
??????????????0??????????????????????????????????????
Kennalestes
11?2?131000040211011120002 2???0?2001110?111120100200110001 00?01130220130
0?02021021100011222203115110011100221020201 1?0100110110100 00?00012012122
21210011100001 02????0010111(01)33200100001101???????????020001 1?????????
??
??????????????2?????????????????????????????1100212211221022311125 11??
210211002(34)1?2001013?????10110020100010010011002110???????21?2???????3213
00?01102000002 00??00?0101212110002022011100210 10?00??1011223???
Asioryctes
11?2?131000040211011120002210301300 1110?111220110200110000 10?01130220130
0?02021021100011201203115110011100221020201 1?0100110010000 00?00012012122
21210011100000010000001011113321010000?101???????????020001111 01??11?110
??????????????????????????0?????0???0?11000??????2?0??00???????0??1?000?012
2100021220302010130111110100000?0200001?00111002122112210223111 25?1??21
02110?241?2001013???11101100201000100100110021 10???????21?2??????32130020
11020000020 0?1001010?212110002022011100210100 00??1011223???
Ukhaatherium
?1???????00?40???????????022???0??00?110?111220110200110000 20?01130220130
0?020?10211000112012031151100111?02210202011?0100110010000 00?00012012122
21210011100000010000000000113321010030?101???????????0200?11???1?011?110
0??0???0?10221011110?211011120022102100?1210?2200000001?101102111000?012
2100021220302010130111110100000???200??1??01??00?1?2????221???3??????????2?
?21????4?0????0???????1????????0?0???1??????21?1?????????2????????21??0?0
?????0????????00?010???21???0????????0??????0?????????????
Zalambdalestes
11?2?1(13)1000(01)40211011120(01)0221030120011 10?111221021220110001 20?0113
02201300?1203102110001102220420511000111022 0?102012?0110110000000000?0001
201212221210011100 00(23)0211?0001101(12)(12)33(23)1010200?111???????????020
0???11010011?1100??0???01?022101111 0?211011120022102100012111220000000 1?
101102111210??122100021220 3?201013?011310000000000200001?001110031221122
1022311125?1??2102110024112001013???111011002010001001001100211 1?????21

?2??????32130020110200000201?100101012111100(01)20210110002101000??10112
23???
Daulestes
11?2?131000140211011120002210301200111 0????1???????0110???00?01130220130
0?020210211000 11?11202115110011100220?102021?0100111110100 00?00012012122
2121001110000?0100??000101113320 0?? 0?100??????????0200?????????????????
??
??1100212011201022311125 11???1
0?????2?????01013???????110?201100??0?001????????1?????2??1??????3???00?0
1?1??000?100?100?000?212110?(01)20???1??00??????00??2?????????
Aspanlestes
?????1????0??0?????????1??????0???0?1?0?11112?1?010?100000?0?0113023113?
??1102102110001 1?11201215110001100220?102032?111031210 0?0000?10012012122
2121001110000?????????????033?0??0????1?0???????????020?????????????????
??
??3?????????1?
0?0?1????0?????1?????????????????00?1?????????1???????????1?????????????
???????0??
Eoungulatum
?????1?????????????????1??????0???0?1???10110???????100?????0113024213?
??1103102110001 1?11201215111001200320?102232?111031210010000?10012000?22
2121001110000?????????????1332???0????1?0???????????020?????????????????
??
??3?????????1?
??0?1????0?????????????????????000???????????1???????????1?????????????
???
Cimolestes
1??2?1010?0140211?111200?2210301 2?01110?10122?1101001100001 0?01130231130
0?020210211000112212031151100112002210102111?0100111100000000?00012012122
2121001110000??200??0?000?113321?00????1?0???????????20200?????????????????
??
??
??????????????????????????????0??
???
Gypsonictops
1??2?101000140211?111200?2210301 2?01110?11122?1212001100011 0?01130231130
0?120210211000112212041151100112002210102111?0100111100000000?00012012122
2121001110000???????0?000?113320?00????1?0???????????20200?????????????????
??
??
??
??
Protungulatum
11?2?101000140211?111200022103012001110?10120?1211001000001 0?01130242130
0?110210211000112112012151110012013 20?102232?111031000000000?10012000122
2121001110000???????0?000?113321?00????100???????????20200?????????????????
??22
2003?2122031 2?10130111312011?????????????????????????????2311125?1??1?

0?0?00??(01)0?????1?????????????11001??????1??21???????????2????????????
??????????????????????????????????1????????????????????????
Erinaceus
11?2?131000141211011120002210301300111O?10110112122001000100?01130220130
0?110310211000110112022151110012112207102122?111020??0000000?10033000122
212111111000020300001001013333420002001110??????????2020011111010011211O
01200?111102(12)10111101211011120022102100012111221?000001110111210121O?1
222003021220512010130111312011000000200101200111003121112010223111251111
210211002311300111 3???111011002011001001001100211121311121220111014213OO
211113000002001100110112121 1?022121011100211100201220112231 11
Leptictis
11?2?131000140211011120002210301300111O?11221121220010001 00?01130222130
0?110310211000112112041151100011012207102111?110011110000000?10012000122
212111111000020200000001001133210002007100???????????0200????????011?110
?1200?101???22??111?012110111200221021????2111221?000001110111221121O?122
2003?2122?312010130111312011007??0200?01??011100312111201022311125111111
020100231130011137??111011002011001001001100211O??????21?20?????32130121
111200000300010011011212111002021011100210100001220112231 ???
Canis
111??131010140211011110002211301300111O?010001001101000000 10?11110230120
0?001010000000000000010210?00121000?001020?211011000110000?31012100121
2100?021000002020000000000233231000000010O??????????2021011111011011211O
0120??101102120111101211111120022112100002111221?000001100110111111O?222
120202122051001013011 1??30110?0?00200001200111003021113111022311125111?11
?3??0?23111101113?????101100200001000000110?112(01)213111212201110142131 1
201114010013000100110112110100220221210002111110012200122311 1
Felis
111??131010140211011110002211301300111O?010001001101000000 10?11110230120
0?001010000000000000000210?00121000?001020?211000?00110000?31012100121
2100?02100???2020000000000344343O?00000100??????????2021011111011011211O
0120??101102120111101211111120022112100002111221?000001100110111111O?222
120202122051001013011 1??30110?0?00200001200111003021113111022311125111?11
?3??0?23111101113?????101100200001000000110?112021311121220111014213112O
111401001300010011011211010022022121000211111001220012231 11
Rattus
1112?111000141211011112000222?011000210??????????0000?????0013???213?
0?13?000?00000000????42041100013?1400??02022??11020??????????003100???2?
??????01?0???3?411112??2??333343???1?02112??????????2020011111010011211O
01200?101102210111000110100021022112000012111211?001011110111211110O?122
100302122050001011011?311011010100010001200111002010110020123111251111 11
010000241101011131??2?101100101001100100211111102131112122011101421300 20
111212001400110011001212011022132121000212 1?200121111223111
Oryctolagus
1112?111000140211011111000222?011?11210?001200001000000001???0013???013?
0?13?000?00000000????210410?00?3?1300??02012??11030??????????0132000?2?
??????01?0???3?411112??2??333343??0??02112??????????2131011111010011211O
01201?101102210111000200101120022102000012111201?001011110111210111O?0?2
111302122050001013010131101101010001000120011100201011002O?2311125111111

0100002411010111131??2?10110010000110010011101110213111212201110152130000
1111121003001 1?02111121201102213212100021 21?200121111223111
Bradypus
111??131010141211011110002211301 3?01110???????????0000??????00??????15?
???????????0??003?????????????????????0?????????????????????0540?????
????????????5?5????1??2??????00??????01????????????30?10111111110112111
0120??101102120111210211111120022112100021113 21?1100011001101201100?122
120102122051001013011 1??30110?0?00200001200111003021113110223111251 11?11
?3??0?23021101013?????10110020000(01)00000110?112021311121220111014213 11
30111103001010 1?0110212110110220?212100021011001122001223111
Tamandua
111??131010141211 0??????0?21?30???1??10?????????????????????0??????????
0??????????0???0?????????????????????0?????????????????????????????
?????????????505????1??2??????????????01????????????3???0111111110112111
0120??101102120111210211110120022112100021113 21?1100011001101101100?222
120102122051001013 0??1??30110?0?00200001200111003121113110223111251 11?11
?3??0?231?1101013?????10110020010000000110?112021311121220111014213 1130
111103001010 02?0110212110110220?212100021011001122001223111
Glyptotherium
111??131010141211011110002211301310111 1???????????0000??????00??????15?
0??????????0??003?????????????????????0?????????????????????0330?????
????????????505????10?2??????00??????01????????????300101111 1?110112111
0120??101102120111200211110120022112100021113 21?1100011001101201210?222
120102122051001013011 1??30110?0?00200001200111103021113110223111251 11?11
?3??0?230?1101013?????10110020000?000000110?1120????11??2201110142131130
111103001010010011021212111 0220?212101021011?01122???22311?
Dasypus
111??131010141211011110002211301310111 1???????????0000??????00??????15?
0??????????0??003?????????????????????0?????????????????????0540?????
????????????505????10?2??????43??????01????????????300101111111110112111
0120??101102120111200211110120022112100021113 21?1100011001111101210?222
120202122051001013011 1??30110?0?00200001200111103021113110223111251 11?11
?3??0?230(12)1101013?????10110020000000000110?112021311121220111014213 11
30111113001010020011011212111 0220?212101021011001122001223111
Chaetophractus
111??131010141211011110002211301310111 1???????????0000??????00??????15?
0??????????0??003?????????????????????0?????????????????????0540?????
????????????505????10?2??????43??????01????????????300101111111110112111
0120??101102120111200211110120022112100021113 21?1100011001111101210?222
120202122051001013011 1??30110?0?00200001200111113021113110223111251 11?11
?3??0?23021101013?????10110020000(01)00000110?112(01)213111212201110142 13
113011111300101002001102121211 0220?212101021011001122001223111
Euphractus
11???131010141211011110002211301310111 1???????????0000??????00??????15?
0??????????0??003?????????????????????0?????????????????????0540?????
????????????505????10?2??????43??????01????????????300101111111110112111
0120??101102120111200211110120022112100021113 21?1100011001111101210?222
120202122051001013011 1??30110?0?00200001200111113021113110223111251 11?11

?3??0?23021101013?????10110020000(01)000000110?112(01)21311121220111014213
113011111300101002001102121211022O?2121010210110011220012231 11
Holoclemensia
??????????????????????????????????0?1?????????????110????????13021013?
0?02011001100011111102115110O?2100120?202011?11000100100111211001 2?12122
2121001000000?????????????????????0?????????????????020??????????????????
??
??
??
??
??
Sinodelphys
11???131010?4021??111?0??2210301300111O?00??11?1010110??00?0?011302??130
0?0101100110001111 11?21151100121??12112?2????110??????0110121100??012122
21?100100000010100000000001132111 20?10?100??????????0200??????00112 1?0
0120??1011?2310111101 2?111112?02211211110 21????00000001?10??0?100000?012
12010??12042202011021?2110001101102100002001 1??0??????????????????????
??
??????0??????10??0???2????0??2?3??????0???????????1?????????
Deltatheridium
11?2?14101012021??1111000421030130011 10?000011000101100000000?01130210130
0?000110(02)1100011111102115110001100121120201 0?11000100100100102201201 21
22212100100000010100??000000222221110 0?12100???????????20200????????????
??
12?????????2???????110212?1??00?????????????11100?020112????2311125 10??
1101002123 12???1013????2?10110??2?00001?????1101111????????2??1???????????0
2?11?2?000?2010100?000121???0?(01)2031????002?011000????????????
Atokatheridium
??????????????????????????????????0????????????????????????1?021013?
??000110211000 11?111021151100?0??0121?202010?11000100100100102201 2?12?22
2121001000000???020??????????????????
??
??
??
??
Sulestes
11?20141010120 21??111100142?1?013101110?000011000101100000000?0?130210130
??000210211000111111211511001221122112?2010?11000100100111102201 2012122
2121001010000??????????00?222221?10????1?????????????020??????????????????
??
??231112510??1?
0????12?1?????????????????????000????????1?1?????????????????????????
????????????????????????????0??2?????????????????0?????????????
Asiatherium
11?1?141010140211?111100142?0?013001110?000011000101100000000?01130220130
0?0103102110001101111221511011221122102020 21?1111211?000100101001201 2122
2121001110000?0?????000?0?222221010?????0???????????0200??????100112110
0??0????11?2310111 10?2110111200221121111021012200000001?10110110010 0?01?
????????2????????????????????????????0?001110?30201120 10?2311125????11

11?0??23??4101013?????10?10?2??0?01?001111???11???????2?????????????020
11?2?00??21??100?0?0?2????0?(01)20???11000??????10??2?????????
Kokopellia
?1?1?1410?012??1??1?1100?(34)2?????3?01110?????1?0001011??00000?0?1302101
3?0?0102102110001100111221511011221022 1?202020?1100111?10011110100120121
222121001110000??1????0?000??222?1?10??0?100??????????2020?????????????
??
??
??
??
Anchistodelphys
??????????????????????????????????0??????????????????1????????0?1?021013?
0?020310211000 11?011122051101132102211 2?2022?121021010101111020012 0???22
2111001110000??????????????????????????????????????020?????????????????
??
??
??
??
Albertatherium
??????????????????????????????????0??????????????????1????????0??3022013?
0??????????0???1???1?????????????????2112020 22?211021011001111120 0?2?12122
2111?????000??????????????????2??????????????????????020?????????????????
??
??
??
??
Didelphodon
11?2?14101011021??1111001421130 1?001110?001???000110100000000?01130220130
0?000310211000112111122051201?321122112020 22?2102010100201102101201212 2
2111001110000?0??????0?000222221?00????1?0??????????20200?????????????????
??2
1201?101203110101102122110 11?????????????????10?302011201022311 12??0????
1??0?1??11?????1??????1??????0?00?1???????0111?????????1?1???????????0??
??????????????????????????????0???1????0???????1?????????????
Pediomys
???2?14101011021??1111001421130 1?001110?????????????100????0?01130220130
0?010310211000111111122051201132112211202022?2210211000011110100120121 22
2111001110000??????????00?222221100??????0??????????20200?????????????????
??2
1201?101204220201102122110 11?????????????????????????????123111???0????
0??0?1???1?????1??????1????????00?1???????0111???????????1?????????????
???2???0?????????????????????????1????????????1?????????????
Turgidodon
???2?14101011021 1?111100?4?11301?001110??????00010?10000000?01130210130
0?010310211000111111132151201132112211202022?2110211000011110200120121 22
2111001110000??????????000222221?00???21?0??????????2020?????????????????
??
??????????????????2?????????????????????????????????????223111???0????

0??0?1??11?????1??????1????????00?1???????0?11???????????1?????????????
??????????????????????????????????1?????????????????????????
Mayulestes
11?2?14101014?2110111100142103013001110?000011000101100000000?01130210130
0?0103102110001111111221512011311022112020222?2200211000010110210120121222
2111001110000001000000000022222110011?100??????????020011111?10011?110
01201?1011?2310111101211111120022112 1?1??2111220000000111011011100000?012
????????2042202011021211101 1??????210??0?00111003020112011123111125????11
0100??24110101013?????1011002100101000011111111??????21?????????????020
1102000002110100100 0?201010?020??011000211111 00??2?????????
Pucadelphys
11?2?141010140211011110014210301300111 0?000011000101100000000?01130210130
0?1203102110001101111221512011321022102020222?2211211100021111100120121222
2111001110000001000000000022222111011121 00??????????020011111110011211 0
01201?1011?2310111101211111121022112?????2111220000000111011011100000?012
1301010120422020110212211011?101?0210??0?00111003020112011123111251 1??11
0100212411010101 3?????1011002100101000011111111??????21?1??????2????020
11?2000002110100111012010100020310110002101110 0?21?????????
Andinodelphys
11?2?141010140211011110014210301300111 0?000011000101100000000?01130210130
0?1203102110001121111221512010321122102020222?2211211100021111100120121222
2111001110000001000000000022222111011 1?100???????????0200????????0??????
???0???0??0???????????
????????2????????????????????????????????0???111003?2011201122311125????11
01002?24110101013?????1011002100101000011111111????????21?1???????????02?
111?1000021?0100110012 01?10?020310110002101111??21?????????
Didelphis
11?2?141010141211011110014210301300111 0?000021000101100000000?01130210130
0?0203102110001101111221512010321122102020222?221120?000021111200120121222
2111001110000001000000000022222111011121 00??????????2020011111110011?110
01201?1011023101111012111111 2(01)022112121102111220000000111011011100000 0
12130101012042202111021231201111011021001020011100302011201112311125111 1
111100212311(01)101013?????1011002000001000111101111121311121210111002212
0020111210000210010011001201010002031001000211111101210112230 02
Marmosa
11?2?141010141211011110014210301300111 0?000021000101100000000?01130210130
0?0203102110001111111211512010321222102020222?221120?000021111100120121222
2111001110000001000000001002222210001112100??????????020011111110011211 0
01201?1011023101111012111111 2002211212110211122000000011101101110000001 2
13010101204220211102122120111101102100102001110030201120111231112511111 1
1100212311110101 3?????1011002000001000111101111121311121210111002212002 0
1112100002100100110112010100020311211002111111012101122300 2
Caenolestes
11???14101014?2110111100142103013001110?????????????0100????0?01?30210130
0?0203102110001111111321512010321222102020222?221120?001021010100120121222
211100111?000101000000000122222101002021 00???????0???020011111?100112110
01201?1011023101111012111111 2002211212110211122000000011101101110000?012
13020?0120422010110212211011110000210100200111003020112 0?112311125111111

13002?23110101013?????10?10020000000002111011111213 1??211101110032120020
11131000021?010011?012010100020 32??10002111?220121???223002
Dasyurus
11?2?14101014021101111001421030130011 10?00(01)021000101100000 00?011302101
300?020310211000111111122151201032122211202022?221120?001021010200120121
22211100111000010200000000003322311000112100?????????? 02001111111001121
1001201?10110231011110121111112002211212110211122000000011101101110000?0
12131201012051001012121 3?11011110000210100200111003020112011323111251111
11130021231011010 13?????10110020000010002111011121?131??2111011100421200
20111112000211010011011201010002032011000211111101210 11223002
Perameles
11???14101014121101111001421030130011 10???????????0000????0?0??30210130
0?020210211000112111132151200032122210202022?221120?001021010200120121 22
211100111?000002000000000122222101002121 01???????????020011111100112110
01201?10110231011110121111112002211212110211122000000011101101100100?012
13020?11205100201212 13?11011110100200100201111003020112021123111251111 11
13002?23114101013?????10110020000010002111011111213 1??211101110042120020
11121000021001001101120101000203212100021110110121???223001
Dromiciops
1112?14101014021101111001421030130011 10?000021000100000000 00?0?130210130
0?020310211000111011132051201032122211202022?221120?000000011100120121 22
211100111000000100000001012222210100212100?????????? 02001111?100112110
01201?10110231011110121111112002211212110211122000000011101101110000?012
13020?11205100201212 13?12011110100210010200111003020112011123111251111 11
13002?231?4101013?????10110020000010002111001110213 1??212201110032130020
11111000031101001100120?0100020321211002101111012101 1223002
Thylacomyidae
111??14101014?21101111001421030130011 10???????????1000????0?01?30?????0
0??????????00011??11132??1????3???4????02042???1120?00100001??0112012122
2101???1100000020000 00???222221??0??2?10??????????? 02001111?100112110
01201?10110231011110121 1?1112002211211110211122000000011101101110000?012
130?0???20510020121213?1??11??0?002?0?00201111030 2?112?1132311125111111
13002?2310?101013?????1011002?000010002?1???11??2131??21??0?1100421?0020
111?1000021?010011?012?101?0020?2??1?0021?1???0121???22300?
Macropus
111??14101014021101111001421030130011 10???????????0000????0?0??3?253130
0?130300200000113301132041310043124 00?302042?21112 0?00100000?30012012122
2101110110???20400001?????332232?1102021 12??1??1?0???020011111100112110
01201?10110231011110121111112002211211110211122001000011101101210010?012
13120?11205100101212 13?11011110100200000201111003021113130323111251111 11
13002?23114101013?????10110020000010003111001111213 1??212201110052130020
11111100131101001100120101000303212110021 01?0(012)0121???223002
Acrobates
111??14101014121101111001421030130011 10???????????0000????0?0??3?353130
0?130210200000110101132151200042124 20?302042?21112 0?00100001110012012122
2101001110???00300000001 0?22223100002021 10???????????020011111?100112110
01201?10110231011110121111112002211211110211122000000011101101110000?012
13020?11205100201212 13?12?11110100 2?0?10201111003021113130323111251111 11

13002?23114101013?????10110020000010001111011202131??212?11110052131020
11131000031101001100120101000203212110021111120121???223002
Phascolarctos
111??131010140211011110014210301300110???????????0000????0?0??3?353130
0?130320200000113301132041300043124 20?302042?211120?00100100?30112012122
2101110110???20400001 0????332233?20010211?????????? 020011111100112110
01201?10110231011110121111112002211211110211122001000011101101110000?012
13020?11205100201212 13?11011110100210010201121003021110010323111251111 11
13002?23114101013?????10110020000010002111011111213 1??211201110032130020
11131100141001001110120101000303201100021111020121???223002
Vombatus
111??141010140211011110014210301300110???????????0000????0?0??3?353130
0?130320200000113301132041310043124 20?302032?211120?00100000?30112012122
2101110110???30401012 0????332233?201?02112?????????? 020011111100112110
01201?10110231011110121111112002211211110211122001000011101101100100?012
13020?11205100201212 13?11011110100210010201121003021110?0032311125111111
13002?23023101013?????10110020000010001111001111213 1??211201110052130020
11131000141101001100120101000303202100021111001121???223002
Phalanger
111??141010140211011110014210301300111 0???????????0000????0?0??3?353130
0?130320200000113300132151200043124 20?302042?211120?00100100?30012012122
2101110110???20300000001 0?222222021020211 1??????????020011111100112110
01201?10110231011110121111112002211211110211122000000011101101110000?012
13020?11205100201212 13?12011110100210010201121003021113130323111251111 11
13002?23114101013?????10110020000010003111001111213 1??212211110052131020
11131100131001001100120101000303202100021111120121???223002
Pseudocheirus
111??141010140211011110014210301300111 0???????????0000??????0??3?353130
0?130320200000113300132041300042124 20?302042?211120?00100100?30112012122
2101110110???20300001001 0?33223200002021 11??????????020011111100112110
01201?10110231011110121111112002211211110211122000000011101101110000?012
13020?11205100201212 13?12011110100210010201121003021113130323111251111 11
13002?23114101013?????10110020000010003111001121213 1??212211110052131020
11121000031101001100120101001203212100021111120121???223002
Petauroides
111??141010140211011110014210301300111 0???????????0?00??????0??3?353130
0?130320200000113300132041300042124 20?302042?211120?00100100?30012012122
2101110110???20300000001 0?33223200002021 11??????????020011111100112110
01201?10110231011110121111112002211211110211122000000011101101110000?012
13120?11205100201212 13?12011110100210010201121003021113130323111251111 11
13002?23114101013?????10110020000010003111001121213 1??212211110052131020
11121000021101001100120101001203212110021011120121???223002
;
End;

APPENDIX 15: Characters used in expanded phylogenetic analysis

Mandible

1 Post-dentary trough (behind the tooth row):
(0) Full presence of the postdentary trough—the plesiomorphic state;
(1) Reduced postdentary trough in angular region and below dentary peduncle—the intermediate state;
(2) (2) Absence of the postdentary trough—the most derived state.

2 Separate scars for the surangular/prearticular in the mandible: (0) Present; (1) Absent.

3 Overhanging medial ridge above the post-dentary trough (behind the tooth row): (0) Present; (1) Absent.

4 Degree of development of Meckel's sulcus: (0) Well developed; (1) Short, and limited to below the mandibular foramen; (2) Vestigial or absent.

5 Curvature of Meckel's sulcus (under the tooth row): (0) Parallel to the ventral border of the mandible; (1) Convergent on the ventral border of the mandible.

6 Groove for the replacement dental lamina (Crompton's groove): (0) Present; (1) Absent.

7 Angular process of the dentary: (0) Weakly developed to absent; (1) Present, distinctive but not inflected; (2) Present and transversely flaring (This is different from character state {4} in having a lateral expansion of the angle and in lacking the anterior shelf); (3) Present and slightly medially inflected; (4) Present, strongly inflected, and continuing anteriorly as the mandibular shelf.

8 Position of the angular process of the dentary relative to the dentary condyle: (0) Anterior position (the angular process is below the main body of the coronoid process, separated widely from the dentary condyle); (1) Posterior position (the angular process is positioned at the level of the posterior end of the coronoid process, either close to, or directly under the dentary condyle).

9 Vertical elevation of the angular process of the dentary relative to the molar alveoli: (0) Angular process low, at or near the level of the ventral border of the mandibular horizontal ramus; (1) Angular process high, at or near the level of the molar alveolar line (and far above the ventral border of the mandibular horizontal ramus).

10 Flat ventral surface of the mandibular angle: (0) Absent; (1) Present.

11 Exoflection of the angular process of mandible: (0) Absent; (1) Present.

12 Coronoid bone (or its attachment scar): (0) Present and significant; (1) Vestigial; (2) Absent.

13 Location of the mandibular foramen (posterior opening of the mandibular canal): (0) Within the postdentary trough or in the posterior part of Meckel's sulcus; (1) In the pterygoid fossa and offset from Meckel's sulcus (the intersection of Meckel's sulcus at the pterygoid margin is ventral and posterior to the foramen); (2) In the pterygoid fossa and in alignment with the posterior end of Meckel's sulcus; (3) In the pterygoid fossa but not associated with Meckel's sulcus; (4) Not associated with any of the above structures.

14 Vertical position of the mandibular foramen: (0) Below the alveolar plane; (1) At or above the alveolar plane.

15 Concavity (fossa) for the reflected lamina of the angular bone on the dentary: (0) Present the medial side; (1) Present on the posterior aspect; (2) Absent.

16 Splenial bone as a separate element (as indicated by its scar on the dentary): (0) Present; (1) Absent.

17 Relationship of the "postdentary" complex (surangular-articular-prearticular) to the craniomandibular joint (CMJ) [CMJ is made of several bones in the stem groups of mammals or mammaliaforms, whereas the temporomandibular joint (TMJ) is the medical and veterinary anatomical term applicable to living mammals in which the jaw hinge is made only of the temporal (squamosal) bone and the dentary. CMJ and TMJ are used interchangeably here as appropriate to the circumstances]: (0) Participating in CMJ; (1) Excluded from CMJ.

18 Contact of the surangular bone (or associated postdentary element) with the squamosal:
(0) Absent; (1) Present.

19 Pterygoid muscle fossa on the medial side of the ramus of the mandible: (0) Absent; (1) Present.

20 Medial pterygoid ridge (shelf) along the ventral border of the body of the mandible: (0) Absent; (1) Present; (2) Pterygoid shelf present and reaching the dentary condyle via a low crest.

21 Ventral border of the masseteric fossa: (0) Absent; (1) Present as a low and broad crest;
(2) Present as a well-defined and thin crest.

22 Crest of the masseteric fossa along the anterior border of the coronoid process: (0) Absent or weakly developed; (1) Present and distinctive; (2) Hypertrophied and laterally flaring.

23 Anteroventral extension of the masseteric fossa: (0) Absent; (1) Extending anteriorly onto the body of the mandible; (2) Further anterior extension below the ultimate premolar/first molar.

24 Labial mandibular foramen inside the masseteric fossa: (0) Absent; (1) Present.

25 Posterior vertical shelf of the masseteric fossa connected to the dentary condyle: (0) Absent; (1) Present, either a thin crest along the curved angular margin of mandible, or a vertically oriented thicker crest, connected to dentary condyle in both configuration.

26 Posterior-most mental foramen: (0) In the canine and anterior premolar (premolariform) region (in the saddle behind the canine eminence of the mandible or behind incisor if canine is absent); (1) Below the penultimate premolar (under the anterior end of the functional postcanine row); (2) Below the ultimate premolar; (3) At the ultimate premolar and the first molar junction; (4) Under the first molar.

27 Articulation of the dentary and the squamosal: (0) Absent; (1) Present, but without condyle/glenoid; (2) Present, with condyle/glenoid.

28 Shape and relative size of the dentary articulation: (0) Condyle small or absent; (1) Condyle massive, bulbous, and transversely broad in its dorsal aspect; (2) Condyle mediolaterally narrow and vertically deep, forming a broad arc in lateral outline, either ovoid or triangular in posterior view.

29 Orientation of the dentary peduncle (condylar process) and condyle: (0) Dentary peduncle more posteriorly directed; (1) Dentary condyle continuous with the semicircular posterior margin of the dentary; the condyle is facing up due to the up-turning of the posterior- most part of the dentary; (2) Dentary articulation extending vertically for the entire depth of the posterior mandibular ramus; it is confluent with the ramus and without a peduncle; the dentary articulation is posteriorly directed; (3) More vertically directed dentary peduncle.

30 (L30). Ventral (inferior) border of the dentary peduncle: (0) Posteriorly tapering; (1) Columnar and with a lateral ridge; (2) Ventrally flaring; (3) Robust and short; (4) Ventral part of the peduncle and condyle continuous with the ventral border of the mandible.

31 Gracile and elongate dentary peduncle: (0) Absent; (1) Present.

32 Position of the dentary condyle relative to the level of the postcanine alveoli: (0) Below or about the same level; (1) Above.

33 Tilting of the coronoid process of the dentary (measured as the angle between the anterior border of the coronoid process and the horizontal alveolar line of all molars): (0) Coronoid process strongly reclined and the

coronoid angle obtuse (≥150 degrees); (1) Coronoid process less reclined (135-145 degrees); (2) Coronoid process less than vertical (110-125 degrees); (3) Coronoid process near vertical (95-105 degrees).

34 Gracile base of the coronoid process: (0) Absent; (1) Present.

35 Height of the coronoid process of the dentary: (0) Not reduced; (1) Reduced.

36 Alignment of the ultimate lower molar (or posterior-most postcanine) to the anterior margin of the dentary coronoid process (and near the coronoid scar if present): (0) Ultimate lower molar medial to the coronoid process; (1) Ultimate lower molar aligned with the coronoid process.

37 Direction of lower jaw movement during occlusion (as inferred from teeth): (0) Dorsal movement; (1) Dorsomedial movement with a significant medial component; (2) Dorsoposterior or dorsal-posterior movement.

38 Dentary symphysis: (0) Fused; (1) Unfused.

39 Rostral mandibular spout: (0) Absent; (1) Present.

40 Relative dentary depth in relation to the length: (0) Shallow; (1) Deep.

Premolars

41 Ultimate upper premolar with two rows of multiple cusps: (0) Absent; (1) Present.

42 Upper ultimate and penultimate premolars basined (with main cusps located peripherally surrounding a shallow and broad central basin): (0) absent; (1) present.

43 Upper ultimate and penultimate premolars central valley: (0) the mesial end open; (1) the mesial end closed (trenched when deeply worn).

44 Ultimate upper premolar width relative to the first upper molar: (0) Ultimate upper premolar transversely narrower than, or subequal to, the first upper molar; (1) Ultimate upper premolar transversely wider than the first upper molar; (2) Ultimate upper premolar with a protruding lingual lobe (wider than M1 by about 50% or more).

45 Enamel ridges or flutings on cusps of upper premolars: (0) absent; (1) present.

46 Ultimate upper premolar with multi-rows of cusps—Labial row of cuspules: (0) Absent;
(1) Present.

47 Ultimate upper premolar—metastylar lobe: (0) Reduced or absent; (1)

Enlarged and wing-like.

48 Ultimate upper premolar—metacone or metaconal swelling: (0) Absent; (1) Present.

49 Ultimate upper premolar—protocone or protoconal swelling: (0) Little or no lingual swelling; (1) Present.

50 Penultimate upper premolar—protocone or protoconal swelling: (0) Little or no lingual swelling; (1) Protoconal swelling; (2) Distinctive and functional protocone.

51 Position the upper premolar with the tallest cusp within the premolar series: (0) No premolar standing out; (1) In ultimate premolar position; (2) In penultimate premolar position.

52 Diastema posterior to the first upper premolar (applicable to taxa with premolar-molar differentiation): (0) Absent; (1) Present.

53 Penultimate upper premolar **with multiple cusp-rows**: tallest cusp position within longitudinal cusp row: (0) Central; (1) Tallest cusp anterior with posterior cusps (if existing) with decreasing heights; (2) Tallest cusp on buccal row; (3) Cusps of even height.

54 Hypertrophic mesial cusp on ultimate lower premolar: (0) Absent; (1) Present.

55 Ultimate lower premolar—symmetry of the main (middle) cusp a (= protoconid): (0) Asymmetrical (anterior edge of cusp a is more convex in outline than the posterior edge); (1) Symmetrical (anterior and posterior cutting edges are equal or subequal in length; neither edge is more convex or concave than the other in lateral profile).

56 Ultimate lower premolar—anterior cusp b (= paraconid): (0) Absent or indistinctive; (1) Present and distinctive; (2) Enlarged.

57 Ultimate lower premolar—arrangement of principal cusp a, cusp b (if present), and cusp c (assuming the cusp to be c if there is only one cusp behind the main cusp a): (0) Aligned in a single straight line or at a slight angle; (1) Distinctive triangulation; (2) Premolar multicuspate in longitudinal row(s).

58 Ultimate lower premolar – posterior-most (distal) cingulid or cingular cuspule (in addition to cusp c or the metaconid if the latter cusp is present on a triangulated trigonid): (0) Absent or indistinctive; (1) Present; (2) Present, in addition to cusp c or the c swelling; (3) Presence of the continuous posterior (distal) cingulid at the base of the crown.

59 Ultimate lower premolar—outline: (0) Laterally compressed (or slightly

angled); (1) Transversely wide (by trigonid); (2) Transversely wide (by talonid); (3) Transversely wide (by inflated anterior cusp and/or distal basined heel).

60 Posterior upper premolar – single enlarged anterior (mesial) sectorial cusp (scored on anterior postcanine in taxa without differentiation of premolars from molars): (0) Absent; (1) Present.

61 Penultimate or ultimate lower premolar with carnassial shearing notch in the middle of the tooth (score on anterior postcanines in taxa where premolars undifferentiated from molars):
(0) Absent (single cusp shearing); (1) Present:

62 Lower premolars – basined heel (score on anterior postcanines in taxa in which premolars are not differentiated from molars): (0) Absent; (1) Weakly developed; (2) Full molarization of posterior premolars.

63 Lower premolar: presence of a distinctive distal cingulid with cuspules or crenulated cingulid, and their topographic relation to the main cusp row: (0) Absence of crenulation or cuspules on cingulid row; (1) Present and labially positioned; (2) Present and lingually positioned.

64 Ultimate lower premolar - labial cingulid: (0) Absent or vestigial; (1) Present (at least along the length of more than half of the crown); (2) cuspate distal cingulid.

65 Ultimate lower premolar - lingual cingulid: (0) Absent or vestigial; (1) Present.

66 Ultimate lower premolar - relative height of primary cusp a to cusp c (measured as the height ratio of a and c from the bottom of the valley between the two adjacent cusps): (0) Indistinctive; (1) Posterior cusp c distinctive but less than 30% of the primary cusp a; (2) Posterior cusp c and primary cusp a equal or subequal in height (c is 40%-100% of a).

67 Penultimate lower premolar - paraconid (=cusp b): (0) Absent; (1) Present but not distinctive; (2) Distinctive and slightly enlarged.

68 Penultimate lower premolar - arrangement of principal cusp a, cusp b (if present), and cusp c (we assume the cusp to be c if there is only one cusp behind the main cusp a): (0) Individual cusps in straight alignment (for a tooth with a single cusp, the anterior and posterior crests from the main cusp are in alignment): (1) Cusps in reversed triangulation; (2) With multicusps or multi-serrations in a single longitudinal row; (3) With multicusps or multi- serrations rows.

69 Penultimate lower premolar – labial cingulid: (0) Absent; (1) Present.

70 Gradation of elongation of posterior penultimate premolars: (0) Absent; (1)

Present.

Molar Morphology

71 (B71). The mesial U-ridge of upper molars with multi-rows of cusps: (0) Absent; (1) Present;
(2) Closed by the cuspules.

72 Cuspules and/or transverse fluting of the central basin on upper molars: (0) Absent; (1) Present.

73 Position of cusp A1 on upper molars: (0) A1 is at the same level as B1; (1) A1 is distal to B1.

74 M1 cusp formula (A row relative to B row): (0) 4:4 or lower; (1)5:4; (2) 6:4 or higher.

75 Alignment of the main cusps of the anterior lower molar(s) (justification for separating this feature from the next character on the list): Several taxa of "obtuse-angled symmetrodonts" and eutriconodont amphilestids show a gradient of variation in cusp triangulation along the molar series; the degree of triangulation may be different between the anterior and posterior molars): (0) Single longitudinal row; (1) Reversed triangle–acute (≤90o); (2) Two or more longitudinal multicuspate rows.

76 Triangulation of cusps in the posterior lower/upper molars: (0) Absent; (1) Multi-row and multi-cuspate; (2) Posterior molars slightly triangulated; (3) Posterior molars fully triangulated.

77 B1 cusp on the upper molar (applicable to molars with triangulation): (0) Absent; (1) Present:

78 Postvallum/prevallid shearing (angle of the main trigonid shear facets, based on the second lower molar): (0) Absent; (1) Present, weakly developed, slightly oblique; (2) Present, strongly developed and more transverse; (3) Present, strongly developed, short and slightly oblique.

79 Rank of postvallum shear (on the upper second molar; applicable to molars with reversed triangulation of cusps) (increasing the ranks of postvallum shear and can be ordered): (0) Present but only by the first rank: postmetacrista; (1) Present, with the addition of a second rank (postprotocrista below postmetacrista) but the second rank does not reach labially below the base of the metacone; (2) Metacingulum/metaconule present, in addition to postprotocrista, but the metacingulum crest does not extend beyond the base of the metacone; (3) Metacingulum extended beyond metacone; (4) Metacingulum extended to the metastylar lobe; (5) Second rank postvallum shear forming a broad shelf (as in selenodonty).

80 Postcingulum: (0) Absent or weak; (1) Present; (2) Present and reaching past the metaconule; (3) Formed by the hypoconal shelf raised

to near the level of the protocone.

81 Precise opposition of the upper and lower molars: (0) Absent; (1) Present (either one- to-one, or occluding at the opposite embrasure or talonid); (2) Present (one lower molar contacts sequentially more than one upper molar).

82 Relationships between the cusps of the opposing upper and lower molars: (0) Absent; (1) Present, lower primary cusp a occludes in the groove between upper cusps A, B; (2) Present, lower main cusp a occludes in front of the upper cusp B and into the embrasure between the opposite upper tooth and the preceding upper tooth; (3) Present, parts of the talonid occluding with the lingual face (or any part) of the upper molar; (4) Lower multicuspate rows alternately occluding between the upper multicuspate rows; (5) Columnar tooth without cusps and with beveled wear across the entire crown contact surface.

83 Lower m1 with multicuspate rows- lingual row occlude into the basin of upper molar: (0) Absent; (1) Present.

84 Lower m2 with multicuspate rows – the lingual cusp row occlude into the basin of upper molar: (0) Absent; (1) Present.

85 The distal end of lower molars with multi-rows of cusps: (0) Absent; (1) Closed by the ridge;(2) Closed by the cuspules.

86 The cuspules or ridges of the central basin on lower molars: (0) Absent; (1) Present.

87 Fusiform (“spindle-shaped”) shearing valley between lingual cusp row and labial cusp row on lower molar: (0) Absent; (1) Present.

88 m1 main lingual row cusp count (distribution revised): (0) 4 or fewer; (1) 5; (2) 6 or more.

89 Lower molars with pyramidal cusps (in contrast to conical cusps): (0) absent; (1) present.

90 Protoconid (cusp a) and metaconid (cusp c) height ratio (on the lower second molar):
(0) Protoconid distinctively higher; (1) Protoconid and metaconid nearly equal in height.

91 Relative height and size of the base of the paraconid (cusp b) and metaconid (cusp c) (on the lower second molar): (0) Paraconid distinctively higher than the metaconid; (1) Paraconid and metaconid nearly equal in height; (2) Paraconid lower than metaconid; (3) Paraconid reduced or absent.

92 Elevation of the cingulid base of the paraconid (cusp b) relative to the cingulid base of the metaconid (cusp c) on the lower molars: (0) Absent; (1) Present.

93 Cristid obliqua (or “oblique cristid”, character definition following Fox, 1975: defined as the oblique crest anterior to, and connected with, the labial-most cusp on the talonid heel, the leading edge of facet 3): presence vs. absence and orientation (applicable only to the molar with at least a hypoconid on the talonid or a distal cingulid cuspule): (0) Absent; (1) Present, contact closest to the middle posterior of the metaconid; (2) Present, contact closest to the lowest point of the protocristid; (3) Present, contact closest to the middle posterior of the protoconid.

94 Lower molar - medial and longitudinal crest (=‘pre-entocristid’ or ‘pre-hypoconulid’) on the talonid heel (only applicable to taxa with talonid or at least a cusp d): (0) Talonid (or cusp d) has no medial and longitudinal crest; (1) Medial-most cristid (‘pre-entoconid cristid’) of the talonid in alignment with the metaconid or with the post-metacristid if the latter is present (the postmetacristid is defined as the posterior crest of metaconid that is parallel to the lingual border of the crown), but widely separated from the latter; (2) Medial-most cristid of the talonid (‘pre- hypoconulid’ cristid) is hypertrophied and in alignment with the postmetacristid and abuts the latter by a V-notch; (3) ‘Pre-entocristid’ crest is offset from the metaconid (and postmetacristid if present), and the ‘pre-entocristid’ extending anterolingually past the base of the metaconid.

95 Posterior lingual cingulid of the lower molars: (0) Absent or weak; (1) Distinctive; (2) Strongly developed, crenulated with distinctive cuspules (such as the kühneocone).

96 Anterior internal (mesio-lingual) cingular cuspule (e) on the lower molars: (0) Present as an anterior cuspule but not at the cingulid level; (1) Present, at the cingulid level; (2) Present, positioned above the cingulid level; (3) Hypertrophied cusp e = pseudo-hypoconulid; (4) Absent.

97 Anterior and labial (mesio-buccal) cingular cuspule (f): (0) Absent; (1) Present; (2) Hypertrophied to form pseudo-hypoconid.

98 Mesial cingulid features above the gum: (0) Absent; (1) Weak and discontinuous, with individualized cuspules below the trigonid (as individual cuspule e, f, or both, but e and f are not connected); (2) Present, in a continuous shelf below the trigonid (with no relations to the protoconid and paraconid), without occlusal function; (3) Present, with occlusal contact to the upper molar.

99 Crest connecting main cusp a to lingual cingulid cusp g or the cusp g position: (0) Absent; (1) Present.

100 Cingulid shelf wrapping around the anterolingual corner of the molar to extend to the lingual side of the trigonid below the paraconid: (0) Absent; (1) Present, without occlusal function to the upper molars; (2) Present, with occlusal function to the upper molars.

101 Postcingulid (distal transverse cingulid above the gum level) on the lower molars: (0) Absent; (1) Present, horizontal above the gum level.

102 Lower molars interlocking: (0) Absent; (1) Present.

103 Lower molars interlocking - types of interlocking mechanisms: (0) Posterior cingular cuspule d (or the base of the hypoconulid) of the preceding molar fits in between cingular cuspules e and f of the succeeding molar; (1) Posterior cingular cuspule d fits between cingular cuspule e and cusp b of the succeeding molar; (2) Posterior cingular cuspule d or cingulum of the preceding molar fits into an embayment or vertical groove of the anterior aspect of the succeeding molar (without any involvement of distinctive cingular cuspules in interlocking). (3) Anterior corner of succeeding lower molar overlapping posterior corner of preceding lower molar.

104 Size ratio of the last three lower postcanines: (0) Ultimate molar is smaller than the penultimate molar (m1≥m2≥m3; or m2≥m3≥m4; or m3≥m4≥m5; or m4≥m5≥m6; or p4≥m1≥m2); (1) Penultimate molar is the largest of the molars (m1≤m2≤m3≥m4; or m1≤m2>m3); (2) Ultimate molar is larger than the penultimate molar (m1≤m2≤m3); (3) Equal size.

105 Paraconid position relative to the other cusps of the trigonid on the lower molars (based on the lower second molar): (0) Paraconid in anterolingual position; (1) Paraconid lingually positioned (within lingual 1/4 of the trigonid width); (2) Paraconid lingually positioned and appressed to the metaconid; (3) Paraconid reduced in the selenodont/lophodont patterns.

106 Orientation of the paracristid (or the crest between cusps a and b) relative to the longitudinal axis of the molar (This is separated from the previous character [“lingual” vs. “labial” position of the paraconid] because of the different distribution of the a-b crest among mammals with non-triangulated molars sampled here): (0) Longitudinal orientation; (1) Oblique; (2) Nearly transverse.

107 Angle of the paracristid (b-a crest) and the protocristid (a-c crest) on the lower molar:
(0) > 90 degrees; (1) 90 ~ 50 degrees; (2) < 35 degrees.

108 Mesiolingual vertical crest of the paraconid on the lower molars (applicable only to taxa with reversed triangulation of the molar cusps): (0) Rounded; (1) Forming a keel.

109 Anteroposterior shortening at the base of the trigonid relative to the talonid (applicable only to taxa with a talonid heel with a distal cusp d; measured at the lingual base of the lower second molar trigonid where possible): (0) Trigonid long (extending over 3/4 of the tooth length);
(1) Swelling on the side walls of the trigonid (taxa assigned to this character state have a trigonid length ratio 45%~50%; but their morphology is different from all other states in

that their side walls are convex); (2) No shortening (trigonid 50-65% of tooth length); (3) Some shortening (the base of trigonid < 50% of tooth length); (4) Anteroposterior compression of trigonid (trigonid 40~45% of the tooth length).

110 Molar (the lower second molar measured where possible) trigonid/talonid heel width ratio: (0) Narrow (talonid ≤40% of trigonid); (1) Wide (talonid is 40-70% of the trigonid in width); (2) Talonid is equal or wider than trigonid.

111 Lower molar hypoflexid (concavity anterolabial to the hypconid or cusp d): (0) Absent or shallow (all "triconodont-like" teeth are coded as "0" here as long as they have cuspule d); (1) Deep (40~50% of talonid width); (2) Very Deep (>65%).

112 Morphology of the talonid (or the posterior heel) of the molar: (0) Absent; (1) Present, as an incipient heel, a cingulid, or cingular cuspule (d); (2) Present, as a transverse 'V-shaped' basin with two functional cusps; (3) Present, as an obtuse 'V-shaped' triangle; (4) Present as a basin (rimmed with 3 functional cusps with at leas is a functional crest to define the medial rim of the basin if the entoconid is not already present) with wear occurs only crests but absent from the bottom of the basin; (5) As a functional basin (rimmed by 3 cusps) with wear occurs inside the basin.

113 Hypoconid (we designate the distal cingulid cuspule d as the homolog to the hypoconid in the teeth with linear alignment of the main cusps; we assume the cusp to be the hypoconid if there is only a single cusp on the talonid in the teeth with reversed triangulation): (0) Present, but not elevated above the cingulid level; (1) Present (as distal cusp d), elevated above the cingulid level, labially positioned (or tilted in the lingual direction); (2) Present (larger than cusp d, with occlusal contact to the upper molar), elevated above the cingulid level, labially positioned.

114 Hypoconulid (if there are only two functional cusps on the talonid, we assume that the second and more lingual cusp on the talonid to be the hypoconulid): (0) Absent; (1) Present, and median (near the mid-point of the transverse talonid width); (2) Present, and placed within the lingual 1/3 of the talonid basin; (3) Incorporated into the crest of lophodont or selenodont conditions.

115 Anterior lower molar (preferably the first, or the second if the first is not available) - hypoconulid - anteroposterior orientation: procumbent vs. reclined (applicable to the taxa with at least two cusps on the talonid): (0) Cusp tip reclined and the posterior wall of the hypoconulid is slanted and overhanging the root; (1) Cusp tip procumbent and the posterior wall of the cusp is vertical; (2) Cusp tip procumbent and the posterior wall is gibbous.

116 Hypoconulid labial postcingulid (shelf) on the lower molars (non-homologous with the postcingulid coded elsewhere in this list because of the

different relationship to the talonid cusps; applicable to taxa with identifiable hypoconid and hypoconulid only): (0) Absent; (1) Present as a crest descending mesiolabially from the apex of the hypoconulid to the base of the hypoconid.

117 Last lower molar - hypoconulid - orientation and relative size (applicable to the taxa with at least a talonid heel; scored on the third molar for *Peramus* and eutherians, the fourth molar for *Kielantherium* and metatherians; justification for separating this character from the character of the anterior molar hypoconulids is that the ultimate molar shows different morphology and distribution, especially in taxa in which there is a posteriorly decreasing size gradient, e.g. *Deltatheridium*): (0) Short and erect; (1) Tall (higher than hypoconid) and recurved.

118 Entoconid (if there are three functional cusps on the talonid, we assume that the third and lingual-most functional cusp on the talonid is the entoconid): (0) Absent; (1) Present, about equal distance to the hypoconulid as to the hypoconid; (2) Present, with slight approximation to the hypoconulid (distance between the hypoconulid and entoconid noticeably shorter than between the hypoconulid and hypoconid); (3) Present, and twinned with the hypoconulid.

119 Height ratio of the medial side of the crown (apex of the hypoconid to the base of the labial crown) vs. the most lingual cusp on the talonid to the base of the labial crown (this character can be based either on the entoconid if the entoconid is present or the hypoconulid if the entoconid cannot be scored): (0) Entoconid absent on the talonid heel; (1) Entoconid lower than the hypoconid; (2) Entoconid near the height of the hypoconid; (3) Entoconid near the height of the hypoconid and linked to the hypoconid by a transverse crest.

120 Alignment of the paraconid, metaconid, and entoconid on the lower molars (applicable only to taxa with triangulation of the trigonid cusps and the entoconid present on the talonid): (0) Cusps not aligned; (1) Cusps aligned.

121 The length vs. width ratio of the functional talonid basin of the lower molars (in occlusal view, measured at the cingulid level, and based on the second molar): (0) Longer than wide (or narrows posteriorly); (1) Length equals width; (2) Wider than long.

122 Elevation of the talonid (measured as the height of the hypoconid from the cingulid on the labial side of the crown) relative to the trigonid (measured as the height of protoconid from the cingulid) (applicable only to the teeth with reversed triangulation): (0) Hypoconid/protoconid height ratio less than 20% (hypoconid or cusp d is on the cingulid); (1) Hypoconid/protoconid height ratio between 25% and 35% (talonid cusp elevated above the cingulid level); (2) Hypoconid/protoconid height ratio between 40% and 60%; (3) Hypoconid/protoconid height ratio between >60% and 80%; (4) Equal height.

123 Size (labiolingual width) of the upper molar labial stylar shelf on the penultimate molar: (0) Absent; (1) Present and narrow; (2) Present and broad.

124 Presence vs. absence of the ectoflexus on the upper second molar (or postcanines in the middle portion of the postcanine row). Comments: justification for separating this character from the next is that only a single upper molar is known for three taxa that are otherwise crucial for assessing the timing and biogeography of the divergence of earliest-known crown therians: *Murtoilestes*, *Atokatheridium*, and *Kokopellia*. *Nanolestes* and *Shuotherium* are also only represented by isolated upper molars. Therefore, the gradient character of the ectoflexus along the tooth row is not applicable for these taxa. Presence vs. absence of the ectoflexus alone does not exhaust the systematic distribution of the ectoflexus-related characters among taxa with isolated upper molars. (0) Absent or weakly developed; (1) Present.

125 Ectoflexus gradient along the molar series (see the above for justification of separating presence/absence from the gradient of the ectoflexus on the upper molar(s)): (0) Present on penultimate molar, but weakly developed or absent on the anterior molars; (1) Present on the penultimate and preceding molars.

126 Morphological features on the labial cingulum or stylar shelf of the upper molars (excluding the parastyle and metastyle): (0) Indistinctive; (1) Distinctive cingulum, without cuspules; (2) Individualized or even hypertrophied cuspules; (3) W-pattern on stylar shelf; (4) Cingulum crenulated with distinctive and even-sized multiple cuspules.

127 Distinctive lingual cingulum on upper molariforms: (0) Absent; (1) Present.

128 Upper molar protocone: (0) Functional cusp and lingual swelling absent; (1) Functional cusp absent, but the lingual side is more swollen than the labial side at the cingular level; (2) Functional cusp present.

129 Degree of labial shift of the protocone (distance from the protocone apex to the lingual border vs. the total tooth width, in %) (applicable only to those taxa with reversed triangulation): (0) Protocone present but no labial shift (10%-20%); (1) Moderate labial shift (25%-30%); (2) Substantial labial shift (≥ 40%).

130 Morphology of the protocone (applicable only to those taxa with reversed triangulation and a lingual swelling of the upper molar): (0) Protoconal region present but no distinct protocone; (1) Protocone present, its apical portion anteroposteriorly compressed; (2) Apical portion slightly expanded; (3) Apical portion expanded; (4) Apical portion forming an obtuse triangle with the protoconal cristae.

131 Height of the protocone/pseudoprotocone relative to the paracone and metacone (whichever is higher of the latter two): (0) Protocone/pseudoprotocone markedly lower (less than 70%); (1) Protocone of intermediate height (70%~80%); (2) Protocone/pseudoprotocone near the height of paracone and metacone (within 80%).

132 Height and size of upper molar cusp B and cusp C of triconodont-type molariform (based on the upper second molar if available): (0) Paracone noticeably higher and larger at the base than metacone; (1) Paracone and metacone of equal size or paracone, or sub-equal.

133 Height and size of the paracone and metacone (applicable only to molars with cusps of triangular arrangement; based on the upper second molar if available): (0) Paracone noticeably higher and larger at the base than metacone; (1) Paracone slightly larger than metacone; (2) Paracone and metacone of equal size or paracone lower than metacone.

134 Metacone position relative to paracone: (0) Metacone labial to paracone; (1) Metacone about the same level as paracone; (2) Metacone lingual to paracone.

135 Base of the paracone and metacone (based on the upper second molar if available, applicable only to triangulated molars): (0) Merged; (1) Separated. Arboroharamiya =?; Shenshou=?; Xianshou linglong=?; Xianshou songae=?

136 Centrocrista between the paracone and the metacone of the upper molars (applicable only to taxa with well-developed metacone and distinctive wear facets 3 and 4): (0) Straight; (1) V-shaped, with labially directed postparacrista and premetacrista.

137 Anteroposterior width of the conular region (with or without conules) on the upper molars (applicable only to taxa with reversed triangulation and an occluding lingual portion of the upper molar; for the taxa with conules, this is measured between the paraconule and metaconule; for those taxa without conules, this is measured as the length of the tooth medial to the base of paracone; the upper second molar measured where possible): (0) Narrow (anteroposterior distance medial to the paracone and metacone less than 0.30 of total tooth length); (1) Moderate development (distance between position of conules = 0.31—0.50 of total tooth length); (2) Wide (distance between conules greater than 0.51 of total tooth length); (3) Expanded.

138 Presence of the paraconule and metaconule on the upper molars: (0) Absent; (1) Present.

139). Relative position of the paraconule and metaconule on the upper first and second molars: (0) Paraconule and metaconule closer to the protocone; (1) Both positioned near the midpoint of the protocone-

metacone; (2) Paraconule and metaconule labial to the midpoint.

140 Internal conular cristae (conular wing): (0) Cristae indistinctive; (1) Cristae distinctive and wing-like.

141 Parastylar groove (on upper second molar): (0) Weak or absent; (1) Moderately to well developed.

142 Stylar cuspule “A”, the parastyle, on the upper molars (of the Bensley-Simpson system; cuspule “E” of the Crompton designation for triconodontan-like molariform): (0) Present (at least a swelling is present); (1) Absent.

143 Preparastyle on the upper first molar (applicable to molars with triangulation): (0) Absent; (1) Present.

144 Stylar cuspule “B” (opposite the paracone) (based on the upper second molar if available): (0) Vestigial to absent; (1) Small but distinctive; (2) Large, or slightly larger than the parastyle.

145 Stylar cuspule "C" (near the ectoflexus) on the penultimate upper molar: (0) Absent;
(1) Present.

146 Stylar cuspule "D" (opposite the metacone) on the penultimate upper molar: (0) Absent; (1) Present.

147 Absence vs. presence and size of the stylar cuspule “E” (Bensley-Simpson designation; not the Crompton cusp E): (0) Absent or poorly developed; (1) Present, less developed than or subequal to stylar cuspule “D”; (2) Present and better developed than cuspule “D”.

148 Position of the stylar cuspule “E” relative to cusp “D” or “D-position”: (0) “E” more lingual to “D” or “D-position”; (1) “E” distal to or at same level as “D” or “D-position”.

149 Size and labial extent of the metastylar lobe and parastylar lobe (based on the upper first molar if available; if not, then based on upper second): (0) Metastylar lobe smaller than the parastylar lobe; (1) Metastylar lobe of similar size and labial extent to the parastylar lobe; (2) Metastylar lobe much larger than the parastylar lobe; (3) Metastylar lobe absent.

150 Salient postmetacrista on the upper molars (applicable to taxa with reversed triangulation): (0) Absent or weakly developed; (1) Well-developed but no longer than the metacone-protocone distance; (2) Hypertrophied and longer than the metacone-protocone distance.

151 Selenodont molar pattern: (0) Absent; (1) Present.

152 Outline of the lower first molar crown (in crown view): (0) Laterally

compressed; (1) Oblong with slight labial bulge; (2) Triangular or tear-drop shaped; (3) Rectangular (or rhomboidal); (4) Oval shaped; (5) Circular.

153 Outline of the lower second molar crown (in crown view): (0) Laterally compressed; (1) Oblong with slight labial bulge; (2) Triangular or tear-drop shaped; (3) Rectangular (or rhomboidal); (4) Circular.

154 Aspect ratio and outline of the upper first molar: (0) Laterally compressed; (1) Longer than transversely wide (oval-shaped or spindle shaped); (2) Transversely wider than long (triangular outline); (3) Rectangular or nearly so; (4) Oval shaped; (5) Circular.

155 Carnassial shearing blades on posterior aspect of the ultimate upper premolar and and anterior aspect of the first lower molar: (0) Absent; (1) Present.

156 Upper molar interlock: (0) Absent; (1) Present.

157 Anterior molar(s) - types of upper molar interlock: (0) Notch interlock (with cingular cusps involved or without); (1) Tongue-in-groove interlock; (2) Parastylar lobe of a succeeding molar lumbricated with the metastylar region of a preceding molar

158 Posterior upper molar(s) - types of upper molar interlock: (0) Posterior end of preceding molar imbricating anterolabial side of ultimate upper molar; (1) Parastylar lobe of a succeeding molar imbricated with the metastylar region of a preceding molar:

Molar Wear Pattern

159 Wear facets on the lingual side of lingual cusps of m1: (0) Absent; (1) Present.

160 Wear facets on buccal side of M2: (0) On all buccal cusps; (1) On buccal side of A1, but not on the buccal side of the mesiobuccal cusp.

161 Functional development of occlusal facets on individual molar cusps: (0) Absent; (1) Absent at eruption but developed later by crown wear; (2) Wear facets match upon tooth eruption (inferred from the flat contact surface upon eruption).

162 Topographic relationships of wear facets to the main cusps: (0) Wear pattern across the entire crown; (1) Lower cusps a, c support two different wear facets (facets 1 and 4) that contact the upper primary cusp A; (2) Lower cusps a, c support a single wear facet (facet 4) that contacts the upper primary cusp B (this facet extends onto cusp A as wear continues, but 1 and 4 do not develop simultaneous in these taxa); (3) Multicuspate series, each cusp may support 2 wear facets.

163 Development and orientation of prevallum/postvallid shearing (based on either upper or the lower molar structures): (0) Absent; (1) Present and obtuse; (2) Present, hypertrophied and transverse.

164 Wear facet 1 (a single facet supported by cusp a and cusp c) and facet 2 (a single facet supported by cusp a and cusp b): (0) Absent; (1) Present.

165 Upper molars - development of facet 1 and the preprotocrista (applicable to molars with reversed triangulation): (0) Facet 1 (prevallum crest) short, not extending to the stylocone area; (1) Facet 1 extending into the hook-like area near the stylocone; (2) Preprotocrista long, extending labially beyond the paracone.

166 Differentiation of wear facet 3 and facet 4 (applicable to taxa with a distal cusp d or "hypoconulid"): (0) Absent; (1) Present; (2) Facets 3 and 4 hypertrophied on the flanks of the strongly V-shaped talonid.

167 Orientation of facet 4 (on the posterior aspect of the hypoconid): (0) Present and oblique to the long axis of the tooth; (1) Present and forming a more transverse angle to the long axis of the tooth.

168 Morphology of the posterolateral aspect of the talonid (the labial face of the hypoconid or equivalent area of Crompton facet 4, applicable to taxa with fully basined talonid): (0) Gently rounded; (1) Angular.

169 Wear pattern within the talonid basin (applicable to those taxa with triangulated molars): (0) Absent; (1) Present; (2) Present apically on the crests of the talonid; (3) Apical wear on crest and lophodont.

170 Development of the distal metacristid (applicable only to taxa with reversed triangulation): (0) Present; (1) Absent.

171 Differentiation of wear facets 5 and 6 on the labial face of the entoconid: (0) Absent;
(1) Present.

172 Surficial features on the occluding surfaces on the talonid (only applicable to taxa with reversed triangulation): (0) Smooth surface on the talonid heel (or on cusp d); (1) Multiple ridges within the talonid basin; (2) Talonid present, but wear occurs apically on the crests of cristid obliqua and hypoconid cristid (V-shaped talonid crests).

173 Molar wear facets pseudo-3 and pseudo-4: (0) Absent; (1) Present.

174 Molar wear facets pseudo-5 and pseudo-6: (0) Absent; (1) Present.

175 Pseudo-cusp e and f hypertrophied: (0) Absent; (1) Present.

176 (New). Medio-lateral compression of the base of cusp a (or protoconid) (applicable only to “triconodont”-like, “symmetrodont”-like, or generalized tribophenic teeth):
(0) Absent (base of cusp a width is 40% or more of tooth length, measured on m1): *Thrinaxodon*, *Probainognathus*, trithelodontids, *Sinoconodon*, morganucodonts, *Hadrocodium*, all docodonts, all spalacotherioids, all cladotherians, all tribosphenic mammals.

(1) Present (base of cusp a width ≥ 30% of tooth length, measured on m1 or other anterior molariforms)
(?) Not applicable: teeth with multi-cusp rows, or simplified teeth.

Other Dental Features

177 Number of upper incisors: (0) Five; (1) Four; (2) Three; (3) Two; (4) One; (5) No incisors.

178 I^2 enlargement: (0) absent; (1) present.

179 Number of cusps on posterior upper incisors: (0) One; (1) two or more.

180 Number of lower incisors: (0) Five or more; (1) Four; (2) Three; (3) Two; (4) One;
(5) No incisors.

181 Lower anterior-most incisor enamel: (0) Covers the whole incisor; (1) Restricted anteriorly.

182 Lower anterior-most incisor with open root: (0) Absent; (1) Present.

183 Upper anterior-most incisor enamel: (0) Covers the whole incisor; (1) Restricted anteriorly.

184 Upper anterior-most incisor with open root: (0) Absent; (1) Present.

185 Upper canine - presence vs. absence, and size: (0) Present and enlarged; (1) Present and small; (2) Absent.

186 Upper canine – number of cusps: (0) Peg-like with single cusp; (1) Two or more cusps.

187 Number of upper canine roots: (0) One; (1) Two.

188 Lower canine - presence vs. absence and size: (0) Present and enlarged; (1) Present and small; (2) Absent.

189 Number of lower canine roots: (0) One; (1) Two.

190 Orientation of lower canine: (0) Erect; (1) Procumbent.

191 Number of upper premolars (only applicable to taxa with premolar vs. molar differentiation): (0) Five or more; (1) Four; (2) Three; (3) Two or less.

192 Number of lower premolars: (0) Five or more; (1) Four; (2) Three; (3) Two or less.

193 Number of lower molars or molariform postcanines: (0) Six or more; (1) Five; (2) Four; (3) Three; (4) Two or less.

194 Number of upper molars or molariform postcanines (applicable only to those taxa that do not have multiple dental replacements): (0) Six or more; (1) Five; (2) Four; (3) Three; (4) Two or less.

195 Total number of upper postcanine loci: (0) More than 8 (including the loci plus the alveoli of shed anterior postcanines); (1) Eight; (2) Seven, (3) Six; (4) Five or less.

196 Total number of lower postcanine loci: (0) Eight or more; (1) Seven; (2) Six; (3) Five or fewer.

197 Procumbency and diastema of first (functional) upper premolar or postcanine in relation to the upper canine: (0) Not procumbent and without diastema; (1) Procumbent and with diastema.

198 Diastema separating the lower first and second premolars (defined as the first and second functioning premolar or premolariform postcanine): (0) Absent (gap less than one tooth root for whichever is smaller of the adjacent teeth); (1) Present, subequal to one tooth-root diameter or more; (2) Present, equal to or more than one-tooth length.

199 Ultimate lower premolar bladed or crenulated: (0) Absent; (1) Present.

200 Upper anterior-most incisor (I^1): (0) Subequal to the remaining incisors, no diastema with the second incisor; (1) Anteriorly projecting, separated from the second incisor (or any following teeth if posterior incisors are absent) by a diastema; (2) Absent (as evidenced by a small median gap between the mesial-most incisors).

201 Ultimate and penultimate upper incisors - morphology: (0) Peg-like/conical; (1) Present, and spoon-shaped to rhomboid-shaped in lateral view; (2) Present, and spatulate in lateral view; (3) Ultimate and/or penultimate upper incisors bicuspate or tricuspate.

202 Staggered lower incisor: (0) Absent; (1) Present.

203 Replacement pattern of incisors and canines: (0) More than one replacement; (1) One replacement; (2) No replacement.

204 Replacement of at least some posterior functional molariform postcanines: (0) Present; (1) Absent.

205 Enlargement of the lower anterior-most incisor: (0) Absent; (1) Present (at least 50% longer than the adjacent incisor).

206 Enlarged diastema in the lower incisor-canine region (better developed in older individuals): (0) Absent; (1) Present and behind the canine; (2) Present and behind the posterior incisor.

207 U-shaped transverse ridge in the lower multi-rowed molars: (0) Absent; (1) Present, at second anterior cusp: (2) Present, at the anterior rim.

208 Fusuliform ("spindle-shaped") shearing valley on anterior upper molars: (0) Absent; (1) Present.

209 Cusp ratio on lingual row of multi-rowed lower molar: (0) Cusps are of subequal height; (1) Mesial cusp on the lingual row the highest.

210 Inflated hook cusp (hypertrophied and recurved) at the mesiolabial end of lower molars (to fit into the fusiliform valley of upper molars). (0) Absent; (1) Present.

211 Cusp ratio on buccal row of multi-rowed lower molar: (0) All cusps are of equal height; (1) The middle cusps higher than the mesial and distal cusps.

212 Enlarged and more centrally placed second cusp of lingual row on lower m1 (applicable only to molars with multi-rows of multiple cusps): (0) Absent; (1) Present.

213 Upper premolar/molar with multi-cusped rows - cusp ratio in the labial row of multi-cusp row on ultimate upper molar: (0) Distal cusp highest, with a gradient of anteriorly decreasing height; (1) Cusps in same row of equal height; (2) Mesial cusp is slightly higher than distal cusp.

214 Antero-lingual wing (in addition to two main cusp rows) on M1: (0) Absent; (1) Present.

215 Last (ultimate) upper molar - alignment of multi-cusped rows: (0) Absence of lingual offset of ultimate molar to penultimate molar; (1) Presence of offset of ultimate molar from the penultimate molar: the lower ultimate molar lingual row occludes with the lingual side of the upper second labial row, or the labial side of the lower ultimate molar occluding with the labial side of the upper ultimate molar.

216 Complete middle valley between lingual cusp row and labial cusp row on lower m2: (0) Absent; (1) Present.

217 Multi-rowed ultimate lower molar, row length difference: (0) Labial cusp row about equal as lingual cusp row; (1) Labial row shorter at the anterior end (by at least half-cusp length) than lingual row; (2) Labial row longer at the posterior end than lingual row (by at least half-cusp length).

218 Enamel microstructure: (0) Synapsida columnar enamel (prismless); (1) 'Transitional' (sheath indistinct, 'prismatic' crystallites inclined at less than 45^{o} to the 'interprismatic' matrix); (2) Full prismatic enamel; (3) Enamel absent.

219 Hypsodonty roots of cheek teeth: (0) Absent; (1) Present.

220 Open root end of the postcanines: (0) Absent; (1) Present.

221 Degrees of postcanine root division: (0) Single root; (1) divided roots connected by dentine sheets; (2) two or three complete divided roots or more; (3) multiple roots coalesced.

222 Orientation of the crown-root of upper molariform row in transverse (coronal) section: (0) Vertical; (1) Oblique.

Vertebrae and Ribs

223 Fusion of the atlas neural arch and intercentrum: (0) Absent; (1) Present.

224 Atlas: fusion of half-neural arches at dorsal midline: (0) Absent; (1) Present.

225 Atlas rib: (0) Present; (1) Absent.

226 Fusion of dens to the axis: (0) Absent; (1) Present.

227 Axis rib: (0) Present; (1) Absent (rib fused to form the transverse process). Note: the base for the axial rib is represented by a stump.

228 Inferior lamina ("tuberculi anterior") on the centra of posterior cervicals: (0) Absent; (1) Present.

229 Postaxial cervical ribs: (0) Unfused; (1) Fused.

230 Number of dorsal vertebrae bearing ribs: (0) 13 or less; (1) 14 or more.

231 Overlapping ventral costal plates: (0) Absent; (1) Present.

232 Overlapping lumbar or posterior thoracic ribs: (0) Present; (1) Absent.

233 Anticlinal vertebra: (0) Absent; (1) Present.

234 Anticlinal vertebra position (not applicable for vertebral column without an anticlinal vertebra): (0) Anticlinal absent; (1) More posterior position (within last 4 lumbar vertebrae); (2) Anteriorly positioned (within the anterior 13 dorsal and the thoracic vertebral region if thoraco- lumbar boundary is distinctive):

235 Mobile lumbar ribs: (0) Present; (1) Absent.

236 Orientation of lumbar ribs or transverse processes: (0) Posterolaterally directed; (1) Laterally or anterolaterally directed.

237 Xenarthrous articulation in addition to the pre- and post-zygapophyses of lumbar vertebrae: (0) Absent; (1) Present.

238 Expanded dorsal end (“flat top”) of neural spine of posterior dorsal vertebrae: (0) Absent; (1) Present.

Shoulder Girdle

239 Interclavicle: (0) Present; (1) Absent.

240 Contact relationships between the interclavicle (embryonic membranous element) and the sternal manubrium (embryonic endochondral element): (0) Two elements distinct from each other, posterior end of the interclavicle abuts with the anterior border of manubrium; (1) Two elements distinct from each other, the interclavicle broadly overlaps the ventral side of the manubrium; (2) Complete fusion of the embryonic membranous and endochondral elements resulting in a single and enlarged manubrium.

241 Inverclavicle distal expansion: (0) Absent; (1) Present.

242 Cranial margin of the interclavicle/manubrium (assuming the interclavicle is fused to the sternal manubrium in living therians): (0) Emarginated or flat; (1) With a median process.

243 Interclavicle to sternal manubrium length ratio: (0) Interclavicle twice the length of manubrium; (1) Interclavicle nearly equal to manubrium in length.

244 Sternoclavicular joint (assuming that homologous elements of the interclavicle and the manubrium are fused to each other in therians): (0) Immobile; (1) Mobile.

245 Interclavico-manubrial craniolateral process: (0) Absent; (1) Present.

246 Acromioclavicular joint: (0) Extensive articulation; (1) Limited articulation (either pointed acromion, pointed distal end of clavicle, or both).

247 Curvature of the clavicle: (0) Boomerang-shaped; (1) Slightly curved.

248 Clavicle - lateral (distal) end expanded with helical articular surface: (0) Tapering or truncated; (1) Expanded with helical articular surface.

249 Scapula - supraspinous fossa: degree of development along the length: (0) Present only in the “acromional region” of the scapula, and on the cranial (dorsal) border of the scapula and positioned anterior to the glenoid); (1) Weakly developed (present only along a part of the scapula and positioned lateral to the glenoid); (2) Fully developed (present along the entire dorsal border of the scapula).

250 Proportion of supraspinous vs. infraspinous fossae (width measured across the "saddle region" of the spine, or near the mid-length of the scapula): (0) Supraspinous “fossa” on the cranial aspect of the scapula and much narrower than infraspinous fossa; (1) Supraspinous width is 50% to 80% that of infraspinous fossa; (2) Fossae subequal; (3) Supraspinous over 150% that of infraspinous fossa.

251 Scapula - acromion process: (0) Short stump, level with or behind the glenoid; (1) Elongate and extending below the glenoid; (2) Pointed process, oriented anteriorly.

252 Scapula - a distinctive fossa for the teres major muscle on the lateral aspect of the scapular plate: (0) Absent; (1) Present.

253 Procoracoid: (0) Present and distinct; (1) Fused to the sternal apparatus.

254 Procoracoid foramen: (0) Present; (1) Absent (assuming the procoracoid is fused to the sternal apparatus in living therians).

255 Coracoid: (0) Large, with posterior process; (1) Small, without posterior process.

256 Anterior process of the coracoid: (0) Indistinctive; (1) Distinctive; (2) Distinctive and forming a broad plate.

257 Coracoid process bridging over posteriorly toward the vertebral border of scapula (or fused with the latter): (0) Absent; (1) Present.

258 Size of the anterior-most element (‘manubrium’) relative to the subsequent sternebrae in the sternal apparatus: (0) Large; (1) Small.

259 Orientation (‘facing’ of the articular surface) of the glenoid (relative to the plane or the long axis of the scapula): (0) Nearly parallel and facing posterolaterally; (1) Oblique and facing more posteriorly; (2) Perpendicular.

260 Shape and curvature of the glenoid: (0) Saddle-shaped, oval and elongate; (1) Uniformly concave and more rounded in outline.

261 Medial surface of the scapula: (0) Convex; (1) Flat.

262 Suprascapular incisure (defined as the prominent emargination on the cranial border of the supraspinus fossa): (0) Absent; (1) Present.

Forelimb and Manus

263 Humeral head: (0) Subspherical, weakly inflected; (1) Spherical, strongly inflected.

264 Intertubercular groove of the humerus: (0) Shallow and broad; (1) Narrow and deep.

265 Size of the lesser tubercle of the humerus relative to the greater tubercle: (0) Wider; (1) Narrower.

266 Torsion between the proximal and distal ends of the humerus: (0) Strong (≥30 degrees); (1) Moderate (30–15 degrees); (2) Weak.

267 Ventral extension of the deltopectoral crest or the position of the deltoid tuberosity: (0) Short and limited to the proximal part of the humeral shaft; (1) Extending ventrally (distally) at least 1/3 the length of the shaft.

268 Teres tuberosity on medial side of humerus. (0) Absent; (1) Present; (2) Hypertrophied.

269 Ulnar articulation on the distal humerus: (0) Bulbous ulnar condyle; (1) Cylindrical trochlea in posterior view with a vestigial ulnar condyle in anterior view; (2) Cylindrical trochlea without an ulnar condyle (cylindrical trochlea extending to the anterior/ventral side).

270 Radial articulation on the distal humerus: (0) Distinct and rounded radial condyle in both anterior (ventral) and posterior (dorsal) aspects (that does not form a continuous synovial surface with the ulnar articulation in the ventral/anterior view of the humerus); (1) Rounded radial condyle anteriorly but cylindrical posteriorly; (2) Capitulum (forming a continuous synovial surface with the ulnar trochlea; cylindrical in both anterior and posterior aspects).

271 Entepicondyle and ectepicondyle of the humerus: (0) Robust; (1) Weak.

272 Sigmoidal shelf for the supinator ridge extending proximally from the ectepicondyle:

273 Coronoid process of semilunar notch of ulna: (0) Absent; (1) Present and level to olecranon process; (2) Present and higher than olecranon process.

274 Styloid process of the radius: (0) Weak; (1) Strong.

275 Enlargement of the scaphoid: (0) Not enlarged (scaphoid ≤150% of the lunate); (1) Enlarged (scaphoid twice the size of the lunate); (2) Enlarged with a distolateral process.

276 Size and shape of the hamate (unciform): (0) About equal size to the triquetrum, anteroposteriorly compressed; (1) Hypertrophied, much larger than the triquetrum, mediolaterally compressed.

277 Trapezium morphology and proportion: (0) Elongate to cuboidal, larger than or subequal to the trapezoid; (1) Bean-shaped or fusiform, smaller than the trapezoid.

278 Triquetrum-lunate proportion: (0) Triquetrum nearly twice the size of the lunate; (1) Triquetrum subequal to the lunate.

279 Relative length of metacarpals (MC) to proximal phalanx (PP) of digit III: (0) PP shorter than MC; (1) PP longer than MC.

Pelvic Girdle

280 Anterior process of the ilium: (0) Short (less than the diameter of the acetabulum);
(1) Long, 1-1.5 times the diameter of the acetabulum; (2) Elongate, more than 1.5 times the diameter of the acetabulum.

281 Posterior process of the ilium: (0) Present; (1) Reduced or absent.

282 Acetabular dorsal emargination: (0) Open (emarginated); (1) Closed (with a complete rim).

283 Sutures of the ilium, ischium, and pubis within the acetabulum: (0) Present; (1) Fused.

284 Ischiatic dorsal margin and tuberosity: (0) Dorsal margin concave (emarginated) and ischiatic tuberosity present; (1) Dorsal margin concave and ischiatic tuberosity hypertrophied; (2) Dorsal margin straight and ischiatic tuberosity small.

285 Posterior spine of the ischium: (0) Short and pointed; (1) Expanded with oblique posterior spine; (2) Expanded and truncated.

286 Epipubic bone: (0) Present; (1) Absent.

287 Width of epipubis: (0) Narrow; (1) Wide.

288 Fusion of the sacral vertebrae with the proximal caudal vertebrae: (0) Absent; (1) Present.

289 Fusion of the ischium with the caudal vertebrae: (0) Absent; (1) Present.

290 Preacetabular tubercle on the ilium for M. rectus femoris: (0) Absent; (1) Present.

291 Fully encircled synovial surface inside the acetabulum: (0) Absent; (1) Present.

292 Lesser psoas tuberosity or process on the pubis: (0) Absent; (1) Present.

Hindlimb and Pes

293 Inflected head of the femur set off from the shaft by a neck: (0) Neck absent and head oriented dorsally; (1) Neck present, head spherical and inflected medially.

294 Fovea for the acetabular ligament on the femoral head: (0) Absent; (1) Present.

295 Orientation of the greater trochanter: (0) Directed dorsolaterally; (1) Directed dorsally.

296 Level of greater trochanter relative to femoral head: (0) Mid-level of femoral head;
(1) Top level of femoral head.

297 Position of the lesser trochanter: (0) On medial side of the shaft; (1) On the ventromedial or ventral side of the shaft.

298 Size of the lesser trochanter: (0) Large; (1) Small to absent.

299 The third trochanter of femur: (0) Absent; (1) Present; (2) Present as a continuous ridge connected to the greater trochanter.

300 Patellar facet (‘groove’) of the femur: (0) Absent; (1) Shallow and weakly developed; (2) Well-developed.

301 Proximo-lateral tubercle or tuberosity of the tibia: (0) Large and hook-like; (1) Indistinct; (2) Fused to fibula

302 Distal tibial malleolus: (0) Weak; (1) Distinctive.

303 Differentiation of lateral tibio-astragalar condyle from the medial tibio-astragalar condyle: (0) Absent; (1) Present.

304 Fibula contacting the distal end of the femur: (0) Present; (1) Absent; (2) Fibula contacting through fusion with the tibia.

305 Fused distal portions of the tibia and fibula: (0) Absent; (1) Present.

306 Enlarged parafibular structure of the fibula: (0) Absent; (1) Present; (3) Present and hypertrophied.

307 Parafibula types: (0) Separate bone and unfused to the fibular; (1) Fused to fibula as an enlarged process:

308 Distal fibular styloid process: (0) Weak or absent; (1) Distinct; (2) Elongate to form a full contact with lateral surface of astraglar trochlea.

309 Fibula contacting the calcaneus (= 'tricontact in upper ankle joint'): (0) Extensive contact; (1) Reduced; (2) Absent.

310 Superposition (overlap) of the astragalus over the calcaneus (lower ankle joint): (0) Little or absent; (1) Weakly developed; (2) Present.

311 Astragalo-navicular articulation – symmetry to the neck: (0) Articulating facet indistinctive; (1) Asymmetrical: present only on the lateral side of the "neck region"; (2) Symmetrical with regard to the astragalar neck.

312 Astragalar neck basal width (justification for separating this character from the navicular facet expansion is that the latter concerns symmetry, whereas this character deals with proportion; the distributions of these two character are different in some stem eutherians and crown marsupials): (0) Neck narrower than the head (constriction posterior to navicular facet); (1) Neck about same width as the head (with parallel sides posterior to navicular facet); (2) Widest point of neck at mid-length (widening is not developed near the base of the neck); (3) Astragalar neck widest at the base.

313 Astragalonavicular contact aspect ratio: (0) Navicular contact transversely wider than dorsoventrally thick; (1) Navicular contact dorsoventrally thicker than transversely wide.

314 Expansion and dorso-ventral orientation of navicular contact in the astragalar head region: (0) Restricted anteriorly (navicular contact narrower than the base of the head); (1) Asymmetrical spread only to the medial side

of the astragalar “head-neck region”; (2) Navicular facet and sides of the neck form a rectangular outline; (3) Symmetrical spread of the navicular facet to both the lateral and the medial sides of the neck (symmetrical with regards to the main axis of the neck); (4) Navicular facet spread underneath the head-neck region so that part of navicular facet faces ventrally, and astragalar head superpositioned on part of the navicular bone.

315 Astragalo-navicular contact shape: (0) Flat to convex; (1) Crest-in-groove: Transverse groove on astralar head to receive crest from navicular.

316 Astragalar trochlea (defined as a saddle-shaped upper ankle joint): (0) Absent; (1) Present, but weak (defining crest on the medial astragalo-tibial facet weakly developed); (2) Present, with clear separation of the medial and lateral tibial facets.

317 Well-defined medio-tibial crest (more or less parallel to the tibio-fibular crest) on the astragalus: (0) Absent; (1) Present.

318 Astragalar medial plantar tuberosity: (0) Absent; (1) Present, but weakly developed;
(2) Present, and ventrally flaring or protruding.

319 Distal end of the calcaneal tubercle: (0) Short, dorso-ventrally compressed, without a terminal swelling; (1) doro-ventrally compressed, with a terminal swelling; (2) Elongate, vertically deep, and mediolaterally compressed, with terminal swelling.

320 Ventral orientation of terminal swelling of calcaneal tuber: (0) Absent; (1) Present.

321 Morphology of the peroneal process of the calcaneus: (0) Laterally expanded shelf, larger than the combined length of the sustentacular and astragalar facets, lateral to the astragalar facet; (1) With a distinct and long peroneal process, laterally projecting; (2) With a distinct peroneal process, demarcated by a deep peroneal groove at the base; (3) Laterally directed, small peroneal shelf demarcated from the anterior (cuboidal) edge of the calcaneus; (4) Anterolaterally directed, hypertrophied peroneal process/shelf; (5) Peroneal structure laterally reduced (lateral surface is straight from the calcaneal tubercle).

322 Placement of the base of the peroneal process relative to the level of the cuboid facet of the calcaneus: (0) Peroneal structure posterior to the level of the cuboid facet; (1) Peroneal structure developed anteriorly at the same level as the cuboid facet; (2) Peroneal structure hypertrophied, extending anteriorly beyond the level of the cuboid facet.

323 Peroneal groove of the calcaneus: (0) Indistinct, on the anterolateral aspect of the lateral shelf; (1) Distinct, located in deep separation of the peroneal process from the calcaneal body; (2) Developed, either on the lateral side of the process or on the anterolateral extremity of the peroneal process.

324 Alignment of the cuboid to the main axis of the calcaneus (horizontal plane): (0) On the anterior (distal) end of the calcaneus (the cuboid is aligned with the long axis of the calcaneus); (1) On the anteromedial aspect of the calcaneus (the cuboid is skewed to the medial side of the long axis of the calcaneus):

325 Orientation of the calcaneocuboid joint in dorso-ventral plane: (0) Calcaneocuboid facet on the calcaneus oriented ventrally (more visible in plantar view than in dorsal view); (1) Calcaneocuboid facet oriented anteriorly (distally); (2) Calcaneocuboid facet oriented ventromedially or medio-obliquely.

326 Saddle-shaped calcaneocuboid joint: (0) Calcaneocuboid facet on the calcaneus relatively flat to slightly concave; (1) Saddle-shaped (differentiation of dorsal vs. proximal calcaneocuboid “facets” so that the whole calcaneocuboidal joint is saddle-shaped).

327 Lower ankle joint - orientation of the sustentacular facet of the calcaneus in relation to the horizontal plane: (0) Nearly vertical; (1) Oblique (≤70 degrees) to nearly horizontal.

328 Antero-posterior placement of the sustentacular facet relative to the astragalar facet on the calcaneus: (0) Directly anterior to the astragalar facet and vertically oriented on the medial edge of the calcaneus; (1) On the dorsal aspect and positioned anteromedial to the astragalar facet on the calcaneus; (2) On the dorsal aspect, medial to the astragalar facet; (3) On the dorsal aspect, anterior to the astragalar facet.

329 Confluence of the sustentacular facet and the astragalar facet on the calcaneus: (0) Absent; (1) Present.

330 Ventral outline of the sustentacular process of the calcaneus: (0) Indistinctive; (1) Medially directed shelf, with rounded outline; (2) Protruding triangle, posteromedially directed

331 Antero-posterior position of the sustentacular facet/process (using the most salient point of the facet/process in ventral view as landmark) relative to the length of the calcaneus: (0) Near the mid-point; (1) Near the anterior (proximal) one-third.

332 Shape of posterior calcaneo-astragalar process/protuberance and its contiguous fibular contact (if the fibula contact is present in medial view) on the calcaneus: (0) Indistinctive (boundary not defined and confluent with fibular contact); (1) Well defined, and oblong to ellipsoidal; (2) Nearly spherical and bulbous, more transversely developed than character state 1; (3) Transversely confluent with the sustentacular facet.

333 Placement of the Calcaneo-Astraglar Facet (CAF) structure (structure of the calcaneoastragalar contact): (0) On the medial side of the body of the calcaneus; (1) On the dorsal side of the body of the calcaneus, but bordering on the body's medial margin (without a protruding outline); (2) On the dorsal side of the body of the calcaneus and protruding beyond the body's medial margin; (3) Withdrawn and separated from the medial margin and placed along the lateral margin of the body of the calcaneus.

334 Orientation of Calcaneo-Astraglar Facet (CAF) relative to Calcaneo-Fibulo-Facet (CFF): (0) CAF anterior to CFF; (1) CAF medial to CFF.

335 Anterior ventral (plantar) tubercle of the calcaneus: (0) Absent; (1) Present, at the anterior edge (just lateral to the cuboid facet); (2) Present, set back from the anterior edge.

336 Anteroventral groove or depression of the calcaneus: (0) Absent; (1) Present.

337 Shape of the body of the calcaneus at the level of the posterior calcaneoastragalar facet: (0) Dorso-ventrally compressed; (1) Mediolaterally compressed.

338 Ventral curvature of the calcaneal tubercle: (0) Present; (1) Absent.

339 Proportion of the navicular and cuboid (transverse width measured in dorsal view):
(0) Navicular narrower than or subequal to cuboid; (1) Navicular wider than cuboid.

340 Proportion of the entocuneiform, mesocuneiform, and ectocuneiform (in ventral view): (0) Mesocuneiform and ectocuneiform small, their combined width smaller than the width of the entocuneiform; (1) Mesocuneiform and ectocuneiform large, their combined width (in dorsal view) exceeding the width of the entocuneiform.

341 Saddle-shaped contact between entocuneiform and proximal end of metatarsal 1:
(0) Absent; (1) Present.

342 Medio-plantar aspect of the cuboid deeply notched by the peroneus longus tendon:
(0) Absent; (1) Present.

343 Prehallux: (0) Absent; (1) Present.

344 End-to-end contact of metatarsal V and the peroneal process of the calcaneus: (0) Absent; (1) Present.

345 Relationships of the proximal end of metatarsal V to the cuboid: (0) Metatarsal V is off-set from the lateral side of the cuboid; (1) Metatarsal V is so far off-set to the side of the cuboid that it contacts the calcaneus; (2) Metatarsal V is level with (not off-set from) the anterior end of the cuboid.

346 Ventrolateral tubercle at the proximal end of metatarsal V: (0) Absent or indistinctive; (1) Present, at or anterior to the anterior edge of the calcaneus; (2) Present, off-set posteriorly from the anterior edge of the calcaneus.

347 Angle of metatarsal III to the calcaneus (which indicates how much the sole of the foot is 'bent' from the long axis of the ankle): (0) Metatarsal III aligned with (or parallel to) the long axis of the calcaneus; (1) Metatarsal III arranged obliquely from the long axis of the calcaneus.

348 (Metatarsal II and metatarsal III proximal ends: (0) II and III even or II more proximal than III; (1) III more proximal than II.

349 Opposable hallux: (0) Absent; (1) Present.

350 Relative length of metatarsals and proximal phalanx of digit III: (0) PP shorter than MT; (1) PP longer than MT.

Other Postcranial Characters

351 Ossified patella: (0) Absent; (1) Present.

352 Sesamoid bones in the digital flexor tendons: (0) Absent; (1) Present, unpaired; (2) Present, paired.

353 External pedal (tarsal) spur: (0) Absent; (1) Present.

354 Pes digital grouping: (0) Didactylous; (1) Syndactylous.

355 Epiphyses in long bones of zeugopodials: (0) Absent; (1) Present.

Basicranium

356 External size of the cranial moiety of the squamosal: (0) Narrow; (1) Broad; (2) Expanded posteriorly to form the skull roof table.

357 Participation of the cranial moiety of the squamosal in the endocranial wall of the braincase: (0) Absent; (1) Present.

358 Multiple vascular foramina (for rami temporales) in the squamosal and parietal: (0) Absent; (1) Present.

359 Multiple vascular foramina (for branches of external ethmoidal artery) in the dorsal surface of the frontal: (0) Absent; (1) Present.

360 Topographic relationships of the dentary-squamosal contact (or glenoid) and the cranial moiety of the squamosal (only applicable to taxa with the dentary-squamosal joint; this character is best seen in ventral view): (0) Contact on the internal aspect of the zygoma, without a constricted neck; (1) Contact on the zygoma, with a constricted neck; (2) Contact on the cranial moiety of squama; (3) On zygoma, without a constricted neck.

361 Cross-section profile of the squamosal anterior to its zygomatic root: (0) Rounded or triangular and tapering anteriorly; (1) Dorsoventrally expanded and mediolaterally compressed, and not tapering anteriorly.

362 Postglenoid depression on the squamosal: (0) Present as the post-craniomandibular joint sulcus ("external auditory meatus" on the zygoma); (1) Absent; (2) Present on the skull base. *Cifelliodon* (UMNH16771) = 1

363 Squamosal - entoglenoid process: (0) Absent or vestigial; (1) Present, but separated from the postglenoid process; (2) Present, enlarged and connected to the postglenoid process.

364 Position of the craniomandibular joint: (0) Posterior or lateral to the level of the fenestra vestibuli; (1) Anterior to the level of the fenestra vestibuli.

365 Orientation of the glenoid on the squamosal: (0) On the inner side of the zygoma and facing ventromedially; (1) On the platform of the zygoma and facing ventrally.

366 Postglenoid process of the squamosal: (0) Absent; (1) Postglenoid crest raised below the fossa, but without a distinctive process; (2) Distinctive process; (3) Distinctive process buttressed by ectotympanic.

367 Postglenoid foramen position: (0) Posterior to the glenoid area; (1) Medial to the postglenoid process; (2) Anterior to the postglenoid process.

368 Postglenoid foramen presence vs. absence and composition: (0) Absent; (1) Present, in the squamosal; (2) Present, between the squamosal and petrosal; (3) Present, between the squamosal and ectotympanic.

369 Medial margin of the glenoid fossa: (0) Formed by the squamosal; (1)

Formed by the alisphenoid.

370 Squamosal - epitympanic recess (this character may be ordered): (0) No contribution to the “epitympanic area” of the petrosal; (1) Small contribution to the posterolateral wall of the epitympanic recess; (2) Large contribution to the lateral wall of the epitympanic recess; (3) Squamosal forming a large part of enlarged epitympanic sinus.

371 Contribution of the basisphenoid wing (parasphenoid ala) to the external bony housing of the cochlea: (0) Participates in the rim of the fenestra vestibuli; (1) Does not reach the rim of the fenestra vestibuli; (2) Absent or excluded from the cochlear housing.

372 Relationship of the cochlear housing to the lateral lappet of the basioccipital: (0) Entirely covered by the basioccipital; (1) Medial aspect covered by the basioccipital; (2) Partially (~about half width on the medial side) covered by the basioccipital; (3) Fully exposed as the promontorium.

373 Thickened rim of the fenestra vestibuli: (0) Present; (1) Absent.

374 Cochlear housing fully formed by the petrosal: (0) Absent; (1) Present.

375 Ventromedial surface of the promontorium: (0) Flat; (1) Inflated and convex.

376 Lateral wall and overall external outline of the promontorium: (0) Triangular, with a steep and slightly concave lateral wall; (1) Elongate and cylindrical; (2) Bulbous and oval shaped.

377 Cochlea: (0) Cochlear recess (without a canal); (1) Short canal; (2) Elongate canal, to the fullest extent of the promontorium; (3) Slightly curved; (4) Elongate and partly coiled; (5) Elongate and coiled to at least 360°.

378 Internal acoustic meatus - cribriform plate: (0) Absent; (1) Present.

379 Internal acoustic meatus depth: (0) Deep with thick prefacial commissure; (1) Shallow with thin prefacial commissure.

380 Primary bony lamina within the cochlear canal: (0) Absent; (1) Present.

381 Secondary bony lamina for the basilar membrane within the cochlear canal: (0) Absent; (1) Present.

382 Crista interfenestralis: (0) Horizontal, broad, and extending to the base of the paroccipital process; (1) Vertical, delimiting the back of the promontorium; (2) Horizontal, narrow, and connecting to the caudal tympanic process.

383 Post-promontorial tympanic recess: (0) Absent; (1) Present.

384 Rostral tympanic process of the petrosal promontorium: (0) Absent or low ridge; (1) present as a ridge of the promontorium.

385 Caudal tympanic process of the petrosal: (0) Absent; (1) Present; (2) Present, notched; (3) Present, hypertrophied and buttressed against the exoccipital paracondylar process.

386 Petrosal - tympanic process: (0) Absent; (1) Present.

387 Rear margin of the auditory region: (0) Marked by a steep wall; (1) Extended onto a flat surface.

388 Prootic canal: (0) Absent; (1) Present, vertical; (2) Present, horizontal and reduced.

389 Position of the sulcus for the anterior distributary of the transverse sinus relative to the subarcuate fossa: (0) Anterolateral; (1) Posterolateral.

390 Lateral trough floor anterior to the tympanic aperture of the prootic canal and/or the primary facial foramen: (0) Open lateral trough, no bony floor; (1) Bony floor present; (2) Lateral trough absent.

391 Anteroventral opening of the cavum epiptericum: (0) Present; (1) Present, with reduced size (due to the anterior expansion of the lateral trough floor); (2) Present, partially enclosed by the petrosal; (3) Present, enclosed by the alisphenoid and petrosal; (4) Present, as large piriform fenestra.

392 Enclosure of the geniculate ganglion by the bony floor of the petrosal in the cavum supracochleare: (0) Absent; (1) Present.

393 Hiatus Fallopii: (0) Present, in the petrosal roof of the middle ear; (1) Present, at the anterior end of the petrosal; (2) Absent (applicable only to those taxa with a cavum supracochleare).

394 Foramen ovale - composition: (0) Between the petrosal and alisphenoid; (1) Secondary foramen partially or fully enclosed by the alisphenoid, in addition to the primary foramen between the petrosal and alisphenoid; (2) In the petrosal (anterior lamina); (3) Between the alisphenoid and squamosal; (4) Within the alisphenoid.

395 Foramen ovale - position: (0) On the lateral wall of the braincase; (1) On the ventral surface of the skull.

396 Number of exit(s) for the mandibular branch of the trigeminal nerve (V3): (0) One;

(1) Two.

397 Quadrate ramus of the alisphenoid: (0) Forming a rod underlying the anterior part of the lateral flange; (1) Absent.

398 Alisphenoid canal (for the ramus inferior and/or ramus infraorbitalis): (0) Absent; (1) Present.

399 Anterior lamina exposure on the lateral braincase wall: (0) Present; (1) Reduced or absent.

400 Orientation of the anterior part of the lateral flange: (0) Horizontal shelf; (1) Ventrally directed; (2) Medially directed and contacting the promontorium; (3) Vestigial or absent.

401 Vertical component of the lateral flange ('L-shaped' and forming a vertical wall to the pterygoparoccipital foramen): (0) Present; (1) Absent.

402 Vascular foramen in the posterior part of the lateral flange (and anterior to the pterygoparoccipital foramen): (0) Present; (1) Absent.

403 Relationship of the lateral flange to the crista parotica (or the anterior paroccipital process that bears the crista): (0) Widely separated; (1) Narrowly separated; (2) Continuous.

404 Pterygoparoccipital foramen (for the ramus superior of the stapedial artery): (0) Laterally open notch; (1) Foramen enclosed by the petrosal or squamosal; (2) Absent.

405 Position of the pterygoparoccipital foramen relative to the level of the fenestra vestibuli: (0) Posterior or lateral; (1) Anterior.

406 "Bifurcation of the paroccipital process" - presence vs. absence (this is modified from the character used in several previous studies): (0) Absent; (1) Present.

407 Posterior paroccipital process of the petrosal: (0) No ventral projection below the level of the surrounding structures; (1) Projecting below the surrounding structures.

408 Morphological differentiation of the anterior paroccipital region: (0) Anterior paroccipital is bulbous and distinctive from the surrounding structures; (1) Anterior paroccipital region has a distinct crista parotica.

409 Epitympanic recess: (0) Absent; (1) Present.

410 Epitympanic recess topographic relationship: (0) Lateral to crista

parotica; (1) Posterior to crista parotica.

411 Tympanohyal contact with the cochlear housing: (0) Absent; (1) Present.

412 Relationship of the squamosal to the paroccipital process: (0) Squamosal covers the entire paroccipital region; (1) No squamosal cover on the anterior paroccipital region; (2) Squamosal covers a part of the paroccipital region, but not the crista parotica (the squamosal wall and the crista parotica are separated by the epitympanic recess).

413 Medial process of the squamosal reaching toward the tympanic cavity: (0) Absent;
(1) Present (near or bordering on the foramen ovale).

414 Stapedial artery sulcus on the petrosal: (0) Absent; (1) Present.

415 Transpromontorial sulcus for the internal carotid artery on the cochlear housing: (0) Absent; (1) Present.

416 Deep groove on the anterior pole of the promontorium: (0) Absent; (1) Present.

417 Perbullar canal or sulcus for the internal carotid artery: (0) Absent; (1) Present.

418 Epitympanic wing medial to the promontorium: (0) Absent; (1) Present.

419 Basioccipital pharyngeal crest: (0) Absent (1) Present.

420 Paired basioccipital foramina (0) Absent; (1) Present.

421 Ectopterygoid process of the alisphenoid: (0) Absent; (1) Present.

422 Tympanic process of the alisphenoid: (0) Absent; (1) Present, but limited to the “piriform” region of the basicranium; (2) Intermediate; (3) Well-developed, extending to near the jugular foramen.

423 Hypotympanic recess in the junction of the alisphenoid, squamosal, and petrosal: (0) Absent; (1) Present.

424 Separation of the fenestra cochleae from the jugular foramen: (0) Absent; (1) Separate but within the same depression; (2) Separate (not within the same depression).

425 Channel of the perilymphatic duct: (0) Open channel and sulcus; (1) At least partially enclosed channel.

426 Jugular foramen size relative to the fenestra cochleae (applicable only

to those taxa with a jugular foramen fully separated from the fenestra cochleae): (0) Jugular subequal to the fenestra cochleae; (1) Jugular larger than the fenestra cochleae.

427 Relationship of the jugular foramen to the opening of the inferior petrosal sinus: (0) Confluent; (1) Separate.

428 Stapedial muscle fossa size: (0) Absent; (1) Present, small; (2) Present, large (twice the size of the fenestra vestibuli).

429 Alignment of the stapedial fossa relative to the crista interfenestralis: (0) Aligned with crista interfenestralis; (1) Lateral to the crista interfenestralis.

430 Hypoglossal foramen: (0) Indistinct, either confluent with the jugular foramen or sharing a depression with the jugular foramen; (1) Separated from the jugular foramen; (2) Separated from the jugular foramen; the latter with a circular, raised external rim.

431 Number of separate hypoglossal foramina: (0) Single; (1) Double.

Middle Ear Ossicle Characters

432 Geometry (shape) of the incudo-mallear contact: (0) Trochlear (convex and cylindrical) surface of the incus; (1) Trough; (2) Saddle-shaped contact on the incus; (3) Flat surface.

433 Alignment of the incus and the malleus: (0) Posterior-anterior; (1) Posteromedial to anterolateral; (2) Dorsoventral.

434 Twisting of the dorsal plate relative to the trochlea on the quadrate: (0) Dorsal plate aligned with the trochlea; (1) Dorsal plate twisted relative to the trochlea, (2) Dorsal plate twisted and elevated from the trochlea; (3) Dorsal plate reduced to a conical process (crus longum).

435 Presence of a quadrate/incus neck (slightly constricted region separating the dorsal plate or crus breve from the trochlea; this represents the differentiation between the ‘body’ and crus breve of the incus): (0) Absent; (1) Present.

436 Dorsal plate (= crus brevis) of the quadrate/incus: (0) Broad plate; (1) Pointed triangle; (2) Reduced.

437 Incus - angle of the crus brevis to crus longum of the incus (this is equivalent to the angle between the dorsal plate and the stapedial process of the quadrate): (0) Alignment of the stapedial process (crus longum) and the dorsal plate (crus breve) (or an obtuse angle between the two structure) (distinctive process is lacking, stapes/incus contact is on the medial side of

the quadrate trochlea); (1) Perpendicular or acute angle of the crus breve and crus longum (“A- shaped” incus).

438 Primary suspension of the incus/quadrate on the basicranium: (0) By quadratojugal in addition to at least one other basicranial bone; (1) By squamosal only; (2) By petrosal (either by the preserved direct contact of the incus or by inference from the presence of a well-defined crista parotica).

439 Quadratojugal: (0) Present; (1) Absent.

440 Morphology of the stapes: (0) Columelliform–macroperforate; (1) Columelliform– imperforate (or microperforate); (2) Bicrurate–perforate.

441 Stapedial ratio: (0) Less than 1.4; (1) 1.4-1.8; (2) ≥1.8.

442 Bullate stapedial footplate: (0) Absent; (1) Present.

443 Malleolar neck: (0) Absent; (1) Present.

444 Length of the malleus manubrium: (0) Shorter than the combined width of the surangular and prearticular anterior to the incudo-malleolar joint; (1) longer than the combined width of surangular and prearticular.

445 Thickness of malleolar manubrium: (0) robust; (1) gracile.

446 Distinctive angle or bending of Meckel’s bone (=anterior portion of ossified postdentary rod) anterior to the level of ectotympanic (angular) bone: (0) Absent; (1) Present.

447 Medio-lateral contact vs. separation of Meckel’s element (either independent or as an ossified component of the “postdentary rod”) from the posterior (pterygoid) region of mandible:
(0) Presence of medio-lateral contact either in adult or in embryonic stage until Meckel’s cartilage re-absorption; (1) Embryonic Meckel’s cartilage medio-laterally separated from the posterior part of mandible; (2) Ossified Meckel’s cartilage medio-laterally separated from the posterior part of mandible:

448 Ectotympanic size/shape (may be ordered): (0) Plate-like; (1) Curved and rod-like;
(2) Ring-shaped; (3) Slightly expanded (fusiform); (4) Expanded; (5) Tube-like.

449 Ectotympanic arc: (0) ≤ 70 degrees: (1) 90 – 135 degrees; (2) ≥ 135 degrees.

450 Anterior process of the ectotympanic (angular): (0) Present; (1) Absent.

451 Position/orientation of the incisura tympanica: (0) Posteroventral; (1)

Posterior; (2)
Postero-dorsal; (3) Dorsal.

452 Fusion of the ectotympanic to other cranial bones: (0) Absent; (1) Fused to other bones.

453 Entotympanic and its contribution to the bullar structure: (0) Absent; (1) Present.

Other Cranial Characters

454 Posterior extent of the bony secondary palate: (0) Anterior to the posterior end of the tooth row; (1) Level with the posterior end of the tooth row; (2) Extending posterior to the tooth row; (3) Extending to the basisphenoid-basioccipital suture.

455 Posterior median spine (or torus) on the palate: (0) Absent; (1) Present.

456 Pterygopalatine ridges: (0) Present; (1) Absent.

457 Transverse process of the pterygoid: (0) Present and massive; (1) Present but reduced (as the hamulus); (2) Greatly reduced (with a vestigial crest on pterygoid) or absent.

458 Pterygoids contact on midline of pharyngeal roof: (0) Present; (1) Absent.

459 Ventral opening of the minor palatine foramen: (0) Encircled by the pterygoid (and ectopterygoid if present) in addition to the palatine; (1) Encircled by the palatine and maxilla, separated widely from the subtemporal margin; (2) Encircled completely by the palatine (or between palatine and maxilla), large, with thin bony bridge from the subtemporal margin; (3) Large, posterior fenestration; (4) Notch.

460 Transverse canal foramen: (0) Absent; (1) Present.

461 Carotid foramen position: (0) Within the basisphenoid; (1) Within the basisphenoid/basioccipital suture; (2) Within the basisphenoid/petrosal suture; (3) Through the opening of the cavum epiptericum.

462 Overhanging roof of the orbit: (0) Absent; (1) Present, formed by the frontal.

463 Exit(s) of the infraorbital canal: (0) Numerous small foramina of similar size; (1) At least a single large, with smaller, anteroventral accessory foramina; (2) One large foramen.

464 Composition of the posterior opening of the infraorbital canal (maxillary foramen):

(0) Between the lacrimal, palatine, and maxilla; (1) Exclusively enclosed by the maxilla; (2) Enclosed by the maxilla, frontal and palatine.

465 Size and shape of the lacrimal: (0) Small, oblong-shaped on the facial part of the rostrum; (1) Large, triangle-shaped on the facial portion of rostrum; (2) Crescent shaped on the facial portion of the rostrum; (3) Reduced to an anteroposteriorly narrow strap confined to the antorbital margin; (4) Absent from the facial portion of the rostrum.

466 Location of the lacrimal foramen: (0) Within the orbit; (1) On the facial side of the lacrimal (anterior to or on the anterior orbital margin).

467 Number of lacrimal foramina: (0) One; (1) Two.

468 Lacrimal foramen composition: (0) Within the lacrimal; (1) Bordered by or within the maxilla.

469 Maximum vertical depth of the zygomatic arch relative to the length of the skull (this character is designed to indicate the robust vs. gracile nature of the zygomatic arch): (0) Between 10-20%; (1) Between 5-7%; (2) Zygoma incomplete.

470 Ultimate upper molar implanted in the anterior root of zygoma: (0) Absent. (1) Present.

471 Maxillary zygomatic tuberosity. (0) Absent; (1) Present.

472 Frontal/alisphenoid contact: (0) Dorsal plate of the alisphenoid contacting the frontal at the anterior corner; (1) Dorsal plate of the alisphenoid with more extensive contact with the frontal (~50% of its dorsal border); (2) Absent.

473 Frontal-maxilla facial contact: (0) Absent; (1) Present.

474 Nasal-frontal suture - medial process of the frontals wedged between the two nasals: (0) Absent; (1) Present.

475 Posterior width of the nasal bones: (0) Broader than the width at the mid-length of the nasal; (1) Reduced/narrow; (2) Parallel-sided with straight sutures (consistent width throughout length).

476 Pila antotica: (0) Present; (1) Absent.

477 Fully ossified medial orbital wall of the orbitosphenoid: (0) Absent; (1) Present, forming the ventral floor of the braincase but not the entire orbital wall; (2) Present, forming both the braincase floor and the medial orbital wall.

478 Separation of the optic foramen from the sphenorbital fissure: (0) Absent; (1) Present.

479 Exit for maxillary nerve: (0) Separate from sphenorbital fissure, behind alisphenoid; (1) Separate from sphenorbital fissure, within alisphenoid; (2) Confluent with sphenorbital fissure.

480 (Separate anterior opening of orbitotemporal canal: (0) Absent; (1) Present.

481 Orbital opening for the minor palatine nerve: (0) Absent; (1) Present.

482 Anterior part of the jugal on the zygoma: (0) Anterior part of the jugal extends to the facial part of the maxilla and forms a part of the anterior orbit; (1) Anterior part of the jugal does not reach the facial part of the maxilla and is excluded from the anterior orbit margin.

483 Jugal lateral exposure on zygoma: (0) Long, extending to at least 2/3 of the zygoma; (1) Short, limited to anterior 1⁄2 of the zygoma; (2) Not exposed on lateral aspect of zygoma.

484 Posterior part of the jugal: (0) Contributes to the squamosal glenoid; (1) Borders on but does not contribute to the squamosal glenoid; (2) Terminates anterior to the squamosal glenoid.

485 Maxillary in the sub-temporal margin of the orbit: (0) Absent; (1) Present; (2) Present and extensive; (3) Present and extremely extended to hamulus.

486 Orbital process of the frontal borders on the maxilla within orbit: (0) Absent; (1) Present.

487 Anterior ascending vascular channel (for the arteria diploëtica magna) in the temporal region: (0) Open groove; (1) Partially enclosed in a canal; (2) Completely enclosed in a canal or endocranial; (3) Absent.

488 Posttemporal canal for the arteria and vena diploëtica: (0) Present, large; (1) Small;
(1) Absent.

489 Nuchal crest: (0) Overhanging the concave or straight supraoccipital; (1) Weakly developed with convex supraoccipital.

490 Sagittal crest: (0) Prominently developed; (1) Weakly developed; (2) Absent.

491 Tabular bone: (0) Present; (1) Absent.

492 Occipital slope: (0) Occiput sloping posterodorsally (or vertically oriented) from the occipital condyle; (1) Occiput sloping anterodorsally from the occipital condyle (such that the lambdoidal crest is leveled anterior to the occipital condyle and condyle is fully visible in dorsal view of the skull).

493 Occipital artery groove on the occiput extending dorsal to the posttemporal foramen: (0) Absent; (1) Present.

494 Foramina on the dorsal surface of the nasals: (0) Absent; (1) Present.

495 Septomaxilla: (0) Present, with the ventromedial shelf; (1) Present, without the ventromedial shelf; (2) Absent.

496 Internarial/dorsal process of the premaxilla: (0) Present on nasal midline suture; (1) Absent/extremely reduced.

497 Posterodorsal process of the premaxilla length: (0) Short (i.e, does not extend beyond level of anterior maxillary tooth); (1) intermediate (i.e., extends beyond level of anterior maxillary tooth); (2) long (i.e., contacts frontal posteriorly).

498 Facial part of the premaxilla borders on the nasal: (0) Absent; (1) Present.

499 Premaxilla - palatal process relative to the canine alveolus: (0) Does not reach to the level of the canine alveolus; (1) Reaches the level of the canine alveolus.

500 Incisive foramina size: (0) Small (one or two incisors); (1) Intermediate (three or four incisors); (2) Large (more than half the palatal length).

501 Palatal vacuities: (0) Absent; (1) Present, near palatomaxillary border; (2) Present, either positioned near or extended to the posterior edge of bony palate.

502 Major palatine foramina: (0) Present. (1) Absent.

503 Ossified ethmoidal cribriform plate of the nasal cavity: (0) Absent; (1) Present.

504 Posterior excavation of the nasal cavity into the bony sphenoid complex: (0) Absent; (1) Present; (2) Present and partitioned from the nasal cavity.

Cranial Vault and Brain Endocast Characters

505 External bulging of the braincase in the parietal region: (0) Absent; (1) Expanded (the parietal part of the cranial vault is wider than the frontal part,

but the expansion does not extend to the lambdoidal region); (2) Greatly expanded (expansion of the cranial vault extends to the lambdoidal region).

506 Anterior expansion of the vermis (central lobe of the cerebellum): (0) (central lobe of the cerebellum): (0) Absent; (1) Present.

507 Overall size of the vermis: (0) Small; (1) Enlarged.

508 Lateral cerebellar hemisphere (excluding the paraflocculus): (0) Absent; (1) Present.

509 External division on the endocast between the olfactory lobe and the cerebral hemisphere (well-defined transverse sulcus separating the olfactory
lobes from the cerebrum): (0) Absence of external separation of the olfactory lobe from cerebral hemisphere; (1) Enlarged olfactory lobes; (2) Clear division of transverse sulcus.

510 Encephalization quotient: (0) Below 0.13; (1) Between 0.15-0.25, (2) Above 0.26.

511 Expansion of the posterior cerebral hemisphere (for each hemisphere, not the combined width of the posterior hemispheres): (0) Absent; (1) Present.

Soft-tissue characters

512 Trophoblasts in the placenta: (0) Absent; (1) Present.

513 Müllerian ducts (oviduct and uterus) pass in between the ureters: (0) Absent; (1) Present.

514 Placental types: (0) Placena absent; (1) Placenta present with vascularized chorio- allantois; (2) Placenta present but without vascularized chorio-allantois.

515 Multi-row and multicuspate molar opposition - Lower molar lingual row tallest anterior cusp a1 occluding into lingual embrasure between upper molars: (0) Absent; (1) Present.

516 Multi-row and multicuspate molar crown: saddle-shaped transverse crest between lingual cusp row (usually the tallest a1 on lowers, or A1 on uppers) and buccal cusp row (usually the tallest b2, or B2 on uppers): (0) AbsenT; (1) Present.

517 Frontal anterior extent location: (0) Posterior to anterior border of orbit; (1) Anterior to orbit but posterior to anterior tip of lacrimal; (2) Anterior to lacrimal.

518 Morphology of frontal-parietal suture in dorsal view: (0) V-shaped, apex directed posteriorly; (1) U-shaped, convex posteriorly; (2) U-shaped, convex anteriorly; 3) Roughly transverse.

519 Contact between nasals and parietals: (0) Absent; (1) Present.

520 Upper incisor alveolus depth: (0) Shallow (approximately 1.5x the alveolar diameter or less); (1) Deep (at least 2x the alveolar diameter or more).

521 Upper incisor alveolus orientation: (0) Vertical; (1) Procumbent: e.g., eleutherodontids, *Vintana*.

522 PMX facial process-nasal suture length (only applicable to taxa coded as '1' for character 497): (0) Less than 75% of maxilla-nasal suture length; (1) 75% to subequal to that of the maxilla.

523 Supraoccipital margin forms horizontal shelf over foramen magnum: (0) Absent;
(1) Present.

524 Supraoccipital dorsal height: (0) Tall, incorporating the nuchal line; (1) Short, restricted from nuchal line.

525 Lambdoidal crest orientation in lateral view: (0) Vertical orientation; (1) Forms a posterior flare and overhang on lateral portion of lambdoidal crest; (2) Forms a posterior flare and overhang on median portion of lambdoidal crest (e.g., therians and stem-therians).

526 Postparietal (if present): (0) Shallow and broad; (1) Forms large, subcircular shield, slightly taller than wide.

527 Parietal contribution to occiput: (0) Slight; (1) Enlarged, forming 30% of the occiput or more.

528 Maxilla-palatine suture orientation in ventral view: (0) Squared or arched; (1) Wedged anteromedially to midline (A-shaped) so that maxilla anterolaterally bounds palatine.

529 (Posterior margin of bony secondary palate shape: (0) Level or truncated; (1) A- shaped notch.

530 Alisphenoid processus ascendens anteroposterior extent: (0) Anteroposteriorly broad; (1) Tall and narrow.

531 Maxilloturbinal supporting ridge: (0) Absent; (1) Present.

532 Ossified maxilloturbinal bones: (0) Absent; (1) Present.

533 Klinorhynchy: (0) Absent; (1) Present, anterior portion of skull is flexed anteroventrally.

534 Preoptic flexure on anteroventral portion of brain endocast: (0) Absent; (1) Present.

535 Mesiolateral divergence of left and right maxillary tooth rows: (0) Absent; (1) Present.

536 Pterygoid anterior expansion in ventral view: (0) Absent; (1) Present, pterygoid extends forward to contact maxilla in ventral view, excluding palatine medially.

537 Parieto-pachyostal sagittal crest: (0) Absent; (1) Present, parietal is greatly thickened on the sagittal midline.

538 Stepwise pattern ("en echelon" pattern of Jenkins et al., 1997) in the profile of upper premolar-molar series (applicable only to molars with more than one rows of multiple cusps). (0) Absent: (1) Present.

539 (New) Dual-Mortar-Pestle occlusion of basined molars that are also partially multi-cusp-row (from Luo et al. 2017 Nature on *Vilevodon*, applicable only to taxa with multiple cusp-rows): (0) Absent; (1) Present.

540 Relative width of calcaneus as measured in length-width ratio. (0) Longer than wide, L/W ratio equal or greater than 150%; (1) length sub-equal to width, L/W is 140%, or less:

New shoulder girdle characters added during Studying of *New Docodontan*

541 (New) Contact of medial ends of the two clavicles at the midline: (0) Present, point-contact or abutting contact; (1) No contact of clavicles at midline – two clavicles respectively contact the interclavicle/sternal manubrium.

New Urogenital Systems Characters

542 (New) Urogenital sinus and vagina morphology: (0) Presence of cloaca (no differentiation of vagina from urogenital sinus, the latter confluent with rectum); (1)
Differentiation of vagina from urogenital sinus: most extant placentals (except tenrecids, golden moles and soricids), and marsupials (except marsupial moles),
(?) Not applicable for all of the fossil taxa in this matrix.

543 (New) Vas deferens looping over ureter in adult males:
(0) Absence: *Ornithorhynchus*, *Tachyglossus*, all extant marsupial species.
(1) Present: all extant placental species. (?) Not observable in fossil mammals.

544 (New) Descent of testis and location of testes in adult males:
(0) No descent of testis (Testes abdominal, or testicondy); (1) Testis descended either ascrotal (testes in pelvic or inguinal position, but ascrotal and not in an external scrotum), or scrotal:

545 (New) Development of scrotum
(0) Acrotal - testes in abdominal, pelvic, or inguinal position;
(1) Scrotal – testes in scrotum.

Hyoid element characters:

546 (New) - Presence of ossified basihyal:
(0) Absent;
(1) Present;
(?) Not preserved: all other fossil taxa of this matrix.

547 (New) - Morphology of basihyal:
(0) Rod-like basihyal;
(1) Antero-posteriorly wide basihyal (strap-like or plate-like basihyal, which is widened in antero-posterior dimension, 25% or more of the transverse length of the bone);
(?) Unknown: not yet investigated in most marsupials (except the taxa listed above); not preserved in many fossils (except those taxa listed above).

548 (New) - Anterior cornu of hyoid apparatus:
(0) Formed by a single, elongate hyoid rod without internal segmentation;
(1) Jointed short segments of anterior cornua (scored for this character state where the cerato- basihyal joint is preserved, and scored also if the cerato-epihyal joint or the dorsal end of ceratohyal is preserved).
(?) Not preserved.

549 (New) - Thyrohyals:
(0) Not ossified:
(1) Ossified, rod-like along the shaft:
(2) Ossified and strap-like in mid shalf:
(3) Ossified, and oblong plate:
(?) No preserved:

550 (New) - The expanded dorsal end of thyrohyal:
(0) Absent:
(1) Present and club-like or fan-like:
(2) Present, broad and rhomboidal or semicircle-like:

551 (New) - Fusion of basihyal and thyrohyals:
(0) Unfused (can be scored if the ends of basihyal are preserved):
(1) Fused:
(?) Not preserved: most Mesozoic mammaliaform fossils

552 (New) – Fused basihyal and thyrohyals form an angled “V-bone”:
(0) Absent:
(1) Present:

553 (New) - Morphology of ceratohyal:
(0) Rod-like:
(1) Strap-like:
(2) Plate-like (broad, semicircle or rhomboidal shape):
(3) Shortened and block-like:

554 (New) – Cartilaginous or ossified epihyal element in adult:
(0) Absent:
(1) Present:
(?) Not preserved:

555 (New) - Ossified stylohyal in adult:
(0) Absent:
(1) Present:
(?) Unknown:

556 (New) - Integro-cornuate versus discreto-cornuate condition of the jointed anterior cornu of hyoids:
(0) Discreto-cornuate:
(1) Integro-cornuate:
(?) Inapplicable:
(?) Unknown (not complete enough to assess):

APPENDIX 16: Changes to characters scores in expanded dataset, and consistency indices (*Borealestes*, based on Zhou et al., 2019)

Characters re-interpreted (from Zhou et al., 2019) for *Agilodocodon* and *Docofossor* in this analysis.

Character	***Borealestes***	***Agilodocodon***	***Docofossor***
32) Position of the dentary condyle relative to the level of the postcanine alveoli: (0) Below or about the same level; (1) Above	1	Changed from 0 to 1	0 (unchanged)
56) Ultimate lower premolar - anterior cusp b (= paraconid): (0) Absent or indistinctive; (1) Present and distinctive; (2) Enlarged.	1	Changed from 2 to 1	1 (unchanged)
67) Penultimate lower premolar - paraconid (=cusp b): (0) Absent; (1) Present but not distinctive; (2) Distinctive and slightly enlarged.	1	Changed from 2 to 1	1 (unchanged)
312) Astragalar neck basal width: (0) Neck narrower than the head (constriction posterior to navicular facet); (1) Neck about same width as the head (with parallel sides posterior to navicular facet); (2) Widest point of neck at mid-length (widening is not developed near the base of the neck); (3) Astragalar neck widest at the base.	3	? (unchanged)	Changed from ? to 3

Results of statistical analyses on phylogenetic analyses. For details of each analysis, see Methods 3.3.4.1. CI = consistency index; HI homoplasy index; RI retention index; RC rescaled consistency index.

Analysis	**Tree length**	**CI**	**HI**	**RI**	**RC**
1	2808	0.320	0.680	0.799	0.256
2	2832	0.317	0.683	0.798	0.252
3 (tree 1)	2838	0.317	0.683	0.798	0.253
3 (tree 2)	2838	0.317	0.683	0.798	0.253
4	2813	0.320	0.680	0.798	0.255
5	2827	0.318	0.682	0.799	0.254

APPENDIX 17: PAUP analysis (*Borealestes* expanded dataset)

```
P A U P *
Version 4.0a (build 164) for 32-bit Microsoft Windows (built on Nov  1 2018 at 19:32:34)
Fri Feb 08 08:39:45 2019

paup> ToNEXUS fromFile=Panciroli2018matrix.txt;

Processing of file "C:\Users\Elsa\Documents\Manuscripts\Block A\Phylogenetic
analysis\PAUP\Panciroli2018matrix.txt" begins...

Data matrix has 113 taxa, 491 characters
Valid character-state symbols: 012345
Missing data identified by '?'
Gaps identified by '-'
Processing of input file "Panciroli2018matrix.txt" completed.
paup> Set maxtrees=200 increase=auto;

paup> Set maxtrees=200;

Maxtrees reset to 200

paup> HSearch addSeq=random nreps=1000;

paup> HSearch steepest;

Heuristic search settings:
  Optimality criterion = parsimony
    Character-status summary:
      Of 491 total characters:
        All characters are of type 'unord'
        All characters have equal weight
        All characters are parsimony-informative
    Gaps are treated as "missing"
    Multistate taxa interpreted as uncertainty
  Starting tree(s) obtained via stepwise addition
    Addition sequence: random
    Number of replicates = 1000
    Starting seed = generated automatically
    Number of trees held at each step = 1
  Branch-swapping algorithm: tree-bisection-reconnection (TBR) with reconnection limit = 8
    Steepest descent option in effect
  Initial 'Maxtrees' setting = 21800 (will be auto-increased by 100)
  Branches collapsed (creating polytomies) if maximum branch length is zero
  'MulTrees' option in effect
  No topological constraints in effect
  Trees are unrooted

Heuristic search completed
  Total number of rearrangements tried = 63961532
  Score of best tree(s) found = 2471
  Number of trees retained = 2
```

Time used = 51.77 sec (CPU time = 50.05 sec)

paup> ShowTrees all / tOrder=right;

Note: No outgroup has been defined; trees are (arbitrarily) rooted at first taxon.

Tree 1 (rooted using default outgroup)

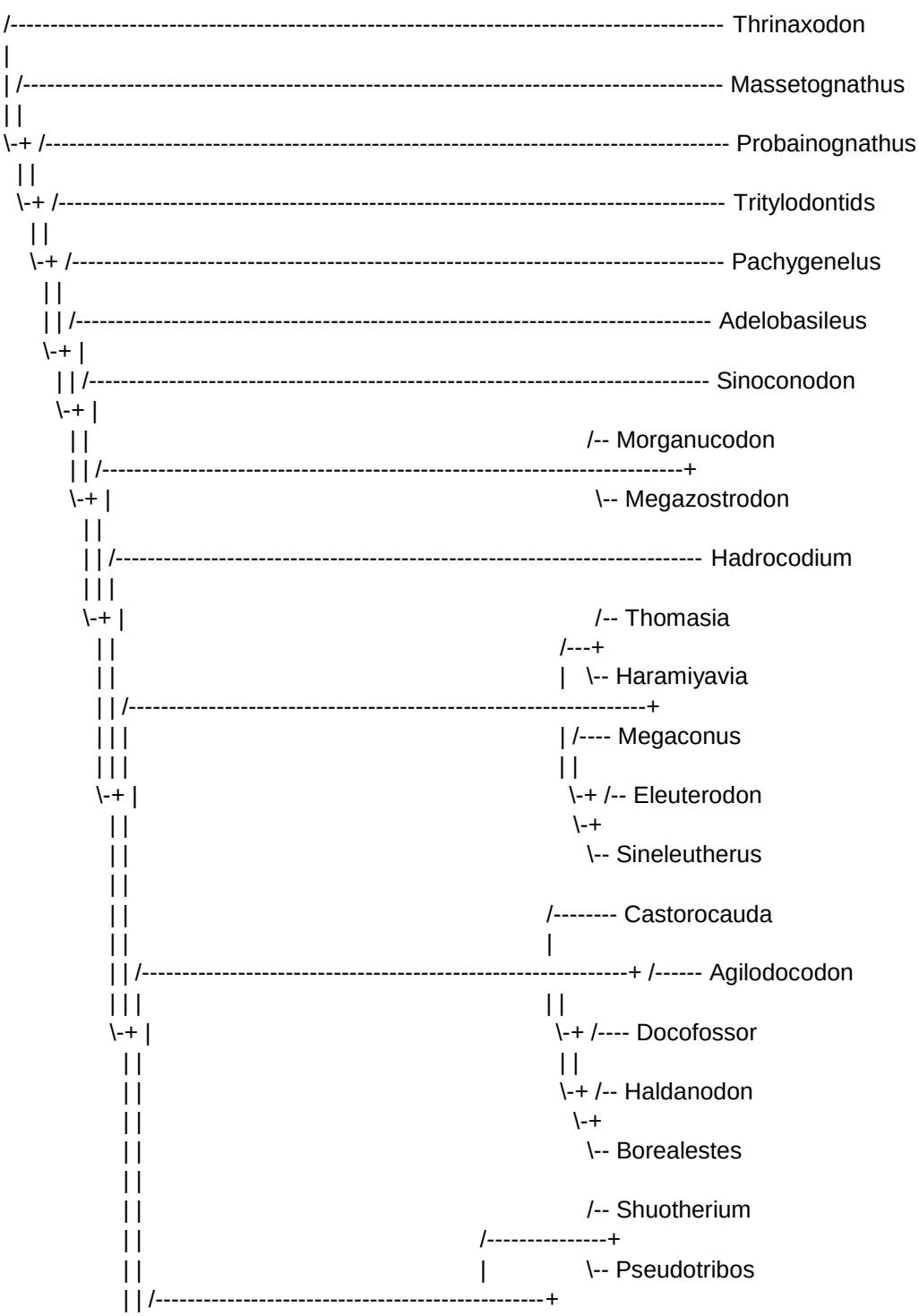

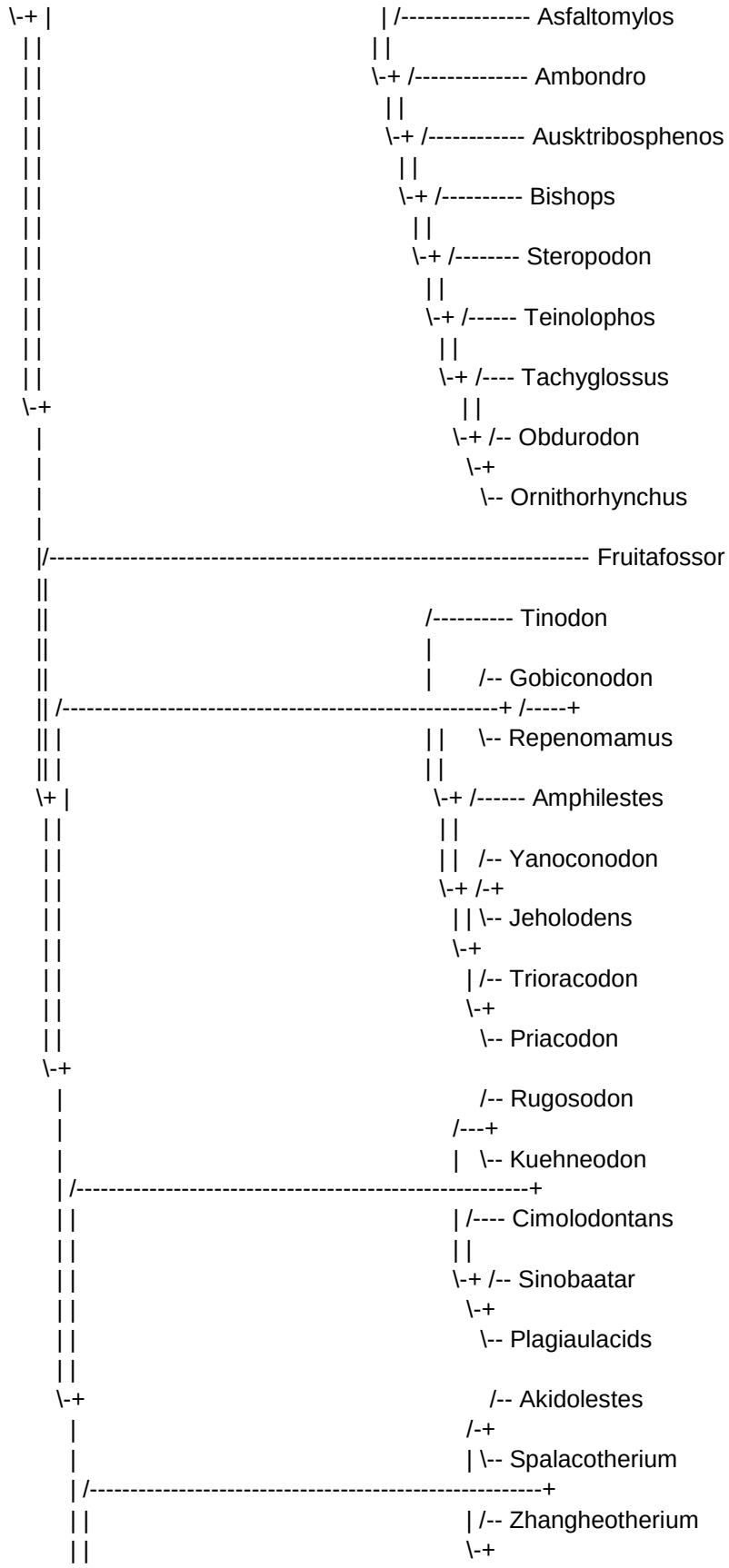
Asfaltomylos
Ambondro
Ausktribosphenos
Bishops
Steropodon
Teinolophos
Tachyglossus
Obdurodon
Ornithorhynchus
Fruitafossor
Tinodon
Gobiconodon
Repenomamus
Amphilestes
Yanoconodon
Jeholodens
Trioracodon
Priacodon
Rugosodon
Kuehneodon
Cimolodontans
Sinobaatar
Plagiaulacids
Akidolestes
Spalacotherium
Zhangheotherium

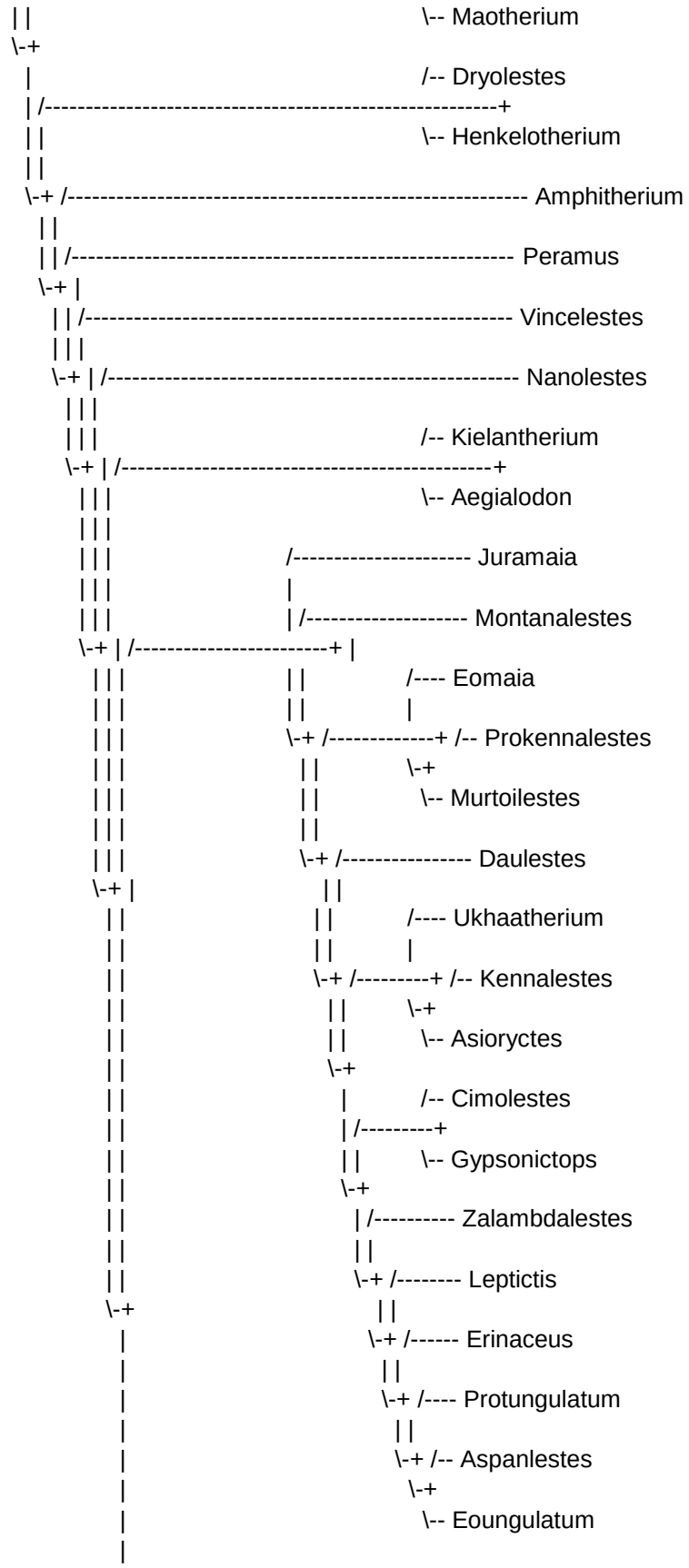
\-- Maotherium
/-- Dryolestes
\-- Henkelotherium
Amphitherium
Peramus
Vincelestes
Nanolestes
/-- Kielantherium
\-- Aegialodon
Juramaia
Montanalestes
/---- Eomaia
/-- Prokennalestes
\-- Murtoilestes
Daulestes
/---- Ukhaatherium
/-- Kennalestes
\-- Asioryctes
/-- Cimolestes
\-- Gypsonictops
Zalambdalestes
Leptictis
Erinaceus
Protungulatum
Aspanlestes
\-- Eoungulatum

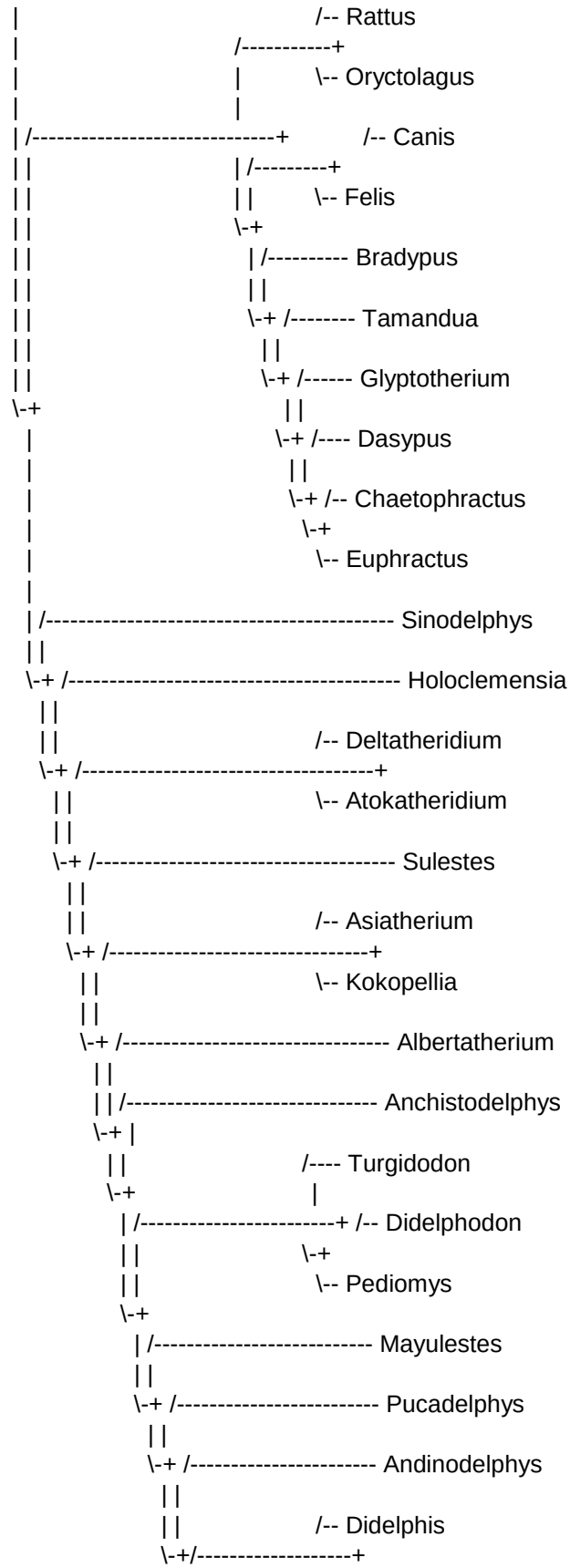
Rattus
Oryctolagus
Canis
Felis
Bradypus
Tamandua
Glyptotherium
Dasypus
Chaetophractus
Euphractus
Sinodelphys
Holoclemensia
Deltatheridium
Atokatheridium
Sulestes
Asiatherium
Kokopellia
Albertatherium
Anchistodelphys
Turgidodon
Didelphodon
Pediomys
Mayulestes
Pucadelphys
Andinodelphys
Didelphis

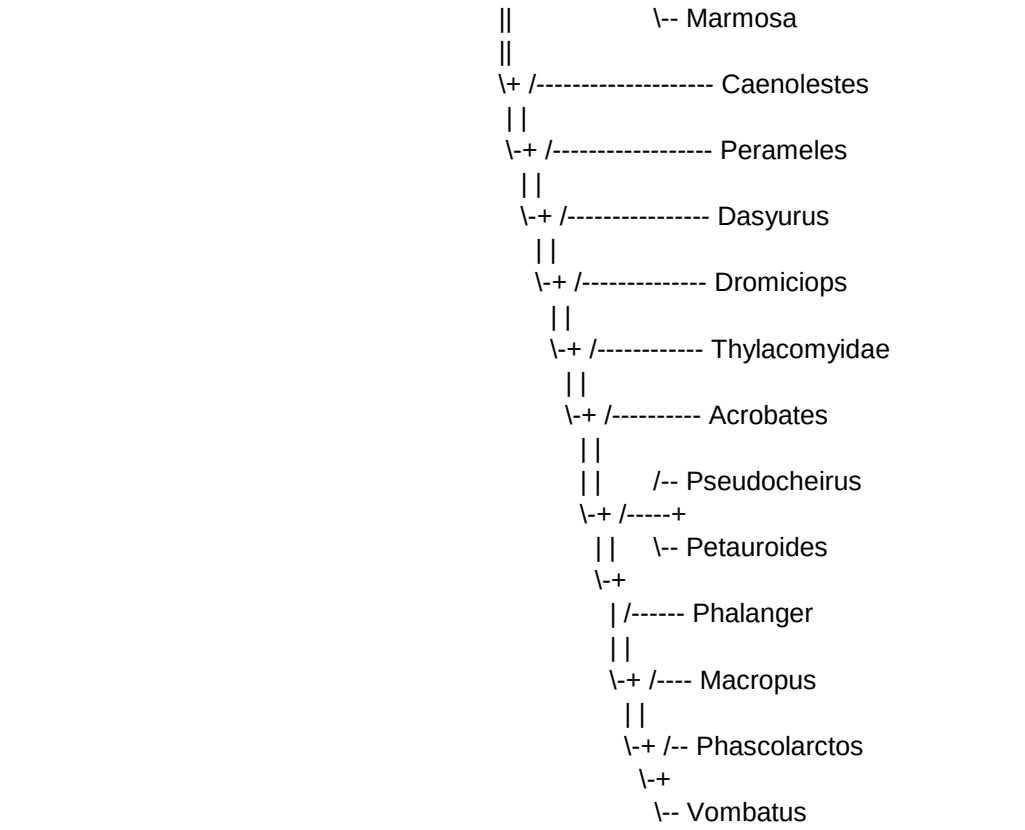

Tree 2 (rooted using default outgroup)

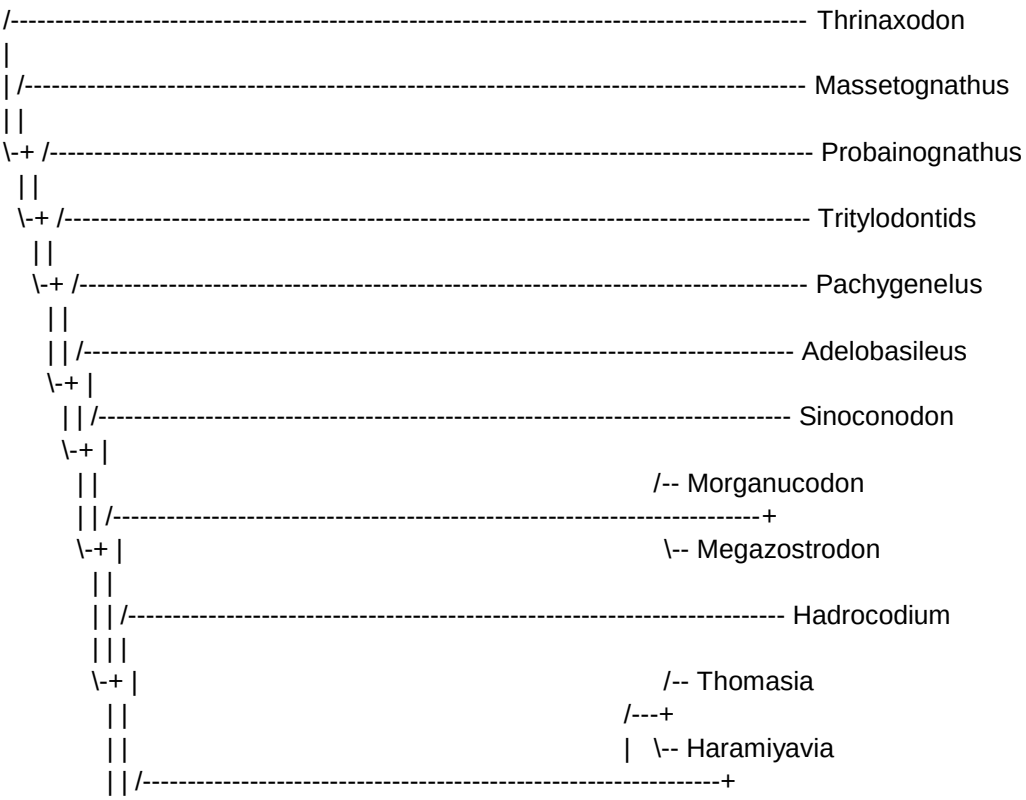

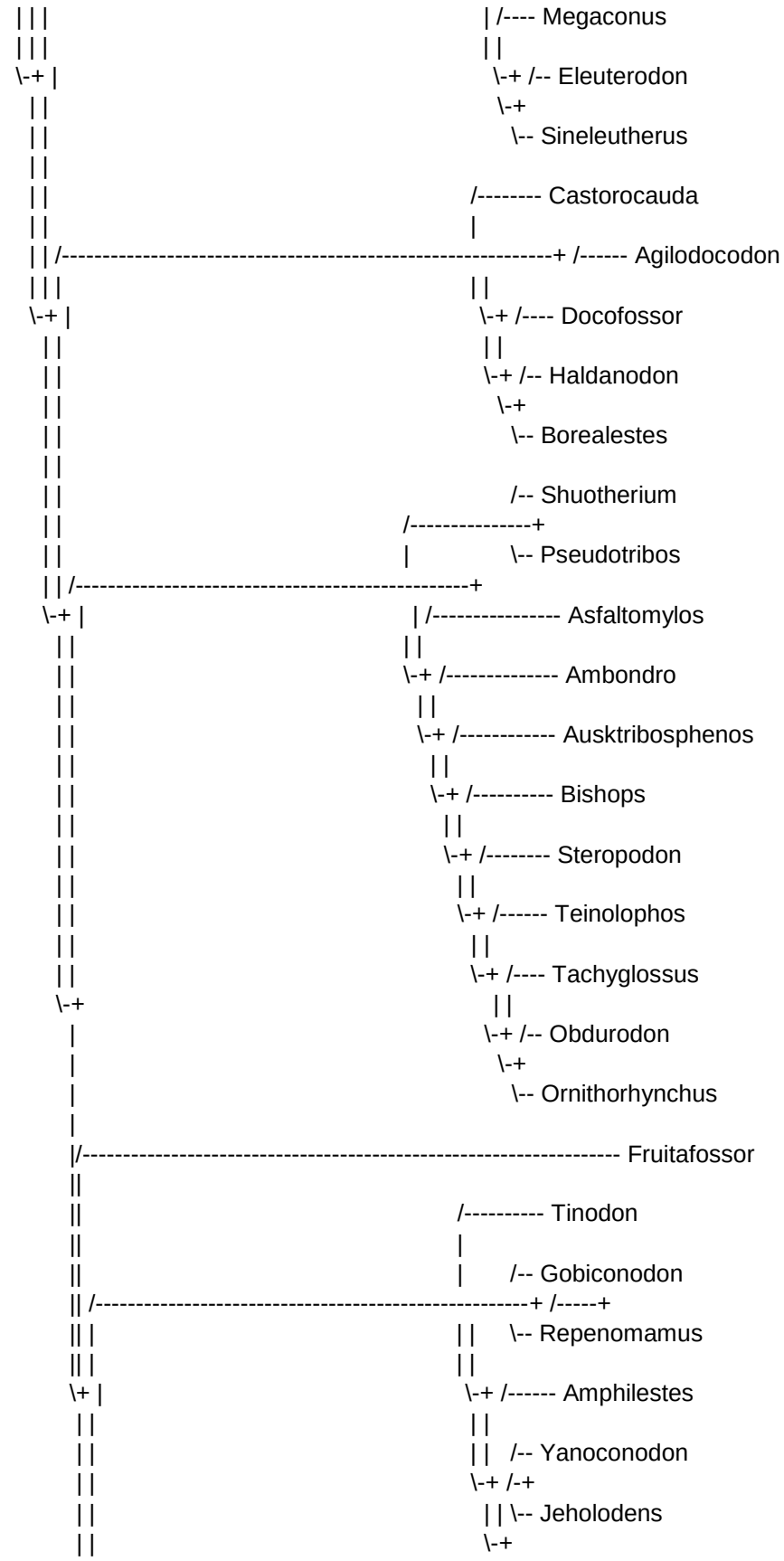
Megaconus
Eleuterodon
Sineleutherus
Castorocauda
Agilodocodon
Docofossor
Haldanodon
Borealestes
Shuotherium
Pseudotribos
Asfaltomylos
Ambondro
Ausktribosphenos
Bishops
Steropodon
Teinolophos
Tachyglossus
Obdurodon
Ornithorhynchus
Fruitafossor
Tinodon
Gobiconodon
Repenomamus
Amphilestes
Yanoconodon
Jeholodens

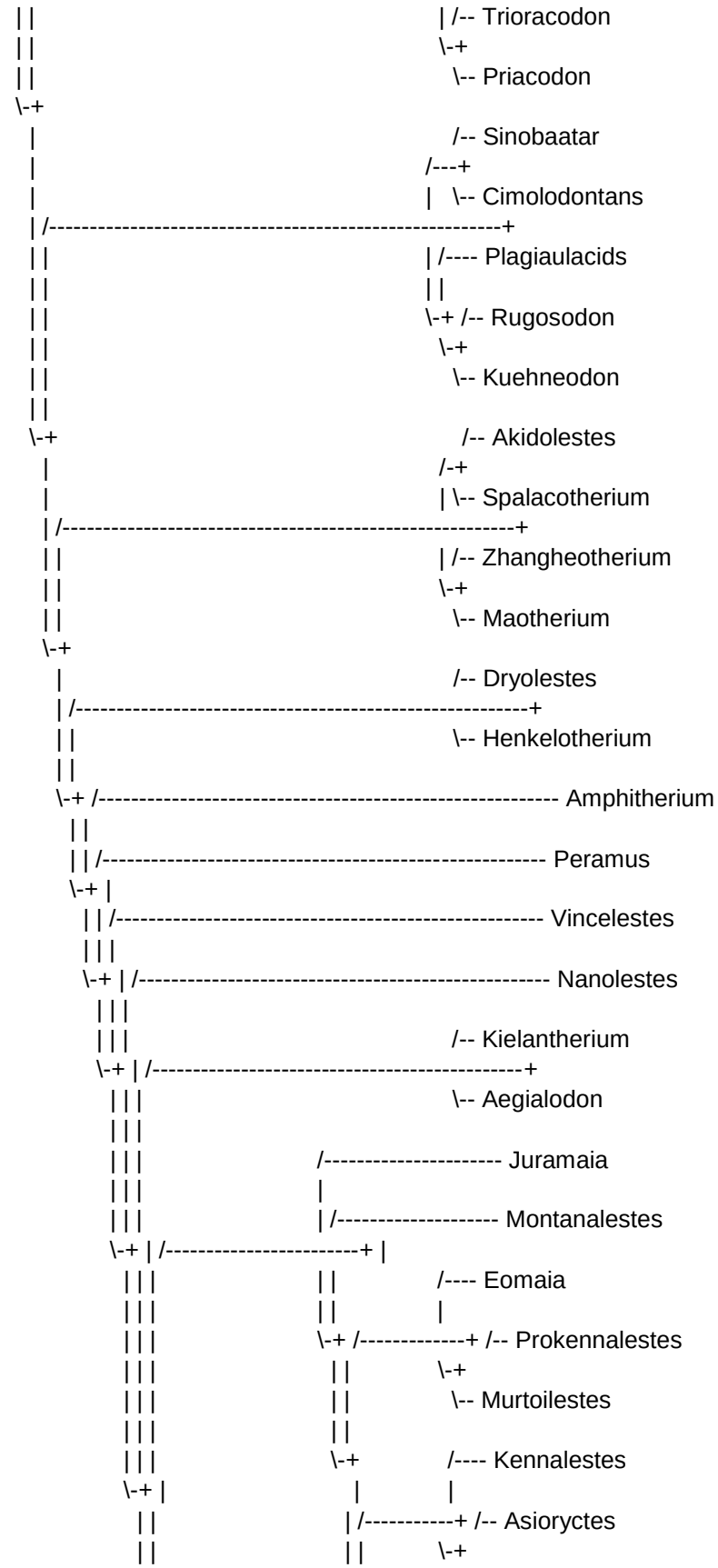
Trioracodon
Priacodon
Sinobaatar
Cimolodontans
Plagiaulacids
Rugosodon
Kuehneodon
Akidolestes
Spalacotherium
Zhangheotherium
Maotherium
Dryolestes
Henkelotherium
Amphitherium
Peramus
Vincelestes
Nanolestes
Kielantherium
Aegialodon
Juramaia
Montanalestes
Eomaia
Prokennalestes
Murtoilestes
Kennalestes
Asioryctes

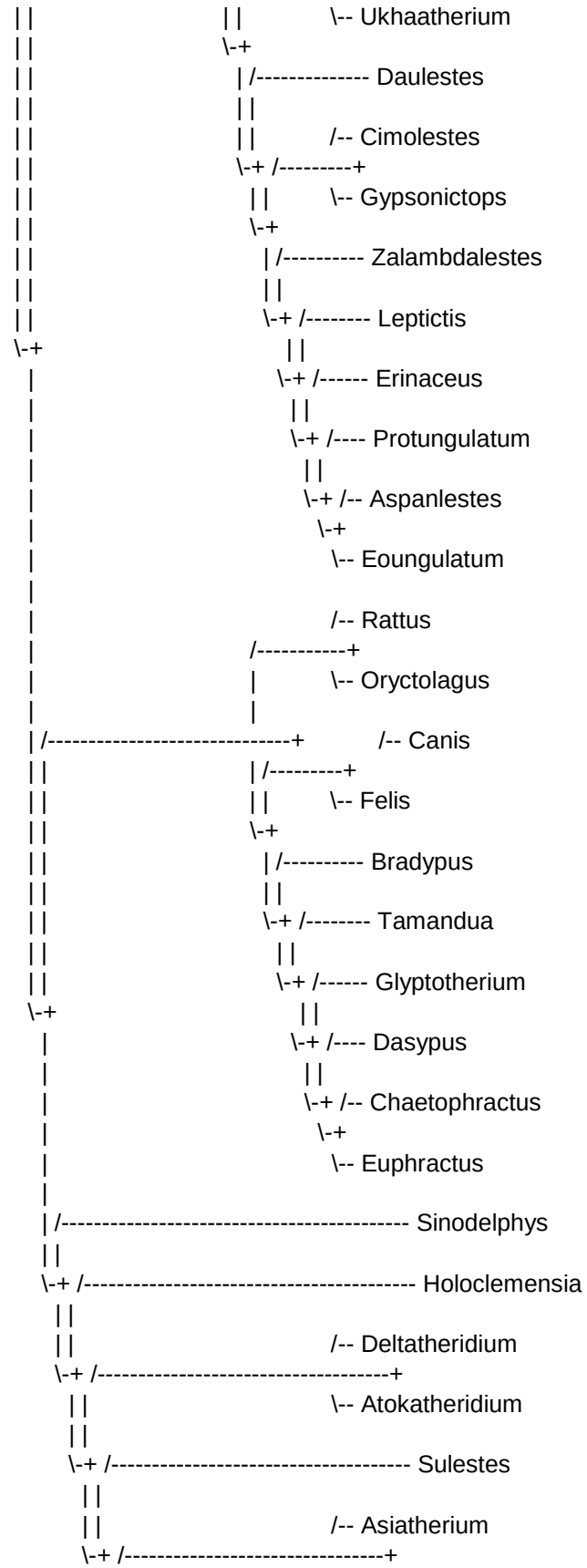
\-- Ukhaatherium
Daulestes
Cimolestes
Gypsonictops
Zalambdalestes
Leptictis
Erinaceus
Protungulatum
Aspanlestes
Eoungulatum
Rattus
Oryctolagus
Canis
Felis
Bradypus
Tamandua
Glyptotherium
Dasypus
Chaetophractus
Euphractus
Sinodelphys
Holoclemensia
Deltatheridium
Atokatheridium
Sulestes
Asiatherium

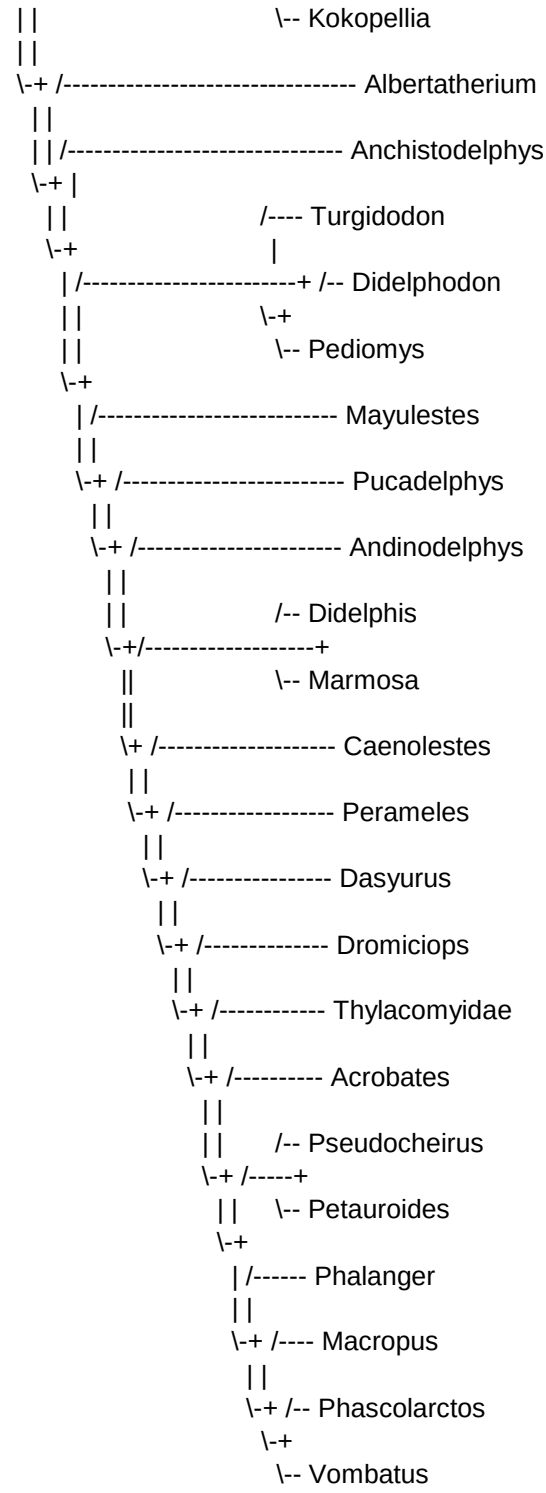


```
paup> PScores / CI RI RC HI Gfit;

Lengths and fit measures of trees in memory:
  Character-status summary:
    Of 491 total characters:
      All characters are of type 'unord'
```

All characters have equal weight
All characters are parsimony-informative
Gaps are treated as "missing"
Multistate taxa interpreted as uncertainty

Sum of min. possible lengths = 817
Sum of max. possible lengths = 8976

Tree #	1	2
Length	2471	2471
CI	0.331	0.331
RI	0.797	0.797
RC	0.264	0.264
HI	0.669	0.669
G-fit	-289.152	-288.986

paup> ConTree;

Strict consensus of 2 trees:

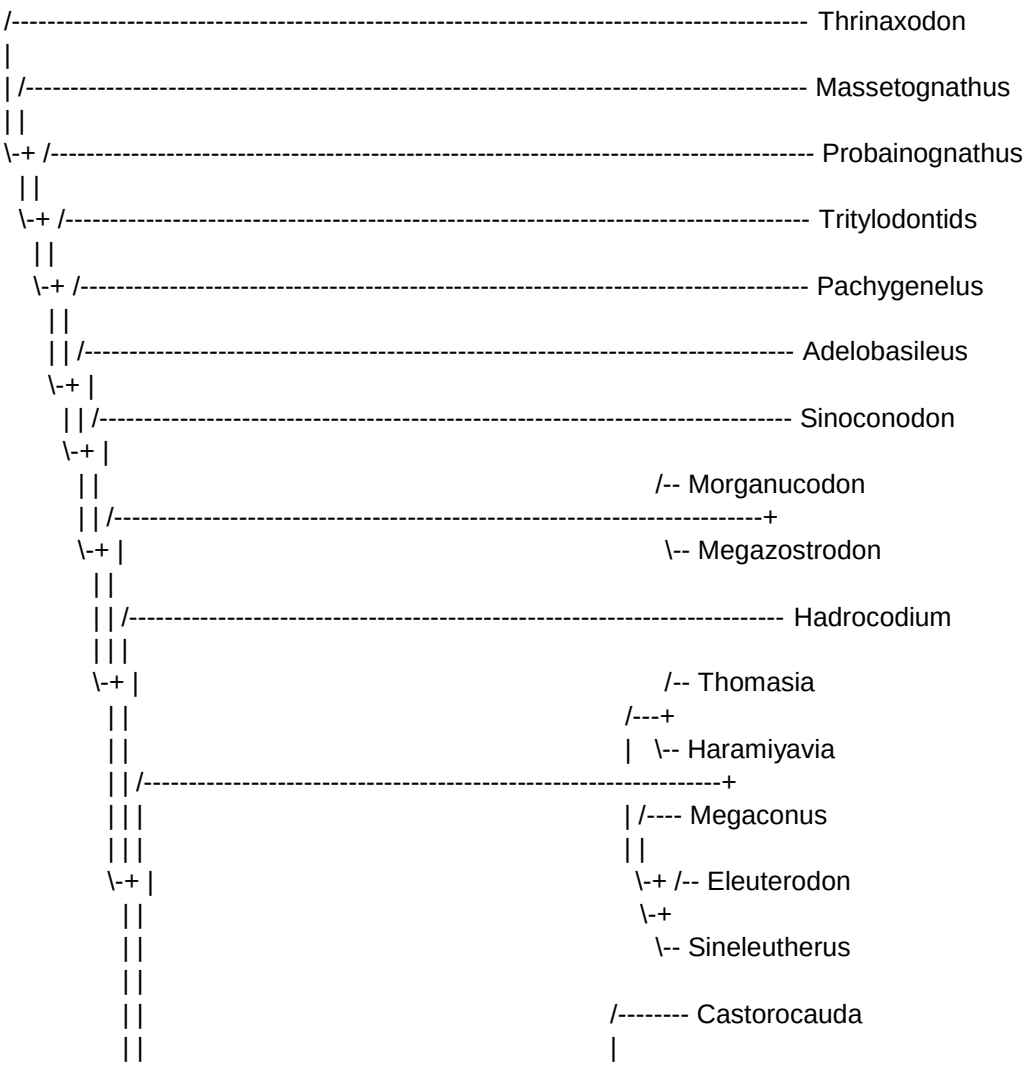

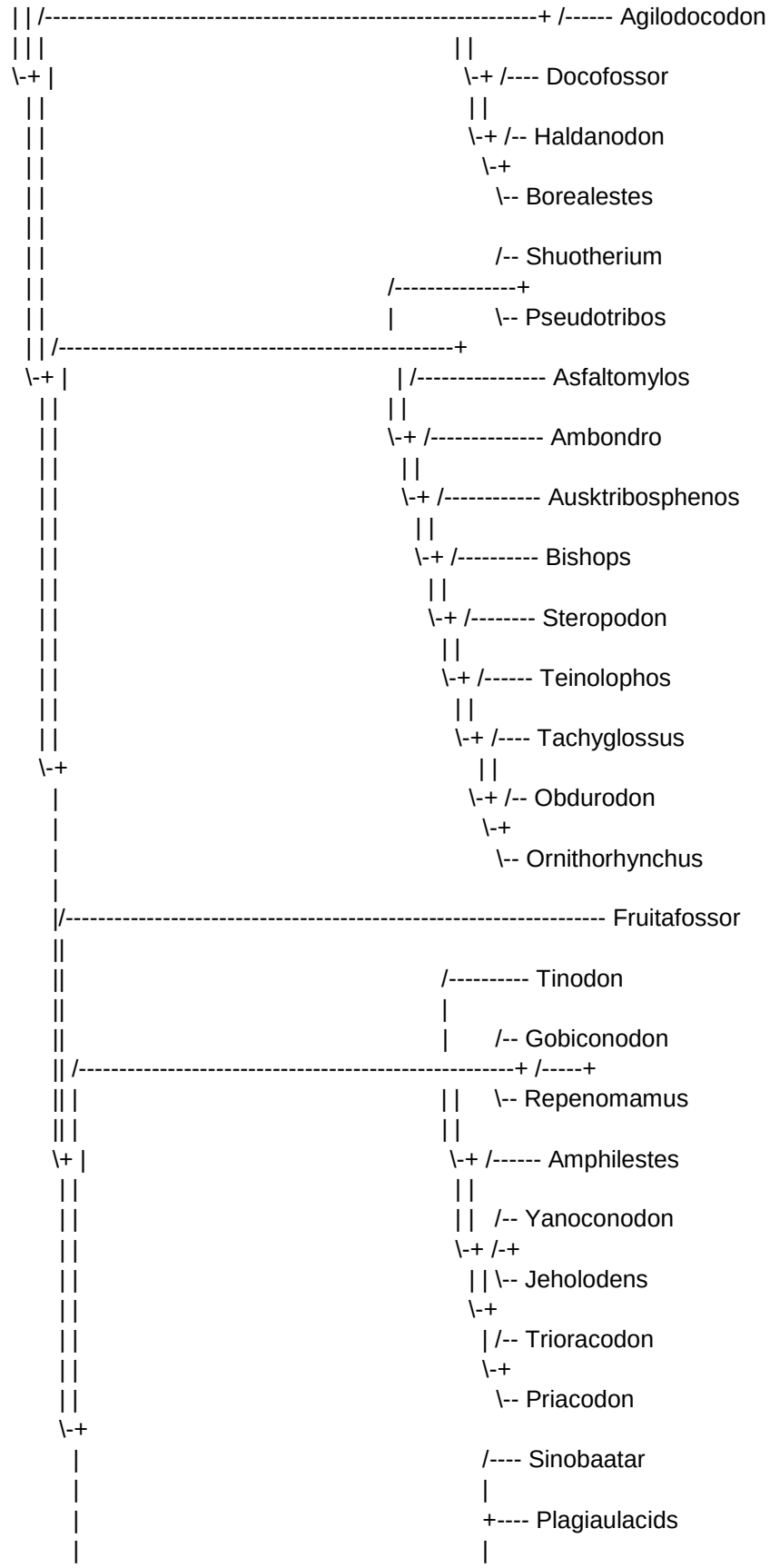
Agilodocodon
Docofossor
Haldanodon
Borealestes
Shuotherium
Pseudotribos
Asfaltomylos
Ambondro
Ausktribosphenos
Bishops
Steropodon
Teinolophos
Tachyglossus
Obdurodon
Ornithorhynchus
Fruitafossor
Tinodon
Gobiconodon
Repenomamus
Amphilestes
Yanoconodon
Jeholodens
Trioracodon
Priacodon
Sinobaatar
Plagiaulacids

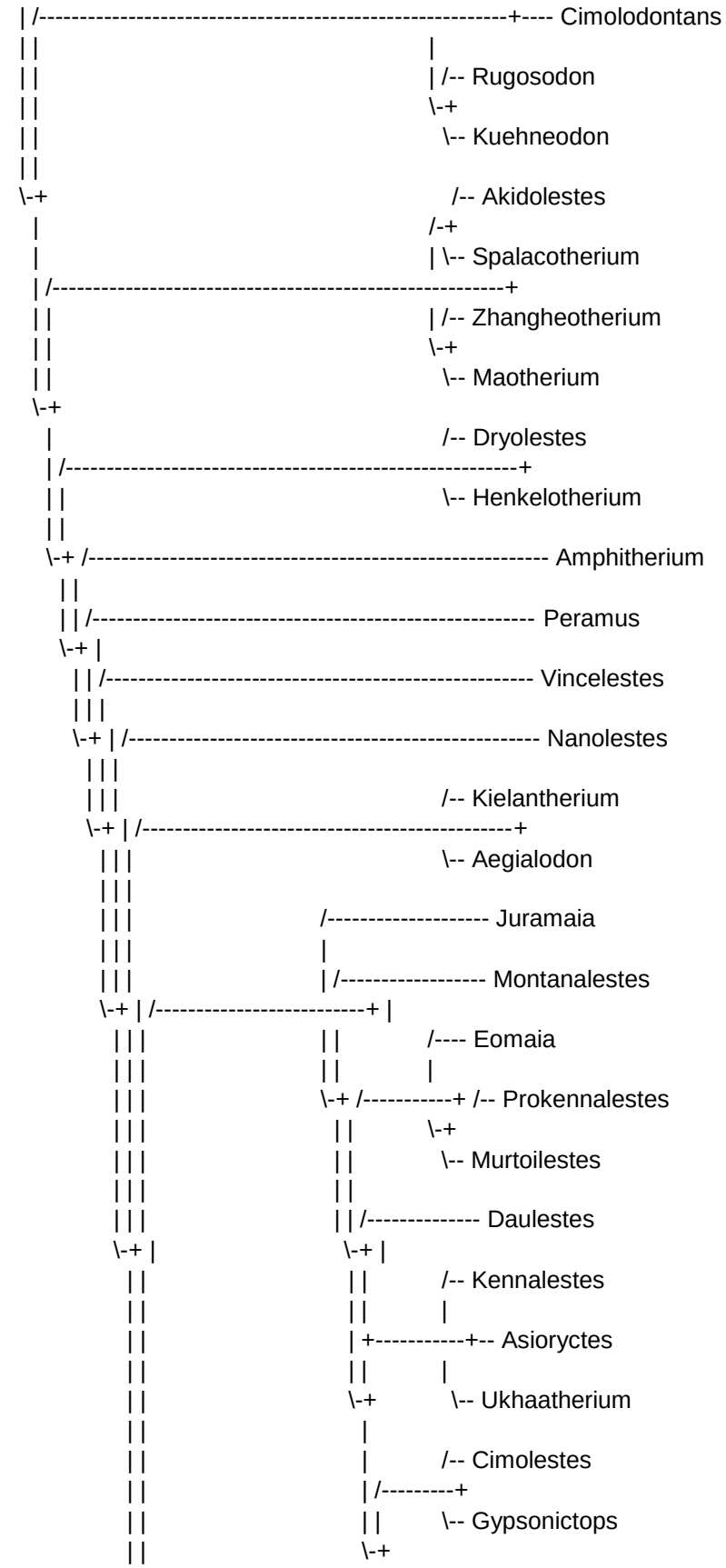
Cimolodontans
Rugosodon
Kuehneodon
Akidolestes
Spalacotherium
Zhangheotherium
Maotherium
Dryolestes
Henkelotherium
Amphitherium
Peramus
Vincelestes
Nanolestes
Kielantherium
Aegialodon
Juramaia
Montanalestes
Eomaia
Prokennalestes
Murtoilestes
Daulestes
Kennalestes
Asioryctes
Ukhaatherium
Cimolestes
Gypsonictops

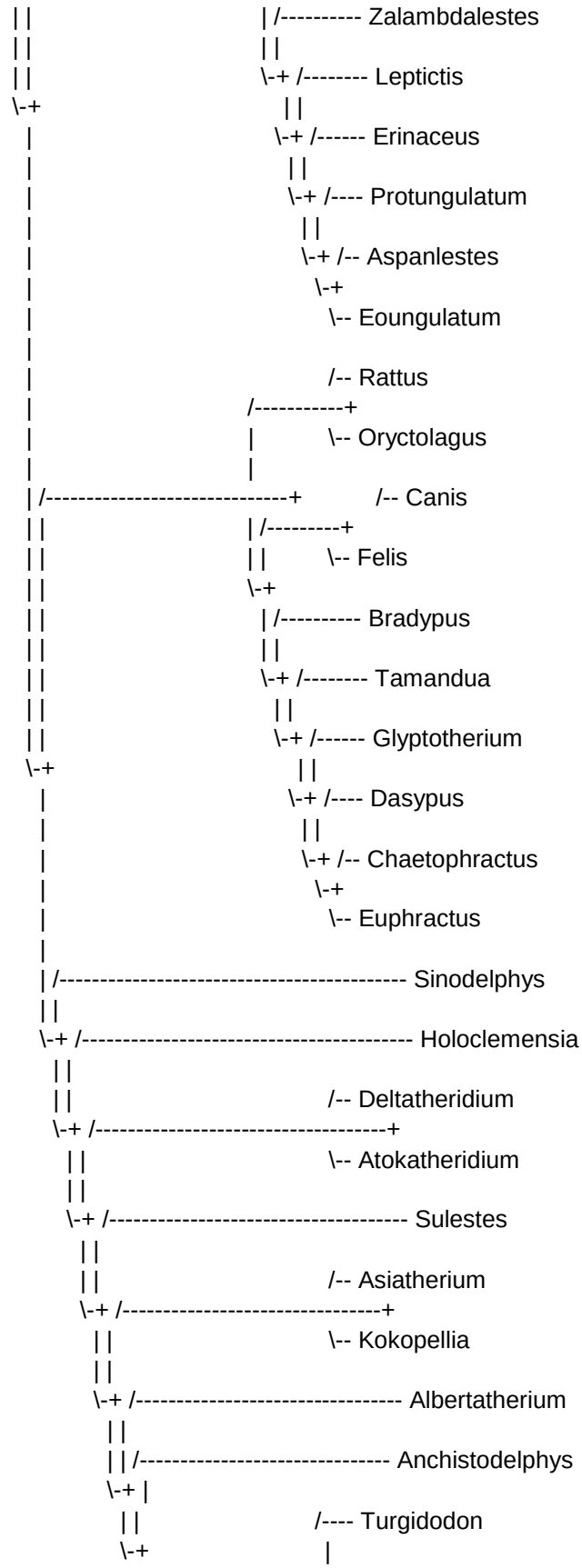
Zalambdalestes
Leptictis
Erinaceus
Protungulatum
Aspanlestes
Eoungulatum
Rattus
Oryctolagus
Canis
Felis
Bradypus
Tamandua
Glyptotherium
Dasypus
Chaetophractus
Euphractus
Sinodelphys
Holoclemensia
Deltatheridium
Atokatheridium
Sulestes
Asiatherium
Kokopellia
Albertatherium
Anchistodelphys
Turgidodon

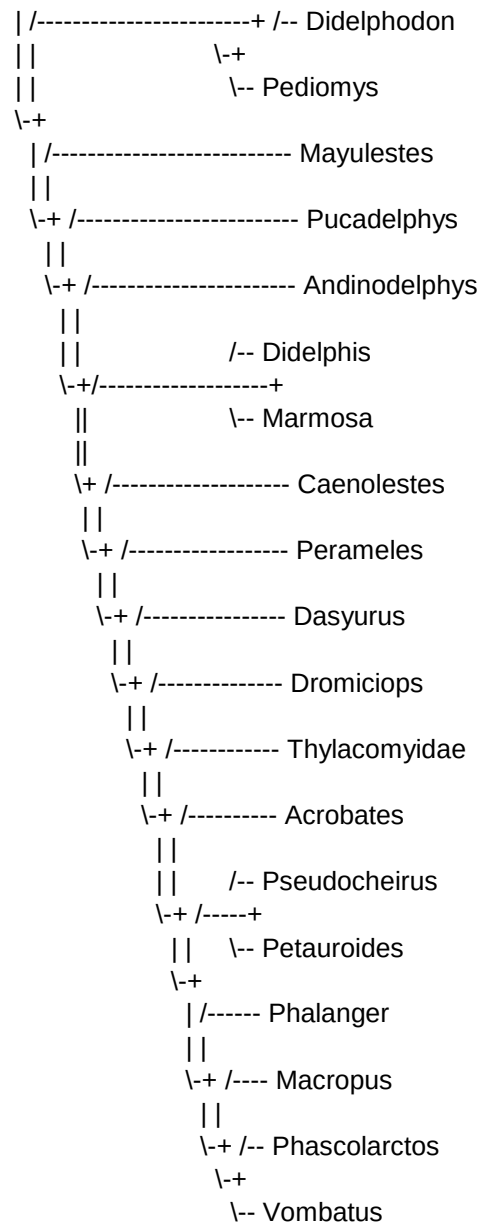

Tree length = 2471
Consistency index (CI) = 0.3306
Homoplasy index (HI) = 0.6694
Retention index (RI) = 0.7973
Rescaled consistency index (RC) = 0.2636
f value = 363272
f-ratio = 0.7263

APPENDIX 18: Newly scored characters for *Palaeoxonodon*.

The following six characters (from Zhou et al., 2013) were newly scored based on morphology present in specimen NMS G.2017.37.1:

12. Coronoid bone (or its attachment scar): (1) absent to (0) present
13. Location of the mandibular foramen (posterior opening of the mandibular canal): ? to (1) in the pterygoid fossa and offset from Meckel's sulcus (the intersection of Meckel's sulcus at the pterygoid margin is ventral and posterior to the foramen).
14. Vertical position of the mandibular foramen: ? to (0) below the alveolar plane.
22. Crest of the masseteric fossa along the anterior border of the coronoid process: ? to (1) present and distinctive.
23. Anteroventral extension of the masseteric fossa: ? to (1) extending anteriorly onto the body of the mandible.
24. Labial mandibular foramen (masseteric foramen) inside the masseteric fossa: ? to (1) present.

Re-scored characters for *Palaeoxonodon*—we re-scored and added the following characters (from Zhou et al., 2013) for *Palaeoxonodon* differently from Close et al. (2016):

6. Groove for the replacement dental lamina (Crompton's groove): (1) absent. Crompton's groove for the replacement dental lam- ina, as seen in Morganucodon and some other stemward mammaliaformes, is not present on any of the specimens of *Palaeoxonodon ooliticus* so far recovered from England or Scotland. We therefore consider it justifiable to score this character as absent.

97. Hypoconid (we designate the distal cingulid cuspule d as the homolog to the hypoconid in the teeth with linear alignment of the main cusps; we assume the cusp to be the hypoconid if there is only a single cusp on the talonid in the teeth with reversed triangulation): (1) present (as distal cusp d, sensu Crompton, 1971), elevated above the cingulid level, labially positioned (or tilted in the lingual direction). We score this based on the morphology of all known material so far.

174. Diastema separating the lower first and second premolars (de- fined as the first and second functioning premolar or premolar- iform postcanine): (0) absent (gap less than one tooth root for whichever is smaller of the adjacent teeth). No diastema sepa- rates the premolars pm1 and pm2, nor is there a diastema pre- or post-canine, in this taxon in any specimens known so far.

182. Enlarged diastema in the lower incisor-canine region (better developed in older individuals): (0) absent; as for 174.

195. Open root end of the postcanines: (1) present; based on NMS G. 2015.17.1.

196. Degrees of root division: (2) two or three complete divided roots. All specimens now recovered confirm that Palaeoxono- don ooliticus has two completely divided roots in all teeth ex- cept incisors, and that they are not connected by dentine sheets.

Re-scored characters for *Arguimus*—we re-scored and added the following characters for *Arguimus* differently from Close et al. (2016):

13. Location of the mandibular foramen (posterior opening of the mandibular canal): 4 to (?) the location of this structure can- not be confirmed in *Arguimus*.

14. Vertical position of the mandibular foramen: 1 to (0) below the alveolar plane.
24. Labial mandibular foramen inside the masseteric fossa: ? to (1) present.
26. Posterior-most mental foramen: ? to variable (1, 2, 3, 4).

Rescored characters for *Amphitherium* and *Peramus*—we re-scored and added the following characters for *Amphitherium* and *Peramus* from Zhou et al. (2013):
12. Coronoid bone (or its attachment scar): (1) absent in *Peramus*.
195. Open root end of the postcanines: (1) present (for both taxa). This character was previously scored as (2) for *Amphitherium* and *Peramus*, which is not an option for this character.

APPENDIX 19 R-scripts for morphometric analyses of *Borealestes*

```
###PCA
setwd("F:/Manuscripts/Block A/R/RatiosWPlacsUnder5Kg/FINAL")
install.packages("moments")
install.packages("geomorph")
library(geomorph)
library(moments)
calcanea<-read.csv("CalcaneaRatios.csv",header=T, row.names=1)
calcanea
attach(calcanea)
names(calcanea)
summary(calcanea)
pca1<-princomp(calcanea, scores=TRUE,cor=TRUE)
summary(pca1)
plot(pca1)
biplot(pca1)
pca1$loadings
write.csv(pca1$summary, file="PCALoadings.csv")
pca1$scores
writes a csv file of PCA scores

##### in excel add columns with presence/absence data so that the ecological bins can
be sorted

calcanea<-read.csv("PCAScoresLocomotor.csv", header=TRUE, row.names=1)
Plot_ConvexHull<-function(xcoord, ycoord, lcolor){
  hpts <- chull(x = xcoord, y = ycoord)
  hpts <- c(hpts, hpts[1])
  lines(xcoord[hpts], ycoord[hpts], col = lcolor)}
datasubset1<-subset(calcanea, Arboreal=="1", select=c(Comp.1:Comp.7))
datasubset2<-subset(calcanea, Scansorial=="1", select=c(Comp.1:Comp.7))
datasubset3<-subset(calcanea, Terrestrial=="1", select=c(Comp.1:Comp.7))
datasubset4<-subset(calcanea, Fossorial=="1", select=c(Comp.1:Comp.7))
datasubset5<-subset(calcanea, SemiFossorial=="1", select=c(Comp.1:Comp.7))
datasubset6<-subset(calcanea, SemiAquatic=="1", select=c(Comp.1:Comp.7))
datasubset7<-subset(calcanea, Fossil=="1", select=c(Comp.1:Comp.7))
datasubset8<-subset(calcanea, Saltatorial=="1", select=c(Comp.1:Comp.7))
datasubset9<-subset(calcanea, Gliding=="1", select=c(Comp.1:Comp.7))
par(mar=c(5,5,3,5), xpd=TRUE)
plot(datasubset1$Comp.1, datasubset1$Comp.2, main="PCA: <5kg, calcaneal ratios",
cex.main=1, ylab="PC2", xlab="PC1", xaxt="n", yaxt="n", xlim=c(-5, 5), ylim=c(-5, 5),
frame=FALSE, cex.lab=1, pch=17, col= "#006600" )
axis(1, at=c(-6:5),labels=c(-6:5),pos=-6, las=0)
axis(2, at=c(-6:5),labels=c(-6:5),pos=-6, las=2)
points(datasubset2$Comp.1, datasubset2$Comp.2, pch=21, col="#FC7E81")
points(datasubset3$Comp.1, datasubset3$Comp.2, pch=22, col="#008000")
```

```
points(datasubset4$Comp.1, datasubset4$Comp.2, pch=6, col="#996633")
points(datasubset5$Comp.1, datasubset5$Comp.2, pch=25, col="#ff9900")
points(datasubset6$Comp.1, datasubset6$Comp.2, pch=10, col="#33ccff")
points(datasubset7$Comp.1, datasubset7$Comp.2, pch=8, col="#000000")
points(datasubset8$Comp.1, datasubset8$Comp.2, pch=13, col="#ffff00")
points(datasubset9$Comp.1, datasubset9$Comp.2, pch=12, col="#cc66ff")
Plot_ConvexHull(xcoord=datasubset1$Comp.1, ycoord= datasubset1$Comp.2,
lcolor="#006600")
Plot_ConvexHull(xcoord=datasubset2$Comp.1, ycoord= datasubset2$Comp.2,
lcolor="#FC7E81")
Plot_ConvexHull(xcoord=datasubset3$Comp.1, ycoord= datasubset3$Comp.2,
lcolor="#008000")
Plot_ConvexHull(xcoord=datasubset4$Comp.1, ycoord= datasubset4$Comp.2,
lcolor="#996633")
Plot_ConvexHull(xcoord=datasubset5$Comp.1, ycoord= datasubset5$Comp.2,
lcolor="#ff9900")
Plot_ConvexHull(xcoord=datasubset6$Comp.1, ycoord= datasubset6$Comp.2,
lcolor="#33ccff")
Plot_ConvexHull(xcoord=datasubset8$Comp.1, ycoord= datasubset8$Comp.2,
lcolor="#ffff00")
Plot_ConvexHull(xcoord=datasubset9$Comp.1, ycoord= datasubset9$Comp.2,
lcolor="#cc66ff")


##LDA
setwd("F:/Manuscripts/Block A/R/LDA/6 Loco")
install.packages("MASS")
library(MASS)
extanttaxa<-read.csv("LDAextant.csv", header=TRUE, row.names=1)
fossiltaxa<-read.csv("LDAfossil.csv", header=TRUE, row.names=1)
extantlda<-lda(Grade ~ Comp.1 + Comp.2 + Comp.3 + Comp.4 + Comp.5 + Comp.6 +
Comp.7, data=extanttaxa)
predict the locomotor grades of extant taxa:
pred.extant<-predict(extantlda, extanttaxa[,c(1:7)])$class
table(pred.extant, extanttaxa[,8])
pred.extant.df<-as.data.frame(pred.extant)
colnames(pred.extant.df)<-"Predicted_l.grade"
extanttaxa<-cbind(extanttaxa, pred.extant.df)
pred.fossil<-predict(extantlda, fossiltaxa)$class
pred.fossil.df<-as.data.frame(pred.fossil)
colnames(pred.fossil.df)<-"Predicted_l.grade"
fossiltaxa<-cbind(fossiltaxa, pred.fossil.df)
write.csv(extanttaxa, file="LDAextantpredic.csv")
write.csv(fossiltaxa, file="LDAfossilpredic.csv")

##ANOVA
setwd("C:/Users/Elsa/Documents/Manuscripts/Block A/R/ANOVA/Astragali")
```

```
library(phytools)
library(paleotree)
tree<-read.newick("TreeEdit.tre")
plot.phylo(tree)
sort<-read.csv("TaxaLocoANOVA.csv", header=TRUE, row.names=1)
data<-read.csv("PCAScoresANOVA.csv", header=TRUE, row.names=1)
data <- data[ tree$tip.label , ]
grades <- sort[ tree$tip.label , 1 ]
names( grades ) <- tree$tip.label
PC1<-data[tree$tip.label,1]
PC2<-data[tree$tip.label,2]
PC3<-data[tree$tip.label,3]
PC4<-data[tree$tip.label,4]
PC5<-data[tree$tip.label,5]
PC6<-data[tree$tip.label,6]
PC7<-data[tree$tip.label,7]
names(PC1) <- names(PC2) <- names(PC3) <- names(PC4) <- names(PC5) <-
names(PC6) <- names(PC7) <- tree$tip.label
phyANOVA1<-phylANOVA(tree, grades, PC1, nsim=10000, posthoc=TRUE,
p.adj="bonferroni")
phyANOVA2<-phylANOVA(tree, grades, PC2, nsim=10000, posthoc=TRUE,
p.adj="bonferroni")
phyANOVA3<-phylANOVA(tree, grades, PC3, nsim=10000, posthoc=TRUE,
p.adj="bonferroni")
phyANOVA4<-phylANOVA(tree, grades, PC4, nsim=10000, posthoc=TRUE,
p.adj="bonferroni")
phyANOVA5<-phylANOVA(tree, grades, PC5, nsim=10000, posthoc=TRUE,
p.adj="bonferroni")
phyANOVA6<-phylANOVA(tree, grades, PC6, nsim=10000, posthoc=TRUE,
p.adj="bonferroni")
phyANOVA7<-phylANOVA(tree, grades, PC7, nsim=10000, posthoc=TRUE,
p.adj="bonferroni")
phyANOVA1
phyANOVA2
phyANOVA3
phyANOVA4
phyANOVA5
phyANOVA6
phyANOVA7
```

APPENDIX 20 Measurements for taxa in calcaneal and astragalar PCA.

Cl = calcaneal length; Cal = calcaneal body length; Ctl = calcaneal tuber length; Csw = calcaneal sustentacular width; Ccw = calcaneal cuboidal width; Ctw = calcaneal tuber width; Al = astragalar length; Anl = astragalar neck width; Atw = astragalar trochlea width. Number (#) corresponds to PCAs in Appendices 21 nd 22.

#	Specimen No.	Taxon	Cl	Cal	Ctl	Csw	Ccw	Ctw	Al	Anl	Atw
1	NMNH 142097	*Aepyprymnus rufescens*	24	5.49	14.37	3.43	9.83	7.92	10.61	3.88	13.13
2	NMNH 155194	*Allactaga sibirica*	11.15	3.18	5.82	2.34	2.19	2.35	4.91	2.51	3.33
3	NMNH 344221	*Amblysomus hottentotus*	4.31	1.24	2.56	0.9	1.83	1.36	2.35	1.35	1.78
4	NMNH 261263	*Aplodontia rufa*	13.22	4.71	5.59	3.09	3.29	4.36	7.77	3.67	5.33
5	NMS R470/98	*Bettongia penicillata*	19.12	3.92	11.44	1.521	6.228	5.994	7.1	3.3	10.3
6	NMNH 582737	*Callimico goeldii*	15.09	6.66	4.82	2.73	4.51	3.75	10.29	4.37	6.18
7	NMNH 399069	*Callithrix argentata*	12.62	6.3	2.95	1.81	3.67	3.25	7.7	4.39	4.04
8	NMNH 582900	*Callithrix geoffroyi*	12.7	6.52	2.99	2.62	3.62	3.12	7.98	4.33	4.42
9	NMNH 464247	*Caluromys derbianus*	7.74	2.79	3.43	1.25	3.46	2.12	5.63	3.37	5.23
10	NMNH 20900	*Cavia porcellus*	12.11	4.45	4.88	2.56	2.76	2.91	6.28	2.44	4.21
11	NMNH A43062	*Chaetodipus fallax*	4.71	1.75	1.86	1.39	0.99	1.07	2.49	1.34	1.74
12	NMNH 241124	*Crossarchus alexanidri*	15.26	5.78	5.69	2.96	5.69	4.62	9.35	4.2	7.27
13	NMNH 296065	*Cryptomys hottentotus*	7.17	2.23	3.43	1.36	1.63	1.83	3.25	1.52	2.29
14	NMS Z.1999.187.009	*Dactylopsila trivirgata*	9.65	3.23	3.978	1.919	2.51	1.81	-	-	-
15	NMNH 396649	*Dasycercus byrnei*	6.86	2.47	3.25	1.53	2.79	2.27	4.12	1.97	4.12
16	NMNH 283979	*Dasyurus hallucatus*	11.91	2.9	5.54	1.61	3.58	3.39	6.78	2.57	6.44
17	NMNH A35089	*Didelphis marsupialis*	15.38	2.47	8.16	3.16	5.83	5.03	9.71	3.22	9.73
18	NMNH A22798	*Dipodomys deserti*	11.08	3.88	4.65	2.21	2.3	2.21	4.76	2.71	2.99
19	NMNH 396674	*Echinosorex gymnura*	18.63	7.04	6.77	1.89	4.39	4.82	8.67	3.64	5.37
20	NMNH 399312	*Elephantulus rufescens*	6.33	2.8	2.54	0.91	1.65	1.56	3.34	1.67	2.31
21	NMNH 578714	*Eliurus webbi*	7.26	2.74	2.78	1.77	1.74	1.63	4.02	2.58	2.64
22	NMS Z.2007.62.61	*Erinaceus europaeus*	10.33	3.01	4.88	2.08	2.53	3.05	6	2.9	3.7
23	NMNH 588791	*Funisciurus pyrropus*	9.28	4.09	3.18	2.1	2.25	2.57	5.91	2.54	3.94
24	NMNH A35259	*Galictis cuja*	15.02	4.97	5.37	3.51	5.33	4.99	10	4.35	7.76
25	NMNH A35400	*Genetta maculata*	21.26	8.64	7.25	3.64	5.88	6.4	12.3	6.33	8.38
26	NMNH A22024	*Geomys pinetis*	9.84	2.25	4.74	2.34	2.34	2.69	4.94	2.15	3.35

27	NMNH 527620	*Glaucomys sabrinus*	6.91	2.67	2.48	1.51	1.73	1.58	4.15	1.93	2.5
28	NMNH 570478	*Glaucomys volans*	5.6	1.95	1.98	1.27	1.73	1.35	3.58	1.58	2.14
29	NMNH 105291	*Glis glis (Myoxus glis)*	6.94	2.74	2.69	1.66	1.9	1.89	3.52	1.92	2.21
30	NMNH 236677	*Gracilinanus microtarsus*	2.59	0.95	1.5	1.32	0.66	0.61	1.82	0.85	1.6
31	NMS Z.1999.187.011	*Gymnobelideus leadbeateri*	7.08	2.59	2.53	0.93	1.428	2.46	3.2	1.6	3.4
32	NMNH 539431	*Heliosciurus rufobrachium*	11.54	4.56	4.13	2.28	2.96	2.82	6.65	3.48	4.4
33	NMNH 354999	*Hemicentetes semispinosus*	4.8	1.65	1.68	0.9	1.98	1.43	3.08	1.18	2.58
34	NMNH 144104	*Herpestes brachyurus*	21.42	8.15	7.62	3.45	5.2	6.21	12.12	5.5	8.86
35	NMNH 238438	*Isoodon macrourus*	22.74	6.05	13.01	2.09	5.21	7.52	7.74	1.25	8.59
36	NMNH 308387	*Jaculus jaculus*	7.72	2.61	3.85	1.08	1.37	1.53	3.21	1.56	2.38
37	NMNH 588175	*Leontopithecus chrysomela*	15.12	6.61	4.67	2.91	4.23	4.47	9.54	4.62	5.85
38	NMNH 172694	*Lophiomys imhausi*	12.84	4.36	4.96	2.8	3.08	3.44	7.08	4.12	5.12
39	NMNH 303065	*Metachirus nudicaudatus*	10.66	3.79	5.04	1.91	2.83	2.55	6.57	2.73	6.35
40	NMNH 577056	*Microgale talazaci*	4.72	2.2	1.21	0.96	1.36	1.14	3.07	1.7	2.11
41	NMNH 519825	*Microtus pennsylvanicus*	4.05	1.53	1.84	1.07	1.44	1.15	2.6	1.09	1.71
42	NMNH 464978	*Monodelphis domestica*	5.81	2.35	2.07	1.01	1.53	1.32	3.05	1.52	2.71
43	NMNH 237730	*Myrmecobius fasciatus*	11.28	3.41	5.21	1.47	3.78	3.49	6.04	2.47	6.58
44	NMNH 529352	*Neotoma bryanti*	9.18	3.14	4	1.98	2.19	2	4.59	2.57	3.16
45	NMNH 256920	*Neovision vison (Mustela vison)*	13.86	4.95	4.8	3.31	3.93	4.05	9.73	4.47	5.57
46	NMNH 449233	*Nesomys rufus*	9.37	4.06	3.77	1.88	2.08	2.25	5.18	3.12	3.22
47	NMS ExG9	*Notoryctes sp.*	5.13	1.21	2.9	0.69	1.02	1.12	3	1.3	2.1
48	NMNH 397332	*Octodon degus*	7.89	3.28	2.91	1.86	2.39	2.4	3.96	1.37	3.05
49	NMNH 397002	*Octodontomys gliroides*	9.13	3.25	2.98	1.76	2.47	2.38	4.47	1.94	2.62
50	NMNH 297847	*Oncifelis geoffroyi*	29.73	11.3	11.56	5.04	11.07	7.39	16.17	8.09	11.32
51	NMNH 564217	*Ondatra zibethicus*	11.48	4.98	3.36	2.32	3.66	3.28	8.4	4.5	5.18
52	NMS	*Ornithorhynchus anatinus*	9.61	5.63	3.31	3.75	2.79	3.3	9.8	3.7	6.6
53	NMNH 540931	*Pappogeomys merriami*	13.2	2.74	6.27	2.41	2.49	3.14	7.25	3.21	5.06
54	NMNH 295211	*Paraxerus cepapi*	9.1	3.8	3.04	2.22	2.23	2.34	5.23	2.58	3.68
55	NMS 18	*Perameles gunnii*	9.57	3.08	4.66	0.83	2.24	2.67	3.9	1.5	4
56	NMS XH2-17.1	*Petauroides volans*	7.1	2.67	1.57	1.07	1.23	1.8	-	-	-
57	NMNH 297823	*Petaurus breviceps*	6.53	2.61	1.93	1.34	2.23	1.36	4.17	2.26	3.71
58	NMNH 241593	*Petrodromus tetradactylus*	10.77	4.37	4.93	2.26	2.53	2.59	6	2.9	3.72

59	NMS PH5504	*Phalanger (Strigocuscus) gymnotis*	16.89	9.03	4.71	2.37	5.2	4.51	7.2	2	6.4
60	NMNH 304647	*Philander opossum*	8.74	3.1	4.43	1.66	3.4	2.89	5.6	2.09	6.02
61	NMNH A49973	*Prionailurus planiceps*	23.6	8.46	8.36	3.68	8.59	6.52	13.43	5.65	9.14
62	NMNH 395048	*Prionodon linsang*	14.61	5.94	4.68	2.42	4.56	3.75	8.92	3.87	5.47
63	NMS W5617	*Pseudocheirus peregrinus*	10.74	4.14	4.3	0.92	2.99	2.88	6.6	3	5.9
64	NMNH 584446	*Rattus andamanensis*	7.62	3.07	3.22	1.97	1.73	1.67	4.3	2.29	2.51
65	NMNH 49703	*Ratufa bicolor*	18.26	6.82	6.32	5.06	4.33	4.66	10.87	6.23	7.53
66	NMNH 270291	*Rhizomys sumatrensis*	15	3.9	8.02	3.24	3.42	5.67	7.94	3.64	5.98
67	NMNH 397270	*Saguinus oedipus*	14.59	5.96	4.26	2.63	4.56	3.64	8.74	3.83	5.75
68	NMNH 448232	*Sciurus aberti*	13.19	4.96	5.48	2.55	3.15	3.41	8.04	4.52	5.36
69	NMNH 521410	*Sciurus carolinensis*	13.35	5.01	4.9	2.73	3.34	3.09	8	4.75	5.6
70	NMS 1995.150	*Setonix brachyurus*	26.5	12	15.5	3.5	11.8	9.5	11.1	2.7	14.2
71	NMNH 290520	*Solenodon paradoxus*	17.85	5.31	7.23	4	6.45	5.14	12.91	7.15	6.42
72	NMNH 564281	*Spilogale putorius*	12.44	4.81	4.11	3.04	3.85	3.57	7.84	3.63	5.05
73	NMNH 395839	*Suricata suricatta*	14.92	5.29	5.87	2.64	4.79	5.25	9.2	3.9	7.39
74	NMNH 252597	*Synaptomys cooperi*	4.01	1.69	1.25	1.03	1.2	0.92	2.59	1.23	1.5
75	NMS Z.2012.144	*Tachyglossus aculeatus*	15.69	7.78	8.13	2.8	4.93	7.43	14.4	4.8	6.5
76	NMS RL 76.97	*Talpa europaea*	5.35	1.513	2.71	1.35	2.28	1.94	3.7	1.7	2.2
77	NMNH 221114	*Trichosurus vulpecula*	19.67	7.55	8.69	4.31	6.99	5.09	11.99	4.29	11.8
78	NMNH 396667	*Tupaia longipes*	10.32	4.62	3.37	2.1	2.88	2.53	6.77	4.25	3
79	NMNH 597840	*Tupaia minor*	5.84	2.45	1.89	1.68	1.72	1.49	4.5	2.54	1.99
80	NMNH 396661	*Tupaia tana*	11.5	4.64	3.85	2.63	3.52	2.82	7.91	4.21	3.95
81	NMNH 244925	*Urocyon cinereoargenteus*	21.7	7.43	8.1	3.36	6.02	5.4	12.9	6.04	7.86
82	NMS Z.2000.159	*Zaglossus bartoni*	21.41	10.5	10.85	4.043	6.5	12.37	17.8	9.3	5.7
-	**NMS G.1992.47.121.1**	***Borealestes serendipitus***	**3.55**	**0.6**	**1.49**	**0.496**	**1.307**	**1.4**	**2.344**	**0.29**	**1.99**

APPENDIX 21 Calcaneal morphospace with all extant taxa labelled

See Appendix 20 for key to taxa.

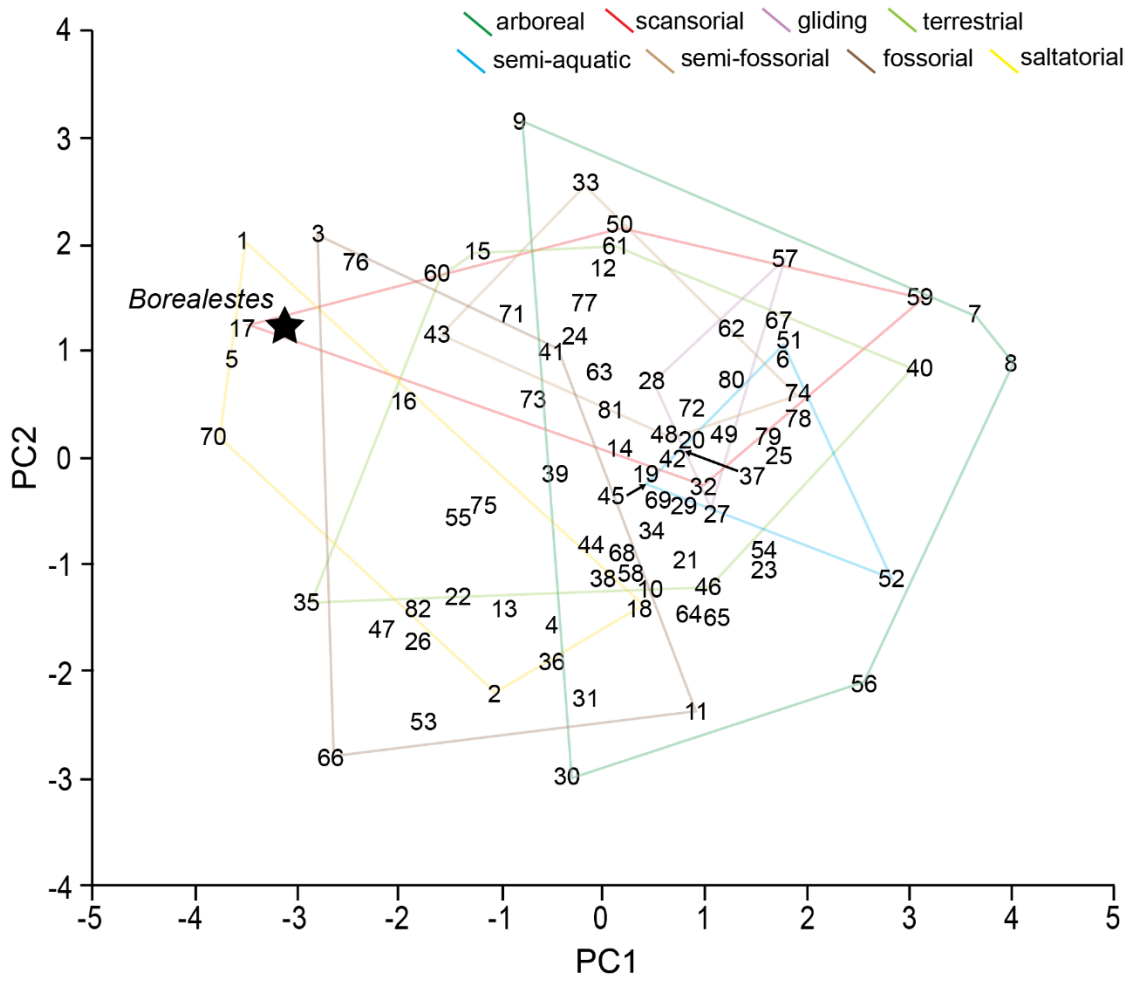

APPENDIX 22 Astragalar morphospace with all extant taxa labelled

See Appendix 20 for key to taxa.

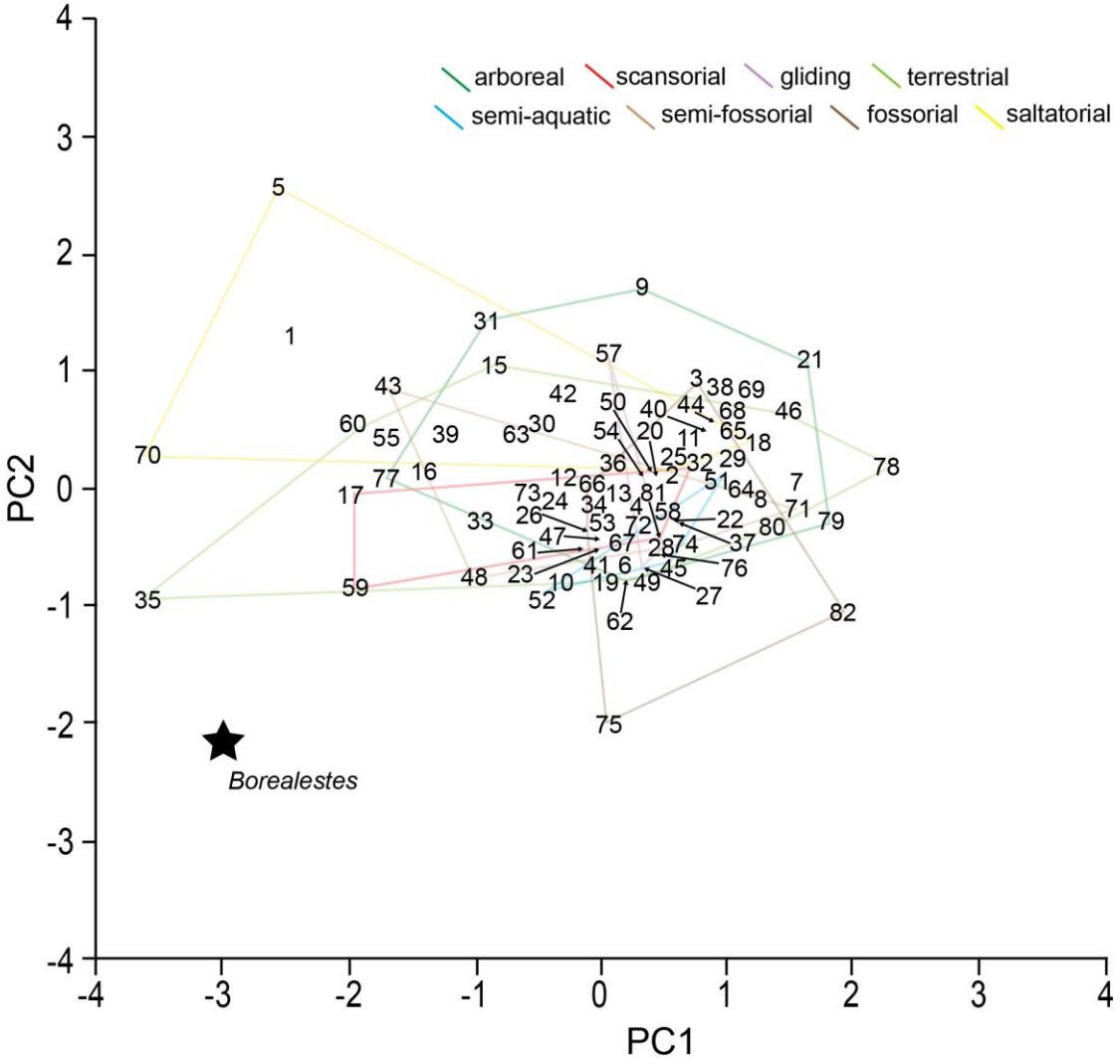

APPENDIX 24 Additional Results of ANOVA and LDA

Within order results: Carnivora. Distribution of principal component axes for PCA on complete dataset of calcaneal ratios, with *F* and *P* values from a phylogenetically corrected ANOVA.

CALCANEA	**PC 1**	**PC 2**	**PC 3**	**PC 4**	**PC 5**	**PC 6**	**PC 7**
Standard deviation	1.722654	1.513376	0.889835	0.837937	0.490237	0.085813	2.27E-02
% Variance	0.423934	0.327187	0.113115	0.100306	0.034333	0.001052	7.39E-05
% Cumulative	0.423934	0.75112	0.864236	0.964541	0.998874	0.999926	1.00E+00
F value	4.768045	0.418455	0.505811	1.439061	0.905962	1.90897	0.072734
P value	0.0703	0.8451	0.8151	0.4306	0.6156	0.3136	0.9928

Within order results: Rodentia. Distribution of principal component axes for PCA on complete dataset of calcaneal, with *F* and *P* values from a phylogenetically corrected ANOVA.

CALCANEA	**PC 1**	**PC 2**	**PC 3**	**PC 4**	**PC 5**	**PC 6**	**PC 7**
Standard deviation	1.92658	1.257767	1.006566	0.654534	0.495513	0.125714	0.058197
% Variance	0.530244	0.225997	0.144739	0.061202	0.035076	0.002258	0.000484
% Cumulative	0.530244	0.756241	0.90098	0.962182	0.997258	0.999516	1
F value	5.875696	1.625266	1.148791	1.57144	0.351823	2.585137	0.436781
P value	0.0066	0.3614	0.555	0.3746	0.9526	0.1328	0.9282

Within order results: Diprotodontia. Distribution of principal component axes for PCA on complete dataset of calcaneal, with *F* and *P* values from a phylogenetically corrected ANOVA.

CALCANEA	**PC 1**	**PC 2**	**PC 3**	**PC 4**	**PC 5**	**PC 6**	**PC 7**
Standard deviation	1.959009	1.372865	0.952712	0.511224	0.27619	0.176713	0.031709
% Variance	0.548245	0.269251	0.129666	0.037336	0.010897	0.004461	0.000144
% Cumulative	0.548245	0.817497	0.947162	0.984498	0.995395	0.999856	1
F value	2.682036	0.65858	0.286242	0.275201	1.314126	6.258237	2.341282
P value	0.2182	0.6978	0.8842	0.8848	0.4608	0.0515	0.2573

Results of LDA assigning extant carnivoran taxa to locomotor mode using PCA results for calcanea. A = arboreal; F = fossorial; G = gliding; S = saltatorial; Sa = semi-aquatic; Sc = scansorial; Sf = semi-fossorial; T = terrestrial.

	A	**Sa**	**Sc**	**Sf**	**T**
A	2	0	0	0	0
Sa	0	1	0	0	0
Sc	0	0	3	0	0
Sf	0	0	0	1	0
T	0	0	0	0	4
% correct	**100**	**100**	**100**	**100**	**100**

Results of LDA assigning extant rodent taxa to locomotor mode using PCA results for calcanea. A = arboreal; F = fossorial; G = gliding; S = saltatorial; Sa = semi-aquatic; Sc = scansorial; Sf = semi-fossorial; T = terrestrial.

	A	**F**	**G**	**S**	**Sa**	**Sc**	**Sf**	**T**
A	7	0	1	0	1	1	3	7
F	0	6	0	0	0	0	0	0
G	0	0	1	0	0	0	0	0
S	0	0	0	1	0	0	0	0
Sa	0	1	0	0	3	0	0	0
Sc	0	0	0	0	0	1	0	0
Sf	2	0	0	0	0	0	1	2
T	9	7	2	1	4	2	4	9
% correct	**78**	**86**	**50**	**100**	**75**	**50**	**25**	**78**

Results of LDA assigning extant diprotodontian taxa to locomotor mode using PCA results for calcanea. A = arboreal; F = fossorial; G = gliding; S = saltatorial; Sa = semi-aquatic; Sc = scansorial; Sf = semi-fossorial; T = terrestrial.

	A	**F**	**G**	**S**	**Sa**	**Sc**	**Sf**	**T**
A	7	0	1	0	1	1	3	7
F	0	6	0	0	0	0	0	0
G	0	0	1	0	0	0	0	0
S	0	0	0	1	0	0	0	0
Sa	0	1	0	0	3	0	0	0
Sc	0	0	0	0	0	1	0	0
Sf	2	0	0	0	0	0	1	2
T	9	7	2	1	4	2	4	9
% correct	**78**	**86**	**50**	**100**	**75**	**50**	**25**	**78**